JAERI-M
85-202

BWR MAIN STEAM LINE BREAK LOCA TESTS RUNS 951, 954 AND 956 AT ROSA-III —BREAK AREA EFFECTS WITH HPCS FAILURE—

December 1985

Mitsuhiro SUZUKI, Kanji TASAKA,
Masahiro KAWAJI, Yoshinari ANODA,
Hiroshige KUMAMARU, Hideo NAKAMURA,
Taisuke YONOMOTO, Hideo MURATA,
and Yasuo KOIZUMI

日本原子力研究所
Japan Atomic Energy Research Institute

JAERI-Mレポートは，日本原子力研究所が不定期に公刊している研究報告書です。
入手の問合わせは，日本原子力研究所技術情報部情報資料課（〒319－11茨城県那珂郡東海村）あて，お申しこしください。なお，このほかに財団法人原子力弘済会資料センター（〒319-11茨城県那珂郡東海村日本原子力研究所内）で複写による実費頒布をおこなっております。

JAERI-M reports are issued irregularly.
Inquiries about availability of the reports should be addressed to Information Division, Department of Technical Information, Japan Atomic Energy Research Institute, Tokai-mura, Naka-gun, Ibaraki-ken 319-11, Japan.

編集兼発行　日本原子力研究所
印　　刷　日立高速印刷株式会社

JAERI-M 85-202

BWR MAIN STEAM LINE BREAK LOCA TESTS RUNS 951, 954 AND 956 AT ROSA-III - BREAK AREA EFFECTS WITH HPCS FAILURE -

Mitsuhiro SUZUKI, Kanji TASAKA, Masahiro KAWAJI,
Yoshinari ANODA, Hiroshige KUMAMARU, Hideo NAKAMURA
Taisuke YONOMOTO, Hideo MURATA and Yasuo KOIZUMI

Department of Nuclear Safety Research,
Tokai Research Establishment, JAERI
(Received November 15, 1985)

This report presents the experimental results of RUNs 951, 954 and 956 in ROSA-III program, which are medium or small main steam line break LOCA tests with assumption of HPCS failure. The ROSA-III test facility simulates a BWR system with volume scale of 1/424 and has four half-length electrically heated fuel bundles, two active recirculation loops, four types of ECCS's, and steam and feedwater systems.

Effects of break area on the depressurization rate, water level and void fraction of the downcomer fluid, and core cooling phenomena were investigated by comparing the present test results with those of RUN 953, a 100% main steam line break test. Namely, (1) the maximum void fraction in the downcomer, which affected the water level swelling, was found to be closely related with the total steam flow area of the main steam line. (2) The ADS actuation affected significantly the system responses in the small steam line break LOCAs. (3) The PCT was higher in a larger steam line break LOCA.

Keywords: BWR, LOCA, ECCS, Integral Test, ROSA-III Program, Main Steam Line Break, Break Area, Downcomer Level, ADS, Data Report

ROSA－ⅢにおけるBWR主蒸気配管破断LOCA実験，RUN 951，954，956
― HPCS故障条件下の破断面積の影響 ―

日本原子力研究所東海研究所原子炉安全工学部
鈴木　光弘・田坂　完二・川路　正裕・安濃田良成
熊丸　博滋・中村　秀夫・与能本泰介・村田　秀夫
小泉　安郎・

（1985年11月15日受理）

本報告は，ROSA－Ⅲ計画において実施された中小口径の主蒸気配管破断LOCA実験であるRUN 951，954，956の実験結果をまとめたものである。実験は高圧炉心スプレイ系（HPCS）の単一故障を仮定した。ROSA－Ⅲ試験装置は，BWR体系を1／424に体積縮小したシステムであり，電気加熱の1／2長さの燃料バンドル4体と，2つの再循環ループ，4種類のECCS，および蒸気・給水系を備えている。

本報では，破断後の減圧速度やダウンカマーの水位とボイド率，炉心冷却状態に及ぼす破断面積の影響を調べるために，以上の実験結果と100％主蒸気配管破断実験RUN 953の実験結果の比較を行った。そして(1)，ダウンカマーの最高ボイド率は，主蒸気配管における全蒸気流出面積により支配され，ダウンカマーの水位スエリングに影響を及ぼす，(2)，自動減圧系（ADS）の作動は，主蒸気配管の小破断時の事象に大きな影響を及ぼす，(3)，最高燃料被ふく管温度（PCT）は，破断面積が大きいほど高いことを明らかにした。

Contents

目　　次

List of Tables for RUNs 951, 954 and 956

List of Figures

List of Figures of Experiment Data for RUN 951

List of Figures of Experiment Data for RUN 954

List of Figures of Experiment Data for RUN 956

List of Figures for Chapter 6

ABBREVIATIONS

ADS	Automatic Depressurization System
AT	Air Tank
AV	Air Actuation Valve
(2)B	(2) inches Pipe of Schedule 80
BN	Boron Nitride
BWR	Boiling Water Reactor
CA	Chromel-Alumel
CCFL	Counter Current Flow Limiting
CHV	Check Valve
CP	Conductivity Prove
CV	Control Valve
CWT	Cooling Water Tank
D	Differential Pressure
d	Diameter
DF	Density of Fluid
DL(+100)	Elevation (+100 mm) from the Bottom of PV
ECCS	Emergency Core Cooling System
ESF	Engineered Safety Features
EX	Heat Exchanger
F	Flow Rate
Fig.	Figure
FS	Full Scale
FW	Feedwater
FWLF	Feedwater Line Flashing
FWP	Feedwater Pump
FWT	Feedwater Tank
HPCS	High Pressure Core Spray
HPCSP	High Pressure Core Spray Pump
HPCST	High Pressure Core Spary Tank

MW	Megawatt
N	Rotation Speed
OR	Orifice
P	Pressure
	Power
PCT	Peak Cladding Temperature
PV	Pressure Vessel
PWT	Pure Water Tank
QOBV	Quick Opening Blowdown Valve
QSV	Quick Shut-off Valve
RCN	Rapid Condencer
ROSA	Rig of Safety Assessment
rpm	Revolution per Minute
S	Signal
s	Second
Sch	Schedule
SUS	Stainless Steel
T	Temperature
T/C	Thermocouple
TC	Temperature of Fluid
TF	Temperature of Fuel
TS	Temperature of Structure Material
UTP	Upper Tie Plate
V	Valve
VF	Void Fraction
W	Watt
WL	Water Level
WSP	Water Supply Pump

HPWP	High Pressure Water Pump
ID	Inner diameter
INC 600	Inconel 600
JP	Jet Pump
K	Kelvin
kg	Kilogram
kPa	Kilopascal
kW	Kilowatt
L	Liter
LB	Liquid Level in Channel Box
LBWR	Large Boiling Water Reactor
LL	Liquid Level
LOCA	Loss-of-Coolant Accident
LOCE	Loss-of-Coolant Experiment
LP	Lower Plenum
LPCI	Low Pressure Coolant Injection
LPCIP	Low Pressure Coolant Injection Pump
LPCIT	Low Pressure Coolant Injection Tank
LPCS	Low Pressure Core Spray
LPCSP	Low Pressure Core Spary Pump
LPCST	Low Pressure Core Spary Tank
LPF	Lower Plenum Flashing
LTP	Lower Tie Plate
M	Momentum Flux
m	Meter
mm	Milimeter
MLHR	Maximum Linear Heat Rate
MPa	Megapascal
MRP	Main Recirculation Pump
MSIV	Main Steam Isolation Valve
MSL	Main Steam Line

1. Introduction

The Rig of Safety Assessment (ROSA)-III program[1] was initiated in 1976 to study the thermal hydraulic behavior of a Boiling Water Reactor (BWR) during a postulated Loss-of-Coolant Accident (LOCA) with the Emergency Core Cooling System (ECCS) actuation and to provide the data base to evaluate the predictability of computer codes developed for reactor safety analysis. The ROSA-III test facility[2] fabricated in 1978 consists of a volumetrically scaled (1/424) primary system of a 3800 MW BWR/6(251-848)[3] with the electrically heated core, the break simulator and the scaled ECCS. Special emphasis of the ROSA-III test program is made on the following objectives, as

(1) To provide the system data required to improve and evaluate the analytical codes currently used to predict the LOCA transients of large BWRs. The performances of the ECCSs are of primary interest.

(2) To identify and investigate any unexpected event(s) or threshold(s) in the response of the plant and to develop analytical techniques that adequately account for such unexpected behavior.

To meet these objectives various kinds of ROSA-III tests have been performed and those results have been published[4]-[33]. Up to the present time, similar experimental studies on the BWR/LOCA phenomena have been performed with respect to some test parameters in TLTA[34], FIST[35] and TBL.[36]

One main steam line break test was performed at the FIST facility with the test conditions of 100% break area at one of the four main steam lines and 2 LPCI failure assumption. Six main steam line break tests have been performed at the ROSA-III facility in 1982 with test objectives to study (1) the effects of steam line break area (2) the effects of break location at upstream-side and downstream-side of MSIV, (3) the effects of downcomer level trip logics on ECCS actuation and (4) the effects of ADS and Safety valve actuation on the small steam line break LOCA. The test data of two tests among the six tests are already published in JAERI.[26][27]

The report presents the experimental test results of three steam line break tests, RUNs 951, 954 and 956 and the effects of break area and ADS actuation on the transient thermal hydraulic phenomena following the steam line break

initiation. RUN 951 is a 34% steam line break test without ADS actuation. RUNs 954 and 956 are 10% steam line break tests with ADS actuation. The trip conditions of the safety valve and MSIV are different between RUNs 954 and 956. All these three tests were performed by assuming failure of the high pressure core spray(HPCS) system. ECCS actuation was tripped by downcomer level trip signals.

Details of the ROSA-III test facility and instrumentations are described in chapters 2 and 3, respectively. Each test conditions and test procedures are described in chapter 4. Chapter 5 shows experiment data of three tests. The effects of break area, ADS and MSIV are descriped in chapter 6 by investigating the three test results and that of RUN 953[27], a 100% steam line break test.

2. ROSA-III Test Facility

The ROSA-III test facility is a volumetrically scaled (1/424) BWR system with an electrically heated core designed to study the response of the primary system, the core and the ECCS during the postulated LOCA. The test facility is instrumented such that various thermal-hydraulic parameters are measured and recorded during the test. Details of the test facility can be refered to the reference (2).

The test facility consists of four subsystems. These subsystems are : (a) the pressure vessel, (b) the steam line and the feedwater line, (c) the recirculation loops and (d) the ECCS. Figures 2.1, 2.2 and 2.3 illustrate configuration of the test facility, the pressure vessel internals and the piping schematics, respectively. The schematic diagram of the test facility and the piping schematic for the test RUN 951 are slightly different as shown later (see Figs.2.11 through 2.13). Table 2.1 compares the major dimensions of the ROSA-III test facility to the corresponding dimensions of the reference BWR system.

The ROSA-III pressure vessel includes various components in it simulating the internal structures of the reactor vessel in the BWR system as shown in Fig. 2.4. The interior of the vessel is divided into the core, the lower plenum, the upper plenum, the downcomer annulus, the steam separator, the steam dome and the steam dryer. The core consists of four simulated fuel assemblies of half length and a control rod simulator. Each fuel assembly contains 62 heater rods (Fig. 2.5) and 2 water rods spaced in a 8 x 8 square array and supported by spacers and upper and lower tie plates. The heater rod is heated electrically with chopped cosine power distribution along the axis as shown in Fig. 2.6. The effective heated length is 1880 mm, one half of the active length of a BWR fuel rod. The high power with radial peaking factor of 1.4 was supplied to the fuel assembly "A" and average power was supplied to the other three bundles "B", "C" and "D" with radial peaking factor of 1.0. The heater rods in each assembly are divided into three groups with respect to heat generation rate as shown in Fig. 2.7. The total electric power is limitted as 4.24 MW by limitation of the power supply system. The relative power generation rate of a heater rod in each group is 1.1, 1.0 and 0.875 respectively. The orifice plate with 44 mm I.D. in one assembly is inserted at each core inlet to control the core inlet flow.

The steam line is connected to the steam dome of the pressure vessel. A control valve is installed in the steam line to control the steam dome pressure in steady state before the initiation of the tests. The steam line has a branch in which the automatic depressurization system (ADS) is installed. The operation of valves in the steam line including the MSIV is described in Chap.4. The feedwater is supplied from the feedwater tank (FWT) through the feedwater line (Fig. 2.8) and the feedwater sparger (Fig.2.9) below the steam separator.

The break unit in the steam line and the recirculation loop are described below. Figure 2.10 shows the main steam line and the recirculation loops for the tests RUN 954 and RUN 956. The steady steam flow is changed to flow through the transient steam line by opening quickly the air valve AV 165 (see Fig.2.3.) immediately after the break initiation and by closing the steady steam line. The steam break flow is lead to the break unit B (break orifice I.D.=9.8mm) and discharged outside the system. The break unit A is isolated both from the steam line and the recirculation loop. The two recirculation loops are similar as shown in Fig.2.10. The steam line and the recirculation loops for the test RUN 951, however, are different from those of the tests RUN 954 and RUN 956. The test RUN 951 was performed prior to the other steam line brak tests by using the recirculation loops for the recirculation loop suction line break tests. Figures 2.11 and 2.12 show the schematic diagram and the piping schematic for the recirculation loop suction line break test. The break units were located at one of the recirculation loops and therfore the two recirculation loops were not the same due to the existence of the break units, which were not exerted during the test RUN 951. The steam discharge flow passed through the steady steam line shown in Fig.2.13 and discharged through the silencer. The steam flow after break was limitted by the orifice (OR-3) with 18.0 mm I.D..

The ROSA-III test facility is furnished with all kinds of the ECCS's available in the BWR system, i.e., the High Pressure Core Spray (HPCS), the Low Pressure Core Spray (LPCS), the Low Pressure Coolant Injection (LPCI), and the ADS. The HPCS and the LPCS spray the cooling water on the top of the core. The LPCI injects the cooling water into the core bypass. Each ECCS consists of a pump, a tank, piping, and a control system. In the all tests of RUNs 951, 954 and 956, a single failure of HPCS diesel generator is assumed.

The water level in the upper downcomer was measured by a differential

pressure transducer and used for the actuations of ECCS's. The LPCS and LPCI in the BWR/6 system are designed to actuate by either the high containment pressure signal or the low downcomer level signal (L1) and to inject the water at their design pressure, P=2.16 MPa and 1.57 MPa, respectively. The actuation signal for the LPCS and LPCI for the present tests, however, is represented by the low downcomer level (L1) and the high containment pressure signal was assumed to be failed. The meanings of this trip logic are as follows. (1)In a case of steam line valve failure such as an abnormal opening of the turbine bypass valve, the containment pressure is kept constant and the system pressure decreases showing an small steam line break LOCA. (2) In a case of small steam line break LOCA, the operators may observe the high downcomer level and make an misjudge such that the high containment pressure signal , which actuates the HPCS, is ignored because the operators are trained to keep the normal water level. In these situations, the LPCS and LPCI must be or may be actuated only by the low downcomer level signal (L1).

The downcomer related trip logics in the present tests are summarized below. The MSIV closure was assumed to actuated at the time of break in RUNs 951 and 954, and by L2 level trip with time delay of 3 s in RUN 956. The LPCS and LPCI were actuated by the low downcomer level with a time delay of 40 s. The ADS was actuated by the low downcomer level with a time delay of 120 s in the tests RUN 954 and RUN 956. In the larger steam line break test, RUN 951, the effect of ADS actuation was neglected.

MSIV Closure = 0 s, L2 + 3 s
LPCS Actuation = (L1 + 40 s) + (P less than 2.16 MPa)
LPCI Actuation = (L1 + 40 s) + (P less than 1.57 MPa)
ADS Actuation = L2 + 120 s

3. Instrumentation

The instrumentation of the ROSA-III is designed to obtain thermal-hydraulic data during the simulated BWR LOCA. The data obtained from the experiments will contribute to assess the analytical computer codes for LOCA analyses and to investigate the transient fluid and fuel responses during the simulated LOCA. Table 3.1 summarizes the No.4 instrumentation list used in the steam line break test RUN 951. In RUNs 954 and 956, smaller number of instrumentations were used as shown in Table 3.1.

Tables 3.2 and 3.3 show the measurement list and the core instrumentation list for RUN 951, respectively. The measurement lists for RUNs 954 and 956 are also shown in Table 3.2. The figure numbers of corresponding measurements for RUNs 954 and 956 are described in the chapter 5. Instrumentation locations are shown in Fig. 3.1 through Fig. 3.6.

Typical measured parameters in the ROSA-III are pressure, differential pressure, flow rate, electric power, pump speed, fluid and metal temperatures, collapsed liquid level, two-phase mixture level, fluid density, trip signals and so on.

Pressure and differential pressure transducers are two-wire, direct-current type which convert diaphragm displacement to electric capacitance. The pressure lead pipes are either the standard single, cylindrical pipes used in conjunction with condensate pots, or dual concentric cylinders capable of the circulation of cooling water to prevent flashing of the fluid.

The flow rate is measured by four types of instrumentations, i.e., turbine flow meter, orifice type flow meter, Venturi type flow meter and momentum flux measurement equipment depending on the fluid condition and measuring location. The turbine flow meter is used for subcooled water flow such as ECCS injection flow and feedwater flow. The orifice type flow meter is used for both flows, one is steam line flow including ADS flow and another one is jet pump discharge flow in the intact loop. The Venturi flow meters used for recirculation flows in both loops and jet pump discharge flow in the intact loop. The momentum flux measurement using drag-disk is shown later.

The temperatures of the fluid, structural material and fuel rod cladding are measured with chromel-alumel thermocouples (CA T/C) of 1.6 or 1.0 mmφ. The thermocouples for fuel rod cladding temperatures are imbedded at the

surface of the cladding as shown in Fig. 2.5. There are seven (maximum) thermocouples for one fuel rod along the axial direction.

Liquid levels are measured by either differential pressure transducers, described above or needle type electrical conductivity probes (CP) developed in the ROSA-III program. The probes are distributed along the vessel height to detect the existence of water or vapor at different levels.

The electric power supplied to the simulated fuel rods is controlled to follow the predetermined power curve with function of time and measured by a fast response electric power meter.

Pump speed is measured by a pulse generator integral of the pump. Trip signals such as selected valve positions and pump coastdown simulation initiations and so on are detected in order to record the exact actuation times of trip signals.

Fluid density in the pipe is measured by means of gamma densitometers. Preliminary studies indicate that two-beam and three-beam densitometers should be used to determine the flow regime. Figures 3.7 and 3.8 show the beam directions of the three-beam and two-beam gamma densitometers. The gamma-ray source is ^{137}Cs and the detector is a water cooled NaI(Tl) scintillation counter.

Momentum flux is measured by a drag disk as shown in Fig. 3.9. The combination of signals from a drag disk and a gamma densitometer is used to determine the two-phase flow rate as shown in Fig. 3.10.

The data acquisition system (DATAC 2000B, Iwasaki Tsushinki Co.) scans all of signals with the frequency up to 30 Hz. The data recorded on magnetic tape are processed by the FACOM M200 system computer at JAERI by off-line control. After evaluation, for example by comparing the initial and final pressure values with standard values, the data is reprocessed using the correct conversion factors as determined from the consistency examination.

More detailed information on the data processing procedure are available in reference (37).

4. Test Conditions and Procedure

The steam line break tests described in the present report, simulated the medium and small steam line breaks (break area of 34 and 10%), which occurred between the reactor pressure vessel and the MSIV in one of the main steam lines of a BWR. Because of simplifications, the test procedures and test conditions for the ROSA-III tests may be different from some BWR steam line LOCA scenarios. The MSIV closure was assumed to occur at the same time of the break in RUNs 951 and 954 and at the trip signal (L2 + 3s) in RUN 956. A single failure of HPCS was assumed in all the tests. The LPCS and LPCI were actuated in all the tests by the downcomer low level trip signal (L1) and by the designed pressures assuming the failure of the high containment pressure signal. The ADS was actuated in the smaller steam line break tests (RUNs 954 and 956).

Test conditions of the steam line break tests, RUNs 951, 954 and 956 are compared in Table 4.1. The major events and test procedures in each test are summarized in Table 4.2 through Table 4.4.

4.1 RUN 951, A 34% Steam Line Break Test

The test RUN 951 is a 34% steam line break scoping test for the ROSA-III facility. The break units in the recirculation loop were not opened but the steam discharged through the steady state steam discharge line. The break area was simulated by an orifice with 18.0 mm I.D. (OR-3) in the third steam line branch. The measured initial test conditions were; steamdome pressure of 7.35 MPa, total core power of 3.965 MW, core inlet mass flow of 16.35 kg/s, core inlet subcooling of 10.0 K, main steam flow of 2.03 kg/s, feedwater flow of 2.02 kg/s, and pressure vessel water level of 5.04 m. The initial average fluid quality in the upper plenum was estimated as 0.13. The initial core power of 3.965 MW in RUN 951 corresponds to 44% of the 1/424 scaled BWR/6 rated power and the initial core flow in RUN 951 corresponds to 25% of one BWR/6 fuel bundle flow.

RUN 951 was performed by the following procedures as shown in Table 4.2. Break was initiated by fully opening the control valve CV-130 in the third steam line shown in Fig. 4.1. At the same time, the power supply to both

recirculation pumps was terminated and the pump speed coasted down rapidly. After the break, the steady state core power was maintained for 9.0 seconds and then decreased along the power curve shown in Fig. 4.2, which simulated the heat transfer rate to coolant during a hypothetical BWR/LOCA.[38] The steam flow to heat up the feedwater from the third steam line was manually stopped immerdiately after the break by closing the valves CV-1 and CV-2. The feedwater line was closed at 2 s after the break.

The MSIV was assumed to close at the time of break and the steam discharged through the steam line orifice. ADS was not actuated in RUN 951. The ECCS actuation signal was tripped by L1 level (4.25 m from PV bottom) signal with a time delay of 40 seconds. The LPCS was actuated at 375 s after the break (at 1.48 MPa of the system pressure) and LPCI was actuated at 415 s after the break (at 1.31 MPa of the system pressure).

The experiment data acquisition system started 119 seconds prior to the break initiation and continued up to 816 seconds after the break. Most of the instruments functioned successfully.

4.2 RUN 954, A 10% Steam Line Break Test

RUN 954 is a small steam line break test with a break area of 10% of the 1/424 scaled main steam line piping flow area assuming both the MSIV closure at the break time and the HPCS failure. The break area was simulated by an orifice with 9.8 mm I.D. (OR-5) in the first steam line branch. The measured initial test conditions were 7.35 MPa of steam dome pressure, 3.975 MW of total core power, 16.7 kg/s of core inlet mass flow, 10.6 K of core inlet subcooling, 2.06 kg/s of main steam flow, 2.07 kg/s of feed water flow, and 5.03 m of the pressure vessel water level. The initial average fluid quality in the upper plenum was estimated as 0.124. The initial core power of 3.975 MW in RUN 954 corresponds to 44% of the BWR/6 rated power and the initial core flow in RUN 954 corresponds to 25% of one BWR/6 bundle flow.

RUN 954 was performed by the following procedures as shown in Table 4.3. Break was initiated by opening the Valve AV165 in the first steam line branch and by closing the valve AV168 in the steady state steam line (third branch) following a break signal which opened the valve of Break B. The characteristics of valves are listed in Table 4.5. At the same time, the power supply to both recirculation pumps was terminated and the pump speed coasted down rapidly. After the break, the steady state core power was

maintained for 9.0 seconds and then decreased along the power curve as in RUN 951. The steam flow to heat up the feedwater from the third steam line was manually stopped immediately after the break by closing the valves CV-1 and CV-2. The feedwater line began to close at 1 s after break.

As the safety/relief valve systems in the BWR/6 system were not simulated in RUN 954, decrease of the steam discharge flow after MSIV closure resulted in rapid pressure increase and consequently the actuation of the plant safety valve to open between 5.4 s (8.4 MPa) and 16.9 s (7.5 MPa).

The ADS was tripped at 153 s by the L2 level (4.76 m from PV bottom) signal with a time delay of 120 s. The ADS actuation signal in BWR/6 system, however, is not the L2 level but the L1 level.

The LPCS and LPCI were initiated by two trip signals, namely a combination of L1 level (4.25 m from PV bottom) signal in the upper downcomer with a time delay of 40 s and a system pressure lower than 2.16 MPa for LPCS initiation, and L1 level signal with a time delay of 40 s and a system pressure lower than 1.57 MPa for LPCI initiation. In RUN 954, L1 level signal was tripped at 403 s after break. Therefore, the LPCS was actuated at 443 s (P = 1.68 MPa) by the L1 signal with a time delay of 40 s. On the other hand, the LPCI was actuated at 455 s by a rather high pressure set-point of 1.63 MPa.

The experimental data acquisition system was started 120 seconds prior to the break initiation and continued up to 1101 seconds after the break. Most of the instrumentation functioned successfully.

4.3 RUN 956, A 10% Steam Line Break Test Assuming MSIV Closure by L2 Level Trip

The test RUN 956 was performed with the same test conditions as those of RUN 954 except for the MSIV trip logic. The initial test conditions of RUN 956 are compared with those of RUN 954 in Table 4.1. In RUN 956, the MSIV was tripped by the low downcomer level signal (L2) with time delay of 3 s (129s after break) and the steam discharged both through the first (transient line) and third (steady state) steam lines during the first 129 s. The ADS was opened by L2 trip signal with time delay of 120 s. The LPCS and LPCI actuation logics were the same as those of RUN 954. The time of major events and test procedures in RUN 956 are summarized in Table 4.4.

5. Data Processing for RUNs 951, 954 and 956

In RUN 951, the data acquisition frequency was 10 Hz, and in RUNs 954 and 956, it was 5 Hz. The test data was processed and reduced to 1000 data points for computer plotting. The time span and frequency of the reduced data for plotting were 1000 s and 1 Hz, respectively.

The test data of RUN 951 are shown in Figs. 5.1 through 5.168. In these figures, the measured quantity is identified by the channel number and the alphabetic characters (ref. Table 3.2). The test data of RUNs 954 and 956 are described after the description of RUN 951 data, in Figs. 5.169 through 5.308 and Figs. 5.309 through 5.448, respectively.

First the test data of RUN 951 are described below.

Figure 5.1 shows the representative pressure data in the pressure vessel (PV) and main steam line (MSL). Figures 5.2 through 5.25 show differential pressure data between various positions in the pressure vessel and the recirculation loop. Figures 5.26 and 5.27 show the liquid levels in the ECCS tanks and downcomer. Figures 5.28 through 5.34 show the flow rates. Figure 5.35 shows the power supplied to the core with the maximum capacities of 2100 and 3150 kW. The pump speeds of the recirculation pumps are shown in Fig. 5.36. The trip signals such as the break initiation signal and the valve positioning signals are shown in Figs. 5.37 through 5.39. Figures 5.40 through 5.47 show the fluid densities measured by the gamma densitometer. Figures 5.48 and 5.49 show momentum fluxes measured by drag disks. Figures 5.50 through 5.52 show the fluid temperatures at various positions in the system. The fuel rod cladding temperature and the surface temperatures of the water rods and the channel boxes measured at positions 1 through 7 are given in Figs. 5.53 through 5.72. Metal temperatures on the inner and outer surfaces of channel boxes are shown in Figs. 5.73 through 5.79. Figures 5.80 through 5.100 show the fuel rod cladding temperatures in a different manner. Figures 5.101 through 5.131 show the fluid temperatures at the inlet and outlet of the channel boxes. The liquid level signals in the core, the upper and lower plena, the guide tube and the downcomer are shown in Figs. 5.132 through 5.152. The peak cladding temperature (PCT) distribution in RUN 951 is given in Table 5.1.

Quantities obtained from reduction of the test data are shown in Figs. 5.153 through 5.168.

Figure 5.153 shows the estimated liquid levels in the core and the pressure vessel obtained by reducing the conductivity probe signals previously shown in Figs. 5.132 through 5.152. Figures 5.154 and 5.155 show the dryout and quenching times of the representative fuel rods in the core. Figures 5.156 through 5.158 show the average fluid density calculated from the data shown in Fig. 5.40 through Fig. 5.47. The average density is calculated as an arithmetic mean of the densities in multi-directions with the weight of each cord length.

For the three beam densitometer at the jet pump outlet spool,

$$\rho_{av} = 0.3221\rho_A + 0.43\rho_B + 0.2479\rho_C \tag{5.1}$$

where,

ρ_{av}: average density obtained from the three-beam gamma densitometer,
ρ_A : density measured by beam A (bottom),
ρ_B : density measured by beam B (middle),
ρ_C : density measured by beam C (top).

For the two-beam densitometer at the break spool piece,

$$\rho_{av} = 0.5863\rho_A + 0.4137\rho_B \tag{5.2}$$

where,

ρ_{av}: average density obtained from the two-beam gamma densitometer,
ρ_A : density measured by beam A (bottom),
ρ_B : density measured by beam B (top).

Figures 5.159 through 5.164 show the fluid flow rates at the channel inlet orifices, the bypass hole and the jet pump outlets. The fluid flow rates are calculated from the test data which are the pressure drop across the orifices or venturi flow meters and the liquid density obtained from the temperature and the pressure condition. The equation used for the calculation is as follows :

$$G = C_D \cdot A \cdot \sqrt{2g \cdot \rho_l \cdot \Delta P} \qquad (5.3)$$

where,

G : flow rate,

ΔP : pressure drop across the orifice,

C_D : discharge coefficient,

= 0.6552 (the orifice to measure the steam discharge flow rate)

= 0.4761 (the channel inlet orifice)

= 0.8032 (the bypass hole)

= 0.7383 (the orifice to measure the jet pump outlet flow rate)

= 1.1260 (the venturi tube to measure the jet pump outlet flow rate)

A : flow area (m^2)

= 2.875×10^{-3} (the orifice to measure the steam discharge flow rate)

= 1.521×10^{-3} (the channel inlet orifice)

= 1.758×10^{-4} (the bypass hole)

= 1.133×10^{-3} (the orifice to measure the jet pump outlet flow rate)

= 9.095×10^{-4} (the venturi tube to measure the jet pump outlet flow rate)

g : gravitational acceleration (= 9.807 m/s^2),

ρ_l : density of the single-phase liquid (kg/m^3),

This calculation method is not applicable for two-phase flow condition after the LPF initiation at the channel inlet orifice, the bypass hole and the jet pump outlet. The calculated value shows only a trend in two-phase flow condition. Total channel inlet flow rate presents the sum of four channel inlet flow rates.

Figures 5.165 and 5.166 show the collapsed water levels in downcomer and inside the core-shroud, respectively. Each level is obtained from corresponding differential pressure. The differential pressure may include the flow resistance effect, however, the flow resistance becomes negligible after completion of the recirculation pump coastdown.

Figure 5.167 shows the fluid mass inventory in downcomer. The fluid mass inventory is determined from the density and configurational data

inside and outside the core shroud,

$$M = \rho_l \cdot Q \tag{5.4}$$

where,

M : fluid inventory,

ρ_l : liquid density estimated from the satulation temperature and/or pressure,

Q : liquid volume calculated from the liquid level.

The volume Q (m^3) inside the shroud is also given as a function of collapsed water level in downcomer (L),

$$\begin{aligned}
Q &= 0.0 && (\ L \leqq 0.494\ ) \\
Q &= 0.0225L - 0.0111 && (\ 0.494 < L \leqq 1.384\ ) \\
Q &= 0.0697L - 0.0769 && (\ 1.384 < L \leqq 1.519\ ) \\
Q &= 0.0225L - 0.0048 && (\ 1.519 < L \leqq 3.355\ ) \\
Q &= 0.0801L - 0.1980 && (\ 3.355 < L \leqq 4.250\ ) \\
Q &= 0.2443L - 0.8959 && (\ 4.250 < L \leqq 4.413\ ) \\
Q &= 0.2611L - 0.9700 && (\ 4.413 < L \leqq 4.578\ ) \\
Q &= 0.2504L - 0.9211 && (\ 4.578 < L \leqq 4.654\ ) \\
Q &= 0.2375L - 0.8610 && (\ 4.654 < L \leqq 4.815\ ) \\
Q &= 0.2866L - 1.0974 && (\ 4.815 < L \leqq 4.915\ ) \\
Q &= 0.3396L - 1.3580 && (\ 4.915 < L \leqq 5.143\ ) \\
Q &= 0.3607L - 1.4665 && (\ 5.143 < L \leqq 5.365\ ) \\
Q &= 0.3848L - 1.5960 && (\ 5.365 < L \leqq 5.995\ ) \\
Q &= 0.7111 && (\ 5.995 < L\ )
\end{aligned} \tag{5.5}$$

Figure 5.168 shows the fluid mass inventory inside core shroud. The fluid mass inventory is determined from the density and configurational data inside and outside the core shroud,

$$M = \rho_l \cdot Q \tag{5.6}$$

where,

M : fluid inventory,

ρ_l : liquid density estimated from the satulation temperature and/or

pressure,

Q : liquid volume calculated from the liquid level.

The volume Q (m^3) inside the shroud is also given as a function of collapsed water level inside core shroud (L),

$$
\begin{aligned}
Q &= 0.0 && (\ L \leqq 0.0\ ) \\
Q &= 0.2350L && (\ 0.0 < L \leqq 0.497\ ) \\
Q &= 0.1245L + 0.0549 && (\ 0.497 < L \leqq 1.354\ ) \\
Q &= 0.0698L + 0.1290 && (\ 1.354 < L \leqq 3.589\ ) \\
Q &= 0.1648L - 0.2120 && (\ 3.589 < L \leqq 3.744\ ) \\
Q &= 0.1963L - 0.3299 && (\ 3.744 < L \leqq 4.243\ ) \\
Q &= 0.0196L + 0.4193 && (\ 4.243 < L \leqq 4.578\ ) \\
Q &= 0.0186L + 0.4244 && (\ 4.578 < L \leqq 4.654\ ) \\
Q &= 0.0410L + 0.3201 && (\ 4.654 < L \leqq 5.099\ ) \\
Q &= 0.0196L + 0.4292 && (\ 5.099 < L \leqq 5.365\ ) \\
Q &= 0.5344 && (\ 5.365 < L\ )
\end{aligned}
\qquad (5.7)
$$

The test data of RUN 954 are presented in Figs. 5.169 through 5.308 in the similar order as RUN 951. Numbers of temperature and liquid level measurements are decreased in RUN 954. On the other hand, the fluid density, momentum flux and therefore the mass flow rate were determined in the main steam line down the break orifice.

Figure 5.169 shows the pressure data in PV and MSL. Figures 5.170 through 5.193 show differential pressure data between various positions in the pressure vessel and recirculation loops. Figures 5.194 and 5.195 show the liquid levels in the ECCS tanks and downcomer. Figures 5.196 through 5.202 show the flow rates. Figure 5.203 shows the power supplied to the core with the maximum capacities of 2100 and 3150 kW. The pump speeds of the recirculation pumps are shown in Fig. 5.204. The trip signals such as the break initiation signal and the valve positioning signals are shown in Fig. 5.205 through 5.207. Figures 5.208 through 5.215 show the fluid densities measured by the gamma densitometers. Figures 5.216 through 5.218 show momentum fluxes measured by the drag-disks. Figures 5.219 through 5.222 show the fluid temperatures at various positions in the system. The fuel rod cladding temperatures and the surface temperatures of the water

rods and the channel boxes are given in the Figs. 5.223 through 5.242. Figures 5.243 through 5.263 show the fuel rod cladding temperatures in a different manner. Figures 5.264 through 5.279 show the fluid temperatures at the inlet and outlet of the channel boxes. The outer surface temperatures of the channel box are shown in Fig. 5.280. The liquid level signals in the core, the upper and lower plena, the guide tube and the downcomer are shown in Figs. 5.281 through 5.292. The peak cladding temperature (PCT) distribution in the core is given in Table 5.2.

Quantities obtained from reduction of the test data are shown in Figs. 5.293 through 5.308.

Figure 5.293 shows the estimated liquid levels in the core and the pressure vessel obtained by reducing the conductivity probe signals previously shown in Figs. 5.281 through 5.292. Figures 5.294 and 5.295 show transients of the dryout and quenching times of the representative fuel rod in the high and average power bundles. Figures 5.296 through 5.298 show the average fluid density calculated from the data shown in Figs. 5.208 through 5.215. Figures 5.229 through 5.304 show the fluid flow rates at the channel inlet orifices, the bypass holes and the jet pump outlets. The fluid flow rates are calculated like as the calculation of RUN 951. Total channel inlet flow rate presents the sum of four channel inlet flow rates.

Figures 5.305 and 5.306 show the collapsed water levels in downcomer and inside the core shroud, respectively. Each level is obtained from corresponding differential pressure. The differential pressure may include the flow resistance effect, however, the flow resistance becomes negligible after completion of coast down of the recirculation flow.

Figures 5.307 and 5.308 show the fluid mass inventories in the pressure vessel. The fluid mass inventory was determined from the fluid density and configurational data inside and outside, like as the data of RUN 951.

Finally, the test data of RUN 956 are described below.

The test data of RUN 956 are presented in Figs. 5.309 through 5.448. These data are processed and presented in the same way as RUN 954. Therefore, the description of data processing for RUN 956 is abbreviated. List of figures for the experiment data of RUN 956 can be refered by Table 3.2. The maximum cladding temperature distribution for RUN 956 is shown in Table 5.3.

6. Test Results

Brief interpretations for the test results of RUNs 951, 954 and 956 are presented in sections 6.1 through 6.3. The effects of break area and actuation times of MSIV and ADS on the transient thermal hydraulic phenomena in the main steam line breaks are presented in sections 6.4 through 6.6.

6.1 Major Events of RUN 951, A 34.% Steam Line Break Test

The test conditions and major events of RUN 951 are shown in Tables 4.1 and 4.2. The recirculation loops for RUN 951 were the same as those for a recirculation loop suction line break test. However, the break units located in the recirculation loop were not used in RUN 951. The steam line break was initiated by fully opening the pressure control valve CV130 (see Fig.2.13) and restricting the steam discharge flow rate by an orifice (OR-3) with a minimum flow area (18.0 mmI.D.). Therefore, the orifice (OR-3) gave steam line break area of 34 % of a 1/424 scaled BWR steam line flow area. At the same time as the break initiation, the main steam isolation valve (MSIV) was assumed to close quickly and two main recirculation pumps were tripped. The feedwater supply (see Fig.5.30) was stopped between 1.9 s and 3.9 s after the break.

The steam flow through the main steam line (MSL) was measured by a flow meter (see Fig.5.28). In general, the steam flow rate, measured by an orifice-type flow meter (F1 in Fig.2.13) gives an accurate value for a single-phase saturated steam flow. In the two-phase flow condition, the flow measurement gives qualitative characteristics of the flow. It is supposed from the test result that single-phase steam passed the flow meter in a short time after the break and probably in a time period after 200s (superheated steam temperature was detected in the MSL ; see Fig.5.51, TE 159). The pressure began to decrease abruptly at 9 s after break due to decrease of core power (see Fig.5.35) and thereafter decreased monotonously due to the continuing steam discharge flow.

After coastdown of the main recirculation pumps, the fluid in the pressure vessel (PV) flowed due to natural circulation. The differential pressures in PV and recirculation loops (see Figs.5.2 through 5.25) showed

abrupt changes from the initial value after the break initiation due to rapid decrease of frictional pressure loss. After the pump coastdown, most of the differential pressure data showed the values close to the static pressure heads.

Fluid remaining in the system began boiling at 19.2 s in the middle downcomer (see Fig.5.4) and at 25 s in the recirculation loops (Figs. 5.11, 5.12, 5.15, 5.17). By the initiation of fluid flashing, the differential pressure began to decrease in the lower downcomer and the downcomer level swelled in the upper downcomer (see Fig.5.27). As the flashing became smaller, flow oscillations with frequency of 0.07-0.08 Hz became obviously in PV and jet pump discharge lines (see Figs.5.2, 5.14, 5.17, 5.18, 5,20 through 5.25). These oscillations are synchronous.

Due to the decrease of fluid mass inventory, the mixture levels were formed in the channel boxes and other regions (see Fig.5.153). Due to the mixture level decrease in the core, the simulated fuel rods (heater rods) began to heat up and showed the surface temperature excursion (see Figs.5.154 and 5.155, Figs.5.53 through 5.100). Figures 5.153 through 5.155 show that the dryout front of the heater rods agreed well with the falling mixture level front except for upper part of the core.

At the time of 245 s after the break, the remained hot water in the feedwarter line began boiling at the saturation pressure of the feedwater temperature (489 K) as shown in Fig.5.30. The low pressure core spray (LPCS) and low pressure core injection (LPCI) were injected at 375 s and 415 s after the break, respectively (see Fig.5.29). The LPCS and LPCI injections caused rapid water accumulation inside core shroud (see Figs.5.2, 5.5) and rapid heater rods quenching (see Fig.5.53 through 5.100, Figs.5.154 and 5.155). The heater rods quenching was completed within 30 s after the LPCI injection. Bottom of the heater rods did not show dryout because the injected LPCS water reached the bottom of core before the mixture level in core fell to the location. The peak cladding temperature in core was observed as 849 K at the middle of the highest power rod A31 at 394 s after the break (19 s after the LPCS injection, 21 s before the LPCI injection).

On the other hand, the injections of LPCI caused rapid condensation inside core shroud and consequently faster depressurization in the system (see Fig.5.1). Large subcooling temperatures were observed at the upper tie plate (UTP) (see Figs.5.102 through 5.131), in the core bypass region and on the channel box walls. The faster depressurization inside core shroud due to the LPCI injection also caused a temporary increase of void fraction in

the downcomer (see Figs.5.4 and 5.27) and continuous higher void fraction in the main recirculation loops (see Fig.5.11, 5.12, 5.15). The continuous higher void fraction may show a counter current flow limitation at the inlets of recirculation loops and the jet pump drive nozzles. The metal stored heat in the recirculation loop walls and the pump casing metals also contributed to the higher void fraction in the recirculation loops.

During the test period, except for time after LPCI actuation, the upper downcomer water level was kept higher than the estimated collapsed water level inside core-shroud as shown in Fig.5.153. The upper downcomer water level was measured by a differential pressure transducer between the middle downcomer (EL 3.9 m) and the top of PV (EL 6.04 m). The total water head between the downcomer bottom (EL 0.938 m) and the PV top (EL 6.04 m) was also higher than the collapsed water level inside core-shroud. The difference between the upper downcomer water level and the total downcomer water head was due to steam void fraction between the two levels (EL 3.9 m, EL 0.938 m). The difference of the total downcomer head and the collapsed water level inside core shroud is due to differences of the locations of level measurements and average steam void fraction between the downcomer and core. The average steam void fraction in the lower downcomer rose up to 0.35 at 100 s after the break and was kept nearly constantly for a long time. This downcomer void fraction was estimated to be larger than that in the lower plenum by comparing the experiment data of the liquid level signals in the downcomer (see Fig.5.151 and 5.152) and lower plenum (see Fig.5.147 and 5.148). And larger friction losses across the core and separator than jet pumps and downcomer also affected the pressure balance in the pressure vessel. It should be noted in a main steam line break LOCA that the upper downcomer water level indicated higher value than the mixture level inside core shroud and that the heater rods in the core were exposed into steam atmosphere. These phenomena are different from the recirculation loop large break LOCA, where the downcomer level fell down in a short time after the break.

6.2 Major Events of RUN954, A 10 % Steam Line Break Test

The test conditions and major events of RUN954 are shown in Tables 4.1 and 4.3. The initial test conditions of RUN954 were similar to those of RUN951. The steam discharge flow path after break, the break orifice diameter and the recirculation loop were changed from the condition of RUN951, to simulate the 10 % steam line break test and to measure the steam discharge flow rate by a gamma densitometer and drag-disk.

The steam line break was initiated by quickly opening the air valve (AV 165) in the transient steam line (see Fig.2.10) and the quick opening blowdown valve (QOBV-B). The steady steam line was simultaneously closed. As the steam discharge flow rate was limitted to 37 % of the initial steam flow by the break orifice (OR-5) in the transient steam line (see Fig.5.196), the system pressure increased rapidly after the break as shown in Fig.5.169. When the system pressure reached the set point of the plant safety valve actuation (P = 8.4 MPa) at 5.4 s after the break, the safety valve opened. It was closed at 16.9 s after the break at the system pressure of 7.5 MPa. The discharged steam flow through the plant safety valve was not measured but estimated as shown in Appendix A-1.

The steam discharge flow through the safety valve was 2.95 kg/s (1.06 x 10^4 kg/hour) and the total discharged steam mass between 5.4 s and 16.9 s was 34 kg.

At the same time of break, the recirculation pumps were tripped off (see Fig.5.204). The feedwater supply was terminated during 1 s and 4 s after the break (see Fig.5.198). The electric power supplied to the core began to decrease at 9 s after the break and thereafter it simulated the BWR/6 decay power curve[38] as shown in Fig.5.203.

The initial water level in the downcomer (see Fig.5.195) was 5.03 m, which included pressure loss of the downward downcomer flow. During the first 5.4 s, the downcomer water level was maintained constant. The steam discharge flow through the plant safety valve caused the temporary level increase after the time of 5.4 s.

At the time of 82 s after the break, the lower downcomer level (pressure head) began to decrease, which indicated the initiation of fluid flashing. At 153 s after the break, the ADS was opened by the L2 trip water level (4.76 m from the bottom of PV) with a time delay of 120 s. By the ADS opening, the system pressure decreased rapidly and the remained water in the

system initiatedto flash violently. The effects of ADS opening are shown in the experiment data of downcomer water level (Fig.5.195) and differential pressures in the recirculation loops (Figs.5.179, 180, 182, 183 and 185). The ADS opening increased the void fraction in the lower downcomer and raised the collapsed water level in the upper downcomer.

At 403 s after break, the upper downcomer water level reached the L1 trip level (4.25 m from the PV bottom) and the LPCS and 3LPCI were actuated with the time delay of 40 s (see Fig.5.197). The LPCI water increased the depressurization rate (see Fig.5.169) and mass inventory in the pressure vessel. The injected LPCS and LPCI water accumulated inside core shroud and then flowed into the downcomer. The mass inventory in the recirculation loop, which are indicated by the differential pressure data, began to decrease rapidly after the LPCI actuation and recovered abruptly about 200 s after the LPCI actuation (see Figs.5.179, 180 and 183).

Fuel rod surface temperatures were measured by CA thermocouples of 1.0 mm O.D inbedded in the fuel rod sheath made of inconel 600. There are seven thermocouples for each fuel rod. Fuel rods in channel A have the channel peaking factor of 1.4 and those in other 3 channels B, C and D have 1.0. Following core cooling behaviors have been observed from the temperature responses shown in Figs.5.223 through 5.263. (1) The peak cladding temperature (PCT) was observed as 683 K at the position 3 of A12 rod at 454 s after break (11 s after LPCS initiation). (2) The major dryout of fuel rods initiated at 300 s from top part of the core but the lower part of the core (below Position 5) were not exposed into steam. The whole core was quenched completely at 467 s after break (12 s after LPCI actuation). (3) Improvement of local core cooling was observed in the upper part of the core before the LPCS actuation due to the fall back water from the upper plenum.

Figures 5.240 and 5.241 show fluid temperatures on the surface of water rods in A and C channels. It should be noted that these water rod surface temperatures were slightly higher than the surface temperatures of the peripheral heater rods after the whole core quench as shown in Figs.5.223 and that they were close to those of central rod of each bundle (Figs.5.227 and 237). And the temperature distribution along the axial direction meant existence of upward flow in the central region including the water rods and downward flow in the peripheral region of the channel box.

Figure 5.280 shows fluid temperatures on the outer surface of channel box A. These temperatures showing large subcooling after LPCI actuation, indicated that the LPCI water caused rapid condensation and depressuriza-

tion. From the temperature responses in the pressure vessel (see Figs.5.219 and 5.220) and recirculation loops, flow path of the ECC water can be found as follows. The steam dome temperature showed the saturation temperature. Fluid temperatures near the MRP1 and MRP2 are close to the saturation temperature. Fluid temperature in the lower downcomer was higher than that in the upper downcomer. Fluid temperature in the lower plenum is higher than that in the upper downcomer and lower that in the lower downcomer. Fluid temperature in the upper plenum was the lowest among these data. It is considered that the injected ECC water filled up the core bypass, core, upper plenum, lower plenum and downcomer, sequentially, and that the recirculation loop pipings near the recirculation pumps were the last part for the ECC water arrival.

Figures 5.281 through 5.292 show liquid level signals in PV. Liquid level fall and its recovery in the core are clearly shown in those figures. The liquid level lowered below the position 1 at 296 s and recovered at 465 s. The position 5 was exposed into steam environment for a few seconds after 443 s and rewetted soon. Difference of the liquid level behaviors among the A, B and C channels was not observed clearly. Figures 5.288 and 5.289 show that no water level was formed in the core inlet chamber. No water levels were also formed below the middle part of downcomers and in the lower plenum.

Figure 5.293 shows the representative fuel rod behaviors, the mixture levels and the collapsed water level in the pressure vessel. The mixture levels in A and C channels were higher than the collapsed water level inside core shroud and they were lower than the collapsed water level in the upper downcomer. It should be noted that the fuel rods in the upper part of the core had been exposed temporarily into steam environment whereas the water level in the upper downcomer stayed higher than the top of core.

Figures 5.294 and 5.295 show dryout and quench times of the fuel rods and the mixture level transients in the core. It is shown from the figures that there was little difference among the dryout and quench behaviors of fuel rods in the same channel box and also in four channel boxes, namely, these dryout and quench behaviors agreed very well with the mixture level transients in the core. It is evident that mixture level controlled the fuel rods cooling conditions in a small break LOCA.

The steam discharge flow rate was measured at the break unit B at the downstream of the orifice OR-5 by using the momentum flux and fluid density (see Fig.5.304). The steam discharge flow rate measured by a gamma densito-

meter and a drag disk should be more accurate in the two-phase flow region than that by the orifice-type meter (see Fig.5.196). These experimental data were corrected at the following two reference conditions; i.e., no steam flow at the initial condition and corrected super-heated steam flow at 150 s after the break.

The experiment data of fluid densities of beams A, B and C in the horizontal pipings at the downstream of the jet pumps, indicated that stratified flow pattern was observed both in blowdown and reflooding phases, and that they were filled up with water at 650 s after break (about 200 s after the LPCI actuation).

Figures 5.214 and 5.215 show fluid densities of beam A and beam B at the downstream of theorifice OR-5. Higher fluid density before break means existence of water level in the horizontal pipe region, which had leaked through the valve AV165 in the first branch of the main steam line and accumulated in the lower horizontal region.

6.3 Major Events of RUN 956, A 10 % Steam Line Break Test Assuming MSIV Closure by L2 Level Trip

The test conditions and major events of RUN956 are shown in Tables 4.1 and 4.4. The test conditions of RUN956 were very similar as those of RUN954 except for the MSIV trip logic. In RUN956, the MSIV was tripped to close by the L2 trip level of the upper downcomer level measurement with time delay of 3 s.

The break was initiated by quickly opening the quick opening valve (QOBV-B) and the air valve (AV 165) in the transient steam line as shown in the previous section. At the same time of break, a part of steady steam flow used to heat up the feedwater was also terminated by closing the valves CV-1 and CV-2 and the recirculation pumps were tripped off. The steam discharged through the following two pathes during 129 s after the break. Those are (1) the steady state steam line, where the initial steam flow rate was 2.06 kg/s and (2) the transient steam line, where the steam flow was limitted by the break orifice (OR-5) with flow area of 7.54×10^{-5} m^2 (10 % of the 1/424 scaled BWR steam line flow area). The steam flow rateshown in Fig. 5.335 is the sum of these two flows during the 129 s. After the MSIV closure at 129 s, the steam flow rate showed only the break steam flow. At 244 s after the break, ADS was actuated to open by the L2 trip level with time delay of 118 s. And the ADS flow rate was added to the break flow rate as shown in Fig.5.335.

According to these steam flow responses, the system pressure dereased after break as shown in Fig.5.309. By the break initiation, the system pressure began to decrease abruptly and then turned to increase due to increased steam generation, which is a result of loss of core inlet nsub-cooling caused by the feedwater stop. When the electric core power began to decrease at 9 s after the break, the system pressure also initiated to decrease. At the system pressure of 6.4 MPa (25 s after break), the lower plenum plashing initiated affecting the depressurization rate. At 129 s after break, the depressurization rate became lower by closing the MSIV (AV 168) and at 244 s after break it began to flow area decrease faster again due to ADS actuation.

These pressure responses affected the void distribution in the system and therefore it affected the differential pressures in the recirculation loops (Figs.5.319, 320, and 323) and downcomer (Figs.5.312 and 5.335), the

fluid densities at the jet pump discharge lines (Figs.5.348 through 5.353) and core inlet flow rates (Figs.5.329 through 5.332). The downcomer head (Fig.5.312) clearly shows theeffects of pressure response on void fraction, which is closely related with the depressurization rate or the steam discharge flow area. This relation is investigated in the next section. The MSIV closure decreased the upward steam flow in PV and supressed the fluid flashing. And the fluid density in the lower region of the vessel and the recirculation loop became higher. Some of the fuel rod surface temperatures at the upper core region, however, showed temperature rise after MSIV closure and quench or rewet after ADS actuation (see Figs.5.363 through 5.403). These temporary temperature rises were observed at the A22, B22, C22, D22, A77, B77, rods, which had the local peaking factor of 1.0, and were not observed at the peripheral peak power rods.

Actuation of the LPCS and 3LPCI resulted in rapid increase of mass inventory inside core shroud (see Figs.5.310, 311, 313 and 327), slower recovery of the downcomer mass inventory (Fig.5.312) and, on the contrary, faster mass depletion in the recirculation loops (Figs.5.319 , 320 and 323) as in the test results of RUN 954.

6.4 Effects of Break Area on Major Events

The effects of break area on the pressure response, mojor events including the ECCS actuation and core cooling phenomena are presented in this section by comparing the test results of RUNs 954, 956, 951 and RUN 953[27], a 100 % steam line break test without HPCS and ADS.

(1) Steam Discharge Flow Area of Each Test

Table 6.1 and Fig.6.1 show the total steam discharge flow area of each test including the break area and ADS flow area. The initial steam flow area at the control valve CV130 (see Fig.2.3) was controlled to keep constantly the system pressure. This flow area of each test was nearly the same under the same initial test conditions (see Table 6.2) and was estimated as 2.21×10^{-4} m^2 (29.3 % of the scaled 100 % steam line flow area) as shown in Appendix A-1. The equivallent flow area through the plant safety valve was calculated as 3.00×10^{-4} m^2 (39.3 %) (see Appendix A-2).

In RUN 956, the steam discharged from the steady state steam line through the CV-130 and the transient steam line through the OR-5 after initiation of the break. If the CV-130 was kept constant after the break initiation, the total steam discharge flow area of RUN 956 became a sum of those two flow areas as 29.3 + 10.0 = 39.3 (%). This value is a little larger than the break area of RUN 951 (33.7%). This larger area, however, can not be consistent with the agreement of pressure responses of RUN 956 with those of RUN 951 in a short time period after the break and a slightly smaller steam discharge flow rate of RUN 956 compared with those of RUN 951 in a time period after initiation of lower plenum flashing. These pressure response and steam discharge flow rate indicate that the CV-130 valve flow area in RUN 956 was throttled slightly from the steady state value after the break so that the total steam discharge flow area of RUN 956 became the same or slightly smaller than that of RUN 951. By using a relationship (see Section 6.5) obtained for the maximum average downcomer void fraction and the total steam discharge flow area, the throttled CV-130 flow area was calculated as 1.731×10^{-4} (m^2) and the total steam discharge flow area after the break was as 2.485×10^{-4} (m^2), (32.9 %).

In RUNs 951 and 953, the steam flow area was kept constant after the break. However, the total steam discharge flow areas of RUNs 954 and 956

were changed by the actuations of the plant safety valve or delayed MSIV and ADS. In the small steam line break LOCAs such as RUNs 954 and 956, the flow areas of MSIV and ADS had the dominating part in the total steam discharge flow area.

(2) Effects of Steam Discharge Flow Area on the Pressure Response and Major Events

The steam dome pressure and steam discharge flow rate of the tests are compared in Figs.6.2 and 6.3. respectively. It is shown that the steam discharge flow rate was affected directly by the total steam discharge flow area and also by the steam dome pressure in each test. The steam discharge flow through the SV in RUN 954 should be added on the measured steam flow rate. It should be noted that these steam flow rates are correct only for the saturated steam flow but not correct for the two-phase flow and super-heated steam flow because of the measuring principle of the orifice-type flow meter and that they can be used as the qualitative flow characteristics.

Afterthe break, the steam dome pressure of RUN 954 increased rapidly by the 10 % break area, those of RUNs 956 and 951 were kept nearly constant and that of RUN 953 decreased rapidly by the 100 % break area. The difference of the pressures during the short time period after the break, depended directly on the total steam discharge flow area. This dependence was very sensitive in the main steam line break LOCA comparing with the recirculation line break LOCA. Moreover, it was reduced from the pressure responses that thetotal steam discharge flow areas of RUNs 951 and 956 were similar during the first 20 s. The pressure responses of RUNs 951, 954 and 956 became similar after the actuation of ADS. The main reason of the similar pressure responses in the later test phase of these three tests was also the similar total steam discharge flow area.

The major events of the four tests are shown in Table 6.3 and Fig. 6.4. The MSIV closure in RUNs 954, 951 and 953 were assumed to occur at the break initiation time, whereas that in RUN 956 was tripped by the low level signal (L2) with time delay of 3s. And the major events of RUN 956 were close to those of RUN 951 due to the similar total steam discharge flow area shown previously. The effects of delayed MSIV actuation is presented in the next section by comparing the test results of RUNs 954 and 956.

Figure 6.4 indicates the following characteristies in the main steam

line break tests. (1) Initiation time of the fuel rod dryout strongly depended on the break area. In the 100 % break test (RUN 953), the fuel rod started the temperature excursion at 33 s after the break and that of the 10 % break test (RUN 954) started at 300 s after the break. Approximately the initiation time of the fuel rod dryout was inversely proportional to the break area. (2) The downcomer water level response indicated some what complicated relation with the break area. The latest L2 trip time was found in the medium break test (RUN 951). Moreover, the L2 level in the 100 % break test (RUN 953) was later than the 10 % break test (RUN 954). On the other hand, the L1 level in each test depends on the break area. One of the reasons of this complicated downcomer level response with respect to the break area was the changes of the downcomer void fraction and therefore the level smelling during the depressurization process, which is shown in the next section. (3) In RUN 954, the L1 level, the actuations of LPCS and LPCI and the final quench of the fuel rods occurred in a rather short time period, whereas those in RUN 953 occurred in the wider time period. This tendancy can be closely related with the response of mass inventory in the pressure vessel as shown later. (4) The longer and earlier time period between the dryout initiation time and the final quench time of fuel rods resulted in the higher peak cladding temperature in the larger break test. (5) The LPCS actuation was tripped by the (L1 + 40s) in all steam line break tests. The LPCI actuation was tripped by the (L1 + 40s) in the 100% break test (RUN 953), the (L1 + 40s) with time delay of 40s in the 34% break test (RUN 951) and the injection setpoint pressure of LPCI in RUNs 954 and 956. The time delay of 40s for the LPCI actuation in RUN 951 was due to missetting.

(3) Mass Inventory Responses

The response of mass inventory in the system can be found from the differential pressure data shown in Figs.6.5 through 6.10. The differential pressure after termination of the initial forced circulation flow mainly consisted of the static water head except for some short time periods after the lower plenum flashing initiation, ADS opening and MSIV closure, when the pressure loss due to the flow resistance can not be neglected.

Figure 6.5 shows the tendencies of PV mass inventories of the four tests. The lowest inventory was observed in the 100 % break test (RUN 953). The mass inventory of RUN 954 was kept higher in the early blowdown phase

(before ADS actuation), and agreed with that of RUN 956 after the ADS actuation. The mass inventory of RUN 956 before the MSIV closure agreed with that of RUN 951. These responses of mass inventory correspond to the change of total steam discharge flow area shown previously. In all tests, the PV mass inventory began to increase after LPCS actuation and it was promoted faster by the 3 LPCI actuation.

Figure 6.6 shows the mass inventories in the jet pump discharge line. As the higher pressure side is at the higher elevation point, the negative differential pressure corresponds to the static head. The tendencies of Fig.6.6 are similar as those of Fig.6.5.

Figures 6.7 and 6.8 show the mass inventory in the upperdowncomer (EL 2.814 to 6.04 m) and lower downcomer (EL 0.94 to 2.814 m), respectively. The differential pressure in the lower downcomer also indicatesthe response of void fraction. The tendencies of downcomer mass inventory in RUN 956 are similar to those of RUN 951. After ADS opening, the differential pressures of RUNs 954 and 956 became similar to that of RUN 951. The constant value at the end of RUNs 954 and 953 show that the downcomer was filled up by water. The recovery of mass inventory in the downcomer was similar as that inside core-shroud (Fig.6.5) in each test.

Figures 6.9 and 6.10 show the differential pressures between the downcomer bottom and the MRP1 suction and between the MRP1 delivery and JP 1 drive line, respectively. After coast down of the initial forced recirculation flow, the differencial pressures indicated static heads in those region. The rapid decrease from the constant static head means initiation of void generation in the region or flashing. The actuations of ADS and MSIV influenced the void fraction in the recirculation loop. Namely, the MSIV closure in RUN 956 decreased rapidly the void fraction at 129 s after the break and therefore increased the corresponding differential pressure value. The ADS actuations in both tests rapidly increased the void fraction and decreased each differential pressure. It is shown in these figures that the recovery of mass inventory in the recirculation loop was delayed from that inside PV and occurred abruptly in the 10 % and 100 % break tests. These rapid mass recovery means a break down of the counter current flow limitation, which was caused by the rising steam flow at the recirculation loop inlet nozzle.

(4) Core Cooling Phenomena

The representative core cooling phenomena of each test are compared in the fuel rod temperature responses at the top (position 1), middle (position 4) and bottom (position 7) of the average power rods in the high and average power bundles. Figures 6.11 and 6.12 show the fuel rod surface temperatures of A22 rod and C22 rod, respectively.

In each test, the temperature responses of A22 and C22 rods are similar except for the slight differences in the dryout and quench times and temperature increasing rates. Figure 6.13 shows the temperature responses of four tests, which recorded the PCT. Figure 6.14 shows relation of PCT and break area in ROSA-III tests. In Fig.6.14, the steam line flow areas of the four tests were normalized by the recirculation linr break area. Namely, the 100% steam line break area corresponded to the 140% recirculation line break area.

From these temperature responses, the following are resulted. (1) The dryout of fuel rods initiated at the top of core and went down in all tests. (2) The dryout initiation time at the top of core was faster in the larger break test. (3) In the middle and small break tests, the lower part of the core was not dryed out due to the existence of two-phase fluid. (4) The dryout fuel rods at the top of core in RUN 956 were cooled down by the actuation of ADS because the ADS opening caused rapid depressurization and fairly strong upward two-phase flow in the core. (5) In steam line break tests, the peak cladding temperature (PCT) was higher for the larger break area. The relation between the PCT and break area in the steam line break tests is different from that in the recirculaion line break tests. Therefore, the break location at the main steam line or the recirculation line results in different core cooling conditions.

It should be noted that the PCTs in these steam line break tests may be lowerd in the following three cases. (1) An updated core power curve [39] gives a slightly lower heat flux on the fuel rods thanthe power curve [38] used in these four tests. (2) In the case of steam line break LOCA in a BWR, the containment pressure measurement detects an increase of the pressure earlier than the low downcomer level trip of L1 and sends an actuation signal to the LPCS and LPCI systems. Therefore, the LPCS and LPCI can be injected at the designed setpoint pressures earlier than these tests. (3) The HPCS system, which is assumed to be failed in these four tests, can cool down the core in the early blowdown phase as shown in the test results of RUN S62 [26].

6.5 Effects of Steam Flow Area on DC Level Responses

In this section, the effects of total steam descharge flow area on the void fraction in the downcomer and the mixture level swelling. The effects of MSIV closure and ADS opening in the small steam line break LOCA are also presented here. Fig.6.15 shows the collapsed water level in PV and the average void fraction in lower downcomer in the 100 % break test (RUN 953). Refer the level responses of RUNs 954 (Fig.5.293), 956 (Fig.5.433) and 951 (Fig.5.153).

(1) The Downcomer Void Fraction

Figure 6.16 shows the average lower downcomer void fractions calculated from the experiment data of the differential pressure (Ch. 24, EL 0.94 to 3.90 m) by neglecting the frictional pressure loss. Practically, the void fraction is correct except for the short time periods after the break, lower plenum flashing and ADS actuation.

Followings were found from the responses of the void fraction in the four tests. (1) The average void fraction in the lower downcomer depended strongly on the total steam discharge flow area including the ADS flow area. (2) The void fraction reached the constant maximum value, increased temporarily after LPCS actuation and finally diminished. (3) The maximun average void fraction was clearly related with the total steam discharge flow area as shown in Table 6.4 and Fig.6.17. The maximum void fractions before ADS opening in RUN 954 and that before MSIV closure in RUN 956 were guessed by extraporating the void fraction increasing rate as shown in Fig.6.17. The relation was reduced in a following form

$$\alpha = 17 \times A^{0.475}$$

where A is the total steam discharge flow area (in m^2) in the steam line break tests. All the data shown in Table 6.4 were included in a error band of 10 %.

By using this relation, the unknown total steam discharge flow area (A_t) of RUN 956 before the MSIV closure was calculated from the void fraction of 0.33 as,

$$A_t = 2.485 \times 10^{-4} \quad (m^2)$$

Which corresponded to 32.9% of the scaled steam line flow area. As the break area of 10% was included in this total steam discharge flow area, the equivallent steam dischrge flow area (A) at the steady state steam line (CV-130) was obtained as,

$$A = A_t - 7.54 \times 10^{-5}$$
$$= 1.731 \times 10^{-4} \quad (m^2),$$

which corresponded to 22.9% of the scaled steam line flow area and the equivallent inner diameter was 14.8 mm. This value was smaller than the initial CV-130 diameter (16.8 mm). As this throttled CV-130 flow area gave a sufficiently consistent explanation on the pressure responses and steam discharge flow rates of RUNs 956 and 951 in a time period between the break and MSIV closure, the estimation of total steam discharge flow area by using the above relation is proved to be useful.

(2) Response of Upper Downcomer Water Level

Figure 6.18 shows collapsed upper downcomer water levels of the four tests. These level measurements were used for the trip signals like as L2 level for the MSIV trip (RUN 956) and the ADS opening (RUNs 954 and 956), and L1 level for the actuation of LPCS in the four tests. The timings of L1 and L2 for each test are shown in Table 6.3.

The followings are derived from the comparison of upper downcomer level responses shown in Fig.6.18 and Table 6.3. (1) In spite of the difference of break areas, the upper downcomer level responses were similar in the four tests and showed very high values during the test periods. These characteristies were completely different from those of the recirculation line break tests.(6),(7) It is concluded that the higher water level in the four tests is one of the characteristic features of the main steam line break LOCA. (2) The water level responses of RUN 956 were almost the same as those of RUN 951 mainly due to the similar total steam discharge flow areas in the test periods. (3) The water level responses of RUN 954 were slightly different from the others. The lower plenum flashing in RUN 954 was initiated at 81 s after the break, which was fairly later than the others due to higher system

pressures shown in the previous section. The delayed lower plenum flashing initiation resulted in earlier level decrease and L2 level trip. (4) The initiation of the lower plenum flashing resulted in the upper downcomer level swelling in RUNs 956, 951 and 953 and hold-up of the level in RUN 954. (5) The ADS opening also resulted in the upper downcomer level swells in RUNs 954 and 956. The reason of higher level swell at the time of ADS actuation in RUN 954 may be attributed to the larger depressurization rate caused by the higher steam discharge flow rate and also to the larger fluid mass in the downcomer by comparing with those of RUN 956. (6) The upper downcomer water level recovered rapidly within 100 s after the LPCS actuation in four tests.

Figure 6.19 shows the swelled mixture levels in the upper downcomer of the four tests. The mixture level was calculated from the collapsed level data (see Fig.6.18) by assuming the uniform void fraction in the whole downcomer region. The transient void fraction data of each test came from the average void fraction in the lower downcomer (see Fig.6.16).

The followings are derived from the mixture level responses shown in Fig.6.19. (1) The swelled mixture level height after initiation of lower plenum flashing was the highest in the 100 % break test (RUN 953) and reached the PV top at 14 s after the break. The highest mixture level was a result of higher void fraction in the downcomer (up to 56 %). (2) The mixture levels of RUNs 951 and 956 were nearly the same. (3) It is shown that the faster and largher the depressurization was, the higher the mixture level swelled. (3) The MSIV closure at 129 s after the break in RUN 956 caused decrease of void fraction and mixture level in the downcomer. (4) The ADS actuations in RUNs 954 and 956 affected the mixture level swell like as in the upper downcomer collapsed level. The ADS effect was greater in RUN 954 due to the larger depressurization rate and larger amount of downcomer fluid.

By comparing the collapsed water levels and the estimated mixture levels in the upper downcomer in the four steam line break tests, the characteristic phenomena in the steam line break tests and the effects of steam discharge flow area including the ADS and MSIV are derived shown above.

6.6 Effects of Steam Discharge Flow area on PV Water Level Responses

The responses of the collapsed water level inside core-shroud, relations between the collapsed water levels across the core shroud and relations between the mixture level and collapsed water level inside core-shroud are presented here with respect to the effects of total steam discharge flow area.

(1) Collapsed Water Level Inside Core-Shroud

Figure 6.20 compares the collapsed water levels inside core-shroud in the four steam line break tests. These water levels was reduced from the corresponding differential pressure data (PD 25) by using the saturation water density and by neglecting the effect of flow resistance. It should be noted that these level responses are important for the estimation of core cooling conditions during the LOCA phenomena because the dryout and quench phenomena of the fuel rods are closely related with the mixture level responses and also related with the collapsed water level responses.

In the case of 100 % break test (RUN 953), the mass inventory inside core-shroud decreased earlier and the bottom of core was exposed into the steam atmosphere at about 200 s after the break. And the mixture level was formed at the top of the lower plenum. In the case of 34 % break test (RUN 951), the decrease of mass nventory inside core-shroud was delayed from that of 100 % break test and the collapsed level reached the bottom of core at 390 s after the break. The core mixture level in the 34 % break test, however, decreased only to the position 6 and the bottom of the core (position 7) was not dryed out. In the 10 % break test (RUN 954), the decrease of the collapsed water level inside core-shroud was delayed more than the 34 % break test and the lowest collapsed level was at the position 6. The core mixture level in RUN 956 decreased to the position 5 and the positions 6 and 7 were not dryed out.

Figure 6.20 also shows the effects of MSIV and ADS trips. The collapsed water levels of RUNs 951 and 956 agreed well until the time of MSIV closure in RUN 956, due to the similar seam discharge flow rates. The MSIV trip in RUN 956 caused the abrupt change of the total steam discharge flow area and resulted in the collapsed water level hold up inside core-shroud. After initiation of ADS opening in both RUNs 954 and 956, the decrease of both

collapsed water levels agreed well. Thus, the responses of collapsed water levels inside core-shroud, which represented the responses of mass inventories in the four steam line break tests, were closely related with the total steam discharge flow area.

The effects of LPCS and LPCI actuations were clearly found on the collapsed water levels inside core-shroud. The collapsed water level began to increase rapidly within 10 to 20 s after the LPCS actuation. And the 3 LPCI actuation further improued the recovery of mass inventory as shown in Fig. 6.20.

(2) Water Level Responses in PV

The collapsed water levels in PV are shown in Figs. 5.153 (RUN 951), 5.293 (RUN 954), 5.433 (RUN 956) and 6.15 (RUN 953). The following relations between the collapsed water level inside core-shroud and those in the downcomer were found by comparing these figures.

(1) In the four steam line break tests, the upper downcomer water levels were kept higher than the collapsed water levels inside core-shroud except for the end of the reflooding phase. The difference of water levels between the upper downcomer and the core-side reached more than 3 m in the 100 % break test (RUN 953) and more than 2 m in the 10 % break tests (RUNs 954 and 956). It must be noted that the heights of ROSA-IV core and PV are scaled down by 1/2 and 1/3 to those of the BWR/6, respectively. This scaling means that the level difference shown above may be scaled up in the BWR LOCA.

(2) The reason of level difference shown in (1) is explained by the static pressure distribution of each test. Tables 6.5 through 6.7 show the pressure balance across the core shroud (see Fig. 6.21) in the test periods of RUNs 951, 956 and 953. Tables 6.5 through 6.7 indicate that the good pressure balance had been established in PV in each test within a small error (less than 7 KPa). It is shown that the higher downcomer water level was caused mainly due to the higher void fraction in the jet pumps.

(3) The total downcomer water head above the elevation of 0.938 m was also higher by more than 1 m compared with the collapsed water level inside core-shroud.

(4) The collapsed water level inside core-shroud recovered rapidly after LPCS actuation and became higher than the upper downcomer water level

after completion of core quenching.

(3) Core Mixture Levels Related with the Collapsed Water Level

The core mixture levels estimeted from the conduction probe data are compared with the collapsed water level inside core-shroud in each test as shown in Figs.6.22 (RUN 954), 5.433 (RUN 956), 6.23 (RUN 951) and 6.24 (RUN 953).

In is found from these figures that the mixture level was kept higher than the collapsed water level inside core-shroud in all tests except for the two phases, namely the temporary dryout phenomena in the upper core region just after the break initiation and the locally delayed quenching regions after the LPCI actuation in the 100 % break test (RUN 953). As it was already mentioned in the test results presentations, the core mixture level responses agreed completely with the dryout and quench behaviors of fuel rods. Therefore, it is concluded that the fuel rod dryout period are observed above the collapsed water level inside core-shroud in all the steam line break tests except for the phases shown above.

7. Conclusions

Three steam line break LOCA tests were performed at the ROSA-III test facility with scaled break areas equalling 34% (RUN 951) and 10% (RUNs 954 and 956) of the BWR main steam line flow area and with a single failure assumption for the HPCS diesel generator. The available ECCS's were the ADS actuated by L2 level in RUNs 954 and 956, and the LPCS and 3 LPCIs, which were actuated by the low downcomer level trip (L1) in the three tests. These test results were compared with those of the 100% steam line break test (RUN 953)[27] to clarify the effects of steam break area on the transient LOCA phenomena and consequently the following conclusions were obtained.

(1) The transient pressure responses, the steam discharge flow rate, the mass inventory in PV and the downcomer water level responses were controlled mainly by the total steam discharge flow area, which was a sum of break area and ADS or MSIV area.

(2) Due to the similar total steam discharge flow areas between the 10% break with MSIV trip by L2 level (RUN 956) and the 34% break with MSIV trip at the break, the mass inventories and the major events of both tests agreed well except for the core cooling conditions which were affected by actuations of MSIV and ADS in RUN 956.

(3) The void fraction in the downcomer began to increase after initiation of the flashing and was held at a maximum value for a long time in every test. An empirical relation was derived from the ROSA-III steam line break test results between the maximum average void fraction (α) in the downcomer and the total steam discharge flow area (A) as shown in the following equation,

$$\alpha = 17 \times A^{0.475},$$

where A is in m^2. This relation is applied also to the time periods after MSIV and ADS actuations and is independent of the time after the break therefore the amount of remaining mass inventory.

(4) The upper downcomer collapsed water level measured by a differential

pressure transducer, showed similar trends in every test and they were kept fairly higher than the collapsed water level inside core-shroud nearly throughout the test. In a large break area test, the higher void fraction compensated the larger mass depletion in the downcomer. These are the important characteristics of the main steam line break LOCA compared with those of the recirculation line break LOCA. An attention should be paid in the BWR operations and LOCA analysis to the fact that the upper downcomer level can be higher than the core level when the steam is discharged from the top of PV.

(5) The core mixture level responses measured by conduction probes were correlated well with the dryout and quench behaviors of fuel rods. The core mixture level was slightly higher than the collapsed water level inside the core-shroud.

(6) The LPCS and LPCI actuations resulted in rapid recovery of mass inventory inside the core-shroud, i.e., fast reflooding of the core. The entire core exposed to the steam atmosphere was completely quenched within 24 s, 70 s and 157 s after the LPCS actuation in the 10%, 34% and 100% steam line break tests. If the LPCS and LPCI were actuated by the high containment pressure trip signal prior to the L1 level trip, the LPCS and LPCI would be injected earlier at their designed pressure setpoints (2.16 MPa and 1.57 MPa). The earlier actuations of LPCS and LPCI are expected to contribute to lower the PCT.

(7) The fuel rod surface temperatures showed excursion due to dryout in all of the steam line break tests. The dryout of fuel rods was initiated earlier and continued longer in a larger break test. The dryout propagated to a lower level in the larger break test. Consequently the PCT was higher in the larger break area test.

(8) The actuation of MSIV by L2 level trip in the 10% break test caused the temporary fuel rod dryout in the upper core region, whereas the actuation of ADS thereafter in the same test rewetted the fuel rods.

Acknowledgment

The authors are grateful to M. SHIBA, Deputy Director of Department of Reactor Safety Research for his coordinating the ROSA-III program, M. OKAZAKI of Institute of Nuclear Safety, Japan for his contribution to the discussion of the steam line break LOCA analysis, and H. ASAHI, T. ODAIRA, T. TAKAYASU, Y. KITANO and T. NUMATA of Nuclear Engineering Corporation for their assistance in conducting the experiment and Y. HIRANO and K. HAKUTA of Information System Laboratory Corpolation for preparing the data plots and M. KIKUCHI of Nihon Computer Bureau for type writing the manuscripts.

References

(1) K.TASAKA, et al., "Study on the Similarity between ROSA-III Experiment and BWR LOCA", JAERI-M 6703 (1976) (in Japanese).

(2) Y.ANODA, et. al.,"ROSA-III System Description for Fuel Assembly No. 4", JAERI-M 9363 (1981) (in Japanese).

(3) General Electric Company, "General Electric Standard Safety Analysis Report, BWR/6", DOCKET-STN-50477 (1978).

(4) K.TASAKA, et. al.,"ROSA-III Base Test Series for a Large Break Loss of Coolant Accident in a Boiling Water Reactor", Nucl. Techn. 57 (1982).

(5) K.SODA, et. al.,"Boiling Water Reactor Loss of Coolant Test (Single Failure Test with ROSA-III)", J. Nucl. Sci. Techn. 20 (1983).

(6) K.TASAKA, et. al.,"Simulation Experiment of Five Percent Small Break LOCA of BWR", J. Nucl. Sci. Techn. 20 (1983).

(7) K.TASAKA, et. al.,"ROSA-III Double-Ended Break Test Series for a Loss-of-Coolant Accident in a Boiling Water Reactor", Nucl. Techn. 68 (1985).

(8) M.SUZUKI, et al.,"Recirculation Pump Discharge Line Break Tests at ROSA-III for a Boiling Water Reactor", Nucl. Techn. 70 (1985).

(9) Y.KOIZUMI, et al., "Experiment Analysis of Power Curve Sensitivity Test Series at ROSA-III", Nuclear Engineering and Design, to be Published.

(10) H.KUMAMARU, et al.,"Five Percent Break BWR LOCA/ECC Test at ROSA-III without HPCS Actuation---Two Dimensional Core Thermal Hydraulic Phenomena", Nuclear Engineering and Design, to be published.

(11) T.YONOMOTO, et.al.,"Investigation of BWR/LOCA at ROSA-III---Effect of

Acknowledgment

The authors are grateful to M. SHIBA, Deputy Director of Department of Reactor Safety Research for his coordinating the ROSA-III program, M. OKAZAKI of Institute of Nuclear Safety, Japan for his contribution to the discussion of the steam line break LOCA analysis, and H. ASAHI, T. ODAIRA, T. TAKAYASU, Y. KITANO and T. NUMATA of Nuclear Engineering Corporation for their assistance in conducting the experiment and Y. HIRANO and K. HAKUTA of Information System Laboratory Corpolation for preparing the data plots and M. KIKUCHI of Nihon Computer Bureau for type writing the manuscripts.

References

(1) K.TASAKA, et al., "Study on the Similarity between ROSA-III Experiment and BWR LOCA", JAERI-M 6703 (1976) (in Japanese).

(2) Y.ANODA, et. al.,"ROSA-III System Description for Fuel Assembly No. 4", JAERI-M 9363 (1981) (in Japanese).

(3) General Electric Company, "General Electric Standard Safety Analysis Report, BWR/6", DOCKET-STN-50477 (1978).

(4) K.TASAKA, et. al.,"ROSA-III Base Test Series for a Large Break Loss of Coolant Accident in a Boiling Water Reactor", Nucl. Techn. 57 (1982).

(5) K.SODA, et. al.,"Boiling Water Reactor Loss of Coolant Test (Single Failure Test with ROSA-III)", J. Nucl. Sci. Techn. 20 (1983).

(6) K.TASAKA, et. al.,"Simulation Experiment of Five Percent Small Break LOCA of BWR", J. Nucl. Sci. Techn. 20 (1983).

(7) K.TASAKA, et. al.,"ROSA-III Double-Ended Break Test Series for a Loss-of-Coolant Accident in a Boiling Water Reactor", Nucl. Techn. 68 (1985).

(8) M.SUZUKI, et al.,"Recirculation Pump Discharge Line Break Tests at ROSA-III for a Boiling Water Reactor", Nucl. Techn. 70 (1985).

(9) Y.KOIZUMI, et al., "Experiment Analysis of Power Curve Sensitivity Test Series at ROSA-III", Nuclear Engineering and Design, to be Published.

(10) H.KUMAMARU, et al.,"Five Percent Break BWR LOCA/ECC Test at ROSA-III without HPCS Actuation---Two Dimensional Core Thermal Hydraulic Phenomena", Nuclear Engineering and Design, to be published.

(11) T.YONOMOTO, et.al.,"Investigation of BWR/LOCA at ROSA-III---Effect of

Break Configuration on System Transient---", Nuclear Engineering and Design, to be published.

(12) K.TASAKA, et. al.,"Analysis of ROSA-III Break Area Spectrum Experiments on BWR Loss-of-Coolant Accident", Nucl. Techn., to be published.

(13) M.SOBAJIMA, et. al.,"Experiment Test Data of ROSA-III Test RUN 701 (Decay Heat Simulation Test with ECCS Actuation)", JAERI-M 8604 (1979).

(14) Y.ANODA et. al.,"Experiment Data of ROSA-III Test RUN 703 (Split Break Simulation Test with ECCS Actuation)", JAERI-M 8967 (1980).

(15) Y.ANODA et. al.,"Experiment Data of ROSA-III Test RUN 704 (Standard Test with ECCS Actuation)", JAERI-M 8968 (1980).

(16) M.OKAZAKI et. al.,"Experimet Test Data of ROSA-III Integral Test RUN 705 (Isothermal Blowdown Test without ECCS Actuation)", JAERI-M 8723 (1980).

(17) M.SUZUKI et. al.,"Experiment Data of ROSA-III Integral Test, RUN 706", JAERI-M 8737 (1980).

(18) M.OKAZAKI et. al.,"Experiment Data of ROSA-III Integral Test RUN 708 (Standard Test without ECCS Actuation)", JAERI-M 8738 (1980).

(19) Y.KOIZUMI et. al.,"Experiment Data of ROSA-III Integral Test, RUN 710", JAERI-M 9249 (1981).

(20) Y.ANODA et. al.,"Experimet Data of ROSA-III Integral Test RUN912 (5% Split Break Test without HPCS Actuation)", JAERI-M 82-010.

(21) H.NAKAMURA et. al.,"Experiment Data of ROSA-III Integral Test RUN 901 (200% Double-Ended Break with Full ECCS Actuation)", JAERI-M 84-007.

(22) H.NAKAMURA et. al.,"Experiment Data of ROSA-III Integral Test RUN 926 (200% Double-Ended Break with HPCS Failure)", JAERI-M 84-008.

(23) M.SUZUKI et. al.,"Experiment Data of 200% Recirculation Pump Discharge Line Break Integral Test RUN 961 with HPCS Failure at ROSA-III and Comparison with Results of Suction Line Break Tests", JAERI-M 84-045, (1984).

(24) M.SUZUKI, et. al.,"Recirculation Pump Suction Line 2.8% Break Integral Test at ROSA-III with HPCS Failure, RUN 984", JAERI-M 84-100, (1984).

(25) M.SUZUKI, et. al.,"Recirculation Pump Suction Line 200% Break Integral Test at ROSA-III with Two LPCI Failures, RUN 983", JAERI-M 84-135, (1984).

(26) M.KAWAJI, et. al.,"A Main Steam Line Break Experiment at ROSA-III RUN 952 (Standard Run with Full ECCS)", JAERI-M 84-229, (1984).

(27) M.KAWAJI, et. al.,"A Main Steam Line Break Experiment at ROSA-III, RUN 953 (100% Break with an HPCS Failure)", JAERI-M 85-029 (1985).

(28) M.SUZUKI, et. al.,"BWR Recirculation Loop Discharge Line Break LOCA Tests with Break Areas of 50 and 100% Assuming HPCS Failure at ROSA-III Facility", JAERI-M 85-037, (1985).

(29) T.YONOMOTO, et. al.,"ROSA-III 50% Break Integral Test RUN 916 (Break Area Parameter Test)", JAERI-M 85-109, (1985).

(30) H.NAKAMURA, et. al.,"Recirculation Pump Suction Line 5% Split Break Test of ROSA-III (RUNs 922 and 923 with HPCS Failure)", JAERI-M 85-128, (1985).

(31) M.SUZUKI, et. al.,"Heat Loss and Fluid Leakage Tests of the ROSA-III Facility", JAERI-M 9834 (1981).

(32) M.SUZUKI, et. al.,"Characteristics of the ROSA-III Test Facility (Characteristics Test of the Jet Pumps in Normal and Reverse Flow)", JAERI-M 8670, (1980) (in Japanese).

(33) M.SUZUKI, et. al.,"Evaluation of a Jet Pump Model for RELAP5 Code", JAERI-M 84-245, (1985) (in Japanese).

(34) W. J. Letzring, et. al.,"BWR Blowdown/ECC Program Preliminary Facility Description Report for the BD/ECC1a Test Phase", GEAP-23592.

(35) GE, EPRI and NRC,"Full Integral Simulation Test (FIST) Program Test Plan", EPRI NP-2313, GEAP 22053, (1981).

(36) M.MURASE et. al.,"BWR Loss-of-Coolant Integral Test -- Parallel Channel Effect", NUREG/CP-0027-Vol.3, (1982).

(37) M.SOBAJIMA et. al.,"Instrumentation and Data Processing Method of the ROSA-III Test", JAERI-M 8499 (1979) (in Japanese).

(38) N.ABE et. al.,"Electric Power Tansient Curve for ROSA-III Tests", JAERI-M 8728 (1980).

(39) M.IRIKO, et. al.,"Updated Core Power Curves for ROSA-III Facility", JAERI-M 84-029, (1984).

Appendix A-1 Estimation of Initial Flow Area of Pressure Control Valve (CV-130)

In RUN 951, the steam discharge flow area was slightly changed by the break initistion. Namely, the flow area of CV-130 was fully opened at the break and thereafter the steam flow was restricted by the orifice (OR-5) with area of $A = 2.54 \times 10^{-4}$ m^2 (18.0 mm I.D.). In a short time after the break, only the single phase steam flow passed through the steam line (the lower plenum flashing initiated at 19 s after break). By selecting a reference point in the short time (9 s after break), the initial steam flow area of CV-130 (A_0) is calculated as.

$$A_0 = A \times (V/V_0) \times (\rho/\rho_0) \times (W_0/W)$$

where A is the choking orifice area, V is sound velocity of saturated steam, ρ is the steam density, W is mass flow rate and the suffix 0 is for the initial test condition. By using the following test data,

$A = 2.54 \times 10^{-4}$	m^2	: Orifice Area (OR-5)
$V_0 = 485$	m/s	: at P = 7.35 MPa
$\rho_0 = 38.59$	kg/m^3	: at P = 7.35 MPa
$V = 487$	m/s	: at P = 7.15 MPa
$\rho = 37.41$	kg/m^3	: at P = 7.15 MPa
$W_0 = 2.04$	kg/s	: Initial Flow Rate
$W = 2.28$	kg/s	: Flow Rate at 9 s.

the initial choking flow area of CV-130 is obtained as,

$$A_0 = 2.21 \times 10^{-4} \text{ m}^2.$$

This value corresponds to 16.8 mm I.D. and 29.3% of the scaled steam line flow area.

Appendix A-2 Estimation of Safety Valve Area and Flow Rate

In RUN 954, the system pressure began to increase after break initiation due to the closure of the steady state pressure control valve and resulted in actuation of the ROSA-III plant safety valve opening. The avarage steam flow rate during the safety valve opening period, the discharged steam mass and the equivallent steam flow area were calculated as follows.

The steam flow rate of the safety valve is defined by the industrial standard as,

$$W = 230 \times AP \times \sqrt{M/T} \qquad (kg/hour)$$

where,

$A = 3.20$	(cm^2)	: Flow Area
$P = 80.9$	(kg/cm^2a)	: Average Pressure
$M = 18$		: Molecular Number
$T = 567.5$	(K)	: Average Steam Temperature

and

$$W = 1.06 \times 10^4 \ (kg/hour)$$
$$= 2.95 \ (kg/s).$$

Therefore, the total discharged mass during the opening time (5.4 and 16.9 s) is obtained as,

$$M = W \times 11.5 = 34 \ (kg).$$

By using the calculated average steam discharge flow rate through the safety valve, an equivallent steam discharge flow area (A_1) is calculated as follows with an assumption that the safety valve has the same geometry as that of the steam break orifice (OR-5),

$$A_1 = A \times (V/V_1) \times (\rho/\rho_1) \times (W_1/W)$$

where A is the choking orifice area, V is sound velocity of saturated steam,

ρ is the steam density, W is mass flow rate and the suffix $_1$ is for the average condition of the valve opening time. By using the following test data and the same reference point as that of the initial CV-130 flow area (see Appendix A-1),

$A = 2.54 \times 10^{-4}$	m^2	: Orifice Area (OR-5)
$V_1 = 483$	m/s	: at P = 7.93 MPa
$\rho_1 = 42.50$	kg/m^3	: at P = 7.93 MPa
$V = 487$	m/s	: at P = 7.15 MPa
$\rho = 37.41$	kg/m^3	: at P = 7.15 MPa
$W_1 = 2.95$	kg/s	: Average Flow Rate at P = 7.93 MPa
$W = 2.28$	kg/s	: Flow Rate at 9 s.

the average safety valve flow area is obtained as,

$$A_1 = 3.00 \times 10^{-4} \quad m^2.$$

This value corresponds to 19.5 mm I.D. and 39.7% of the scaled steam line flow area.

Table 2.1 Primary chracteristics of ROSA-III and BWR/6

	BWR-6	ROSA-III	BWR/ROSA
No. of Recirc. Loops	2	2	1
No. of Jet Pumps	24	4	6
No. of Separators	251	1	251
No. of Fuel Assemblies	848	4	212
Active Fuel Length (m)	3.76	1.88	2
Total Volume (m^3)	621	1.42	437
Power (MW)	3800	4.40	864
Pressure (MPa)	7.23	7.23	1
Core Flow (kg/s)	1.54×10^4	36.4	424
Recirculation Flow (l/s)	2970	7.01	424
Feedwater Flow (kg/s)	2060	4.86	424
Feedwater Temp (K)	489	489	1

Table 3.1 ROSA-III instrumentation summary list

TYPE	SENSOR	NUMBER	NOTE	
PRESSURE	PRESSURE TRANSDUCER	20		
DIFFERENTIAL PRESSURE	DP CELL	60	PV AND LOOP LEVEL MEASUREMENT FLOW METER	44 5 11
FLUID TEMPERATURE	CA THERMOCOUPLE	129	PRIMARY LOOP DTT TIE ROD UPPER PLENUM LOWER PLENUM TIE PLATE BY PASS	23 4 28 10 10 40 14
FUEL ROD TEMPERATURE	CA THERMOCOUPLE	213		
SLAB SURFACE TEMPERATURE	CA THERMOCOUPLE	70	CORE BARREL PRESSURE VESSEL CHANNEL BOX SHROUD SUPPORT	24 3 35 8
SLAB INNER TEMPERATURE	CA THERMOCOUPLE	9	JP DIFFUSER PV WALL	4 5
VOLUMETRIC FLOW RATE	TURBINE METER VENTURI METER ORIFICE METER	3 4 6	ECCS LOOP PRIMARY LOOP	3 10
MASS FLOW RATE	TURBINE METER ORIFICE METER	4 3	RECIC. LOOP STEAM LINE	4 3
LIQUID LEVEL	CONDUCTIVITY PROBE CAPACITANCE PROBE	138 2		
DENSITY	GAMMA DENSITOMETER	10	2 BEAM GD 3 BEAM GD	2 2
MOMENTUMR FLUX	DRAG DISK	7		
SIGNAL	ON/OFF SWITCH	14		
PUMP SPEED	REVOLUTION COUNTER	2		
ELECTRIC POWER	VA METER	2		
TOTAL		696		

Table 3.2 Measurement list for RUNs 951, 954 and 956

1Ch.- 50Ch.

Ch.	Item	Symbol	ID.		Location	Fig.No.	Range			Unit	Accuracy
1	Press.	P- 1	PA	1	Lower Plenum	5. 1,169,309	0.100	-	10.0	MPa	1.08%FS
2	Press.	P- 2	PA	2	Upper Plenum		0.100	-	10.0	MPa	1.08%FS
3	Press.	P- 3	PA	3	Steam Dome	5. 1,169,309	0.100	-	10.0	MPa	1.08%FS
4	Press.	P- 4	PA	4	Downcomer Bottom		0.100	-	10.0	MPa	1.08%FS
5	Press.	P- 5	PA	5	JP-3 Drive		0.100	-	10.0	MPa	1.08%FS
6	Press.	P- 6	PA	6	JP-4 Drive		0.100	-	10.0	MPa	1.08%FS
7	Press.	P- 7	PA	7	JP-3 Suction		0.100	-	10.0	MPa	1.08%FS
8	Press.	P- 8	PA	8	JP-4 Suction		0.100	-	10.0	MPa	1.08%FS
9	Press.	P- 9	PA	9	MRP-1 Suction		0.100	-	10.0	MPa	1.08%FS
10	Press.	P-10	PA	10	MRP-2 Suction		0.100	-	10.0	MPa	1.08%FS
11	Press.	P-11	PA	11	MRP-2 Delivery		0.100	-	10.0	MPa	1.08%FS
12	Press.	P-12	PA	12	Break A Upstream		0.100	-	10.0	MPa	1.08%FS
13	Press.	P-13	PA	13	Break A Downstream		0.100	-	10.0	MPa	1.08%FS
14	Press.	P-14	PA	14	Break B Upstream		0.100	-	10.0	MPa	1.08%FS
15	Press.	P-15	PA	15	Break B Downstream		0.100	-	10.0	MPa	1.08%FS
16	Press.	P-16	PA	16	Steam Line	5. 1,169,309	0.100	-	10.0	MPa	1.08%FS
17	Press.	P-17	PA	17	JP-1,2 Outlet Spool		0.100	-	10.0	MPa	1.08%FS
18	Press.	P-18	PA	18	JP-3,4 Outlet Spool		0.100	-	10.0	MPa	1.08%FS
19	Press.	P-19	PA	19	Break A Spool Piece		0.100	-	10.0	MPa	1.08%FS
20	Press.	P-30	PA	20	Break B Spool Piece		0.100	-	10.0	MPa	1.08%FS
21	Diff.P.	D- 1	PD	21	Lower Pl.-Upper Pl.	5. 2,170,310	-50.0	-	350.	kPa	0.63%FS
22	Diff.P.	D- 2	PD	22	Upper Pl.-Steam Dome	5. 3,171,311	-10.0	-	90.0	kPa	0.63%FS
23	Diff.P.	D- 3	PD	23	Lower Plenum Head	NM, NM, NM					
24	Diff.P.	D- 4	PD	24	Downcomer Head	5. 4,172,312	0.0	-	100.	kPa	0.63%FS
25	Diff.P.	D- 5	PD	25	PV Bottom-Top	5. 5,173,313	-100.	-	900.	kPa	0.63%FS
26	Diff.P.	D- 6	PD	26	JP-1 Disch.-Suction	5. 6,174,314	-100.	-	300.	kPa	0.63%FS
27	Diff.P.	D- 7	PD	27	JP-1 Drive -Suction	5. 7,175,315	0.0	-	2.50	MPa	0.63%FS
28	Diff.P.	D- 8	PD	28	JP-2 Disch.-Suction	5. 6,174,314	-100.	-	300.	kPa	0.63%FS
29	Diff.P.	D- 9	PD	29	JP-2 Drive -Suction	5. 7,175,315	0.0	-	2.50	MPa	0.63%FS
30	Diff.P.	D-10	PD	30	JP-3 Disch.-Suction	5. 8,176,316	-100.	-	300.	kPa	0.63%FS
31	Diff.P.	D-11	PD	31	JP-3 Drive -Suction	5. 9,177,317	-4.00	-	2.00	MPa	0.63%FS
32	Diff.P.	D-12	PD	32	JP-4 Disch.-Suction	5. 8,176,316	-100.	-	300.	kPa	0.63%FS
33	Diff.P.	D-13	PD	33	JP-4 Drive -Suction	5. 9,177,317	-4.00	-	2.00	MPa	0.63%FS
34	Diff.P.	D-14	PD	34	MRP-1 Deliv.-Suction	5. 10,178,318	-0.100	-	2.50	MPa	0.63%FS
35	Diff.P.	D-15	PD	35	MRP-2 Deliv.-Suction	5. 10,178,318	-0.100	-	2.50	MPa	0.63%FS
36	Diff.P.	D-16	PD	36	DC Bottom- MRP-1 Suc.	5. 11,179,319	-50.0	-	50.0	kPa	0.63%FS
37	Diff.P.	D-17	PD	37	MRP1 Deliv.-JP1 Drive	5. 12,180,320	0.0	-	250.	kPa	0.63%FS
38	Diff.P.	D-18	PD	38	MRP1 Deliv.-JP2 Drive	5. 12,180,320	0.0	-	250.	kPa	0.63%FS
39	Diff.P.	D-19	PD	39	DC Middle-JP1 Suction	5. 13,181,321	0.0	-	250.	kPa	0.63%FS
40	Diff.P.	D-20	PD	40	DC Middle-JP2 Suction	5. 13,181,321	0.0	-	250.	kPa	0.63%FS
41	Diff.P.	D-21	PD	41	JP1 Disch.-Lower Pl.	5. 14,182,322	-100.	-	100.	kPa	0.63%FS
42	Diff.P.	D-22	PD	42	JP2 Disch.-Lower Pl.	5. 14,182,322	-100.	-	100.	kPa	0.63%FS
43	Diff.P.	D-23	PD	43	DC Bottom- Break B		-60.0	-	540.	kPa	0.63%FS
44	Diff.P.	D-24	PD	44	Break B- Break A		0.0	-	100.	kPa	0.63%FS
45	Diff.P.	D-25	PD	45	Break A- MRP2 Suction		-500.	-	100.	kPa	0.63%FS
46	Diff.P.	D-26	PD	46	MRP2 Deliv.-JP3 Drive	5. 15,183,323	-500.	-	500.	kPa	0.63%FS
47	Diff.P.	D-27	PD	47	MRP2 Deliv.-JP4 Drive	5. 15,183,323	-500.	-	500.	kPa	0.63%FS
48	Diff.P.	D-28	PD	48	DC Middle-JP3 Suction	5. 16,184,324	-250.	-	250.	kPa	0.63%FS
49	Diff.P.	D-29	PD	49	DC Middle-JP4 Suction	5. 16,184,324	-250.	-	250.	kPa	0.63%FS
50	Diff.P.	D-30	PD	50	JP3 Disch.-Confluence	5. 17,185,325	-100.	-	100.	kPa	0.63%FS

Table 3.2 Measurement List (Continued)

51Ch.- 100Ch.

Ch.	Item	Symbol	ID.		Location	Fig.No.	Range			Unit	Accuracy
51	Diff.P.	D-31	PD	51	JP4 Disch.-Confluence	5. 17,185,325	-100.	-	100.	kPa	0.63%FS
52	Diff.P.	D-32	PD	52	Confluence -Lower Pl.	5. 18,186,326	-50.0	-	50.0	kPa	0.63%FS
53	Diff.P.	D-33	PD	53	Lower Pl.-DC Middle		-250.	-	250.	kPa	0.63%FS
54	Diff.P.	D-34	PD	54	Lower Pl.-DC Bottom		-250.	-	250.	kPa	0.63%FS
55	Diff.P.	D-35	PD	55	DC Bottom-DC Middle		-50.0	-	50.0	kPa	0.63%FS
56	Diff.P.	D-36	PD	56	DC Middle-Steam Dome	5. 19,187,327	-50.0	-	50.0	kPa	0.63%FS
57	Diff.P.	D-37	PD	57	Lower Pl.Mid-Upper PL	NM,187,327					
58	Diff.P.	D-38	PD	58	Lower Pl.Bottom-Mid.	5. 20,188,328	0.0	-	50.0	kPa	0.63%FS
59	Diff.P.	D-39	PD	59	Upper Pl.-DC High	NU, NM, NM	-20.0	-	100.	kPa	0.63%FS
60	Diff.P.	D-40	PD	60	Channel Orifice A	5. 21,189,329	-50.0	-	50.0	kPa	0.63%FS
61	Diff.P.	D-41	PD	61	Channel Orifice B	5. 22,190,330	-50.0	-	50.0	kPa	0.63%FS
62	Diff.P.	D-42	PD	62	Channel Orifice C	5. 23,191,331	-25.0	-	75.0	kPa	0.63%FS
63	Diff.P.	D-43	PD	63	Channel Orifice D	5. 24,192,332	-50.0	-	50.0	kPa	0.63%FS
64	Diff.P.	D-44	PD	64	Bypass Hole	5. 25,193,333	-100.	-	100.	KPA	0.63%FS
65	Level	WL- 1	LM	65	HPCS Tank	NU NU, NU	0.0	-	2.30	m	1.00%FS
66	Level	WL- 2	LM	66	LPCS Tank	5. 26,194,334	0.0	-	2.30	m	1.00%FS
67	Level	WL- 3	LM	67	LPCI Tank	5. 26,194,334	0.0	-	4.25	m	1.00%FS
68	Level	WL- 4	LM	68	Upper Downcomer	5. 27,195,335	3.90	-	6.04	m	1.00%FS
69	Level	WL- 5	LM	69	Lower Downcomer	5. 27,195,335	0.938	-	3.90	m	1.00%FS
70	Mass.F.	F- 1	FM	70	Steam Line (Low Range)	5. 28,196,336	0.0	-	1.13	kg/s	0.92%FS
71	Mass.F.	F- 2	FM	71	Steam Line(High Range)	5. 28,196,336	0.0	-	3.00	kg/s	0.92%FS
72	Mass.F.	F- 3	FM	72	Steam Line (Mid Range)	5. 28,196,336	0.0	-	1.94	kg/s	1.40%FS
73	Vol.F.	F- 7	FV	73	HPCS (Upper Plenum)	NU,197,337	0.0	-	0.250E-02	m3/s	0.79%FS
74	Vol.F.	F- 9	FV	74	LPCS (Upper Plenum)	5. 29,197,337	0.0	-	0.250E-02	m3/s	0.79%FS
75	Vol.F.	F-11	FV	75	LPCI (Core Bypass)	5. 29,197,337	0.0	-	0.830E-02	m3/s	0.79%FS
76	Vol.F.	F-15	FV	76	Feedwater	5. 30,198,338	0.0	-	0.100E-01	m3/s	0.79%FS
77	Vol.F.	F-16	FV	77	PWT Flow	NU, NU, NU	0.0	-	0.420E-02	m3/s	0.79%FS
78	Vol.F.	F-17	FV	78	JP1 Discharge	5. 31,199,339	0.0	-	0.170E-01	m3/s	0.88%FS
79	Vol.F.	F-18	FV	79	JP2 Discharge	5. 31,199,339	0.0	-	0.170E-01	m3/s	0.88%FS
80	Vol.F.	F-19	FV	80	JP3 Disch. Positive	5. 32,200,340	0.0	-	0.170E-01	m3/s	0.92%FS
81	Vol.F.	F-20	FV	81	JP3 Disch. Negative	5. 33,201,341	0.0	-	0.500E-02	m3/s	0.92%FS
82	Vol.F.	F-21	FV	82	JP4 Disch. Positive	5. 32,200,340	0.0	-	0.170E-01	m3/s	0.92%FS
83	Vol.F.	F-22	FV	83	JP4 Disch. Negative	5. 33,201,341	0.0	-	0.500E-02	m3/s	0.92%FS
84	Mass.F.	F-23	FM	84	JP1,2 Outlet Spool	NM, NM, NM	0.0	-	30.0	kg/s	1.40%FS
85	Mass.F.	F-24	FM	85	JP3,4 Outlet Spool	NM, NM, NM	0.0	-	30.0	kg/s	1.40%FS
86	Mass.F.	F-25	FM	86	Break A Spool Piece	NM, NM, NM	0.0	-	30.0	kg/s	1.40%FS
87	Mass.F.	F-26	FM	87	Break B Spool Piece	NM, NM. NM	0.0	-	30.0	kg/s	1.40%FS
88	Vol.F.	F-27	FV	88	MRP-1	5. 34,202,342	0.0	-	0.120E-01	m3/s	0.88%FS
89	Vol.F.	F-28	FV	89	MRP-2	5. 34,202,342	0.0	-	0.120E-01	m3/s	0.63%FS
90	Diff.P.	D-F1	PD	90	F1 Orifice		0.0	-	4.90	kPa	0.63%FS
91	Diff.P.	D-F2	PD	91	F2 Orifice		0.0	-	34.9	kPa	0.63%FS
92	Diff.P.	D-F3	PD	92	F3 Orifice		0.0	-	14.6	kPa	0.63%FS
93	Diff.P.	D-F17	PD	93	F17 Venturi		0.0	-	98.1	kPa	0.63%FS
94	Diff.P.	D-F18	PD	94	F18 Venturi		0.0	-	98.1	kPa	0.63%FS
95	Diff.P.	D-F19	PD	95	F19 Orifice		0.0	-	147.	kPa	0.63%FS
96	Diff.P.	D-F20	PD	96	F20 Orifice		0.0	-	13.2	kPa	0.63%FS
97	Diff.P.	D-F21	PD	97	F21 Orifice		0.0	-	147.	kPa	0.63%FS
98	Diff.P.	D-F22	PD	98	F22 Orifice		0.0	-	13.2	kPa	0.63%FS
99	Diff.P.	D-F27	PD	99	F27 Venturi		0.0	-	200.	kPa	0.63%FS
100	Diff.P.	D-F28	PD	100	F28 Venturi		0.0	-	200.	kPa	0.63%FS

Table 3.2 Measurement List (Continued)

101Ch.- 150Ch.

Ch.	Item	Symbol	ID.		Location	Fig.No.	Range			Unit	Accuracy
101	Power	W- 1	WE	101	2100 kW Power Supplier	5. 35,203,343	0.0	-	0.210E+04	kW	1.00%FS
102	Power	W- 2	WE	102	3150 kW Power Supplier	5. 35,203,343	0.0	-	0.315E+04	kW	1.00%FS
103											
104	Rev.	N- 1	SR	104	MRP-1 Revolution	5. 36,204,344	0.0	-	0.500E+04	RPM	1.08%FS
105	Rev.	N- 2	SR	105	MRP-2 Revolution	5. 36,204,344	0.0	-	0.500E+04	RPM	1.08%FS
106	Signal	S- 1	EV	106	Break Signal A	NU, NU, NU					
107	Signal	S- 2	EV	107	Break Signal B	5. 37,205,345					
108	Signal	S- 3	EV	108	QSV Signal						
109	Signal	S- 6	EV	109	HPCS Valve	NU, NU, NU					
110	Signal	S- 7	EV	110	LPCS Valve	5. 38,206,346					
111	Signal	S- 8	EV	111	LPCI Valve	5. 38,206,346					
112	Signal	S- 9	EV	112	Feedwater Control	5. 37,205,345					
113	Signal	S-10	EV	113	MSIV Signal	5. 37,205,345					
114	Signal	S-11	EV	114	Steam Line Valve	NU,205,345					
115	Signal	S-12	EV	115	ADS Valve	NU,206,346					
116	Signal	S-13	EV	116	MRP-1 Power OFF	5. 39,207,347					
117	Signal	S-14	EV	117	MRP-2 Power OFF	5. 39,207,347					
118	Signal	RD- 1	EV	118	MRP-1 Rev. Direction	NU, NU, NU					
119	Signal	RD- 2	EV	119	MRP-2 Rev. Direction	NU, NU, NU					
120	Density	DF- 1	DE	120	JP1,2 Outlet Beam A	5. 40,208,348	0.0	-	0.100E+04	kg/m3	1.00%FS
121	Density	DF- 2	DE	121	JP1,2 Outlet Beam B	5. 41,209,349	0.0	-	0.100E+04	kg/m3	1.00%FS
122	Density	DF- 3	DE	122	JP1,2 Outlet Beam C	5. 42,210,350	0.0	-	0.100E+04	kg/m3	1.00%FS
123	Density	DF- 4	DE	123	JP3,4 Outlet Beam A	5. 43,211,351	0.0	-	0.100E+04	kg/m3	1.00%FS
124	Density	DF- 5	DE	124	JP3,4 Outlet Beam B	5. 44,212,352	0.0	-	0.100E+04	kg/m3	1.00%FS
125	Density	DF- 6	DE	125	JP3,4 Outlet Beam C	5. 45,213,353	0.0	-	0.100E+04	kg/m3	1.00%FS
126	Density	DF- 7	DE	126	Break A Beam A	NM, NM	0.0	-	0.100E+04	kg/m3	1.00%FS
127	Density	DF- 8	DE	127	Break A Beam B	NM, NM	0.0	-	0.100E+04	kg/m3	1.00%FS
128	Density	DF- 9	DE	128	Break B Beam A	5. 46,214,354	0.0	-	0.100E+04	kg/m3	1.00%FS
129	Density	DF-10	DE	129	Break B Beam B	5. 47,215,355	0.0	-	0.100E+04	kg/m3	1.00%FS
130	Mo.Flux	M- 1	MF	130	JP1,2 Outlet Spool	5. 48,216,356	0.0	-	0.220E+05	kg/ms2	1.00%FS
131	Mo.Flux	M- 2	MF	131	JP3,4 Outlet Spool	5. 49,217,357	0.0	-	0.220E+05	kg/ms2	1.00%FS
132	Mo.Flux	M- 3	MF	132	Break A (Low Range)	NU, NU	0.0	-	0.220E+05	kg/ms2	1.00%FS
133	Mo.Flux	M- 4	MF	133	Break B (Low Range)	FL, FL, FL	0.0	-	0.220E+05	kg/ms2	1.00%FS
134	Mo.Flux	M- 5	MF	134	Break A (High Range)	NU, NU	0.0	-	0.220E+06	kg/ms2	1.00%FS
135	Mo.Flux	M- 6	MF	135	Break B (High Range)	218,358	0.0	-	0.220E+06	kg/ms2	1.00%FS
136	Mo.Flux	M- 7	MF	136	Break Orifice	NM, NM, NM	0.0	-	0.220E+05	kg/ms2	1.00%FS
137											
138	Fluid T.	T- 1	TE	138	Lower Plenum	5. 50,219,359	273.	-	673.	K	0.64%FS
139	Fluid T.	T- 2	TE	139	Upper Plenum	5. 50,219,359	273.	-	673.	K	0.64%FS
140	Fluid T.	T- 3	TE	140	Steam Dome	5. 51,220,360	273.	-	673.	K	0.64%FS
141	Fluid T.	T- 4	TE	141	Upper Downcomer	5. 50,219,359	273.	-	673.	K	0.64%FS
142	Fluid T.	T- 5	TE	142	Lower Downcomer	FL,219,359	273.	-	673.	K	0.64%FS
143	Fluid T.	T- 6	TE	143	JP-1 Drive		273.	-	673.	K	0.64%FS
144	Fluid T.	T- 7	TE	144	JP-2 Drive		273.	-	673.	K	0.64%FS
145	Fluid T.	T- 8	TE	145	JP-3 Drive		273.	-	673.	K	0.64%FS
146	Fluid T.	T- 9	TE	146	JP-4 Drive		273.	-	673.	K	0.64%FS
147	Fluid T.	T-10	TE	147	JP-1 Discharge		273.	-	673.	K	0.64%FS
148	Fluid T.	T-11	TE	148	JP-2 Discharge		273.	-	673.	K	0.64%FS
149	Fluid T.	T-12	TE	149	JP-3 Discharge		273.	-	673.	K	0.64%FS
150	Fluid T.	T-13	TE	150	JP-4 Discharge		273.	-	673.	K	0.64%FS

Table 3.2 Measurement List (Continued)

151Ch.- 200Ch.

Ch.	Item	Symbol	ID.		Location	Fig.No.	Range			Unit	Accuracy
151	Fluid T.	T-14	TE	151	MRP-1 Suction		273.	-	673.	K	0.64%FS
152	Fluid T.	T-15	TE	152	MRP-1 Delivery		273.	-	673.	K	0.64%FS
153	Fluid T.	T-16	TE	153	MRP-2 Suction		273.	-	673.	K	0.64%FS
154	Fluid T.	T-17	TE	154	MRP-2 Delivery		273.	-	673.	K	0.64%FS
155	Fluid T.	T-18	TE	155	Break A Upstream		273.	-	673.	K	0.64%FS
156	Fluid T.	T-19	TE	156	Break B Upstream	221,361	273.	-	673.	K	0.64%FS
157	Fluid T.	T-20	TE	157	RCN A Condenced Water	NU, NU, NU	273.	-	698.	K	0.64%FS
158	Fluid T.	T-21	TE	158	RCN B Condenced Water	NU, NU, NU	273.	-	698.	K	0.64%FS
159	Fluid T.	T-22	TE	159	Discharged Steam	5. 51,220,360	273.	-	673.	K	0.64%FS
160	Fluid T.	T-24	TE	160	JP-1,2 Outlet Spool		273.	-	763.	K	0.64%FS
161	Fluid T.	T-25	TE	161	JP-3,4 Outlet Spool		273.	-	763.	K	0.64%FS
162	Fluid T.	T-26	TE	162	Break A Spool Piece		273.	-	763.	K	0.64%FS
163	Fluid T.	T-27	TE	163	Break B Spool Piece		273.	-	763.	K	0.64%FS
164	Fluid T.	T-28	TE	164	Feedwater	5. 52,222,362	273.	-	673.	K	0.64%FS
165	Fluid T.	T-29	TE	165	Break Orifice 1	NM, NM, NM	273.	-	673.	K	0.64%FS
166	Fluid T.	T-30	TE	166	Break Orifice 2	NM, NM, NM	273.	-	673.	K	0.64%FS
167	Fluid T.	T-31	TE	167	Break A Down DD(Low)	NM, NM, NM	273.	-	673.	K	0.64%FS
168	Fluid T.	T-32	TE	168	Break B Down DD(Low)	NM, NM, NM	273.	-	673.	K	0.64%FS
169	Fluid T.	T-33	TE	169	Break A Up. DD(High)	NM, NM, NM	273.	-	673.	K	0.64%FS
170	Fluid T.	T-34	TE	170	Break B Up. DD(High)	NM, NM, NM	273.	-	673.	K	0.64%FS
171	Fluid T.	T-F17	TE	171	JP1 Fluid D. Correc.	NM, NM, NM	273.	-	673.	K	0.64%FS
172	Fluid T.	T-F18	TE	172	JP2 Fluid D. Correc.	NM, NM, NM	273.	-	673.	K	0.64%FS
173	Fluid T.	T-F19	TE	173	JP3 Fluid D. Correc.	NM, NM, NM	273.	-	673.	K	0.64%FS
174	Fluid T.	T-F21	TE	174	JP4 Fluid D. Correc.	NM, NM, NM	273.	-	673.	K	0.64%FS
175	Slab T.	TS-11	TE	175	Core Barrel A Pos.5	NM, NM, NM	273.	-	673.	K	0.64%FS
176	Slab T.	TS-12	TE	176	Core Barrel A Pos.6	NM, NM, NM	273.	-	673.	K	0.64%FS
177	Slab T.	TS-13	TE	177	Filler Block C Pos.1	NM, NM, NM	273.	-	673.	K	0.64%FS
178	Slab T.	TS-14	TE	178	Filler Block C Pos.2	NM, NM, NM	273.	-	673.	K	0.64%FS
179	Slab T.	TS-15	TE	179	Filler Block C Pos.3	NM, NM, NM	273.	-	673.	K	0.64%FS
180	Slab T.	TS-16	TE	180	Filler Block C Pos.4	NM, NM, NM	273.	-	673.	K	0.64%FS
181	Slab T.	TS-17	TE	181	Filler Block C Pos.5	NM, NM, NM	273.	-	673.	K	0.64%FS
182	Slab T.	TS-18	TE	182	Filler Block C Pos.6	NM, NM, NM	273.	-	673.	K	0.64%FS
183	Slab T.	TS-19	TE	183	Filler Block A Pos.1	NM, NM, NM	273.	-	673.	K	0.64%FS
184	Slab T.	TS-20	TE	184	Filler Block A Pos.2	NM, NM, NM	273.	-	673.	K	0.64%FS
185	Slab T.	TS-21	TE	185	Filler Block A Pos.3	NM, NM, NM	273.	-	673.	K	0.64%FS
186	Slab T.	TS-22	TE	186	Filler Block A Pos.4	NM, NM, NM	273.	-	673.	K	0.64%FS
187	Slab T.	TS-23	TE	187	Filler Block A Pos.5	NM, NM, NM	273.	-	673.	K	0.64%FS
188	Slab T.	TS-24	TE	188	Filler Block A Pos.6	NM, NM, NM	273.	-	673.	K	0.64%FS
189	Slab T.	TS-25	TE	189	JP-1 Diffuser Wall	NM, NM, NM	273.	-	673.	K	0.64%FS
190	Slab T.	TS-26	TE	190	JP-2 Diffuser Wall	NM, NM, NM	273.	-	673.	K	0.64%FS
191	Slab T.	TS-27	TE	191	JP-3 Diffuser Wall	NM, NM, NM	273.	-	673.	K	0.64%FS
192	Slab T.	TS-28	TE	192	JP-4 Diffuser Wall	NM, NM, NM	273.	-	673.	K	0.64%FS
193	Slab T.	TS-29	TE	193	PV Wall Inside 1-1	NM, NM, NM	273.	-	673.	K	0.64%FS
194	Slab T.	TS-30	TE	194	PV Inner Surface 1-2	NM, NM, NM	273.	-	673.	K	0.64%FS
195	Slab T.	TS-31	TE	195	PV Inner Surface 1-3	NM, NM, NM	273.	-	673.	K	0.64%FS
196	Slab T.	TS-32	TE	196	PV Wall Inside 2	NM, NM, NM	273.	-	673.	K	0.64%FS
197	Slab T.	TS-33	TE	197	PV Wall Inside 3	NM, NM, NM	273.	-	673.	K	0.64%FS
198	Slab T.	TS-34	TE	198	PV Wall Inside 4	NM, NM, NM	273.	-	673.	K	0.64%FS
199	Slab T.	TS-35	TE	199	L.P. Inner Surface	NM, NM, NM	273.	-	673.	K	0.64%FS
200	Slab T.	TS-36	TE	200	L.P. Wall Inside	NM, NM, NM	273.	-	673.	K	0.64%FS

Table 3.2 Measurement List (Continued)

201Ch.- 250Ch.

Ch.	Item	Symbol	ID.	Location	Fig.No.	Range	Unit	Accuracy
201	Temp.	TF- 1	TE 201	A11 Fuel Rod Pos.1	5. 53,223,363	273. - 0.147E+04	K	0.64%FS
202	Temp.	TF- 2	TE 202	A11 Fuel Rod Pos.2	5. 53,223,363	273. - 0.147E+04	K	0.64%FS
203	Temp.	TF- 3	TE 203	A11 Fuel Rod Pos.3	5. 53,223,363	273. - 0.147E+04	K	0.64%FS
204	Temp.	TF- 4	TE 204	A11 Fuel Rod Pos.4	5. 53,223,363	273. - 0.147E+04	K	0.64%FS
205	Temp.	TF- 5	TE 205	A11 Fuel Rod Pos.5	5. 53,223,363	273. - 0.147E+04	K	0.64%FS
206	Temp.	TF- 6	TE 206	A11 Fuel Rod Pos.6	5. 53,223,363	273. - 0.147E+04	K	0.64%FS
207	Temp.	TF- 7	TE 207	A11 Fuel Rod Pos.7	5. 53,223,363	273. - 0.147E+04	K	0.64%FS
208	Temp.	TF- 8	TE 208	A12 Fuel Rod Pos.1	5. 54,224,364	273. - 0.147E+04	K	0.64%FS
209	Temp.	TF- 9	TE 209	A12 Fuel Rod Pos.2	5. 54,224,364	273. - 0.147E+04	K	0.64%FS
210	Temp.	TF- 10	TE 210	A12 Fuel Rod Pos.3	5. 54,224,364	273. - 0.147E+04	K	0.64%FS
211	Temp.	TF- 11	TE 211	A12 Fuel Rod Pos.4	5. 54,224,364	273. - 0.147E+04	K	0.64%FS
212	Temp.	TF- 12	TE 212	A12 Fuel Rod Pos.5	5. 54,224,364	273. - 0.147E+04	K	0.64%FS
213	Temp.	TF- 13	TE 213	A12 Fuel Rod Pos.6	5. 54,224,364	273. - 0.147E+04	K	0.64%FS
214	Temp.	TF- 14	TE 214	A12 Fuel Rod Pos.7	5. 54,224,364	273. - 0.147E+04	K	0.64%FS
215	Temp.	TF- 15	TE 215	A13 Fuel Rod Pos.1	5. 55,225,365	273. - 0.147E+04	K	0.64%FS
216	Temp.	TF- 16	TE 216	A13 Fuel Rod Pos.2	5. 55,225,365	273. - 0.147E+04	K	0.64%FS
217	Temp.	TF- 17	TE 217	A13 Fuel Rod Pos.3	5. 55,225,365	273. - 0.147E+04	K	0.64%FS
218	Temp.	TF- 18	TE 218	A13 Fuel Rod Pos.4	5. 55,225,365	273. - 0.147E+04	K	0.64%FS
219	Temp.	TF- 19	TE 219	A13 Fuel Rod Pos.5	5. 55,225,365	273. - 0.147E+04	K	0.64%FS
220	Temp.	TF- 20	TE 220	A13 Fuel Rod Pos.6	FL,225,365	273. - 0.147E+04	K	0.64%FS
221	Temp.	TF- 21	TE 221	A13 Fuel Rod Pos.7	5. 55,225,365	273. - 0.147E+04	K	0.64%FS
222	Temp.	TF- 22	TE 222	A14 Fuel Rod Pos.1	5. 56, NM, NM	273. - 0.147E+04	K	0.64%FS
223	Temp.	TF- 23	TE 223	A14 Fuel Rod Pos.2	5. 56, NM, NM	273. - 0.147E+04	K	0.64%FS
224	Temp.	TF- 24	TE 224	A14 Fuel Rod Pos.3	5. 56, NM, NM	273. - 0.147E+04	K	0.64%FS
225	Temp.	TF- 25	TE 225	A14 Fuel Rod Pos.4	5. 56, NM, NM	273. - 0.147E+04	K	0.64%FS
226	Temp.	TF- 26	TE 226	A14 Fuel Rod Pos.5	5. 56, NM, NM	273. - 0.147E+04	K	0.64%FS
227	Temp.	TF- 27	TE 227	A14 Fuel Rod Pos.6	5. 56, NM, NM	273. - 0.147E+04	K	0.64%FS
228	Temp.	TF- 28	TE 228	A14 Fuel Rod Pos.7	FL, NM, NM	273. - 0.147E+04	K	0.64%FS
229	Temp.	TF- 29	TE 229	A15 Fuel Rod Pos.1	NM, NM	273. - 0.147E+04	K	0.64%FS
230	Temp.	TF- 30	TE 230	A15 Fuel Rod Pos.4	NM, NM	273. - 0.147E+04	K	0.64%FS
231	Temp.	TF- 31	TE 231	A17 Fuel Rod Pos.1	NM, NM	273. - 0.147E+04	K	0.64%FS
232	Temp.	TF- 32	TE 232	A17 Fuel Rod Pos.4	NM, NM	273. - 0.147E+04	K	0.64%FS
233	Temp.	TF- 33	TE 233	A22 Fuel Rod Pos.1	FL, FL, FL	273. - 0.147E+04	K	0.64%FS
234	Temp.	TF- 34	TE 234	A22 Fuel Rod Pos.2	5. 57,226,366	273. - 0.147E+04	K	0.64%FS
235	Temp.	TF- 35	TE 235	A22 Fuel Rod Pos.3	5. 57,226,366	273. - 0.147E+04	K	0.64%FS
236	Temp.	TF- 36	TE 236	A22 Fuel Rod Pos.4	5. 57,226,366	273. - 0.125E+04	K	0.64%FS
237	Temp.	TF- 37	TE 237	A22 Fuel Rod Pos.5	5. 57,226,366	273. - 0.125E+04	K	0.64%FS
238	Temp.	TF- 38	TE 238	A22 Fuel Rod Pos.6	5. 57,226,366	273. - 0.125E+04	K	0.64%FS
239	Temp.	TF- 39	TE 239	A22 Fuel Rod Pos.7	5. 57,226,366	273. - 0.125E+04	K	0.64%FS
240	Temp.	TF- 40	TE 240	A24 Fuel Rod Pos.1	NM, NM	273. - 0.125E+04	K	0.64%FS
241	Temp.	TF- 41	TE 241	A24 Fuel Rod Pos.2	NM, NM	273. - 0.125E+04	K	0.64%FS
242	Temp.	TF- 42	TE 242	A24 Fuel Rod Pos.3	NM, NM	273. - 0.125E+04	K	0.64%FS
243	Temp.	TF- 43	TE 243	A24 Fuel Rod Pos.4	NM, NM	273. - 0.125E+04	K	0.64%FS
244	Temp.	TF- 44	TE 244	A24 Fuel Rod Pos.5	NM, NM	273. - 0.125E+04	K	0.64%FS
245	Temp.	TF- 45	TE 245	A24 Fuel Rod Pos.6	NM, NM	273. - 0.125E+04	K	0.64%FS
246	Temp.	TF- 46	TE 246	A24 Fuel Rod Pos.7	NM, NM	273. - 0.125E+04	K	0.64%FS
247	Temp.	TF- 47	TE 247	A26 Fuel Rod Pos.1	NM, NM	273. - 0.125E+04	K	0.64%FS
248	Temp.	TF- 48	TE 248	A26 Fuel Rod Pos.2	NM, NM	273. - 0.125E+04	K	0.64%FS
249	Temp.	TF- 49	TE 249	A28 Fuel Rod Pos.1	NM, NM	273. - 0.125E+04	K	0.64%FS
250	Temp.	TF- 50	TE 250	A28 Fuel Rod Pos.4		273. - 0.125E+04	K	0.64%FS

Table 3.2 Measurement List (Continued)

251Ch.- 300Ch.

Ch.	Item	Symbol	ID.		Location	Fig.No.	Range		Unit	Accuracy
251	Temp.	TF- 51	TE	251	A31 Fuel Rod Pos.1	NM, NM	273.	- 0.125E+04	K	0.64%FS
252	Temp.	TF- 52	TE	252	A31 Fuel Rod Pos.4		273.	- 0.125E+04	K	0.64%FS
253	Temp.	TF- 53	TE	253	A33 Fuel Rod Pos.1	5. 58,227,367	273.	- 0.125E+04	K	0.64%FS
254	Temp.	TF- 54	TE	254	A33 Fuel Rod Pos.2	5. 58,227,367	273.	- 0.125E+04	K	0.64%FS
255	Temp.	TF- 55	TE	255	A33 Fuel Rod Pos.3	5. 58,227,367	273.	- 0.125E+04	K	0.64%FS
256	Temp.	TF- 56	TE	256	A33 Fuel Rod Pos.4	5. 58,227,367	273.	- 0.125E+04	K	0.64%FS
257	Temp.	TF- 57	TE	257	A33 Fuel Rod Pos.5	5. 58,227,367	273.	- 0.125E+04	K	0.64%FS
258	Temp.	TF- 58	TE	258	A33 Fuel Rod Pos.6	5. 58,227,367	273.	- 0.125E+04	K	0.64%FS
259	Temp.	TF- 59	TE	259	A33 Fuel Rod Pos.7	5. 58,227,367	273.	- 0.125E+04	K	0.64%FS
260	Temp.	TF- 60	TE	260	A34 Fuel Rod Pos.1	NN, NM	273.	- 0.125E+04	K	0.64%FS
261	Temp.	TF- 61	TE	261	A34 Fuel Rod Pos.2	NM, NM	273.	- 0.125E+04	K	0.64%FS
262	Temp.	TF- 62	TE	262	A34 Fuel Rod Pos.3	NM, NM	273.	- 0.125E+04	K	0.64%FS
263	Temp.	TF- 63	TE	263	A34 Fuel Rod Pos.4	NM, NM	273.	- 0.125E+04	K	0.64%FS
264	Temp.	TF- 64	TE	264	A34 Fuel Rod Pos.5	NM, NM	273.	- 0.125E+04	K	0.64%FS
265	Temp.	TF- 65	TE	265	A34 Fuel Rod Pos.6	NM, NM	273.	- 0.125E+04	K	0.64%FS
266	Temp.	TF- 66	TE	266	A34 Fuel Rod Pos.7	NM, NM	273.	- 0.125E+04	K	0.64%FS
267	Temp.	TF- 67	TE	267	A37 Fuel Rod Pos.1	NM, NM	273.	- 0.125E+04	K	0.64%FS
268	Temp.	TF- 68	TE	268	A37 Fuel Rod Pos.4	NM, NM	273.	- 0.125E+04	K	0.64%FS
269	Temp.	TF- 69	TE	269	A42 Fuel Rod Pos.1	NM, NM	273.	- 0.125E+04	K	0.64%FS
270	Temp.	TF- 70	TE	270	A42 Fuel Rod Pos.4	NM, NM	273.	- 0.125E+04	K	0.64%FS
271	Temp.	TF- 71	TE	271	A44 Fuel Rod Pos.1	NM, NM	273.	- 0.125E+04	K	0.64%FS
272	Temp.	TF- 72	TE	272	A44 Fuel Rod Pos.2	NM, NM	273.	- 0.125E+04	K	0.64%FS
273	Temp.	TF- 73	TE	273	A44 Fuel Rod Pos.3	NM, NM	273.	- 0.125E+04	K	0.64%FS
274	Temp.	TF- 74	TE	274	A44 Fuel Rod Pos.4	NM, NM	273.	- 0.125E+04	K	0.64%FS
275	Temp.	TF- 75	TE	275	A44 Fuel Rod Pos.5	NM, NM	273.	- 0.125E+04	K	0.64%FS
276	Temp.	TF- 76	TE	276	A44 Fuel Rod Pos.6	NM, NM	273.	- 0.125E+04	K	0.64%FS
277	Temp.	TF- 77	TE	277	A44 Fuel Rod Pos.7	NM, NM	273.	- 0.125E+04	K	0.64%FS
278	Temp.	TF- 78	TE	278	A48 Fuel Rod Pos.1	NM, NM	273.	- 0.125E+04	K	0.64%FS
279	Temp.	TF- 79	TE	279	A48 Fuel Rod Pos.4	NM, NM	273.	- 0.125E+04	K	0.64%FS
280	Temp.	TF- 80	TE	280	A51 Fuel Rod Pos.1	NM, NM	273.	- 0.125E+04	K	0.64%FS
281	Temp.	TF- 81	TE	281	A51 Fuel Rod Pos.4	NM, NM	273.	- 0.125E+04	K	0.64%FS
282	Temp.	TF- 82	TE	282	A53 Fuel Rod Pos.1	NM, NM	273.	- 0.125E+04	K	0.64%FS
283	Temp.	TF- 83	TE	283	A53 Fuel Rod Pos.4	NM, NM	273.	- 0.125E+04	K	0.64%FS
284	Temp.	TF- 84	TE	284	A57 Fuel Rod Pos.1		273.	- 0.125E+04	K	0.64%FS
285	Temp.	TF- 85	TE	285	A57 Fuel Rod Pos.4	NM, NM	273.	- 0.125E+04	K	0.64%FS
286	Temp.	TF- 86	TE	286	A62 Fuel Rod Pos.1	NM, NM	273.	- 0.125E+04	K	0.64%FS
287	Temp.	TF- 87	TE	287	A62 Fuel Rod Pos.4	NM, NM	273.	- 0.125E+04	K	0.64%FS
288	Temp.	TF- 88	TE	288	A66 Fuel Rod Pos.1	NM, NM	273.	- 0.125E+04	K	0.64%FS
289	Temp.	TF- 89	TE	289	A66 Fuel Rod Pos.4	NM, NM	273.	- 0.125E+04	K	0.64%FS
290	Temp.	TF- 90	TE	290	A68 Fuel Rod Pos.1		273.	- 0.125E+04	K	0.64%FS
291	Temp.	TF- 91	TE	291	A68 Fuel Rod Pos.4	NM, NM	273.	- 0.125E+04	K	0.64%FS
292	Temp.	TF- 92	TE	292	A71 Fuel Rod Pos.1		273.	- 0.125E+04	K	0.64%FS
293	Temp.	TF- 93	TE	293	A71 Fuel Rod Pos.4	NM, NM	273.	- 0.125E+04	K	0.64%FS
294	Temp.	TF- 94	TE	294	A73 Fuel Rod Pos.1		273.	- 0.125E+04	K	0.64%FS
295	Temp.	TF- 95	TE	295	A73 Fuel Rod Pos.4	NM, NM	273.	- 0.125E+04	K	0.64%FS
296	Temp.	TF- 96	TE	296	A75 Fuel Rod Pos.1	NM, NM	273.	- 0.125E+04	K	0.64%FS
297	Temp.	TF- 97	TE	297	A75 Fuel Rod Pos.4	5. 59,228,368	273.	- 0.125E+04	K	0.64%FS
298	Temp.	TF- 98	TE	298	A77 Fuel Rod Pos.1	5. 59,228,368	273.	- 0.125E+04	K	0.64%FS
299	Temp.	TF- 99	TE	299	A77 Fuel Rod Pos.2	5. 59,228,368	273.	- 0.125E+04	K	0.64%FS
300	Temp.	TF-100	TE	300	A77 Fuel Rod Pos.3					

Table 3.2 Measurement List (Continued)

301Ch.- 350Ch.

Ch.	Item	Symbol	ID.	Location	Fig.No.	Range	Unit	Accuracy
301	Temp.	TF-101	TE 301	A77 Fuel Rod Pos.4	5. 59,228,368	273. - 0.125E+04	K	0.64%FS
302	Temp.	TF-102	TE 302	A77 Fuel Rod Pos.5	5. 59,228,368	273. - 0.125E+04	K	0.64%FS
303	Temp.	TF-103	TE 303	A77 Fuel Rod Pos.6	5. 59,228,368	273. - 0.125E+04	K	0.64%FS
304	Temp.	TF-104	TE 304	A77 Fuel Rod Pos.7	FL, FL, FL	273. - 0.125E+04	K	0.64%FS
305	Temp.	TF-105	TE 305	A82 Fuel Rod Pos.1	NM, NM	273. - 0.125E+04	K	0.64%FS
306	Temp.	TF-106	TE 306	A82 Fuel Rod Pos.4	NM, NM	273. - 0.125E+04	K	0.64%FS
307	Temp.	TF-107	TE 307	A84 Fuel Rod Pos.1		273. - 0.125E+04	K	0.64%FS
308	Temp.	TF-108	TE 308	A84 Fuel Rod Pos.4		273. - 0.125E+04	K	0.64%FS
309	Temp.	TF-109	TE 309	A85 Fuel Rod Pos.1	NM, NM	273. - 0.125E+04	K	0.64%FS
310	Temp.	TF-110	TE 310	A85 Fuel Rod Pos.2	NM, NM	273. - 0.125E+04	K	0.64%FS
311	Temp.	TF-111	TE 311	A85 Fuel Rod Pos.3	NM, NM	273. - 0.125E+04	K	0.64%FS
312	Temp.	TF-112	TE 312	A85 Fuel Rod Pos.4	NM, NM	273. - 0.125E+04	K	0.64%FS
313	Temp.	TF-113	TE 313	A85 Fuel Rod Pos.5	NM, NM	273. - 0.125E+04	K	0.64%FS
314	Temp.	TF-114	TE 314	A85 Fuel Rod Pos.6	NM, NM	273. - 0.125E+04	K	0.64%FS
315	Temp.	TF-115	TE 315	A85 Fuel Rod Pos.7	NM, NM	273. - 0.125E+04	K	0.64%FS
316	Temp.	TF-116	TE 316	A87 Fuel Rod Pos.1	5. 60,229,369	273. - 0.125E+04	K	0.64%FS
317	Temp.	TF-117	TE 317	A87 Fuel Rod Pos.2	5. 60,229,369	273. - 0.125E+04	K	0.64%FS
318	Temp.	TF-118	TE 318	A87 Fuel Rod Pos.3	5. 60,229,369	273. - 0.125E+04	K	0.64%FS
319	Temp.	TF-119	TE 319	A87 Fuel Rod Pos.4	5. 60,229,369	273. - 0.125E+04	K	0.64%FS
320	Temp.	TF-120	TE 320	A87 Fuel Rod Pos.5	5. 60,229,369	273. - 0.125E+04	K	0.64%FS
321	Temp.	TF-121	TE 321	A87 Fuel Rod Pos.6	5. 60,229,369	273. - 0.125E+04	K	0.64%FS
322	Temp.	TF-122	TE 322	A87 Fuel Rod Pos.7	5. 60,229,369	273. - 0.125E+04	K	0.64%FS
323	Temp.	TF-123	TE 323	A88 Fuel Rod Pos.1	5. 61,230,370	273. - 0.125E+04	K	0.64%FS
324	Temp.	TF-124	TE 324	A88 Fuel Rod Pos.2	5. 61,230,370	273. - 0.125E+04	K	0.64%FS
325	Temp.	TF-125	TE 325	A88 Fuel Rod Pos.3	5. 61,230,370	273. - 0.125E+04	K	0.64%FS
326	Temp.	TF-126	TE 326	A88 Fuel Rod Pos.4	5. 61,230,370	273. - 0.125E+04	K	0.64%FS
327	Temp.	TF-127	TE 327	A88 Fuel Rod Pos.5	5. 61,230,370	273. - 0.125E+04	K	0.64%FS
328	Temp.	TF-128	TE 328	A88 Fuel Rod Pos.6	5. 61,230,370	273. - 0.125E+04	K	0.64%FS
329	Temp.	TF-129	TE 329	A88 Fuel Rod Pos.7	5. 61,230,370	273. - 0.125E+04	K	0.64%FS
330	Temp.	TF-130	TE 330	B11 Fuel Rod Pos.1	5. 62,231,371	273. - 0.125E+04	K	0.64%FS
331	Temp.	TF-131	TE 331	B11 Fuel Rod Pos.2	5. 62,231,371	273. - 0.125E+04	K	0.64%FS
332	Temp.	TF-132	TE 332	B11 Fuel Rod Pos.3	5. 62,231,371	273. - 0.125E+04	K	0.64%FS
333	Temp.	TF-133	TE 333	B11 Fuel Rod Pos.4	5. 62,231,371	273. - 0.125E+04	K	0.64%FS
334	Temp.	TF-134	TE 334	B11 Fuel Rod Pos.5	5. 62,231,371	273. - 0.125E+04	K	0.64%FS
335	Temp.	TF-135	TE 335	B11 Fuel Rod Pos.6	5. 62,231,371	273. - 0.125E+04	K	0.64%FS
336	Temp.	TF-136	TE 336	B11 Fuel Rod Pos.7	FL, FL, FL	273. - 0.125E+04	K	0.64%FS
337	Temp.	TF-137	TE 337	B13 Fuel Rod Pos.4		273. - 0.125E+04	K	0.64%FS
338	Temp.	TF-138	TE 338	B22 Fuel Rod Pos.1	5. 63,232,372	273. - 0.125E+04	K	0.64%FS
339	Temp.	TF-139	TE 339	B22 Fuel Rod Pos.2	5. 63,232,372	273. - 0.125E+04	K	0.64%FS
340	Temp.	TF-140	TE 340	B22 Fuel Rod Pos.3	5. 63,232,372	273. - 0.125E+04	K	0.64%FS
341	Temp.	TF-141	TE 341	B22 Fuel Rod Pos.4	5. 63,232,372	273. - 0.125E+04	K	0.64%FS
342	Temp.	TF-142	TE 342	B22 Fuel Rod Pos.5	5. 63,232,372	273. - 0.125E+04	K	0.64%FS
343	Temp.	TF-143	TE 343	B22 Fuel Rod Pos.6	5. 63,232,372	273. - 0.125E+04	K	0.64%FS
344	Temp.	TF-144	TE 344	B22 Fuel Rod Pos.7	5. 63,232,372	273. - 0.125E+04	K	0.64%FS
345	Temp.	TF-145	TE 345	B31 Fuel Rod Pos.4	NM, NM	273. - 0.125E+04	K	0.64%FS
346	Temp.	TF-146	TE 346	B33 Fuel Rod Pos.4	NM, NM	273. - 0.125E+04	K	0.64%FS
347	Temp.	TF-147	TE 347	B51 Fuel Rod Pos.4	NM, NM	273. - 0.125E+04	K	0.64%FS
348	Temp.	TF-148	TE 348	B53 Fuel Rod Pos.4	NM, NM	273. - 0.125E+04	K	0.64%FS
349	Temp.	TF-149	TE 349	B66 Fuel Rod Pos.4	NM, NM	273. - 0.125E+04	K	0.64%FS
350	Temp.	TF-150	TE 350	B77 Fuel Rod Pos.1	5. 64,233,373	273. - 0.125E+04	K	0.64%FS

Table 3.2 Measurement List (Continued)

351Ch.- 400Ch.

Ch.	Item	Symbol	ID.		Location	Fig.No.	Range		Unit	Accuracy
351	Temp.	TF-151	TE	351	B77 Fuel Rod Pos.2	5. 64,233,373	273.	- 0.125E+04	K	0.64%FS
352	Temp.	TF-152	TE	352	B77 Fuel Rod Pos.3	5. 64,233,373	273.	- 0.125E+04	K	0.64%FS
353	Temp.	TF-153	TE	353	B77 Fuel Rod Pos.4	5. 64,233,373	273.	- 0.125E+04	K	0.64%FS
354	Temp.	TF-154	TE	354	B77 Fuel Rod Pos.5	5. 64,233,373	273.	- 0.125E+04	K	0.64%FS
355	Temp.	TF-155	TE	355	B77 Fuel Rod Pos.6	5. 64,233,373	273.	- 0.125E+04	K	0.64%FS
356	Temp.	TF-156	TE	356	B77 Fuel Rod Pos.7	5. 64,233,373	273.	- 0.125E+04	K	0.64%FS
357	Temp.	TF-157	TE	357	B86 Fuel Rod Pos.4	NM, NM, NM	273.	- 0.125E+04	K	0.64%FS
358	Temp.	TF-158	TE	358	C11 Fuel Rod Pos.1	5. 65,234,374	273.	- 0.125E+04	K	0.64%FS
359	Temp.	TF-159	TE	359	C11 Fuel Rod Pos.2	5. 65,234,374	273.	- 0.125E+04	K	0.64%FS
360	Temp.	TF-160	TE	360	C11 Fuel Rod Pos.3	5. 65,234,374	273.	- 0.125E+04	K	0.64%FS
361	Temp.	TF-161	TE	361	C11 Fuel Rod Pos.4	5. 65,234,374	273.	- 0.125E+04	K	0.64%FS
362	Temp.	TF-162	TE	362	C11 Fuel Rod Pos.5	5. 65,234,374	273.	- 0.125E+04	K	0.64%FS
363	Temp.	TF-163	TE	363	C11 Fuel Rod Pos.6	5. 65,234,374	273.	- 0.125E+04	K	0.64%FS
364	Temp.	TF-164	TE	364	C11 Fuel Rod Pos.7	5. 65,234,374	273.	- 0.125E+04	K	0.64%FS
365	Temp.	TF-165	TE	365	C13 Fuel Rod Pos.1	5. 66,235,375	273.	- 0.125E+04	K	0.64%FS
366	Temp.	TF-166	TE	366	C13 Fuel Rod Pos.2	5. 66,235,375	273.	- 0.125E+04	K	0.64%FS
367	Temp.	TF-167	TE	367	C13 Fuel Rod Pos.3	5. 66,235,375	273.	- 0.125E+04	K	0.64%FS
368	Temp.	TF-168	TE	368	C13 Fuel Rod Pos.4	5. 66,235,375	273.	- 0.125E+04	K	0.64%FS
369	Temp.	TF-169	TE	369	C13 Fuel Rod Pos.5	5. 66,235,375	273.	- 0.125E+04	K	0.64%FS
370	Temp.	TF-170	TE	370	C13 Fuel Rod Pos.6	5. 66,235,375	273.	- 0.125E+04	K	0.64%FS
371	Temp.	TF-171	TE	371	C13 Fuel Rod Pos.7	NM, NM, NM	273.	- 0.125E+04	K	0.64%FS
372	Temp.	TF-172	TE	372	C15 Fuel Rod Pos.4	5. 67,236,376	273.	- 0.125E+04	K	0.64%FS
373	Temp.	TF-173	TE	373	C22 Fuel Rod Pos.1	5. 67,236,376	273.	- 0.125E+04	K	0.64%FS
374	Temp.	TF-174	TE	374	C22 Fuel Rod Pos.2	5. 67,236,376	273.	- 0.125E+04	K	0.64%FS
375	Temp.	TF-175	TE	375	C22 Fuel Rod Pos.3	5. 67,236,376	273.	- 0.125E+04	K	0.64%FS
376	Temp.	TF-176	TE	376	C22 Fuel Rod Pos.4	5. 67,236,376	273.	- 0.125E+04	K	0.64%FS
377	Temp.	TF-177	TE	377	C22 Fuel Rod Pos.5	5. 67,236,376	273.	- 0.125E+04	K	0.64%FS
378	Temp.	TF-178	TE	378	C22 Fuel Rod Pos.6	5. 67,236,376	273.	- 0.125E+04	K	0.64%FS
379	Temp.	TF-179	TE	379	C22 Fuel Rod Pos.7	NM, NM, NM	273.	- 0.125E+04	K	0.64%FS
380	Temp.	TF-180	TE	380	C31 Fuel Rod Pos.4	5. 68,237,377	273.	- 0.125E+04	K	0.64%FS
381	Temp.	TF-181	TE	381	C33 Fuel Rod Pos.1	5. 68,237,377	273.	- 0.125E+04	K	0.64%FS
382	Temp.	TF-182	TE	382	C33 Fuel Rod Pos.2	5. 68,237,377	273.	- 0.125E+04	K	0.64%FS
383	Temp.	TF-183	TE	383	C33 Fuel Rod Pos.3	5. 68,237,377	273.	- 0.125E+04	K	0.64%FS
384	Temp.	TF-184	TE	384	C33 Fuel Rod Pos.4	5. 68,237,377	273.	- 0.125E+04	K	0.64%FS
385	Temp.	TF-185	TE	385	C33 Fuel Rod Pos.5	5. 68,237,377	273.	- 0.125E+04	K	0.64%FS
386	Temp.	TF-186	TE	386	C33 Fuel Rod Pos.6	5. 68,237,377	273.	- 0.125E+04	K	0.64%FS
387	Temp.	TF-187	TE	387	C33 Fuel Rod Pos.7	5. 68,237,377	273.	- 0.125E+04	K	0.64%FS
388	Temp.	TF-188	TE	388	C35 Fuel Rod Pos.4		273.	- 0.125E+04	K	0.64%FS
389	Temp.	TF-189	TE	389	C66 Fuel Rod Pos.4		273.	- 0.125E+04	K	0.64%FS
390	Temp.	TF-190	TE	390	C68 Fuel Rod Pos.4		273.	- 0.125E+04	K	0.64%FS
391	Temp.	TF-191	TE	391	C77 Fuel Rod Pos.1	5. 69,238,378	273.	- 0.125E+04	K	0.64%FS
392	Temp.	TF-192	TE	392	C77 Fuel Rod Pos.2	5. 69,238,378	273.	- 0.125E+04	K	0.64%FS
393	Temp.	TF-193	TE	393	C77 Fuel Rod Pos.3	5. 69,238,378	273.	- 0.125E+04	K	0.64%FS
394	Temp.	TF-194	TE	394	C77 Fuel Rod Pos.4	5. 69,238,378	273.	- 0.125E+04	K	0.64%FS
395	Temp.	TF-195	TE	395	C77 Fuel Rod Pos.5	5. 69,238,378	273.	- 0.125E+04	K	0.64%FS
396	Temp.	TF-196	TE	396	C77 Fuel Rod Pos.6	5. 69,238,378	273.	- 0.125E+04	K	0.64%FS
397	Temp.	TF-197	TE	397	C77 Fuel Rod Pos.7	5. 69,238,378	273.	- 0.125E+04	K	0.64%FS
398	Temp.	TF-198	TE	398	D11 Fuel Rod Pos.4		273.	- 0.125E+04	K	0.64%FS
399	Temp.	TF-199	TE	399	D13 Fuel Rod Pos.4		273.	- 0.125E+04	K	0.64%FS
400	Temp.	TF-200	TE	400	D22 Fuel Rod Pos.1	5. 70,239,379	273.	- 0.125E+04	K	0.64%FS

Table 3.2 Measurement List (Continued)

401Ch.- 450Ch.

Ch.	Item	Symbol	ID.		Location	Fig.No.	Range			Unit	Accuracy
401	Temp.	TF-201	TE	401	D22 Fuel Rod Pos.2	5. 70,239,379	273.	-	0.125E+04	K	0.64%FS
402	Temp.	TF-202	TE	402	D22 Fuel Rod Pos.3	5. 70,239,379	273.	-	0.125E+04	K	0.64%FS
403	Temp.	TF-203	TE	403	D22 Fuel Rod Pos.4	5. 70,239,379	273.	-	0.125E+04	K	0.64%FS
404	Temp.	TF-204	TE	404	D22 Fuel Rod Pos.5	5. 70,239,379	273.	-	0.125E+04	K	0.64%FS
405	Temp.	TF-205	TE	405	D22 Fuel Rod Pos.6	5. 70,239,379	273.	-	0.125E+04	K	0.64%FS
406	Temp.	TF-206	TE	406	D22 Fuel Rod Pos.7	5. 70,239,379	273.	-	0.125E+04	K	0.64%FS
407	Temp.	TF-207	TE	407	D31 Fuel Rod Pos.4	NM, NM	273.	-	0.125E+04	K	0.64%FS
408	Temp.	TF-208	TE	408	D33 Fuel Rod Pos.4	NM, NM	273.	-	0.125E+04	K	0.64%FS
409	Temp.	TF-209	TE	409	D51 Fuel Rod Pos.4	NM, NM	273.	-	0.125E+04	K	0.64%FS
410	Temp.	TF-210	TE	410	D53 Fuel Rod Pos.4	NM, NM	273.	-	0.125E+04	K	0.64%FS
411	Temp.	TF-211	TE	411	D66 Fuel Rod Pos.4	NM, NM	273.	-	0.125E+04	K	0.64%FS
412	Temp.	TF-212	TE	412	D77 Fuel Rod Pos.4	NM, NM	273.	-	0.125E+04	K	0.64%FS
413	Temp.	TF-213	TE	413	D86 Fuel Rod Pos.4	NM, NM	273.	-	0.125E+04	K	0.64%FS
414	Fluid T.	TW- 1	TE	414	A45 Tie Rod Pos.1	5. 71,240,380	273.	-	0.125E+04	K	0.64%FS
415	Fluid T.	TW- 2	TE	415	A45 Tie Rod Pos.2	5. 71,240,380	273.	-	0.125E+04	K	0.64%FS
416	Fluid T.	TW- 3	TE	416	A45 Tie Rod Pos.3	5. 71,240,380	273.	-	0.125E+04	K	0.64%FS
417	Fluid T.	TW- 4	TE	417	A45 Tie Rod Pos.4	5. 71,240,380	273.	-	0.125E+04	K	0.64%FS
418	Fluid T.	TW- 5	TE	418	A45 Tie Rod Pos.5	5. 71,240,380	273.	-	0.125E+04	K	0.64%FS
419	Fluid T.	TW- 6	TE	419	A45 Tie Rod Pos.6	5. 71,240,380	273.	-	0.125E+04	K	0.64%FS
420	Fluid T.	TW- 7	TE	420	A45 Tie Rod Pos.7	5. 71,240,380	273.	-	0.125E+04	K	0.64%FS
421	Fluid T.	TW- 8	TE	421	B45 Tie Rod Pos.1	NM, NM	273.	-	0.125E+04	K	0.64%FS
422	Fluid T.	TW- 9	TE	422	B45 Tie Rod Pos.2	NM, NM	273.	-	0.125E+04	K	0.64%FS
423	Fluid T.	TW-10	TE	423	B45 Tie Rod Pos.3	NM, NM	273.	-	0.125E+04	K	0.64%FS
424	Fluid T.	TW-11	TE	424	B45 Tie Rod Pos.4	NM, NM	273.	-	0.125E+04	K	0.64%FS
425	Fluid T.	TW-12	TE	425	B45 Tie Rod Pos.5	NM, NM	273.	-	0.125E+04	K	0.64%FS
426	Fluid T.	TW-13	TE	426	B45 Tie Rod Pos.6	NM, NM	273.	-	0.125E+04	K	0.64%FS
427	Fluid T.	TW-14	TE	427	B45 Tie Rod Pos.7	NM, NM	273.	-	0.125E+04	K	0.64%FS
428	Fluid T.	TW-15	TE	428	C45 Tie Rod Pos.1	5. 72,241,381	273.	-	0.125E+04	K	0.64%FS
429	Fluid T.	TW-16	TE	429	C45 Tie Rod Pos.2	5. 72,241,381	273.	-	0.125E+04	K	0.64%FS
430	Fluid T.	TW-17	TE	430	C45 Tie Rod Pos.3	5. 72,241,381	273.	-	0.125E+04	K	0.64%FS
431	Fluid T.	TW-18	TE	431	C45 Tie Rod Pos.4	5. 72,241,381	273.	-	0.125E+04	K	0.64%FS
432	Fluid T.	TW-19	TE	432	C45 Tie Rod Pos.5	5. 72,241,381	273.	-	0.125E+04	K	0.64%FS
433	Fluid T.	TW-20	TE	433	C45 Tie Rod Pos.6	5. 72,241,381	273.	-	0.125E+04	K	0.64%FS
434	Fluid T.	TW-21	TE	434	C45 Tie Rod Pos.7	5. 72,241,381	273.	-	0.125E+04	K	0.64%FS
435	Fluid T.	TW-22	TE	435	D45 Tie Rod Pos.1	NM, NM	273.	-	0.125E+04	K	0.64%FS
436	Fluid T.	TW-23	TE	436	D45 Tie Rod Pos.2	NM, NM	273.	-	0.125E+04	K	0.64%FS
437	Fluid T.	TW-24	TE	437	D45 Tie Rod Pos.3	FL, NM, NM	273.	-	0.125E+04	K	0.64%FS
438	Fluid T.	TW-25	TE	438	D45 Tie Rod Pos.4	NM, NM	273.	-	0.125E+04	K	0.64%FS
439	Fluid T.	TW-26	TE	439	D45 Tie Rod Pos.5	NM, NM	273.	-	0.125E+04	K	0.64%FS
440	Fluid T.	TW-27	TE	440	D45 Tie Rod Pos.6	FL, N	273.	-	0.125E+04	K	0.64%FS
441	Fluid T.	TW-28	TE	441	D45 Tie Rod Pos.7	NM, NM	273.	-	0.125E+04	K	0.64%FS
442	Fluid T.	TC- 1	TE	442	Channel Box A Inlet	5.101,	273.	-	0.125E+04	K	0.64%FS
443	Fluid T.	TC- 2	TE	443	Channel Box B Inlet	5.101,	273.	-	0.125E+04	K	0.64%FS
444	Fluid T.	TC- 3	TE	444	Channel Box C Inlet	5.101,	273.	-	0.125E+04	K	0.64%FS
445	Fluid T.	TC- 4	TE	445	Channel Box D Inlet	5.101,	273.	-	0.125E+04	K	0.64%FS
446	Fluid T.	TC- 5	TE	446	Channel Box Outlet A-1	5.102,264,404	273.	-	0.125E+04	K	0.64%FS
447	Fluid T.	TC- 6	TE	447	Channel Box Outlet A-2	5.102,264,404	273.	-	0.125E+04	K	0.64%FS
448	Fluid T.	TC- 7	TE	448	Channel Box Outlet A-3	5.102,264,404	273.	-	0.125E+04	K	0.64%FS
449	Fluid T.	TC- 8	TE	449	Channel Box Outlet A-4	5.102,264,404	273.	-	0.125E+04	K	0.64%FS
450	Fluid T.	TC- 9	TE	450	Channel Box Outlet A-6	5.102,264,404	273.	-	0.125E+04	K	0.64%FS

Table 3.2 Measurement List (Continued)

451Ch.- 500Ch.

Ch.	Item	Symbol	ID.		Location	Fig.No.	Range			Unit	Accuracy
451	Fluid T.	TC-10	TE	451	Channel Box Outlet C-1	5.103,265,405	273.	-	0.125E+04	K	0.64%FS
452	Fluid T.	TC-11	TE	452	Channel Box Outlet C-2	5.103,265,405	273.	-	0.125E+04	K	0.64%FS
453	Fluid T.	TC-12	TE	453	Channel Box Outlet C-3	5.103,265,405	273.	-	0.125E+04	K	0.64%FS
454	Fluid T.	TC-13	TE	454	Channel Box Outlet C-4	5.103,265,405	273.	-	0.125E+04	K	0.64%FS
455	Fluid T.	TC-14	TE	455	Channel Box Outlet C-6	5.103,265,405	273.	-	0.125E+04	K	0.64%FS
456	Fluid T.	TG- 1	TE	456	Upper Tieplate A Up.1	5.104,266,406	273.	-	0.125E+04	K	0.64%FS
457	Fluid T.	TG- 2	TE	457	Upper Tieplate A Up.2	5.104, NM, NM	273.	-	0.125E+04	K	0.64%FS
458	Fluid T.	TG- 3	TE	458	Upper Tieplate A Up.3	5.104, NM, NM	273.	-	0.125E+04	K	0.64%FS
459	Fluid T.	TG- 4	TE	459	Upper Tieplate A Up.4	5.104,266,406	273.	-	0.125E+04	K	0.64%FS
460	Fluid T.	TG- 5	TE	460	Upper Tieplate A Up.5	5.104, NM, NM	273.	-	0.125E+04	K	0.64%FS
461	Fluid T.	TG- 6	TE	461	Upper Tieplate A Up.6	5.105, NM, NM	273.	-	0.125E+04	K	0.64%FS
462	Fluid T.	TG- 7	TE	462	Upper Tieplate A Up.7	5.105, NM, NM	273.	-	0.125E+04	K	0.64%FS
463	Fluid T.	TG- 8	TE	463	Upper Tieplate A Up.8	5.105, NM, NM	273.	-	0.125E+04	K	0.64%FS
464	Fluid T.	TG- 9	TE	464	Upper Tieplate A Up.9	5.105, NM, NM	273.	-	0.125E+04	K	0.64%FS
465	Fluid T.	TG-10	TE	465	Upper Tieplate A Up.10	5.105,267,407	273.	-	0.125E+04	K	0.64%FS
466	Fluid T.	TG-11	TE	466	Upper Tieplate A Lo.1	5.106,268,408	273.	-	0.125E+04	K	0.64%FS
467	Fluid T.	TG-12	TE	467	Upper Tieplate A Lo.2	5.106, NM, NM	273.	-	0.125E+04	K	0.64%FS
468	Fluid T.	TG-13	TE	468	Upper Tieplate A Lo.3	5.106, NM, NM	273.	-	0.125E+04	K	0.64%FS
469	Fluid T.	TG-14	TE	469	Upper Tieplate A Lo.4	5.106,268,408	273.	-	0.125E+04	K	0.64%FS
470	Fluid T.	TG-15	TE	470	Upper Tieplate A Lo.5	5.106, NM, NM	273.	-	0.125E+04	K	0.64%FS
471	Fluid T.	TG-16	TE	471	Upper Tieplate A Lo.6	5.107, NM, NM	273.	-	0.125E+04	K	0.64%FS
472	Fluid T.	TG-17	TE	472	Upper Tieplate A Lo.7	5.107, NM, NM	273.	-	0.125E+04	K	0.64%FS
473	Fluid T.	TG-18	TE	473	Upper Tieplate A Lo.8	5.107, NM, NM	273.	-	0.125E+04	K	0.64%FS
474	Fluid T.	TG-19	TE	474	Upper Tieplate A Lo.9	5.107, NM, NM	273.	-	0.125E+04	K	0.64%FS
475	Fluid T.	TG-20	TE	475	Upper Tieplate A Lo.10	5.107,269,409	273.	-	0.125E+04	K	0.64%FS
476	Fluid T.	TG-21	TE	476	Upper Tieplate C Up.1	5.118,273,413	273.	-	0.125E+04	K	0.64%FS
477	Fluid T.	TG-22	TE	477	Upper Tieplate C Up.2	5.118, NM, NM	273.	-	0.125E+04	K	0.64%FS
478	Fluid T.	TG-23	TE	478	Upper Tieplate C Up.3	5.118, NM, NM	273.	-	0.125E+04	K	0.64%FS
479	Fluid T.	TG-24	TE	479	Upper Tieplate C Up.4	5.118,273,413	273.	-	0.125E+04	K	0.64%FS
480	Fluid T.	TG-25	TE	480	Upper Tieplate C Up.5	5.118, NM, NM	273.	-	0.125E+04	K	0.64%FS
481	Fluid T.	TG-26	TE	481	Upper Tieplate C Up.6	5.119, NM, NM	273.	-	0.125E+04	K	0.64%FS
482	Fluid T.	TG-27	TE	482	Upper Tieplate C Up.7	5.119, NM, NM	273.	-	0.125E+04	K	0.64%FS
483	Fluid T.	TG-28	TE	483	Upper Tieplate C Up.8	5.119, NM, NM	273.	-	0.125E+04	K	0.64%FS
484	Fluid T.	TG-29	TE	484	Upper Tieplate C Up.9	5.119, NM, NM	273.	-	0.125E+04	K	0.64%FS
485	Fluid T.	TG-30	TE	485	Upper Tieplate C Up.10	5.119,274,414	273.	-	0.125E+04	K	0.64%FS
486	Fluid T.	TG-31	TE	486	Upper Tieplate C Lo.1	5.120,275,415	273.	-	0.125E+04	K	0.64%FS
487	Fluid T.	TG-32	TE	487	Upper Tieplate C Lo.2	5.120, NM, NM	273.	-	0.125E+04	K	0.64%FS
488	Fluid T.	TG-33	TE	488	Upper Tieplate C Lo.3	5.120, NM, NM	273.	-	0.125E+04	K	0.64%FS
489	Fluid T.	TG-34	TE	489	Upper Tieplate C Lo.4	5.120,275,415	273.	-	0.125E+04	K	0.64%FS
490	Fluid T.	TG-35	TE	490	Upper Tieplate C Lo.5	5.120, NM, NM	273.	-	0.125E+04	K	0.64%FS
491	Fluid T.	TG-36	TE	491	Upper Tieplate C Lo.6	5.121, NM, NM	273.	-	0.125E+04	K	0.64%FS
492	Fluid T.	TG-37	TE	492	Upper Tieplate C Lo.7	5.121, NM, NM	273.	-	0.125E+04	K	0.64%FS
493	Fluid T.	TG-38	TE	493	Upper Tieplate C Lo.8	5.121, NM, NM	273.	-	0.125E+04	K	0.64%FS
494	Fluid T.	TG-39	TE	494	Upper Tieplate C Lo.9	5.121, NM, NM	273.	-	0.125E+04	K	0.64%FS
495	Fluid T.	TG-40	TE	495	Upper Tieplate C Lo.10	5.121,276,416	273.	-	0.125E+04	K	0.64%FS
496	Slab T.	TB- 1	TE	496	C.B. A1 Inner ,Pos.1	5. 73, NM, NM	273.	-	0.125E+04	K	0.64%FS
497	Slab T.	TB- 2	TE	497	C.B. A1 Inner ,Pos.2	5. 73, NM, NM	273.	-	0.125E+04	K	0.64%FS
498	Slab T.	TB- 3	TE	498	C.B. A1 Inner ,Pos.3	5. 73, NM, NM	273.	-	0.125E+04	K	0.64%FS
499	Slab T.	TB- 4	TE	499	C.B. A1 Inner ,Pos.4	5. 73, NM, NM	273.	-	0.125E+04	K	0.64%FS
500	Slab T.	TB- 5	TE	500	C.B. A1 Inner ,Pos.5	5. 73, NM, NM	273.	-	0.125E+04	K	0.64%FS

Table 3.2 Measurement List (Continued)

501Ch.- 550Ch.

Ch.	Item	Symbol	ID.		Location	Fig.No.	Range			Unit	Accuracy
501	Slab T.	TB- 6	TE	501	C.B. A1 Inner ,Pos.6	5. 73, NM, NM	273.	-	0.125E+04	K	0.64%FS
502	Slab T.	TB- 7	TE	502	C.B. A1 Inner ,Pos.7	5. 73, NM, NM	273.	-	0.125E+04	K	0.64%FS
503	Slab T.	TB- 8	TE	503	C.B. A2 Inner ,Pos.1	FL, FL, FL	273.	-	0.125E+04	K	0.64%FS
504	Slab T.	TB- 9	TE	504	C.B. A2 Inner ,Pos.2	5. 74, NM, NM	273.	-	0.125E+04	K	0.64%FS
505	Slab T.	TB-10	TE	505	C.B. A2 Inner ,Pos.3	5. 74, NM, NM	273.	-	0.125E+04	K	0.64%FS
506	Slab T.	TB-11	TE	506	C.B. A2 Inner ,Pos.4	5. 74, NM, NM	273.	-	0.125E+04	K	0.64%FS
507	Slab T.	TB-12	TE	507	C.B. A2 Inner ,Pos.5	5. 74, NM, NM	273.	-	0.125E+04	K	0.64%FS
508	Slab T.	TB-13	TE	508	C.B. A2 Inner ,Pos.6	5. 74, NM, NM	273.	-	0.125E+04	K	0.64%FS
509	Slab T.	TB-14	TE	509	C.B. A2 Inner ,Pos.7	5. 74, NM, NM	273.	-	0.125E+04	K	0.64%FS
510	Slab T.	TB-15	TE	510	C.B. B Inner ,Pos.1	5. 75, NM, NM	273.	-	0.125E+04	K	0.64%FS
511	Slab T.	TB-16	TE	511	C.B. B Inner ,Pos.2	5. 75, NM, NM	273.	-	0.125E+04	K	0.64%FS
512	Slab T.	TB-17	TE	512	C.B. B Inner ,Pos.3	5. 75, NM, NM	273.	-	0.125E+04	K	0.64%FS
513	Slab T.	TB-18	TE	513	C.B. B Inner ,Pos.4	5. 75, NM, NM	273.	-	0.125E+04	K	0.64%FS
514	Slab T.	TB-19	TE	514	C.B. B Inner ,Pos.5	5. 75, NM, NM	273.	-	0.125E+04	K	0.64%FS
515	Slab T.	TB-20	TE	515	C.B. B Inner ,Pos.6	5. 75, NM, NM	273.	-	0.125E+04	K	0.64%FS
516	Slab T.	TB-21	TE	516	C.B. B Inner ,Pos.7	5. 75, NM, NM	273.	-	0.125E+04	K	0.64%FS
517	Slab T.	TB-22	TE	517	C.B. C Inner ,Pos.1	5. 76, NM, NM	273.	-	0.125E+04	K	0.64%FS
518	Slab T.	TB-23	TE	518	C.B. C Inner ,Pos.2	5. 76, NM, NM	273.	-	0.125E+04	K	0.64%FS
519	Slab T.	TB-24	TE	519	C.B. C Inner ,Pos.3	5. 76, NM, NM	273.	-	0.125E+04	K	0.64%FS
520	Slab T.	TB-25	TE	520	C.B. C Inner ,Pos.4	5. 76, NM, NM	273.	-	0.125E+04	K	0.64%FS
521	Slab T.	TB-26	TE	521	C.B. C Inner ,Pos.5	5. 76, NM, NM	273.	-	0.125E+04	K	0.64%FS
522	Slab T.	TB-27	TE	522	C.B. C Inner ,Pos.6	5. 76, NM, NM	273.	-	0.125E+04	K	0.64%FS
523	Slab T.	TB-28	TE	523	C.B. C Inner ,Pos.7	5. 76, NM, NM	273.	-	0.125E+04	K	0.64%FS
524	Slab T.	TB-29	TE	524	C.B. D Inner ,Pos.1	5. 77, NM, NM	273.	-	0.125E+04	K	0.64%FS
525	Slab T.	TB-30	TE	525	C.B. D Inner ,Pos.2	5. 77, NM, NM	273.	-	0.125E+04	K	0.64%FS
526	Slab T.	TB-31	TE	526	C.B. D Inner ,Pos.3	5. 77, NM, NM	273.	-	0.125E+04	K	0.64%FS
527	Slab T.	TB-32	TE	527	C.B. D Inner ,Pos.4	5. 77, NM, NM	273.	-	0.125E+04	K	0.64%FS
528	Slab T.	TB-33	TE	528	C.B. D Inner ,Pos.5	5. 77, NM, NM	273.	-	0.125E+04	K	0.64%FS
529	Slab T.	TB-34	TE	529	C.B. D Inner ,Pos.6	5. 77, NM, NM	273.	-	0.125E+04	K	0.64%FS
530	Slab T.	TB-35	TE	530	C.B. D Inner ,Pos.7	5. 77, NM, NM	273.	-	0.125E+04	K	0.64%FS
531	Fluid T.	TB-36	TE	531	C.B. A Outer ,Pos.1	5. 78,242,382	273.	-	0.125E+04	K	0.64%FS
532	Fluid T.	TB-37	TE	532	C.B. A Outer ,Pos.2	5. 78,242,382	273.	-	0.125E+04	K	0.64%FS
533	Fluid T.	TB-38	TE	533	C.B. A Outer ,Pos.3	5. 78,242,382	273.	-	0.125E+04	K	0.64%FS
534	Fluid T.	TB-39	TE	534	C.B. A Outer ,Pos.4	5. 78,242,382	273.	-	0.125E+04	K	0.64%FS
535	Fluid T.	TB-40	TE	535	C.B. A Outer ,Pos.5	5. 78,242,382	273.	-	0.125E+04	K	0.64%FS
536	Fluid T.	TB-41	TE	536	C.B. A Outer ,Pos.6	5. 78,242,382	273.	-	0.125E+04	K	0.64%FS
537	Fluid T.	TB-42	TE	537	C.B. A Outer ,Pos.7	5. 78,242,382	273.	-	0.125E+04	K	0.64%FS
538	Fluid T.	TB-43	TE	538	C.B. C Outer ,Pos.1	5. 79, NM, NM	273.	-	0.125E+04	K	0.64%FS
539	Fluid T.	TB-44	TE	539	C.B. C Outer ,Pos.2	5. 79, NM, NM	273.	-	0.125E+04	K	0.64%FS
540	Fluid T.	TB-45	TE	540	C.B. C Outer ,Pos.3	5. 79, NM, NM	273.	-	0.125E+04	K	0.64%FS
541	Fluid T.	TB-46	TE	541	C.B. C Outer ,Pos.4	5. 79, NM, NM	273.	-	0.125E+04	K	0.64%FS
542	Fluid T.	TB-47	TE	542	C.B. C Outer ,Pos.5	5. 79, NM, NM	273.	-	0.125E+04	K	0.64%FS
543	Fluid T.	TB-48	TE	543	C.B. C Outer ,Pos.6	5. 79, NM, NM	273.	-	0.125E+04	K	0.64%FS
544	Fluid T.	TB-49	TE	544	C.B. C Outer ,Pos.7	5. 79, NM, NM	273.	-	0.125E+04	K	0.64%FS
545	Fluid T.	TP- 1	TE	545	Lower Pl. Center 1		273.	-	0.125E+04	K	0.64%FS
546	Fluid T.	TP- 2	TE	546	Lower Pl. Center 2		273.	-	0.125E+04	K	0.64%FS
547	Fluid T.	TP- 3	TE	547	Lower Pl. Center 3		273.	-	0.125E+04	K	0.64%FS
548	Fluid T.	TP- 4	TE	548	Lower Pl. Center 4		273.	-	0.125E+04	K	0.64%FS
549	Fluid T.	TP- 5	TE	549	Lower Pl. Center 5		273.	-	0.125E+04	K	0.64%FS
550	Fluid T.	TP- 6	TE	550	Lower Pl. Center 7		273.	-	0.125E+04	K	0.64%FS

Table 3.2 Measurement List (Continued)

551Ch.- 600Ch.

Ch.	Item	Symbol	ID.		Location	Fig.No.	Range			Unit	Accuracy
551	Slab T.	TP- 7	TE	551	Lower Pl. North	1	273.	-	0.125E+04	K	0.64%FS
552	Slab T.	TP- 8	TE	552	Lower Pl. North	2	273.	-	673.	K	0.64%FS
553	Slab T.	TP- 9	TE	553	Lower Pl. North	4	273.	-	673.	K	0.64%FS
554	Slab T.	TP-10	TE	554	Lower Pl. North	6	273.	-	673.	K	0.64%FS
555	Slab T.	TP-11	TE	555	Lower Pl. South	1	273.	-	673.	K	0.64%FS
556	Slab T.	TP-12	TE	556	Lower Pl. South	2	273.	-	673.	K	0.64%FS
557	Slab T.	TP-13	TE	557	Lower Pl. South	4	273.	-	673.	K	0.64%FS
558	Slab T.	TP-14	TE	558	Lower Pl. South	6	273.	-	673.	K	0.64%FS
559	Level	LB- 1	LM	559	C.B.Liquid Level	A1-1 FL, NM, NM					
560	Level	LB- 2	LM	560	C.B.Liquid Level	A1-2 FL, NM, NM					
561	Level	LB- 3	LM	561	C.B.Liquid Level	A1-3 5.132, NM, NM					
562	Level	LB- 4	LM	562	C.B.Liquid Level	A1-4 5.132, NM, NM					
563	Level	LB- 5	LM	563	C.B.Liquid Level	A1-5 5.132, NM, NM					
564	Level	LB- 6	LM	564	C.B.Liquid Level	A1-6 5.132, NM, NM					
565	Level	LB- 7	LM	565	C.B.Liquid Level	A1-7 5.132, NM, NM					
566	Level	LB- 8	LM	566	C.B.Liquid Level	A2-1 FL,281,421					
567	Level	LB- 9	LM	567	C.B.Liquid Level	A2-2 FL,281,421					
568	Level	LB-10	LM	568	C.B.Liquid Level	A2-3 FL,281,421					
569	Level	LB-11	LM	569	C.B.Liquid Level	A2-4 FL,281,421					
570	Level	LB-12	LM	570	C.B.Liquid Level	A2-5 FL,281,421					
571	Level	LB-13	LM	571	C.B.Liquid Level	A2-6 FL,281,421					
572	Level	LB-14	LM	572	C.B.Liquid Level	A2-7 FL,281,421					
573	Level	LB-15	LM	573	C.B.Liquid Level	B-1 5.134,282,422					
574	Level	LB-16	LM	574	C.B.Liquid Level	B-2 5.134,282,422					
575	Level	LB-17	LM	575	C.B.Liquid Level	B-3 5.134,282,422					
576	Level	LB-18	LM	576	C.B.Liquid Level	B-4 5.134,282,422					
577	Level	LB-19	LM	577	C.B.Liquid Level	B-5 5.134,282,422					
578	Level	LB-20	LM	578	C.B.Liquid Level	B-6 5.134,282,422					
579	Level	LB-21	LM	579	C.B.Liquid Level	B-7 5.134,282,422					
580	Level	LB-22	LM	580	C.B.Liquid Level	C-1 5.135,283,423					
581	Level	LB-23	LM	581	C.B.Liquid Level	C-2 FL,283,423					
582	Level	LB-24	LM	582	C.B.Liquid Level	C-3 5.135,283,423					
583	Level	LB-25	LM	583	C.B.Liquid Level	C-4 5.135, FL, FL					
584	Level	LB-26	LM	584	C.B.Liquid Level	C-5 5.135,283,423					
585	Level	LB-27	LM	585	C.B.Liquid Level	C-6 5.135,283,423					
586	Level	LB-28	LM	586	C.B.Liquid Level	C-7 5.135,283,423					
587	Level	LB-29	LM	587	C.B.Liquid Level	D-1 5.135,283,423					
588	Level	LB-30	LM	588	C.B.Liquid Level	D-2 5.136, NM, NM					
589	Level	LB-31	LM	589	C.B.Liquid Level	D-3 5.136, NM, NM					
590	Level	LB-32	LM	590	C.B.Liquid Level	D-4 5.136, NM, NM					
591	Level	LB-33	LM	591	C.B.Liquid Level	D-5 5.136, NM, NM					
592	Level	LB-34	LM	592	C.B.Liquid Level	D-6 5.136, NM, NM					
593	Level	LB-35	LM	593	C.B.Liquid Level	D-7 5.136, NM, NM					
594	Level	LL- 1	LM	594	Ch.Box Outlet	A1-5 5.137, NM, NM					
595	Level	LL- 2	LM	595	Ch.Box Outlet	A1-6 5.137, NM, NM					
596	Level	LL- 3	LM	596	Ch.Box Outlet	A1-7 FL, FL, FL					
597	Level	LL- 4	LM	597	Ch.Box Outlet	A2-5 5.138, FL, FL					
598	Level	LL- 5	LM	598	Ch.Box Outlet	A2-6 5.138,284,424					
599	Level	LL- 6	LM	599	Ch.Box Outlet	A2-7 5.138,284,424					
600	Level	LL- 7	LM	600	Ch.Box Outlet	A-1 5.139,285,425					

Table 3.2 Measurement List (Continued)

601Ch.- 650Ch.

Ch.	Item	Symbol	ID.		Location	Fig.No.	Range	Unit	Accuracy
601	Level	LL- 8	LM	601	Ch.Box Outlet A-2	FL, FL, FL			
602	Level	LL- 9	LM	602	Ch.Box Outlet A-3	5.139,285,425			
603	Level	LL-10	LM	603	Ch.Box Outlet A-4	5.139,285,425			
604	Level	LL-11	LM	604	Ch.Box Outlet A-6	5.139,285,425			
605	Level	LL-12	LM	605	Ch.Box Outlet C1-5	5.140,286,426			
606	Level	LL-13	LM	606	Ch.Box Outlet C1-6	5.140,286,426			
607	Level	LL-14	LM	607	Ch.Box Outlet C1-7	5.140,286,426			
608	Level	LL-15	LM	608	Ch.Box Outlet C2-5	5.141, NM, NM			
609	Level	LL-16	LM	609	Ch.Box Outlet C2-6	5.141, NM, NM			
610	Level	LL-17	LM	610	Ch.Box Outlet C2-7	5.141, NM, NM			
611	Level	LL-18	LM	611	Ch.Box Outlet C-1	5.142,287,427			
612	Level	LL-19	LM	612	Ch.Box Outlet C-2	5.142,287,427			
613	Level	LL-20	LM	613	Ch.Box Outlet C-3	5.142,287,427			
614	Level	LL-21	LM	614	Ch.Box Outlet C-4	5.142,287,427			
615	Level	LL-22	LM	615	Ch.Box Outlet C-6	5.142,287,427			
616	Level	LL-23	LM	616	Ch.Box Inlet A-1	5.143,288,428			
617	Level	LL-24	LM	617	Ch.Box Inlet A-2	5.143,288,428			
618	Level	LL-25	LM	618	Ch.Box Inlet B-1	5.144, NM, NM			
619	Level	LL-26	LM	619	Ch.Box Inlet B-2	5.144, NM, NM			
620	Level	LL-27	LM	620	Ch.Box Inlet C-1	5.145,289,429			
621	Level	LL-28	LM	621	Ch.Box Inlet C-2	5.145,289,429			
622	Level	LL-29	LM	622	Ch.Box Inlet D-1	5.146, NM, NM			
623	Level	LL-30	LM	623	Ch.Box Inlet D-2	5.146, NM, NM			
624	Level	LL-31	LM	624	Lower Pl. North 1	5.147,290,430			
625	Level	LL-32	LM	625	Lower Pl. North 2	5.147,290,430			
626	Level	LL-33	LM	626	Lower Pl. North 3	5.147,290,430			
627	Level	LL-34	LM	627	Lower Pl. North 4	5.147,290,430			
628	Level	LL-35	LM	628	Lower Pl. North 5	5.147,290,430			
629	Level	LL-36	LM	629	Lower Pl. North 6	FL, FL, FL			
630	Level	LL-37	LM	630	Lower Pl. South 1	5.148, NM, NM			
631	Level	LL-38	LM	631	Lower Pl. South 2	5.148, NM, NM			
632	Level	LL-39	LM	632	Lower Pl. South 3	5.148, NM, NM			
633	Level	LL-40	LM	633	Lower Pl. South 4	5.148, NM, NM			
634	Level	LL-41	LM	634	Lower Pl. South 5	5.148, NM, NM			
635	Level	LL-42	LM	635	Lower Pl. South 6	5.148, NM, NM			
636	Level	LL-43	LM	636	Guide Tube North 0	5.149,291,431			
637	Level	LL-44	LM	637	Guide Tube North 1	5.149,291,431			
638	Level	LL-45	LM	638	Guide Tube North 3	5.149,291,431			
639	Level	LL-46	LM	639	Guide Tube North 6	5.149,291,431			
640	Level	LL-47	LM	640	Guide Tube South 0	5.150, NM, NM			
641	Level	LL-48	LM	641	Guide Tube South 1	5.150, NM, NM			
642	Level	LL-49	LM	642	Guide Tube South 3	5.150, NM, NM			
643	Level	LL-50	LM	643	Guide Tube South 6	5.150, NM, NM			
644	Level	L- 1	LM	644	Downcomer D-Side 1	5.151,292,432			
645	Level	L- 2	LM	645	Downcomer D-Side 2	5.151,292,432			
646	Level	L- 3	LM	646	Downcomer D-Side 3	5.151,292,432			
647	Level	L- 4	LM	647	Downcomer D-Side 4	5.151,292,432			
648	Level	L- 5	LM	648	Downcomer D-Side 5	5.151, FL, FL			
649	Level	L- 6	LM	649	Downcomer B-Side 1	5.152, NM, NM			
650	Level	L- 7	LM	650	Downcomer B-Side 2	5.152, NM, NM			

Table 3.2 Measurement List (Continued)

651Ch.- 700Ch.

Ch.	Item	Symbol	ID.		Location	Fig.No.	Range			Unit	Accuracy
651	Level	L- 8	LM	651	Downcomer B-Side 3	5.152, NM, NM					
652	Level	L- 9	LM	652	Downcomer B-Side 4	5.152, NM, NM					
653	Level	L-10	LM	653	Downcomer B-Side 5	FL, FL, FL					
654	Void	VF- 1	VD	654	A54 Tie Rod Pos.1	NM, NM, NM	0.0	-	1.00		
655	Void	VF- 2	VD	655	A54 Tie Rod Pos.2	NM, NM, NM	0.0	-	1.00		
656	Void	VF- 3	VD	656	A54 Tie Rod Pos.3	NM, NM, NM	0.0	-	1.00		
657	Void	VF- 4	VD	657	A54 Tie Rod Pos.4	NM, NM, NM	0.0	-	1.00		
658	Void	VF- 5	VD	658	A54 Tie Rod Pos.5	NM, NM, NM	0.0	-	1.00		
659	Void	VF- 6	VD	659	A54 Tie Rod Pos.6	NM, NM, NM	0.0	-	1.00		
660	Void	VF- 7	VD	660	A54 Tie Rod Pos.7	NM, NM, NM	0.0	-	1.00		
661	Void	VF- 8	VD	661	B54 Tie Rod Pos.1	NM, NM, NM	0.0	-	1.00		
662	Void	VF- 9	VD	662	B54 Tie Rod Pos.2	NM, NM, NM	0.0	-	1.00		
663	Void	VF-10	VD	663	B54 Tie Rod Pos.3	NM, NM, NM	0.0	-	1.00		
664	Void	VF-11	VD	664	B54 Tie Rod Pos.4	NM, NM, NM	0.0	-	1.00		
665	Void	VF-12	VD	665	B54 Tie Rod Pos.5	NM, NM, NM	0.0	-	1.00		
666	Void	VF-13	VD	666	B54 Tie Rod Pos.6	NM, NM, NM	0.0	-	1.00		
667	Void	VF-14	VD	667	B54 Tie Rod Pos.7	NM, NM, NM	0.0	-	1.00		
668	Void	VF-15	VD	668	C54 Tie Rod Pos.1	NM, NM, NM	0.0	-	1.00		
669	Void	VF-16	VD	669	C54 Tie Rod Pos.2	NM, NM, NM	0.0	-	1.00		
670	Void	VF-17	VD	670	C54 Tie Rod Pos.3	NM, NM, NM	0.0	-	1.00		
671	Void	VF-18	VD	671	C54 Tie Rod Pos.4	NM, NM, NM	0.0	-	1.00		
672	Void	VF-19	VD	672	C54 Tie Rod Pos.5	NM, NM, NM	0.0	-	1.00		
673	Void	VF-20	VD	673	C54 Tie Rod Pos.6	NM, NM, NM	0.0	-	1.00		
674	Void	VF-21	VD	674	C54 Tie Rod Pos.7	NM, NM, NM	0.0	-	1.00		
675	Void	VF-22	VD	675	D54 Tie Rod Pos.7	NM, NM, NM	0.0	-	1.00		
676	Void	VF-23	VD	676	D54 Tie Rod Pos.7	NM, NM, NM	0.0	-	1.00		
677	Void	VF-24	VD	677	D54 Tie Rod Pos.7	NM, NM, NM	0.0	-	1.00		
678	Void	VF-25	VD	678	D54 Tie Rod Pos.7	NM, NM, NM	0.0	-	1.00		
679	Void	VF-26	VD	679	D54 Tie Rod Pos.7	NM, NM, NM	0.0	-	1.00		
680	Void	VF-27	VD	680	D54 Tie Rod Pos.7	NM, NM, NM	0.0	-	1.00		
681	Void	VF-28	VD	681	D54 Tie Rod Pos.7	NM, NM, NM	0.0	-	1.00		
682	Void	VE- 1	VD	682	Channel A Outlet 1	NM, NM, NM	0.0	-	1.00		
683	Void	VE- 2	VD	683	Channel A Outlet 2	NM, NM, NM	0.0	-	1.00		
684	Void	VE- 3	VD	684	Channel A Outlet 3	NM, NM, NM	0.0	-	1.00		
685	Void	VE- 4	VD	685	Channel B Outlet 1	NM, NM, NM	0.0	-	1.00		
686	Void	VE- 5	VD	686	Channel B Outlet 2	NM, NM, NM	0.0	-	1.00		
687	Void	VE- 6	VD	687	Channel B Outlet 3	NM, NM, NM	0.0	-	1.00		
688	Void	VE- 7	VD	688	Channel C Outlet 1	NM, NM, NM	0.0	-	1.00		
689	Void	VE- 8	VD	689	Channel C Outlet 2	NM, NM, NM	0.0	-	1.00		
690	Void	VE- 9	VD	690	Channel C Outlet 3	NM, NM, NM	0.0	-	1.00		
691	Void	VE-10	VD	691	Channel D Outlet 1	NM, NM, NM	0.0	-	1.00		
692	Void	VE-11	VD	692	Channel D Outlet 2	NM, NM, NM	0.0	-	1.00		
693	Void	VE-12	VD	693	Channel D Outlet 3	NM, NM, NM	0.0	-	1.00		
694	Void	VE-13	VD	694	Lower Plenum Bottom 1	NM, NM, NM	0.0	-	1.00		
695	Void	VE-14	VD	695	Lower Plenum Bottom 2	NM, NM, NM	0.0	-	1.00		
696	Void	VE-15	VD	696	Lower Plenum Bottom 3	NM, NM, NM	0.0	-	1.00		
697	Void	VP- 1	VD	697	Lower Plenum Inlet	NM, NM, NM	0.0	-	1.00		
698	Void	VP- 2	VD	698	Lower Plenum Inlet	NM, NM, NM	0.0	-	1.00		

Table 3.3 Core instrumentation map

Item	Pos. / DL / Rod NO.	Core Outlet	Pos.1	Pos.2	Pos.3	Pos.4	Pos.5	Pos.6	Pos.7	Core Inlet
		3660	3417	3114.5	2879.5	2527	2174.5	1939.5	1637	1454
Surface Temp.	A11		TF 1	TF 2	TF 3	TF 4	TF 5	TF 6	TF 7	
	A12		TF 8	TF 9	TF 10	TF 11	TF 12	TF 13	TF 14	
	A13		TF 15	TF 16	TF 17	TF 18	TF 19	TF 20	TF 21	
	A14		TF 22	TF 23	TF 24	TF 25	TF 26	TF 27	TF 28	
	A15		TF 29			TF 30				
	A17		TF 31			TF 32				
	A22		TF 33	TF 34	TF 35	TF 36	TF 37	TF 38	TF 39	
	A23		TF 40	TF 41	TF 42	TF 43	TF 44	TF 45	TF 46	
	A24		TF 47	TF 48	TF 49	TF 50	TF.51	TF 52	TF 53	
	A26		TF 54			TF 55				
	A28		TF 56			TF 57				
	A31		TF 58			TF 59				
	A33		TF 60	TF 61	TF 62	TF 63	TF 64	TF 65	TF 66	
	A34		TF 67	TF 68	TF 69	TF 70	TF 71	TF 72	TF 73	
	A35		TF 74			TF 75				
	A37		TF 76			TF 77				
	A42		TF 78			TF 79				
Fluid Temp.	A44	TC 1	TF180	TF181	TF182	TF183	TF184	TF185	TF186	TC 2
Surface Temp.	A45		TF 80			TF 81				
	A46		TF 82			TF 83				
	A48		TF 84			TF 85				
	A51		TF 86			TF 87				
	A53		TF 88			TF 89				
	A54		TF 90							
	A57		TF 91			TF 92				
	A62		TF 93			TF 94				
	A64		TF 95			TF 96				
	A66		TF 97			TF 98				
	A68		TF 99			TF100				
	A71		TF101			TF102				
	A73		TF103			TF104				
	A75		TF105			TF106				
	A77		TF107			TF108				

Table 3.3 Core instrumentation map (Continued)

Item	Pos. / Rod NO. / DL	Core Outlet	Pos.1	Pos.2	Pos.3	Pos.4	Pos.5	Pos.6	Pos.7	Core Inlet
		3660	3417	3114.5	2879.5	2527	2174.5	1939.5	1637	1454
Surface Temp.	A82		TF109			TF110				
	A84		TF111			TF112				
	A86		TF113			TF114				
	A88		TF115			TF116				
	B11					TF117				
	B13					TF118				
	B15		TF119	TF120	TF121	TF122	TF123	TF124	TF125	
	B31					TF126				
	B33					TF127				
	B35					TF128				
Fluid Temp.	B44	TC 3	TF187	TF188	TF189	TF190	TF191	TF192	TF193	TC 4
Surface Temp.	B51					TF129				
	B53					TF130				
	B85		TF131	TF132	TF133	TF134	TF135	TF136	TF137	
	C11					TF138				
	C13					TF139				
	C15					TF140				
	C31					TF141				
	C33		TF142	TF143	TF144	TF145	TF146	TF147	TF148	
	C35					TF149				
Fluid Temp.	C44	TC 5	TF194	TF195	TF196	TF197	TF198	TF199	TF200	TC 6
Surface Temp.	C51					TF150				
	C53					TF151				
	C77		TF152	TF153	TF154	TF155	TF156	TF157	TF158	
	D11					TF159				
	D13					TF160				
	D27		TF161	TF162	TF163	TF164	TF165	TF166	TF167	
	D31					TF168				
	D33					TF169				
	D35					TF170				
Fluid Temp.	D44	TC 7	TF201	TF202	TF203	TF204	TF205	TF206	TF207	TC 8
Surface Temp.	D51					TF171				
	D53					TF172				
	D88		TF173	TF174	TF175	TF176	TF177	TF178	TF179	

Table 3.3 Core instrumentation map (Continued)

Item	Pos. / Rod NO. / DL	Core Outlet	Pos.1	Pos.2	Pos.3	Pos.4	Pos.5	Pos.6	Pos.7	Core Inlet
		3660	3417	3114.5	2879.5	2527	2174.5	1939.5	1673	1454
Void	A5S		VF 1	VF 2	VF 3	VF 4	VF 5	VF 6	VF 7	
	B5S		VF 8	VF 9	VF 10	VF 11	VF 12	VF 13	VF 14	
	C5S		VF 15	VF 16	VF 17	VF 18	VF 19	VF 20	VF 21	
	D5S		VF 22	VF 23	VF 24	VF 25	VF 26	VF 27	VF 28	
Channel Box Surface Temp.	A1*		TB 1	TB 2	TB 3	TB 4	TB 5	TB 6	TB 7	
	A2*		TB 8	TB 9	TB 10	TB 11	TB 12	TB 13	TB 14	
	B*		TB 15	TB 16	TB 17	TB 18	TB 19	TB 20	TB 21	
	C*		TB 22	TB 23	TB 24	TB 25	TB 26	TB 27	TB 28	
	D*		TB 29	TB 30	TB 31	TB 32	TB 33	TB 34	TB 35	
Liquid Level in the Channel Box	A1*		LB 1	LB 2	LB 3	LB 4	LB 5	LB 6	LB 7	
	A2*		LB 8	LB 9	LB 10	LB 11	LB 12	LB 13	LB 14	
	B*		LB 15	LB 16	LB 17	LB 18	LB 19	LB 20	LB 21	
	C*		LB 22	LB 23	LB 24	LB 25	LB 26	LB 27	LB 28	
	D*		LB 29	LB 30	LB 31	LB 32	LB 33	LB 34	LB 35	

Table 4.1 Test conditions of RUNs 951, 954 and 956

Items	Unit	RUN951	RUN954	RUN956
Break Orifice I.D./Area	mm/%	18.0 (34)	9.8 (10)	9.8 (10)
Initial S.D. Pressure	MPa	7.35	7.35	7.35
" L.P. Subcooling	K	10.0	10.6	10.6
" Core Flow Rate	kg/s	16.4	16.7	16.8
" Core Power	MW	3.965	3.975	3.972
" U.P. Quality	%	13.0	12.4	12.4
" D.C. Water Level	m	5.04	5.03	5.03
" Steam Flow Rate	kg/s	2.03	2.06	2.05
MSIV Trip Logic/Time	- /s	Time/0.0	Time/0.0	L2+3/129
S/R Valve Opening Pressure	MPa	-	8.4-7.5	8.34-8.24
Feedwater Trip Time	s	2-4	2-4	2-4
Recirculation Pump Trip Time	s	0.0	0.0	0.0
ADS Actuation Logic/Time	- /s	-	L2+120/153	L2+120/244
ADS Orifice I.D.	mm	-	15.5	15.5
HPCS Actuation	-	Failure	Failure	Failure
LPCS " Time/Pressure	s/MPa	L1+40/P≤2.2	L1+40/P≤2.2	L1+40/P≤2.2
LPCI " "	s/MPa	" /P≤1.6	" /P≤1.6	" /P≤1.6
ECC Water Temperature	K	313	313	313
L2 Level	m	-	4.76	4.76
L1 Level	m	-	4.25	4.25

Table 4.2 Major events and test procedures of RUN951

Time (s)	Procedures and Events
-119	. Initiation of data recording by DATAC 2000B system
-9	. Initiation of data plotting in the figures
0.0	. Initiation of break in the main steam line (CV-130 full opening, CV-1 and CV-2 closure)
	. MRP1 coast down
	. MRP2 coast down
1.9	. Initiation of feedwater line closure (completed at 3.9 s)
9.0	. Initiation of core power decrease
19.2	. Initiation of flashing in the downcomer
23	. Initiation of water level recovery in the upper downcomer
25	. Initiation of lower plenum flashing
42	. Re-decrease of water level in the upper downcomer
131	. Initiation of upper core uncovery
245	. Initiation of feedwater flashing
335	. L1 level in the upper downcomer
375	. LPCS actuation
390	. Initiation of mass recovery in the core shroud
394	. PCT at Position 4 of A31 rod (Ch.252), 849 K
415	. LPCI actuation
445	. Completion of core quenching
591	. Termination of data plotting
816	. Termination of data recording

Table 4.3 Major events and test procedures of RUN 954

Time (s)	Procedures and Events
-120	Initiation of data recording
-12	Initiation of data plotting in figures
0	Initiation of break in steam line
	Closure of steady state steam line
	MRP1 and MRP2 coast down
	Pressure increase
2∿4	Feedwater line closure
5.4	Safety valve opening at P=8.4 MPa
	(Closed at 16.9 s)
9.0	Initiation of core power decrease
33	L2 level (4.76 m from PV Bottom)
153	ADS actuation
300	Top of core uncovering
403	L1 level (4.25 m from PV Bottom)
443	LPCS actuation at P=1.7 MPa
454	PCT 683 K at Position 3 of A12 rod
455	LPCI actuation at P=1.6 MPa
467	Completion of core quenching
656	PV filled up by liquid water
658	Recirculation loop filled up by liquid water
776	Termination of data plotting
1101	Termination of data recording

Table 4.4 Major events and test procedures of RUN956

Time (s)	Procedures and Events
-120	Initiation of data recording
-9	" of data plotting
0	" of break in steam line
	MRP1 and MRP2 coast down
2∿4	Feedwater line closure
9	Initiation of core power decrease
126	L2 level trip
129	MSIV closure (L2+3s)
145	Top of core temporal dryout
244	ADS actuation (L2+118s)
	PCT 583K at position 1 of A77 rod
334	Top of core redryout
350	L1 level trip
390	LPCS actuation (L1+40s)
408	Completion of core quench
432	LPCI actuation ($P \leq 1.65$MPa)
591	Termination of data plotting
1012	" of data recording

Table 4.5 Characteristics of steam discharge line valves

Valve	Close to Open	Open to Close
AV165 (Transient Line)	0.1 s	1.5 s
AV168 (Steady Line)	-	0.1 s
AV169 (ADS)	0.3 s	2.0 s

Table 4.6 Control sequence for steam line valves in RUNs 951, 954 and 956

(a) RUN951

Valves	Before Break	After Break
CV-130	Open	Full Open
AV-168	Open	Open
AV-165	Not Used	Not Used
AV-169	Not Used	Not Used
CV-1	Open	Close
CV-2	Open	Close

(b) RUN954

Valves	Before Break	After Break
CV-130	Open	Close
AV-168	Open	Close
AV-165	Close	Open
AV-169	Close	Open by L2+120s (ADS)
CV-1	Open	Close
CV-2	Open	Close
Safety Valve	Close	Open during 5.4∿16.9s

(c) RUN956

Valves	Before Break	After Break
CV-130	Open	Throttled
AV-168	Open	Close by L2+3 (MSIV)
AV-165	Close	Open
AV-169	Close	Open by L2+120s (ADS)
CV-1	Open	Close
CV-2	Open	Close

Table 5.1 Maximum cladding temperatures distribution in RUN 951

	Pos.1	Pos.2	Pos.3	Pos.4	Pos.5	Pos.6	Pos.7
A-11 rod	TE 201	TE 202	TE 203	TE 204	TE 205	TE 206	TE 207
PCT (K)	565.9	562.5	834.7	827.5	708.7	566.9	568.3
Time (s)	0.6	0.0	383.4	394.8	394.8	0.0	0.0
A-12 rod	TE 208	TE 209	TE 210	TE 211	TE 212	TE 213	TE 214
PCT (K)	562.6	747.1	811.9	808.3	684.7	567.5	564.3
Time (s)	0.0	381.0	383.4	398.4	394.2	0.0	0.0
A-13 rod	TE 215	TE 216	TE 217	TE 218	TE 219	TE 220	TE 221
PCT (K)	565.0	771.1	792.7	804.7	688.3	------	566.0
Time (s)	0.0	382.2	384.0	396.6	393.6	------	0.0
A-14 rod	TE 222	TE 223	TE 224	TE 225	TE 226	TE 227	TE 228
PCT (K)	564.7	678.7	736.3	774.7	673.9	569.5	------
Time (s)	0.0	310.8	391.8	391.8	395.4	0.0	------
A-15 rod	TE 229			TE 230			
PCT (K)	563.6			735.1			
Time (s)	0.0			355.2			
A-17 rod	TE 231			TE 232			
PCT (K)	560.9			653.5			
Time (s)	0.0			281.4			
A-22 rod	TE 233	TE 234	TE 235	TE 236	TE 237	TE 238	TE 239
PCT (K)	663.1	798.7	832.4	820.1	692.2	570.3	565.2
Time (s)	376.8	385.2	385.2	394.2	393.6	0.0	0.0
A-24 rod	TE 240	TE 241	TE 242	TE 243	TE 244	TE 245	TE 246
PCT (K)	566.9	694.1	747.8	788.2	675.2	564.5	563.4
Time (s)	0.0	382.2	396.6	405.0	389.4	0.0	0.0

Table 5.1 Maximum Cladding Temperature Distribution in the Core of RUN 951 (Continued)

	Pos.1	Pos.2	Pos.3	Pos.4	Pos.5	Pos.6	Pos.7
A-26 rod	TE 247			TE 248			
PCT (K)	565.6			567.2			
Time (s)	0.0			0.0			
A-28 rod	TE 249			TE 250			
PCT (K)	566.9			570.1			
Time (s)	0.0			0.0			
A-31 rod	TE 251			TE 252			
PCT (K)	563.4			844.5			
Time (s)	0.0			394.2			
A-33 rod	TE 253	TE 254	TE 255	TE 256	TE 257	TE 258	TE 259
PCT (K)	566.2	631.4	781.6	767.5	650.5	567.3	565.4
Time (s)	11.4	305.4	412.8	404.4	394.8	0.0	0.0
A-34 rod	TE 260	TE 261	TE 262	TE 263	TE 264	TE 265	TE 266
PCT (K)	566.5	567.2	715.8	754.4	651.4	568.1	564.5
Time (s)	0.0	0.0	355.8	406.2	391.8	0.0	0.0
A-37 rod	TE 267			TE 268			
PCT (K)	567.4			567.1			
Time (s)	0.0			0.0			
A-42 rod	TE 269			TE 270			
PCT (K)	565.5			824.7			
Time (s)	0.0			405.0			
A-44 rod	TE 271	TE 272	TE 273	TE 274	TE 275	TE 276	TE 277
PCT (K)	565.1	567.7	573.9	624.8	642.9	569.4	563.2
Time (s)	0.0	0.0	207.6	279.6	385.8	0.0	0.0

Table 5.1 Maximum Cladding Temperature Distribution in the Core of RUN 951 (Continued)

	Pos.1	Pos.2	Pos.3	Pos.4	Pos.5	Pos.6	Pos.7
A-48 rod	TE 278			TE 279			
PCT (K)	565.3			601.8			
Time (s)	0.0			261.6			
A-51 rod	TE 280			TE 281			
PCT (K)	564.9			823.8			
Time (s)	0.0			402.6			
A-53 rod	TE 282			TE 283			
PCT (K)	563.2			756.2			
Time (s)	0.0			406.8			
A-57 rod	TE 284			TE 285			
PCT (K)	566.1			778.8			
Time (s)	0.0			396.6			
A-62 rod	TE 286			TE 287			
PCT (K)	565.4			825.7			
Time (s)	0.0			396.0			
A-66 rod	TE 288			TE 289			
PCT (K)	563.8			764.7			
Time (s)	0.0			408.6			
A-68 rod	TE 290			TE 291			
PCT (K)	592.2			795.7			
Time (s)	382.2			395.4			
A-71 rod	TE 292			TE 293			
PCT (K)	564.5			840.7			
Time (s)	0.0			384.0			

Table 5.1 Maximum Cladding Temperature Distribution in the Core of RUN 951 (Continued)

	Pos.1	Pos.2	Pos.3	Pos.4	Pos.5	Pos.6	Pos.7
A-73 rod	TE 294			TE 295			
PCT (K)	565.3			822.9			
Time (s)	0.0			394.2			
A-75 rod	TE 296			TE 297			
PCT (K)	565.0			797.5			
Time (s)	0.0			405.6			
A-77 rod	TE 298	TE 299	TE 300	TE 301	TE 302	TE 303	TE 304
PCT (K)	710.1	798.5	826.6	792.8	675.2	564.7	------
Time (s)	417.0	405.0	394.8	394.2	394.2	0.0	------
A-82 rod	TE 305			TE 306			
PCT (K)	564.0			------			
Time (s)	0.0			------			
A-84 rod	TE 307			TE 308			
PCT (K)	565.5			821.9			
Time (s)	0.0			396.6			
A-85 rod	TE 309	TE 310	TE 311	TE 312	TE 313	TE 314	TE 315
PCT (K)	563.4	759.1	839.8	819.1	693.1	568.1	565.2
Time (s)	0.0	418.8	384.0	395.4	393.0	0.0	0.0
A-87 rod	TE 316	TE 317	TE 318	TE 319	TE 320	TE 321	TE 322
PCT (K)	684.6	777.8	836.0	811.6	690.3	568.6	563.6
Time (s)	388.2	418.8	387.6	397.2	393.0	0.0	0.0
A-88 rod	TE 323	TE 324	TE 325	TE 326	TE 327	TE 328	TE 329
PCT (K)	662.8	760.9	812.5	806.0	693.1	567.6	565.3
Time (s)	384.0	411.6	387.0	393.6	392.4	0.0	0.0

Table 5.1 Maximum Cladding Temperature Distribution in the Core of RUN 951 (Continued)

	Pos.1	Pos.2	Pos.3	Pos.4	Pos.5	Pos.6	Pos.7
B-11 rod	TE 330	TE 331	TE 332	TE 333	TE 334	TE 335	TE 336
PCT (K)	562.5	563.3	640.0	717.7	647.6	565.3	------
Time (s)	0.0	0.0	247.2	379.8	394.8	0.0	------
B-13 rod				TE 337			
PCT (K)				695.0			
Time (s)				381.6			
B-22 rod	TE 338	TE 339	TE 340	TE 341	TE 342	TE 343	TE 344
PCT (K)	599.9	666.6	713.9	715.8	629.5	566.2	563.2
Time (s)	326.4	378.0	378.6	379.2	393.6	0.0	0.0
B-31 rod				TE 345			
PCT (K)				729.0			
Time (s)				383.4			
B-33 rod				TE 346			
PCT (K)				674.2			
Time (s)				384.0			
B-51 rod				TE 347			
PCT (K)				719.5			
Time (s)				399.0			
B-53 rod				TE 348			
PCT (K)				685.6			
Time (s)				393.0			
B-66 rod				TE 349			
PCT (K)				566.2			
Time (s)				0.0			

Table 5.1 Maximum Cladding Temperature Distribution in the Core of RUN 951 (Continued)

	Pos.1	Pos.2	Pos.3	Pos.4	Pos.5	Pos.6	Pos.7
B-77 rod	TE 350	TE 351	TE 352	TE 353	TE 354	TE 355	TE 356
PCT (K)	564.5	656.2	693.1	696.9	639.1	566.5	564.3
Time (s)	0.0	381.6	381.0	401.4	385.8	0.0	0.0
B-86 rod				TE 357			
PCT (K)				665.7			
Time (s)				388.2			
C-11 rod	TE 358	TE 359	TE 360	TE 361	TE 362	TE 363	TE 364
PCT (K)	565.4	566.4	610.4	742.1	649.5	568.1	564.4
Time (s)	0.0	0.0	270.6	397.8	393.6	0.0	0.0
C-13 rod	TE 365	TE 366	TE 367	TE 368	TE 369	TE 370	TE 371
PCT (K)	563.5	565.4	565.3	630.5	646.7	567.8	564.8
Time (s)	0.0	0.0	0.0	279.6	384.6	0.0	0.0
C-15 rod				TE 372			
PCT (K)				726.1			
Time (s)				381.6			
C-22 rod	TE 373	TE 374	TE 375	TE 376	TE 377	TE 378	TE 379
PCT (K)	566.2	641.9	691.2	709.2	632.4	569.7	564.2
Time (s)	381.0	383.4	380.4	384.6	385.2	0.0	0.0
C-31 rod				TE 380			
PCT (K)				731.8			
Time (s)				390.0			
C-33 rod	TE 381	TE 382	TE 383	TE 384	TE 385	TE 386	TE 387
PCT (K)	563.3	566.9	565.4	567.2	565.3	564.2	560.9
Time (s)	0.0	0.0	0.0	0.6	0.0	0.0	0.0

Table 5.1 Maximum Cladding Temperature Distribution in the Core of RUN 951 (Continued)

	Pos.1	Pos.2	Pos.3	Pos.4	Pos.5	Pos.6	Pos.7
C-35 rod				TE 388			
PCT (K)				680.8			
Time (s)				396.0			
C-66 rod				TE 389			
PCT (K)				574.9			
Time (s)				414.6			
C-68 rod				TE 390			
PCT (K)				745.9			
Time (s)				402.6			
C-77 rod	TE 391	TE 392	TE 393	TE 394	TE 395	TE 396	TE 397
PCT (K)	585.5	666.6	722.4	739.3	645.7	565.3	563.3
Time (s)	387.0	412.2	415.2	408.6	392.4	0.0	0.0
D-11 rod				TE 398			
PCT (K)				752.5			
Time (s)				390.0			
D-13 rod				TE 399			
PCT (K)				755.3			
Time (s)				382.8			
D-22 rod	TE 400	TE 401	TE 402	TE 403	TE 404	TE 405	TE 406
PCT (K)	606.6	678.0	725.2	746.8	641.9	566.7	563.1
Time (s)	380.4	381.6	382.2	388.2	393.6	0.0	0.0
D-31 rod				TE 407			
PCT (K)				759.1			
Time (s)				389.4			

Table 5.1 Maximum Cladding Temperature Distribution in the Core of RUN 951 (Continued)

	Pos.1	Pos.2	Pos.3	Pos.4	Pos.5	Pos.6	Pos.7
D-33 rod				TE 408			
PCT (K)				686.5			
Time (s)				385.2			
D-51 rod				TE 409			
PCT (K)				731.8			
Time (s)				396.0			
D-53 rod				TE 410			
PCT (K)				702.6			
Time (s)				400.8			
D-66 rod				TE 411			
PCT (K)				699.3			
Time (s)				410.4			
D-77 rod				TE 412			
PCT (K)				------			
Time (s)				------			
D-86 rod				TE 413			
PCT (K)				751.5			
Time (s)				404.4			

Table 5.1 Maximum Cladding Temperature Distribution in the Core of RUN 951 (Continued)

** Order of PCT (RUN 951) **

No. 1	A-31 rod	Pos. 4	PCT =	844.5 (K)	Time =	394.2 (s)
No. 2	A-71 rod	Pos. 4	PCT =	840.7 (K)	Time =	384.0 (s)
No. 3	A-85 rod	Pos. 3	PCT =	839.8 (K)	Time =	384.0 (s)
No. 4	A-87 rod	Pos. 3	PCT =	836.0 (K)	Time =	387.6 (s)
No. 5	A-11 rod	Pos. 3	PCT =	834.7 (K)	Time =	383.4 (s)
No. 6	A-22 rod	Pos. 3	PCT =	832.4 (K)	Time =	385.2 (s)
No. 7	A-11 rod	Pos. 4	PCT =	827.5 (K)	Time =	394.8 (s)
No. 8	A-77 rod	Pos. 3	PCT =	826.6 (K)	Time =	394.8 (s)
No. 9	A-62 rod	Pos. 4	PCT =	825.7 (K)	Time =	396.0 (s)
No.10	A-42 rod	Pos. 4	PCT =	824.7 (K)	Time =	405.0 (s)

Table 5.2 Maximum cladding temperatures distribution in RUN 954

	Pos.1	Pos.2	Pos.3	Pos.4	Pos.5	Pos.6	Pos.7
A-11 rod	TE 201	TE 202	TE 203	TE 204	TE 205	TE 206	TE 207
PCT (K)	575.5	604.3	629.5	636.7	579.1	575.5	577.9
Time (s)	5.6	11.2	453.6	458.4	6.4	5.6	6.4
A-12 rod	TE 208	TE 209	TE 210	TE 211	TE 212	TE 213	TE 214
PCT (K)	573.1	658.3	683.5	633.1	576.7	575.5	574.3
Time (s)	6.4	451.2	454.4	457.6	5.6	5.6	5.6
A-13 rod	TE 215	TE 216	TE 217	TE 218	TE 219	TE 220	TE 221
PCT (K)	574.3	660.7	682.3	634.3	577.9	576.7	576.7
Time (s)	5.6	450.4	453.6	458.4	5.6	5.6	4.8
A-14 rod	TE 222	TE 223	TE 224	TE 225	TE 226	TE 227	TE 228
PCT (K)	------	------	------	------	------	------	------
Time (s)	------	------	------	------	------	------	------
A-15 rod	TE 229			TE 230			
PCT (K)	------			------			
Time (s)	------			------			
A-17 rod	TE 231			TE 232			
PCT (K)	------			630.7			
Time (s)	------			457.6			
A-22 rod	TE 233	TE 234	TE 235	TE 236	TE 237	TE 238	TE 239
PCT (K)	594.7	655.9	671.5	622.8	578.8	576.6	571.4
Time (s)	452.8	452.8	457.6	460.0	5.6	5.6	5.6
A-24 rod	TE 240	TE 241	TE 242	TE 243	TE 244	TE 245	TE 246
PCT (K)	------	------	------	------	------	------	------
Time (s)	------	------	------	------	------	------	------

Table 5.2 Maximum Cladding Temperature Distribution in the Core of RUN 954 (Continued)

	Pos.1	Pos.2	Pos.3	Pos.4	Pos.5	Pos.6	Pos.7
A-26 rod	TE 247			TE 248			
PCT (K)	------			------			
Time (s)	------			------			
A-28 rod	TE 249			TE 250			
PCT (K)	------			580.0			
Time (s)	------			5.6			
A-31 rod	TE 251			TE 252			
PCT (K)	------			629.5			
Time (s)	------			458.4			
A-33 rod	TE 253	TE 254	TE 255	TE 256	TE 257	TE 258	TE 259
PCT (K)	571.7	616.9	637.5	597.3	574.9	575.9	574.9
Time (s)	5.6	449.6	454.4	458.4	5.6	5.6	5.6
A-34 rod	TE 260	TE 261	TE 262	TE 263	TE 264	TE 265	TE 266
PCT (K)	------	------	------	------	------	------	------
Time (s)	------	------	------	------	------	------	------
A-37 rod	TE 267			TE 268			
PCT (K)	------			------			
Time (s)	------			------			
A-42 rod	TE 269			TE 270			
PCT (K)	------			------			
Time (s)	------			------			
A-44 rod	TE 271	TE 272	TE 273	TE 274	TE 275	TE 276	TE 277
PCT (K)	------	------	------	------	------	------	------
Time (s)	------	------	------	------	------	------	------

Table 5.2 Maximum Cladding Temperature Distribution in the Core of RUN 954 (Continued)

	Pos.1	Pos.2	Pos.3	Pos.4	Pos.5	Pos.6	Pos.7
A-48 rod	TE 278			TE 279			
PCT (K)	------			------			
Time (s)	------			------			
A-51 rod	TE 280			TE 281			
PCT (K)	------			------			
Time (s)	------			------			
A-53 rod	TE 282			TE 283			
PCT (K)	------			------			
Time (s)	------			------			
A-57 rod	TE 284			TE 285			
PCT (K)	------			615.2			
Time (s)	------			459.2			
A-62 rod	TE 286			TE 287			
PCT (K)	------			------			
Time (s)	------			------			
A-66 rod	TE 288			TE 289			
PCT (K)	------			------			
Time (s)	------			------			
A-68 rod	TE 290			TE 291			
PCT (K)	------			624.8			
Time (s)	------			459.2			
A-71 rod	TE 292			TE 293			
PCT (K)	------			638.1			
Time (s)	------			459.2			

Table 5.2 Maximum Cladding Temperature Distribution in the Core of RUN 954 (Continued)

	Pos.1	Pos.2	Pos.3	Pos.4	Pos.5	Pos.6	Pos.7
A-73 rod	TE 294			TE 295			
PCT (K)	------			620.9			
Time (s)	------			457.6			
A-75 rod	TE 296			TE 297			
PCT (K)	------			------			
Time (s)	------			------			
A-77 rod	TE 298	TE 299	TE 300	TE 301	TE 302	TE 303	TE 304
PCT (K)	598.0	649.5	659.0	607.6	560.7	574.9	------
Time (s)	460.0	460.0	458.4	459.2	0.0	5.6	------
A-82 rod	TE 305			TE 306			
PCT (K)	------			------			
Time (s)	------			------			
A-84 rod	TE 307			TE 308			
PCT (K)	628.6			626.7			
Time (s)	454.4			458.4			
A-85 rod	TE 309	TE 310	TE 311	TE 312	TE 313	TE 314	TE 315
PCT (K)	------	------	------	------	------	------	------
Time (s)	------	------	------	------	------	------	------
A-87 rod	TE 316	TE 317	TE 318	TE 319	TE 320	TE 321	TE 322
PCT (K)	599.9	654.3	673.3	624.8	576.8	576.8	573.9
Time (s)	456.0	456.8	457.6	459.2	5.6	5.6	5.6
A-88 rod	TE 323	TE 324	TE 325	TE 326	TE 327	TE 328	TE 329
PCT (K)	607.6	650.5	671.4	627.6	577.8	577.8	574.9
Time (s)	12.0	460.8	457.6	457.6	5.6	5.6	4.8

Table 5.2 Maximum Cladding Temperature Distribution in the Core of RUN 954 (Continued)

	Pos.1	Pos.2	Pos.3	Pos.4	Pos.5	Pos.6	Pos.7
B-11 rod	TE 330	TE 331	TE 332	TE 333	TE 334	TE 335	TE 336
PCT (K)	573.9	573.9	576.8	574.9	573.0	573.9	------
Time (s)	5.6	5.6	5.6	4.8	4.8	4.8	------
B-13 rod				TE 337			
PCT (K)				574.9			
Time (s)				4.8			
B-22 rod	TE 338	TE 339	TE 340	TE 341	TE 342	TE 343	TE 344
PCT (K)	574.9	585.5	605.6	579.7	574.9	573.9	571.0
Time (s)	5.6	448.8	455.2	456.0	5.6	5.6	4.8
B-31 rod				TE 345			
PCT (K)				------			
Time (s)				------			
B-33 rod				TE 346			
PCT (K)				------			
Time (s)				------			
B-51 rod				TE 347			
PCT (K)				------			
Time (s)				------			
B-53 rod				TE 348			
PCT (K)				------			
Time (s)				------			
B-66 rod				TE 349			
PCT (K)				------			
Time (s)				------			

Table 5.2 Maximum Cladding Temperature Distribution in the Core of RUN 954 (Continued)

	Pos.1	Pos.2	Pos.3	Pos.4	Pos.5	Pos.6	Pos.7
B-77 rod	TE 350	TE 351	TE 352	TE 353	TE 354	TE 355	TE 356
PCT (K)	572.0	600.8	620.9	587.4	------	574.9	573.9
Time (s)	5.6	454.4	454.4	454.4	------	5.6	5.6
B-86 rod				TE 357			
PCT (K)				------			
Time (s)				------			
C-11 rod	TE 358	TE 359	TE 360	TE 361	TE 362	TE 363	TE 364
PCT (K)	575.9	574.9	573.9	574.9	571.0	575.9	570.1
Time (s)	5.6	5.6	5.6	5.6	5.6	5.6	5.6
C-13 rod	TE 365	TE 366	TE 367	TE 368	TE 369	TE 370	TE 371
PCT (K)	570.1	571.0	613.3	589.3	576.8	576.8	573.9
Time (s)	5.6	4.8	449.6	457.6	5.6	5.6	5.6
C-15 rod				TE 372			
PCT (K)				------			
Time (s)				------			
C-22 rod	TE 373	TE 374	TE 375	TE 376	TE 377	TE 378	TE 379
PCT (K)	571.0	591.3	606.6	578.8	576.8	577.8	572.0
Time (s)	5.6	452.0	459.2	457.6	5.6	5.6	5.6
C-31 rod				TE 380			
PCT (K)				------			
Time (s)				------			
C-33 rod	TE 381	TE 382	TE 383	TE 384	TE 385	TE 386	TE 387
PCT (K)	572.0	573.9	573.0	574.9	574.9	573.0	570.1
Time (s)	5.6	5.6	5.6	5.6	5.6	5.6	6.4

Table 5.2 Maximum Cladding Temperature Distribution in the Core of RUN 954 (Continued)

	Pos.1	Pos.2	Pos.3	Pos.4	Pos.5	Pos.6	Pos.7
C-35 rod				TE 388			
PCT (K)				------			
Time (s)				------			
C-66 rod				TE 389			
PCT (K)				------			
Time (s)				------			
C-68 rod				TE 390			
PCT (K)				------			
Time (s)				------			
C-77 rod	TE 391	TE 392	TE 393	TE 394	TE 395	TE 396	TE 397
PCT (K)	573.0	617.1	626.7	596.1	576.8	574.9	573.0
Time (s)	5.6	457.6	457.6	457.6	5.6	5.6	5.6
D-11 rod				TE 398			
PCT (K)				601.8			
Time (s)				457.6			
D-13 rod				TE 399			
PCT (K)				599.9			
Time (s)				457.6			
D-22 rod	TE 400	TE 401	TE 402	TE 403	TE 404	TE 405	TE 406
PCT (K)	572.0	612.3	623.8	583.6	575.9	576.8	573.0
Time (s)	5.6	447.2	456.8	449.6	5.6	5.6	5.6
D-31 rod				TE 407			
PCT (K)				------			
Time (s)				------			

Table 5.2 Maximum Cladding Temperature Distribution in the Core of RUN 954 (Continued)

	Pos.1	Pos.2	Pos.3	Pos.4	Pos.5	Pos.6	Pos.7
D-33 rod				TE 408			
PCT (K)				------			
Time (s)				------			
D-51 rod				TE 409			
PCT (K)				------			
Time (s)				------			
D-53 rod				TE 410			
PCT (K)				------			
Time (s)				------			
D-66 rod				TE 411			
PCT (K)				------			
Time (s)				------			
D-77 rod				TE 412			
PCT (K)				587.4			
Time (s)				458.4			
D-86 rod				TE 413			
PCT (K)				594.1			
Time (s)				459.2			

Table 5.2 Maximum Cladding Temperature Distribution in the Core of RUN 954 (Continued)

** Order of PCT (RUN 954) **

No. 1	A-12 rod	Pos. 3	PCT = 683.5 (K)	Time = 454.4 (s)
No. 2	A-13 rod	Pos. 3	PCT = 682.3 (K)	Time = 453.6 (s)
No. 3	A-87 rod	Pos. 3	PCT = 673.3 (K)	Time = 457.6 (s)
No. 4	A-22 rod	Pos. 3	PCT = 671.5 (K)	Time = 457.6 (s)
No. 5	A-88 rod	Pos. 3	PCT = 671.4 (K)	Time = 457.6 (s)
No. 6	A-13 rod	Pos. 2	PCT = 660.7 (K)	Time = 450.4 (s)
No. 7	A-77 rod	Pos. 3	PCT = 659.0 (K)	Time = 458.4 (s)
No. 8	A-12 rod	Pos. 2	PCT = 658.3 (K)	Time = 451.2 (s)
No. 9	A-22 rod	Pos. 2	PCT = 655.9 (K)	Time = 452.8 (s)
No.10	A-87 rod	Pos. 2	PCT = 654.3 (K)	Time = 456.8 (s)

Table 5.3 Maximum cladding temperatures distribution in RUN 956

	Pos.1	Pos.2	Pos.3	Pos.4	Pos.5	Pos.6	Pos.7
A-11 rod	TE 201	TE 202	TE 203	TE 204	TE 205	TE 206	TE 207
PCT (K)	566.6	569.5	568.5	570.8	569.8	567.3	569.5
Time (s)	0.0	0.0	0.0	0.0	0.0	0.0	0.0
A-12 rod	TE 208	TE 209	TE 210	TE 211	TE 212	TE 213	TE 214
PCT (K)	565.4	566.2	567.5	568.7	568.7	567.3	565.8
Time (s)	0.0	0.0	0.0	0.0	0.0	0.0	0.0
A-13 rod	TE 215	TE 216	TE 217	TE 218	TE 219	TE 220	TE 221
PCT (K)	567.0	569.6	568.4	570.8	568.2	568.3	567.3
Time (s)	0.0	0.0	0.0	0.0	0.0	0.0	0.0
A-14 rod	TE 222	TE 223	TE 224	TE 225	TE 226	TE 227	TE 228
PCT (K)	------	------	------	------	------	------	------
Time (s)	------	------	------	------	------	------	------
A-15 rod	TE 229			TE 230			
PCT (K)	------			------			
Time (s)	------			------			
A-17 rod	TE 231			TE 232			
PCT (K)	------			569.1			
Time (s)	------			0.0			
A-22 rod	TE 233	TE 234	TE 235	TE 236	TE 237	TE 238	TE 239
PCT (K)	575.5	566.2	567.0	569.9	570.3	573.0	566.8
Time (s)	242.4	0.0	0.0	0.0	0.0	1.8	0.0
A-24 rod	TE 240	TE 241	TE 242	TE 243	TE 244	TE 245	TE 246
PCT (K)	------	------	------	------	------	------	------
Time (s)	------	------	------	------	------	------	------

Table 5.3 Maximum Cladding Temperature Distribution in the Core of RUN 956 (Continued)

	Pos.1	Pos.2	Pos.3	Pos.4	Pos.5	Pos.6	Pos.7
A-26 rod	TE 247			TE 248			
PCT (K)	------			------			
Time (s)	------			------			
A-28 rod	TE 249			TE 250			
PCT (K)	------			570.7			
Time (s)	------			0.0			
A-31 rod	TE 251			TE 252			
PCT (K)	------			569.8			
Time (s)	------			0.0			
A-33 rod	TE 253	TE 254	TE 255	TE 256	TE 257	TE 258	TE 259
PCT (K)	565.5	569.0	568.2	565.9	565.3	568.2	562.1
Time (s)	0.0	0.0	0.0	0.0	0.0	0.0	0.0
A-34 rod	TE 260	TE 261	TE 262	TE 263	TE 264	TE 265	TE 266
PCT (K)	------	------	------	------	------	------	------
Time (s)	------	------	------	------	------	------	------
A-37 rod	TE 267			TE 268			
PCT (K)	------			------			
Time (s)	------			------			
A-42 rod	TE 269			TE 270			
PCT (K)	------			------			
Time (s)	------			------			
A-44 rod	TE 271	TE 272	TE 273	TE 274	TE 275	TE 276	TE 277
PCT (K)	------	------	------	------	------	------	------
Time (s)	------	------	------	------	------	------	------

Table 5.3 Maximum Cladding Temperature Distribution in the Core of RUN 956 (Continued)

	Pos.1	Pos.2	Pos.3	Pos.4	Pos.5	Pos.6	Pos.7
A-48 rod	TE 278			TE 279			
PCT (K)	------			------			
Time (s)	------			------			
A-51 rod	TE 280			TE 281			
PCT (K)	------			------			
Time (s)	------			------			
A-53 rod	TE 282			TE 283			
PCT (K)	------			------			
Time (s)	------			------			
A-57 rod	TE 284			TE 285			
PCT (K)	------			569.1			
Time (s)	------			0.0			
A-62 rod	TE 286			TE 287			
PCT (K)	------			------			
Time (s)	------			------			
A-66 rod	TE 288			TE 289			
PCT (K)	------			------			
Time (s)	------			------			
A-68 rod	TE 290			TE 291			
PCT (K)	------			567.6			
Time (s)	------			0.0			
A-71 rod	TE 292			TE 293			
PCT (K)	------			565.6			
Time (s)	------			0.0			

Table 5.3 Maximum Cladding Temperature Distribution in the Core of RUN 956 (Continued)

	Pos.1	Pos.2	Pos.3	Pos.4	Pos.5	Pos.6	Pos.7
A-73 rod	TE 294			TE 295			
PCT (K)	------			567.1			
Time (s)	------			0.0			
A-75 rod	TE 296			TE 297			
PCT (K)	------			------			
Time (s)	------			------			
A-77 rod	TE 298	TE 299	TE 300	TE 301	TE 302	TE 303	TE 304
PCT (K)	586.4	568.5	569.7	562.8	------	567.4	------
Time (s)	244.2	0.0	0.0	0.0	------	0.0	------
A-82 rod	TE 305			TE 306			
PCT (K)	------			------			
Time (s)	------			------			
A-84 rod	TE 307			TE 308			
PCT (K)	565.1			569.4			
Time (s)	0.0			0.0			
A-85 rod	TE 309	TE 310	TE 311	TE 312	TE 313	TE 314	TE 315
PCT (K)	------	------	------	------	------	------	------
Time (s)	------	------	------	------	------	------	------
A-87 rod	TE 316	TE 317	TE 318	TE 319	TE 320	TE 321	TE 322
PCT (K)	567.3	567.2	567.0	565.3	568.1	568.4	565.3
Time (s)	0.0	0.0	0.0	0.0	0.0	0.0	0.0
A-88 rod	TE 323	TE 324	TE 325	TE 326	TE 327	TE 328	TE 329
PCT (K)	567.3	567.3	568.1	569.6	569.1	567.2	567.4
Time (s)	0.0	0.0	0.0	0.0	0.0	0.0	0.0

Table 5.3 Maximum Cladding Temperature Distribution in the Core of RUN 956 (Continued)

	Pos.1	Pos.2	Pos.3	Pos.4	Pos.5	Pos.6	Pos.7
B-11 rod	TE 330	TE 331	TE 332	TE 333	TE 334	TE 335	TE 336
PCT (K)	564.5	565.3	568.5	564.9	565.4	567.4	------
Time (s)	0.0	0.0	0.0	0.0	0.0	0.0	------
B-13 rod				TE 337			
PCT (K)				568.9			
Time (s)				0.0			
B-22 rod	TE 338	TE 339	TE 340	TE 341	TE 342	TE 343	TE 344
PCT (K)	570.1	568.5	570.5	570.3	569.1	567.3	568.1
Time (s)	245.4	0.0	0.0	0.0	0.0	0.0	0.0
B-31 rod				TE 345			
PCT (K)				------			
Time (s)				------			
B-33 rod				TE 346			
PCT (K)				------			
Time (s)				------			
B-51 rod				TE 347			
PCT (K)				------			
Time (s)				------			
B-53 rod				TE 348			
PCT (K)				------			
Time (s)				------			
B-66 rod				TE 349			
PCT (K)				------			
Time (s)				------			

Table 5.3 Maximum Cladding Temperature Distribution in the Core of RUN 956 (Continued)

	Pos.1	Pos.2	Pos.3	Pos.4	Pos.5	Pos.6	Pos.7
B-77 rod	TE 350	TE 351	TE 352	TE 353	TE 354	TE 355	TE 356
PCT (K)	566.6	572.3	573.1	568.3	567.8	569.0	566.4
Time (s)	0.0	0.0	0.0	0.0	0.0	0.0	0.0
B-86 rod				TE 357			
PCT (K)				------			
Time (s)				------			
C-11 rod	TE 358	TE 359	TE 360	TE 361	TE 362	TE 363	TE 364
PCT (K)	570.1	566.5	565.6	566.5	564.2	569.3	560.9
Time (s)	0.0	0.0	0.0	0.0	0.0	0.0	0.0
C-13 rod	TE 365	TE 366	TE 367	TE 368	TE 369	TE 370	TE 371
PCT (K)	562.2	566.3	565.3	567.1	568.5	567.3	565.3
Time (s)	0.0	0.0	0.0	0.0	0.0	0.0	0.0
C-15 rod				TE 372			
PCT (K)				------			
Time (s)				------			
C-22 rod	TE 373	TE 374	TE 375	TE 376	TE 377	TE 378	TE 379
PCT (K)	565.3	568.1	570.2	570.9	569.2	570.0	564.7
Time (s)	0.0	0.0	0.0	0.0	0.0	0.0	0.0
C-31 rod				TE 380			
PCT (K)				------			
Time (s)				------			
C-33 rod	TE 381	TE 382	TE 383	TE 384	TE 385	TE 386	TE 387
PCT (K)	566.1	567.4	567.5	568.2	568.5	566.4	562.7
Time (s)	0.0	0.0	0.0	0.0	0.0	0.0	0.0

Table 5.3 Maximum Cladding Temperature Distribution in the Core of RUN 956 (Continued)

	Pos.1	Pos.2	Pos.3	Pos.4	Pos.5	Pos.6	Pos.7
C-35 rod				TE 388			
PCT (K)				------			
Time (s)				------			
C-66 rod				TE 389			
PCT (K)				------			
Time (s)				------			
C-68 rod				TE 390			
PCT (K)				------			
Time (s)				------			
C-77 rod	TE 391	TE 392	TE 393	TE 394	TE 395	TE 396	TE 397
PCT (K)	565.5	567.8	567.4	567.7	568.3	566.5	564.7
Time (s)	0.0	0.0	0.0	0.0	0.0	0.0	0.0
D-11 rod				TE 398			
PCT (K)				567.4			
Time (s)				0.0			
D-13 rod				TE 399			
PCT (K)				568.9			
Time (s)				0.0			
D-22 rod	TE 400	TE 401	TE 402	TE 403	TE 404	TE 405	TE 406
PCT (K)	573.9	567.7	567.6	568.9	567.6	567.4	565.0
Time (s)	244.2	0.0	0.0	0.0	0.0	0.0	0.0
D-31 rod				TE 407			
PCT (K)				------			
Time (s)				------			

Table 5.3 Maximum Cladding Temperature Distribution in the Core of RUN 956 (Continued)

	Pos.1	Pos.2	Pos.3	Pos.4	Pos.5	Pos.6	Pos.7
D-33 rod				TE 408			
PCT (K)				------			
Time (s)				------			
D-51 rod				TE 409			
PCT (K)				------			
Time (s)				------			
D-53 rod				TE 410			
PCT (K)				------			
Time (s)				------			
D-66 rod				TE 411			
PCT (K)				------			
Time (s)				------			
D-77 rod				TE 412			
PCT (K)				568.3			
Time (s)				0.0			
D-86 rod				TE 413			
PCT (K)				568.3			
Time (s)				0.0			

Table 5.3 Maximum Cladding Temperature Distribution in the Core of RUN 956 (Continued)

** Order of PCT (RUN 956) **

No. 1	A-77 rod	Pos. 1	PCT =	586.4 (K)	Time =	244.2 (s)
No. 2	A-22 rod	Pos. 1	PCT =	575.5 (K)	Time =	242.4 (s)
No. 3	D-22 rod	Pos. 1	PCT =	573.9 (K)	Time =	244.2 (s)
No. 4	B-77 rod	Pos. 3	PCT =	573.1 (K)	Time =	0.0 (s)
No. 5	A-22 rod	Pos. 6	PCT =	573.0 (K)	Time =	1.8 (s)
No. 6	B-77 rod	Pos. 2	PCT =	572.3 (K)	Time =	0.0 (s)
No. 7	C-22 rod	Pos. 4	PCT =	570.9 (K)	Time =	0.0 (s)
No. 8	A-11 rod	Pos. 4	PCT =	570.8 (K)	Time =	0.0 (s)
No. 9	A-13 rod	Pos. 4	PCT =	570.8 (K)	Time =	0.0 (s)
No.10	A-28 rod	Pos. 4	PCT =	570.7 (K)	Time =	0.0 (s)

Table 6.1 Steam discharge flow areas in steam line break tests

RUN No.	Break Area (%)	Before Break	Steam Discharge Flow Area (%)			
			Immediately after Break	After MSIV Closure	Plant SV Opening	After ADS Opening
954	10.0	29.3	10.0	10.0	49.7	35.0
956	10.0	"	(32.9)	10.0	-	35.0
951	33.7	"	33.7	33.7	-	-
953	100.0	"	100.0	100.0	-	-

Table 6.2 Test conditions of steam line break tests

Items	Unit	RUN954	RUN956	RUN951	RUN953
Break Area	%	10.0	10.0	33.7	100.0
(Rec. Line Reference)	"	(14.0)	(14.0)	(47.2)	(140.0)
Initial Pressure	MPa	7.35	7.35	7.35	7.35
Initial Core Power	MW	3.975	3.972	3.965	3.977
LP Subcooling	K	10.6	10.6	10.0	10.7
Initial Core Flow	kg/s	16.7	16.8	16.4	16.6
Initial Steam Flow	"	2.06	2.05	2.03	2.08
ECCS Mode	-	HP-Fail.	HP-Fail.	HP-Fail.	HP-Fail.
ADS Actuation		ON	ON	-	-
MSIV Trip		at Break	L2 + 3s	at Break	at Break
Safety Valve Actuation		ON	-	-	-

Table 6.3 Major events of steam line break tests

Events	RUN954	RUN956	RUN951	RUN953
Break Initiation (MRPs Coastdown)	0.0s	0.0s	0.0s	0.0s
Feedwater Stops	2.0∿4.0	2.0∿4.0	2.0∿4.0	2.0∿4.0
Power Decay	9.0	9.0	9.0	9.0
SV Actuation	5.4∿16.9	-	-	-
L.P. Flashing	81.	27.7	19.2	6.2
DC Level (L2)	33.	126.	142.	74.
" (L1)	403.	350.	335.	241.
MSIV Closure	0.0	129.	0.0	0.0
ADS Actuation	153.	244.	-	-
LPCS "	443.	390.	375.	281.
LPCI "	455.	432.	415.	281.
Top of Core Uncovering	300.	334.	131.	27.
Final Core Quenching	467.	408.	445.	438.

Table 6.4 Maximum void fraction in the lower downcomer related with the total steam discharge flow area

Run No.	Phase after Break	Steam Flow Area		Void Fraction
		Ratio (%)	A (m^2)	α (%)
954	before ADS opening	10.0	7.54×10^{-5}	(17.)
	after ADS opening	35.0	2.64×10^{-4}	34.
956	before MSIV trip	(32.9)	2.49× "	(33.)
	MSIV - ADS	10.0	7.54×10^{-5}	17.
	after ADS opening	35.0	2.64×10^{-4}	36.
951		33.7	2.54× "	35.
953		100.0	7.55× "	56.

Ref. Initial steam line flow area was limitted as $2.21\times10^{-4}m^2$ (29.3%) at CV-130 to maintain the constant pressure.

Table 6.5 Pressure balance in PV in RUN951

T(s)	D5 (kPa)	-D1 (kPa)	D2 (kPa)	-D3 (kPa)	D4 (kPa)	$\sum_{1}^{4} D_i$ (kPa)	D5- $\sum_{1}^{4} D_i$ (kPa)
0	90	8	84	-23	15	84	6
10	36	15	-1	-1	17	30	6
50	25	7	-3	1	14	19	6
100	23	7	-3	1	13	18	5
200	18	5	-3	1	11	14	4
300	16	4	-3	1	10	12	4
400	15	5	-3	1	9	12	3
500	46	10	9	8	14	41	5
590	58	13	8	5	25	51	7

Measurement location of each differential pressure is shown in Fig. 6.21.

Table 6.6 Pressure balance in PV in RUN956

T(s)	D5 (kPa)	-D1 (kPa)	D2 (kPa)	-D3 (kPa)	D4 (kPa)	$\sum_{1}^{4} D_i$ (kPa)	D5- $\sum_{1}^{4} D_i$ (kPa)
0	92	9	87	-23	16	89	3
10	36	16	1	-2	18	33	3
50	27	10	-1	0	15	24	3
100	24	9	-2	0	14	21	3
150	22	7	-2	0	14	19	3
200	22	8	-1	0	13	20	2
250	24	11	-1	0	11	21	3
300	21	10	-1	0	10	19	2
350	20	9	-1	0	10	18	2
400	19	6	-1	1	10	16	3
500	38	9	10	6	12	37	1

Table 6.7 Pressure balance in PV in RUN953

T(s)	D5 (kPa)	-D1 (kPa)	D2 (kPa)	-D3 (kPa)	D4 (kPa)	$\sum_{1}^{4} D_i$ (kPa)	D5- $\sum_{1}^{4} D_i$ (kPa)
0	93	9	86	-23	16	88	5
10	45	12	8	3	18	41	4
20	29	8	0	0	16	24	5
50	23	6	-1	0	13	18	5
100	16	2	-1	1	11	13	3
150	14	2	-1	0	10	11	3
200	12	1	-1	0	9	9	3
250	11	1	-1	0	8	8	3
300	14	3	1	2	7	13	1
350	33	6	10	4	9	29	4
400	43	9	11	6	15	41	2
500	58	16	6	3	29	54	4

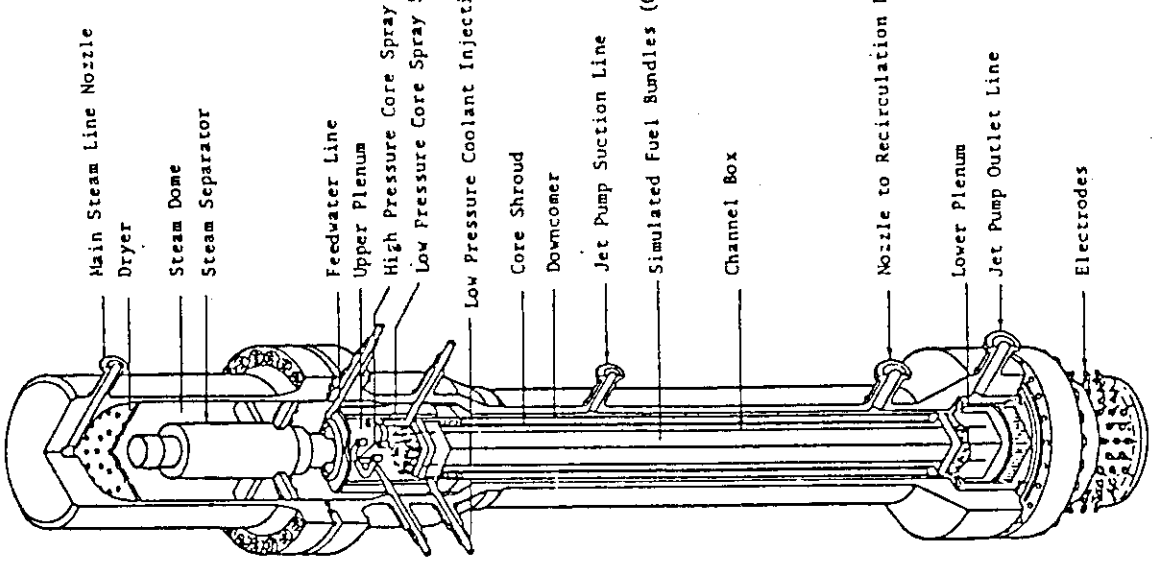

Fig. 2.2 Internal structure of pressure vessel of ROSA-III

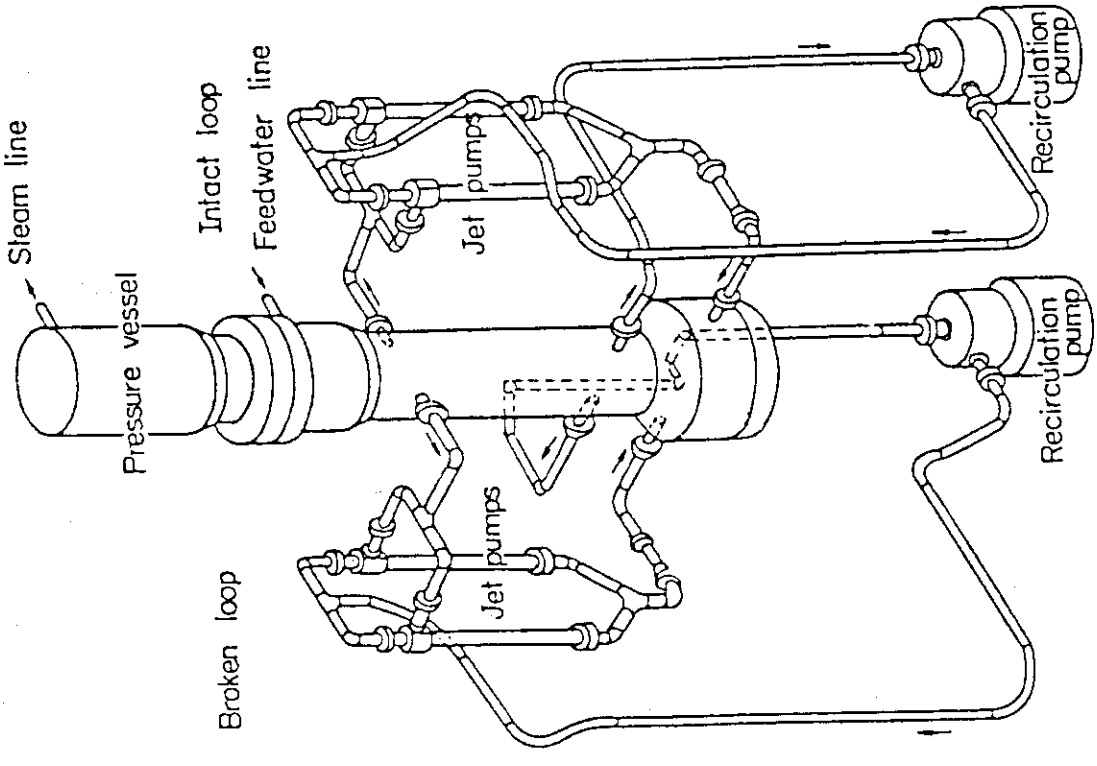

Fig. 2.1 Schematic diagram of ROSA-III test facility for RUNs 954 and 956

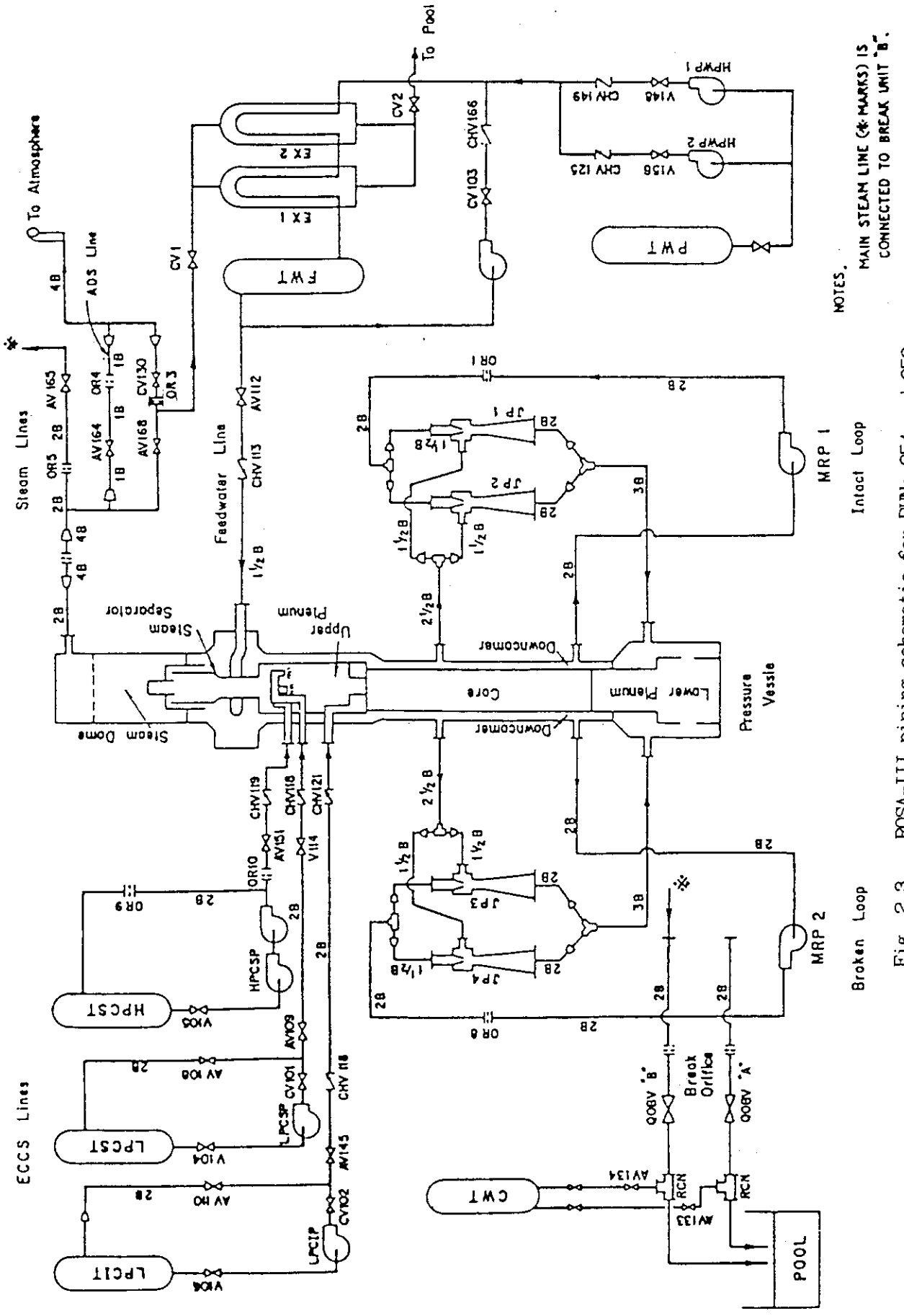

Fig. 2.3 ROSA-III piping schematic for RUNs 954 and 956

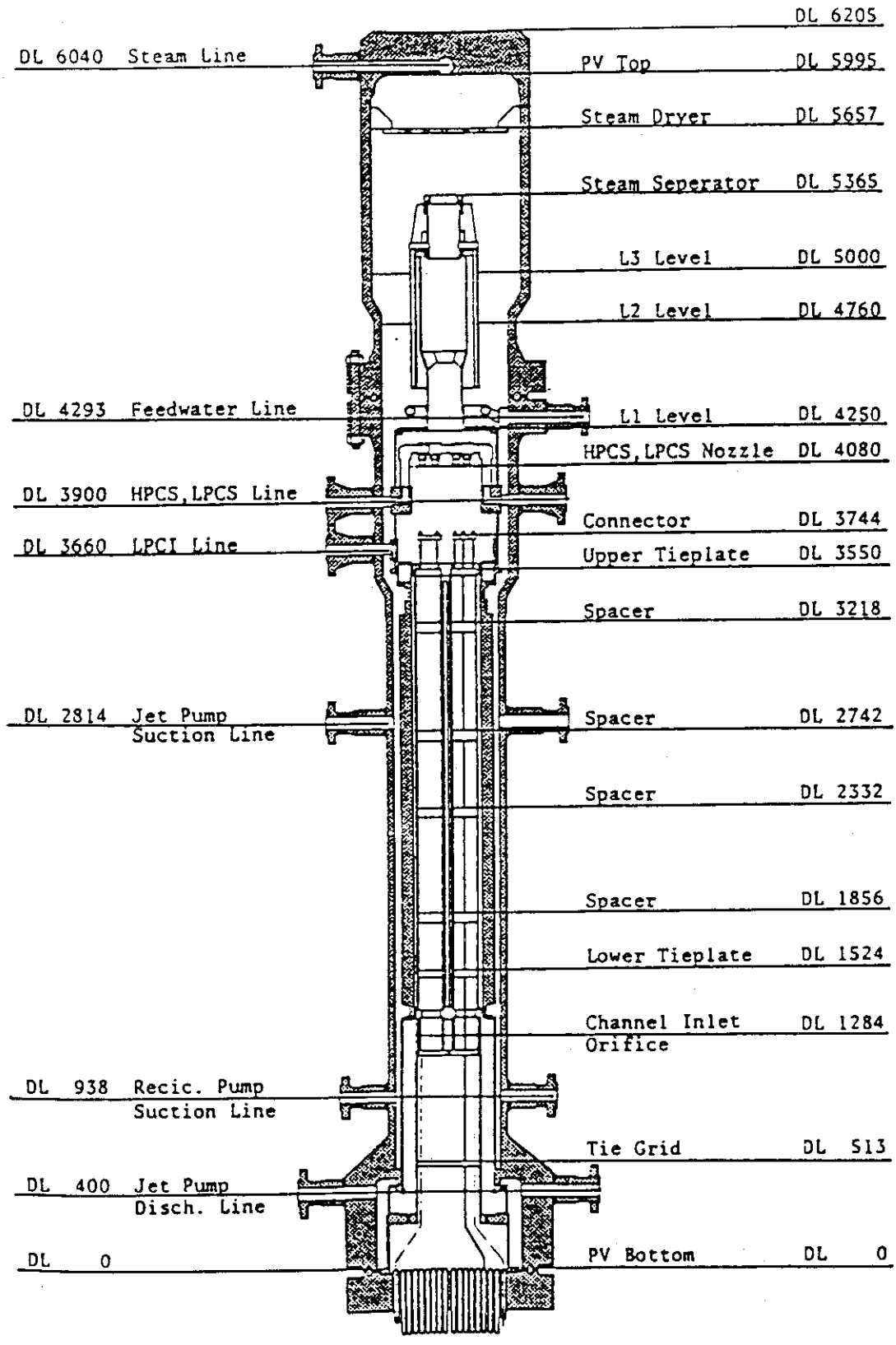

Fig. 2.4 Pressure vessel internals arrangement

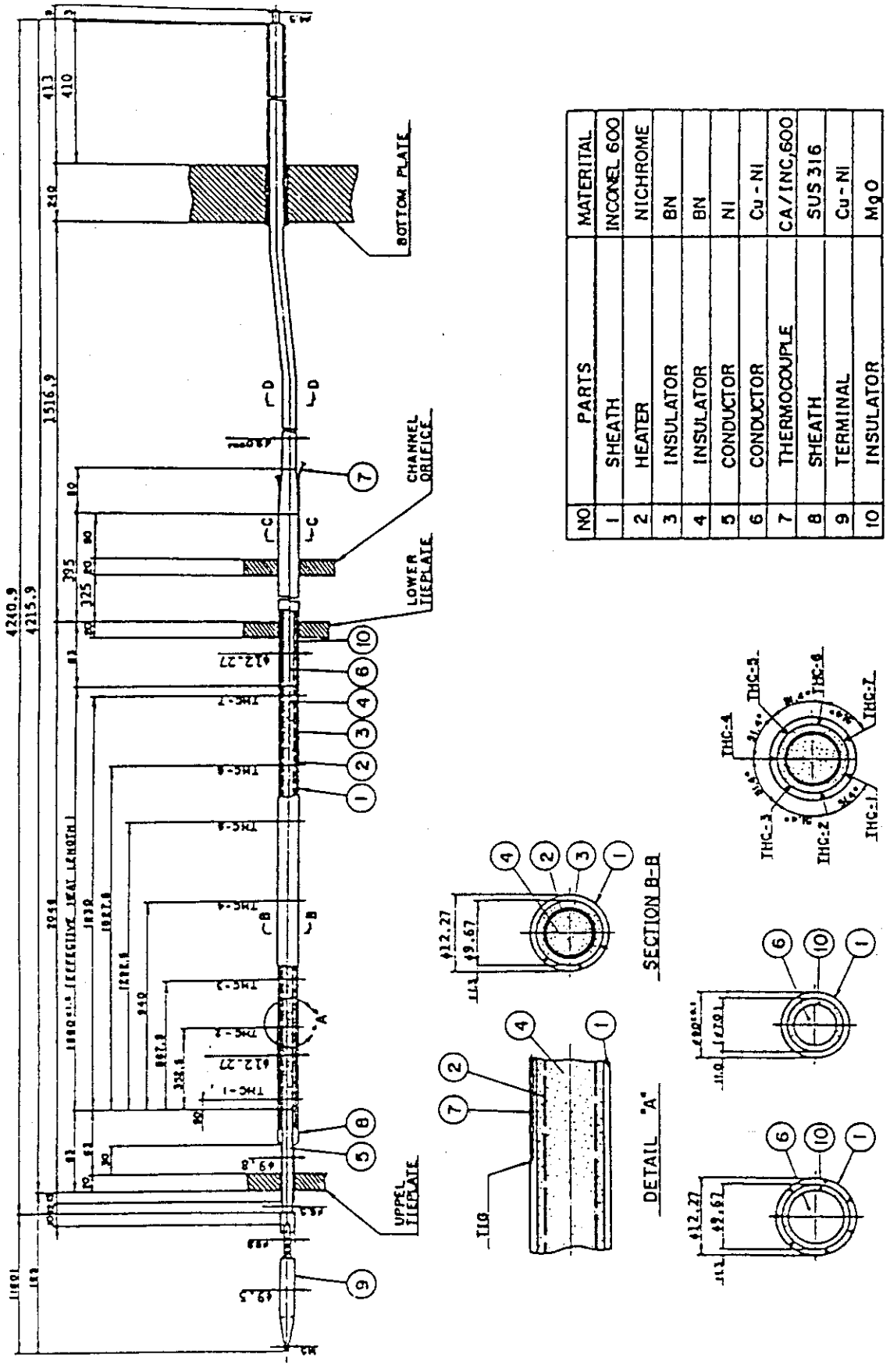

NO	PARTS	MATERITAL
1	SHEATH	INCONEL 600
2	HEATER	NICHROME
3	INSULATOR	BN
4	INSULATOR	BN
5	CONDUCTOR	NI
6	CONDUCTOR	Cu - NI
7	THERMOCOUPLE	CA/INC,600
8	SHEATH	SUS 316
9	TERMINAL	Cu - NI
10	INSULATOR	MgO

Fig. 2.5 Simulated fuel rod of ROSA-III

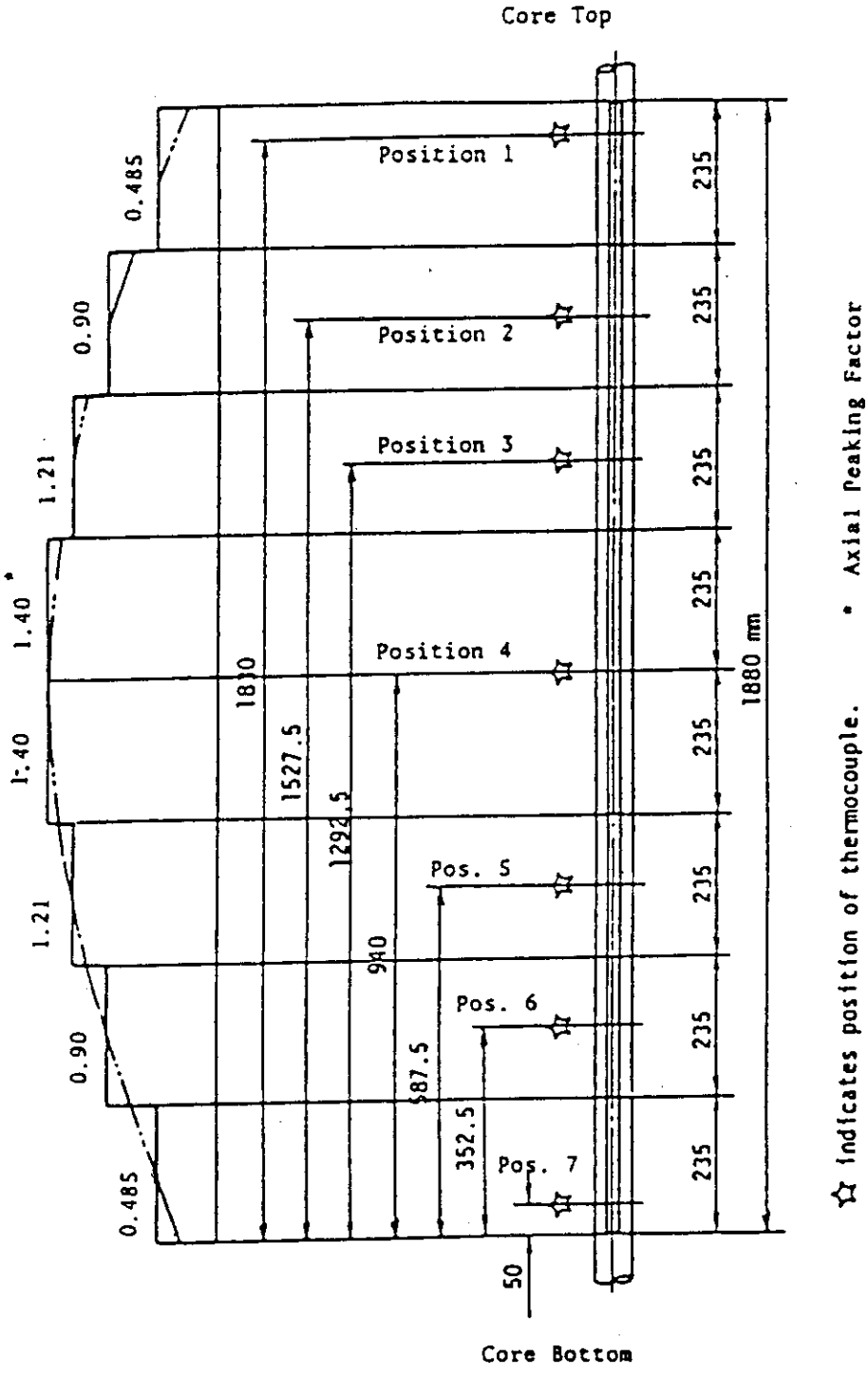

Fig. 2.6 Axial power distribution of heater rod

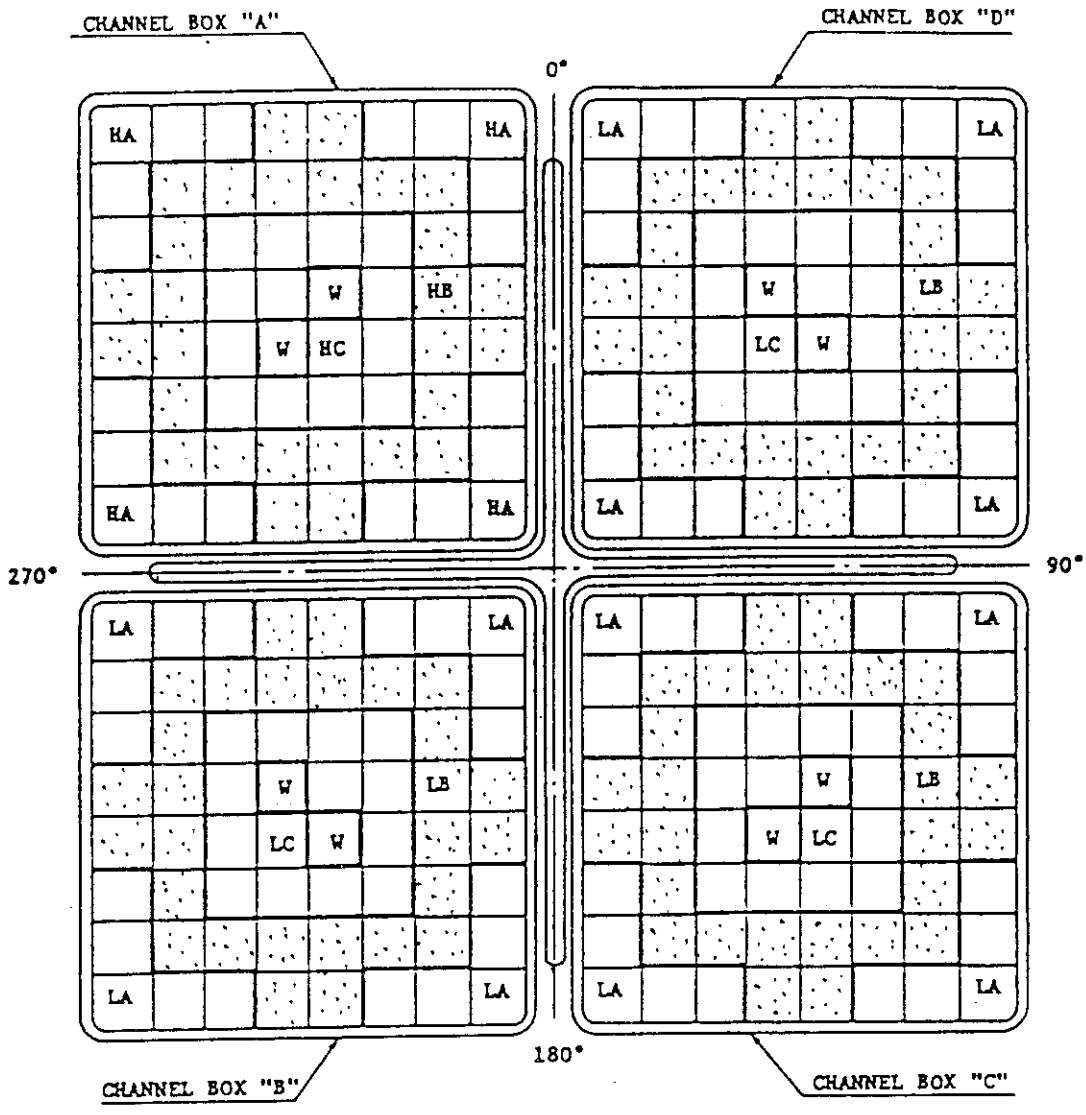

Region	HA	HB	HC	LA	LB	LC	W
Lenear Heat Rate (kW/m)	18.5	16.81	14.41	13.21	12.01	10.29	0.0
Local peaking factor	1.1	1.0	0.875	1.1	1.0	0.875	0.0
No. of Rods	20	28	14	60	84	42	8

* note : Radial peaking factor is 1.4

Fig. 2.7 Radial power distribution of core

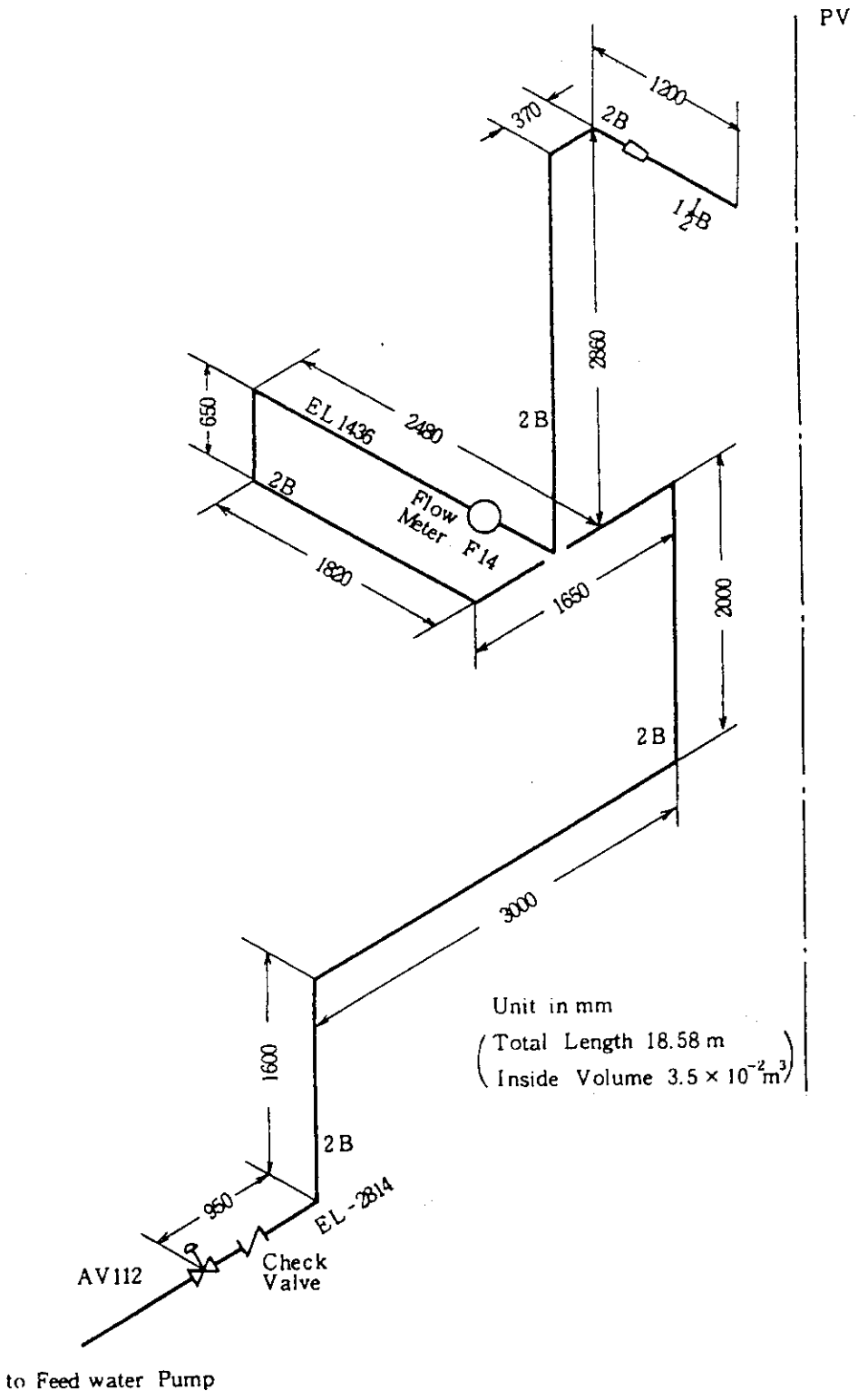

Fig. 2.8 Feedwater line between PV and AV-112

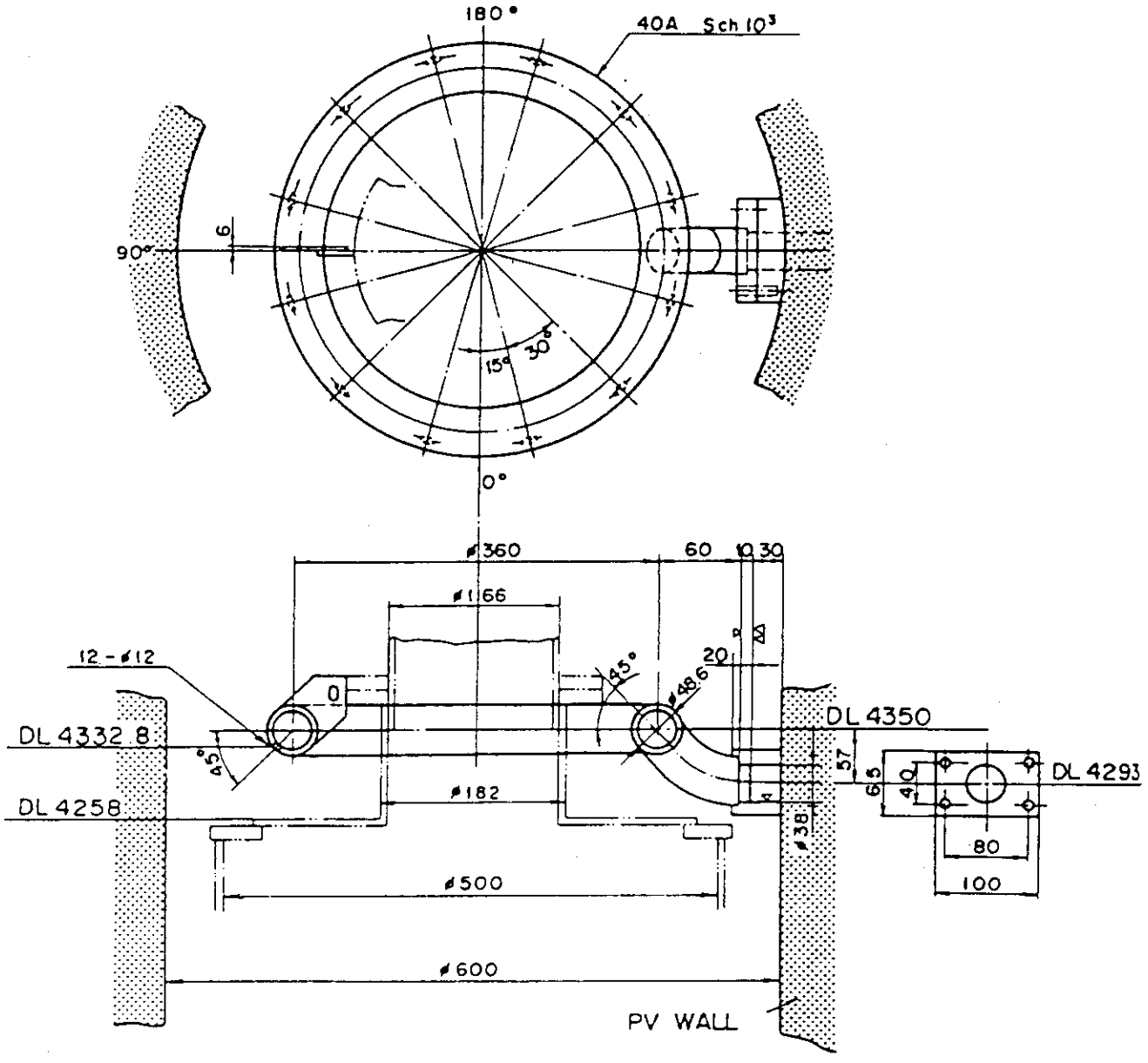

Fig. 2.9 Feedwater sparger configuration

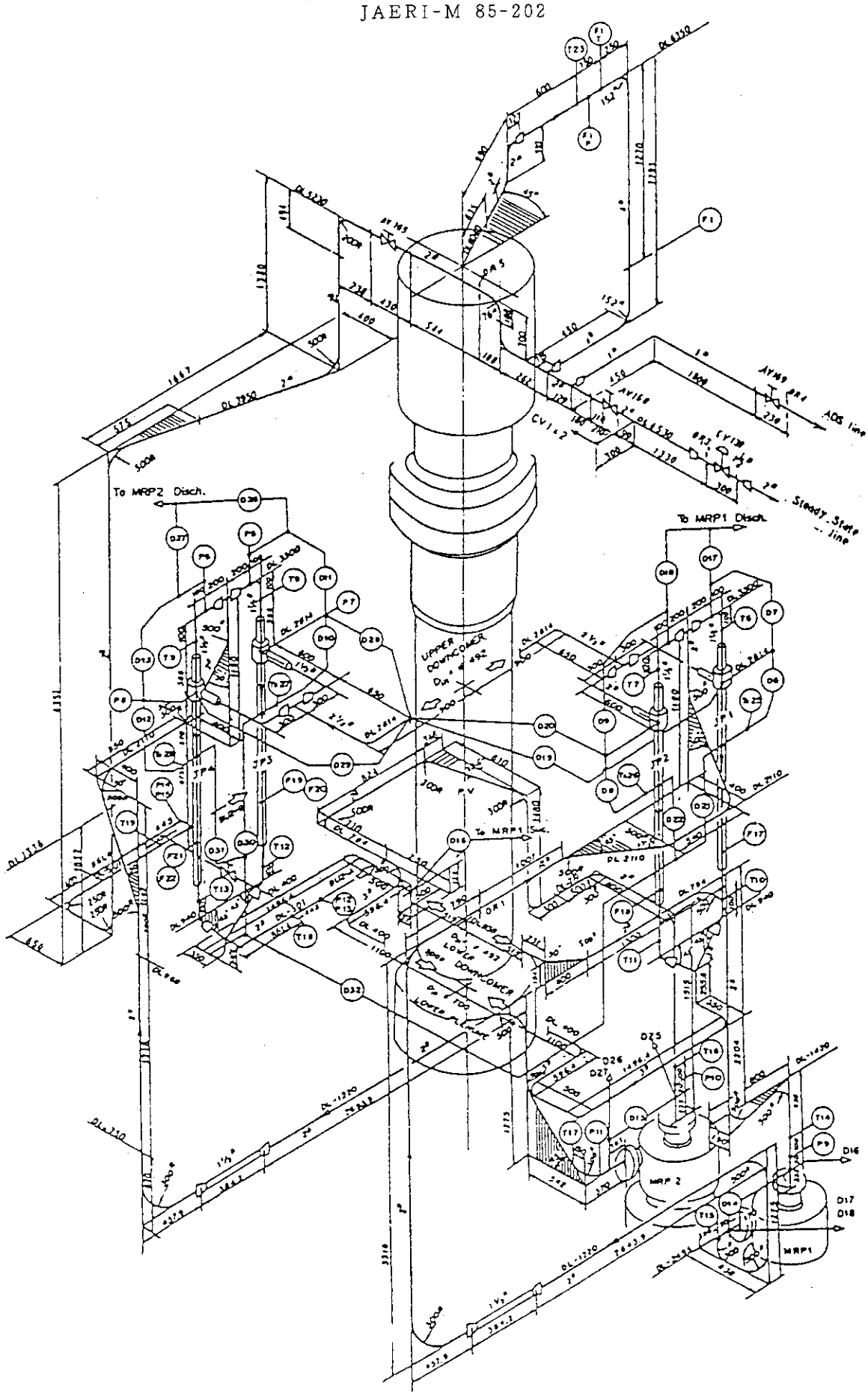

Fig. 2.10 Details of ROSA-III system piping for RUNs 954 and 956

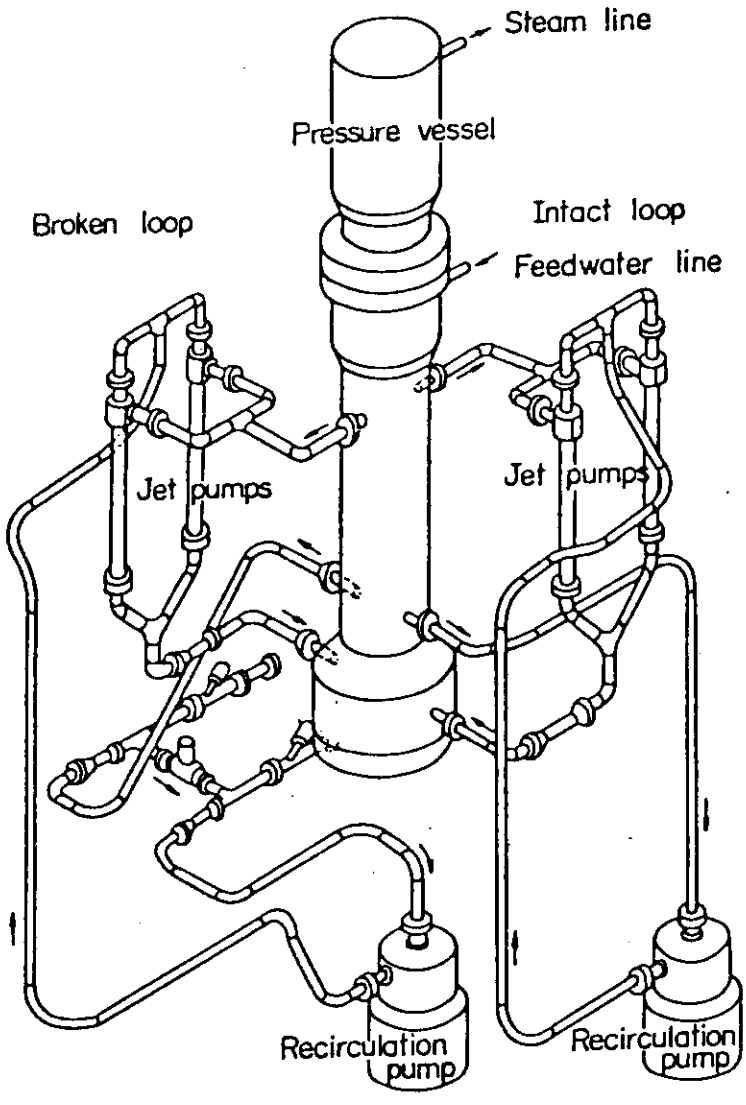

Fig. 2.11 Schematic diagram of ROSA-III facility for RUN 951

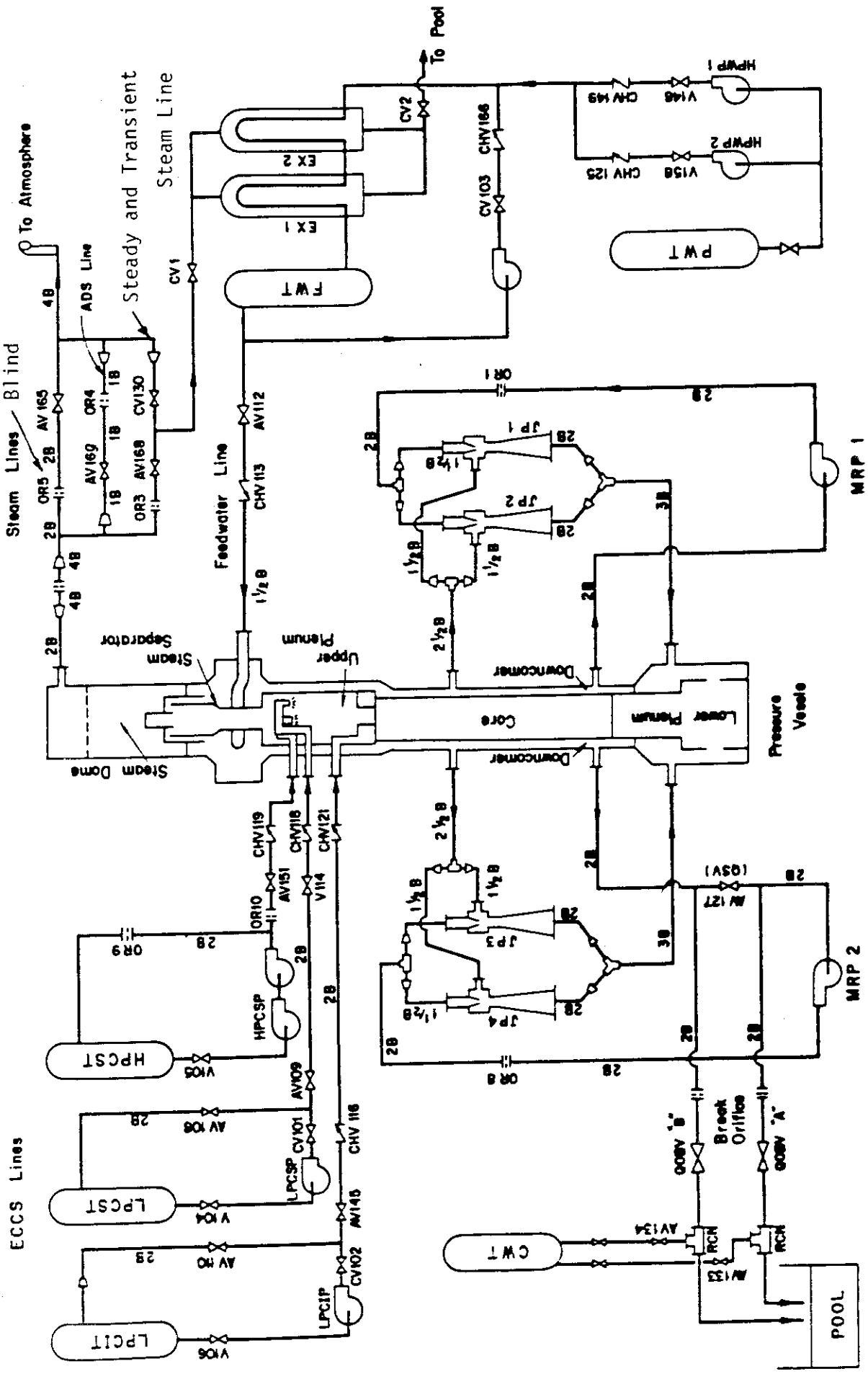

Fig. 2.12 ROSA-III piping schematic for RUN 951

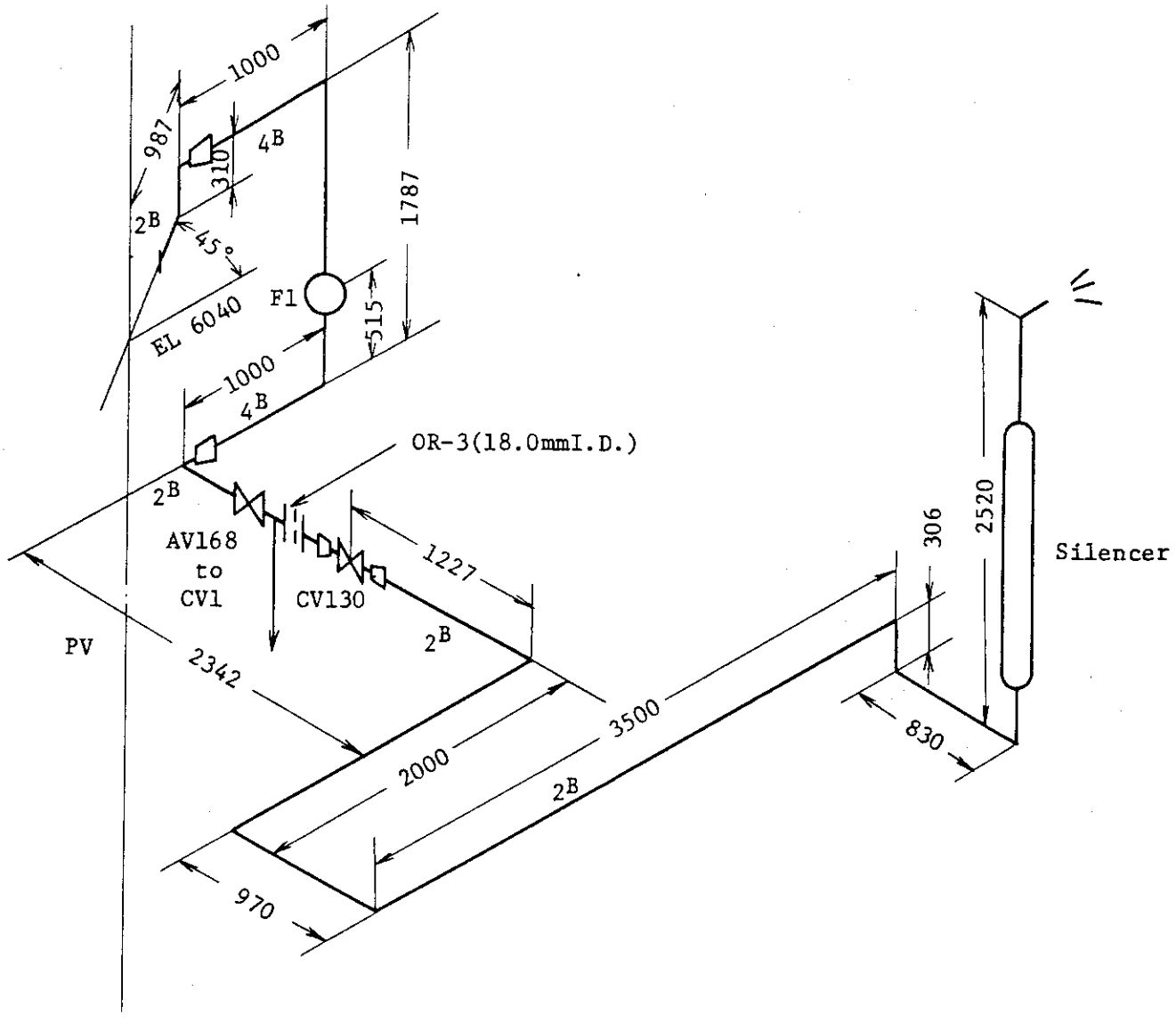

Fig. 2.13 Steam discharge flow path for RUN 951

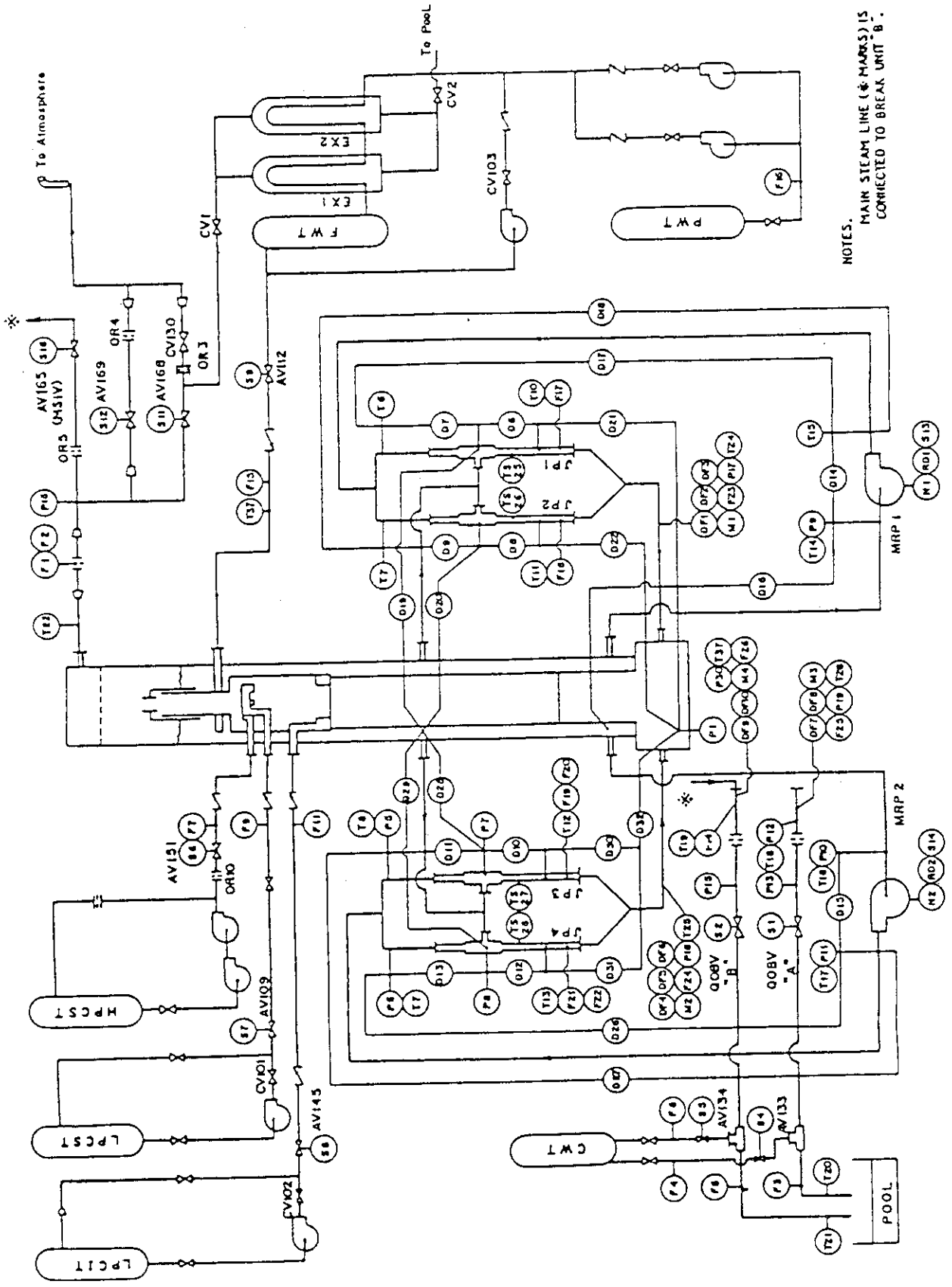

Fig. 3.1 Instrumentation location of ROSA-III test facility

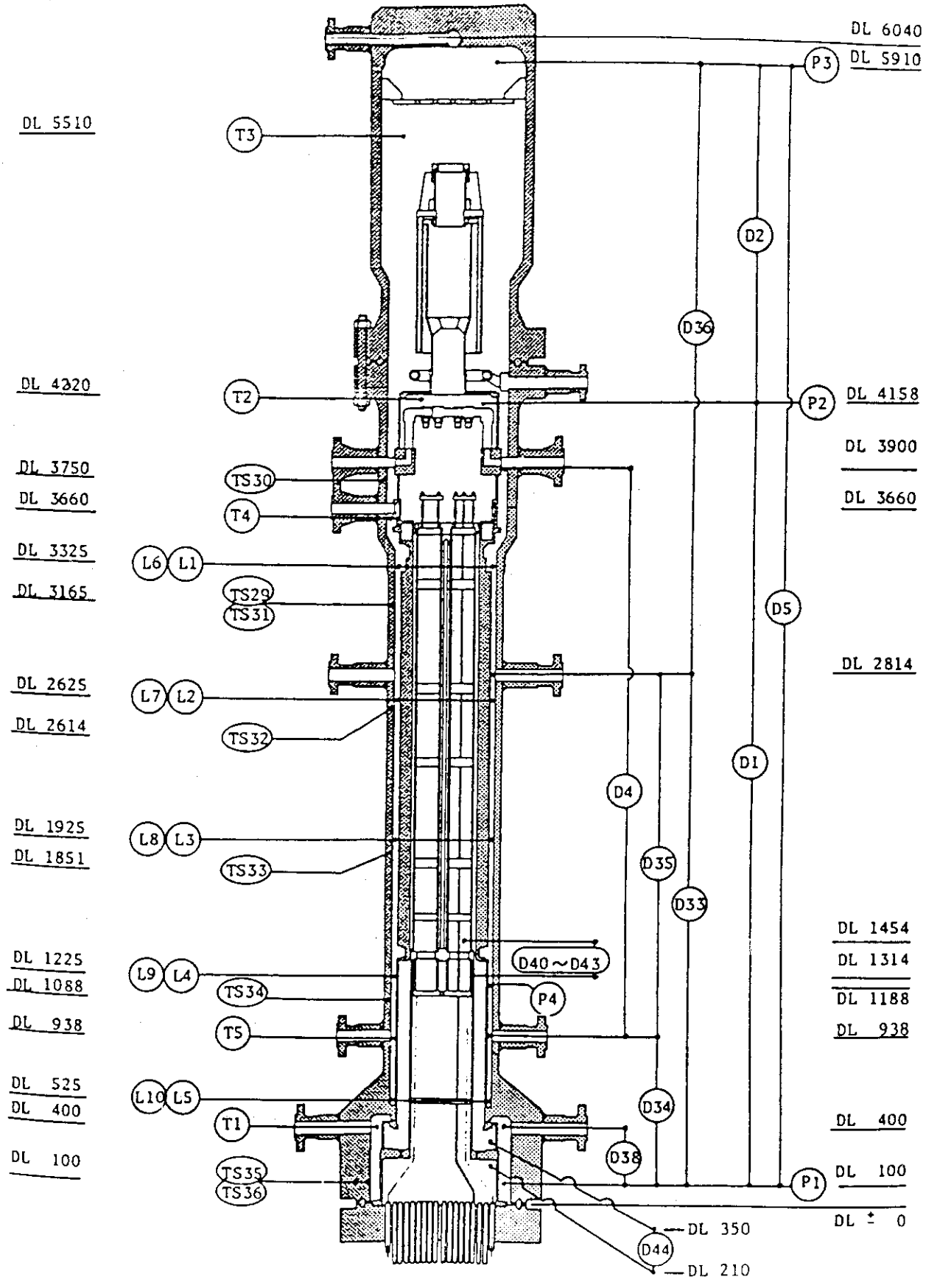

Fig. 3.2 Instrumentation location in pressure vessel

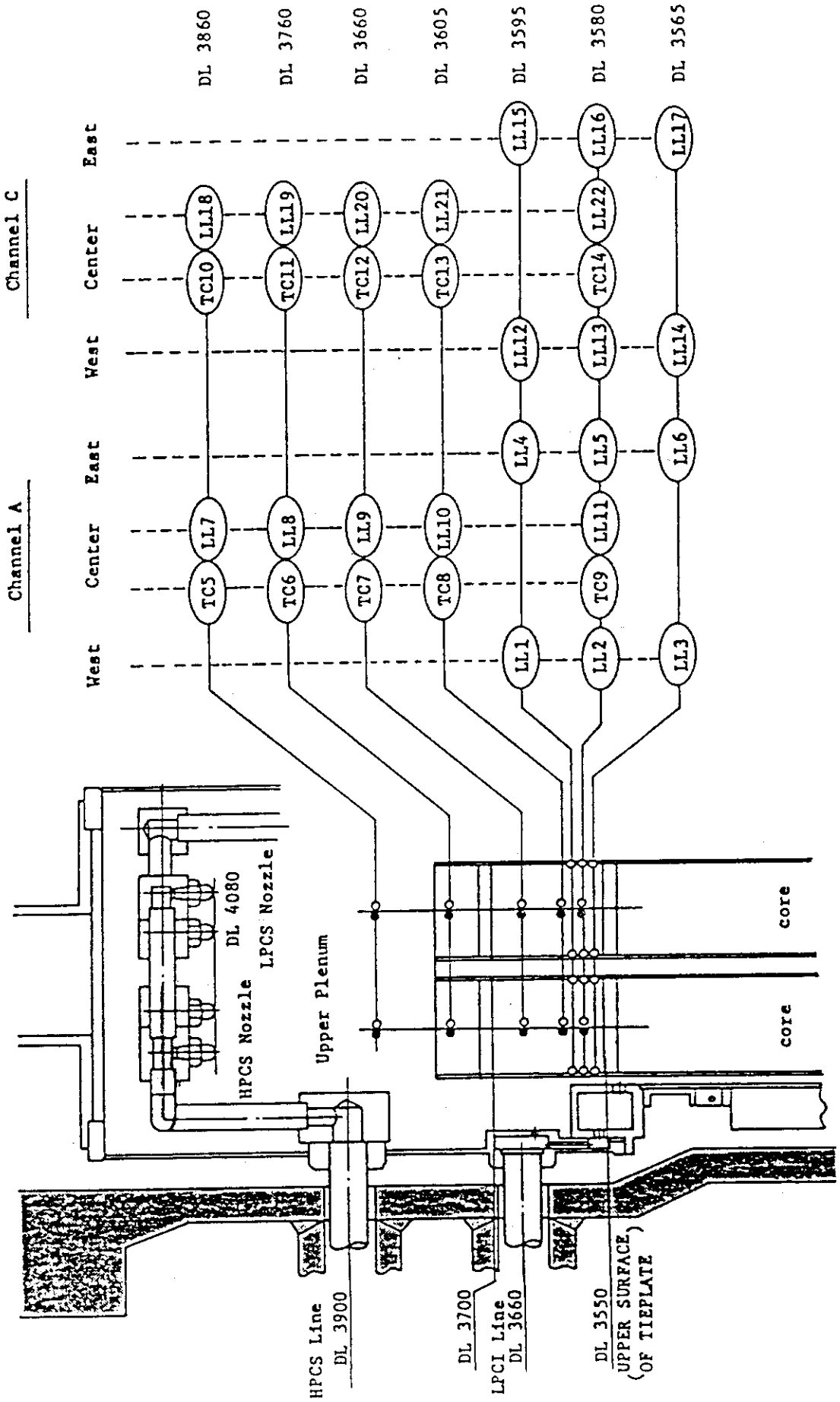

Fig. 3.3 Upper plenum instrumentation

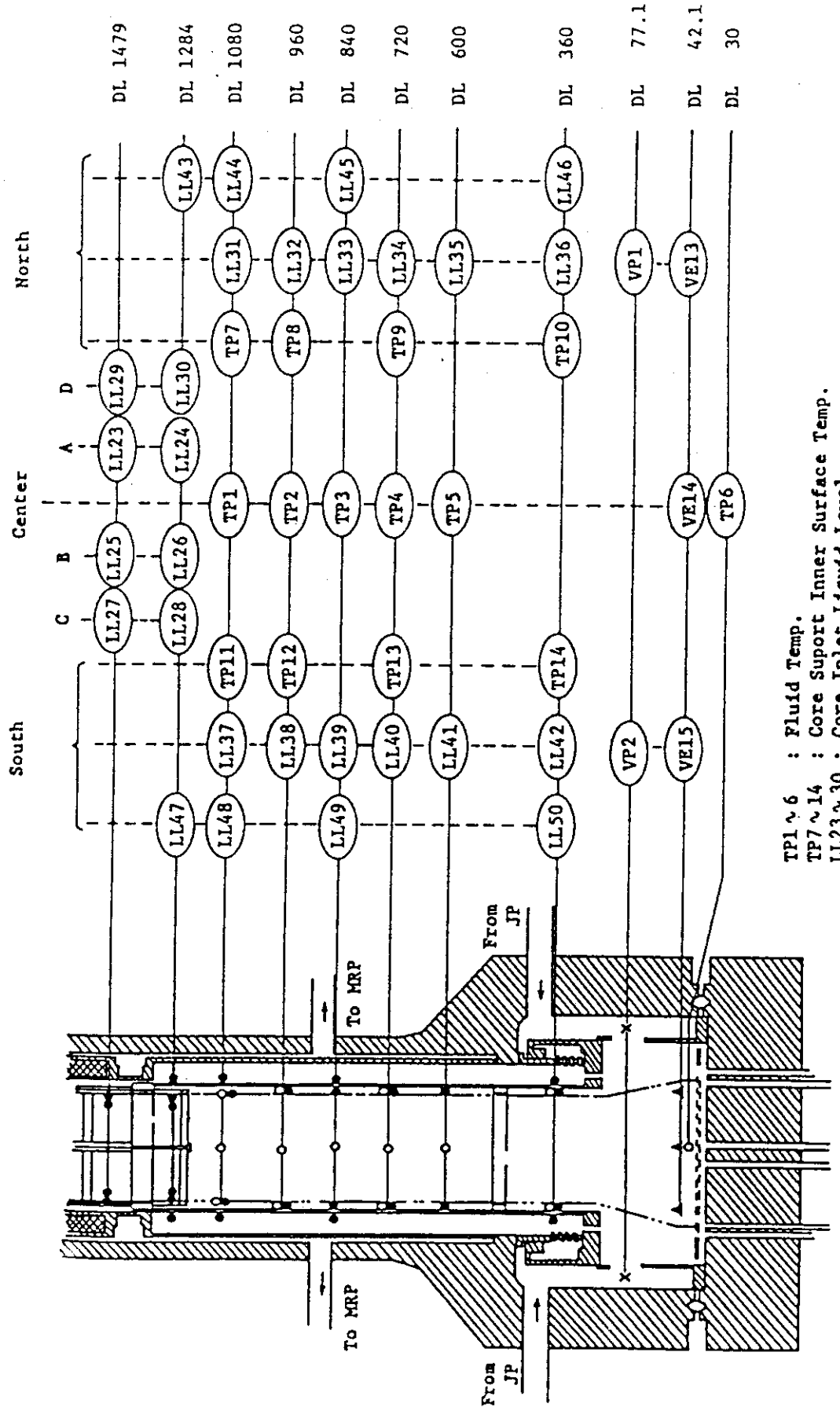

Fig. 3.4 Lower plenum instrumentation

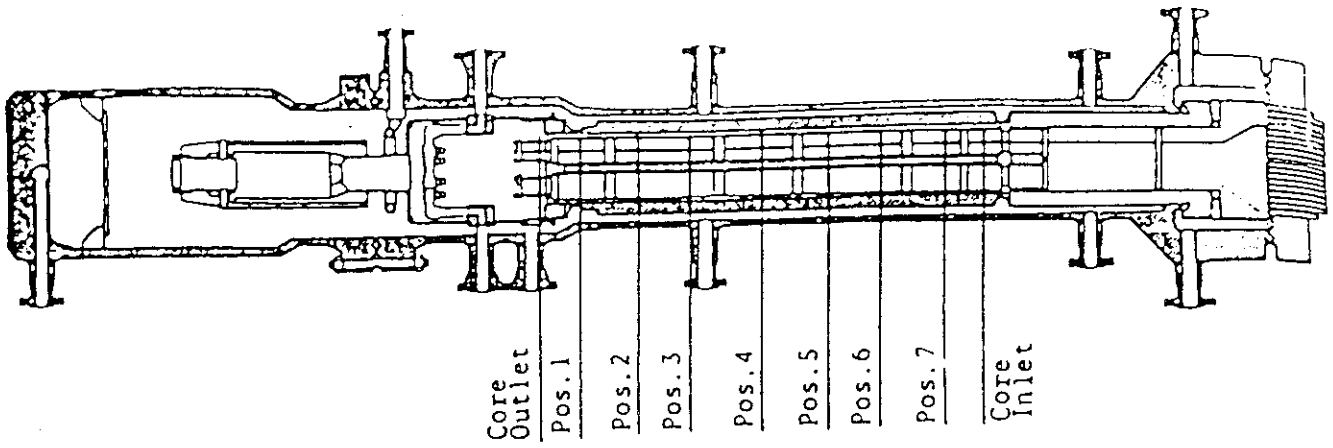

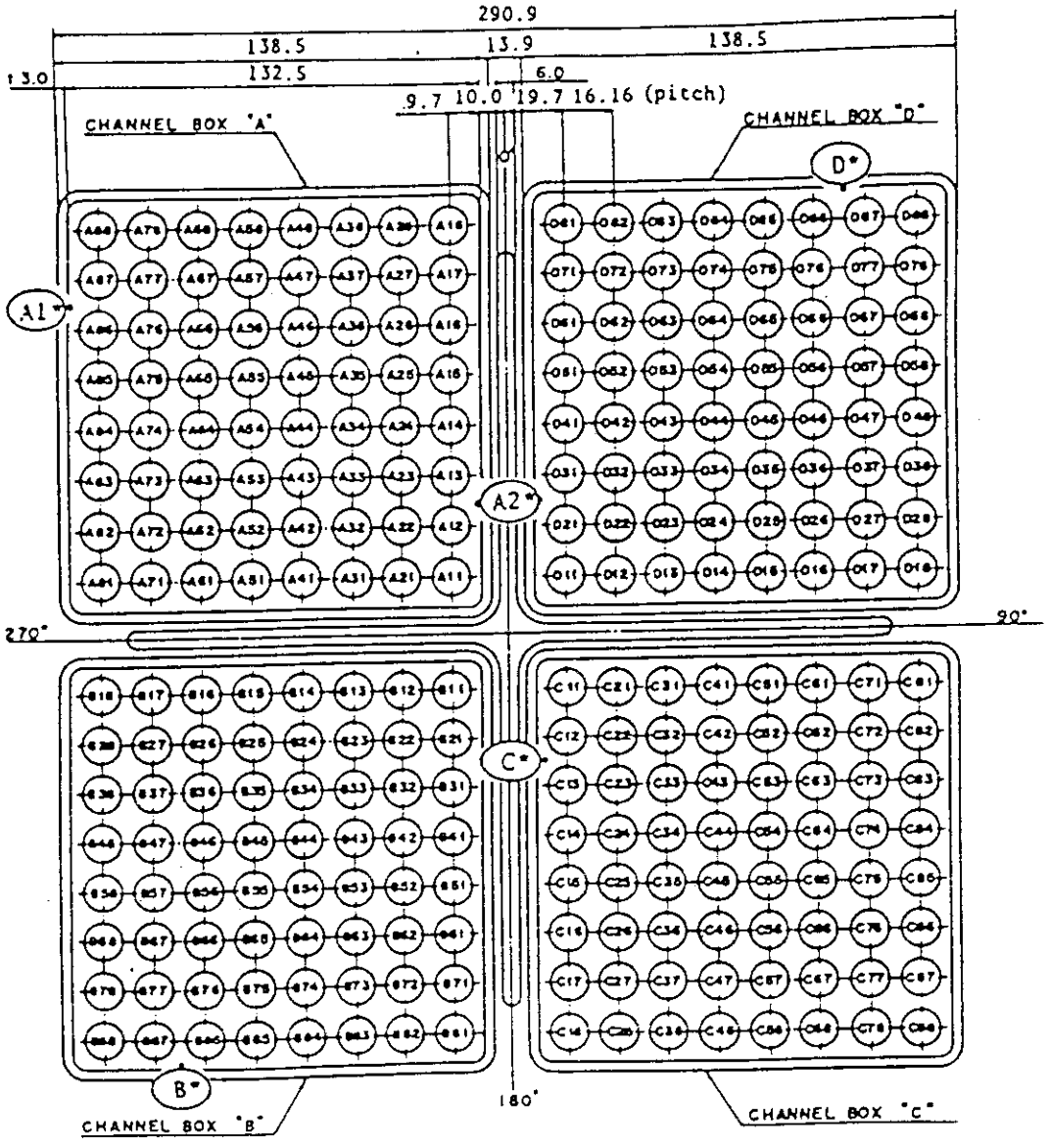

Heater rod O.D. is 12.27mm

A54,B54,C54 and D54 are water rod simulators with void probes, O.D.= 15.01mm

A45,B45,C45 and D45 are water rod simulators with thermocouples, O.D.= 15.01mm

Fig. 3.5 Core instrumentation (cf. Table 3.3)

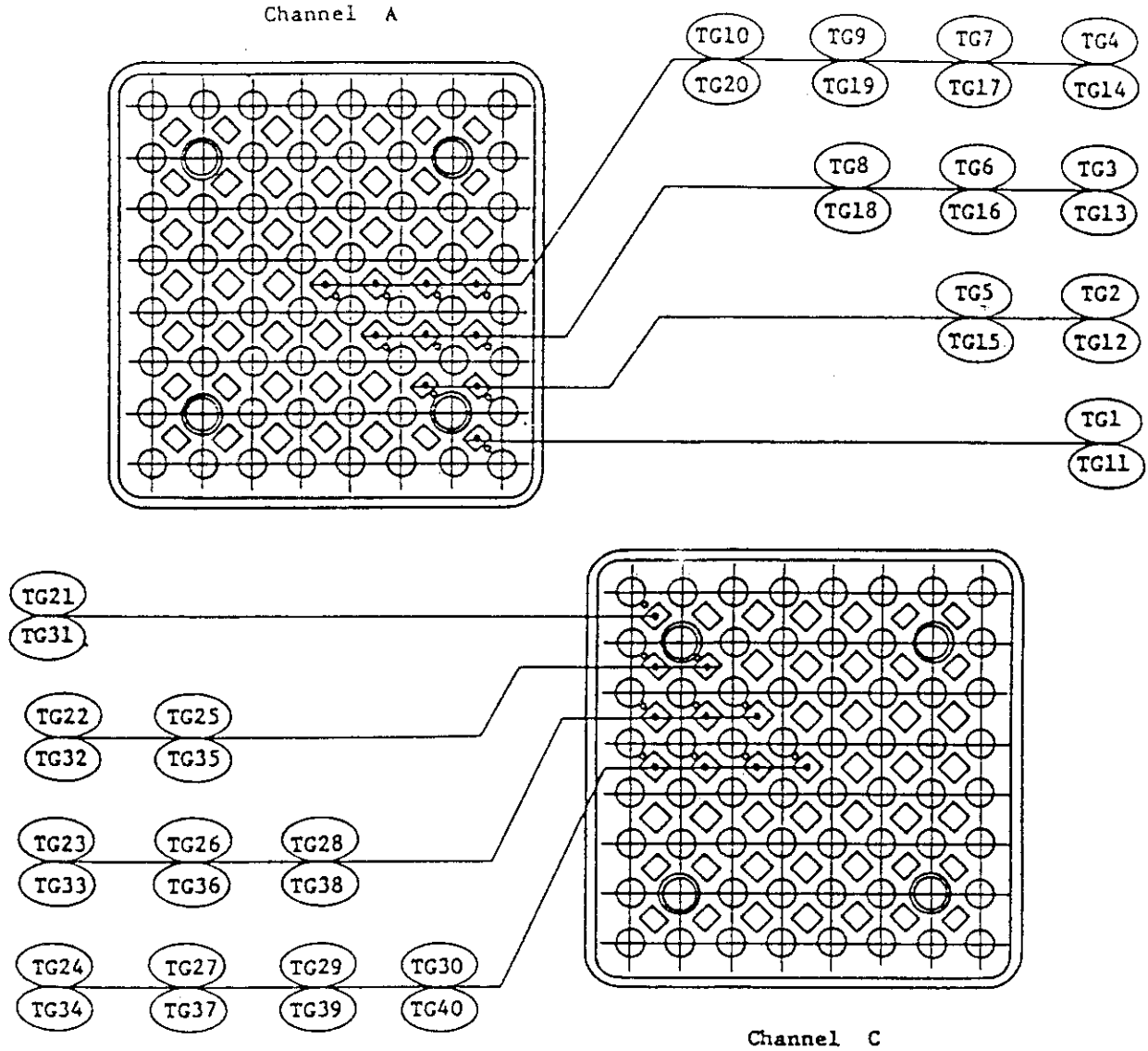

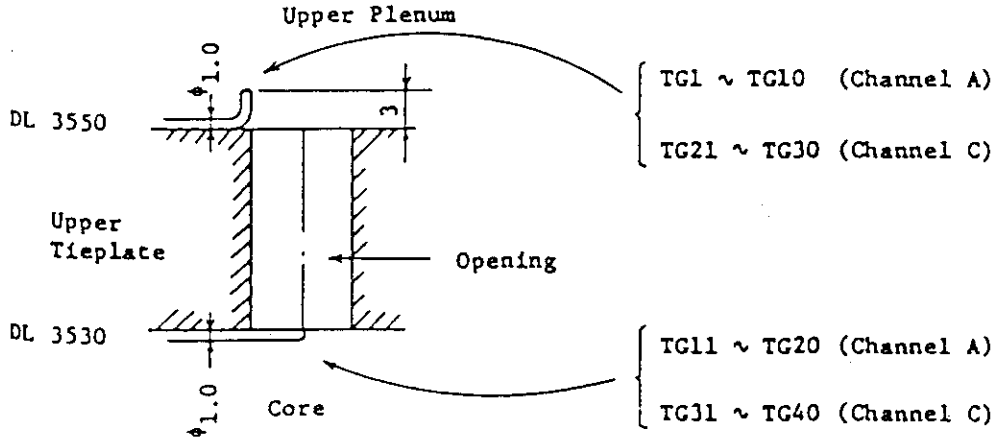

Fig. 3.6 Upper tieplate instrumentations

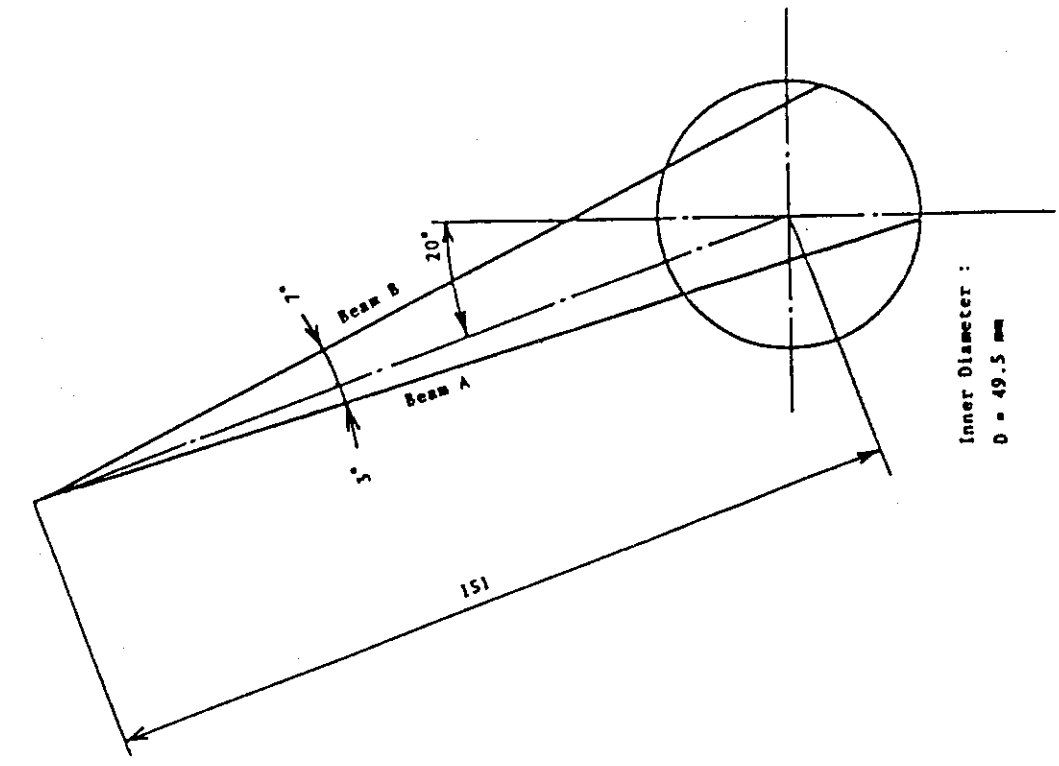

Fig. 3.8 Beam directions of two-beam gamma densitometer

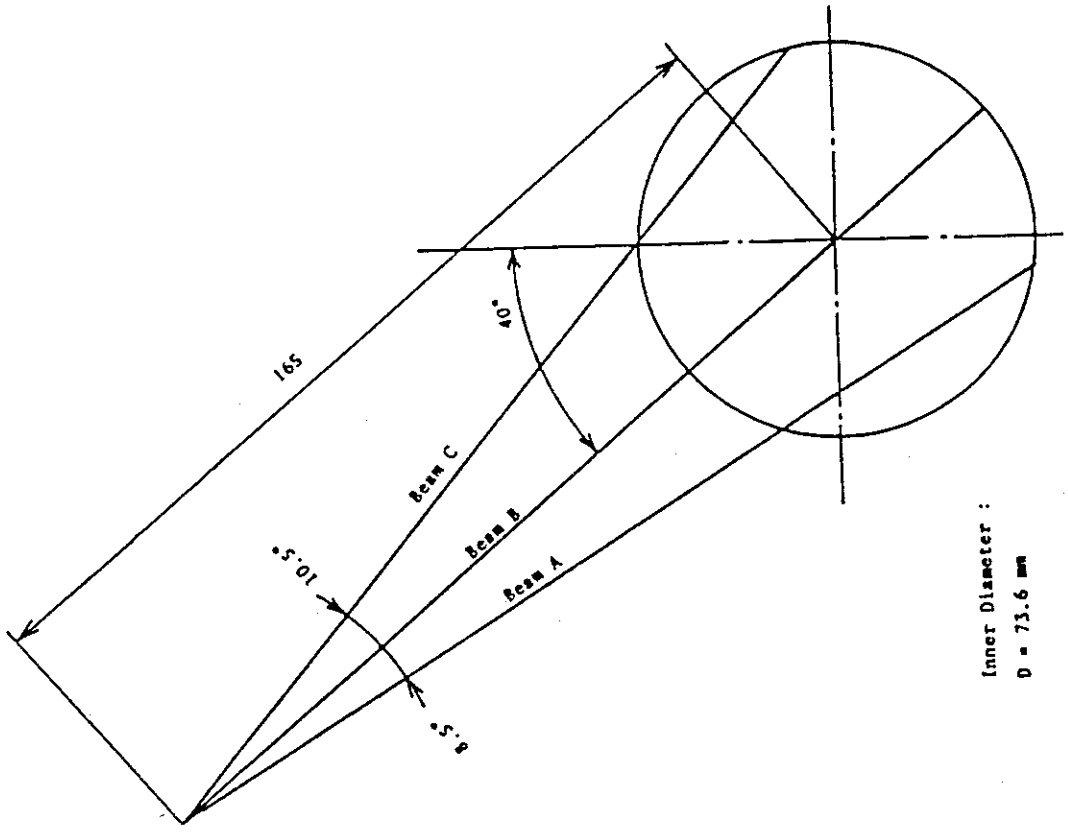

Fig. 3.7 Beam directions of three-beam gamma densitometer

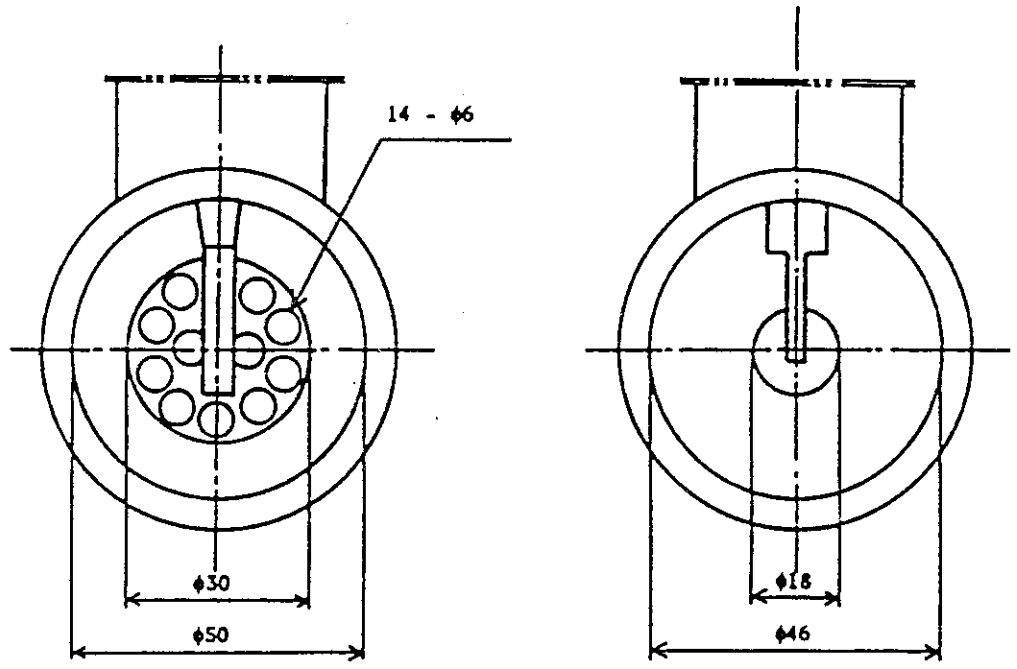

(a) High Range Drag Disc

(b) Low Range Drag Disc

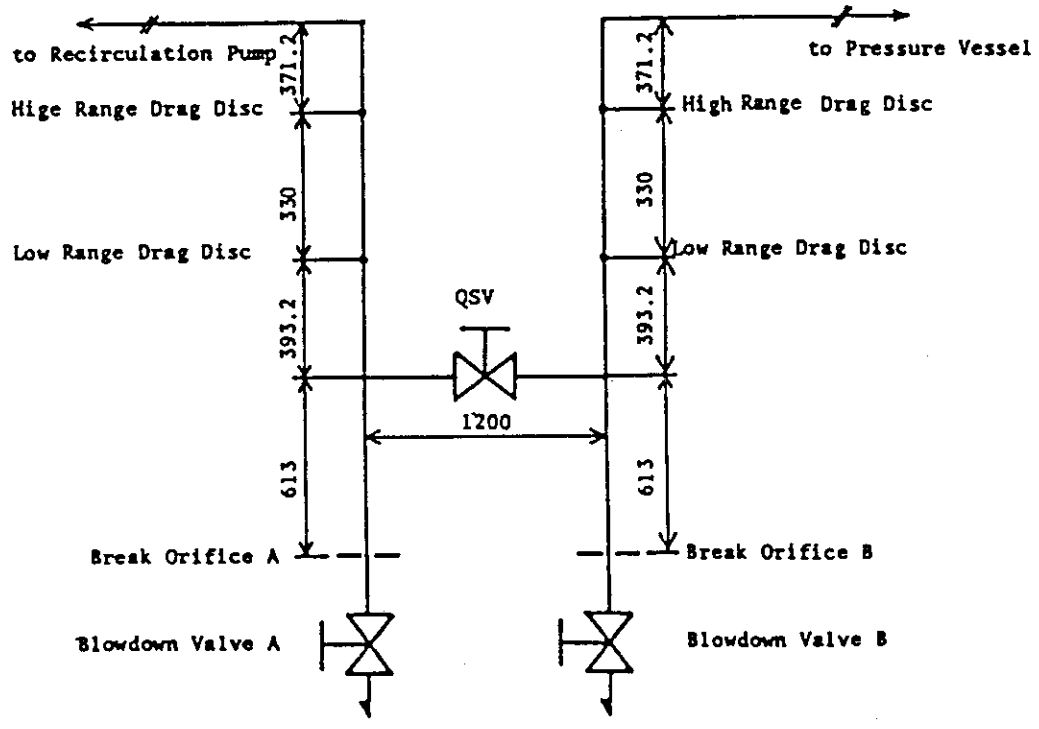

(c) Location of Drag Discs

Fig. 3.9 Arrangement and location of drag disks

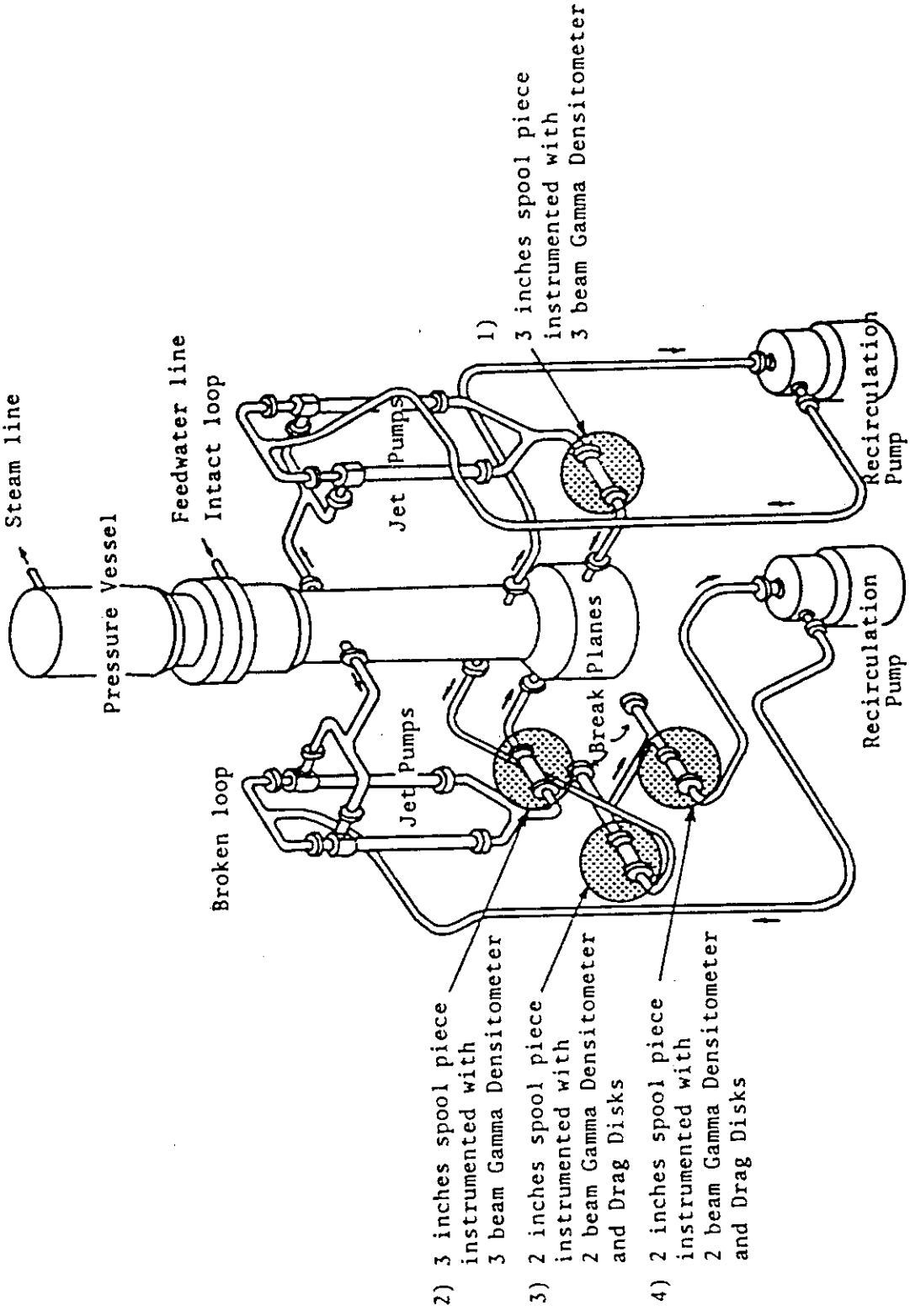

Fig. 3.10 Location of two-phase flow measurement spool pieces

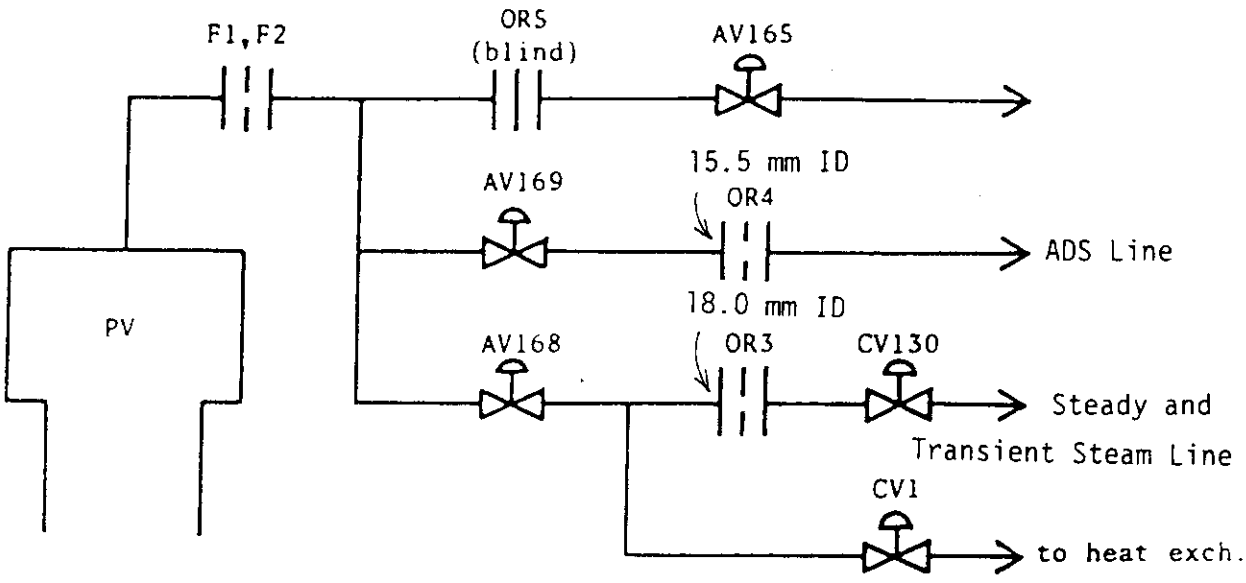

Fig. 4.1 Main steam line schematic

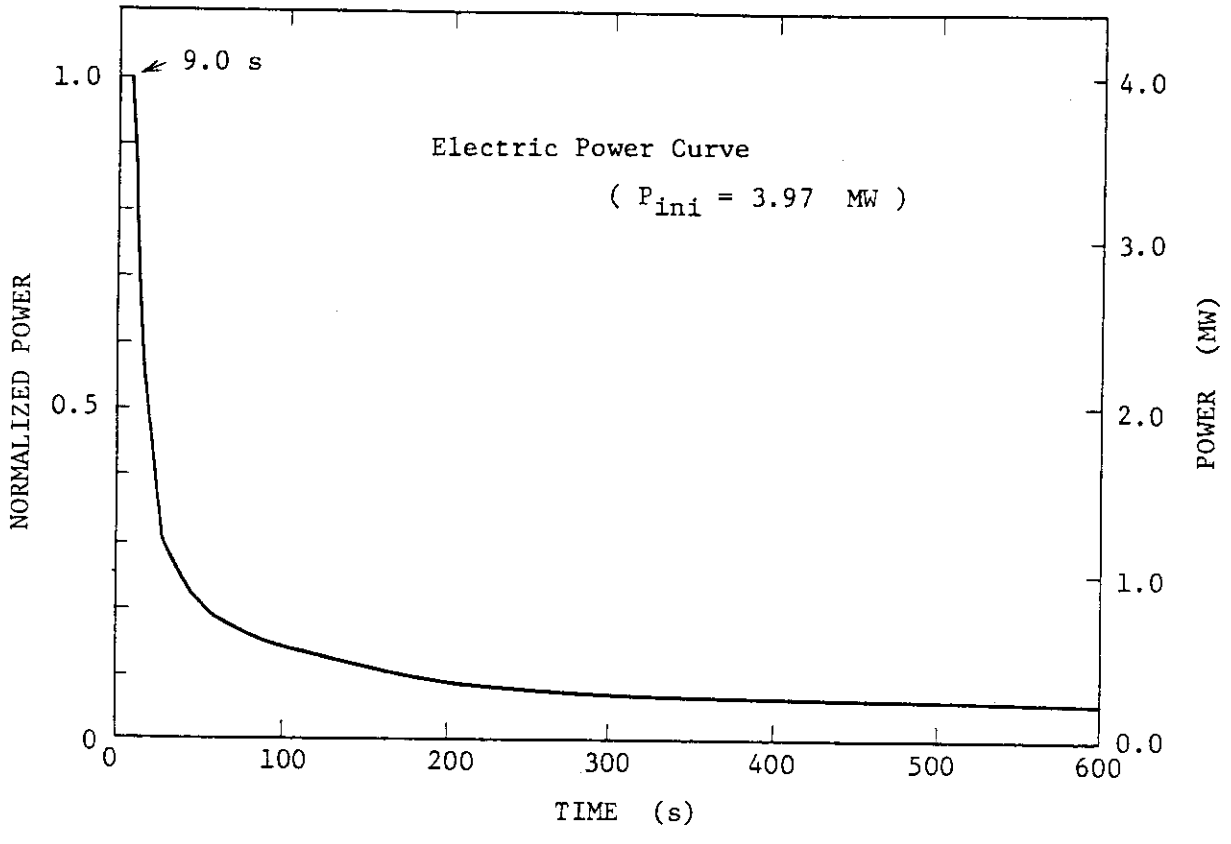

Fig. 4.2 Normalized power transient for ROSA-III test

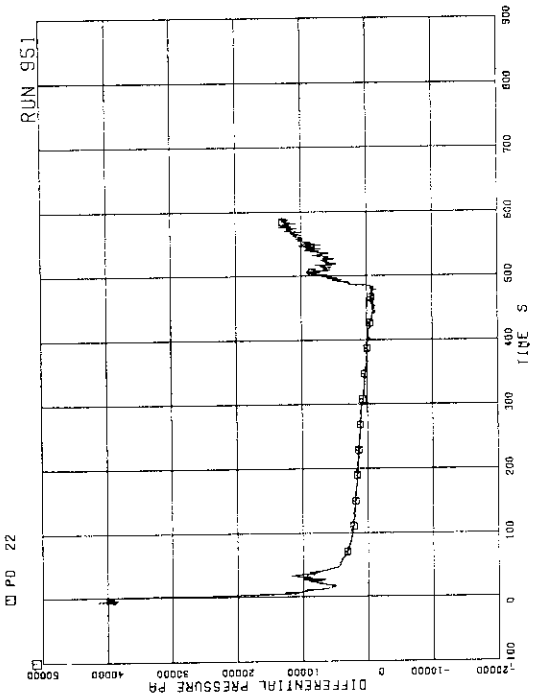

FIG.5. 3 DIFFERENTIAL PRESSURE BETWEEN UP AND STEAM DOME

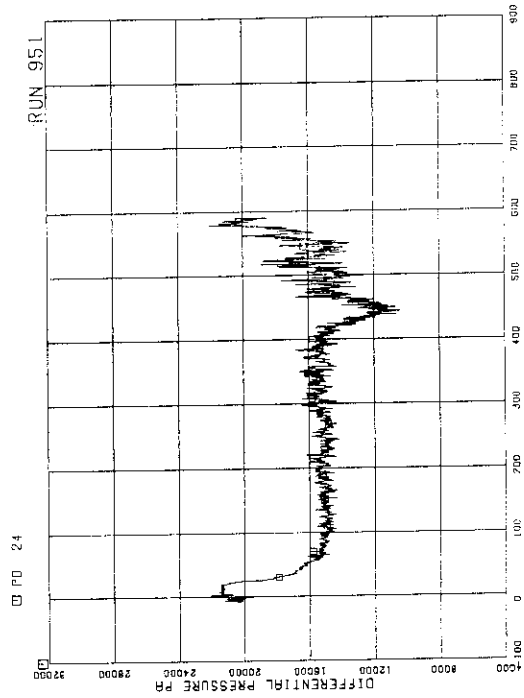

FIG.5. 4 DC (DOWNCOMER) HEAD

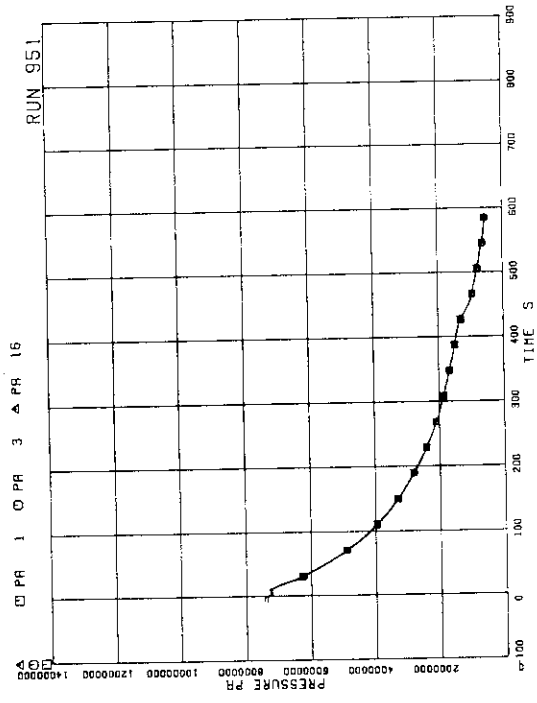

FIG.5. 1 PRESSURES IN PV (PRESSURE VESSEL) AND MSL (MAIN STEAM LINE)

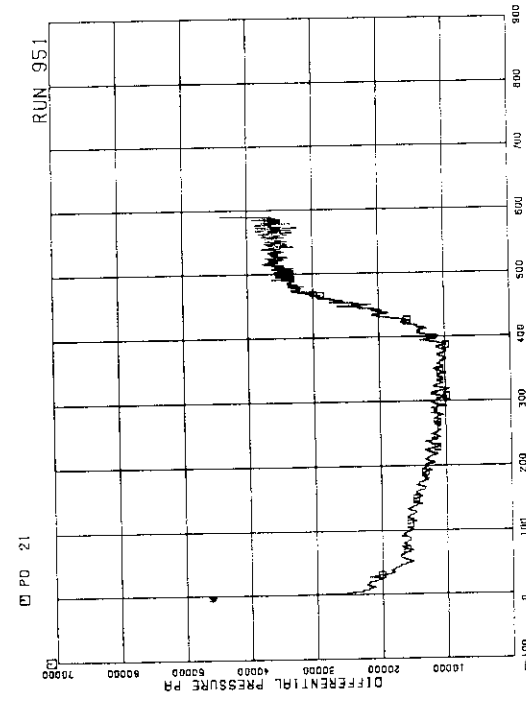

FIG.5. 2 DIFFERENTIAL PRESSURE BETWEEN LOWER PLENUM (LP) AND UPPER PLENUM (UP)

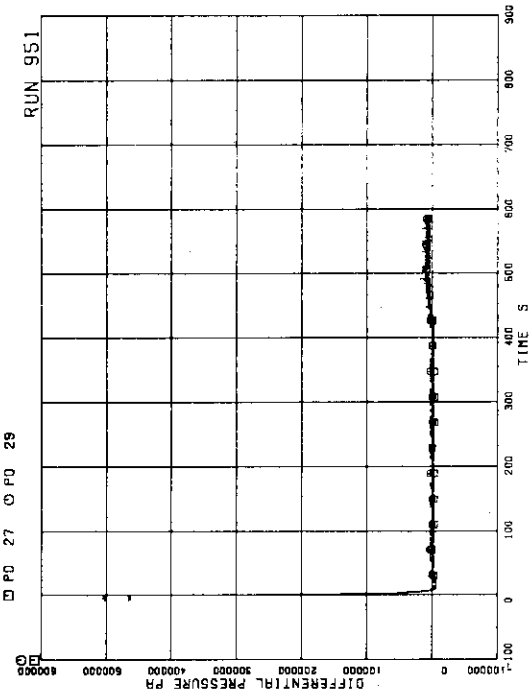

FIG.5. 7 DIFFERENTIAL PRESSURE BETWEEN JP-1.2 DRIVE AND SUCTION

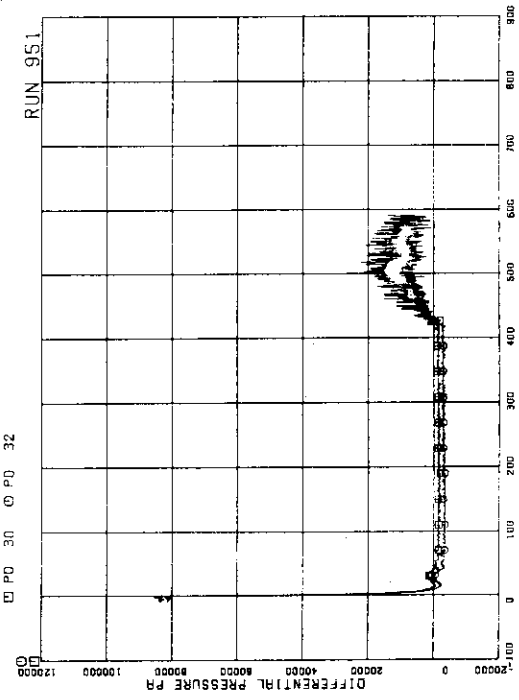

FIG.5. 8 DIFFERENTIAL PRESSURE BETWEEN JP-3.4 DISCHARGE AND SUCTION

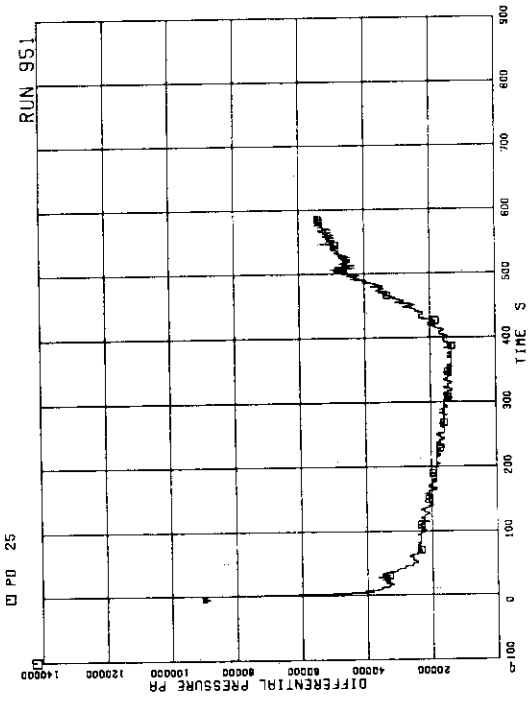

FIG.5. 5 DIFFERENTIAL PRESSURE BETWEEN PV BOTTOM AND TOP

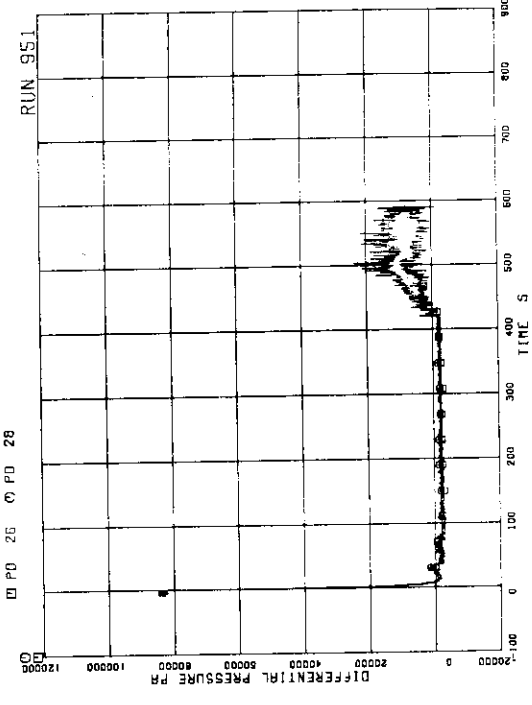

FIG.5. 6 DIFFERENTIAL PRESSURE BETWEEN JP-1.2 DISCHARGE AND SUCTION

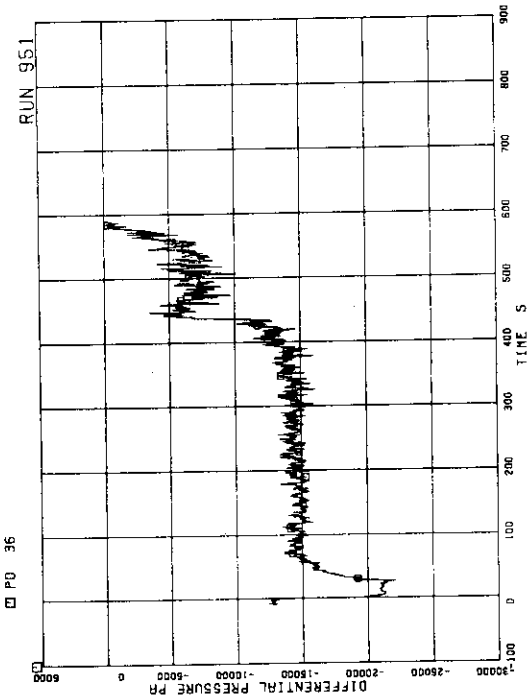

FIG.5. 11 DIFFERENTIAL PRESSURE BETWEEN DC BOTTOM AND MRP1 SUCTION

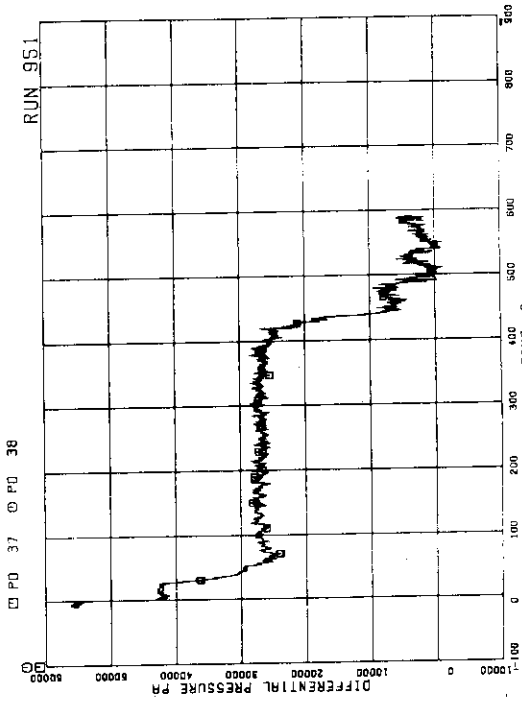

FIG.5. 12 DIFFERENTIAL PRESSURE BETWEEN MRP DELIVERY AND JP-1.2 DRIVE

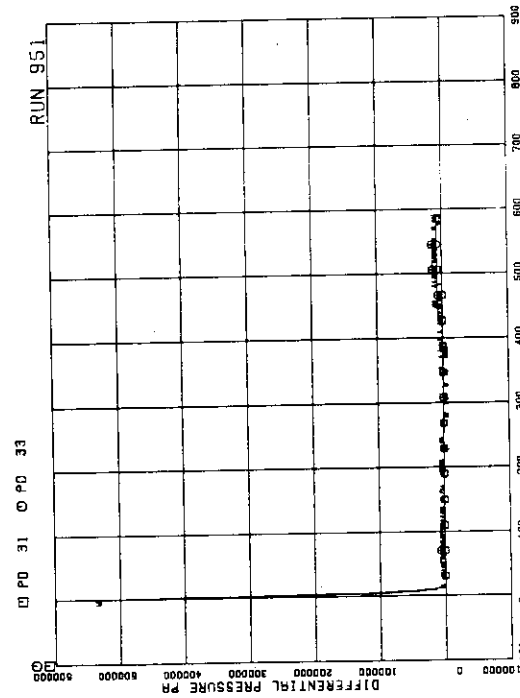

FIG.5. 9 DIFFERENTIAL PRESSURE BETWEEN JP-3.4 DRIVE AND SUCTION

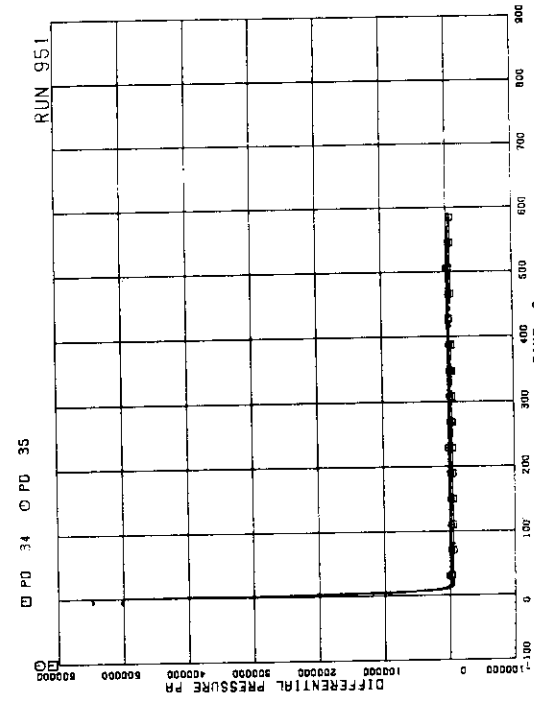

FIG.5. 10 DIFFERENTIAL PRESSURE BETWEEN MRP DELIVERY AND SUCTION

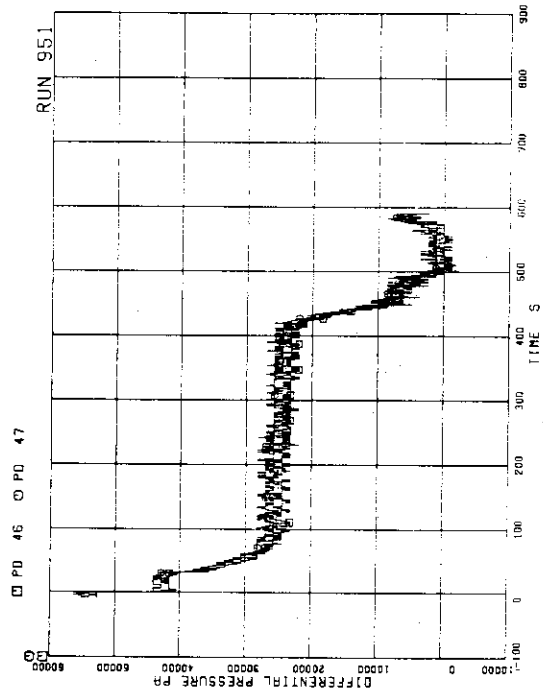

FIG.5. 15 DIFFERENTIAL PRESSURE BETWEEN MRP2 DELIVERY AND JP 3.4 DRIVE

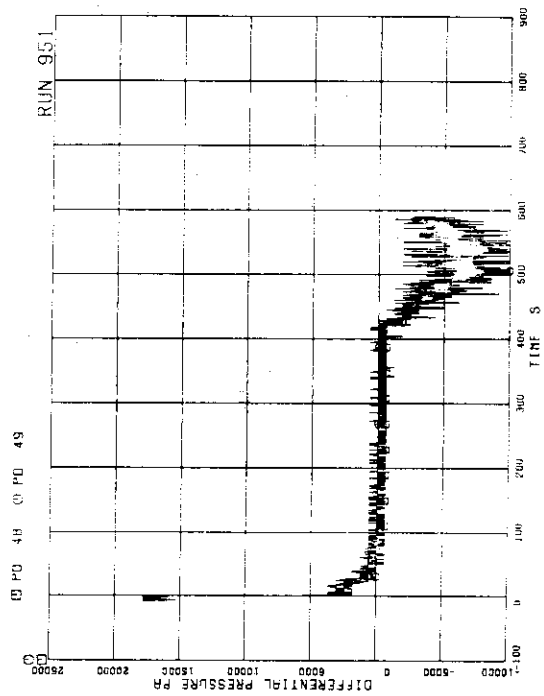

FIG.5. 16 DIFFERENTIAL PRESSURE BETWEEN DC MIDDLE AND JP 3.4 SUCTION

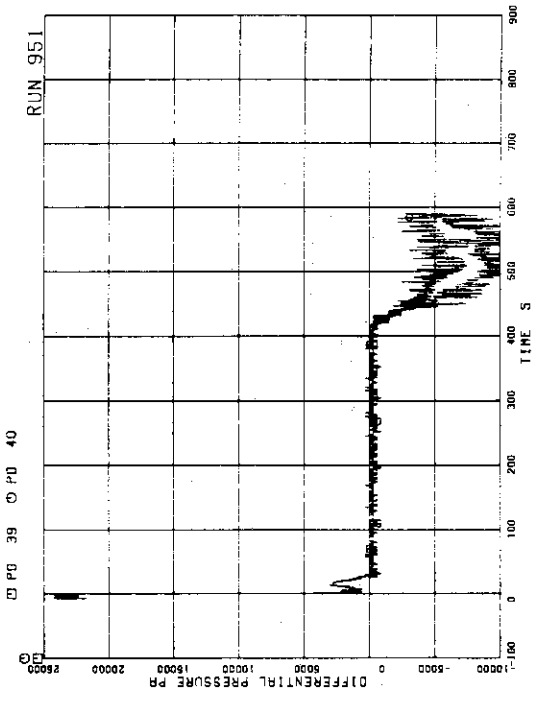

FIG.5. 13 DIFFERENTIAL PRESSURE BETWEEN DC MIDDLE AND JP 1.2 SUCTION

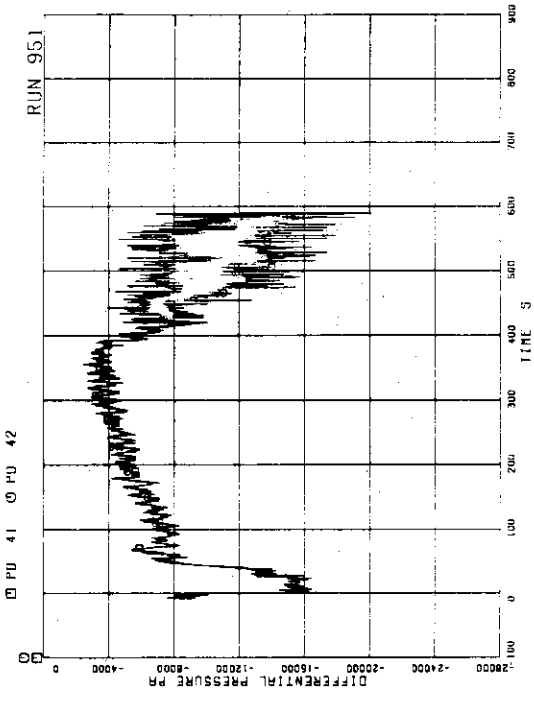

FIG.5. 14 DIFFERENTIAL PRESSURE BETWEEN JP 1.2 DISCHARGE AND LP

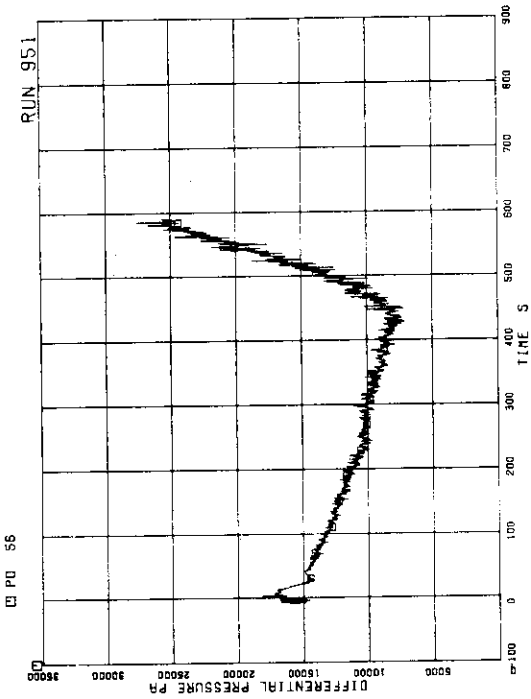

FIG.5. 19 DIFFERENTIAL PRESSURE BETWEEN OC MIDDLE AND STEAM DOME

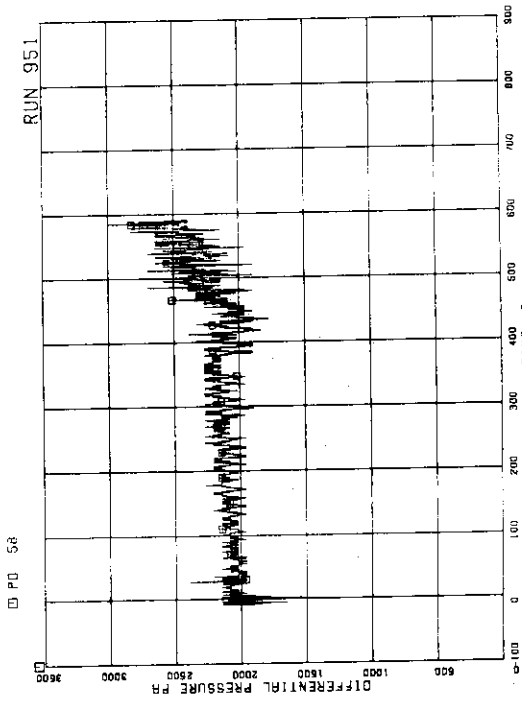

FIG.5. 20 DIFFERENTIAL PRESSURE BETWEEN LP BOTTOM AND LP MIDDLE

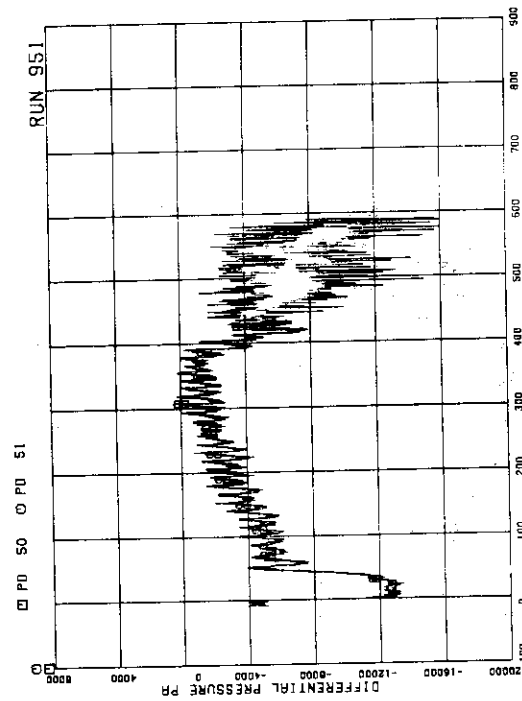

FIG.5. 17 DIFFERENTIAL PRESSURE BETWEEN JP-3.4 DISCHARGE AND CONFLURNCE

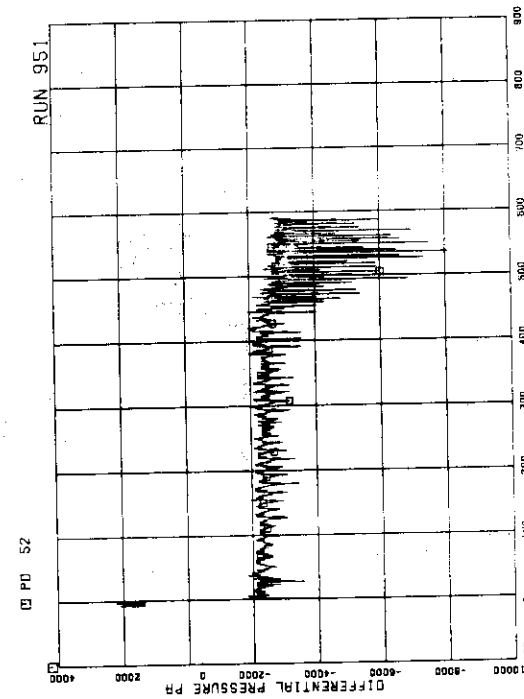

FIG.5. 18 DIFFERENTIAL PRESSURE BETWEEN JP-3.4 CONFLUENCE AND LP

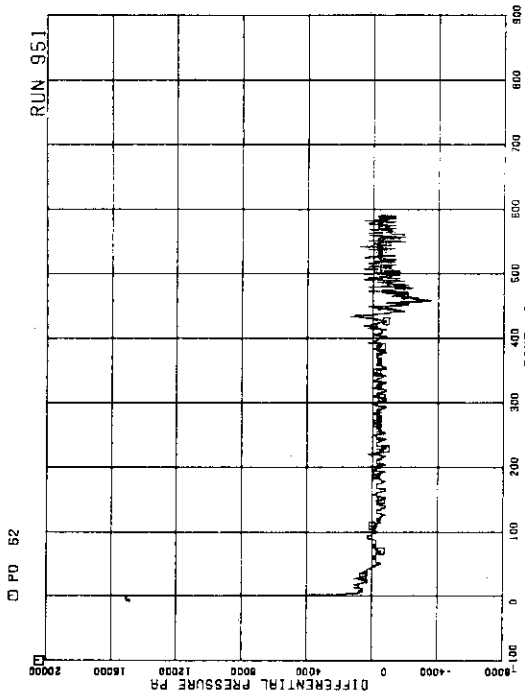

FIG.5. 23 DIFFERENTIAL PRESSURE ACROSS CHANNEL INLET ORIFICE C

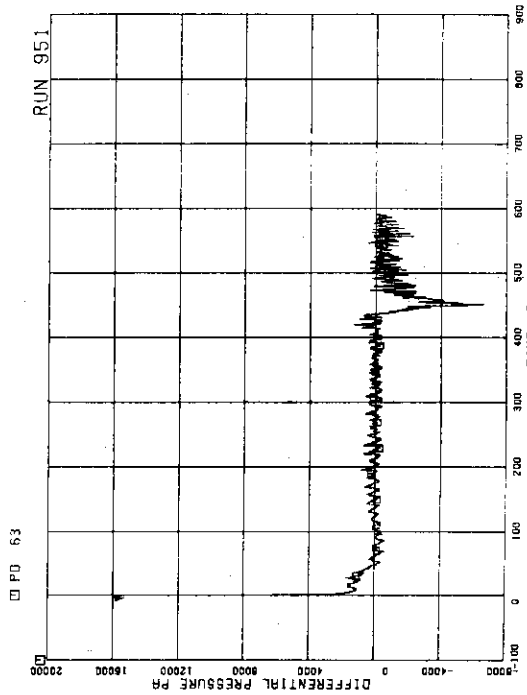

FIG.5. 24 DIFFERENTIAL PRESSURE ACROSS CHANNEL INLET ORIFICE D

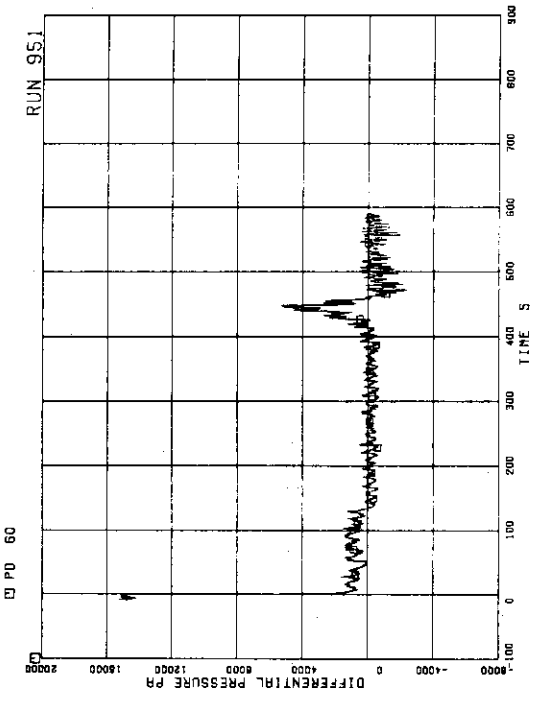

FIG.5. 21 DIFFERENTIAL PRESSURE ACROSS CHANNEL INLET ORIFICE A

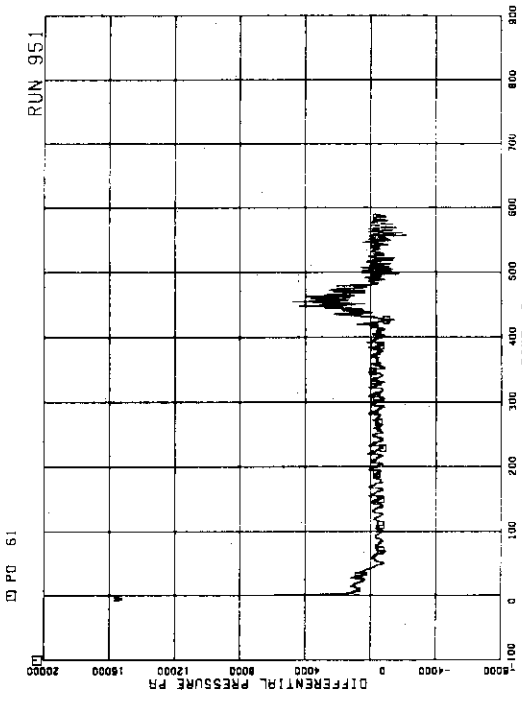

FIG.5. 22 DIFFERENTIAL PRESSURE ACROSS CHANNEL INLET ORIFICE B

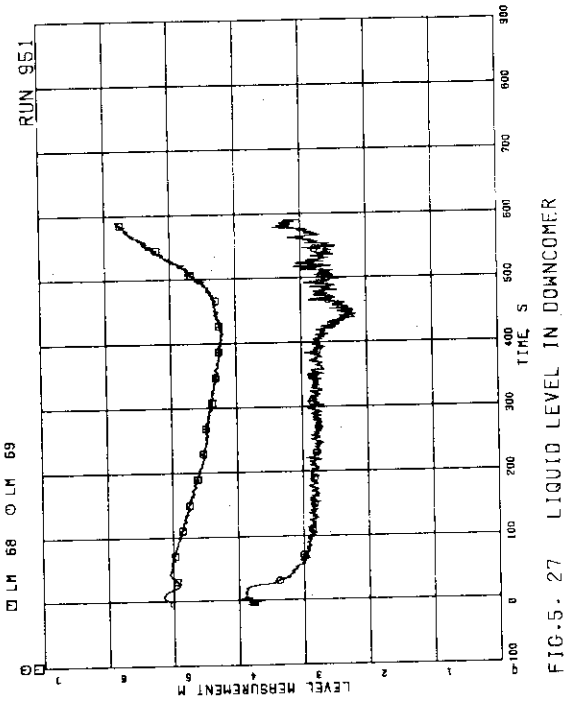

FIG.5. 27 LIQUID LEVEL IN DOWNCOMER

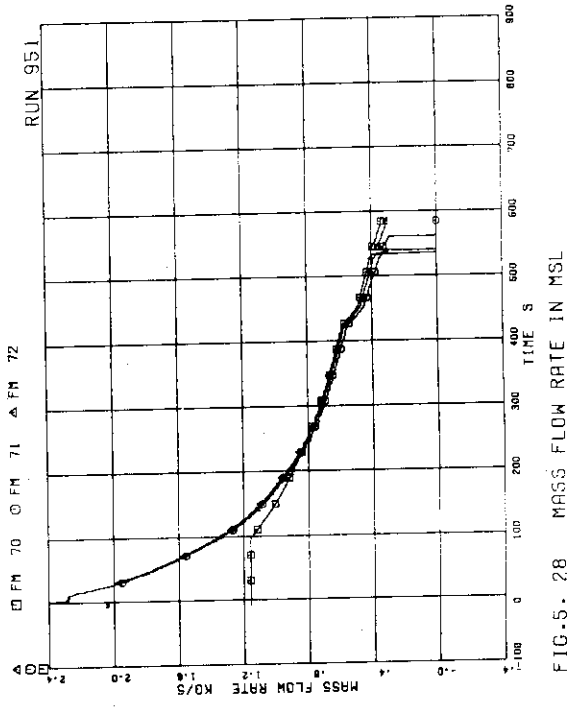

FIG.5. 28 MASS FLOW RATE IN MSL

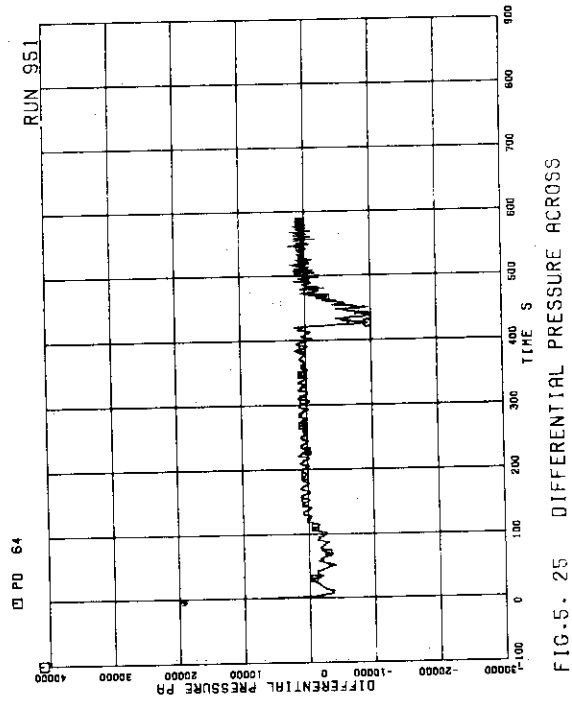

FIG.5. 25 DIFFERENTIAL PRESSURE ACROSS BYPASS HOLE

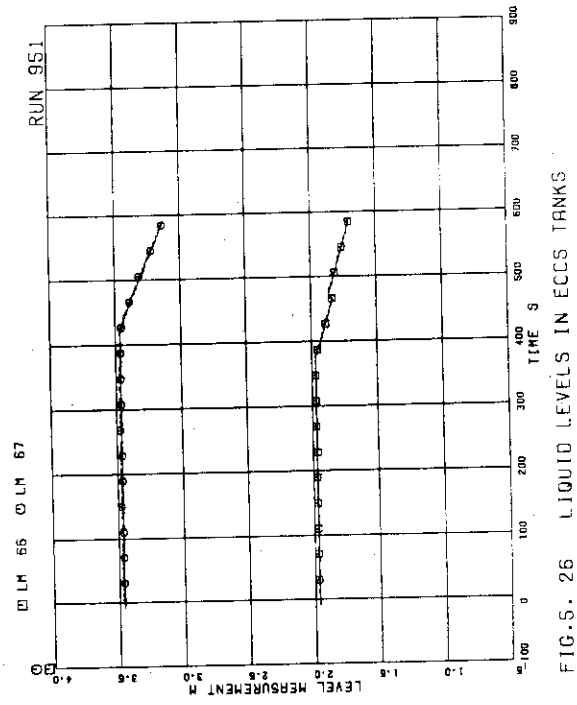

FIG.5. 26 LIQUID LEVELS IN ECCS TANKS

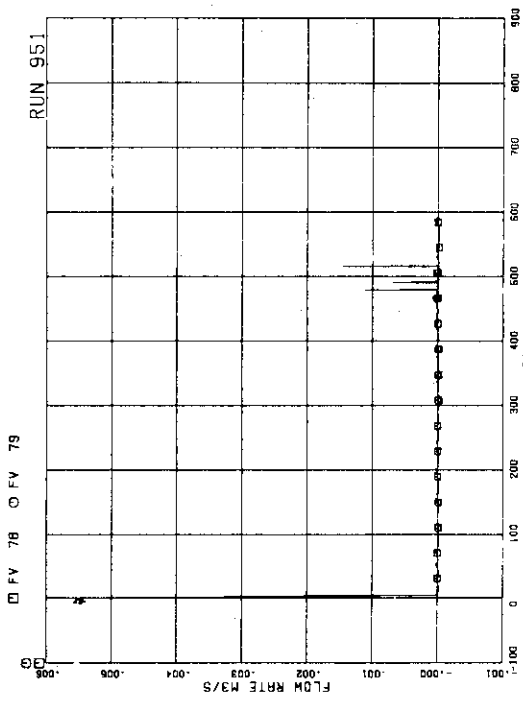

FIG.5. 31 JP-1.2 DISCHARGE FLOW RATES (POS-FLOW)

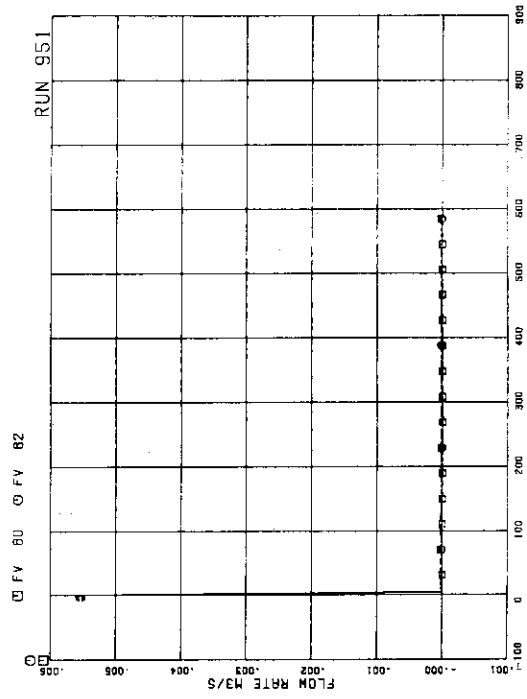

FIG.5. 32 JP-3.4 DISCHARGE FLOW RATES (POS-FLOW)

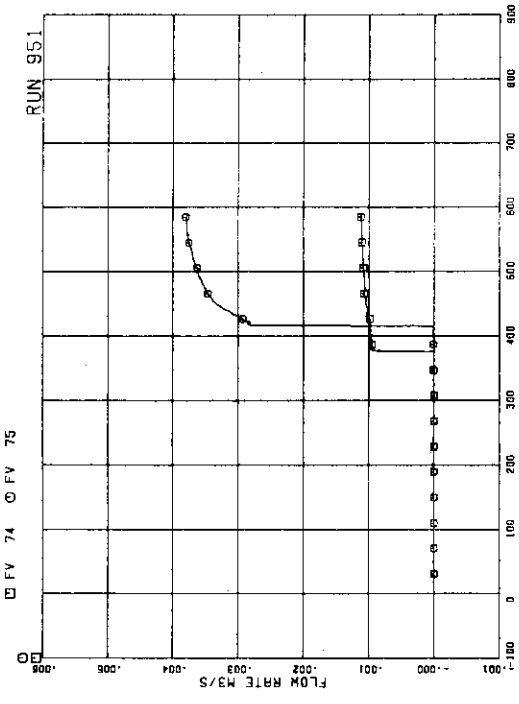

FIG.5. 29 ECC INJECTION FLOW RATES

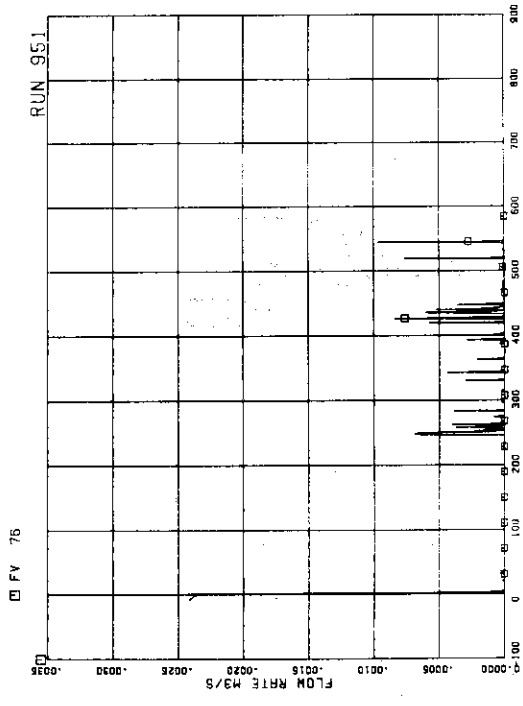

FIG.5. 30 FEEDWATER FLOW RATE

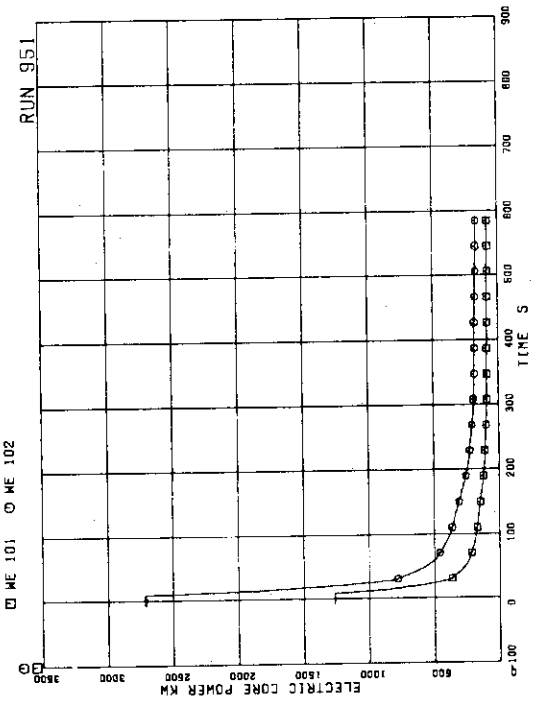

FIG.5. 35 ELECTRIC CORE POWER

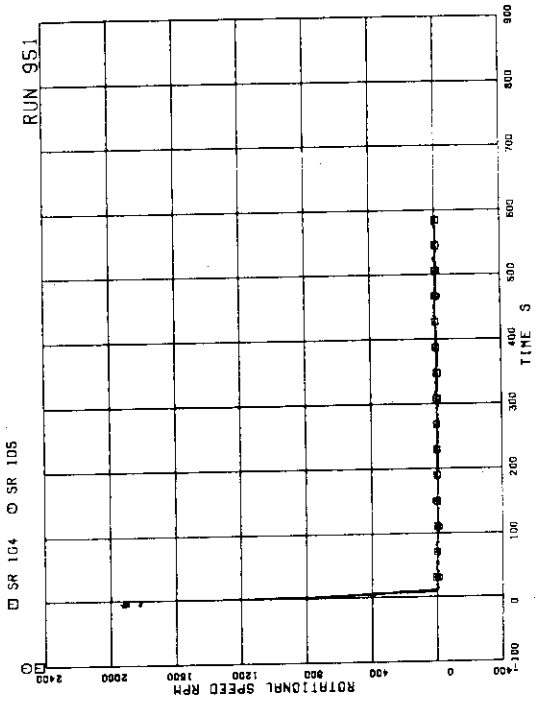

FIG.5. 36 MRP PUMP SPEEDS

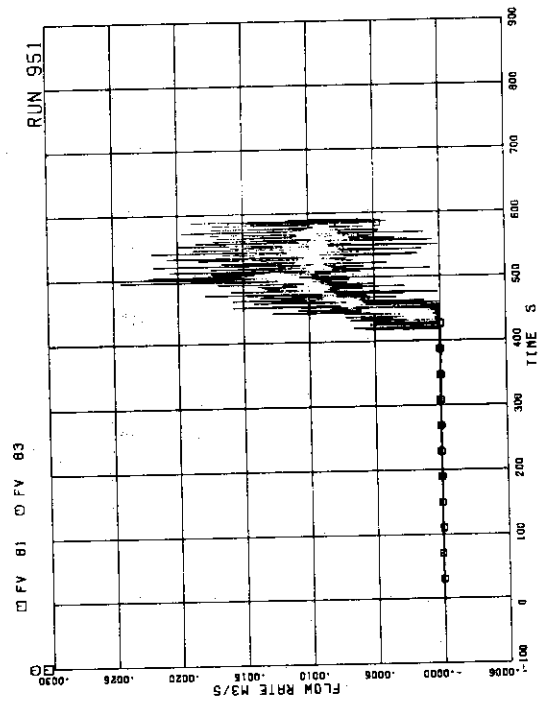

FIG.5. 33 JP-3,4 DISCHARGE FLOW RATES (NEG-FLOW)

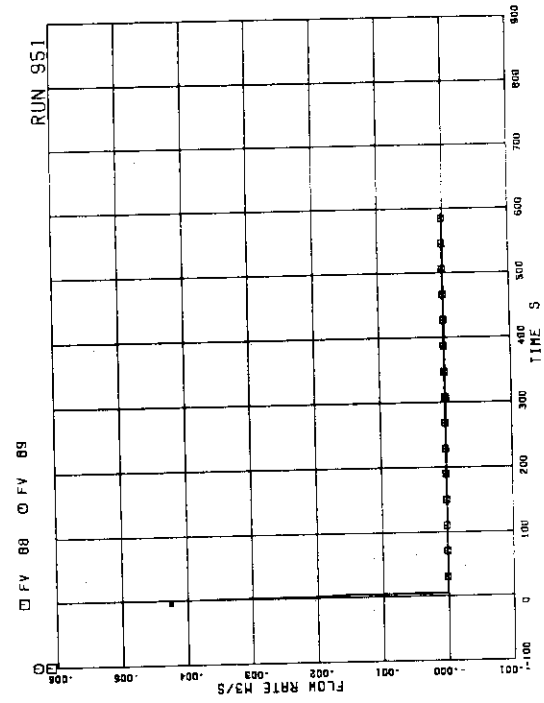

FIG.5. 34 MRP DISCHARGE FLOW RATES

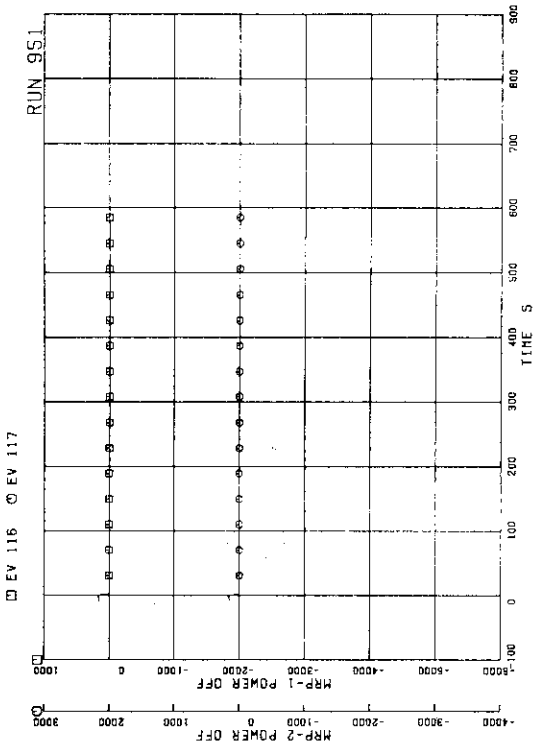

FIG.5. 39 MRP OPERATION SIGNALS

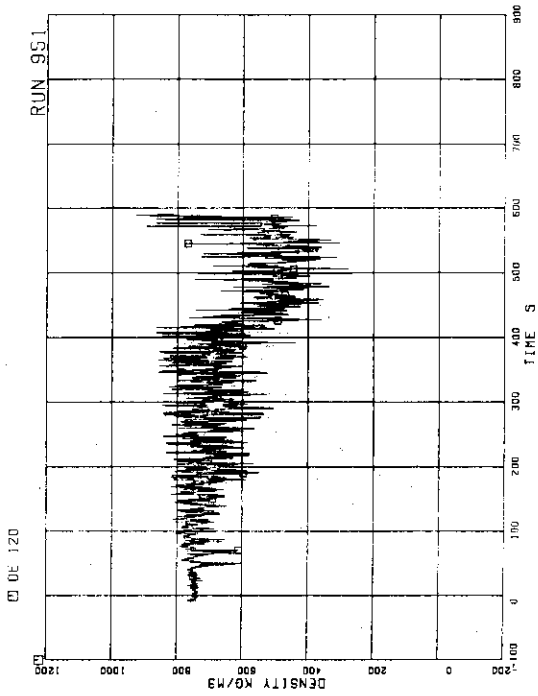

FIG.5. 40 FLUID DENSITY AT JP-1.2 OUTLET, BEAM A

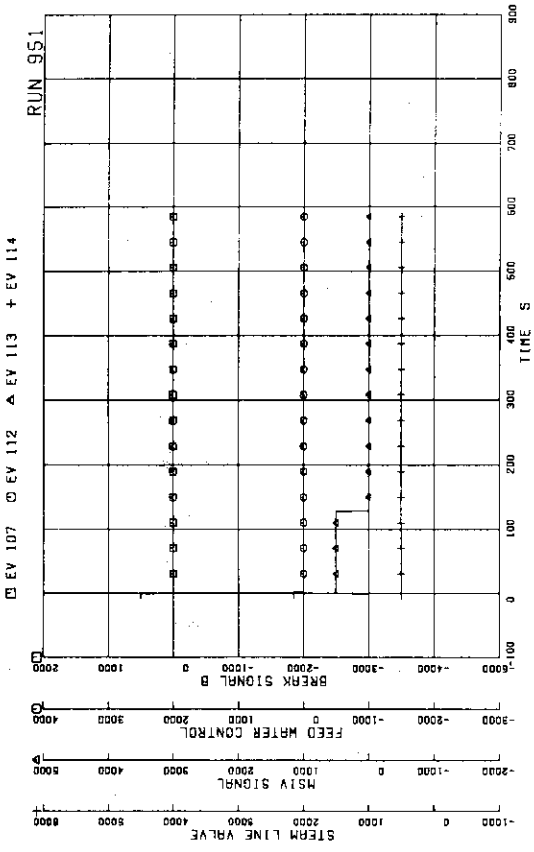

FIG.5. 37 VALVE OPERATION SIGNALS

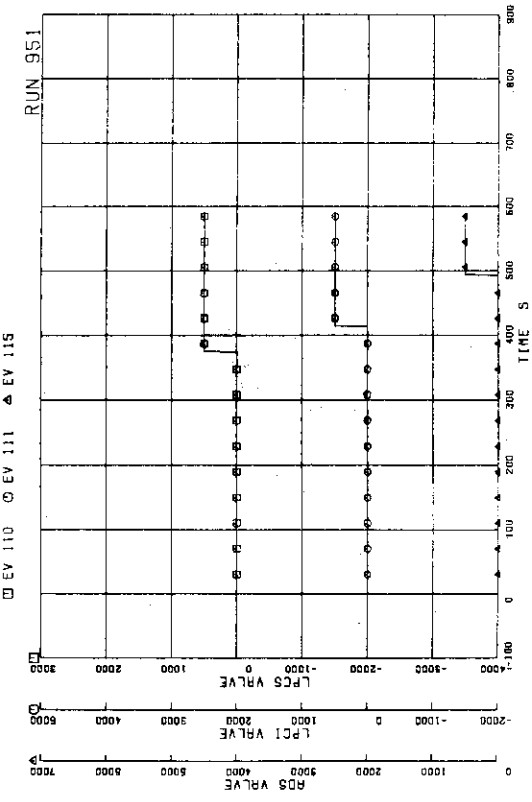

FIG.5. 38 ECCS OPERATION SIGNALS

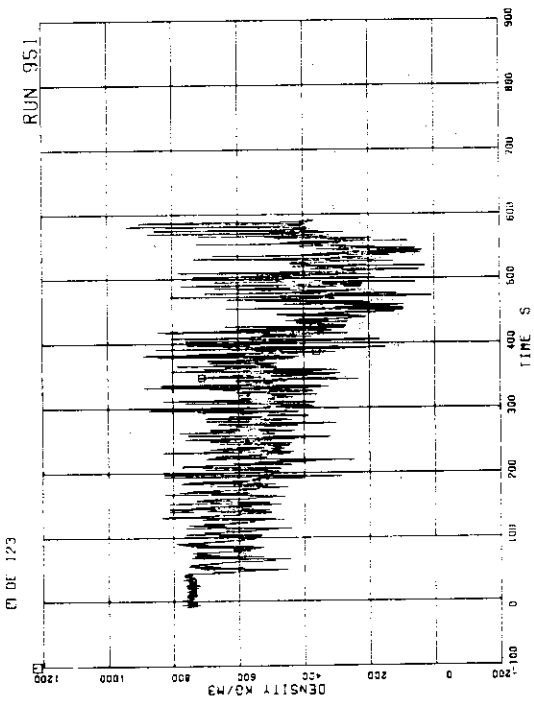

FIG.5. 43 FLUID DENSITY AT JP-3.4 OUTLET, BEAM A

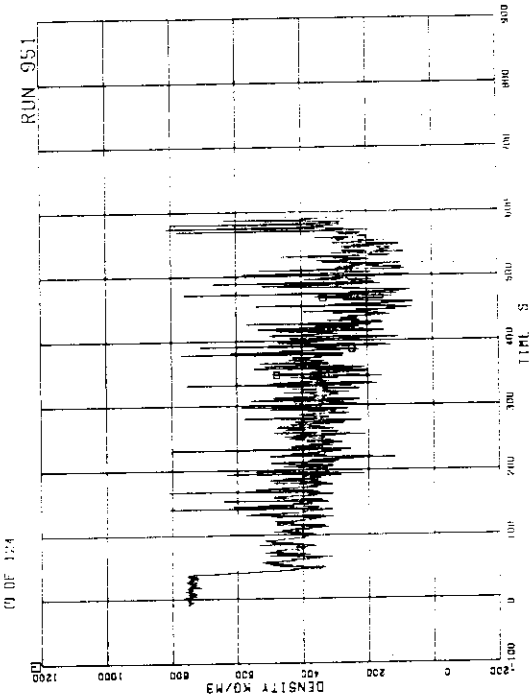

FIG.5. 44 FLUID DENSITY AT JP-3.4 OUTLET, BEAM B

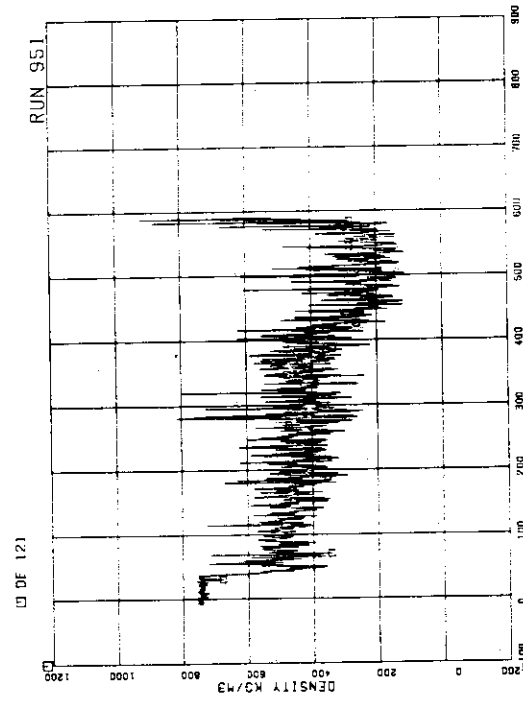

FIG.5. 41 FLUID DENSITY AT JP-1.2 OUTLET, BEAM B

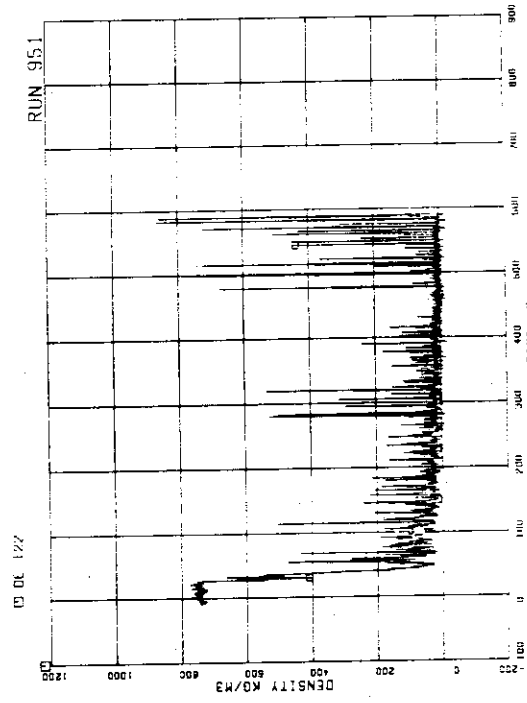

FIG.5. 42 FLUID DENSITY AT JP-1.2 OUTLET, BEAM C

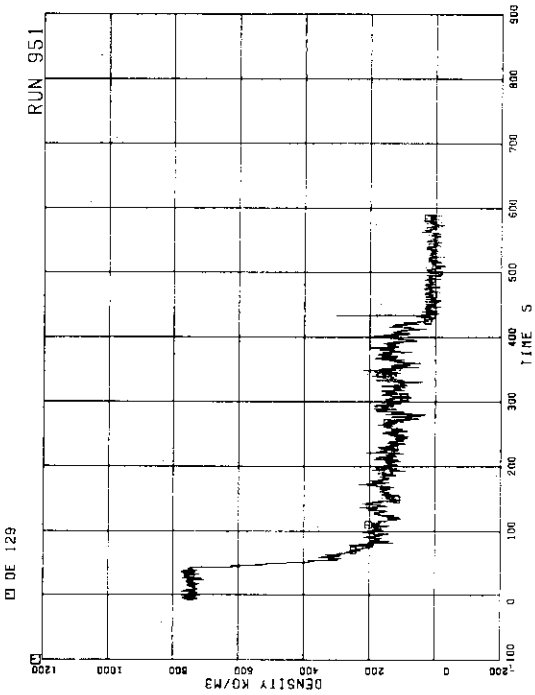

FIG.5. 47 FLUID DENSITY AT PV SIDE OF LOOP, BEAM B

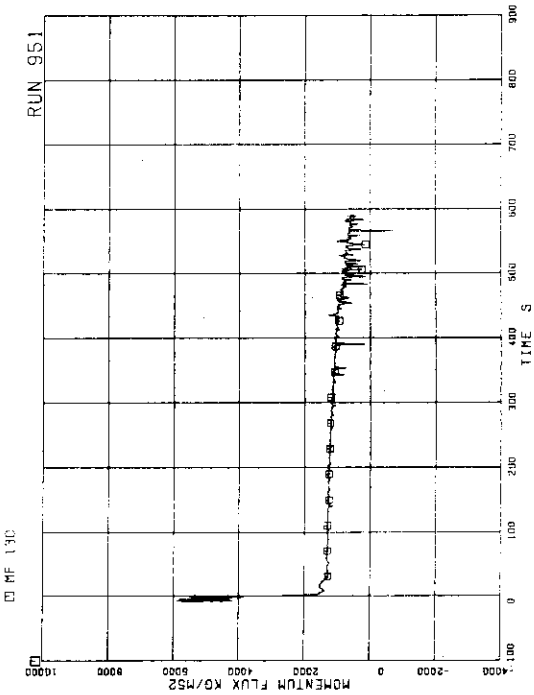

FIG.5. 48 MOMENTUM FLUX AT JP-1,2 OUTLET SPOOL

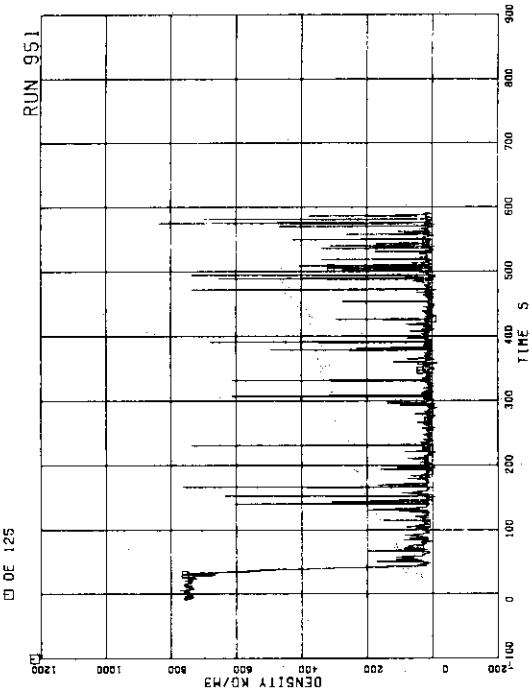

FIG.5. 45 FLUID DENSITY AT JP-3,4 OUTLET, BEAM C

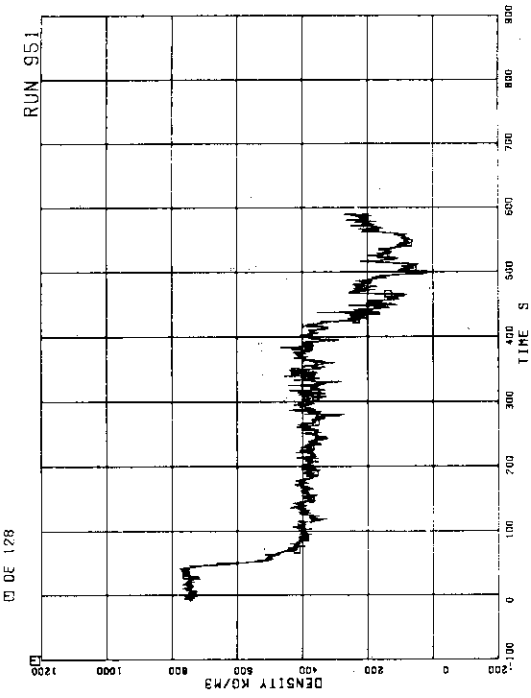

FIG.5. 46 FLUID DENSITY AT PV SIDE OF LOOP, BEAM A

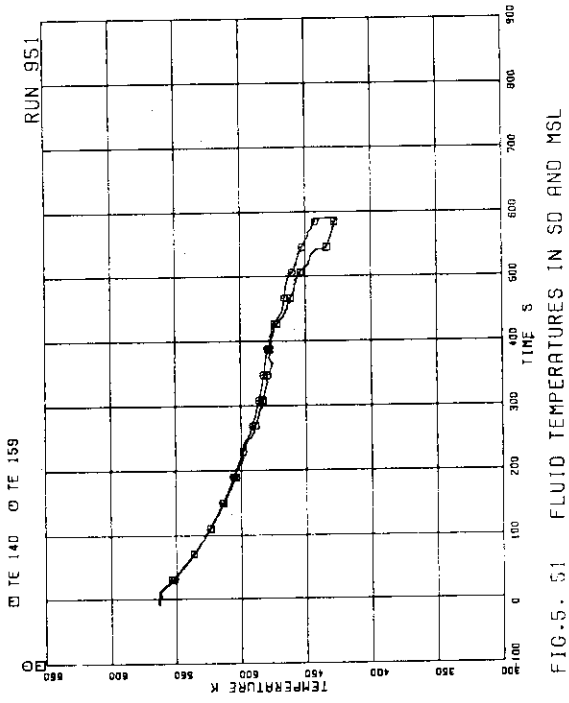

FIG.5. 51 FLUID TEMPERATURES IN SD AND MSL

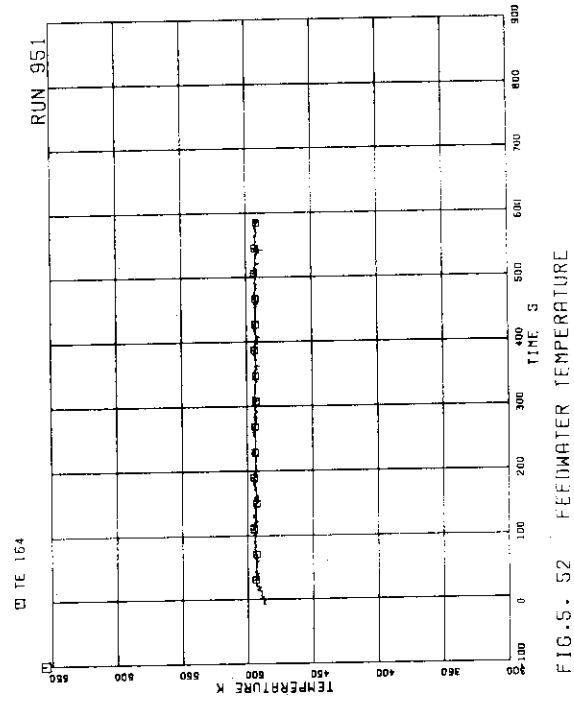

FIG.5. 52 FEEDWATER TEMPERATURE

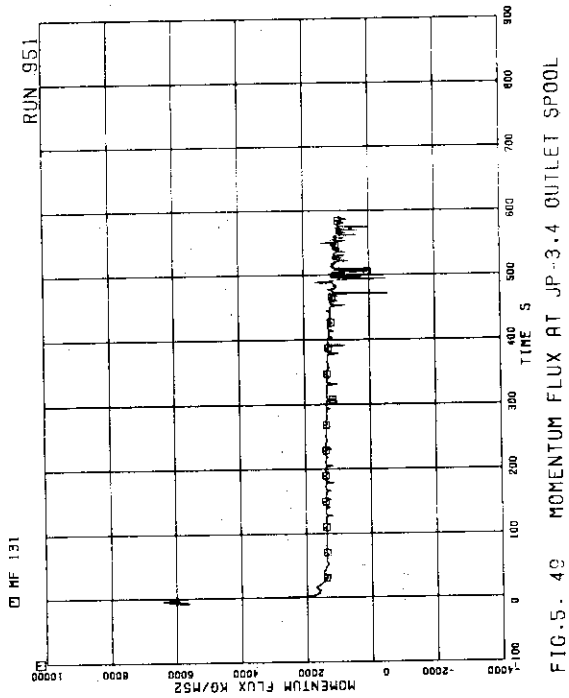

FIG.5. 49 MOMENTUM FLUX AT JP-3.4 OUTLET SPOOL

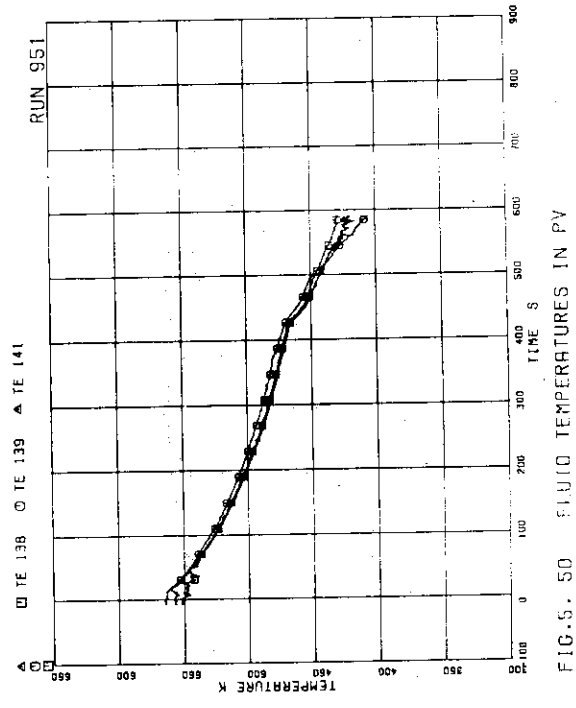

FIG.5. 50 FLUID TEMPERATURES IN PV

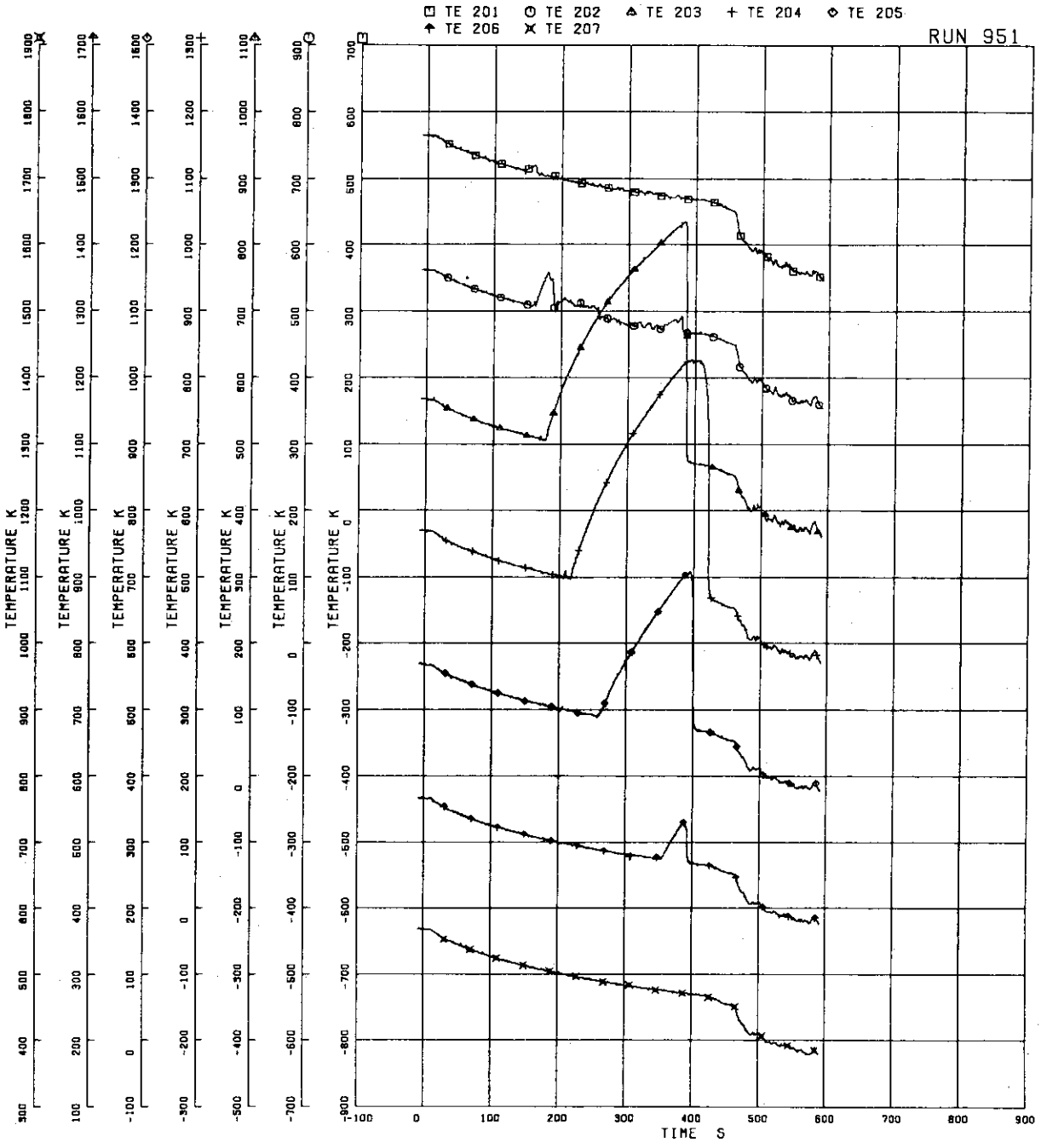

FIG.5. 53 FUEL ROD SURFACE TEMPERATURE OF A11 ROD

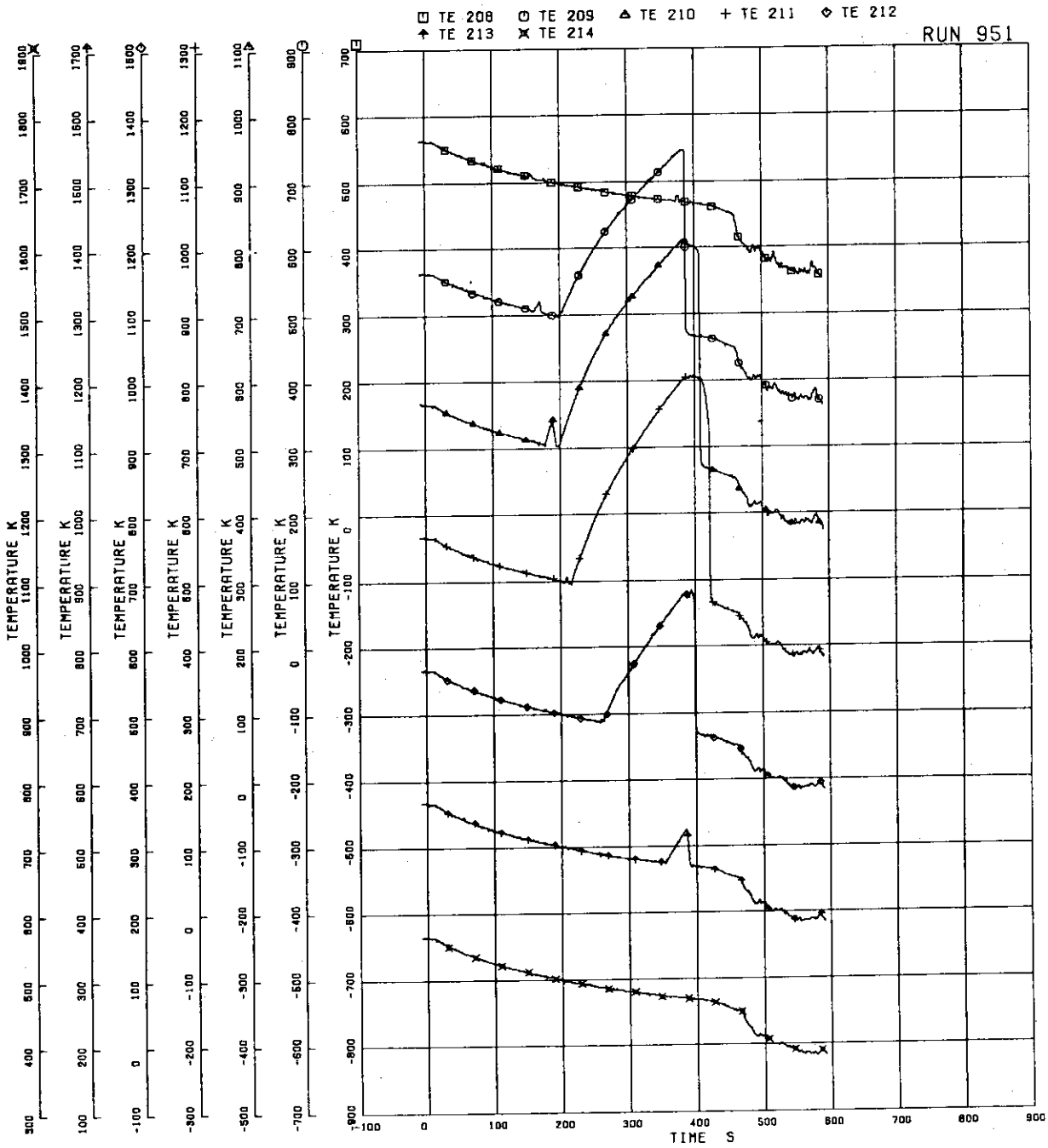

FIG.5. 54 FUEL ROD SURFACE TEMPERATURE OF A12 ROD

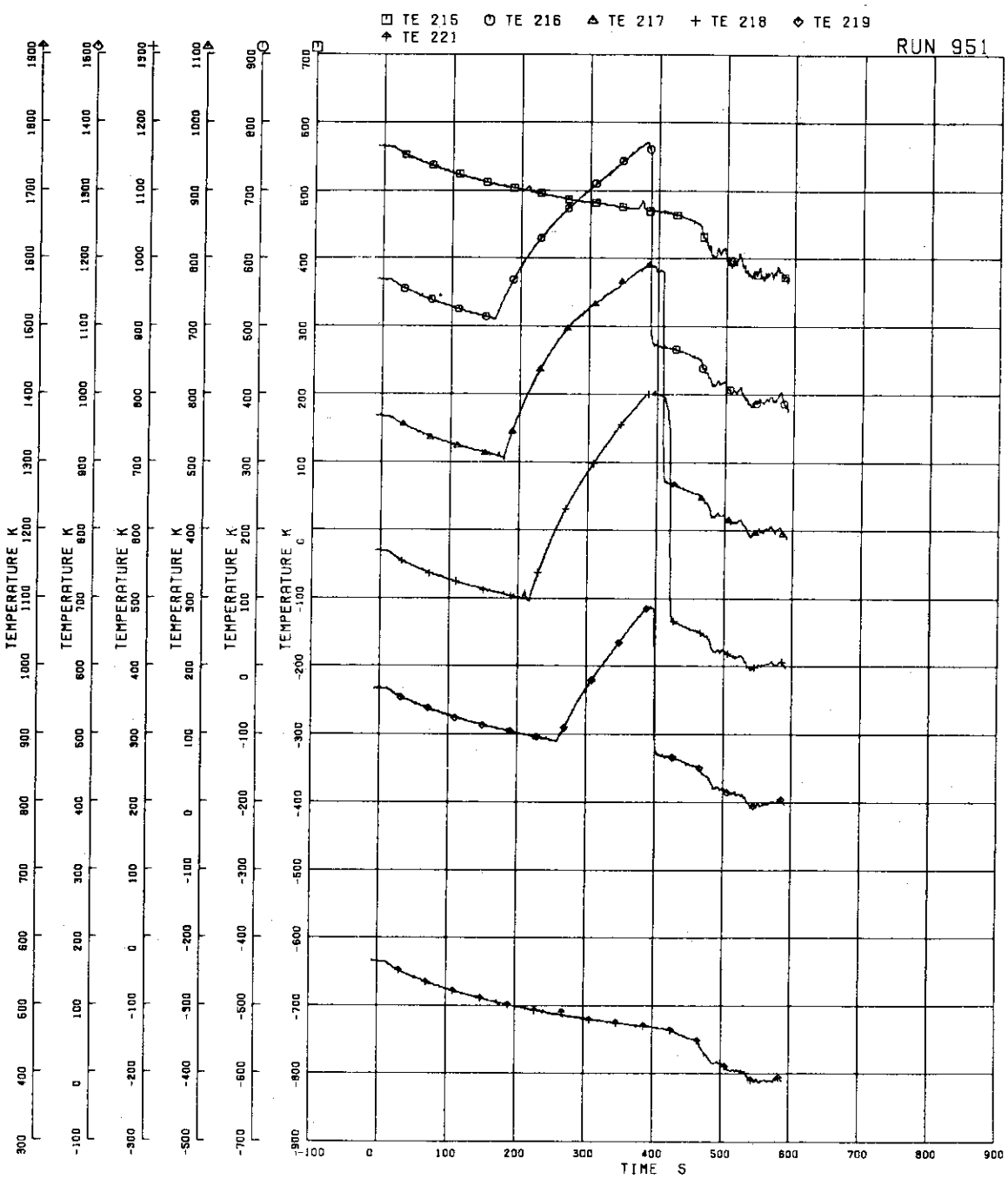

FIG.5. 55 FUEL ROD SURFACE TEMPERATURE OF A13 ROD

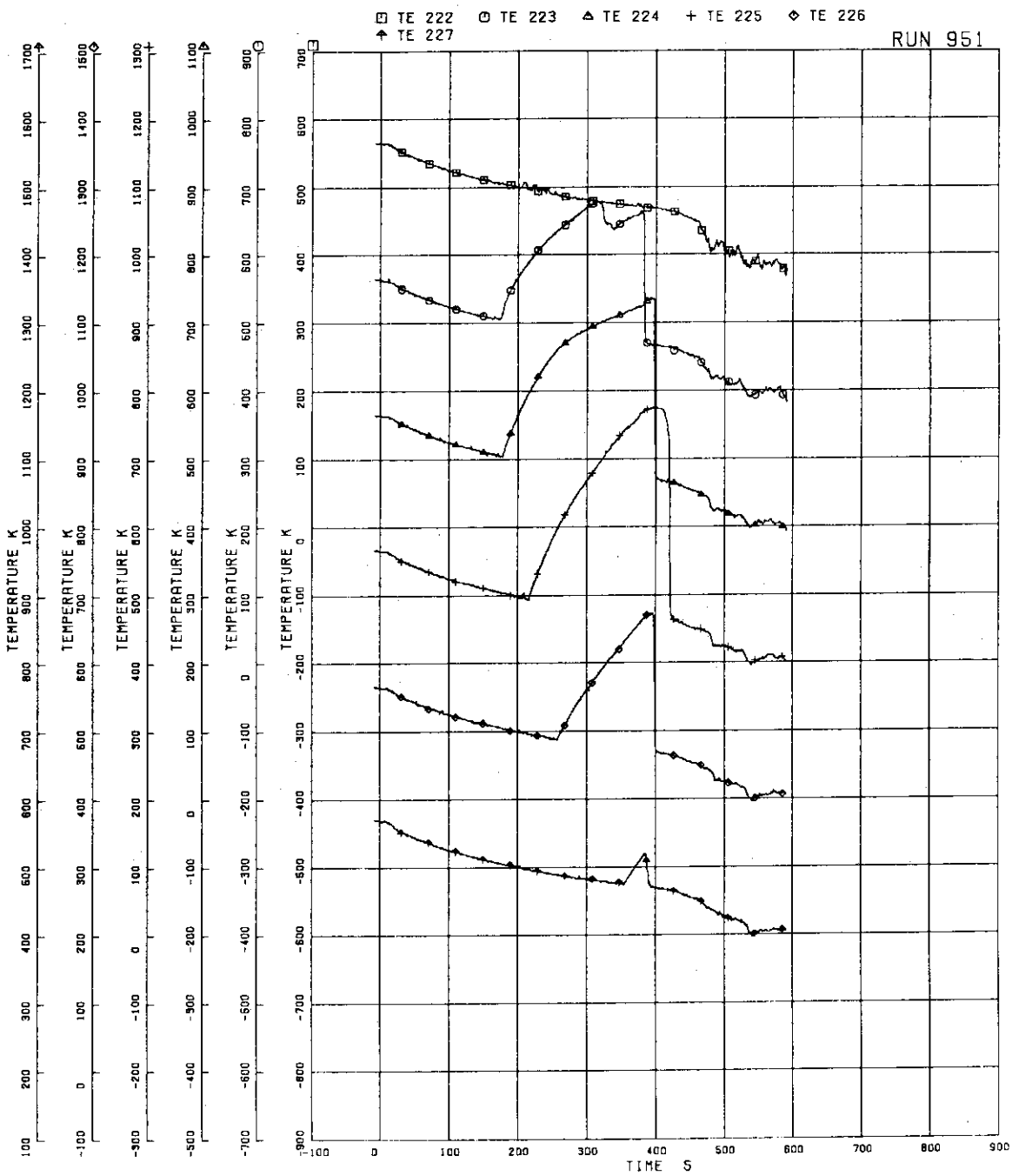

FIG.5. 56 FUEL ROD SURFACE TEMPERATURE OF A14 ROD

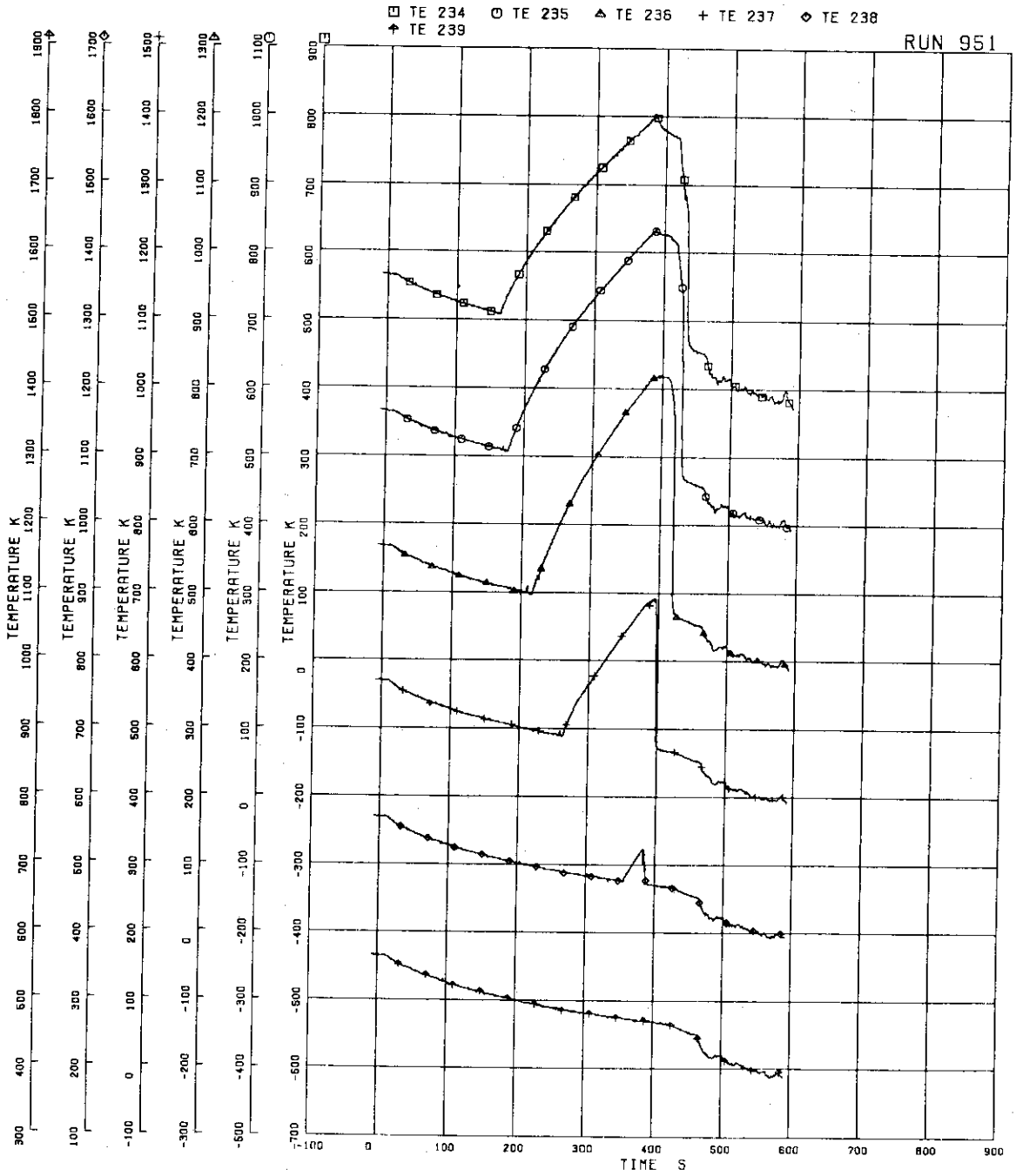

FIG.5. 57 FUEL ROD SURFACE TEMPERATURE OF A22 ROD

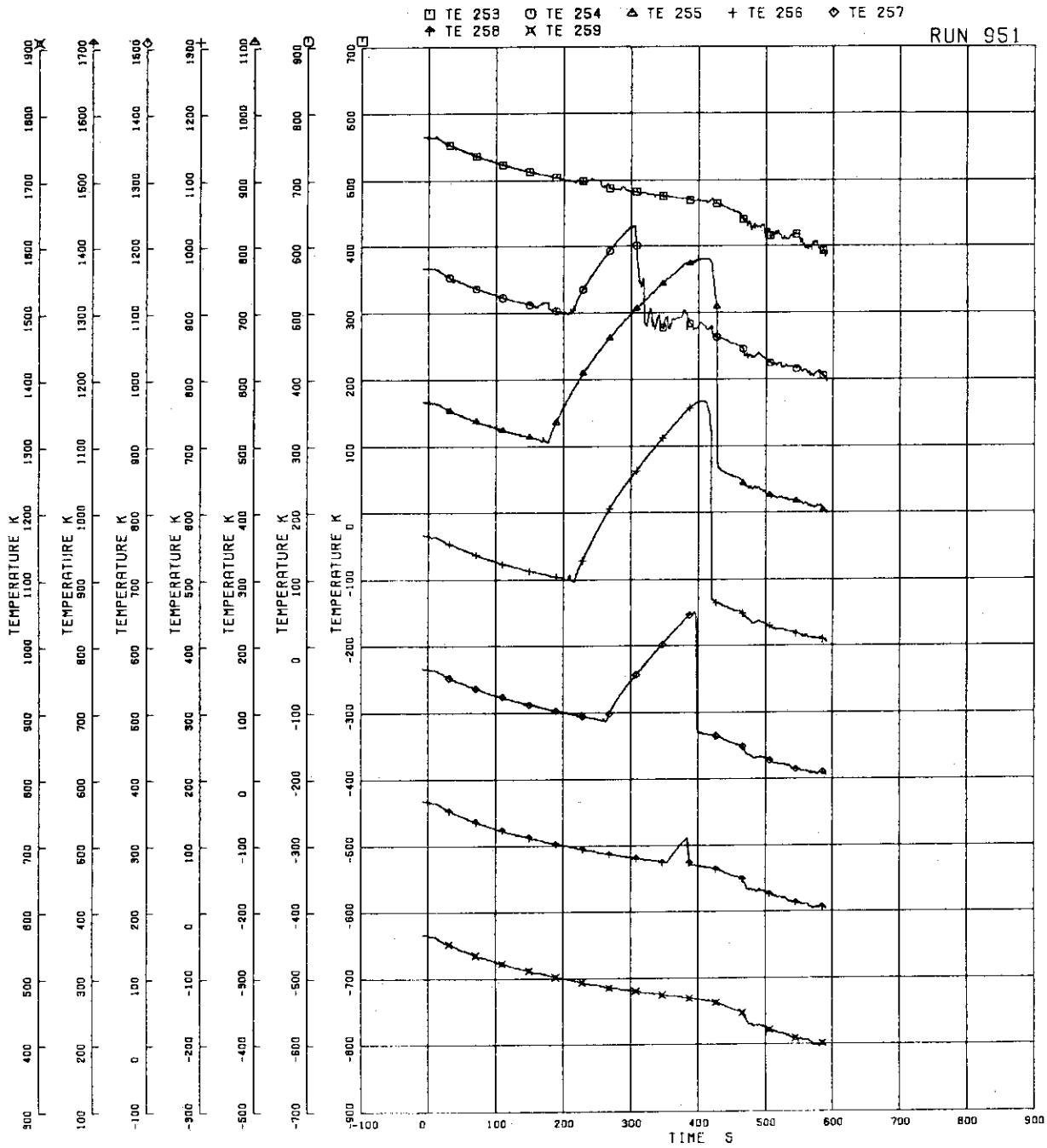

FIG.5. 58 FUEL ROD SURFACE TEMPERATURE OF A33 ROD

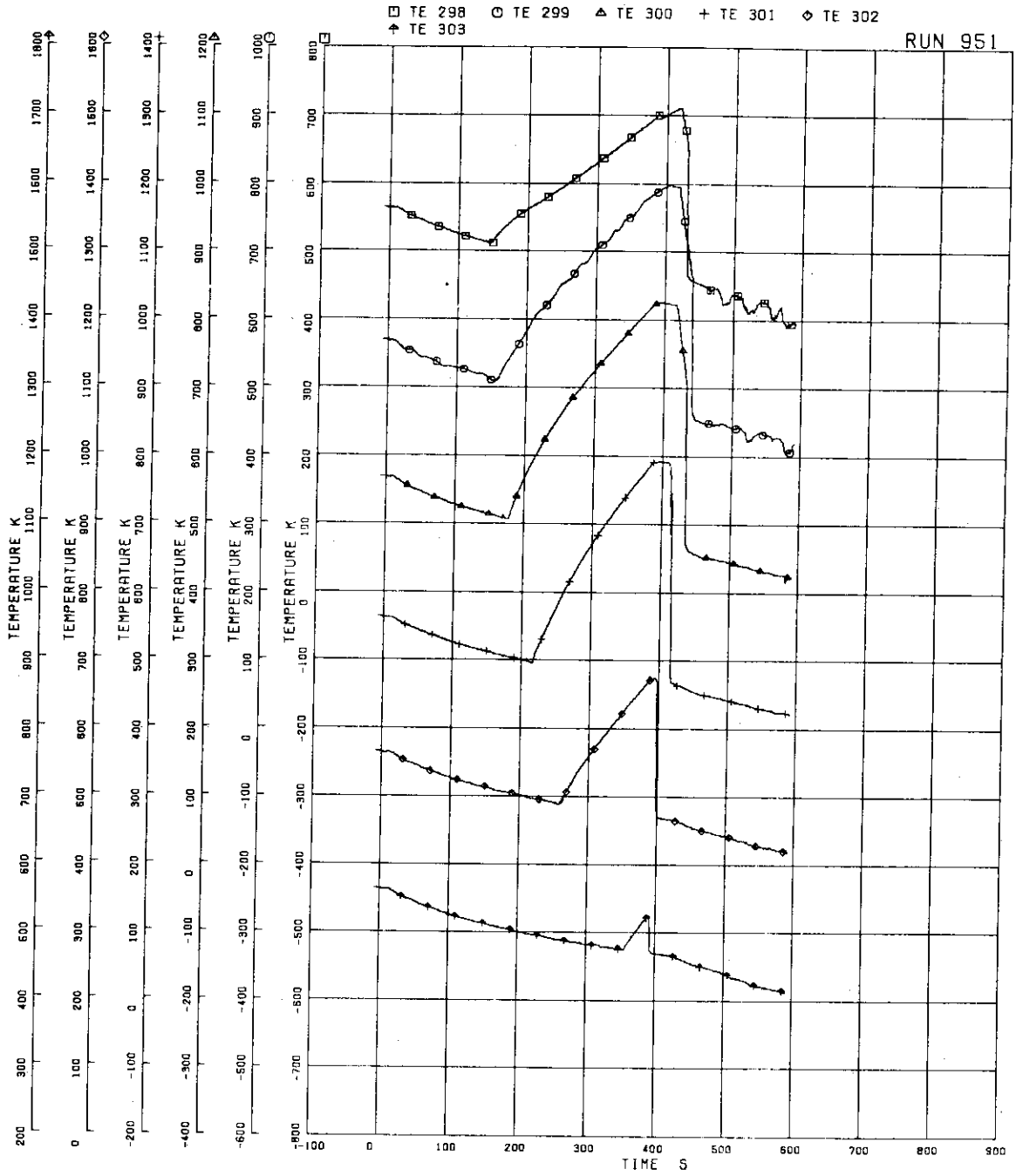

FIG.5. 59 FUEL ROD SURFACE TEMPERATURE OF A77 ROD

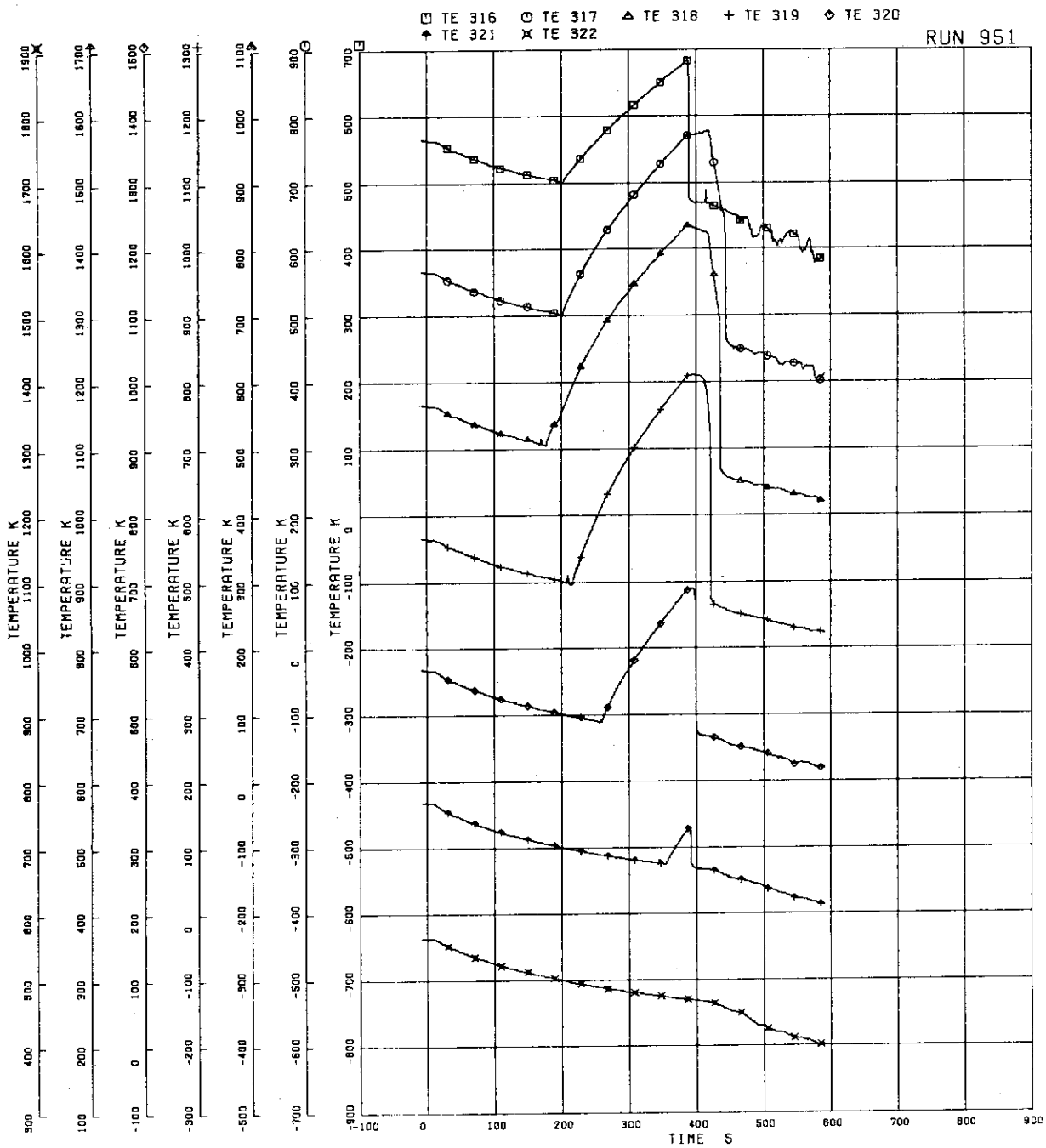

FIG.5. 60 FUEL ROD SURFACE TEMPERATURE OF A87 ROD

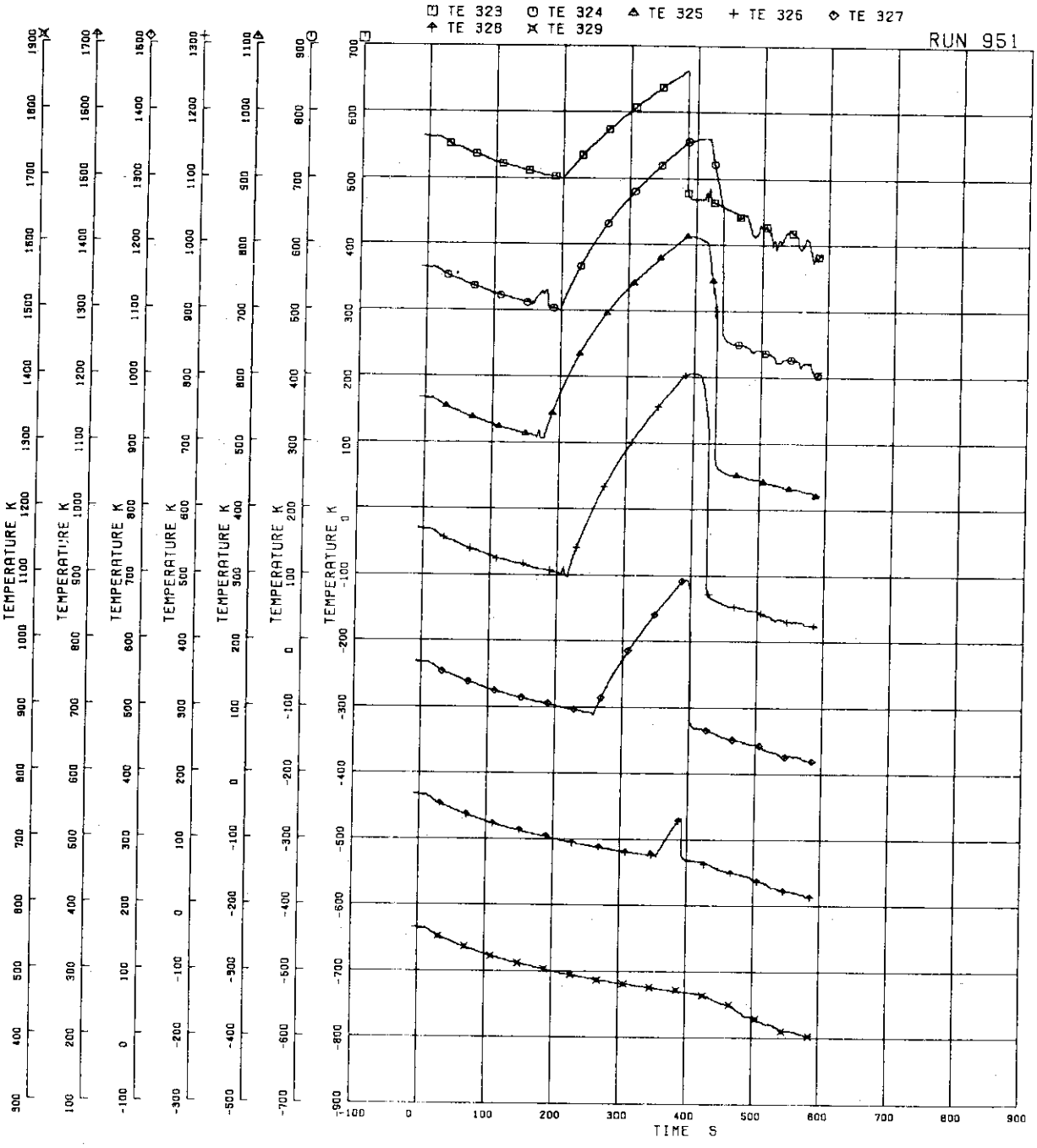

FIG.5. 61 FUEL ROD SURFACE TEMPERATURE OF A88 ROD

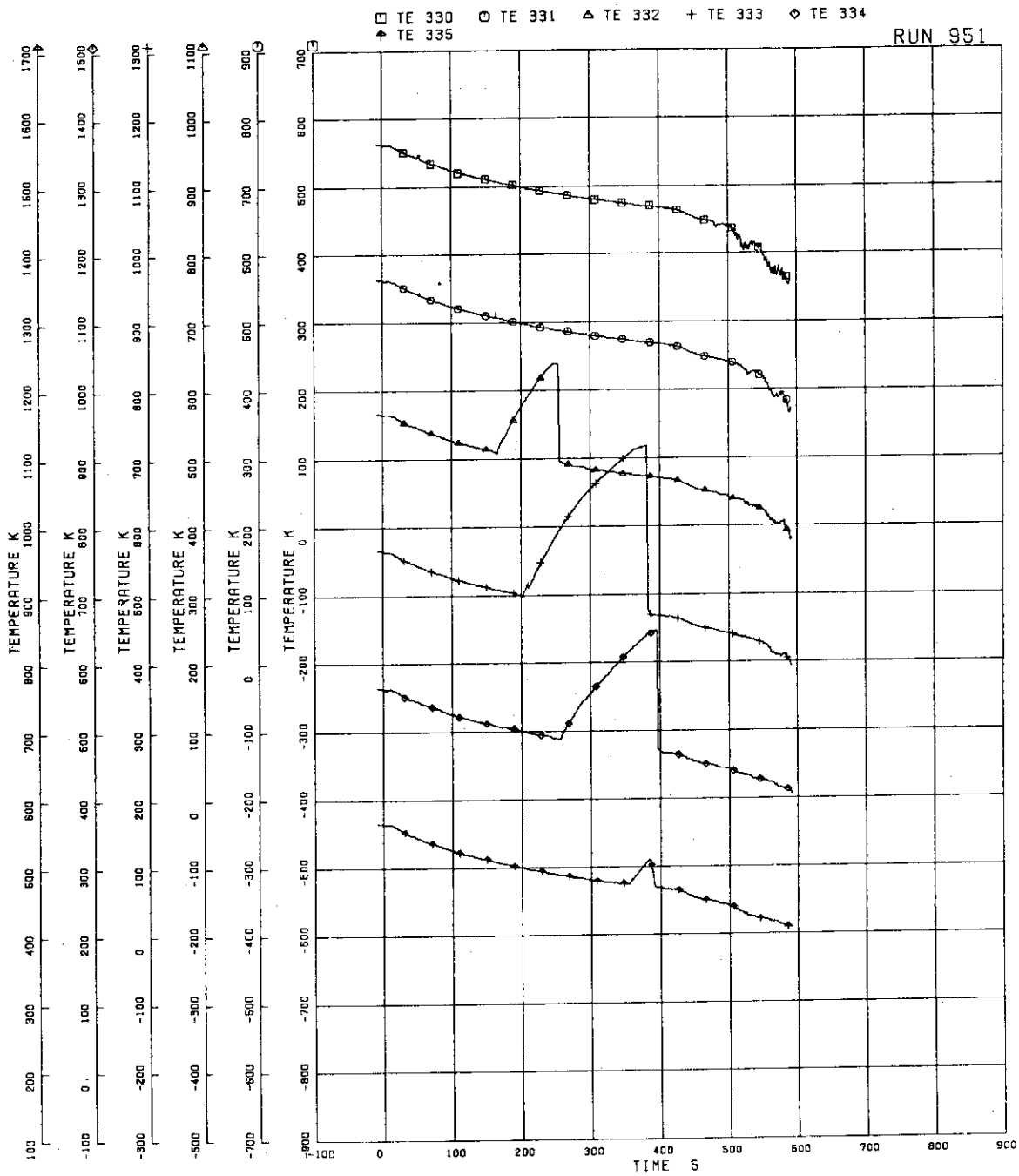

FIG.5. 62 FUEL ROD SURFACE TEMPERATURE OF B11 ROD

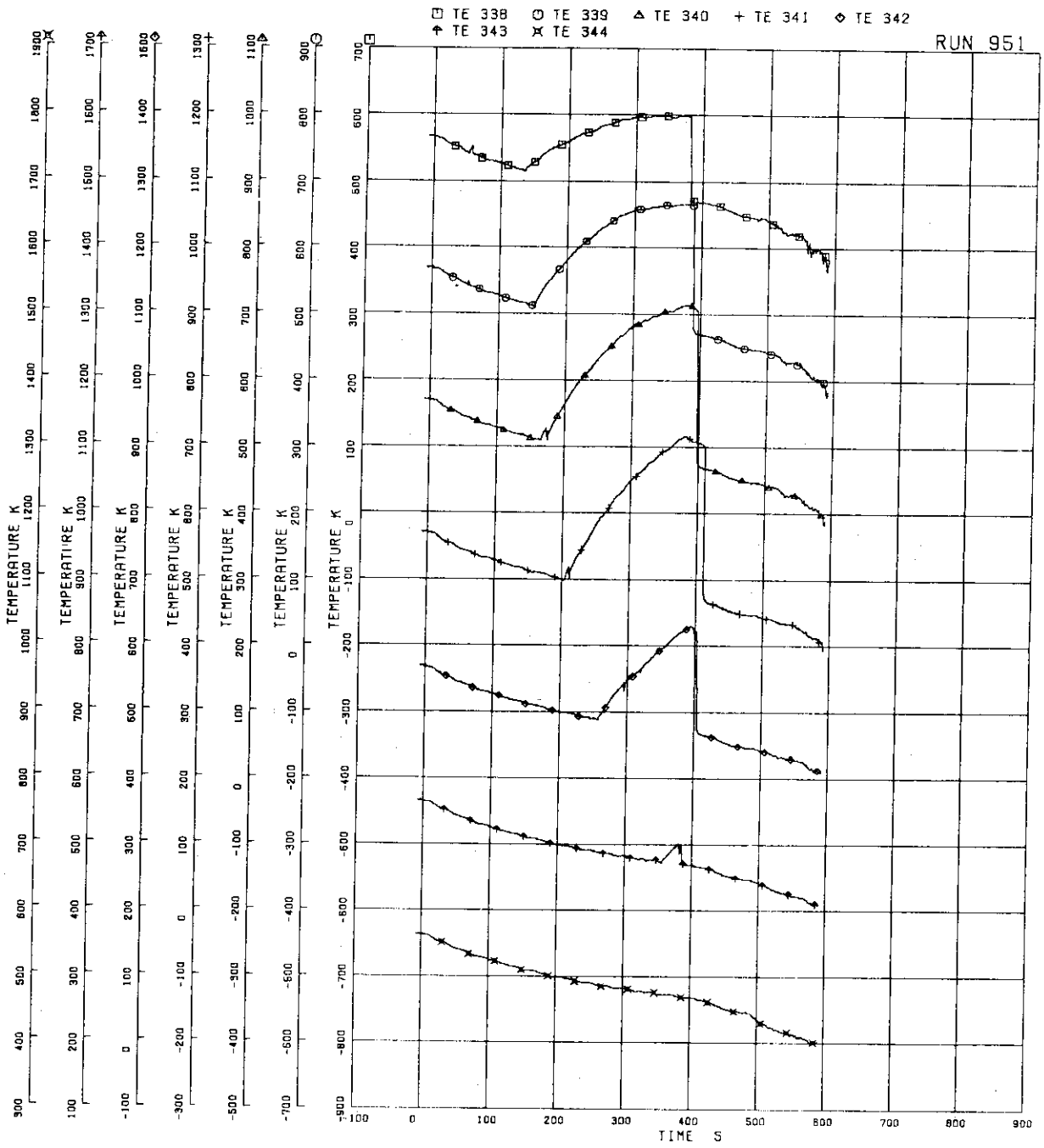

FIG.5. 63 FUEL ROD SURFACE TEMPERATURE OF B22 ROD

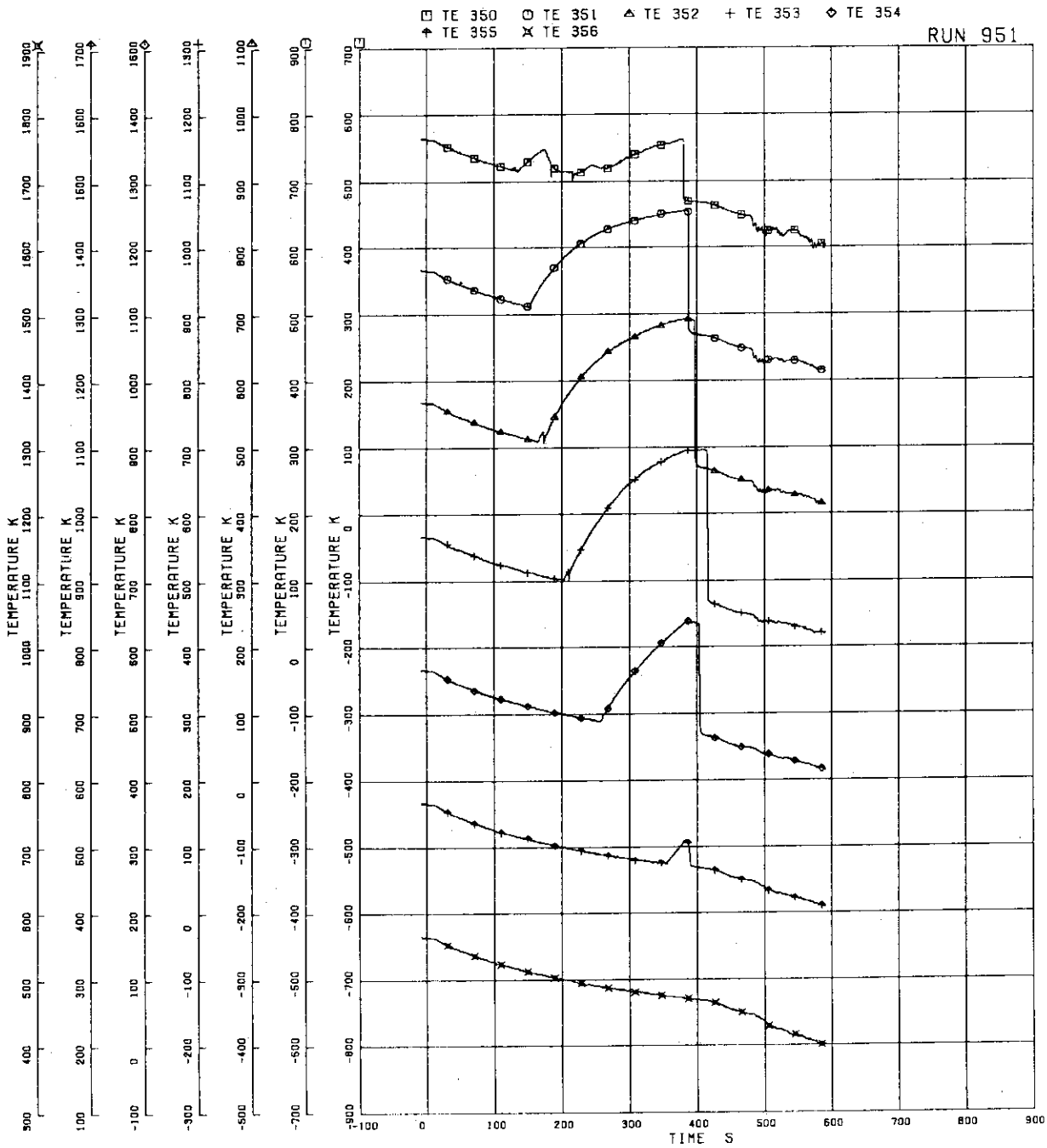

FIG.5. 64 FUEL ROD SURFACE TEMPERATURE OF B77 ROD

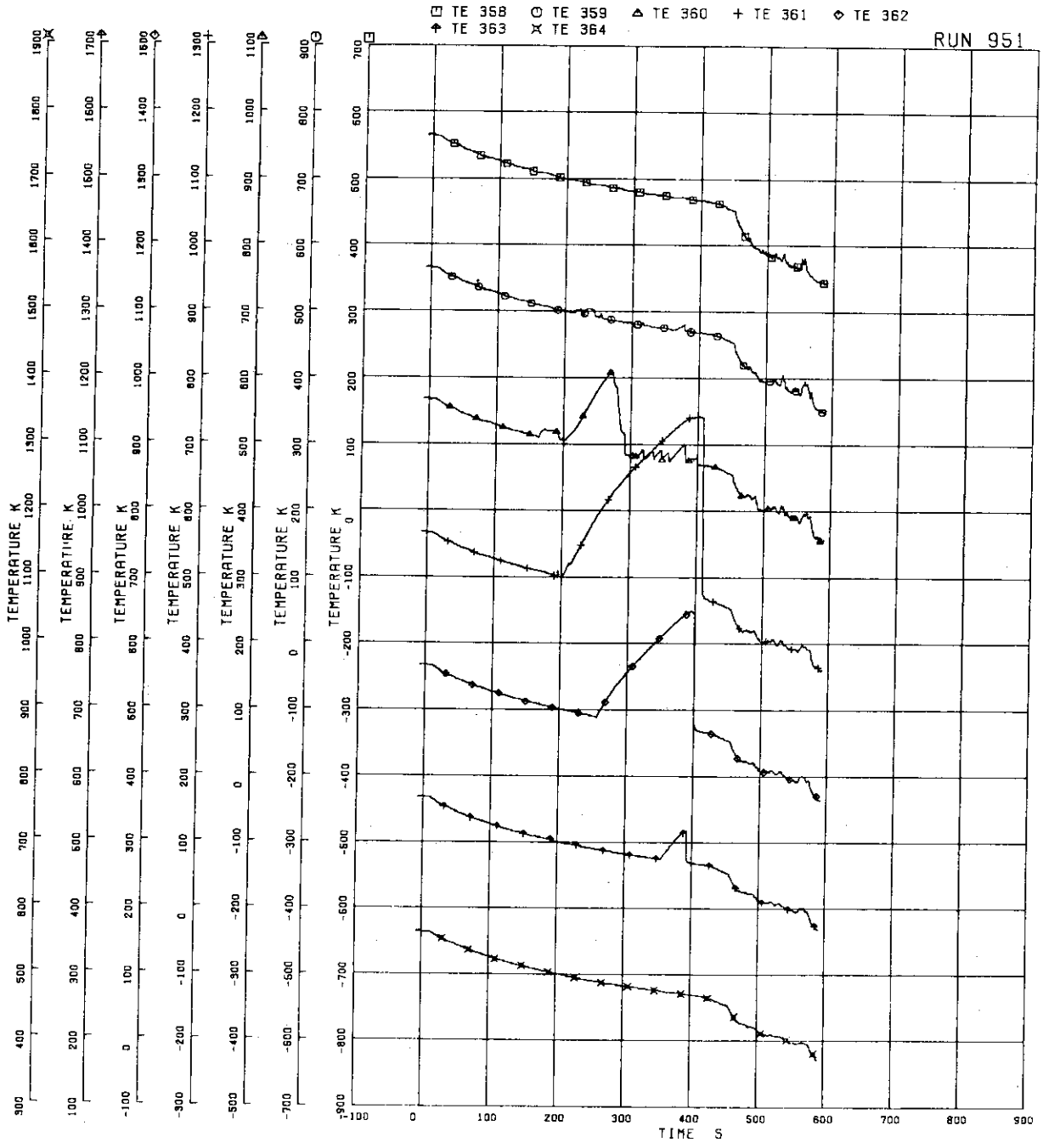

FIG.5. 65 FUEL ROD SURFACE TEMPERATURE OF C11 ROD

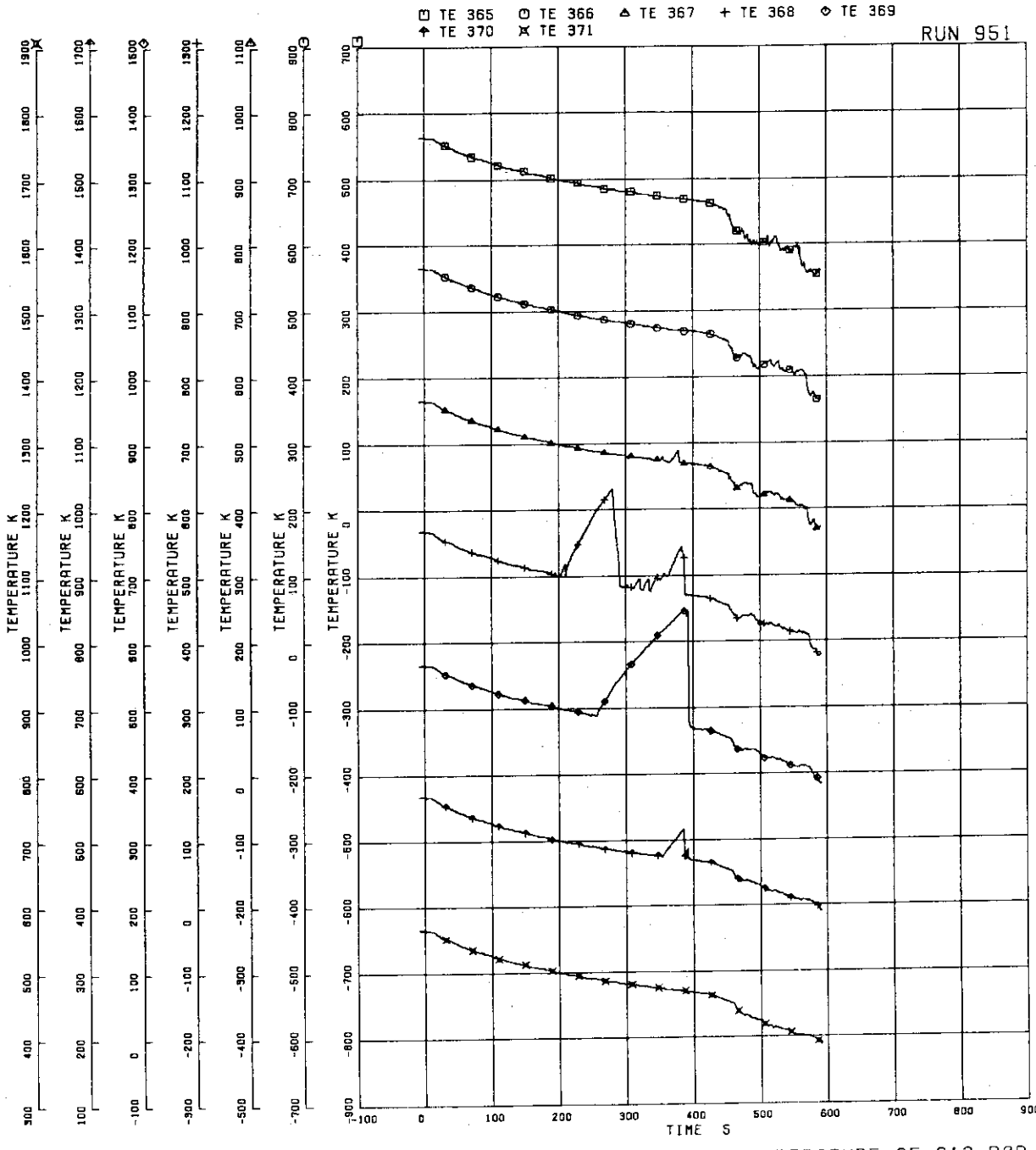

FIG.5. 66 FUEL ROD SURFACE TEMPERATURE OF C13 ROD

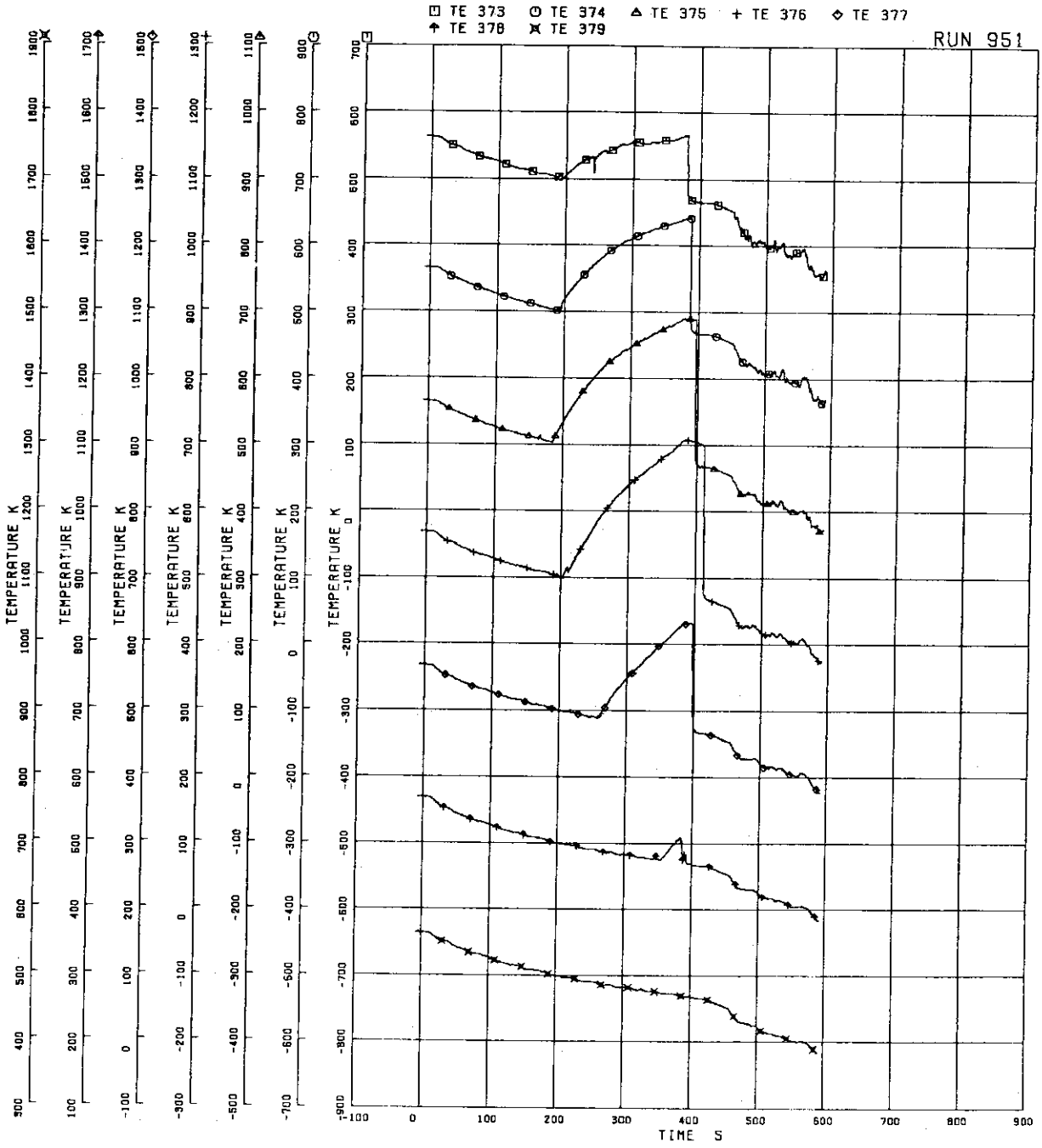

FIG.5. 67 FUEL ROD SURFACE TEMPERATURE OF C22 ROD

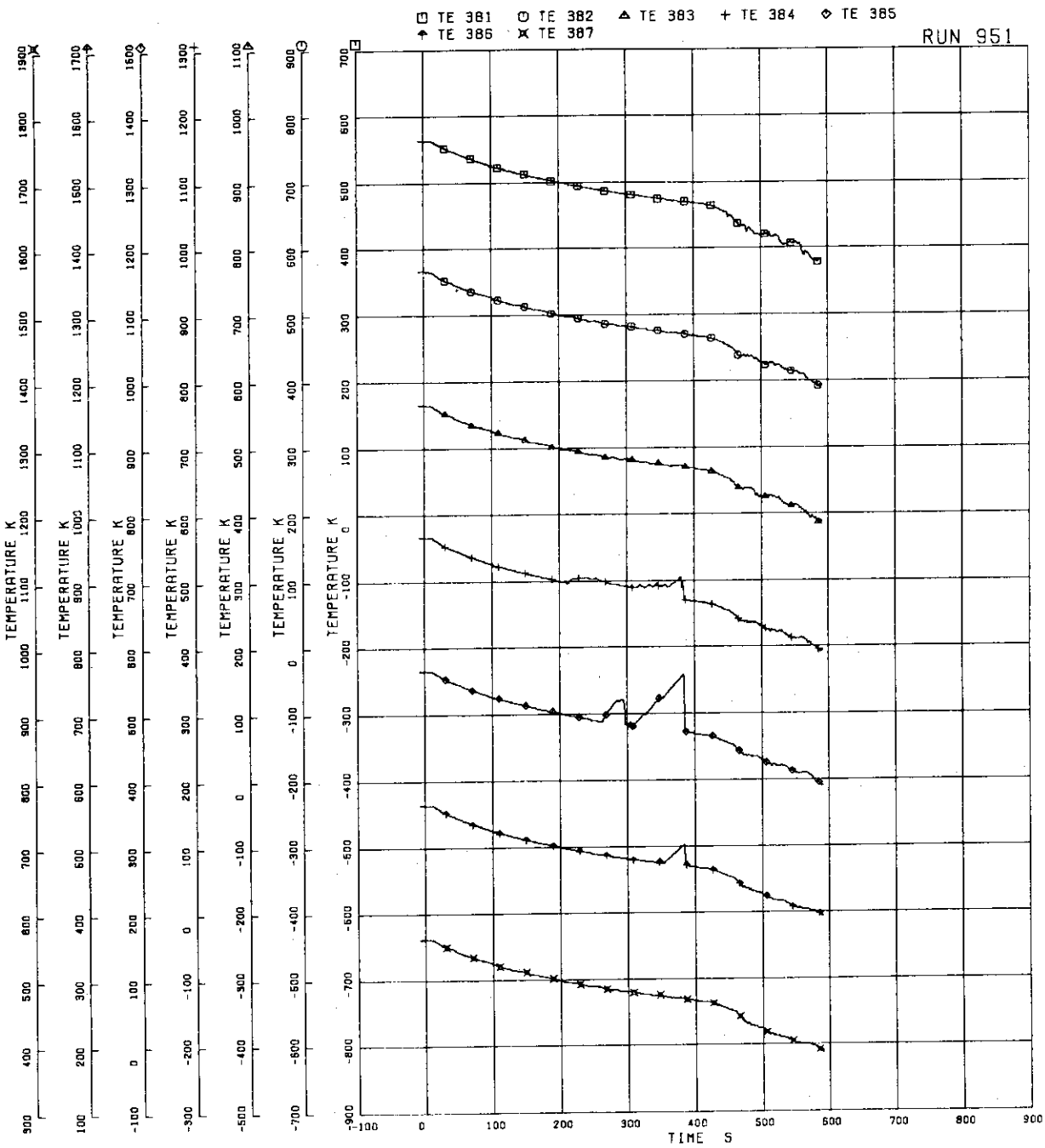

FIG.5. 68 FUEL ROD SURFACE TEMPERATURE OF C33 ROD

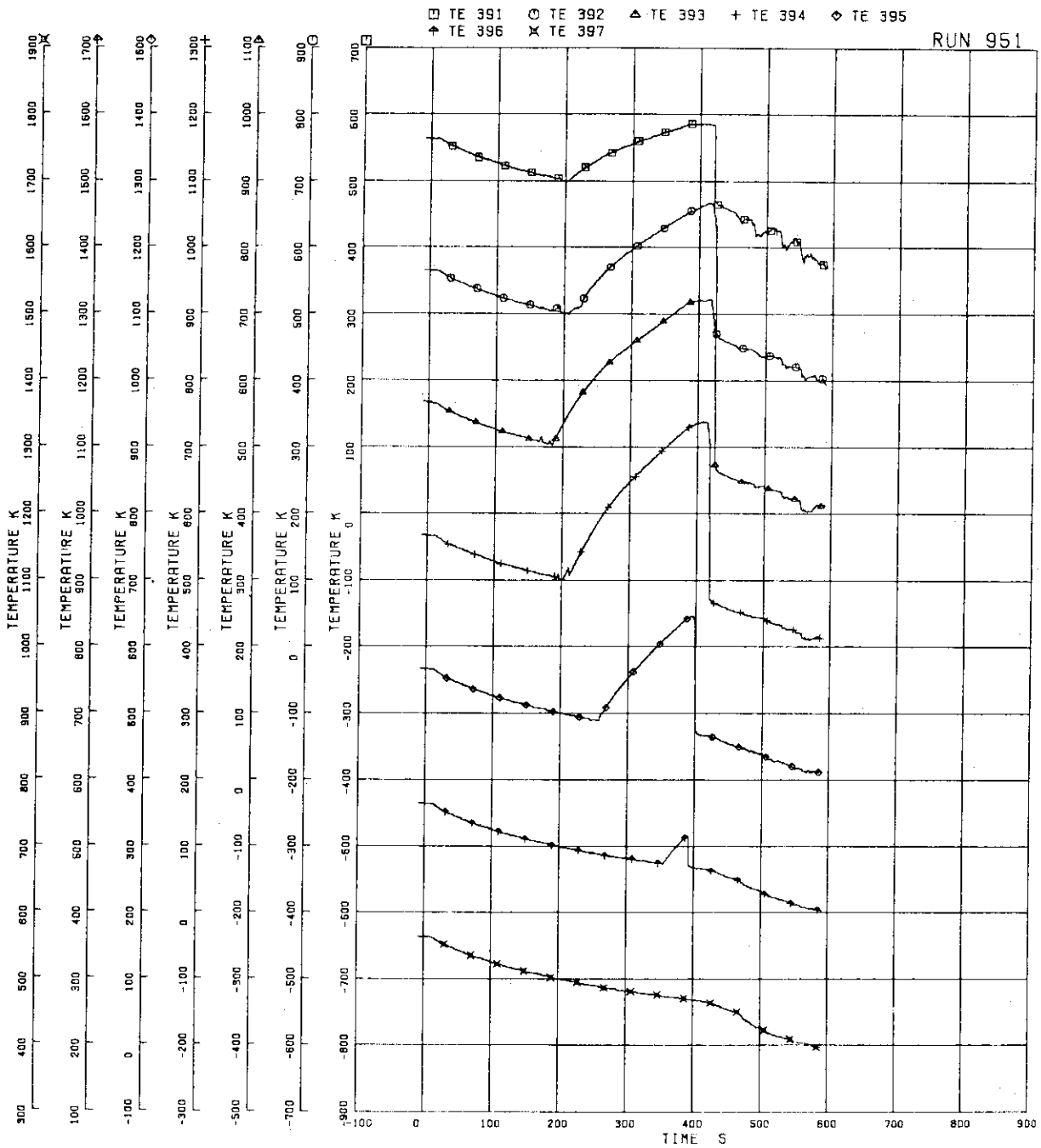

FIG.5. 69 FUEL ROD SURFACE TEMPERATURE OF C77 ROD

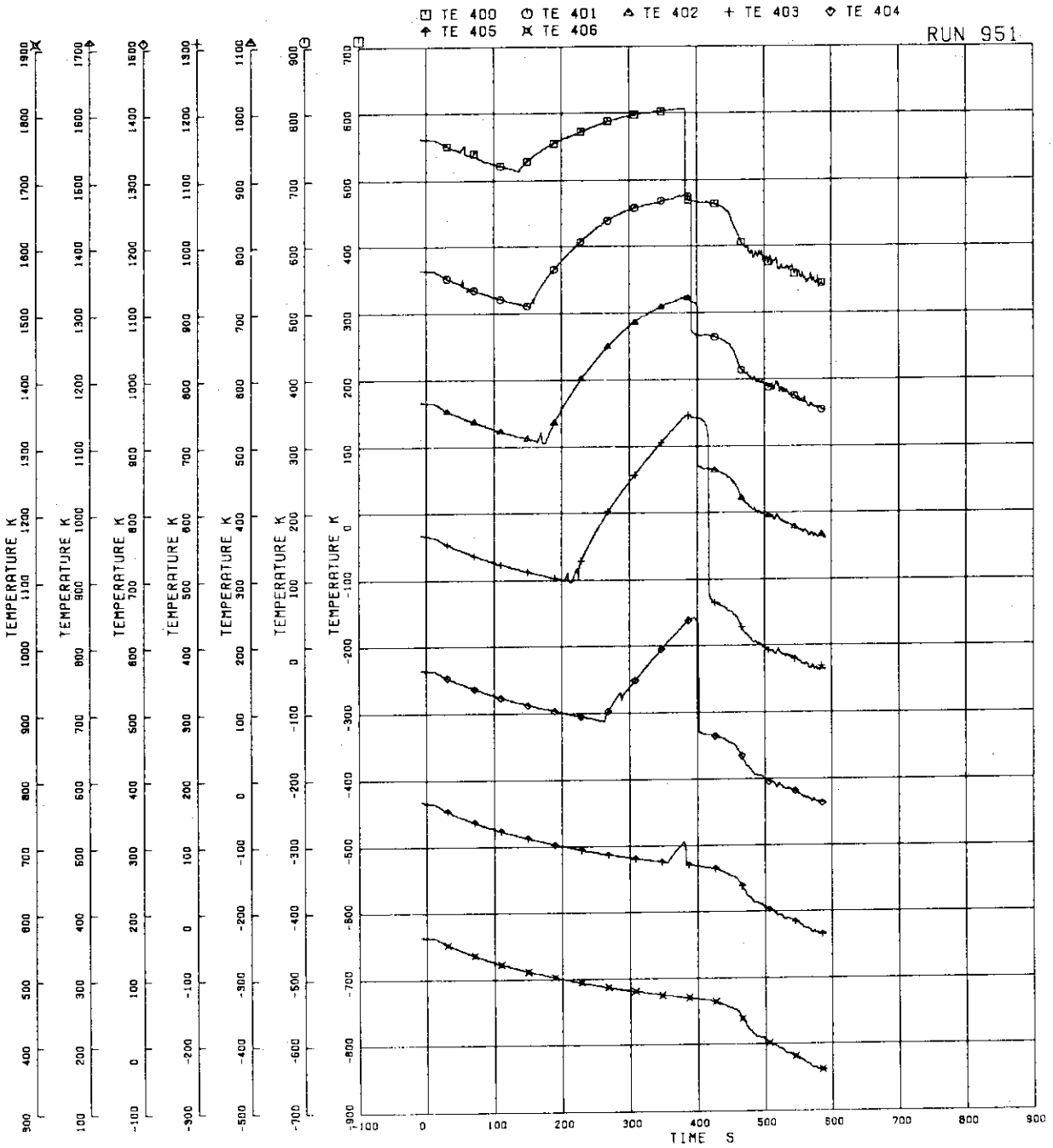

FIG.5. 70 FUEL ROD SURFACE TEMPERATURE OF D22 ROD

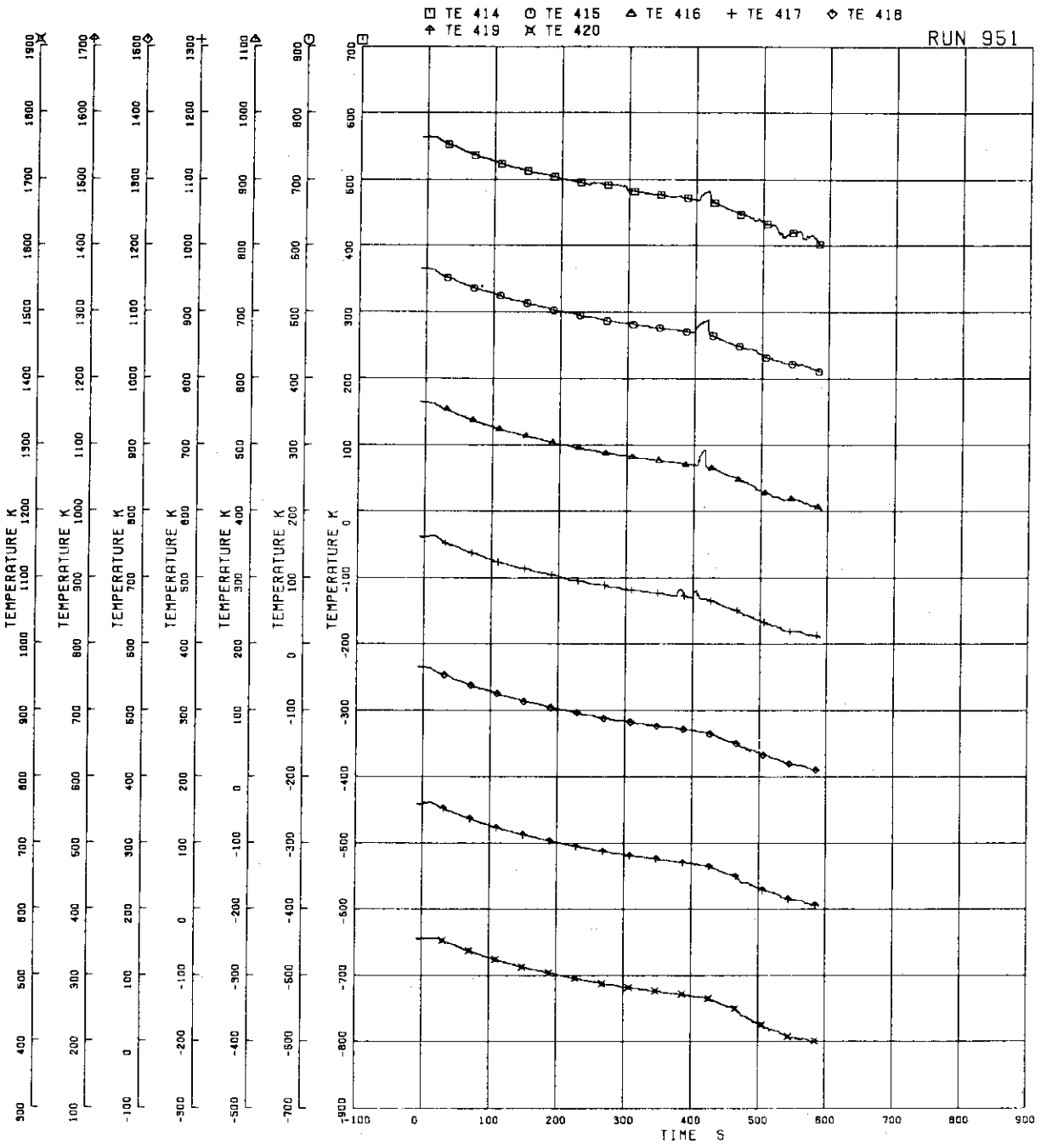

FIG.5. 71 SURFACE TEMPERATURE OF WATER ROD SIMULATOR A45

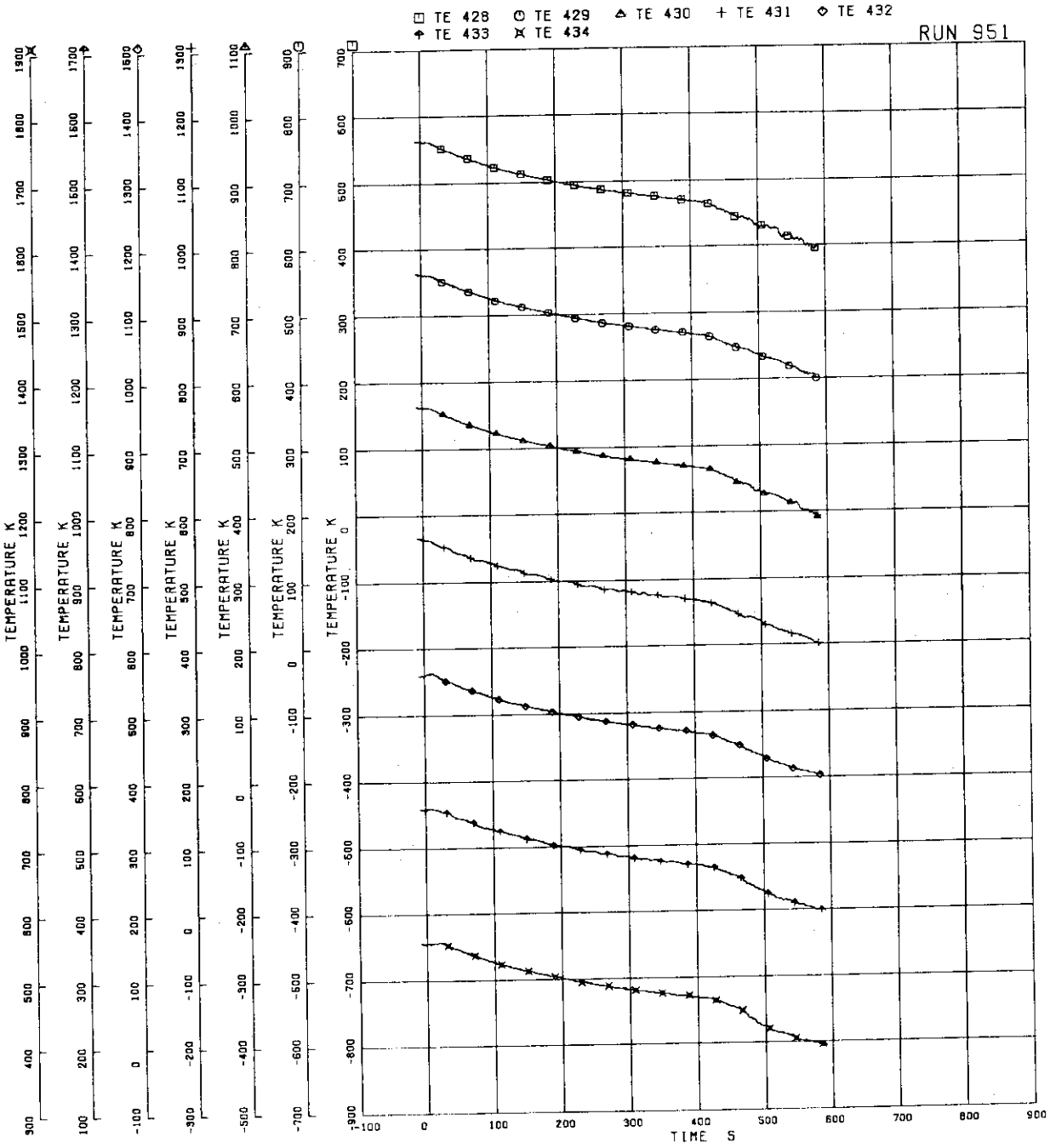

FIG.5. 72 SURFACE TEMPERATURE OF WATER ROD SIMULATOR C45

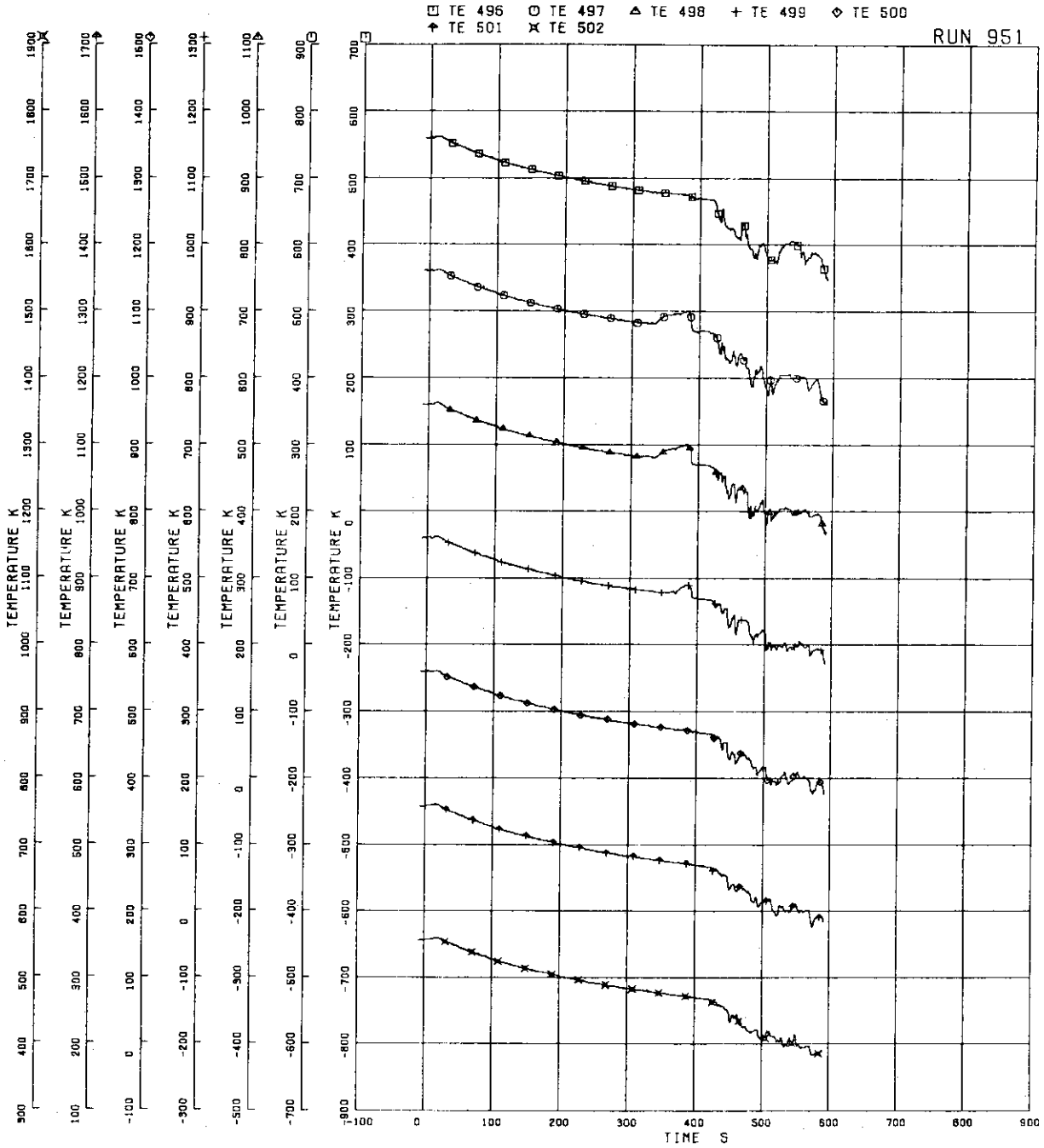

FIG.5. 73 INNER SURFACE TEMPERATURE OF CHANNEL BOX A, LOCATION A1

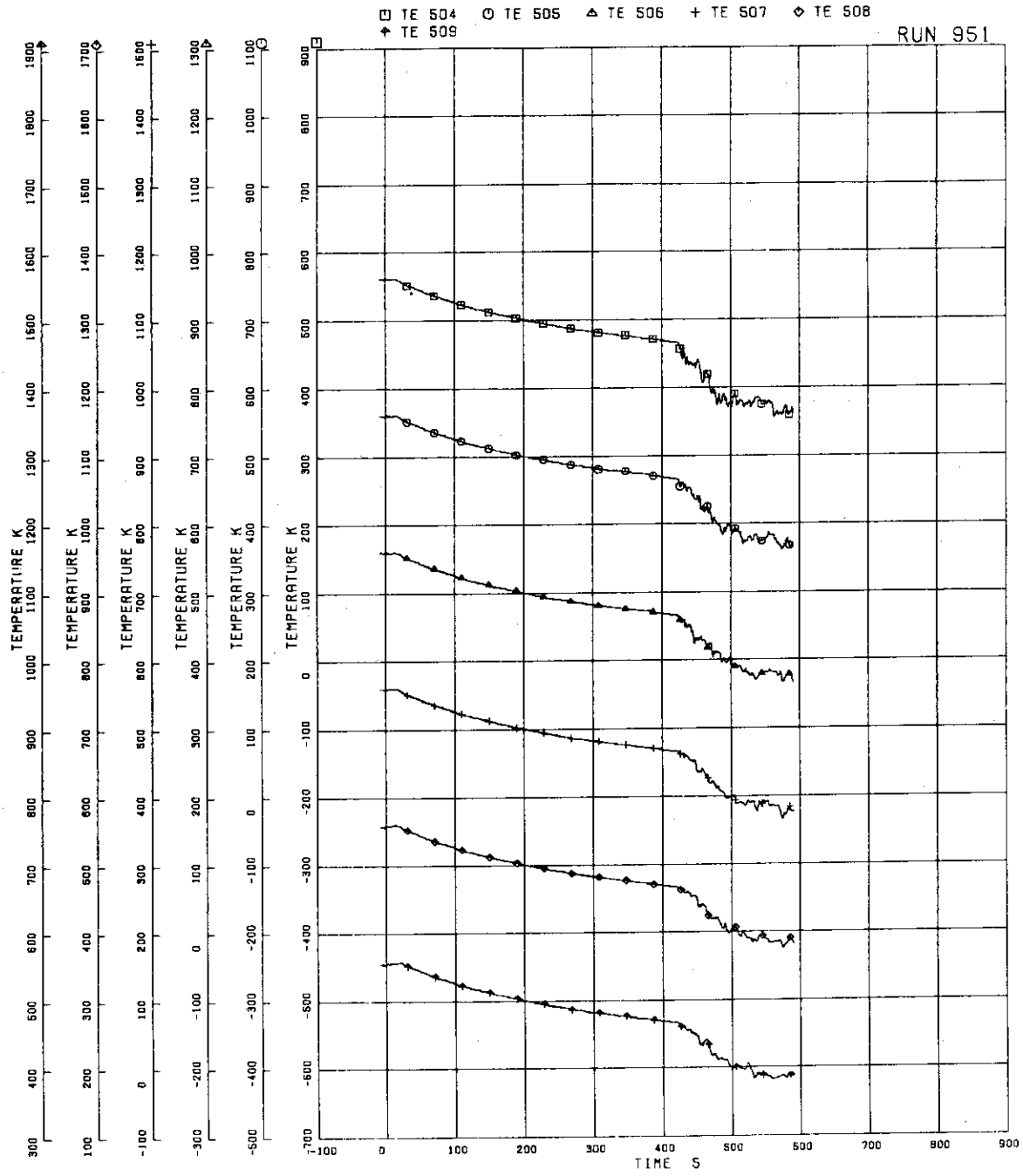

FIG.5. 74 INNER SURFACE TEMPERATURE OF CHANNEL BOX A, LOCATION A2

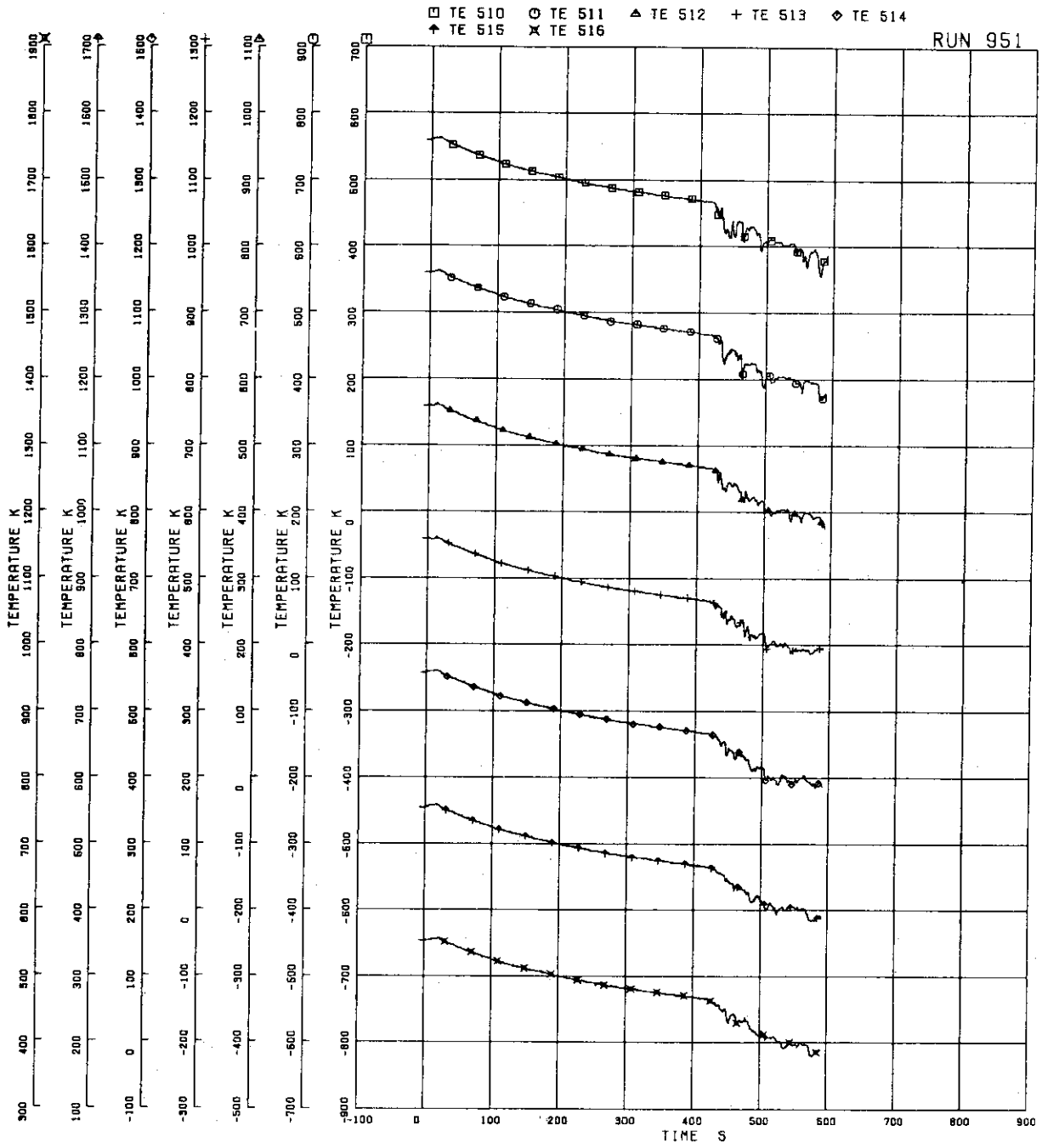

FIG.5. 75 INNER SURFACE TEMPERATURE OF CHANNEL BOX B

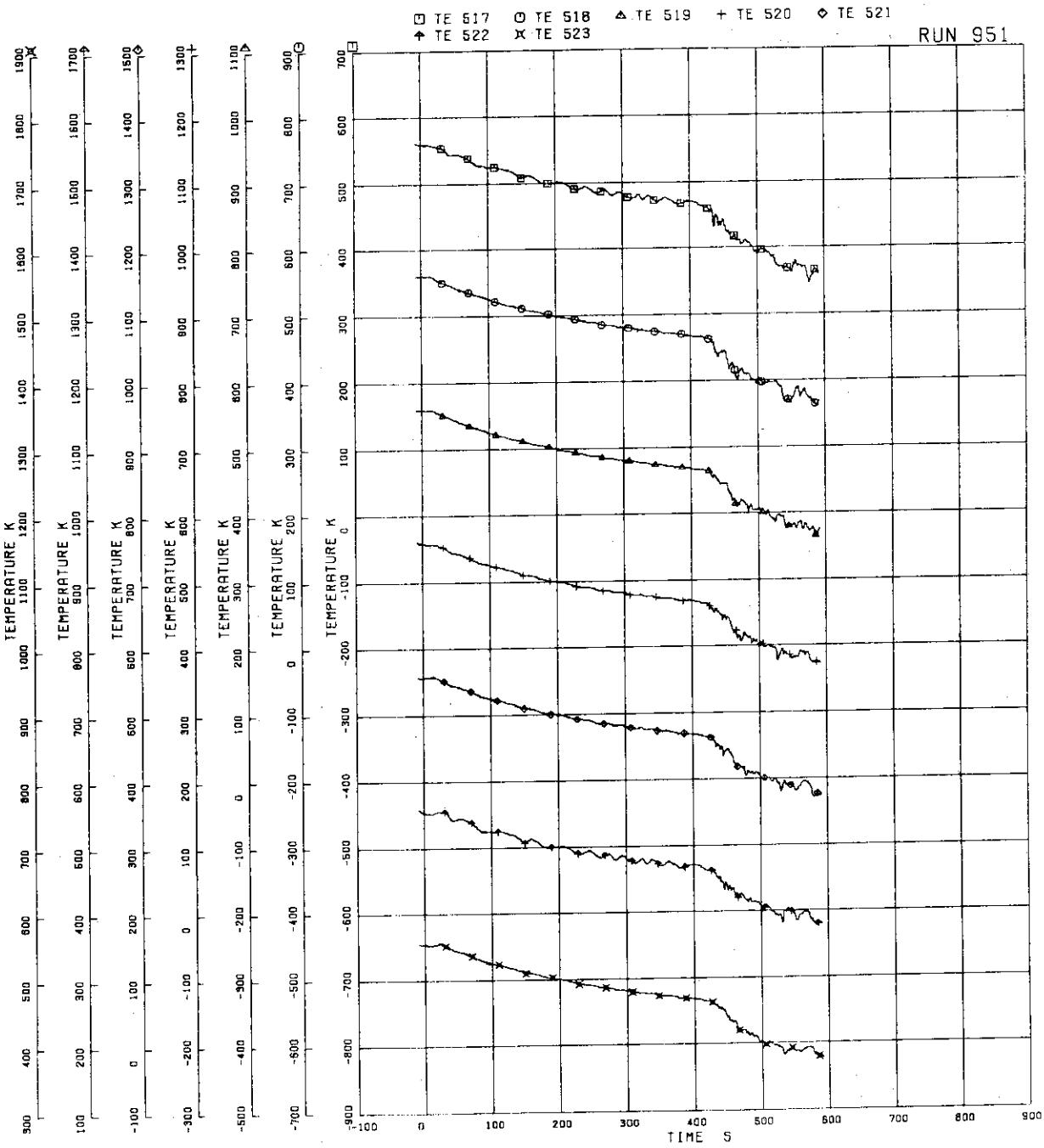

FIG.5. 76 INNER SURFACE TEMPERATURE OF CHANNEL BOX C

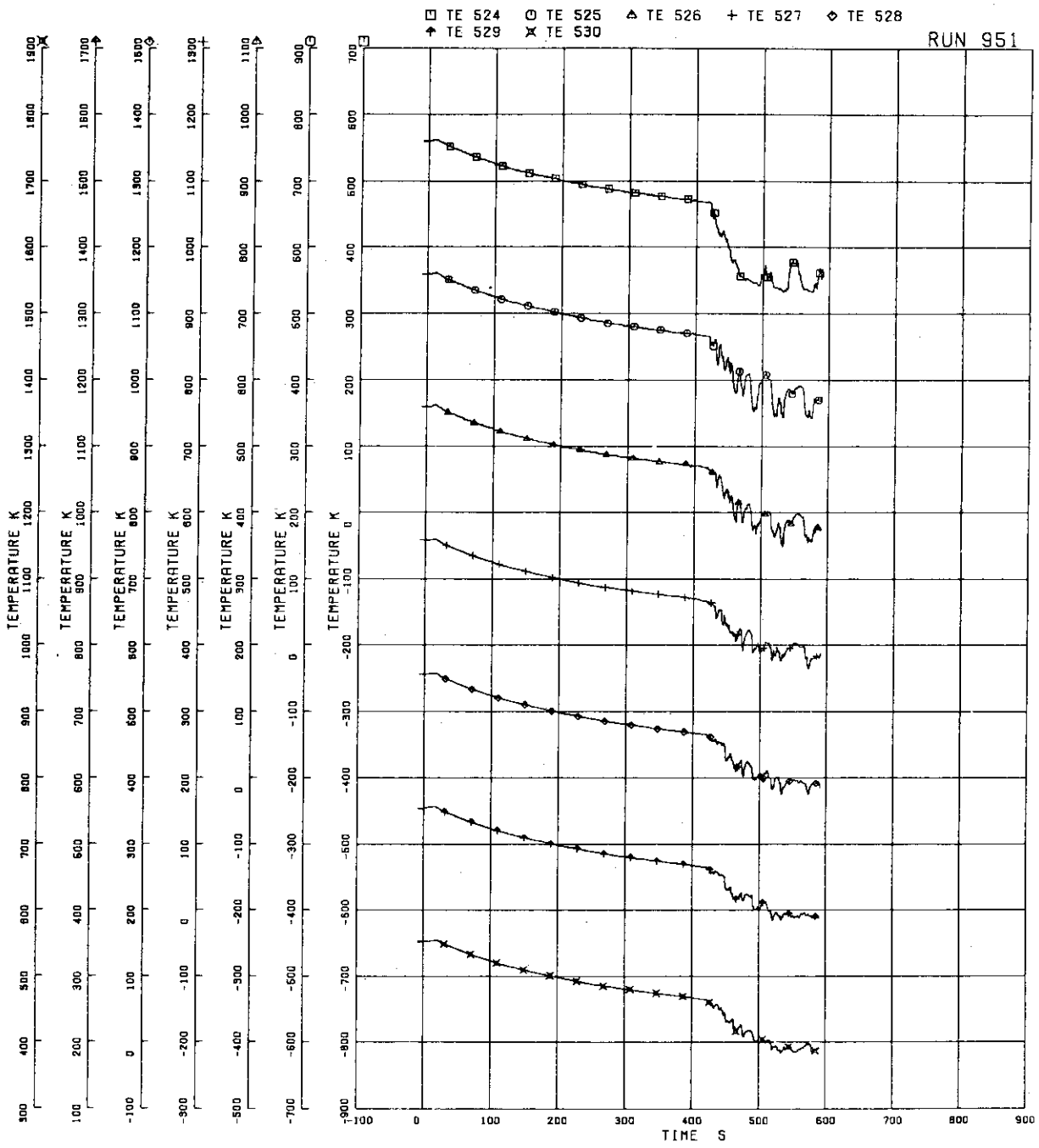

FIG.5. 77 INNER SURFACE TEMPERATURE OF CHANNEL BOX D

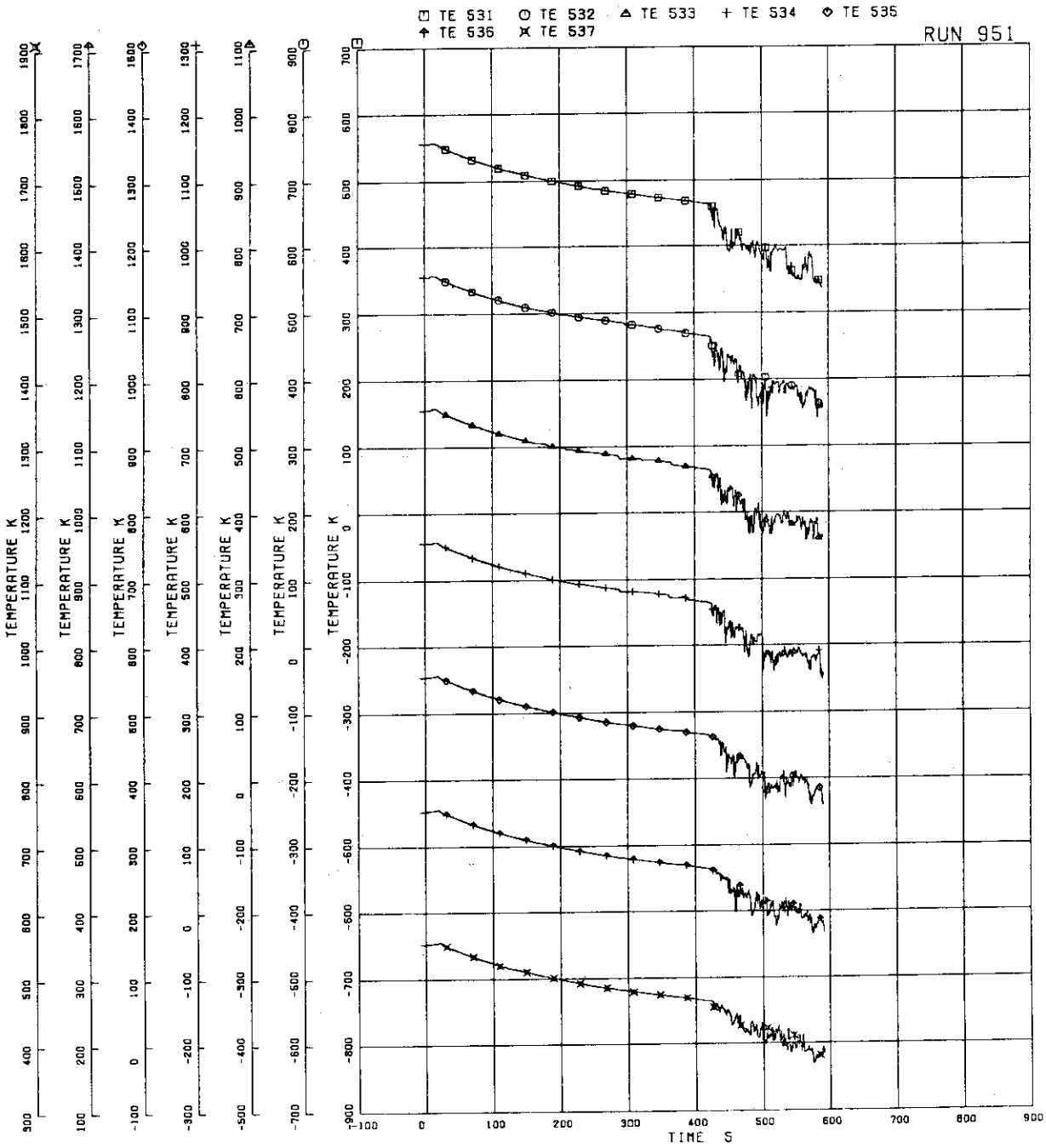

FIG.5. 78 OUTER SURFACE TEMPERATURE OF CHANNEL BOX A

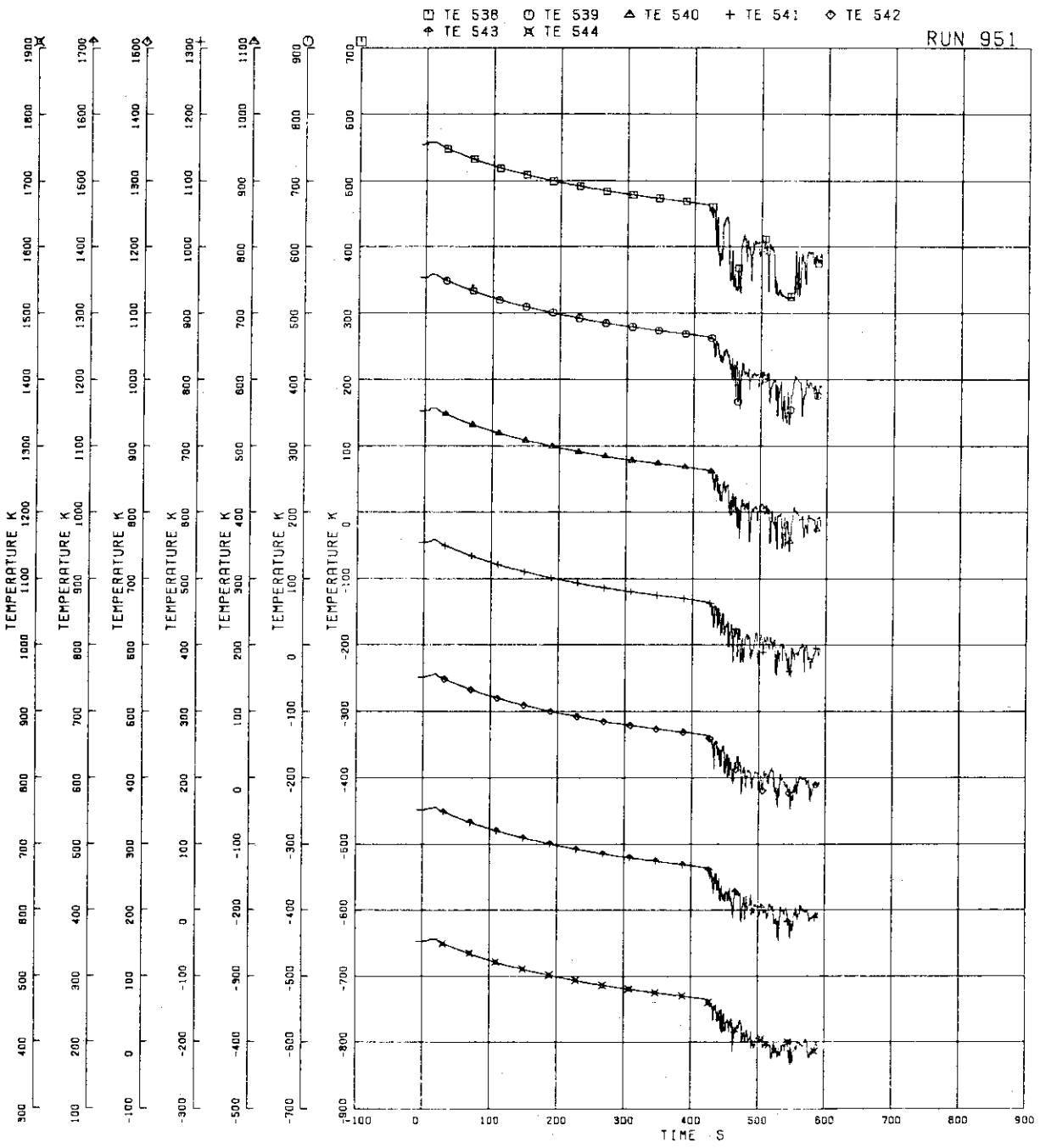

FIG.5. 79 OUTER SURFACE TEMPERATURE OF CHANNEL BOX C

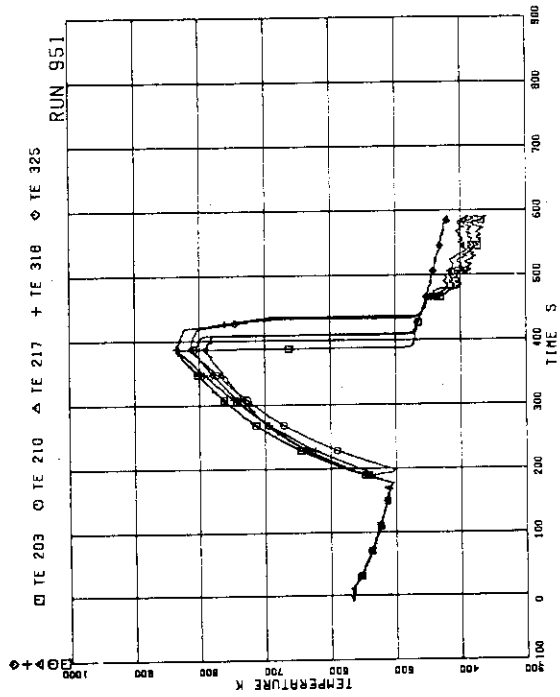

FIG.5. 82 FUEL ROD SURFACE TEMPERATURE OF A11,A12,A13,A87,A88 RODS AT POSITION 3

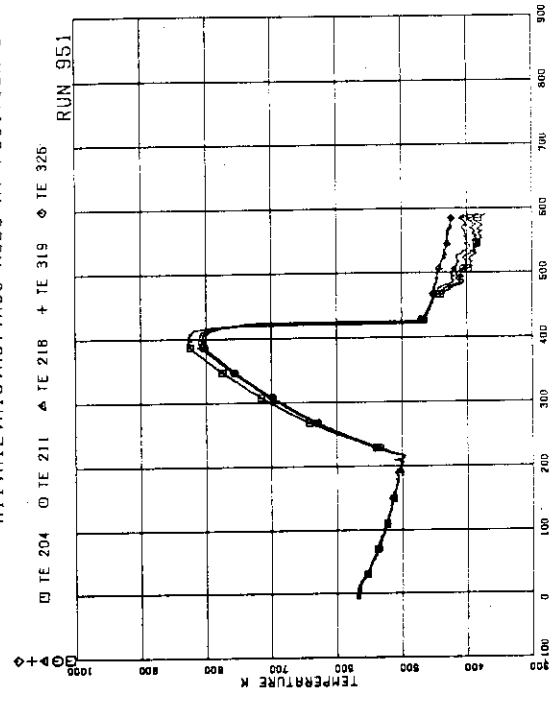

FIG.5. 83 FUEL ROD SURFACE TEMPERATURE OF A11,A12,A13,A87,A88 RODS AT POSITION 4

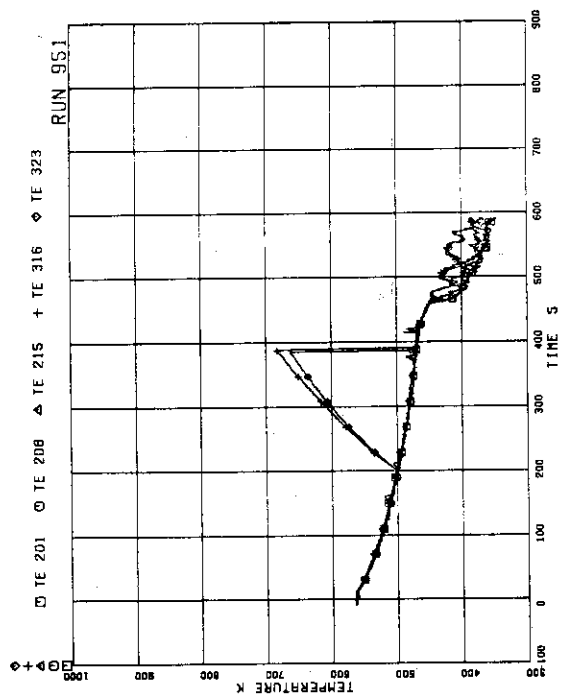

FIG.5. 80 FUEL ROD SURFACE TEMPERATURE OF A11,A12,A13,A87,A88 RODS AT POSITION 1

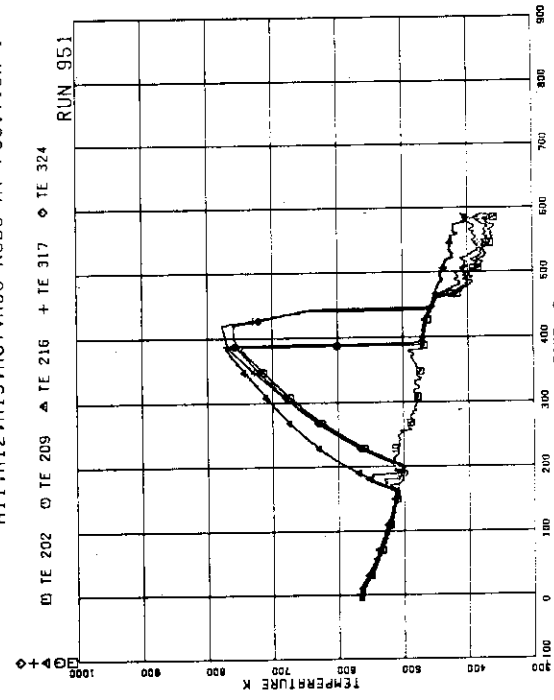

FIG.5. 81 FUEL ROD SURFACE TEMPERATURE OF A11,A12,A13,A87,A88 RODS AT POSITION 2

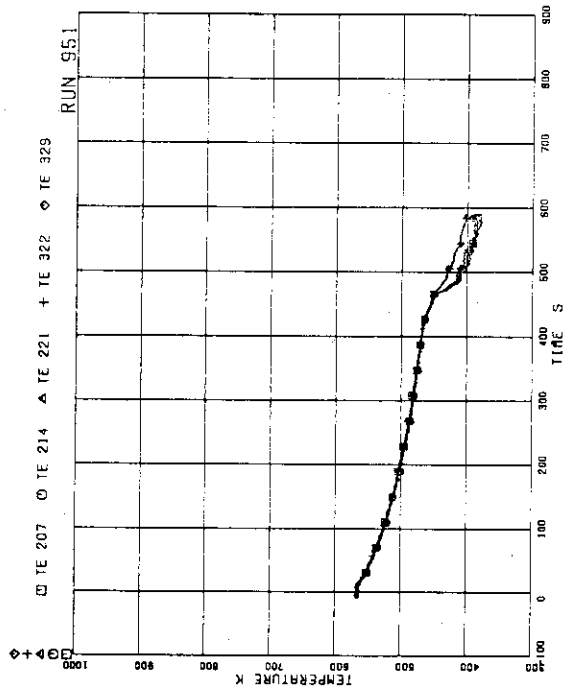

FIG.5. 86 FUEL ROD SURFACE TEMPERATURE OF A11,A12,A13,A87,A88 RODS AT POSITION 7

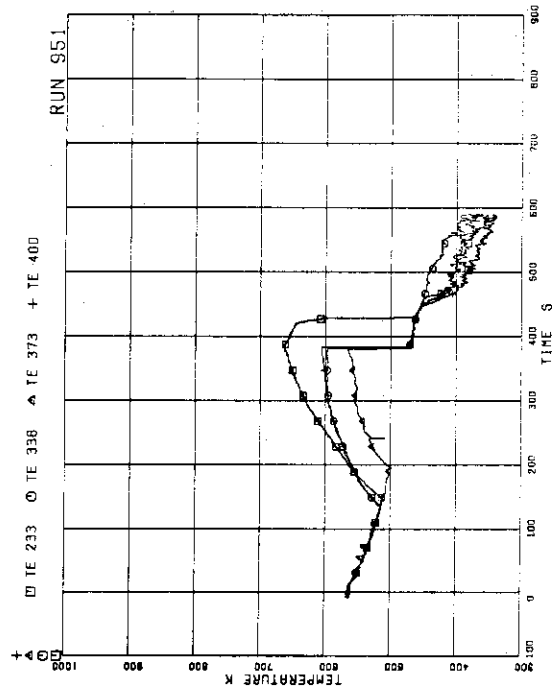

FIG.5. 87 FUEL ROD SURFACE TEMPERATURE OF A22,B22,C22,D22 RODS AT POSITION 1

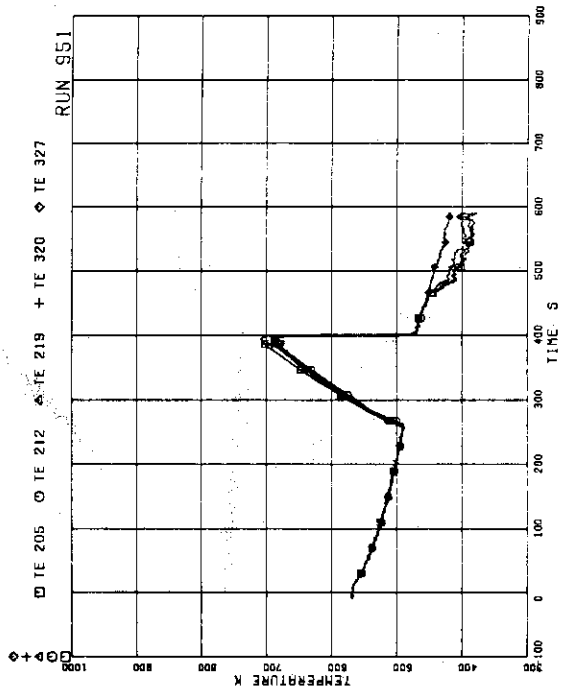

FIG.5. 84 FUEL ROD SURFACE TEMPERATURE OF A11,A12,A13,A87,A88 RODS AT POSITION 5

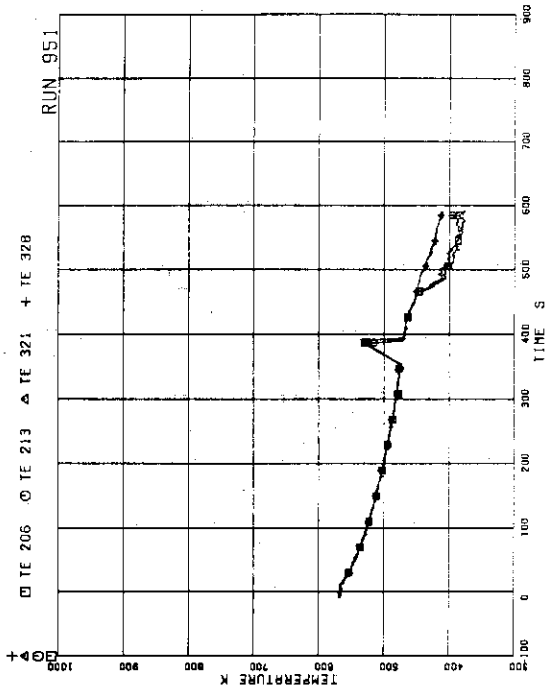

FIG.5. 85 FUEL ROD SURFACE TEMPERATURE OF A11,A12,A13,A87,A88 RODS AT POSITION 6

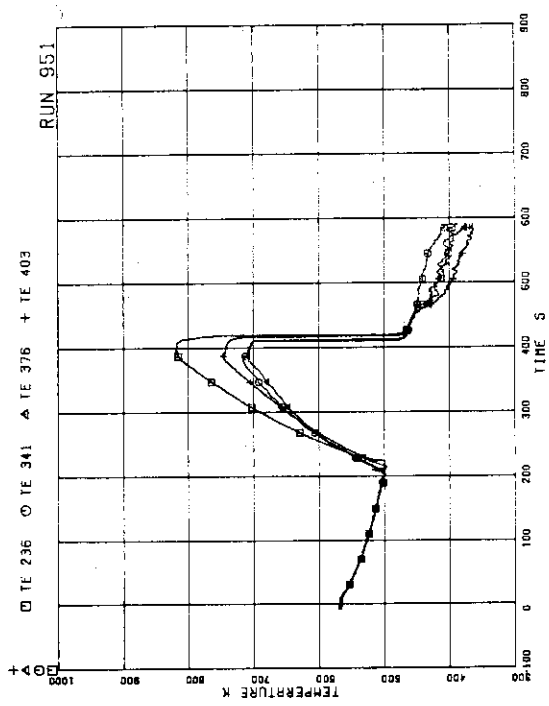

FIG.5. 90 FUEL ROD SURFACE TEMPERATURE OF A22.B22.C22.D22 RODS AT POSITION 4

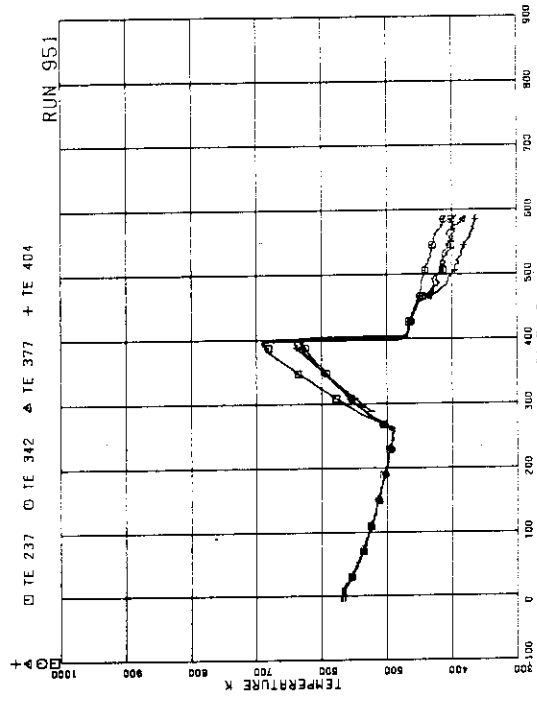

FIG.5. 91 FUEL ROD SURFACE TEMPERATURE OF A22.B22.C22.D22 RODS AT POSITION 5

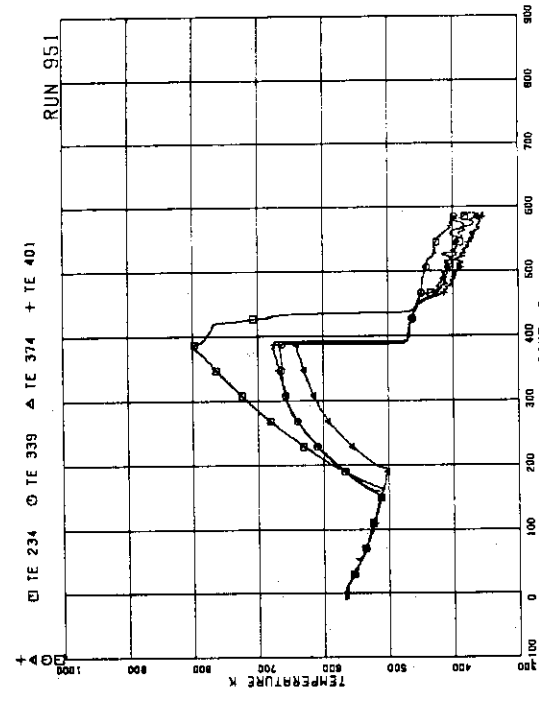

FIG.5. 88 FUEL ROD SURFACE TEMPERATURE OF A22.B22.C22.D22 RODS AT POSITION 2

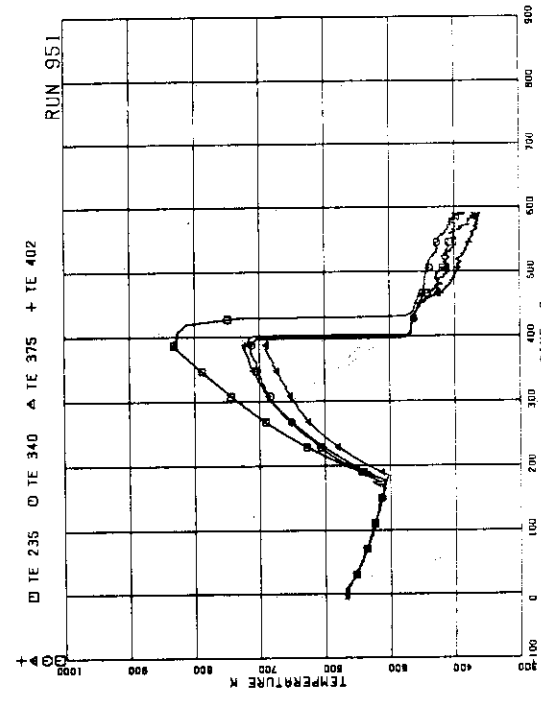

FIG.5. 89 FUEL ROD SURFACE TEMPERATURE OF A22.B22.C22.D22 RODS AT POSITION 3

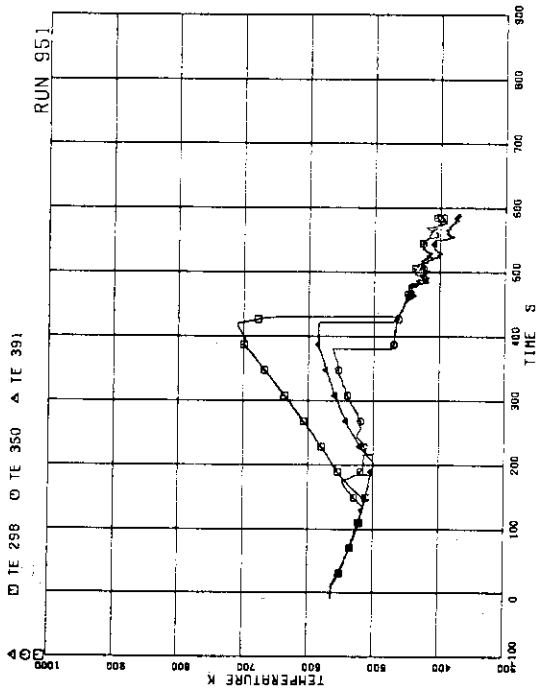

FIG.5. 94 FUEL ROD SURFACE TEMPERATURE OF A77,B77,C77 RODS AT POSITION 1

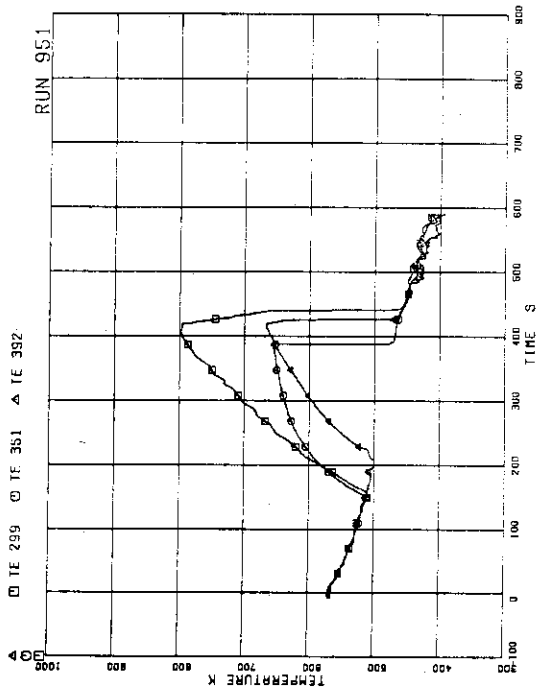

FIG.5. 95 FUEL ROD SURFACE TEMPERATURE OF A77,B77,C77 RODS AT POSITION 2

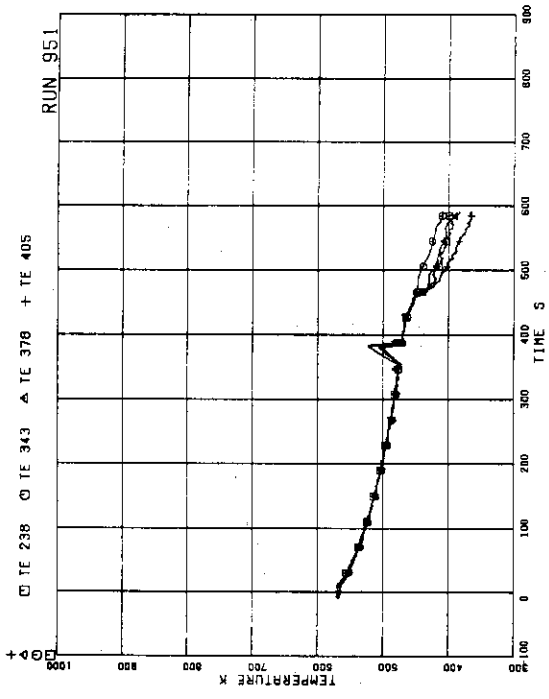

FIG.5. 92 FUEL ROD SURFACE TEMPERATURE OF A22,B22,C22,D22 RODS AT POSITION 6

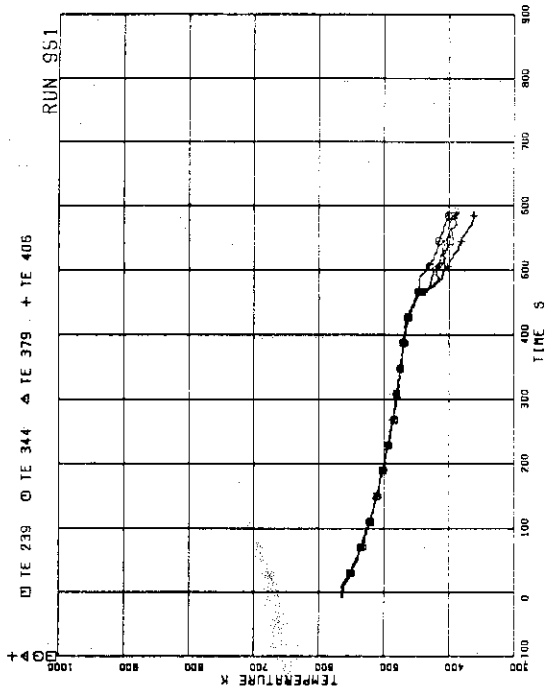

FIG.5. 93 FULL ROD SURFACE TEMPERATURE OF A22,B22,C22,D22 RODS AT POSITION 7

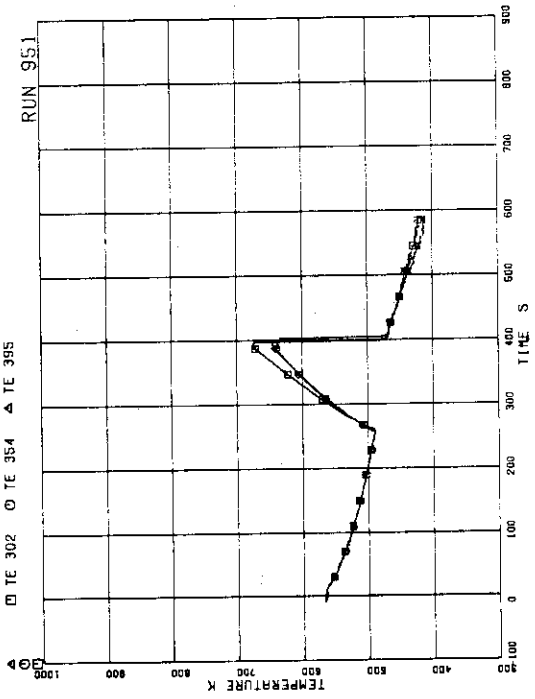

FIG.5. 98 FUEL ROD SURFACE TEMPERATURE OF A77,B77,C77 RODS AT POSITION 5

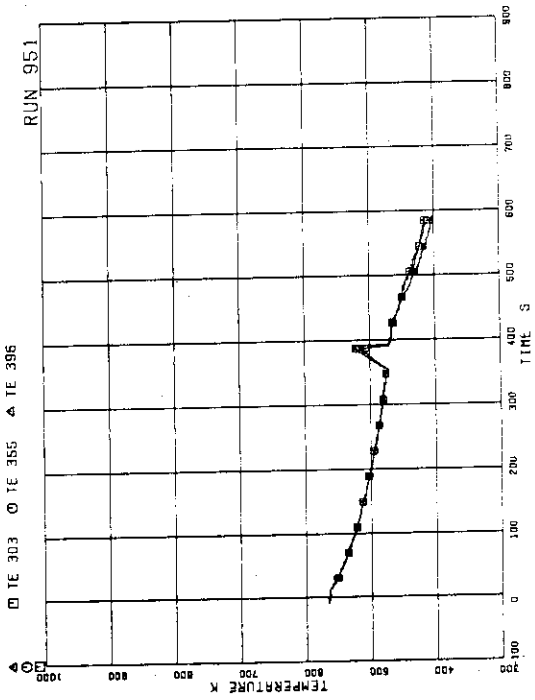

FIG.5. 99 FUEL ROD SURFACE TEMPERATURE OF A77,B77,C77 RODS AT POSITION 6

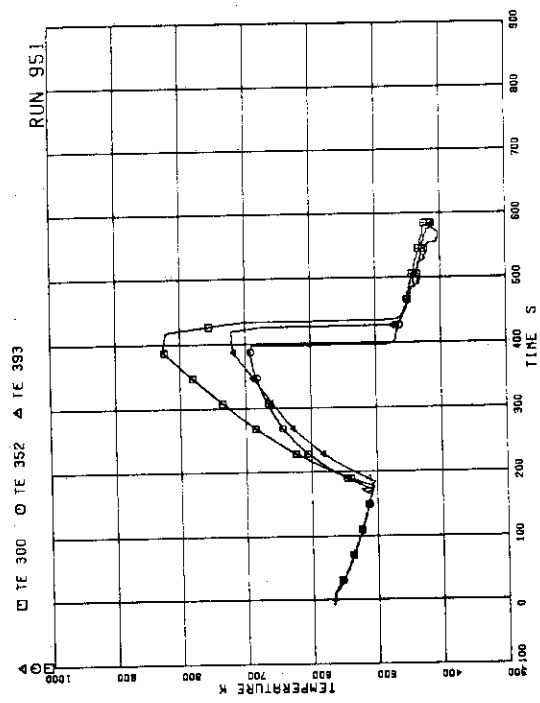

FIG.5. 96 FUEL ROD SURFACE TEMPERATURE OF A77,B77,C77 RODS AT POSITION 3

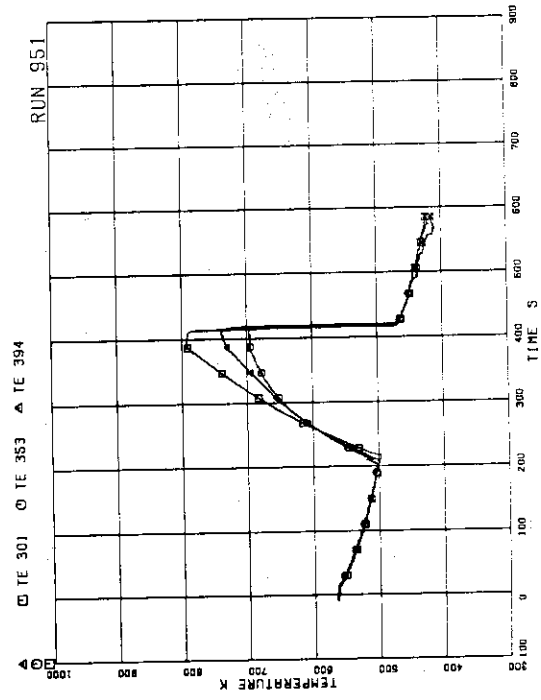

FIG.5. 97 FUEL ROD SURFACE TEMPERATURE OF A77,B77,C77 RODS AT POSITION 4

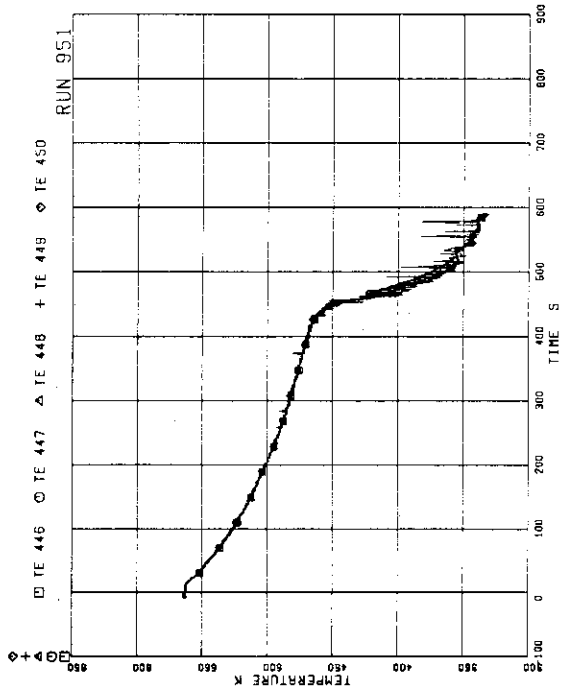

FIG.5.102 FLUID TEMPERATURE AT CHANNEL A OUTLET

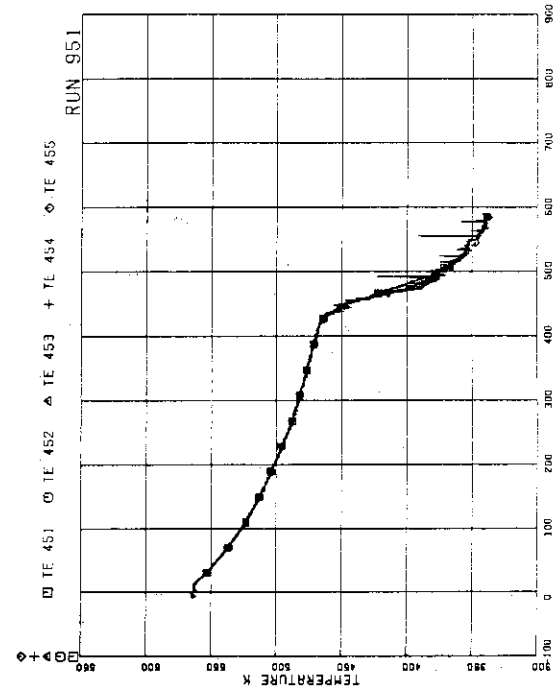

FIG.5.103 FLUID TEMPERATURE AT CHANNEL C OUTLET

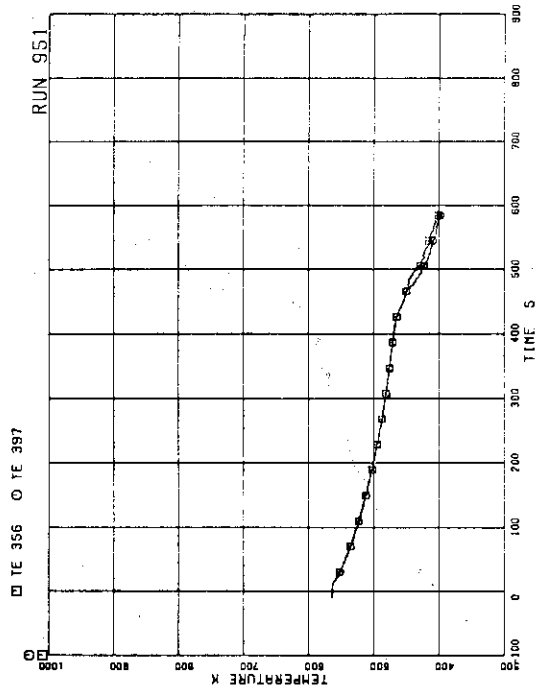

FIG.5.100 FUEL ROD SURFACE TEMPERATURE OF B77.C77 RODS AT POSITION 7

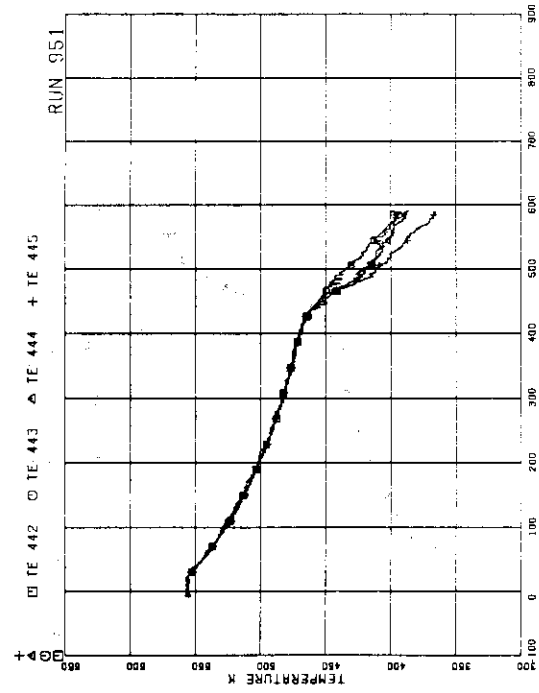

FIG.5.101 FLUID TEMPERATURE AT CHANNEL INLET

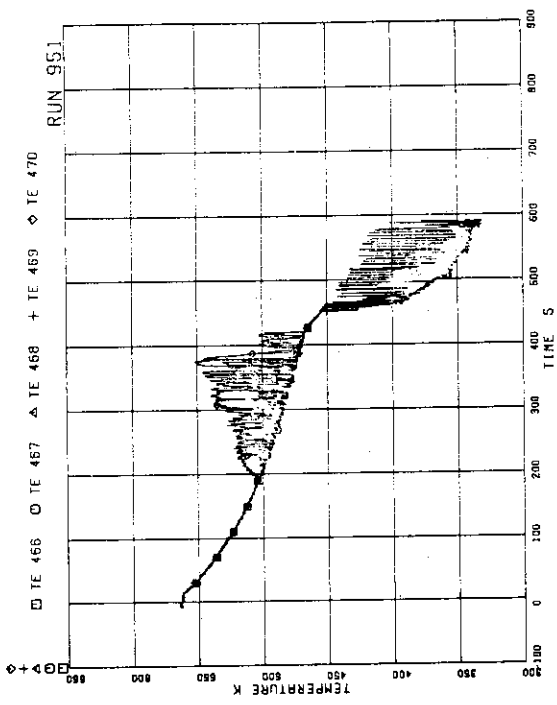

FIG.5.104 FLUID TEMPERATURE ABOVE UTP OF CHANNEL A, OPENINGS 1 TO 5

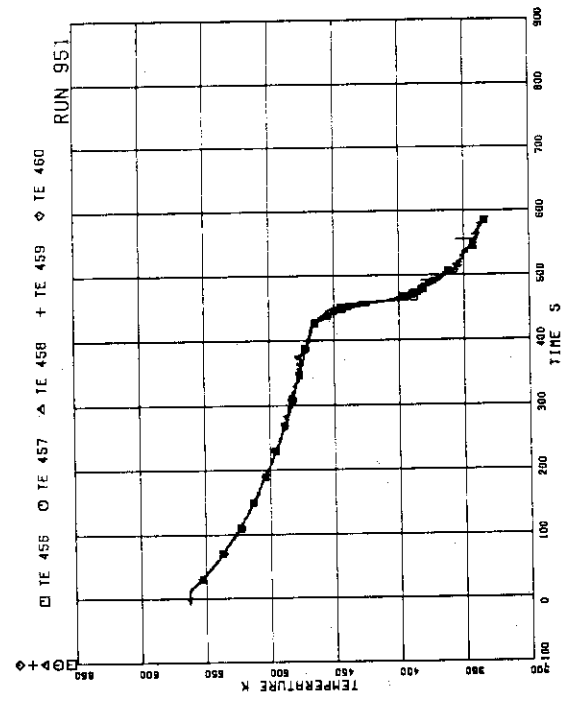

FIG.5.105 FLUID TEMPERATURE ABOVE UTP OF CHANNEL A, OPENINGS 6 TO 10

FIG.5.106 FLUID TEMPERATURE BELOW UTP OF CHANNEL A, OPENINGS 1 TO 5

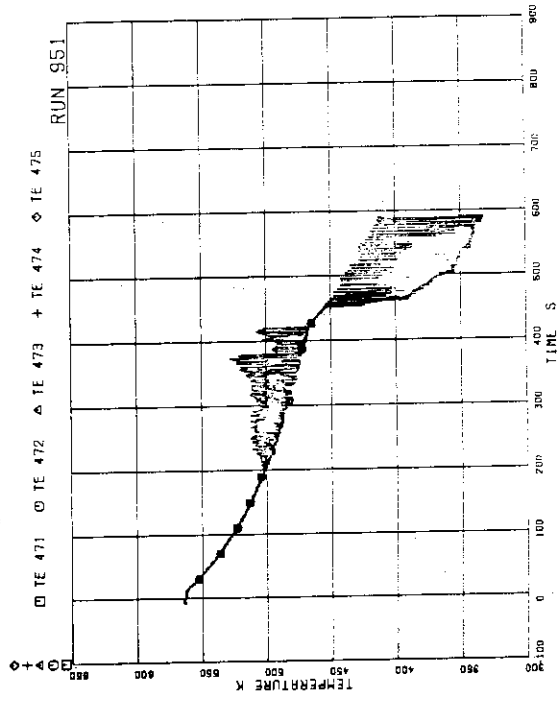

FIG.5.107 FLUID TEMPERATURE BELOW UTP OF CHANNEL A, OPENINGS 6 TO 10

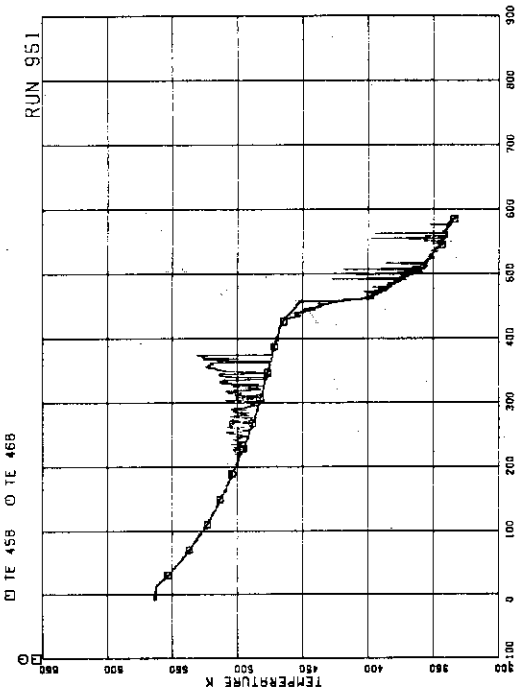

FIG.5.110 FLUID TEMPERATURE AT UTP IN CHANNEL A. OPENING 3

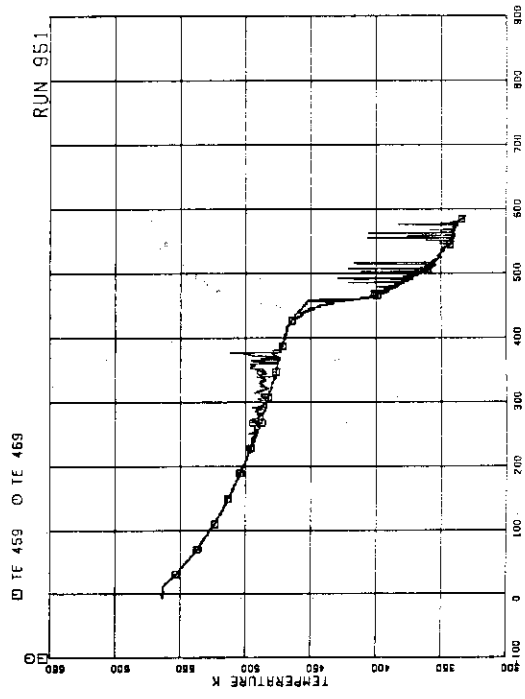

FIG.5.111 FLUID TEMPERATURE AT UTP IN CHANNEL A. OPENING 4

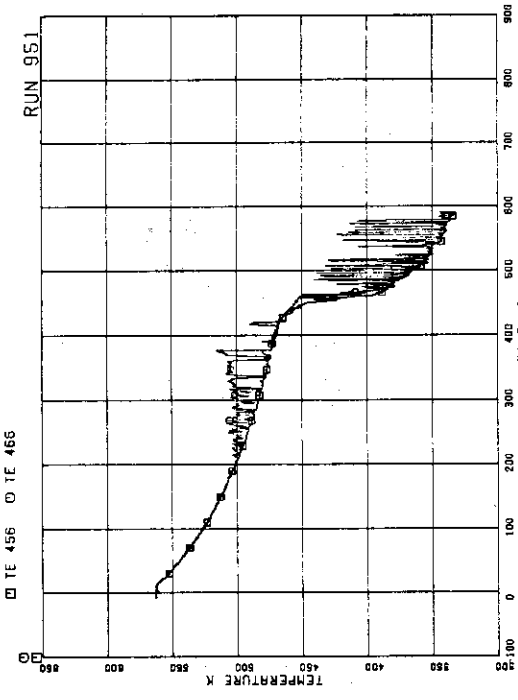

FIG.5.108 FLUID TEMPERATURE AT UTP IN CHANNEL A. OPENING 1

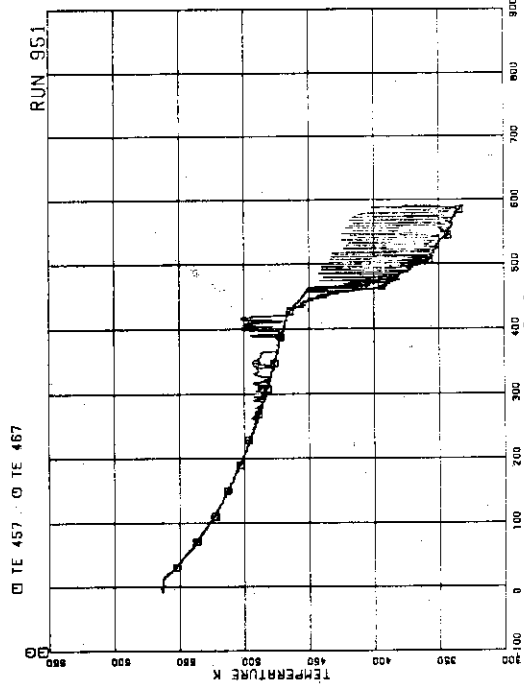

FIG.5.109 FLUID TEMPERATURE AT UTP IN CHANNEL A. OPENING 2

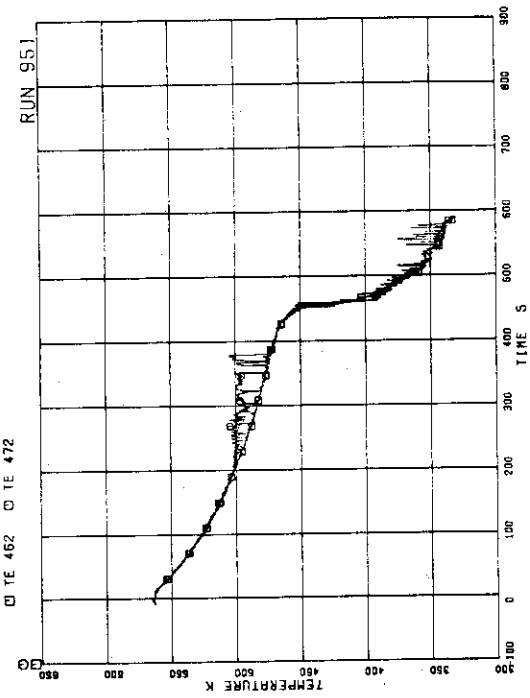

FIG.5.114 FLUID TEMPERATURE AT UTP IN CHANNEL A. OPENING 7

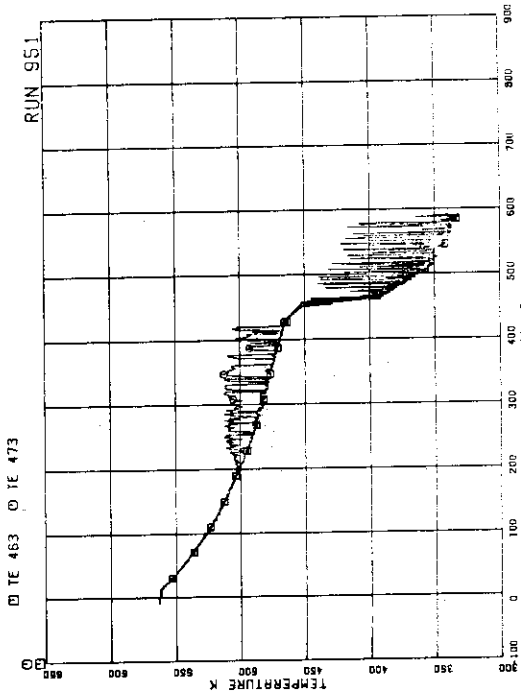

FIG.5.115 FLUID TEMPERATURE AT UTP IN CHANNEL A. OPENING 8

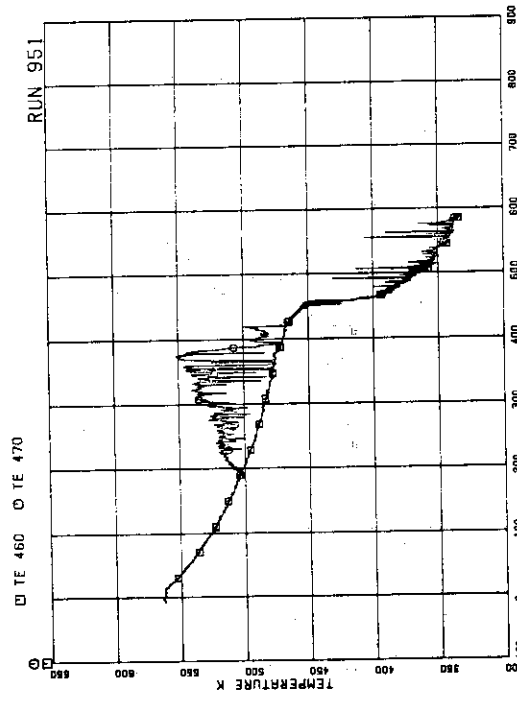

FIG.5.112 FLUID TEMPERATURE AT UTP IN CHANNEL A. OPENING 5

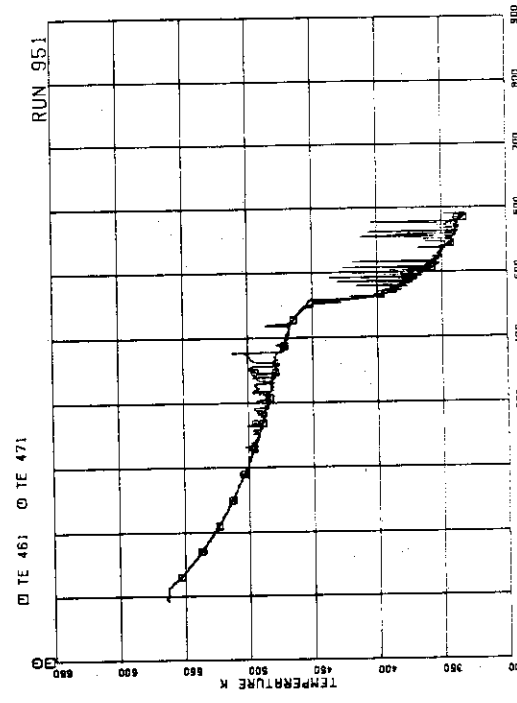

FIG.5.113 FLUID TEMPERATURE AT UTP IN CHANNEL A. OPENING 6

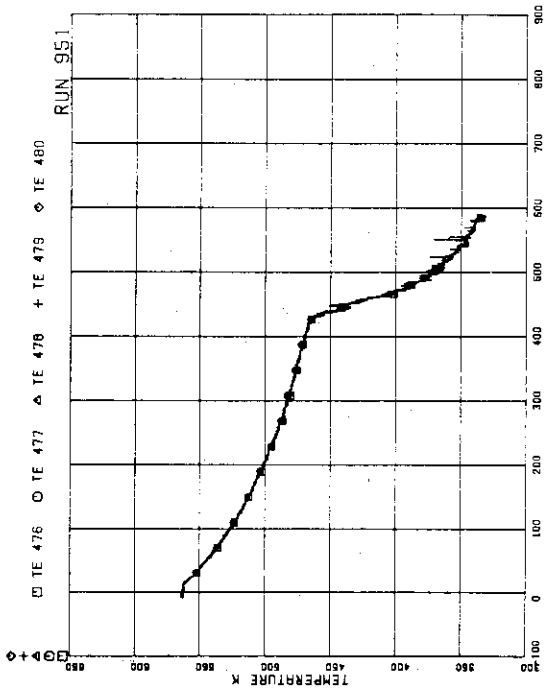

FIG.5.118 FLUID TEMPERATURE ABOVE UTP OF CHANNEL C, OPENING 1 TO 5

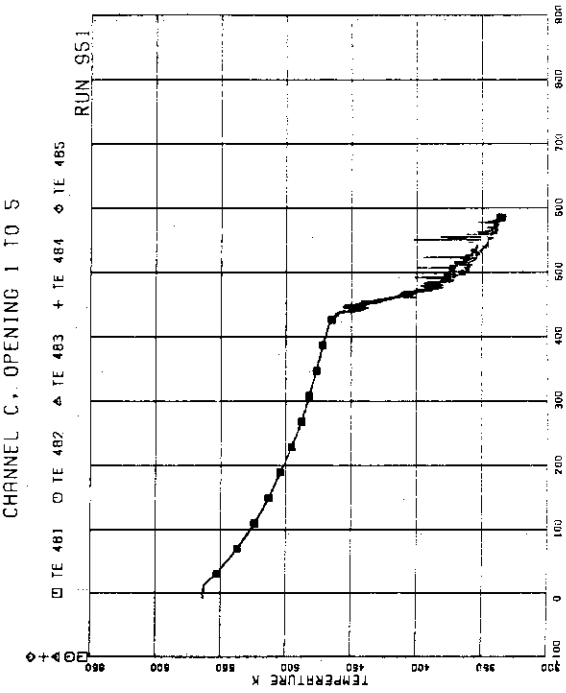

FIG.5.119 FLUID TEMPERATURE ABOVE UTP OF CHANNEL C, OPENING 6 TO 10

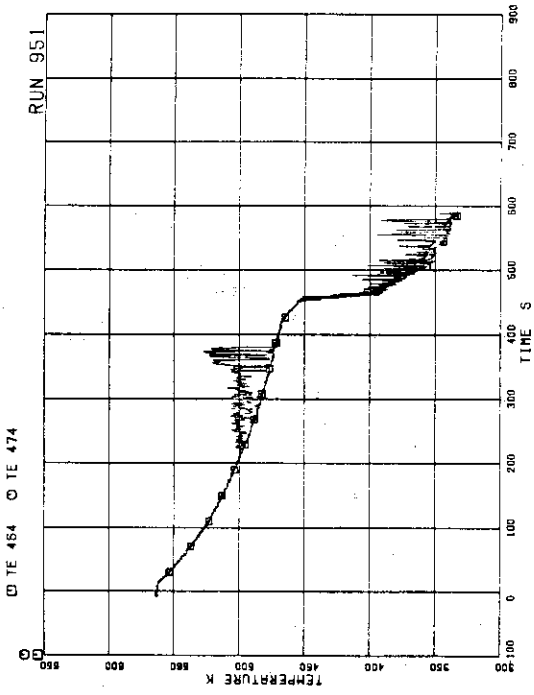

FIG.5.116 FLUID TEMPERATURE AT UTP IN CHANNEL A, OPENING 9

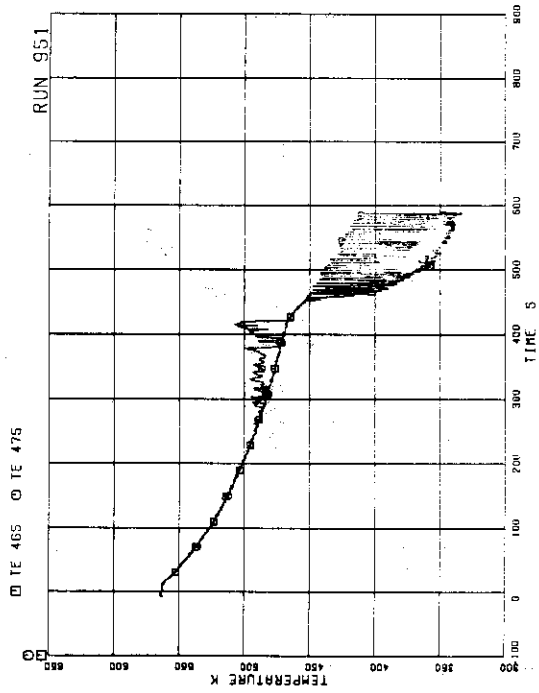

FIG.5.117 FLUID TEMPERATURE AT UTP IN CHANNEL A, OPENING 10

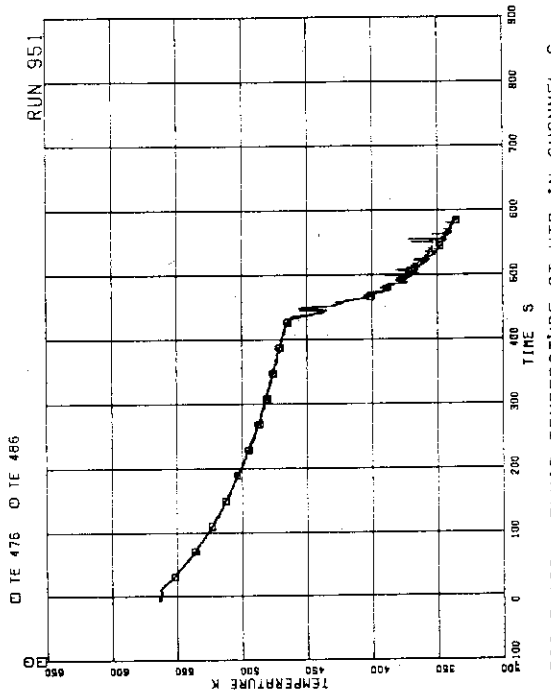

FIG.5.122 FLUID TEMPERATURE AT UTP IN CHANNEL C, OPENING 1

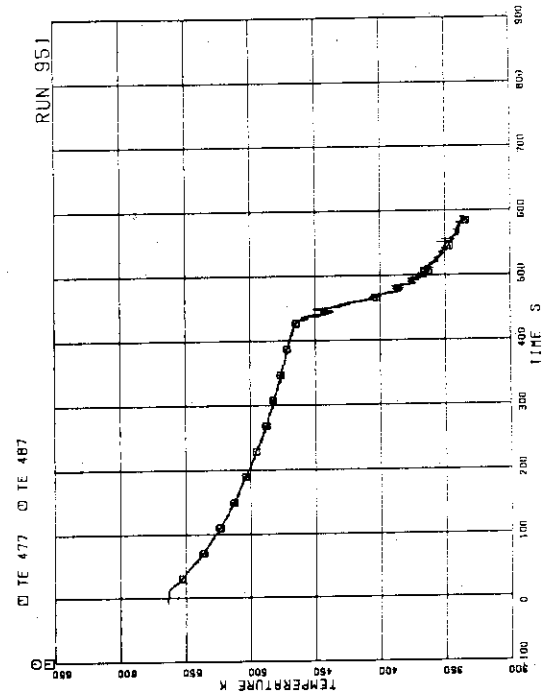

FIG.5.123 FLUID TEMPERATURE AT UTP IN CHANNEL C, OPENING 2

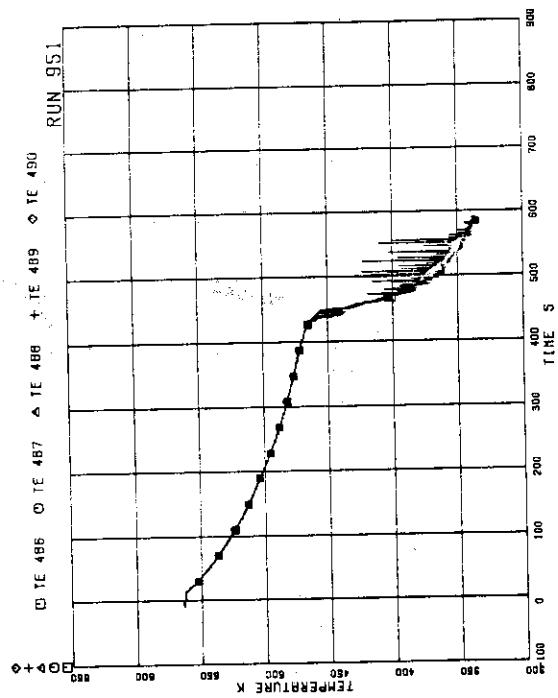

FIG.5.120 FLUID TEMPERATURE BELOW UTP OF CHANNEL C, OPENING 1 TO 5

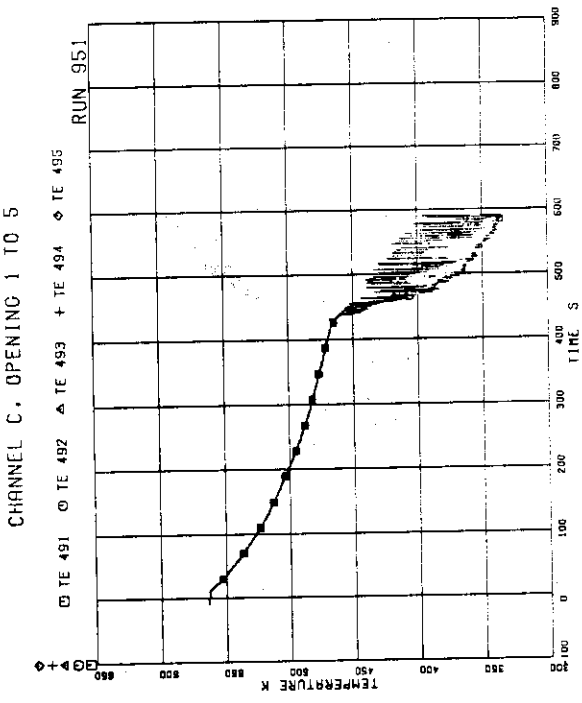

FIG.5.121 FLUID TEMPERATURE BELOW UTP OF CHANNEL C, OPENING 6 TO 10

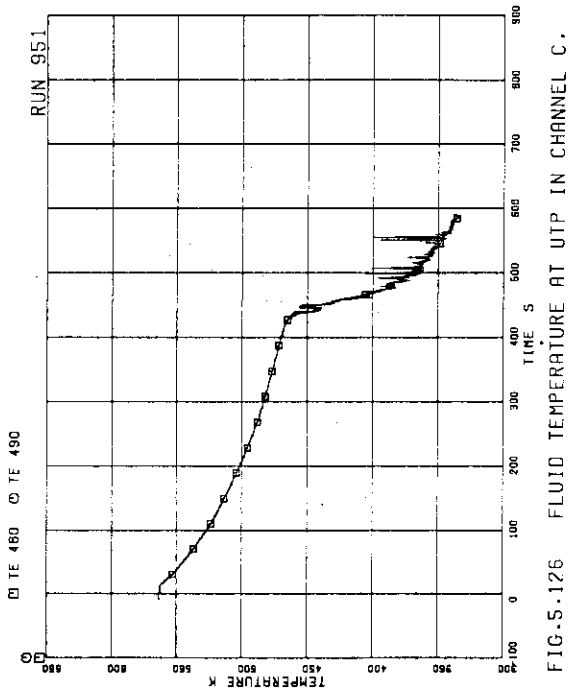

FIG.5.126 FLUID TEMPERATURE AT UTP IN CHANNEL C. OPENING 5

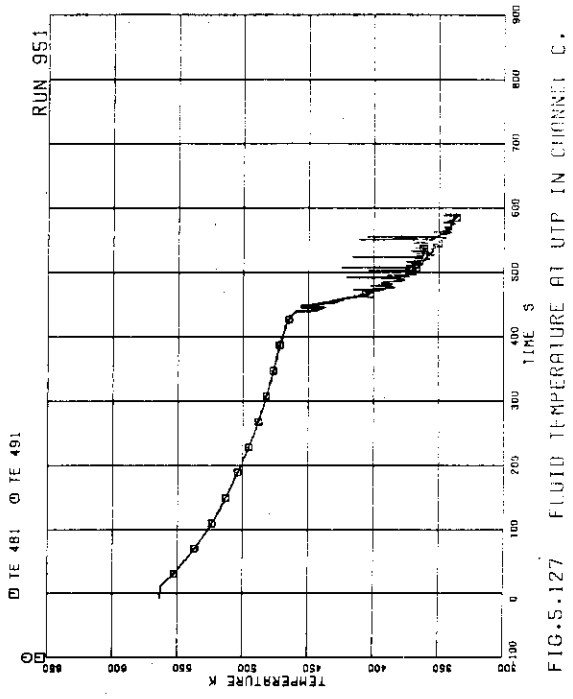

FIG.5.127 FLUID TEMPERATURE AT UTP IN CHANNEL C. OPENING 6

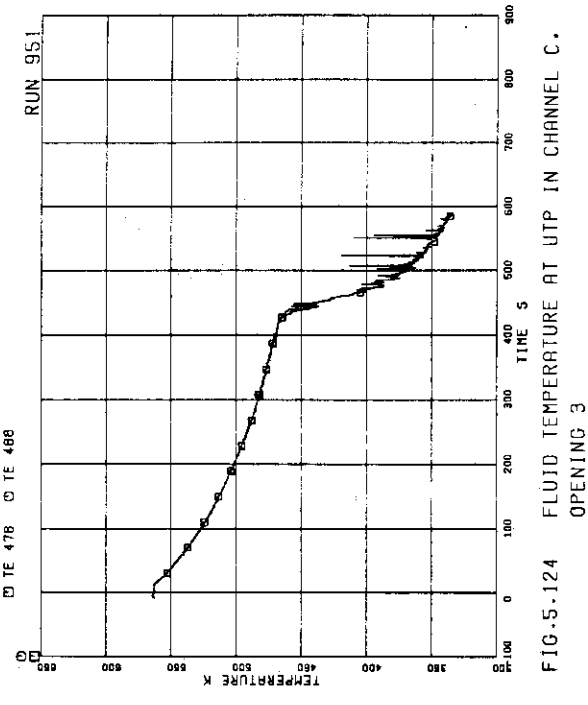

FIG.5.124 FLUID TEMPERATURE AT UTP IN CHANNEL C. OPENING 3

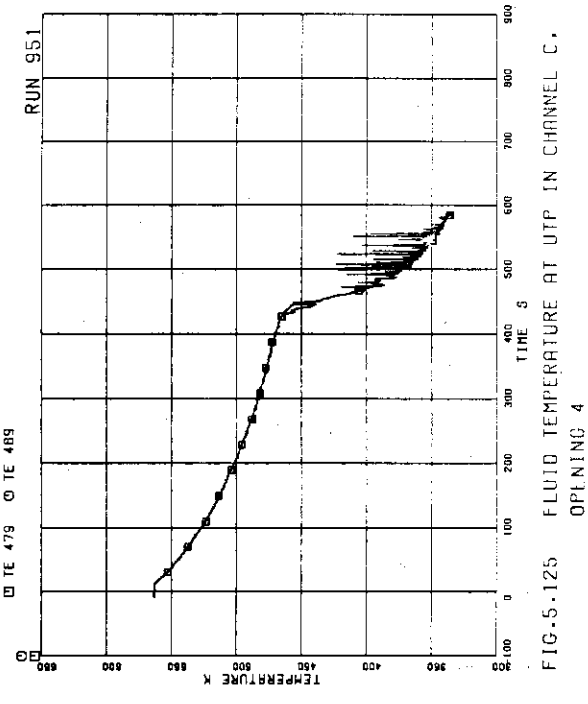

FIG.5.125 FLUID TEMPERATURE AT UTP IN CHANNEL C. OPENING 4

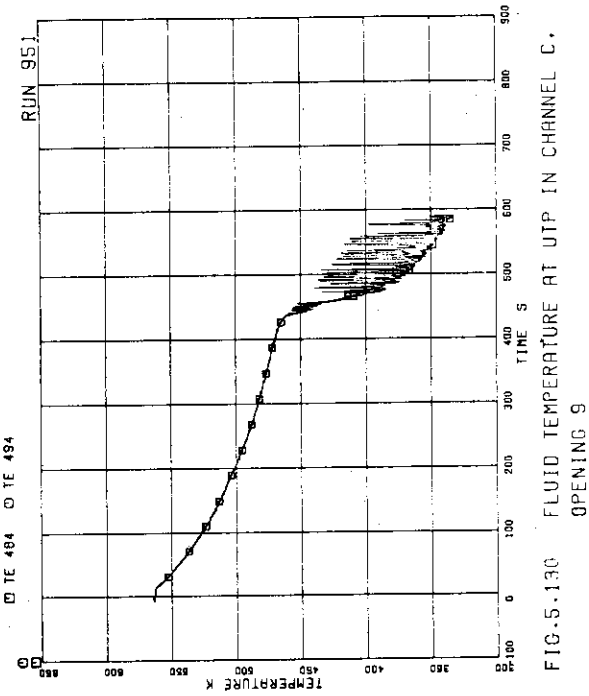

FIG.5.130 FLUID TEMPERATURE AT UTP IN CHANNEL C. OPENING 9

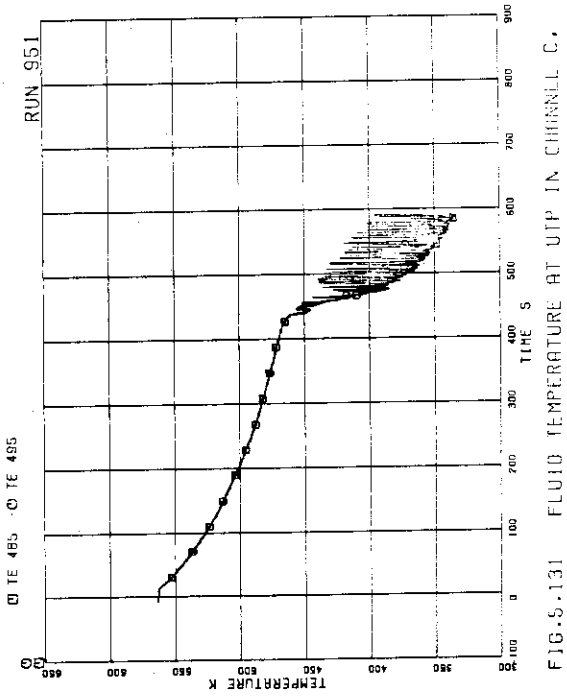

FIG.5.131 FLUID TEMPERATURE AT UTP IN CHANNEL C. OPENING 10

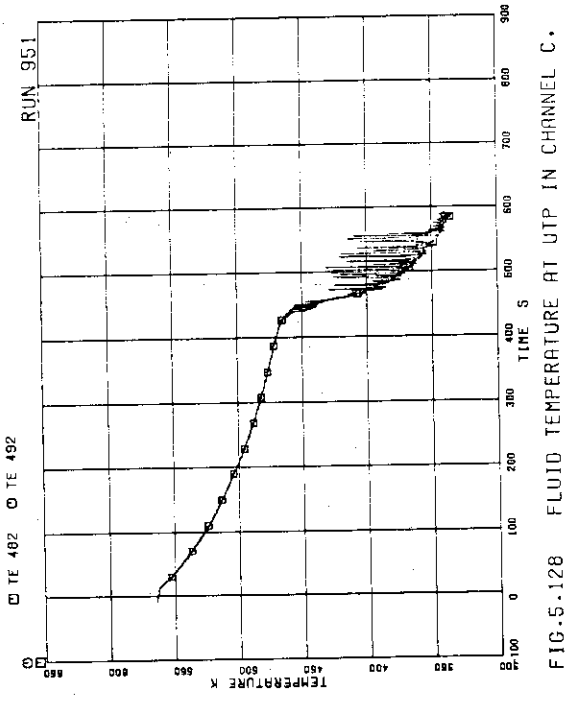

FIG.5.128 FLUID TEMPERATURE AT UTP IN CHANNEL C. OPENING 7

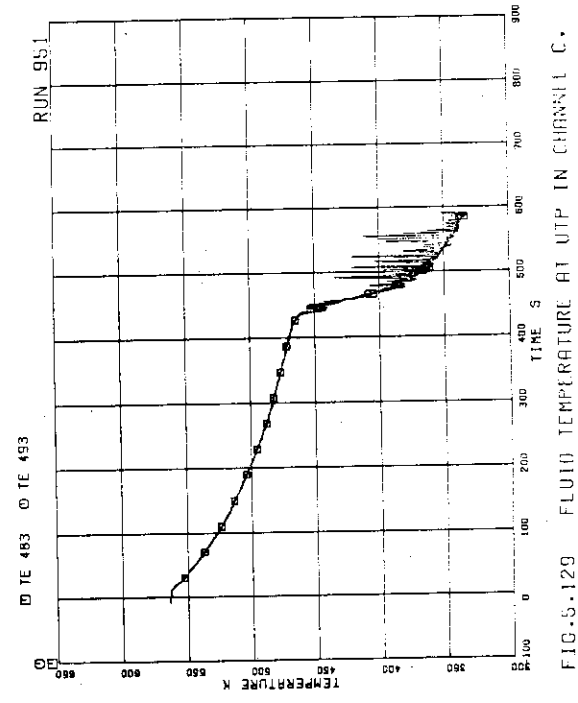

FIG.5.129 FLUID TEMPERATURE AT UTP IN CHANNEL C. OPENING 8

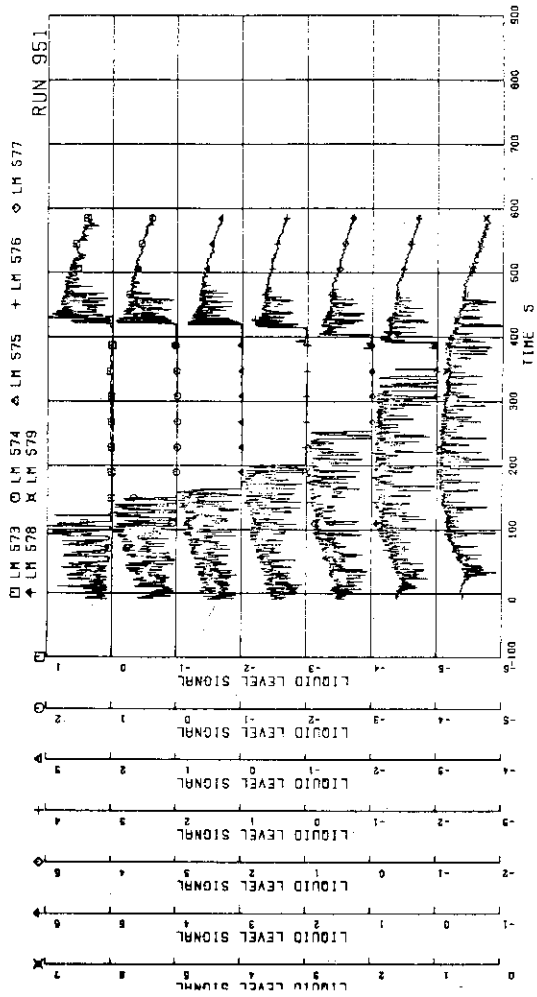

FIG.5.134 LIQUID LEVEL SIGNAL IN CHANNEL BOX B

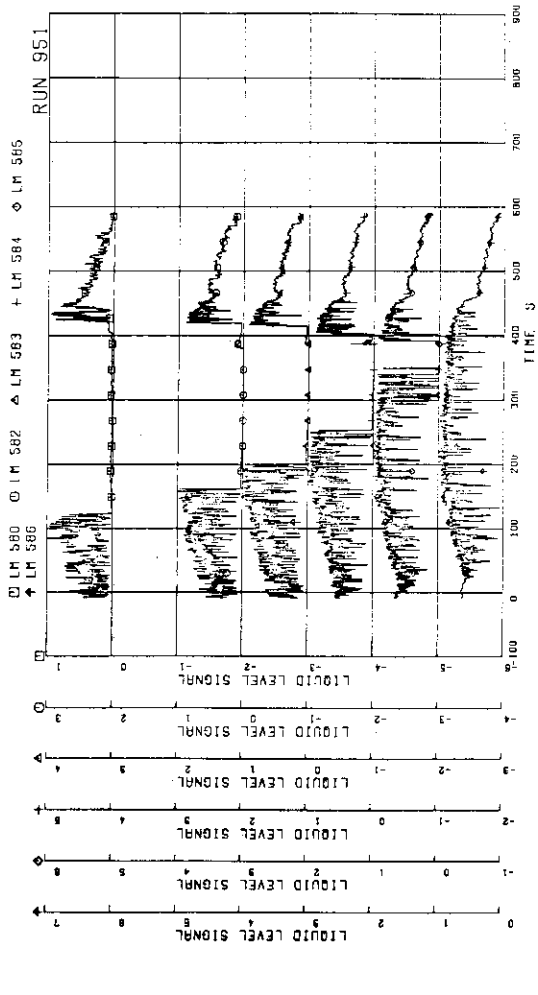

FIG.5.135 LIQUID LEVEL SIGNAL IN CHANNEL BOX C

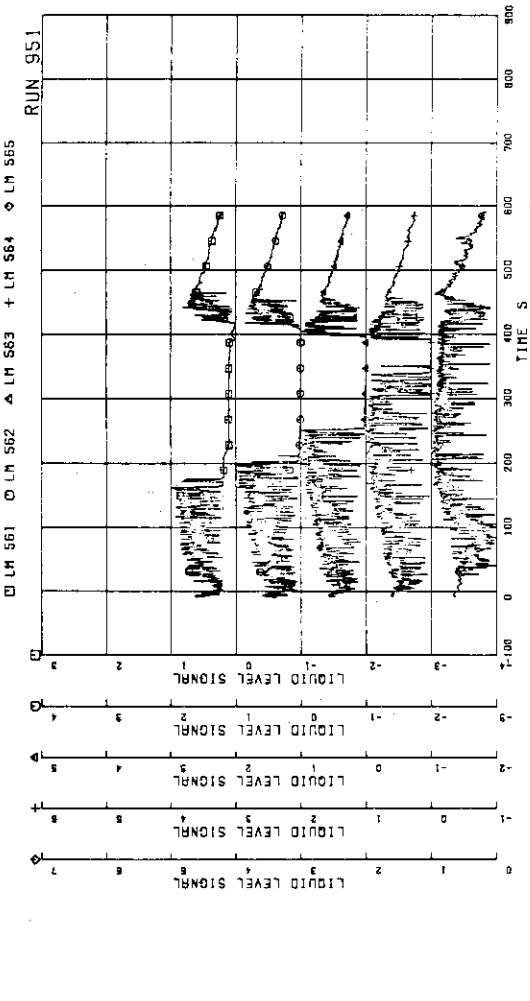

FIG.5.132 LIQUID LEVEL SIGNAL IN CHANNEL BOX A, LOCATION A1

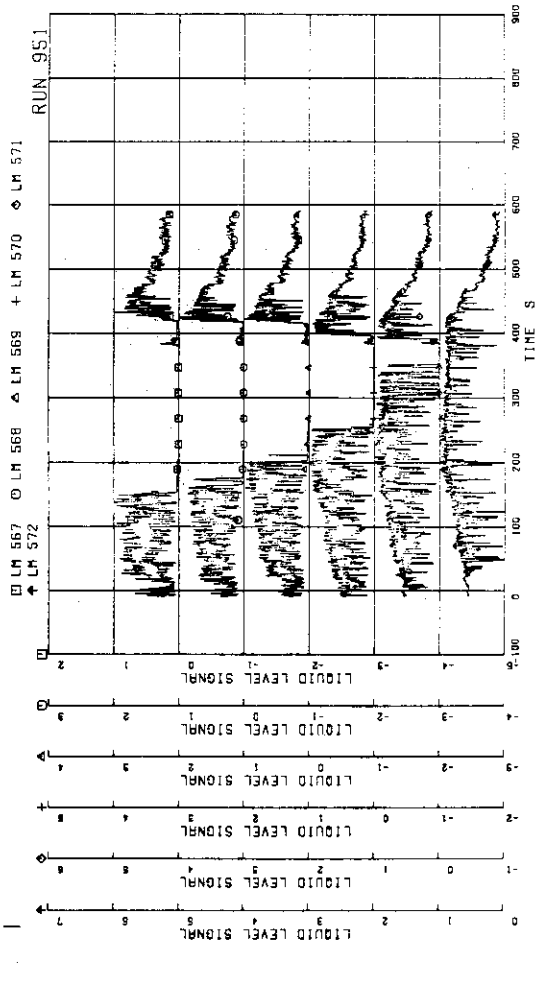

FIG.5.133 LIQUID LEVEL SIGNAL IN CHANNEL BOX A, LOCATION A2

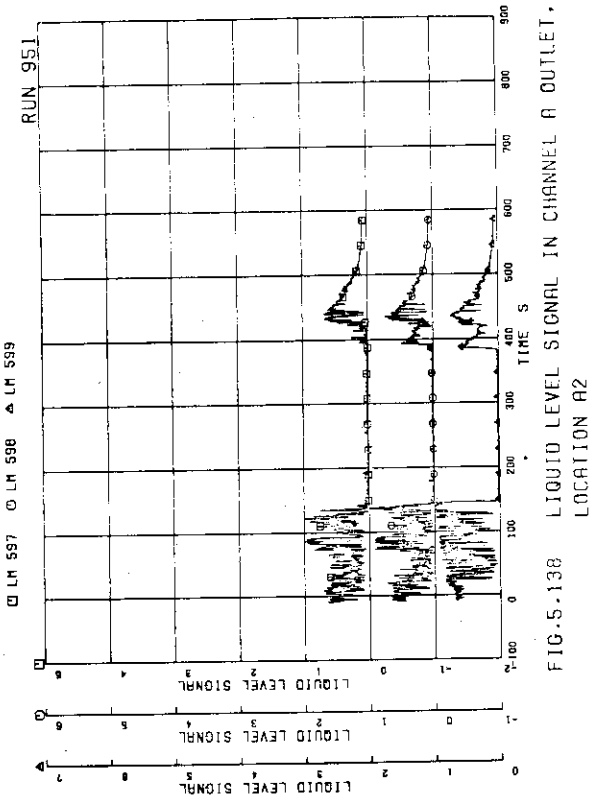

FIG.5.138 LIQUID LEVEL SIGNAL IN CHANNEL A OUTLET, LOCATION A2

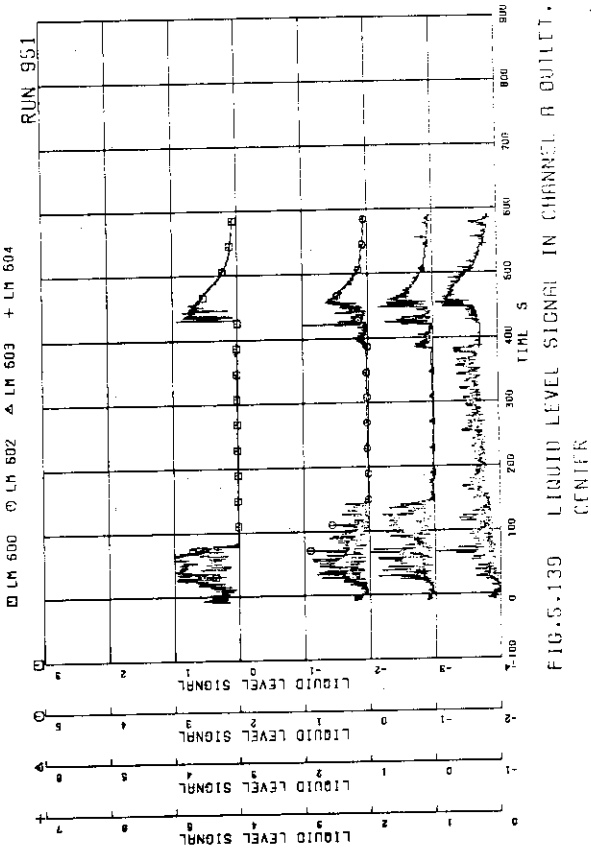

FIG.5.139 LIQUID LEVEL SIGNAL IN CHANNEL A OUTLET, CENTER

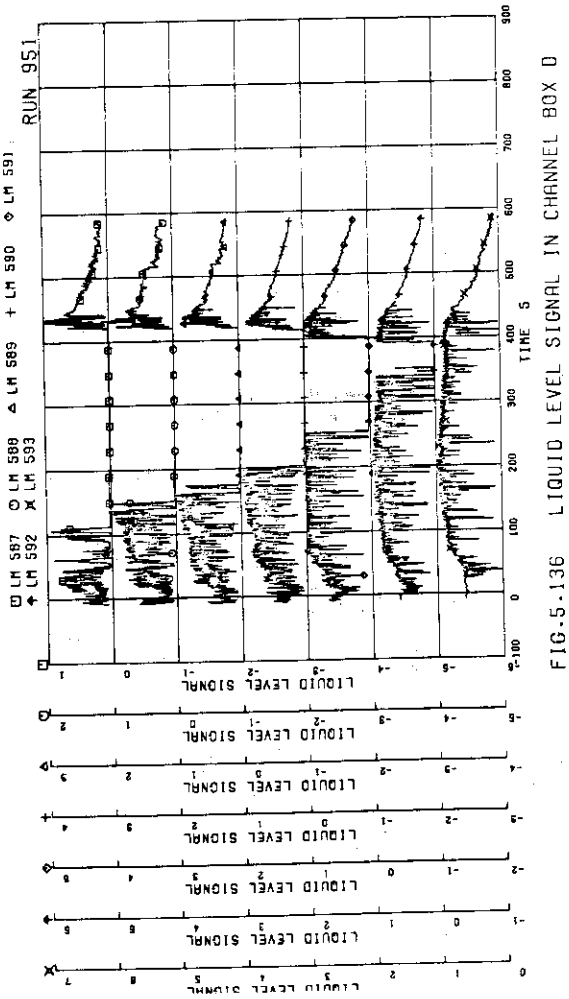

FIG.5.136 LIQUID LEVEL SIGNAL IN CHANNEL BOX D

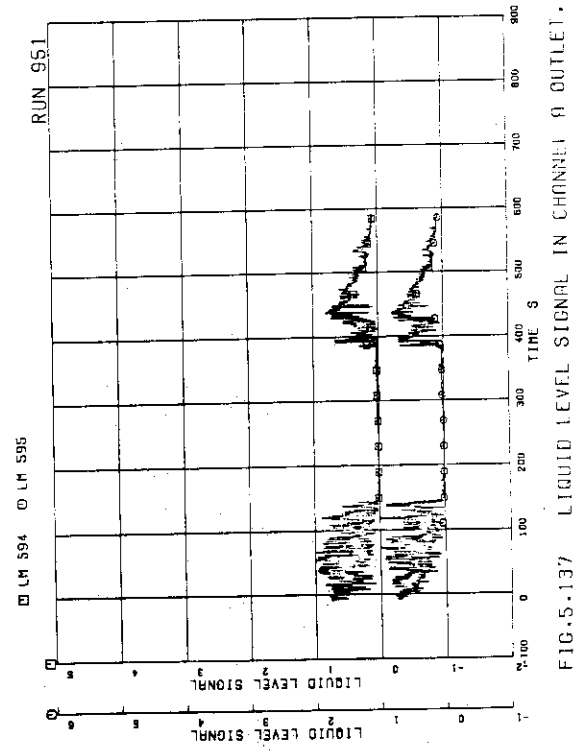

FIG.5.137 LIQUID LEVEL SIGNAL IN CHANNEL A OUTLET, LOCATION A1

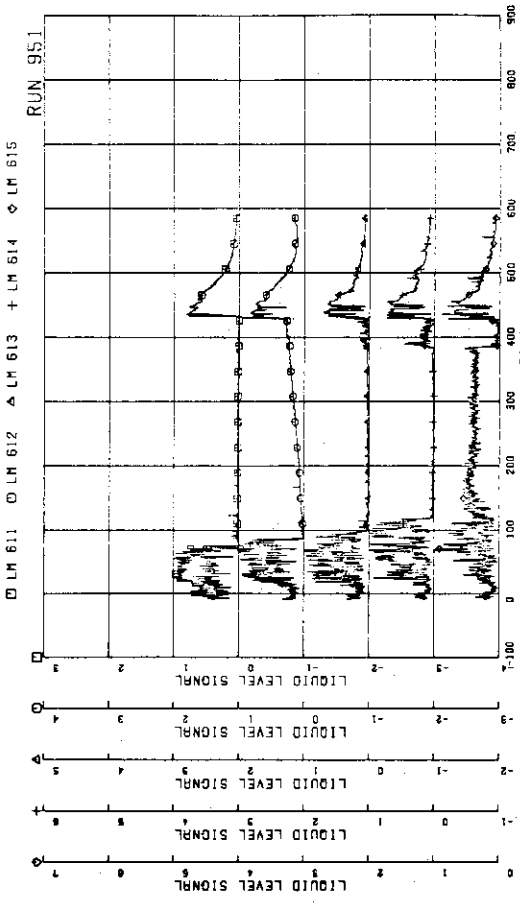

FIG.5.142 LIQUID LEVEL SIGNAL IN CHANNEL C OUTLET, CENTER

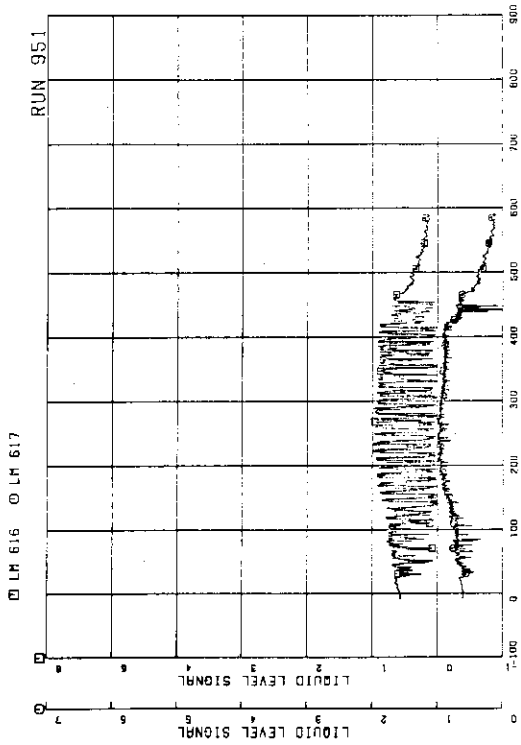

FIG.5.143 LIQUID LEVEL SIGNAL IN CHANNEL A INLET

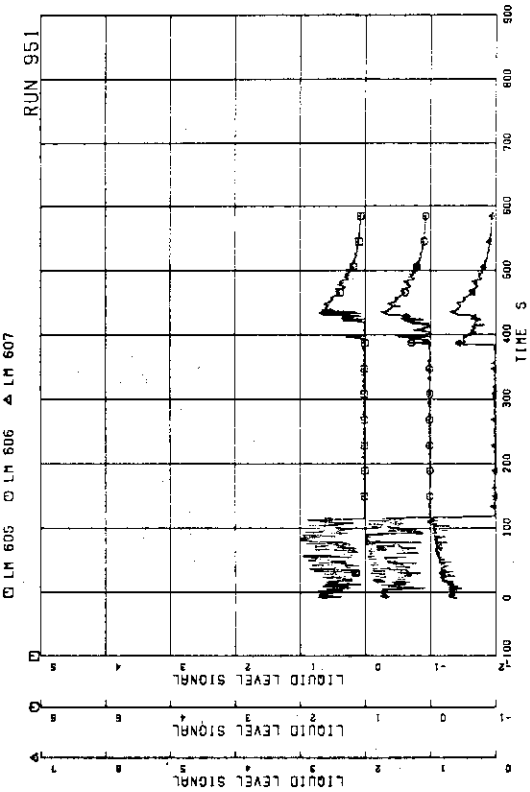

FIG.5.140 LIQUID LEVEL SIGNAL IN CHANNEL C OUTLET, LOCATION C1

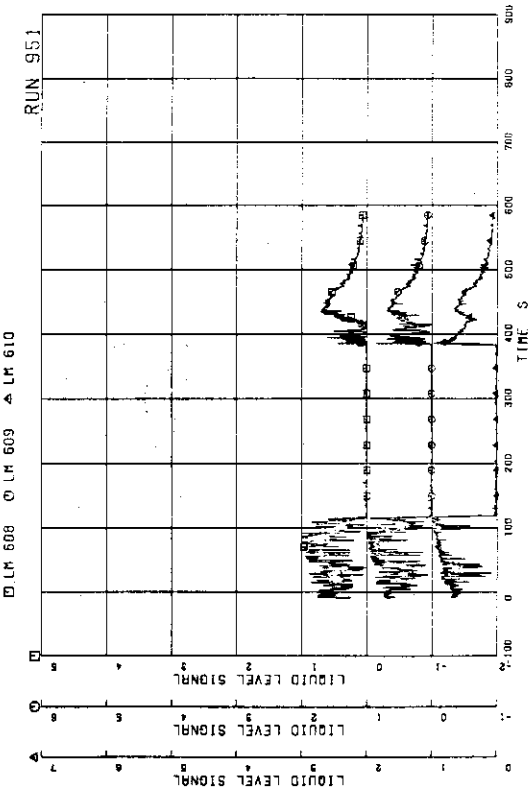

FIG.5.141 LIQUID LEVEL SIGNAL IN CHANNEL C OUTLET, LOCATION C2

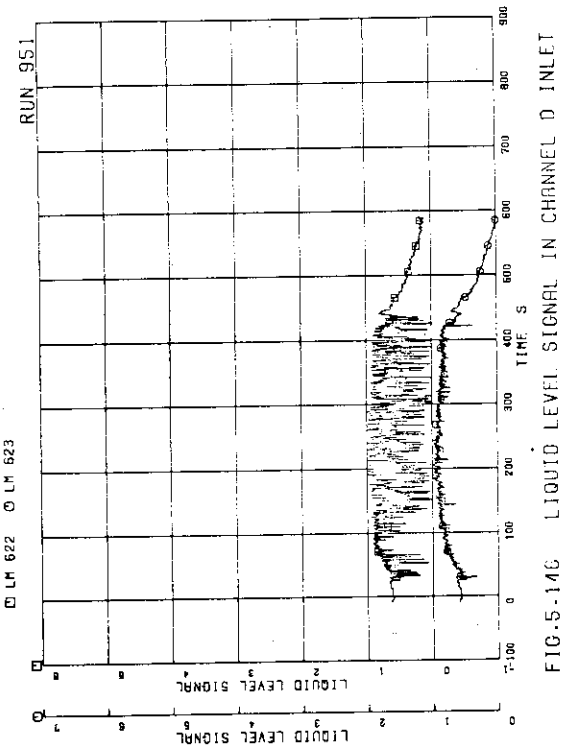

FIG.5.146 LIQUID LEVEL SIGNAL IN CHANNEL D INLET

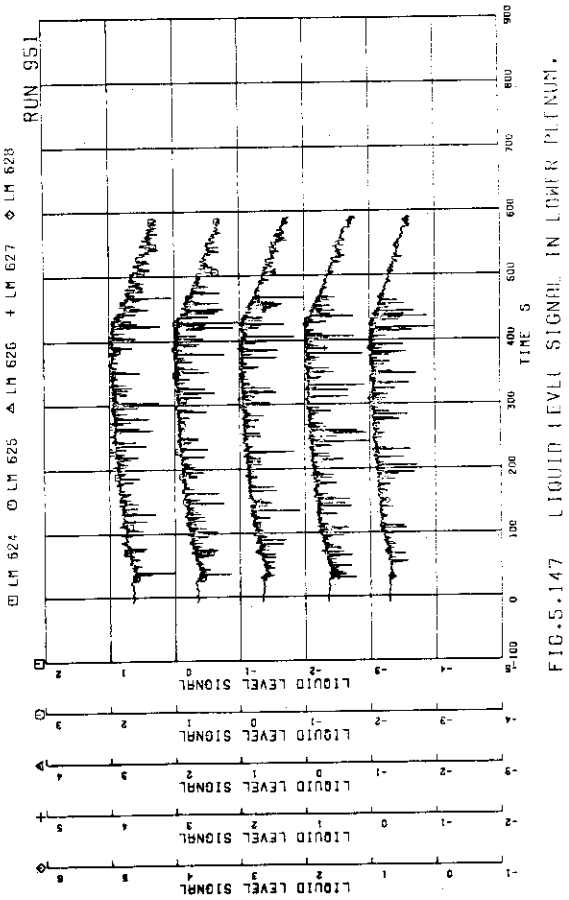

FIG.5.147 LIQUID LEVEL SIGNAL IN LOWER PLENUM, NORTH

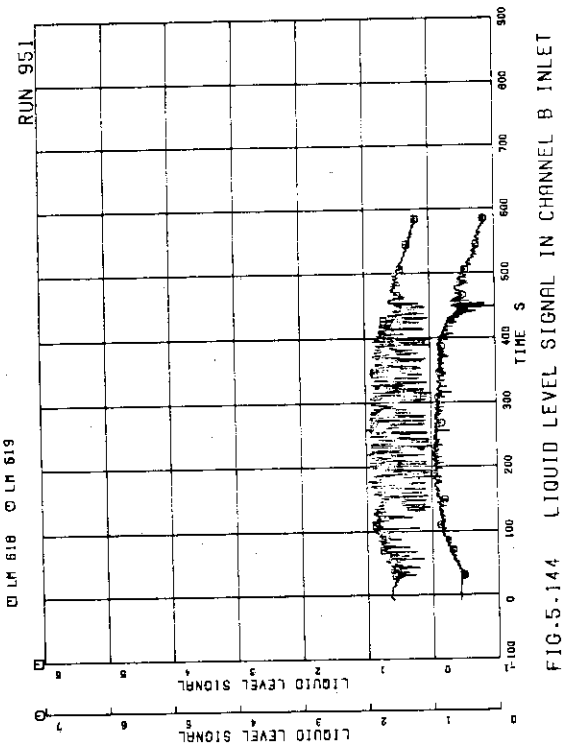

FIG.5.144 LIQUID LEVEL SIGNAL IN CHANNEL B INLET

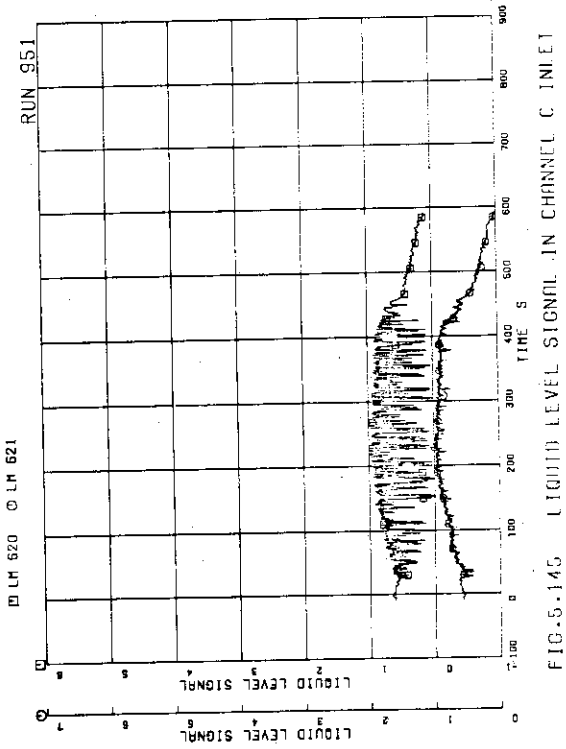

FIG.5.145 LIQUID LEVEL SIGNAL IN CHANNEL C INLET

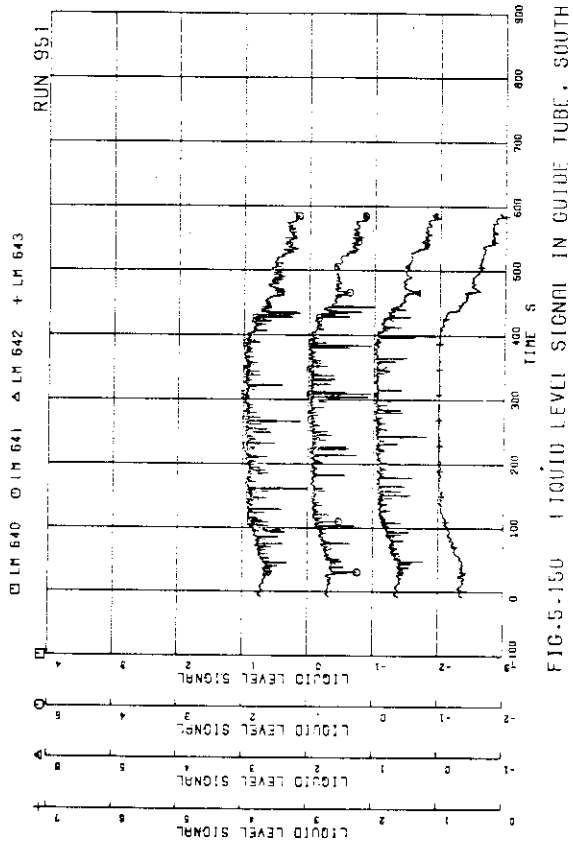

FIG.5-150 LIQUID LEVEL SIGNAL IN GUIDE TUBE, SOUTH

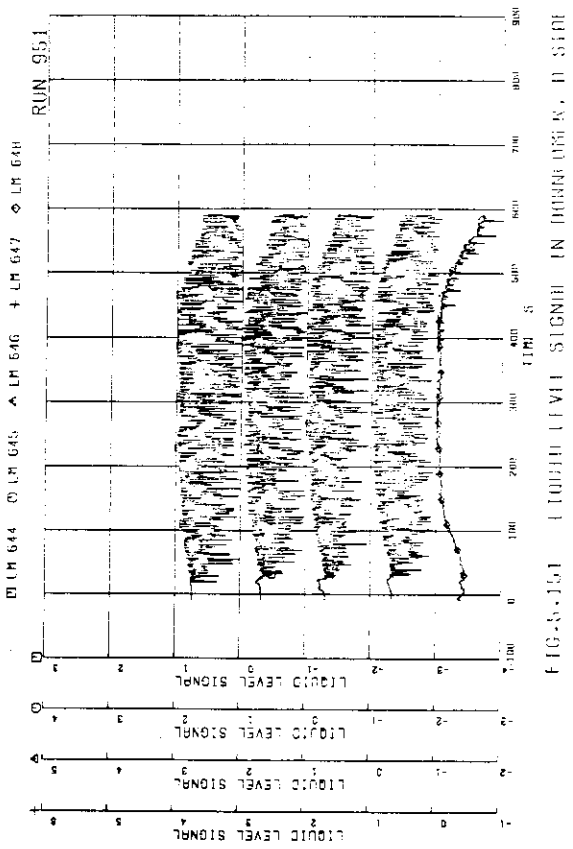

FIG.5-151 LIQUID LEVEL SIGNAL IN DOWNCOMER, N SIDE

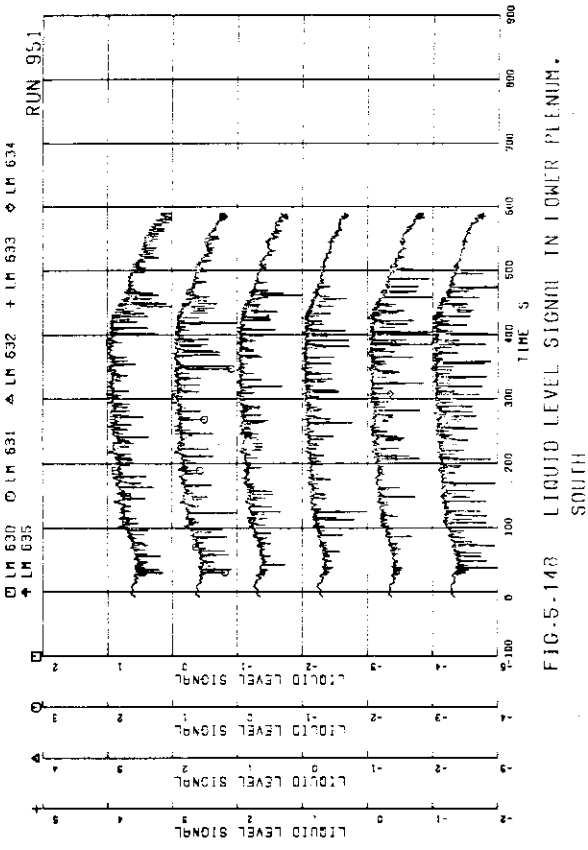

FIG.5-148 LIQUID LEVEL SIGNAL IN LOWER PLENUM, SOUTH

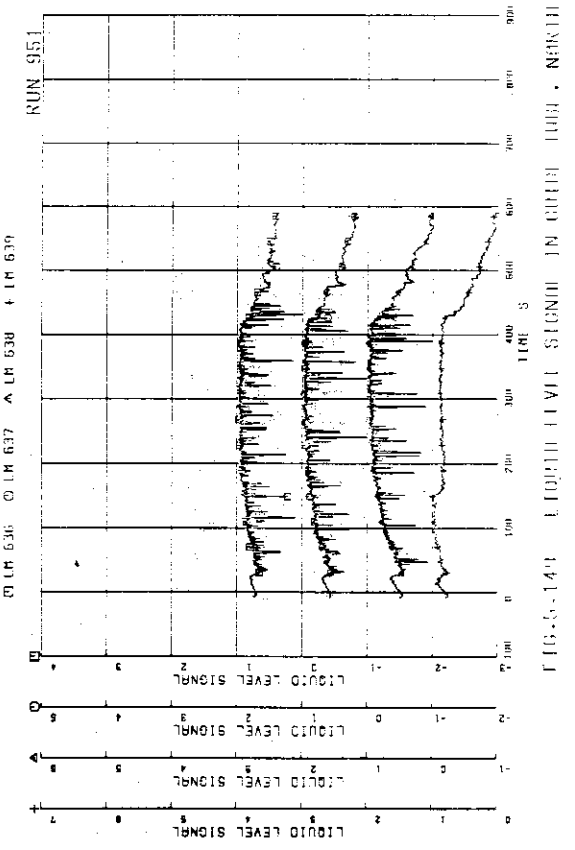

FIG.5-147 LIQUID LEVEL SIGNAL IN CORE TUBE, NORTH

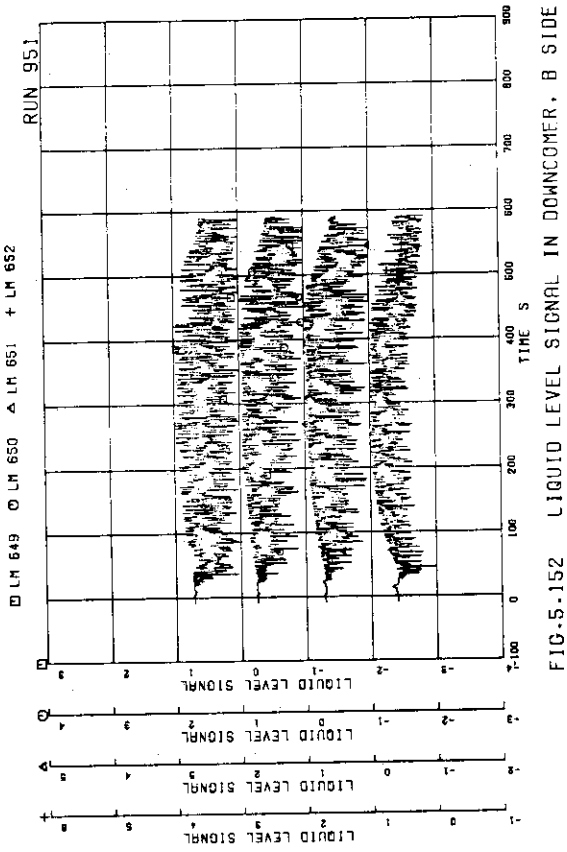

FIG.5.152 LIQUID LEVEL SIGNAL IN DOWNCOMER, B SIDE

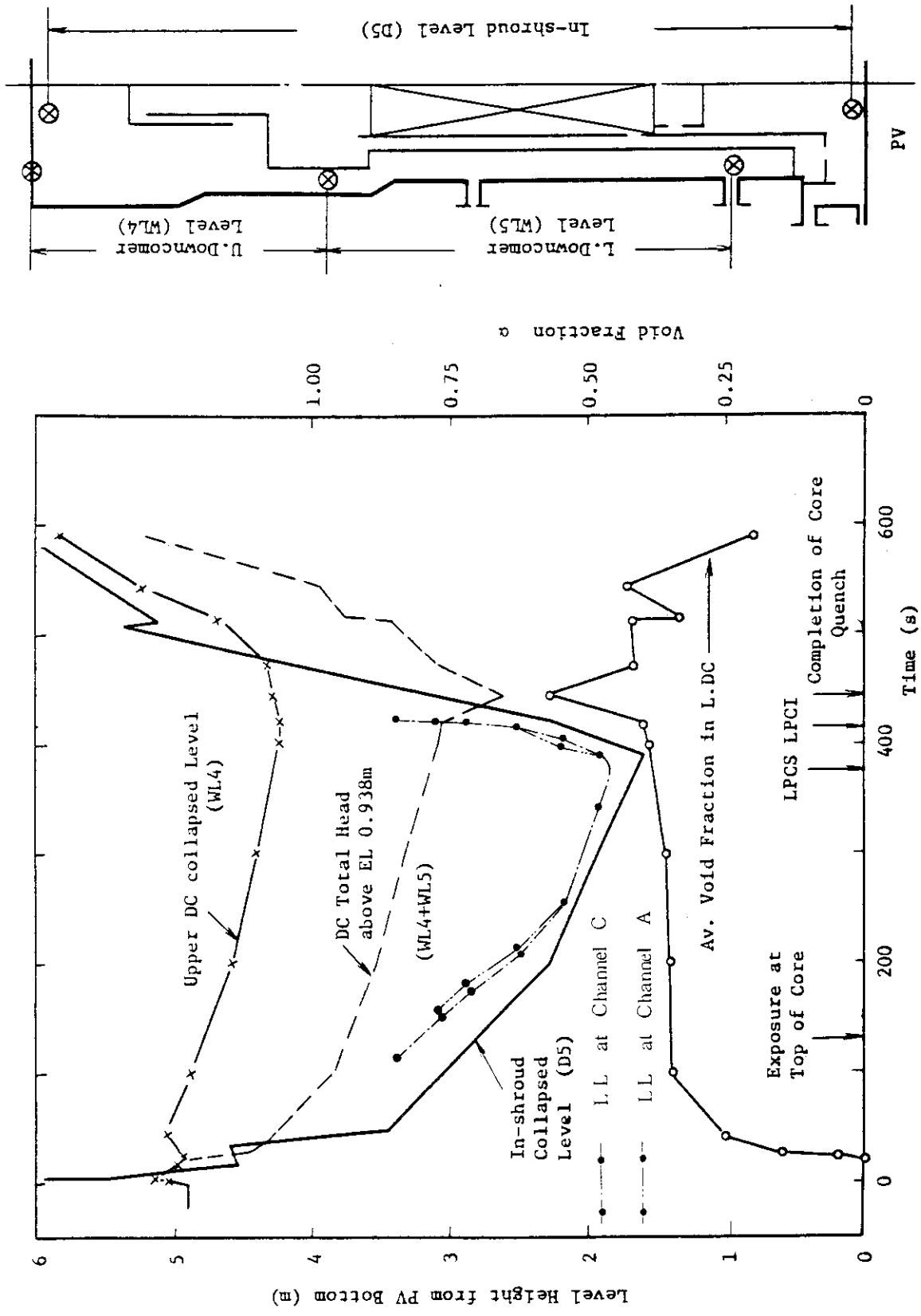

Fig. 5.153 Estimated liquid levels in pressure vessel

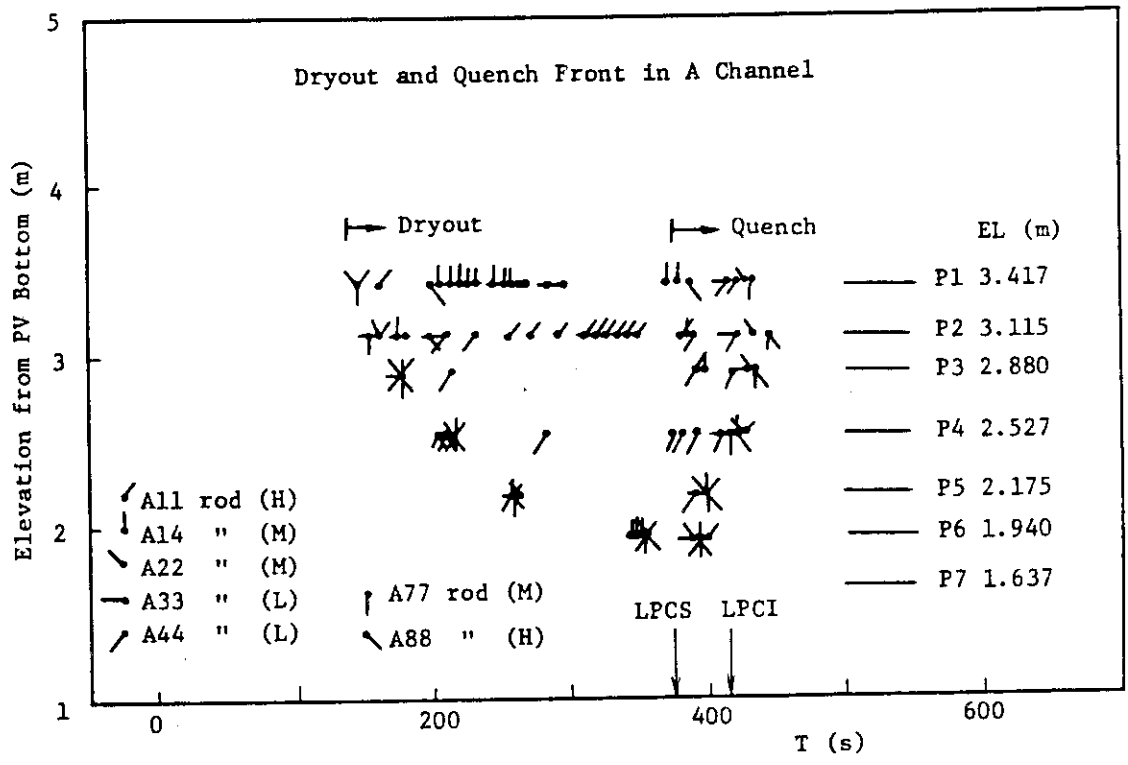

Fig. 5.154 Dryout and quench times of fuel rods in bundle A

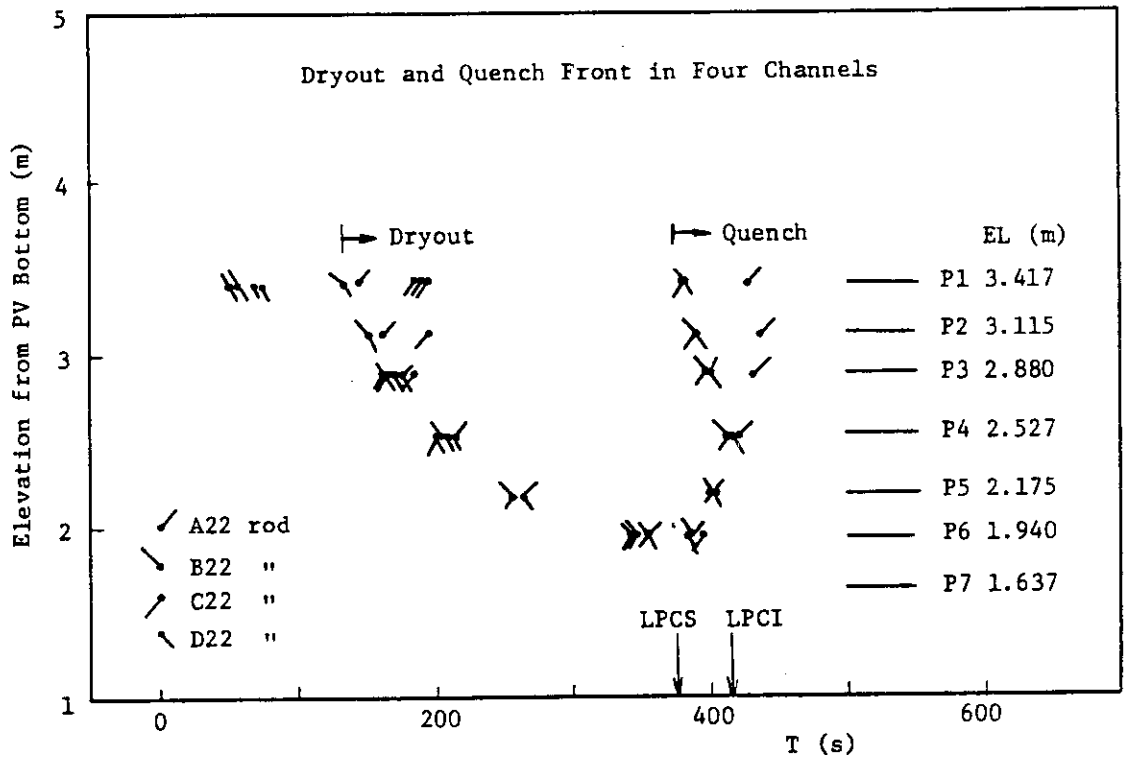

Fig. 5.155 Dryout and quench times of fuel rods in four bundles

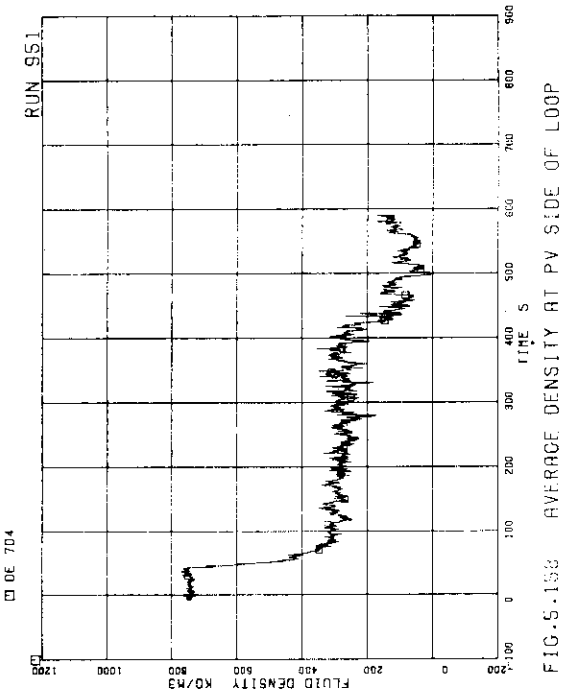

FIG.5.153 AVERAGE DENSITY AT PV SIDE OF LOOP

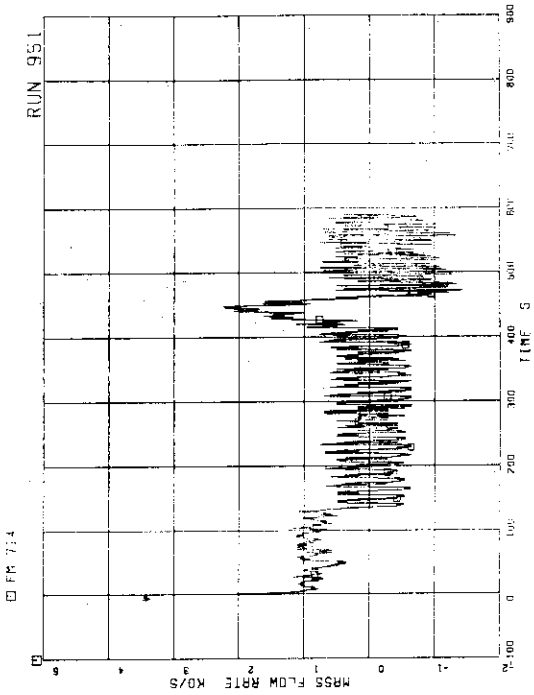

FIG.5.159 FLOW RATE AT CHANNEL A INLET

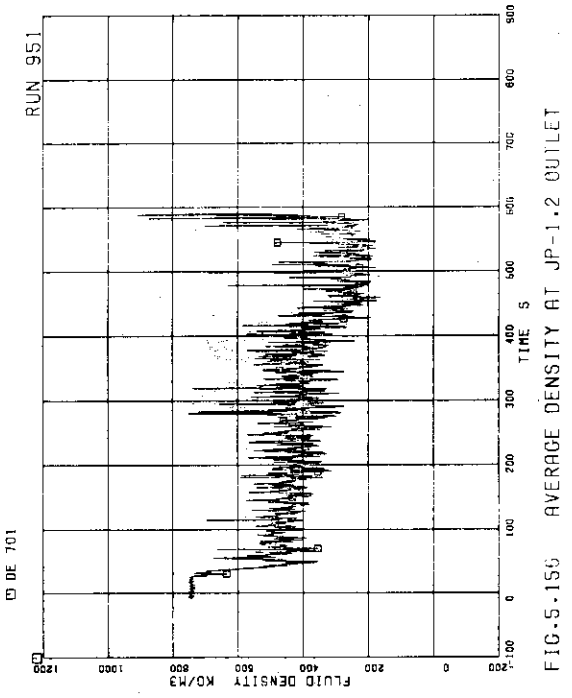

FIG.5.156 AVERAGE DENSITY AT JP-1.2 OUTLET

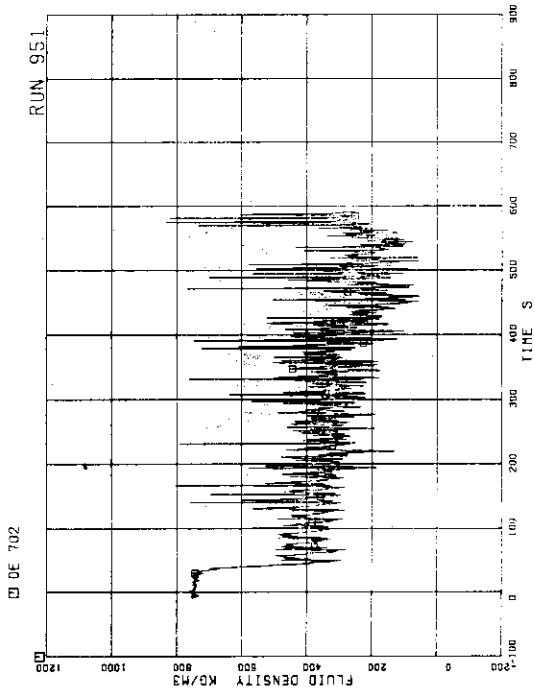

FIG.5.157 AVERAGE DENSITY AT JP-3.4 OUTLET

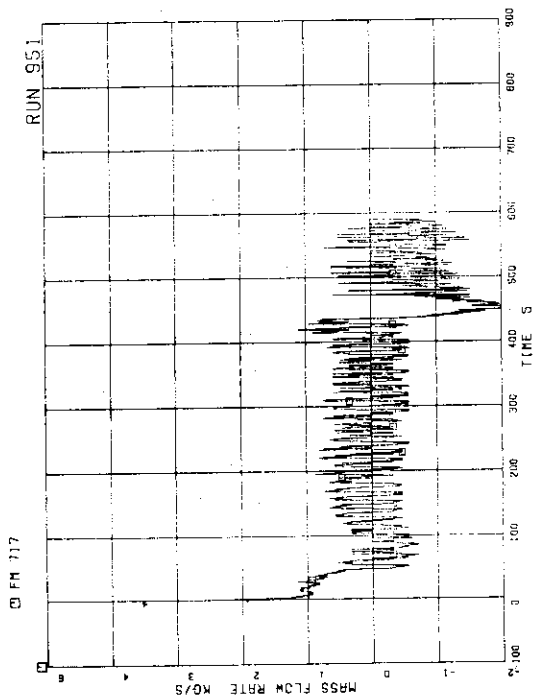

FIG.5.162 FLOW RATE AT CHANNEL D INLET

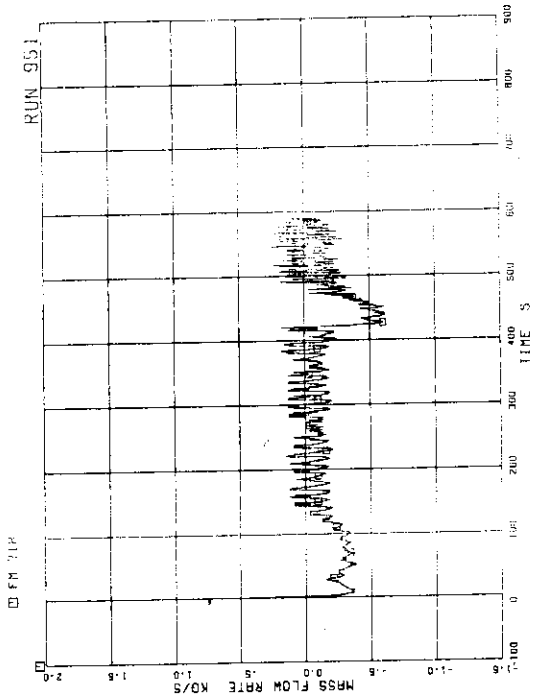

FIG.5.163 FLOW RATE AT BYPASS HOLE

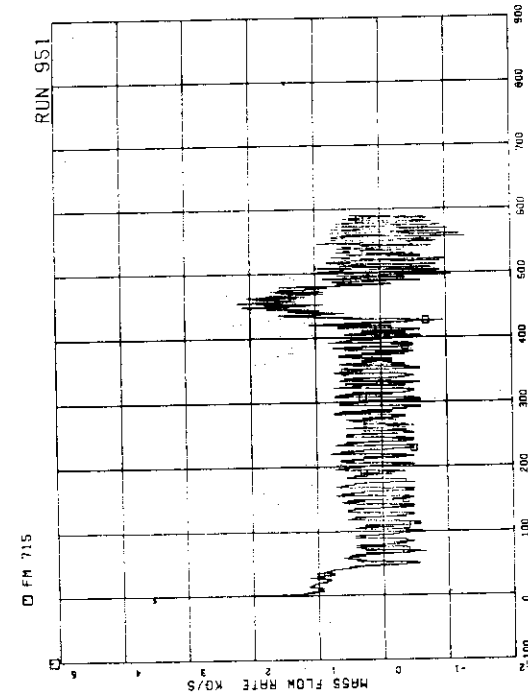

FIG.5.160 FLOW RATE AT CHANNEL B INLET

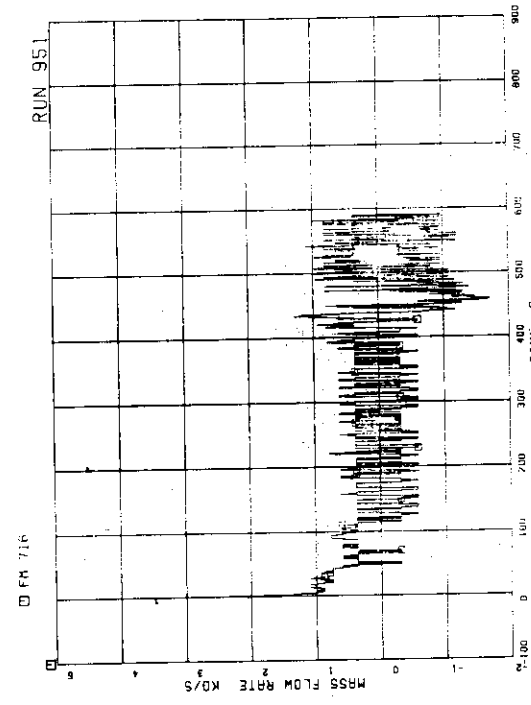

FIG.5.161 FLOW RATE AT CHANNEL C INLET

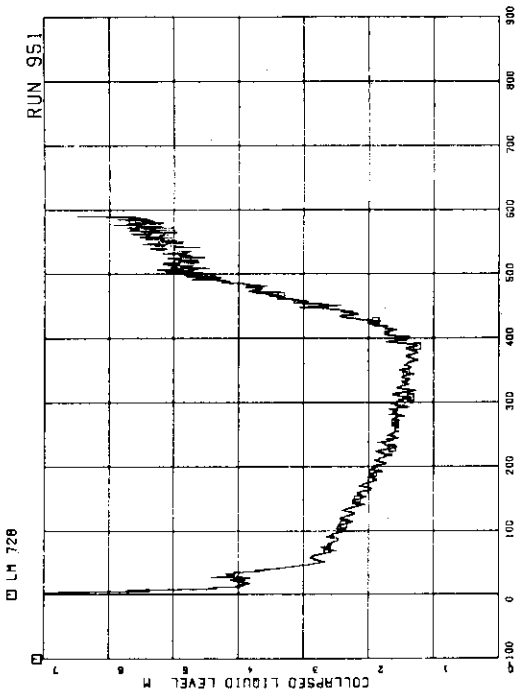

FIG.5.166 COLLAPSED LIQUID LEVEL INSIDE CORE SHROUD

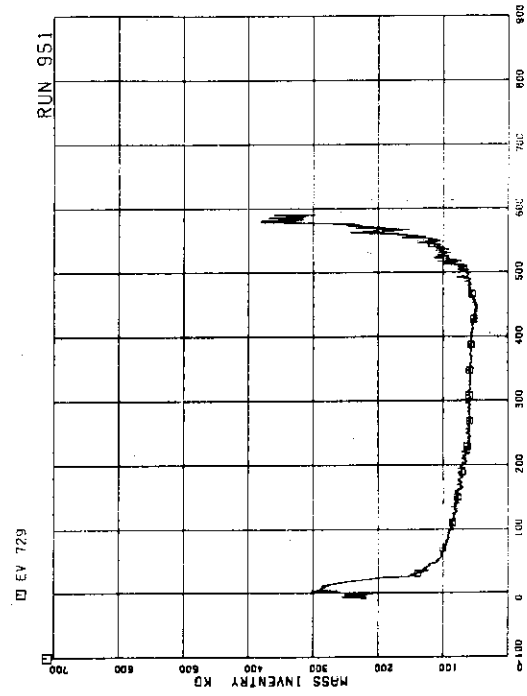

FIG.5.167 FLUID INVENTORY IN DOWNCOMER

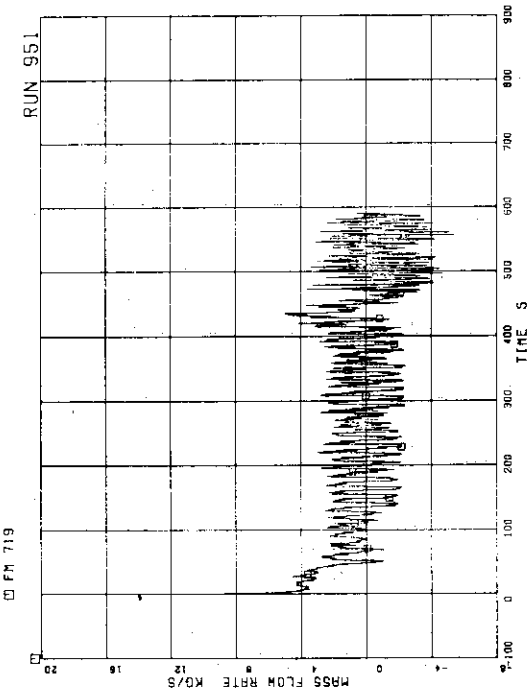

FIG.5.164 TOTAL CHANNEL INLET FLOW RATE

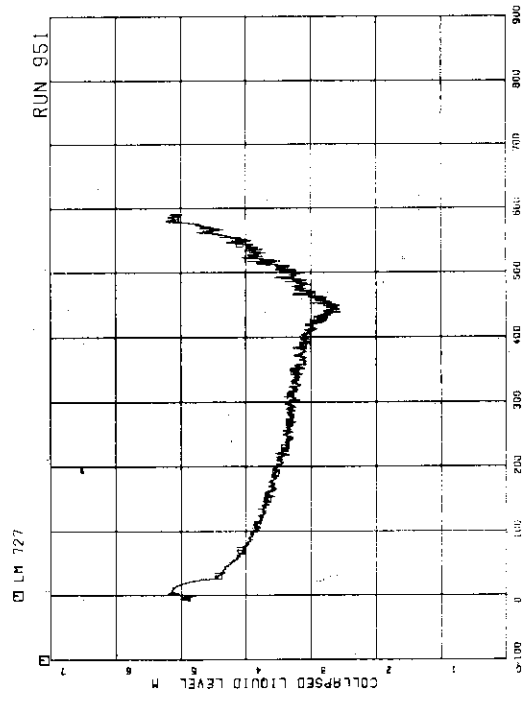

FIG.5.165 COLLAPSED LIQUID LEVEL IN DOWNCOMER

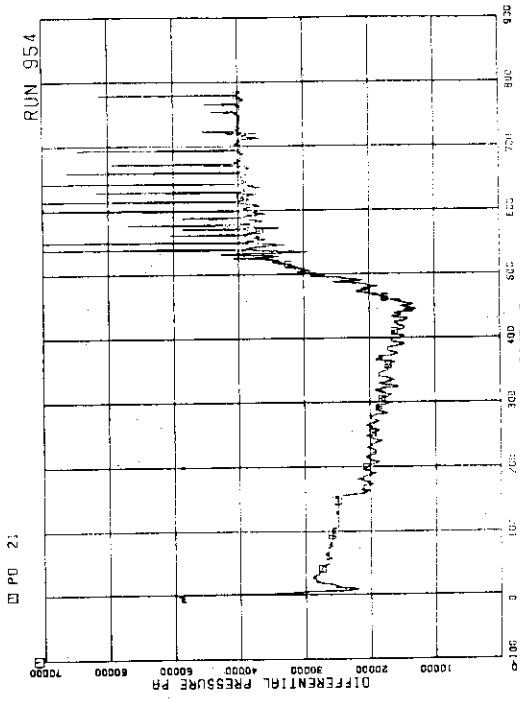

FIG.5.170 DIFFERENTIAL PRESSURE BETWEEN LOWER PLENUM (LP) AND UPPER PLENUM (UP)

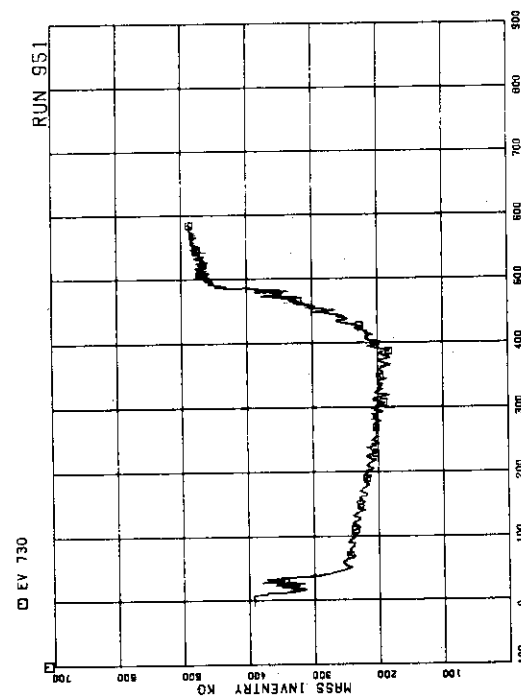

FIG.5.168 FLUID INVENTORY INSIDE CORE SHROUD

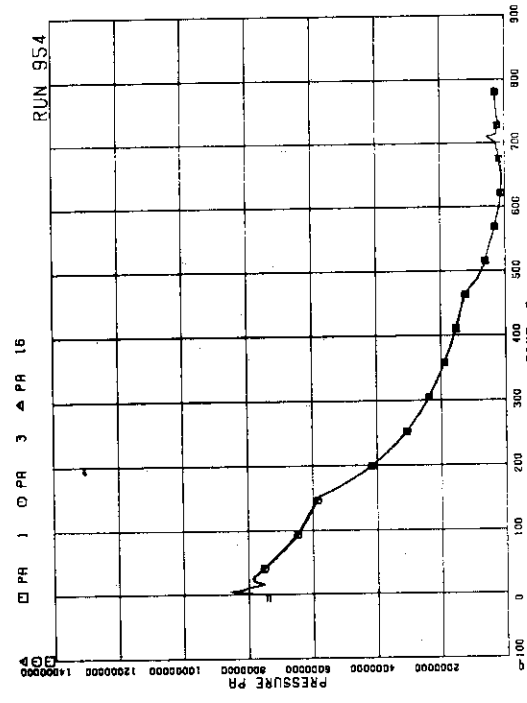

FIG.5.169 PRESSURES IN PV (PRESSURE VESSEL) AND MSL (MAIN STEAM LINE)

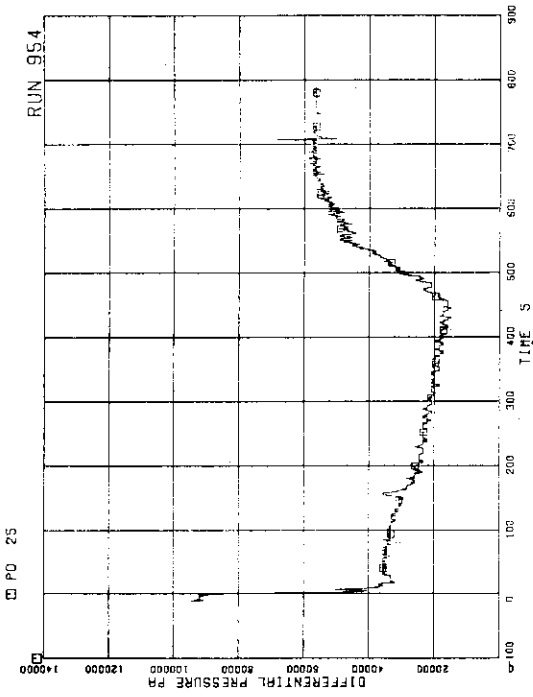

FIG.5.173 DIFFERENTIAL PRESSURE BETWEEN PV BOTTOM AND TOP

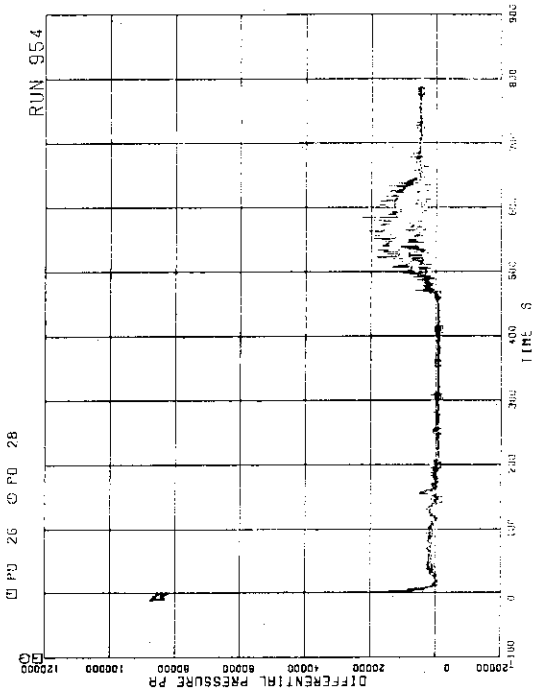

FIG.5.174 DIFFERENTIAL PRESSURE BETWEEN JP 1,2 DISCHARGE AND SUCTION

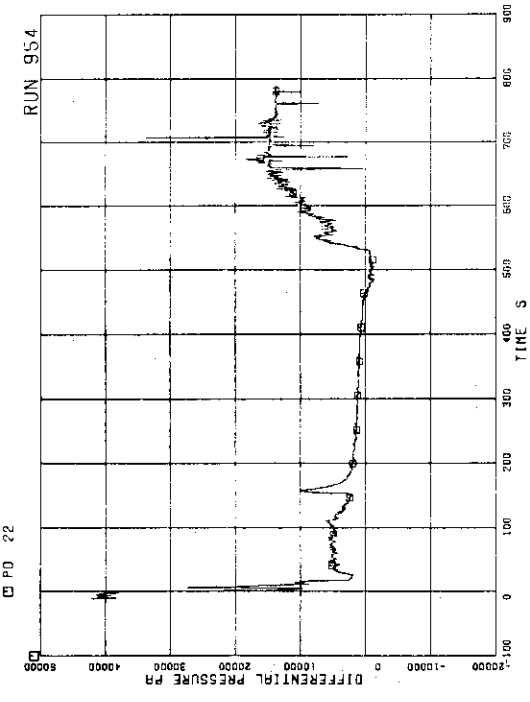

FIG.5.171 DIFFERENTIAL PRESSURE BETWEEN UP AND STEAM DOME

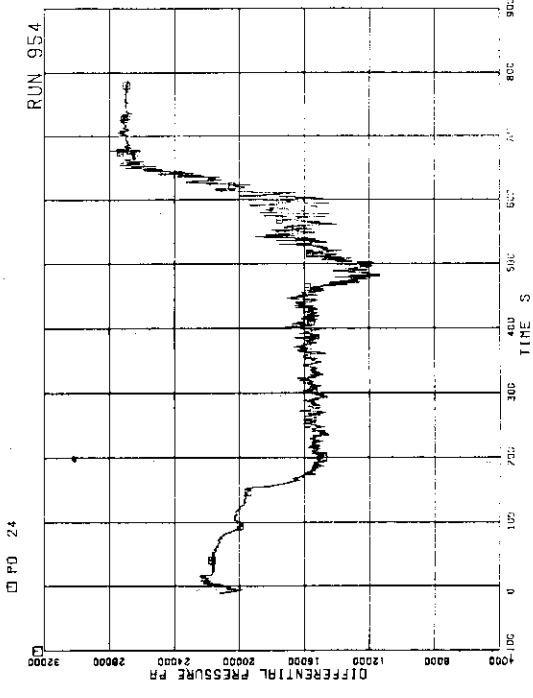

FIG.5.172 DIFFERENTIAL PRESSURE BETWEEN DOWNCOMER AND LOWER HEAD

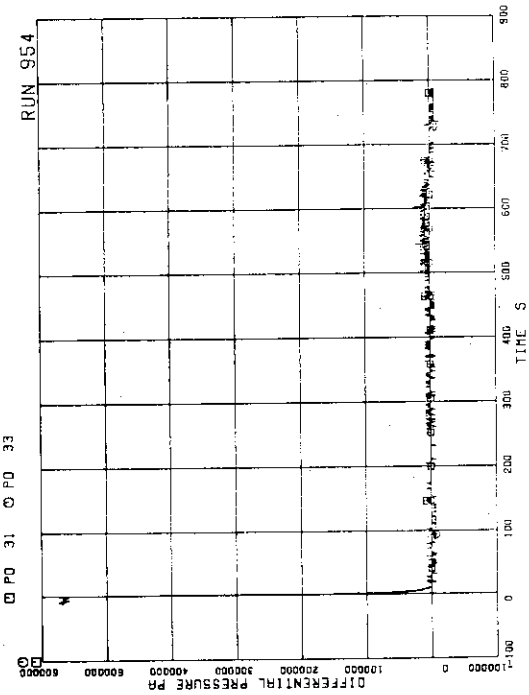

FIG.5.174 DIFFERENTIAL PRESSURE BETWEEN JP 3,4 DRIVE AND SUCTION

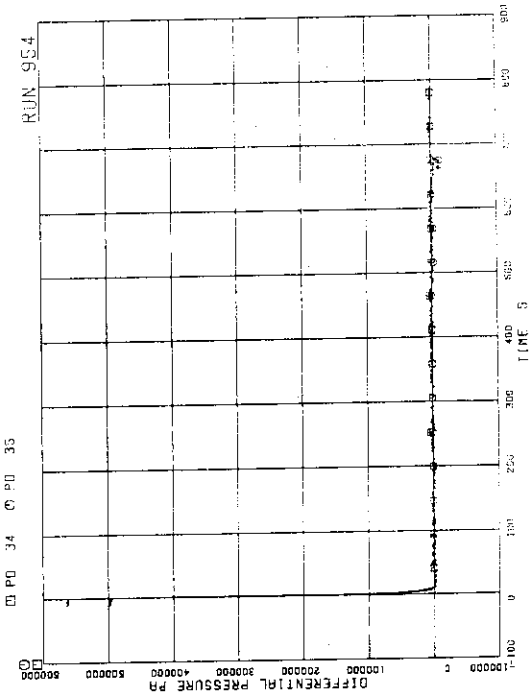

FIG.5.178 DIFFERENTIAL PRESSURE BETWEEN MRP DELIVERY AND SUCTION

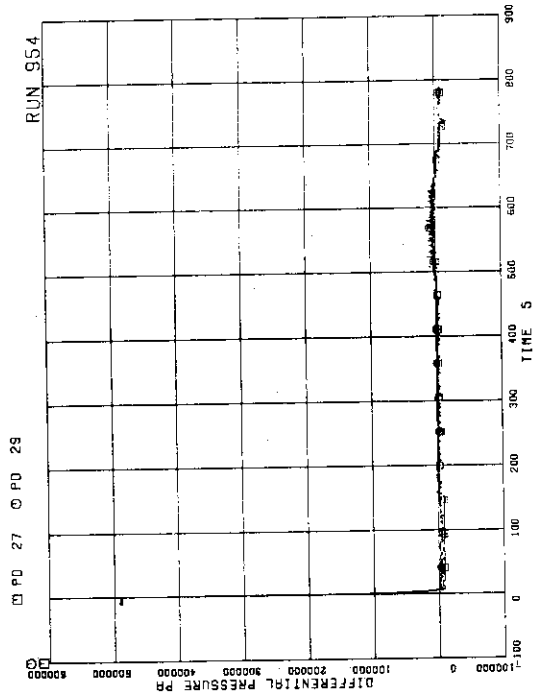

FIG.5.175 DIFFERENTIAL PRESSURE BETWEEN JP-1,2 DRIVE AND SUCTION

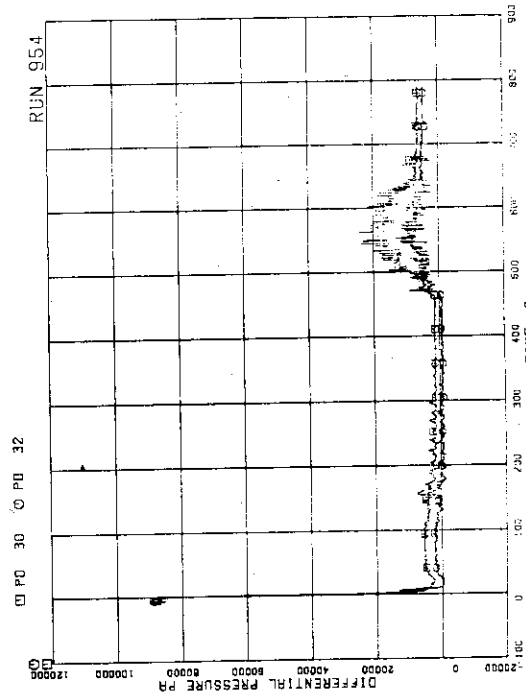

FIG.5.176 DIFFERENTIAL PRESSURE BETWEEN JP 3,4 DISCHARGE AND SUCTION

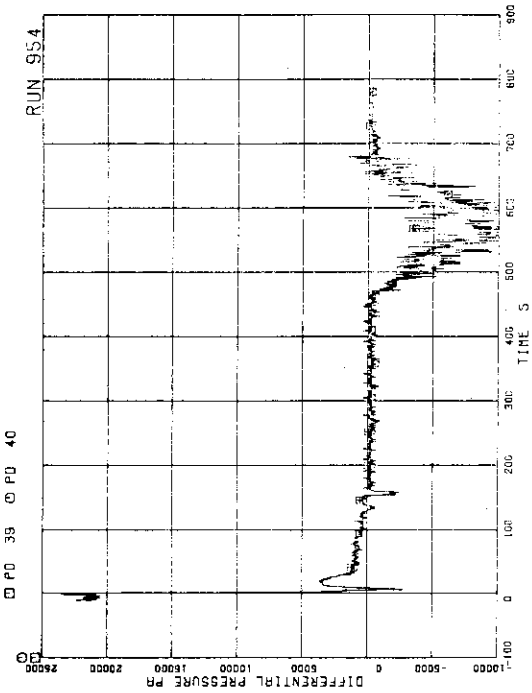

FIG.5-181 DIFFERENTIAL PRESSURE BETWEEN OC MIDDLE AND JP-1,2 SUCTION

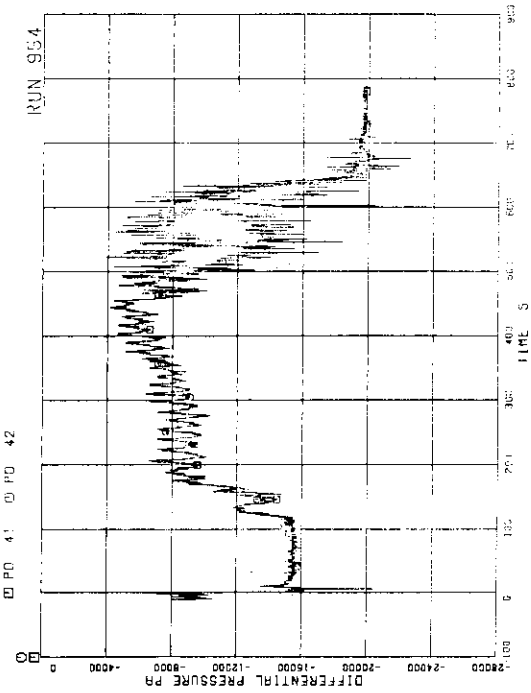

FIG.5-182 DIFFERENTIAL PRESSURE BETWEEN JP 1,2 DISCHARGE AND LP

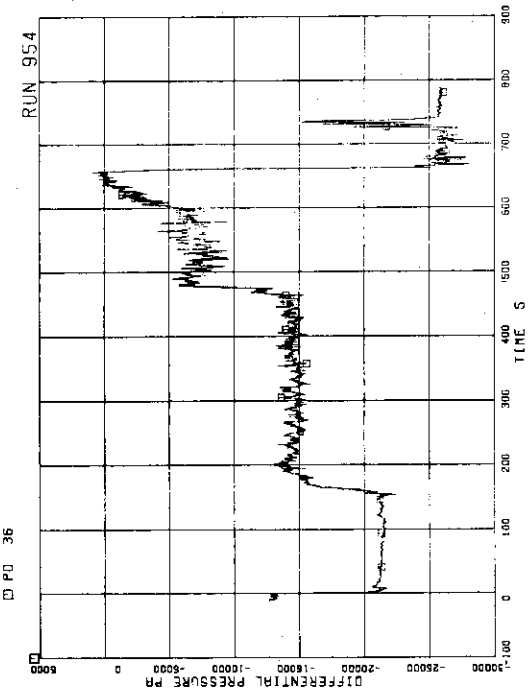

FIG.5-179 DIFFERENTIAL PRESSURE BETWEEN OC BOTTOM AND MRP1 SUCTION

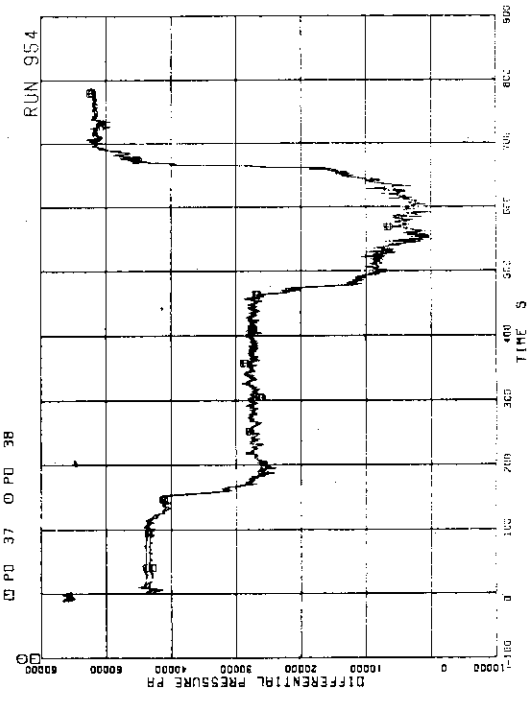

FIG.5-180 DIFFERENTIAL PRESSURE BETWEEN MRP1 DELIVERY AND JP 1,2 DRIVE

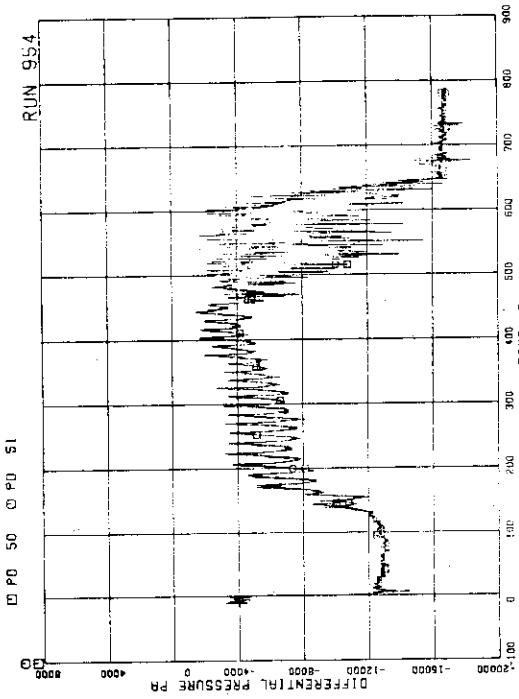

FIG.5.183 DIFFERENTIAL PRESSURE BETWEEN MRP2 DELIVERY AND JP-3,4 DRIVE

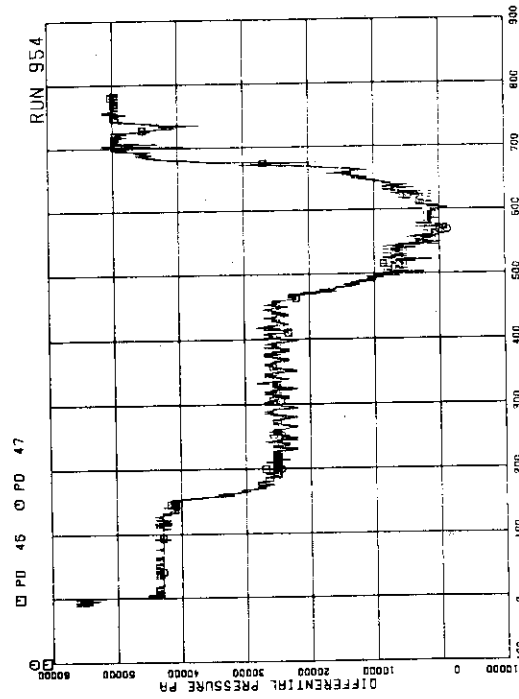

FIG.5.184 DIFFERENTIAL PRESSURE BETWEEN DC MIDDLE AND JP 3,4 SUCTION

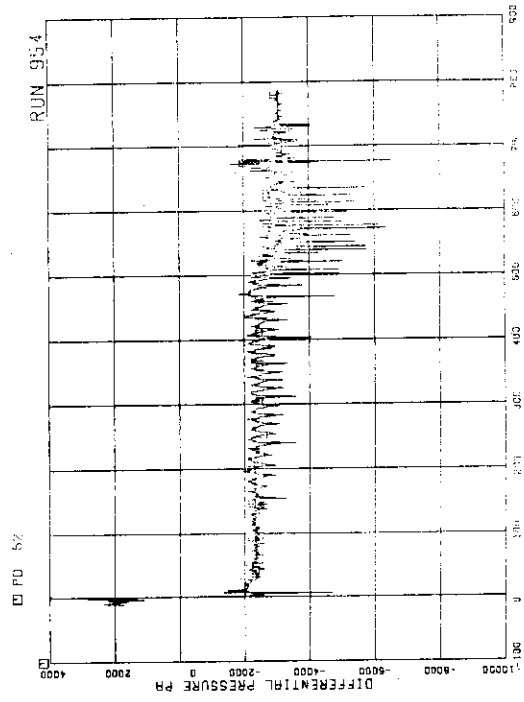

FIG.5.185 DIFFERENTIAL PRESSURE BETWEEN JP 3,4 DISCHARGE AND CONFLUENCE

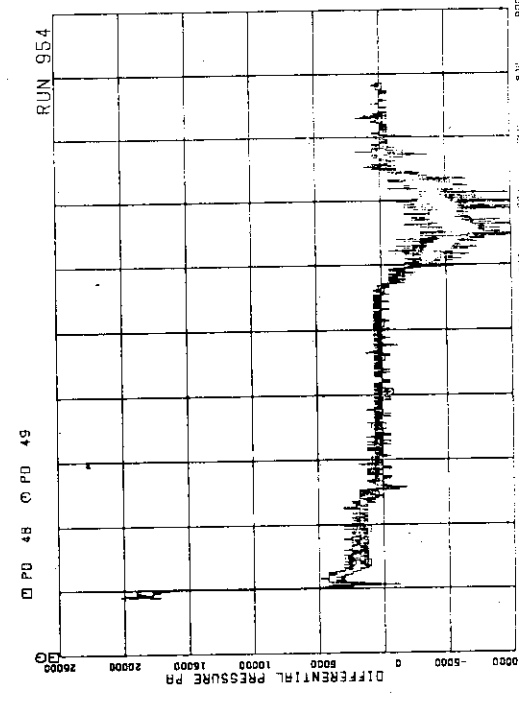

FIG.5.186 DIFFERENTIAL PRESSURE BETWEEN JP 3,4 CONFLUENCE AND LP

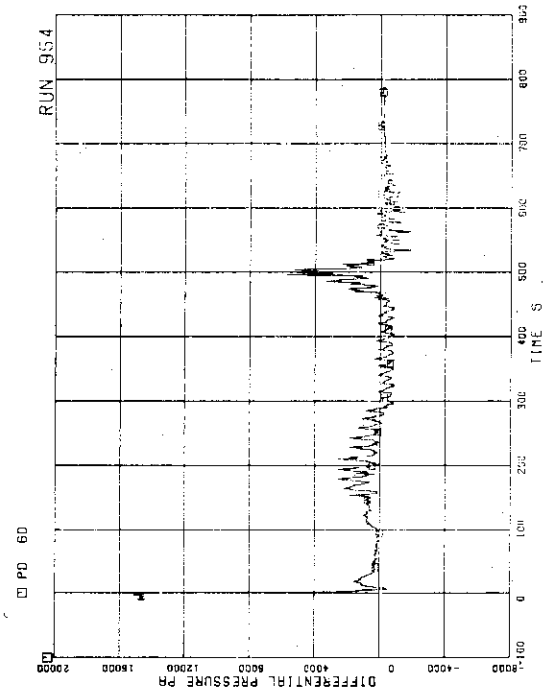

FIG.5.186 DIFFERENTIAL PRESSURE ACROSS CHANNEL INLET ORIFICE A

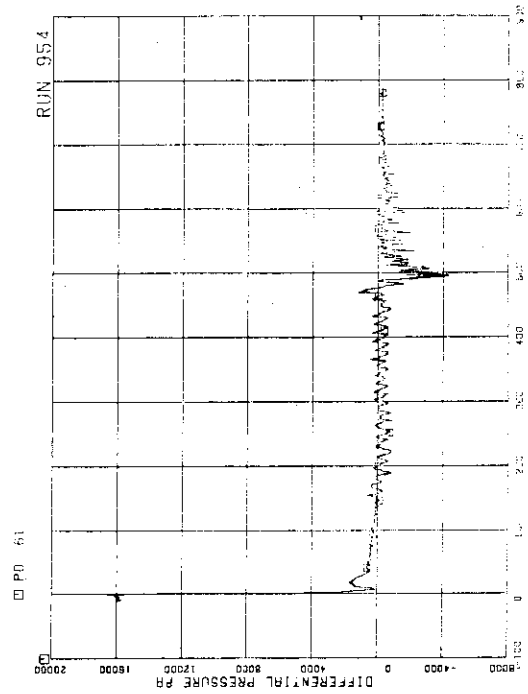

FIG.5.190 DIFFERENTIAL PRESSURE ACROSS CHANNEL INLET ORIFICE B

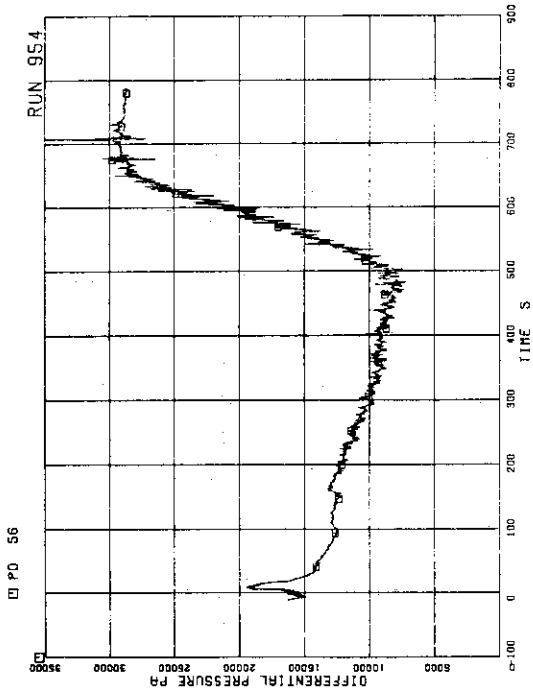

FIG.5.187 DIFFERENTIAL PRESSURE BETWEEN DC MIDDLE AND STEAM DOME

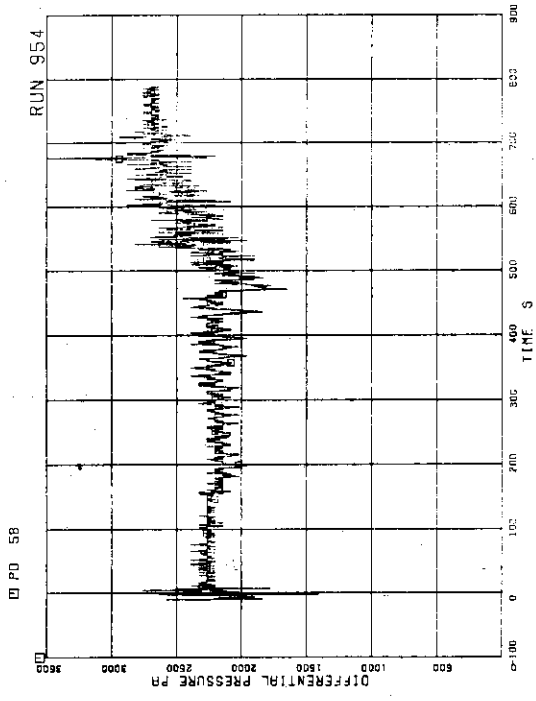

FIG.5.188 DIFFERENTIAL PRESSURE BETWEEN LP BOTTOM AND LP MIDDLE

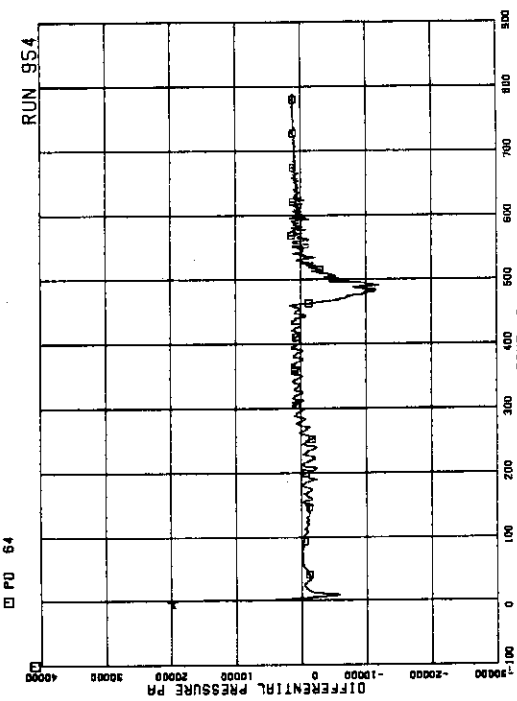

FIG.5.193 DIFFERENTIAL PRESSURE ACROSS BYPASS HOLE

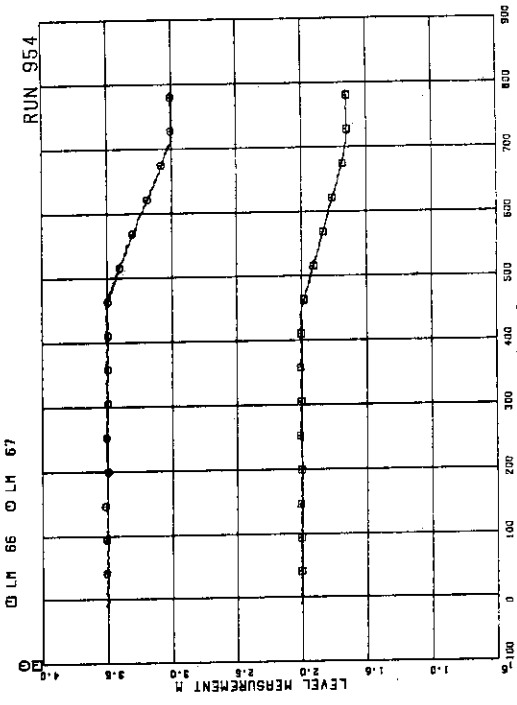

FIG.5.194 LIQUID LEVELS IN ECCS TANKS

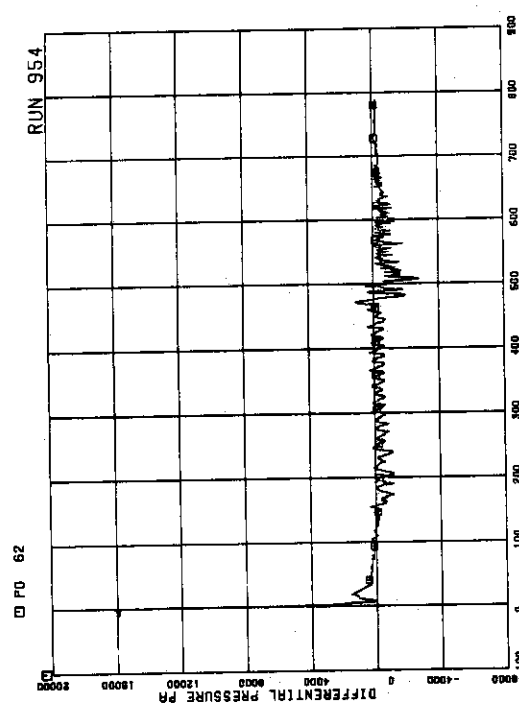

FIG.5.191 DIFFERENTIAL PRESSURE ACROSS CHANNEL INLET ORIFICE C

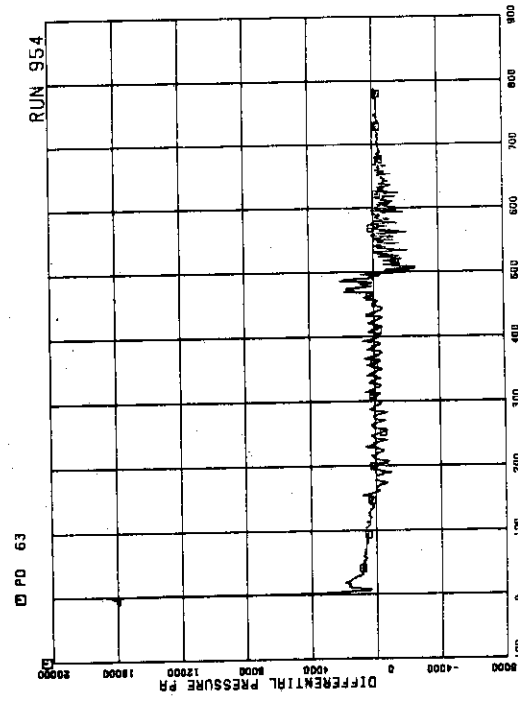

FIG.5.192 DIFFERENTIAL PRESSURE ACROSS CHANNEL INLET ORIFICE D

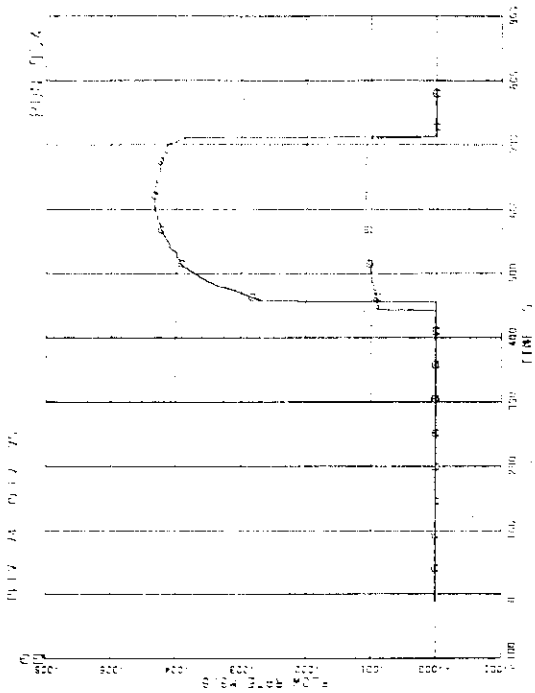

FIG.5.19(2) ECC INJECTION FLOW RATE

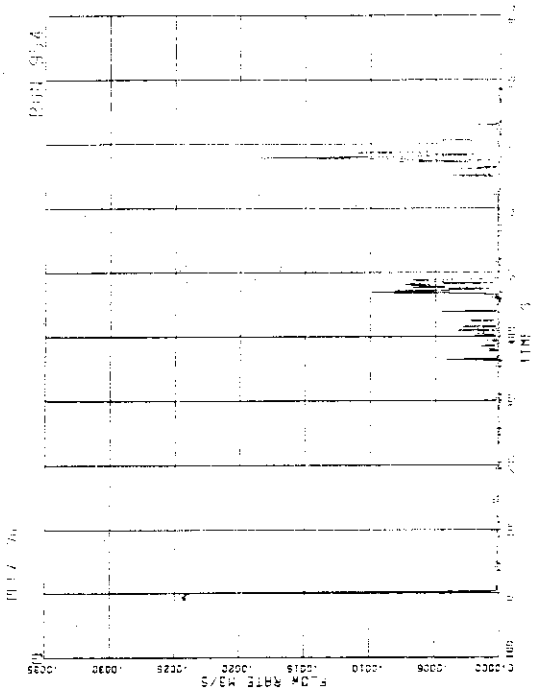

FIG.5.19(3) ACCUMULATOR FLOW RATE

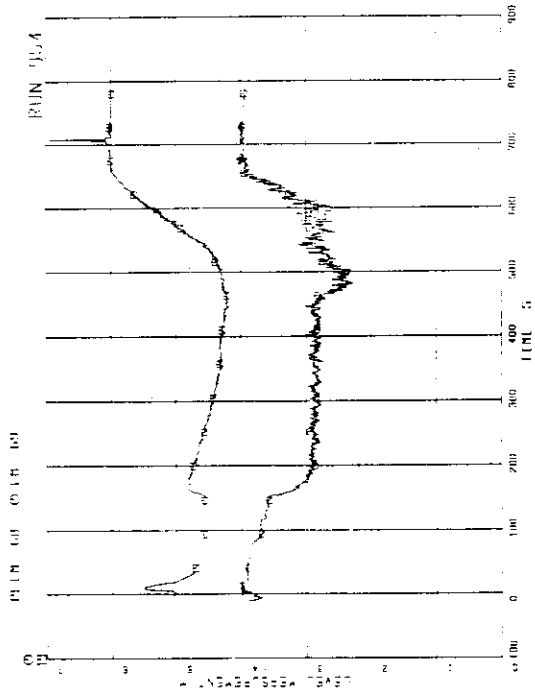

FIG.5.19(4) LIQUID LEVEL IN DOWNCOMER

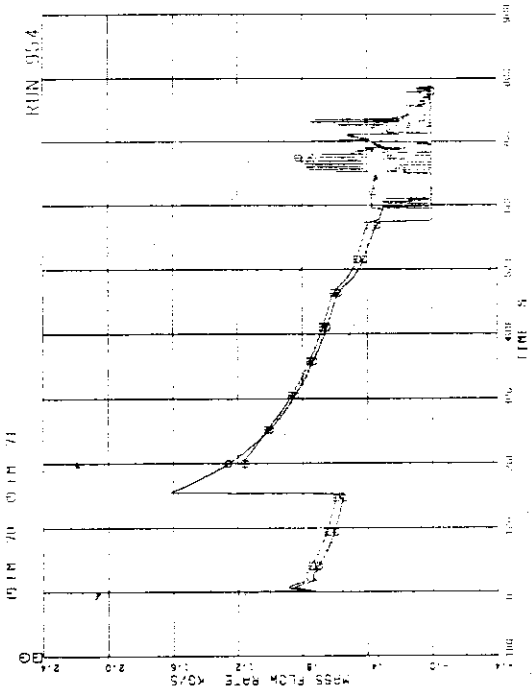

FIG.5.19(5) MASS FLOW RATE IN MCL

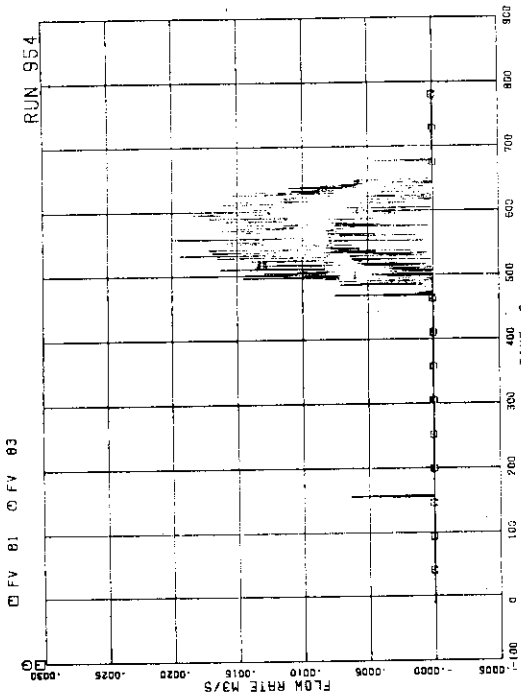

FIG.5.201 JP-3.4 DISCHARGE FLOW RATES (NEG.FLOW)

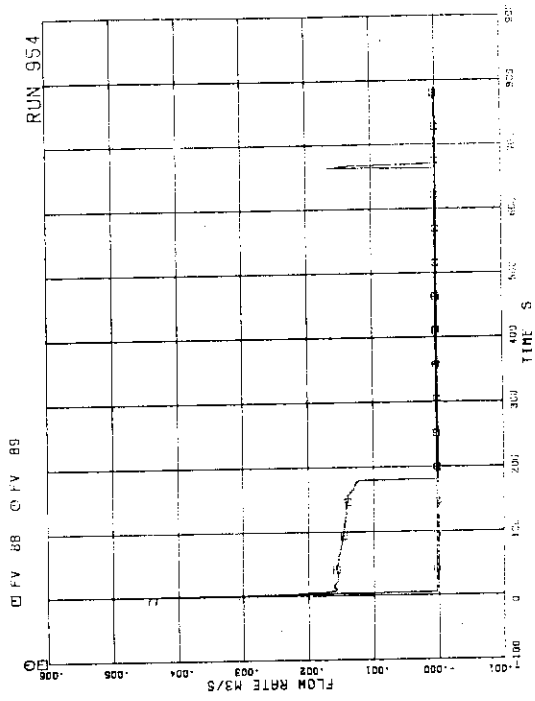

FIG.5.202 MSP DISCHARGE FLOW RATES

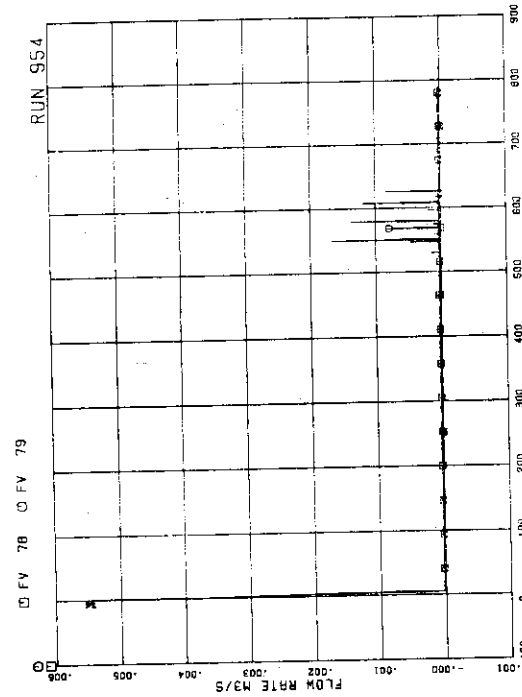

FIG.5.199 JP-1.2 DISCHARGE FLOW RATES (POS.FLOW)

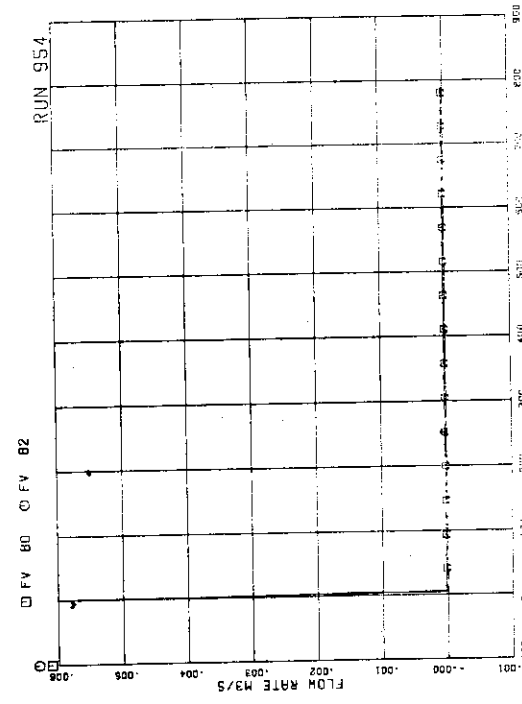

FIG.5.200 JP-3.4 DISCHARGE FLOW RATES (POS.FLOW)

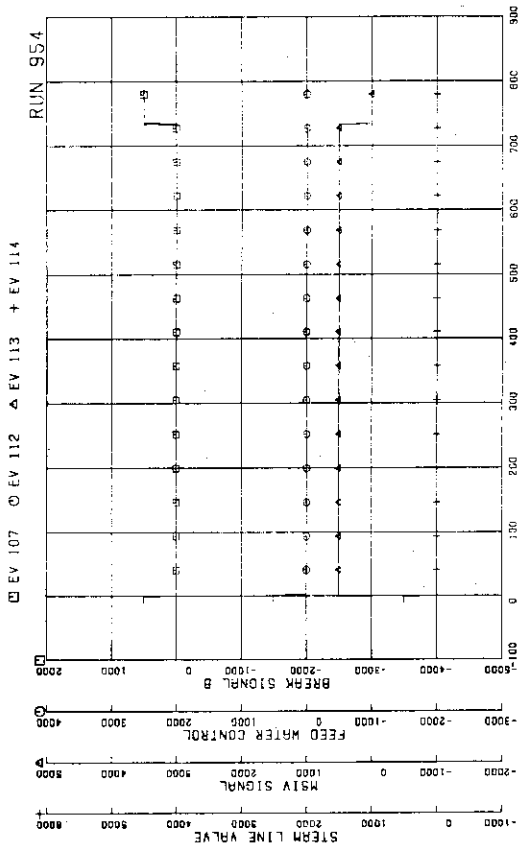

FIG.5-203 VALVE OPERATION SIGNALS

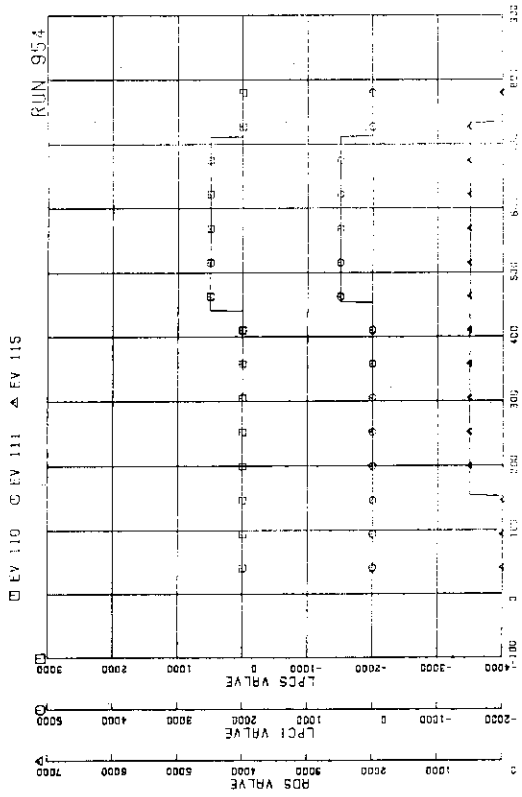

FIG.5-204 ECCS OPERATION SIGNALS

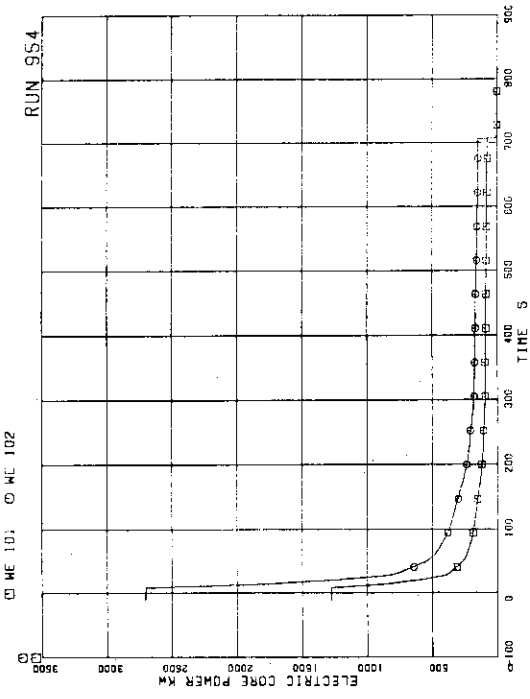

FIG.5-205 ELECTRIC CORE POWER

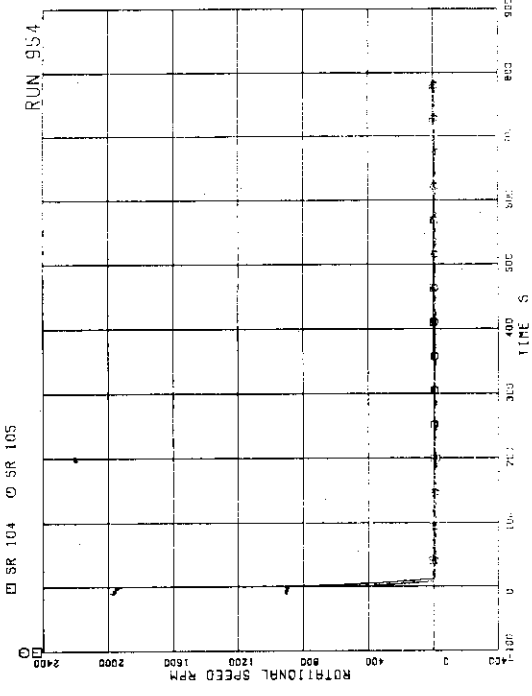

FIG.5-206 RCIC PUMP SPEEDS

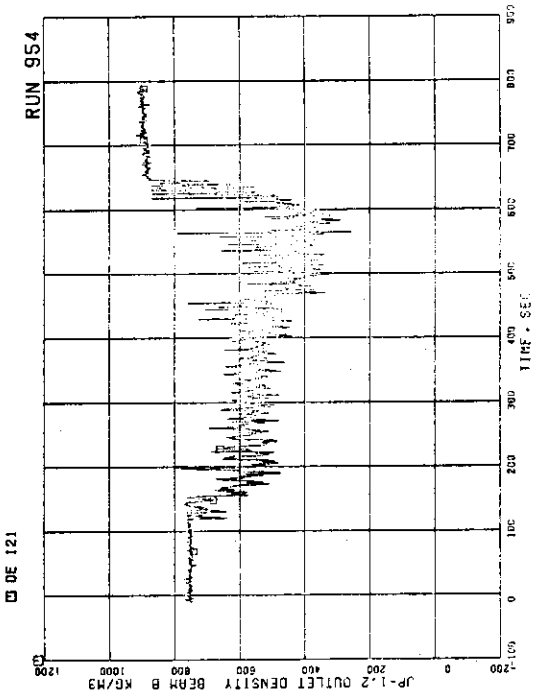

FIG.5.209 FLUID DENSITY AT JP-1,2 OUTLET, BEAM B

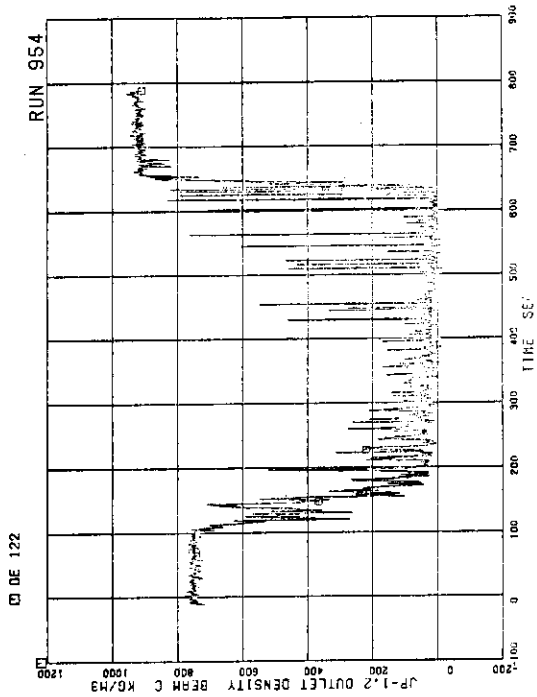

FIG.5.210 FLUID DENSITY AT JP-1,2 OUTLET, BEAM C

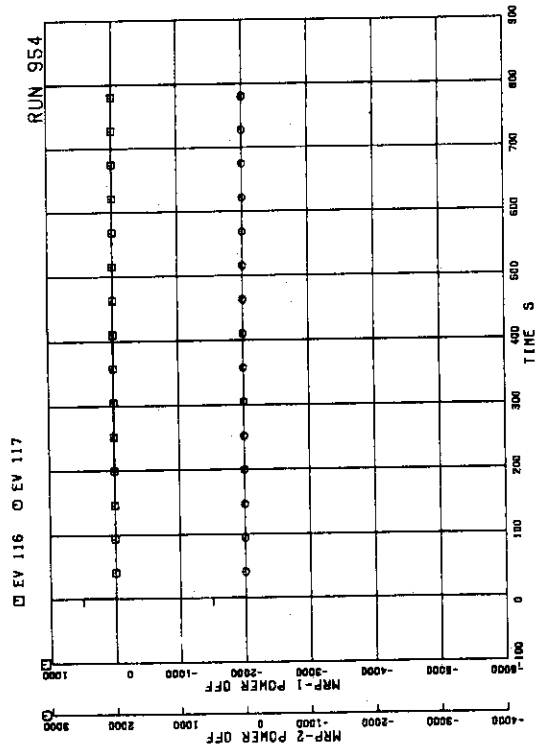

FIG.5.207 MRP OPERATION SIGNALS

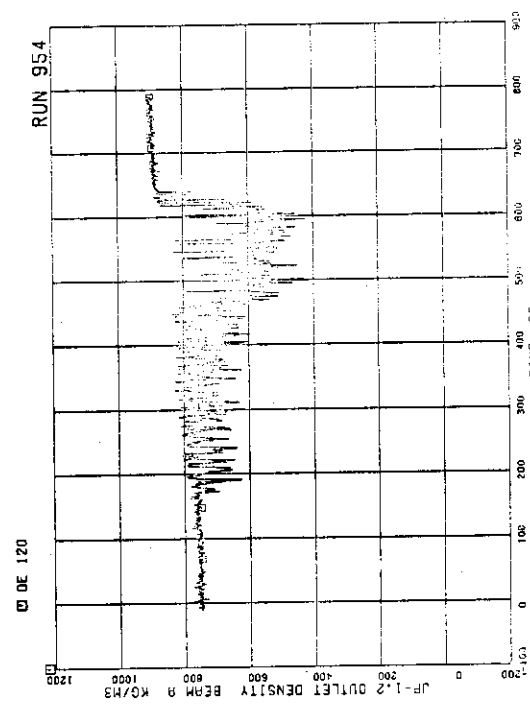

FIG.5.208 FLUID DENSITY AT JP-1,2 OUTLET, BEAM A

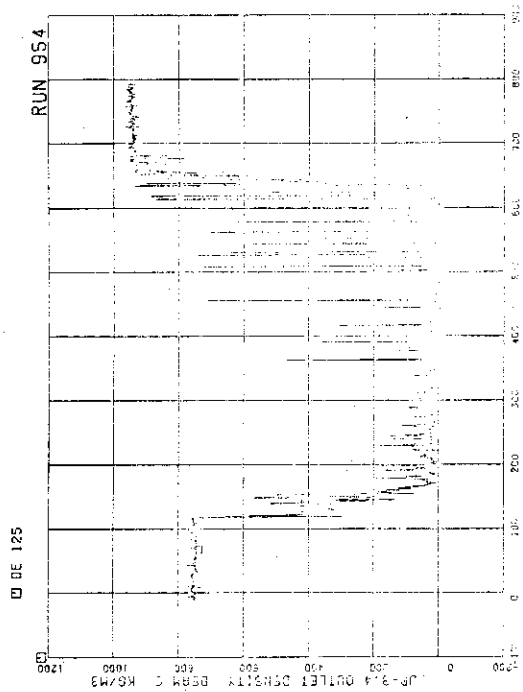

FIG.5.213 FLUID DENSITY AT JP-3.4 OUTLET, BEAM C

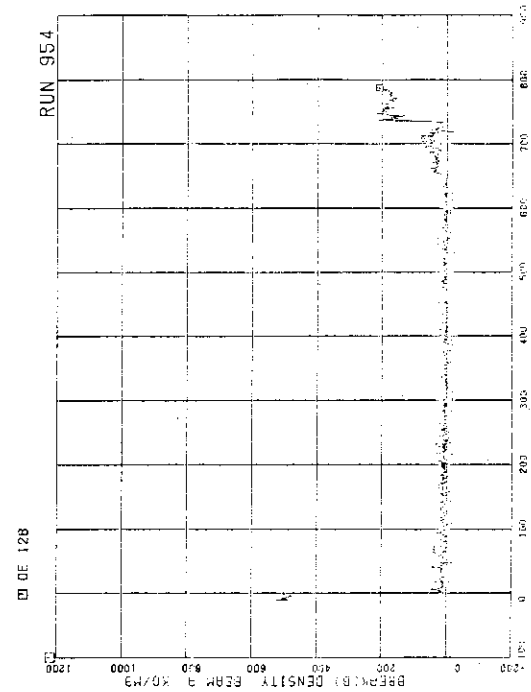

FIG.5.214 FLUID DENSITY IN MSL DOWN THE ORFAK ORIFICE, BEAM A

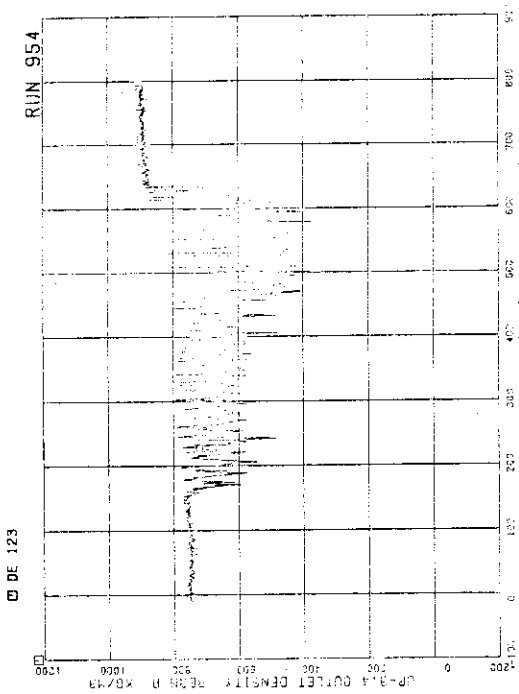

FIG.5.211 FLUID DENSITY AT JP-3.4 OUTLET, BEAM A

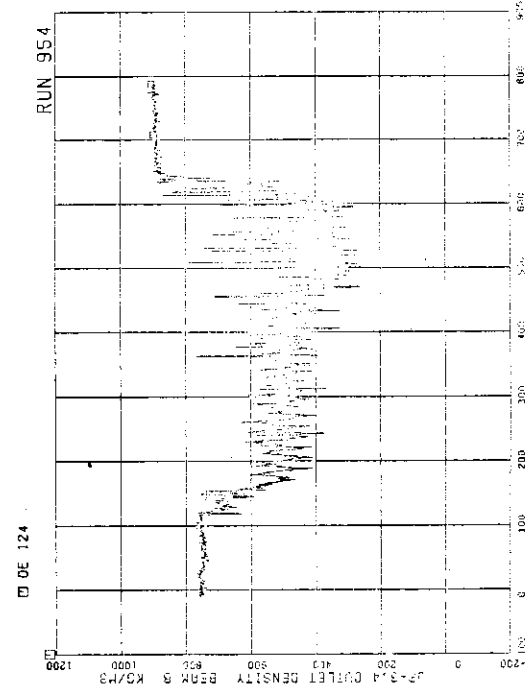

FIG.5.212 FLUID DENSITY AT JP 3.4 OUTLET, BEAM B

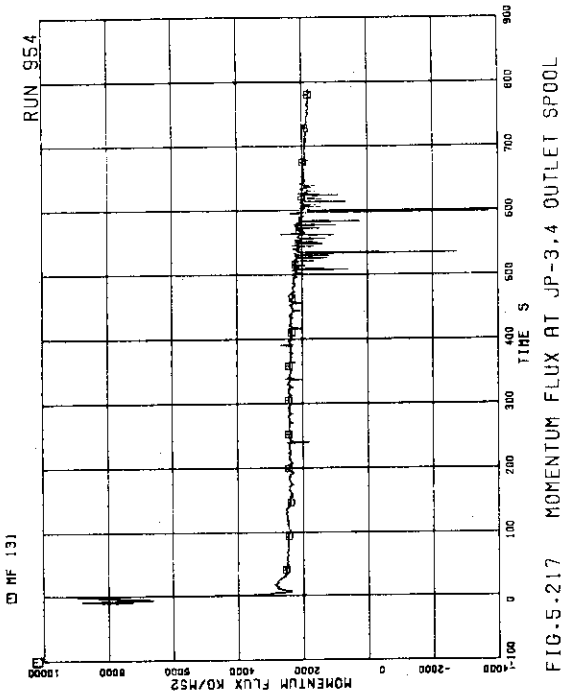

FIG.5.217 MOMENTUM FLUX AT JP-3,4 OUTLET SPOOL

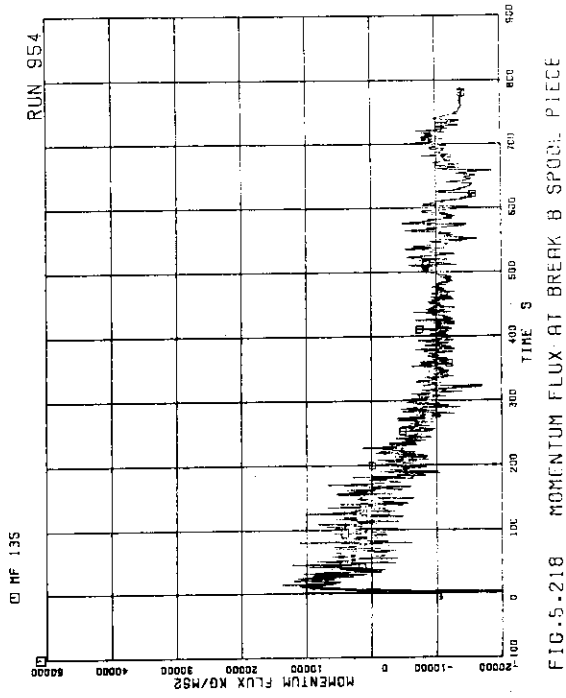

FIG.5.218 MOMENTUM FLUX AT BREAK B SPOOL PIECE (HIGH RANGE)

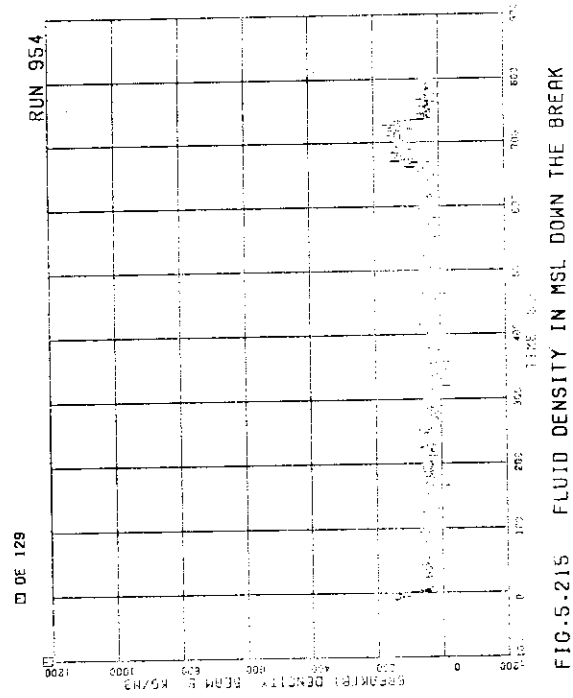

FIG.5.215 FLUID DENSITY IN MSL DOWN THE BREAK ORIFICE, BEAM B

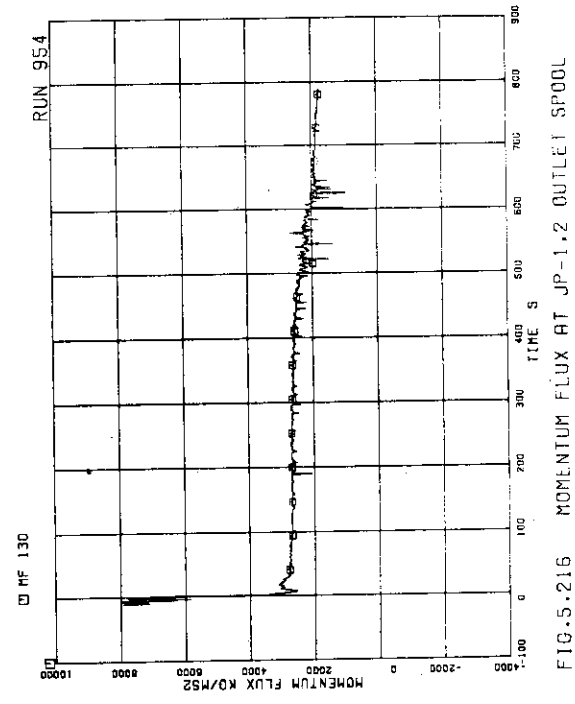

FIG.5.216 MOMENTUM FLUX AT JP-1,2 OUTLET SPOOL

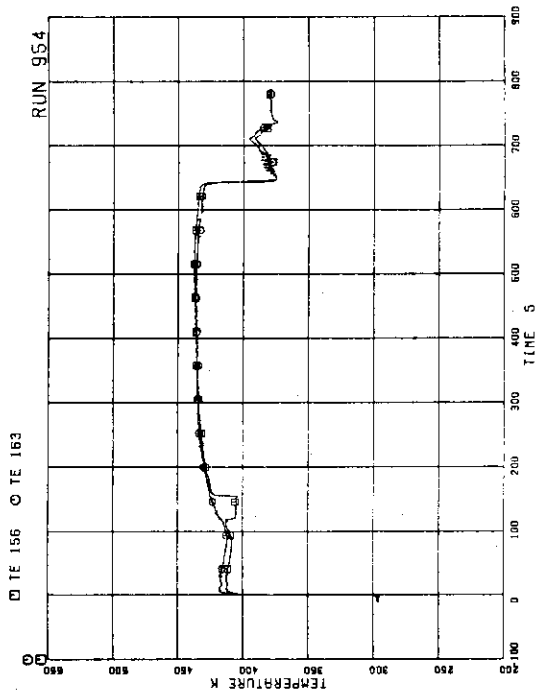

FIG.5-221 FLUID TEMPERATURE IN MSL DOWN THE BREAK ORIFICE

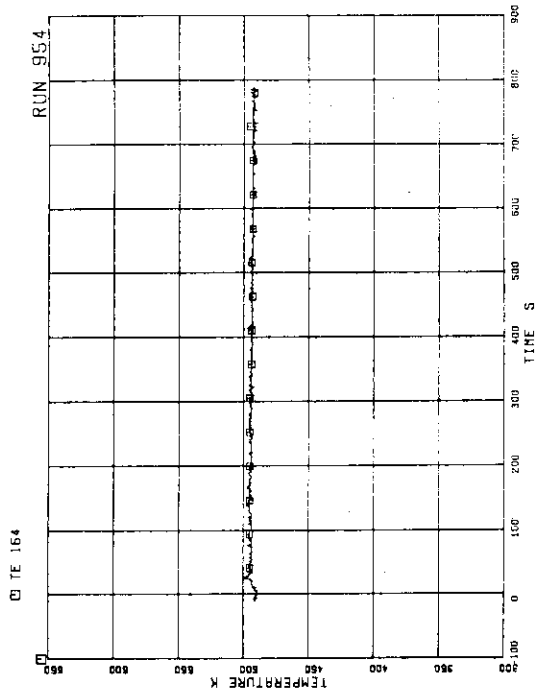

FIG.5-222 FEEDWATER TEMPERATURE

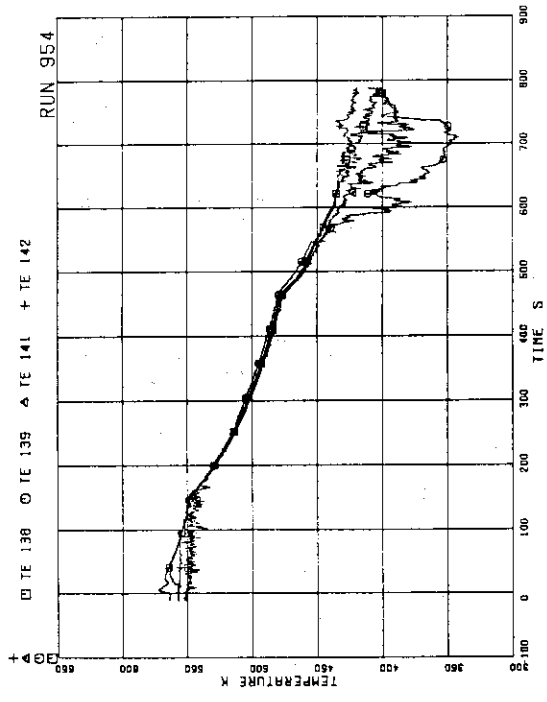

FIG.5-219 FLUID TEMPERATURES IN PV

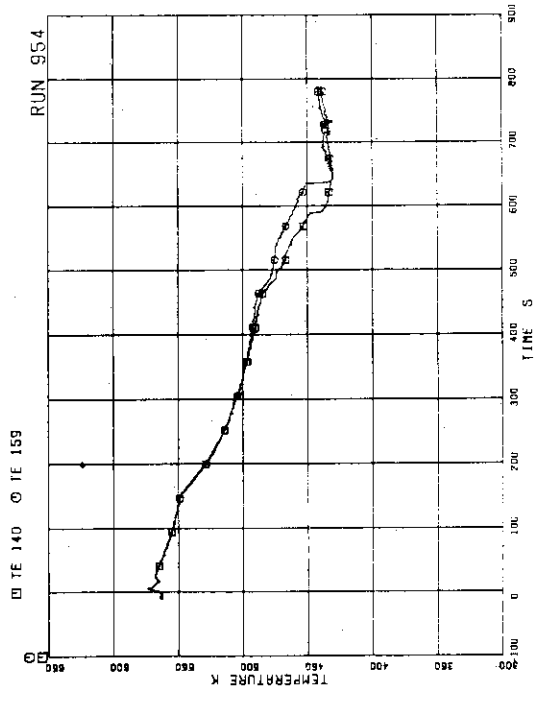

FIG.5-220 FLUID TEMPERATURE IN STEAM DOME AND MSL

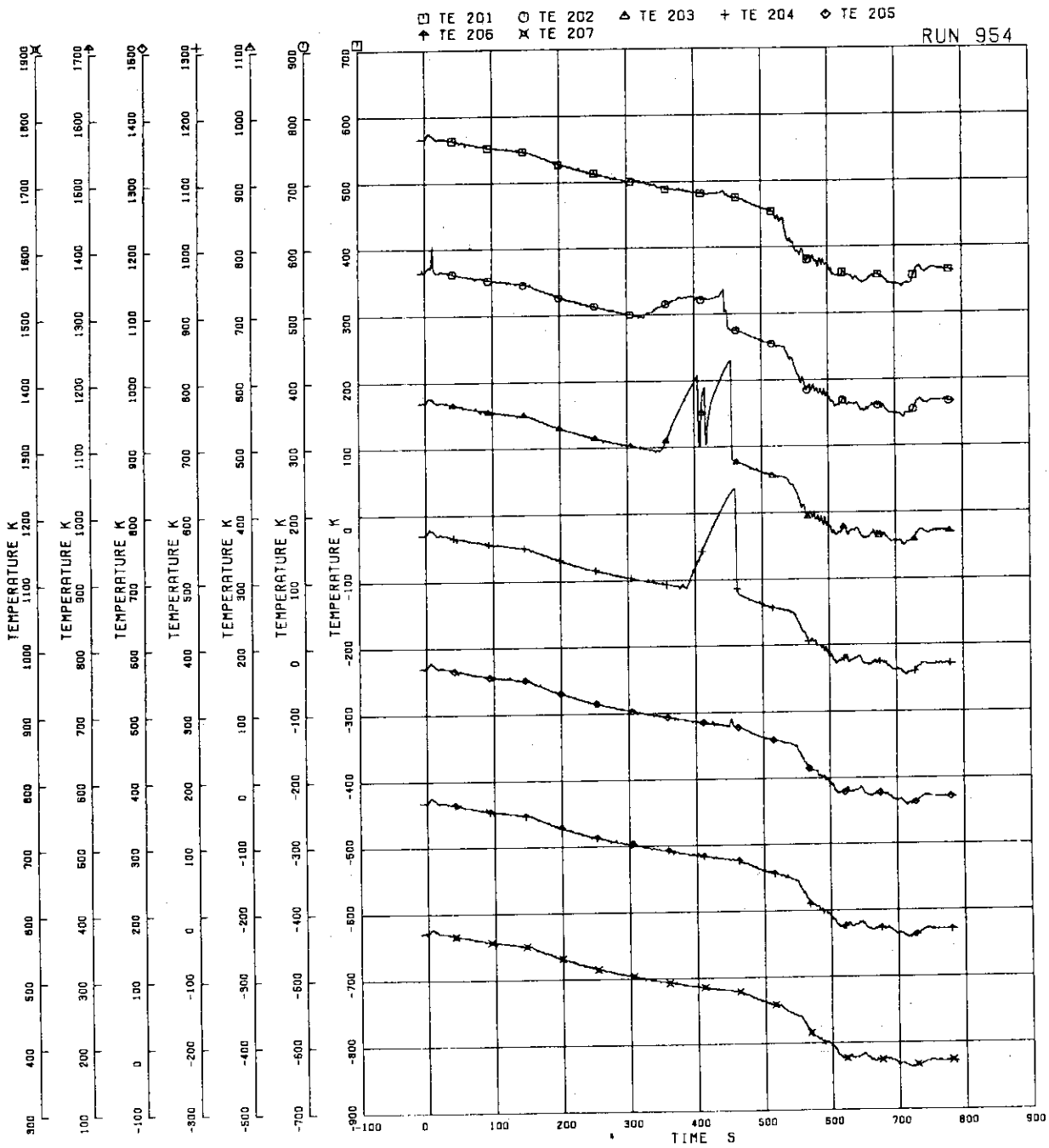

FIG.5.223 FUEL ROD SURFACE TEMPERATURE OF A11 ROD

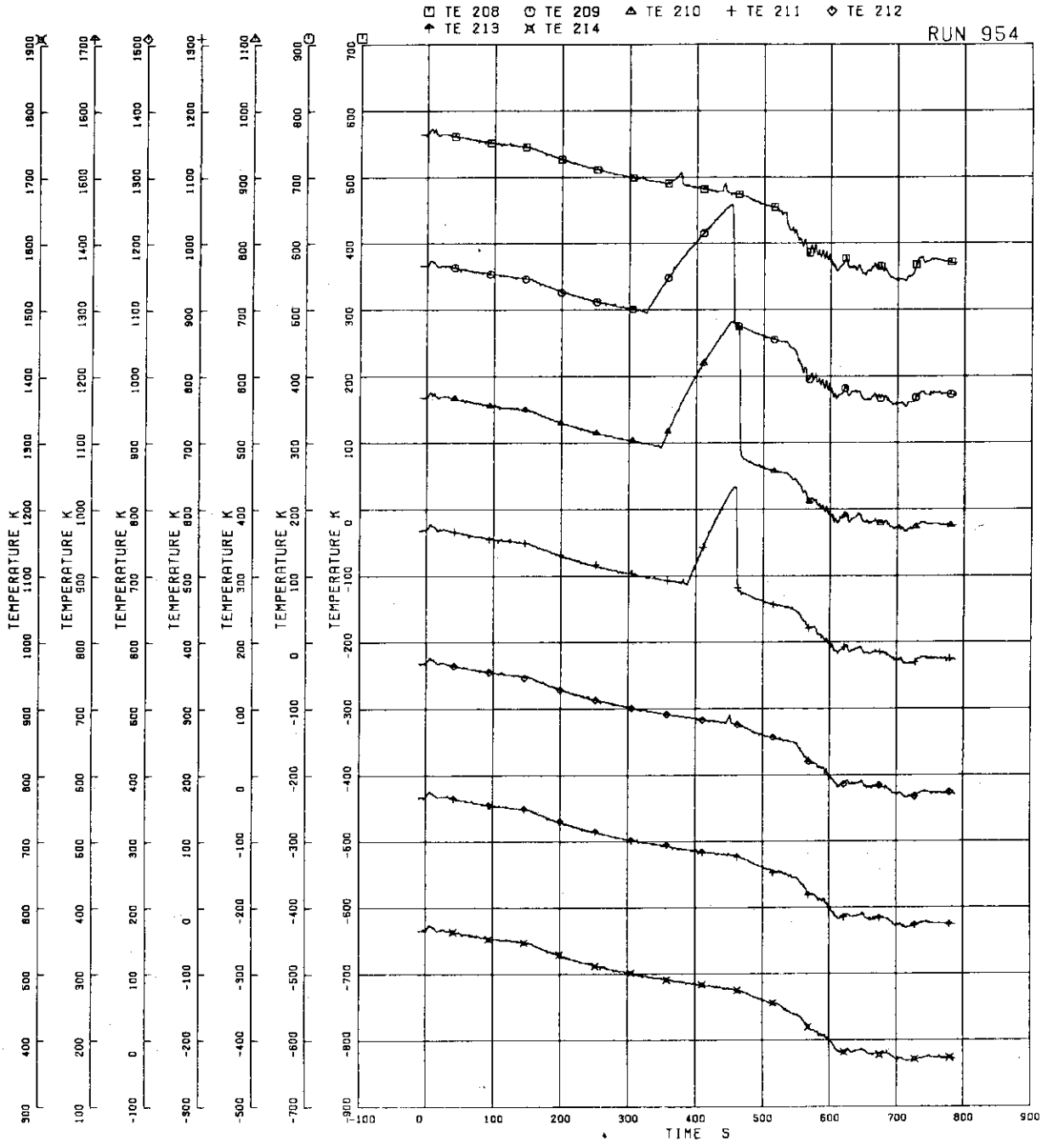

FIG.5-224 FUEL ROD SURFACE TEMPERATURE OF A12 ROD

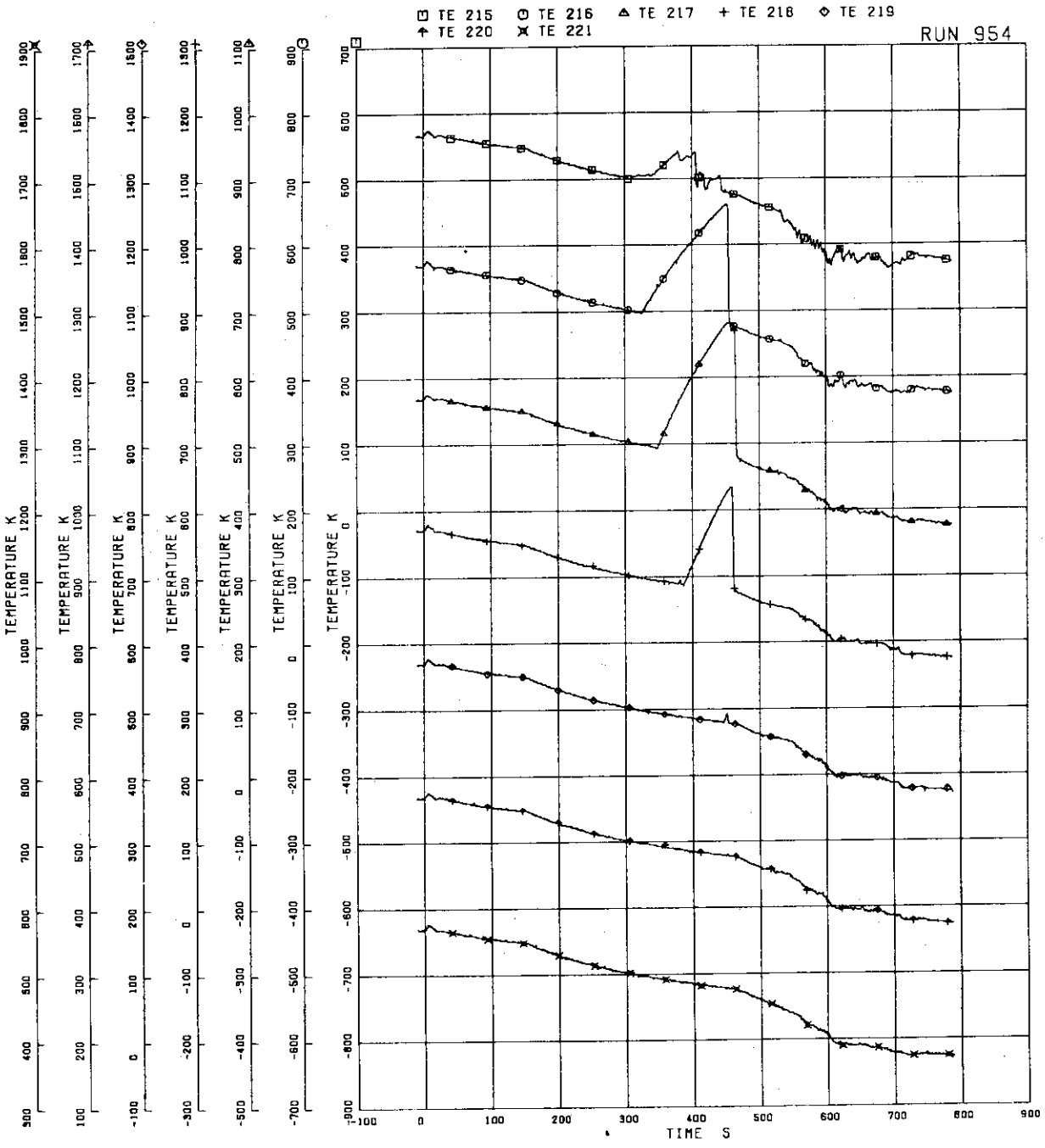

FIG.5.225 FUEL ROD SURFACE TEMPERATURE OF A13 ROD

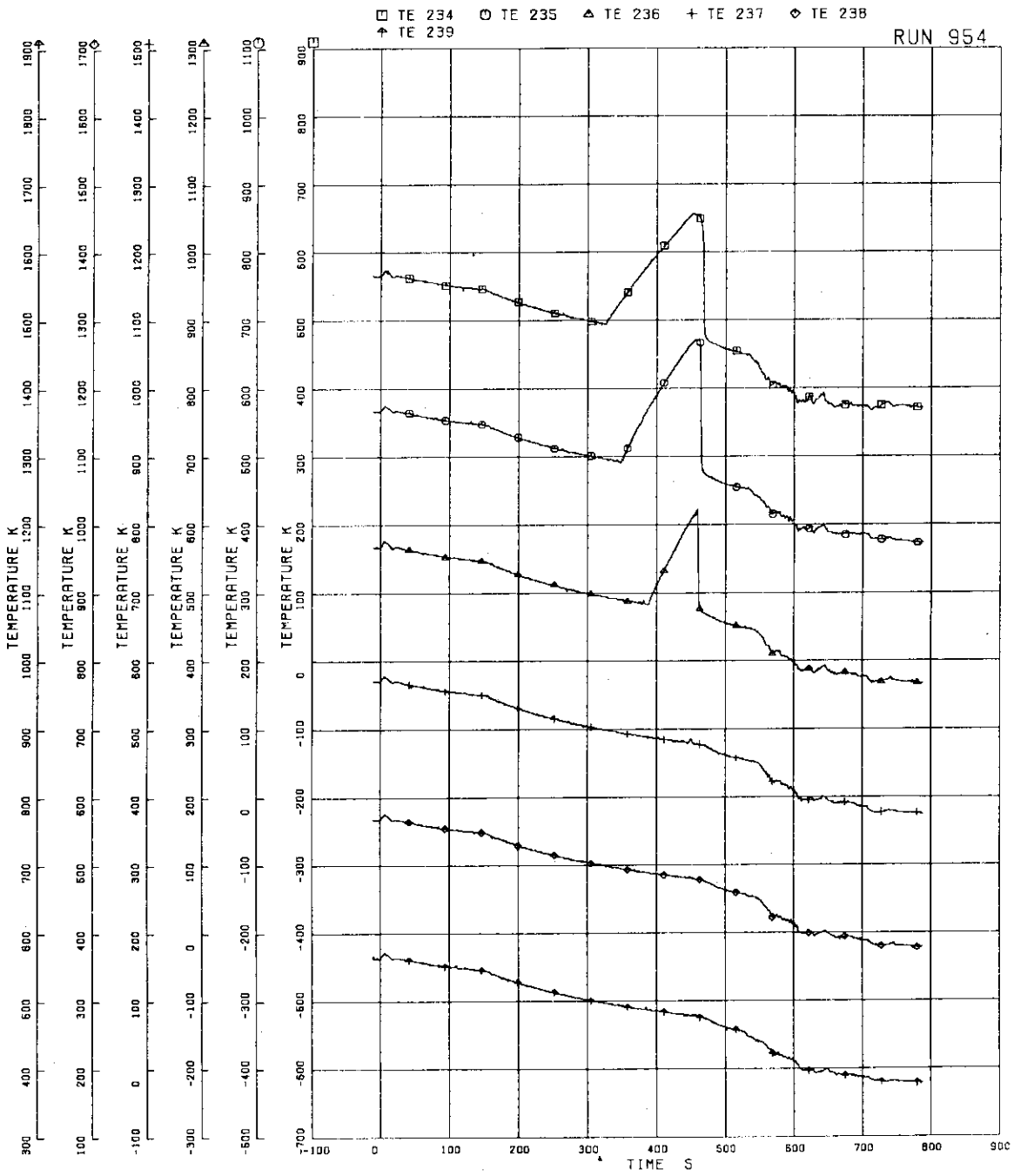

FIG.5.226 FUEL ROD SURFACE TEMPERATURE OF A22 ROD

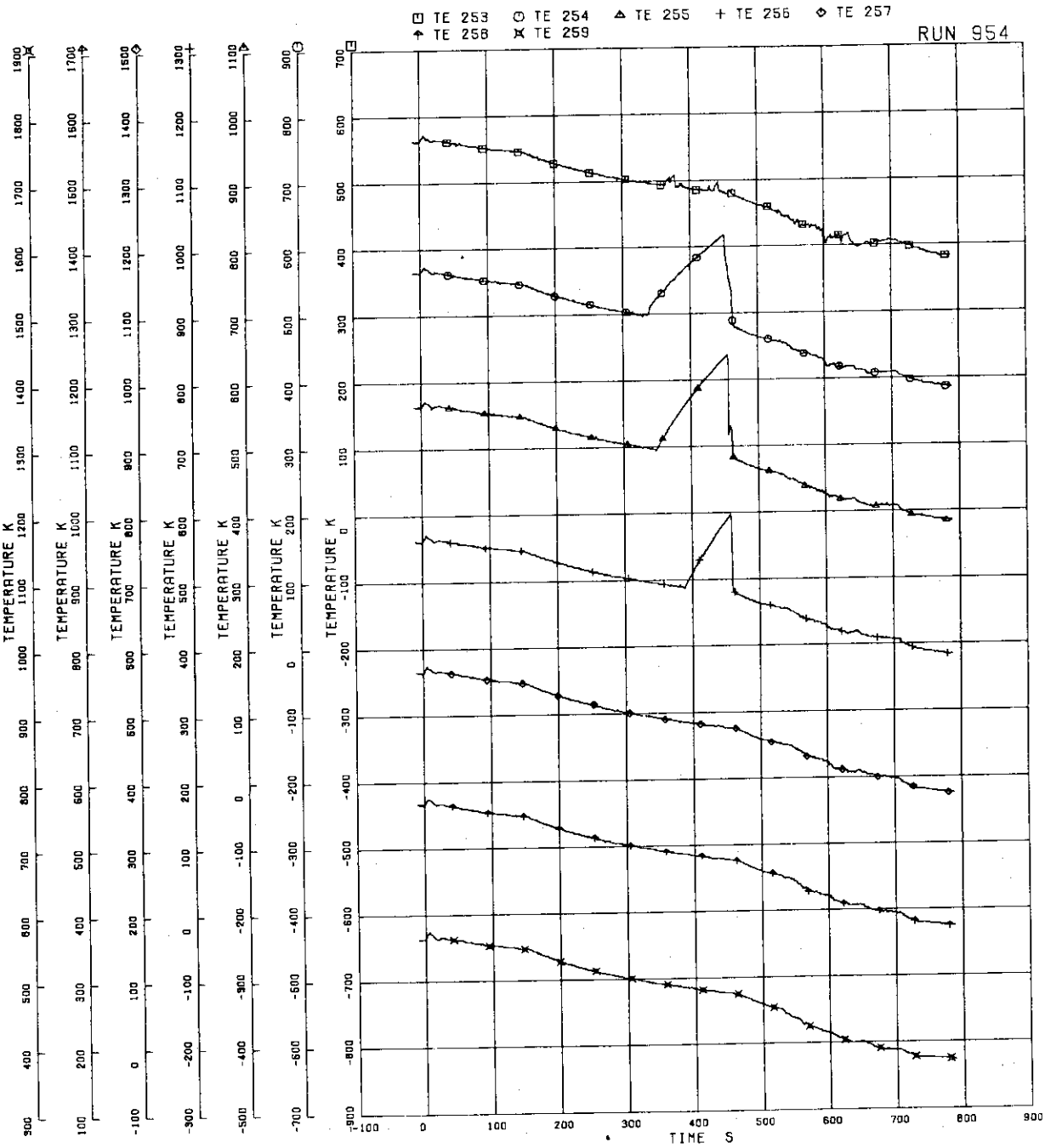

FIG.5.227 FUEL ROD SURFACE TEMPERATURE OF A33 ROD

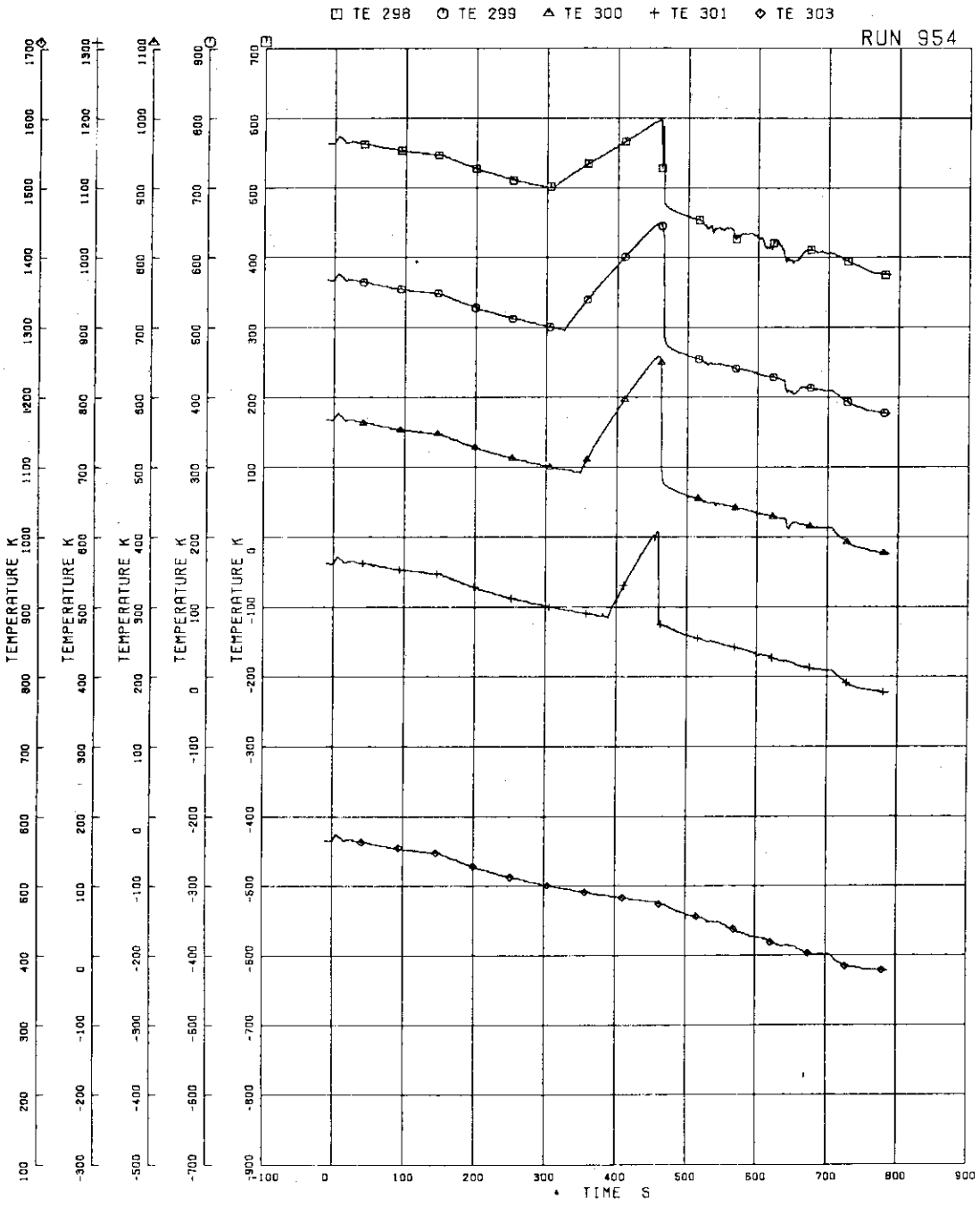

FIG.5.228 FUEL ROD SURFACE TEMPERATURE OF A77 ROD

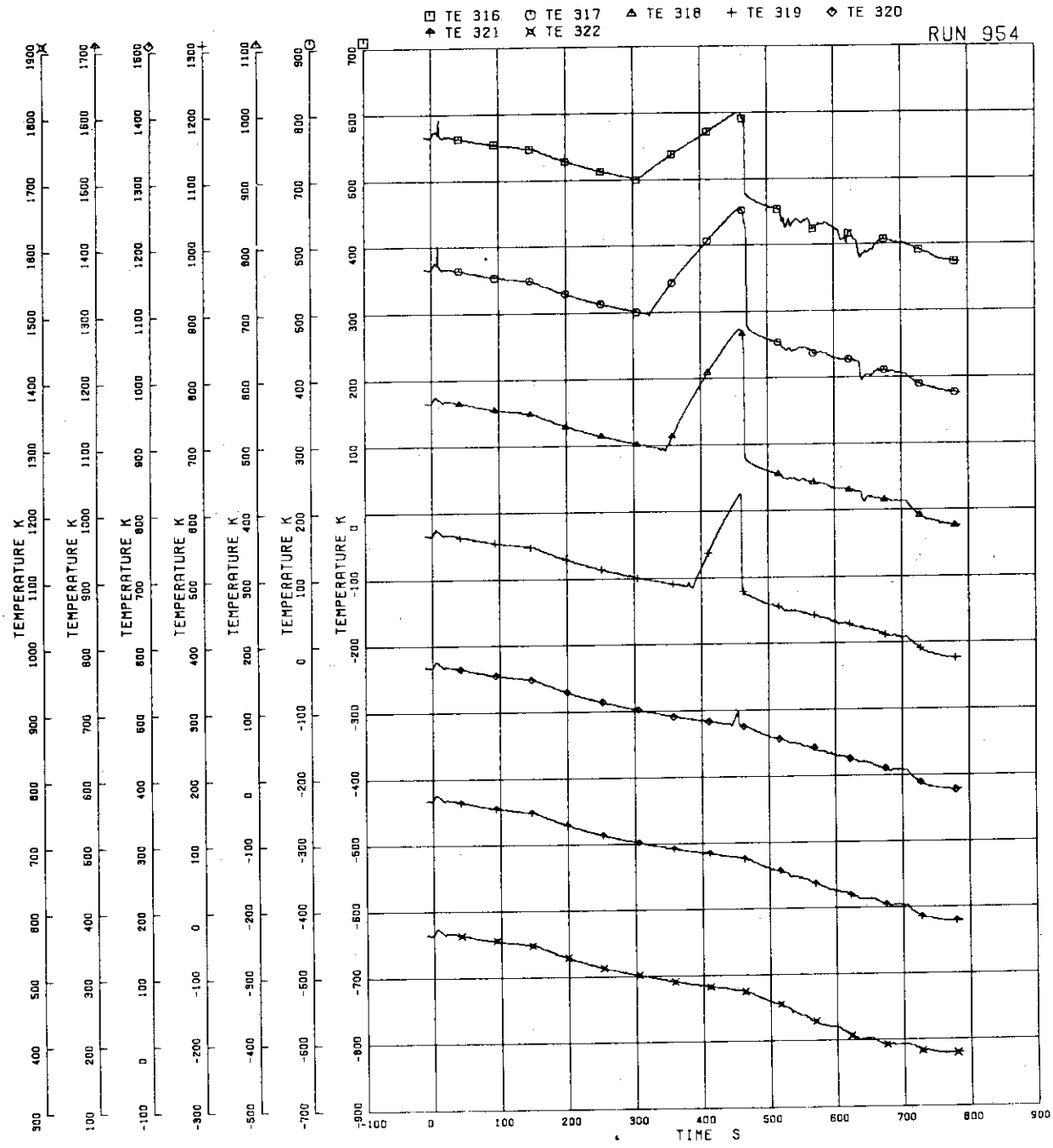

FIG.5.229 FUEL ROD SURFACE TEMPERATURE OF A87 ROD

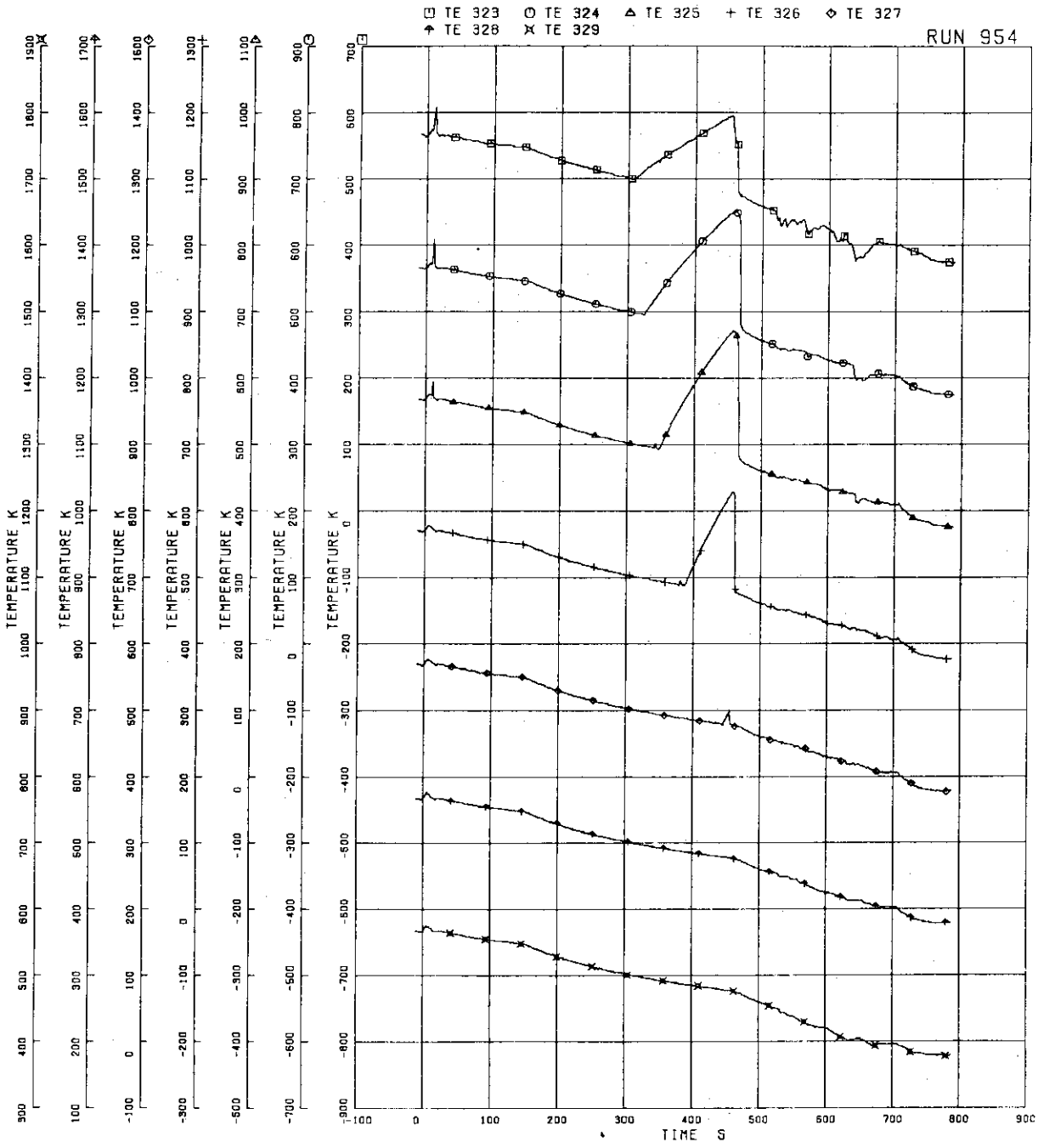

FIG.5.230 FUEL ROD SURFACE TEMPERATURE OF A88 ROD

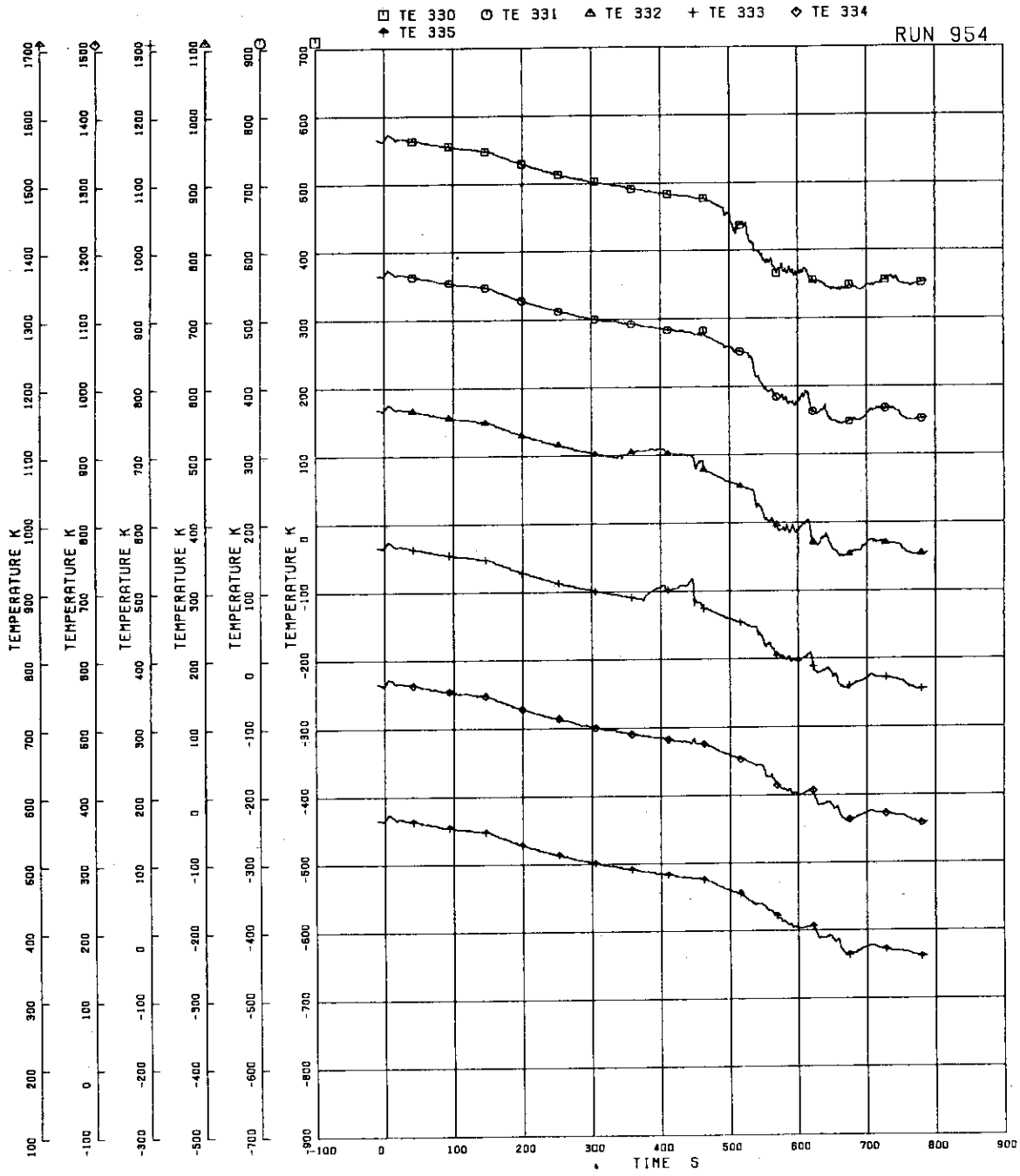

FIG.5.231 FUEL ROD SURFACE TEMPERATURE OF B11 ROD

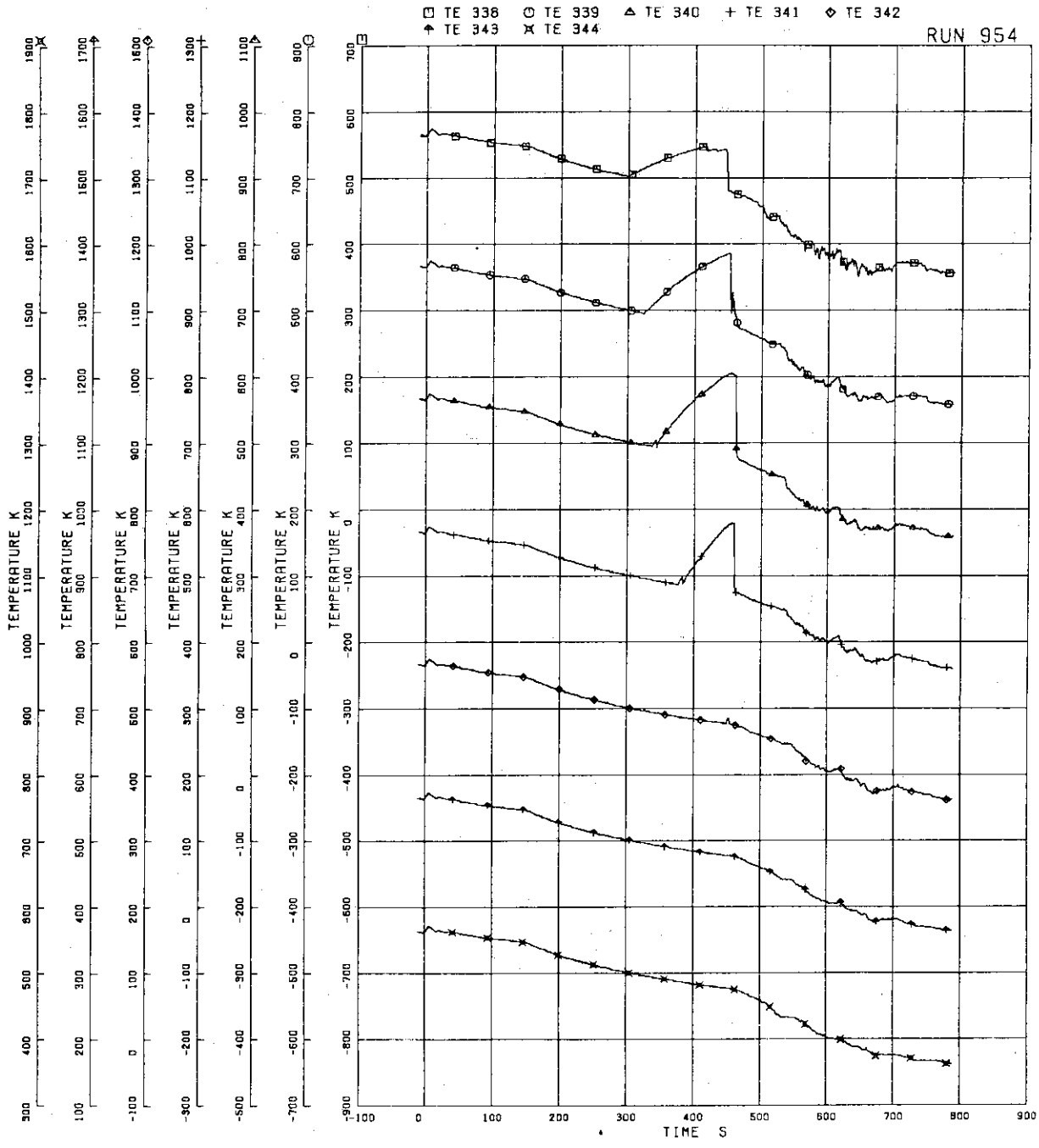

FIG.5.232 FUEL ROD SURFACE TEMPERATURE OF B22 ROD

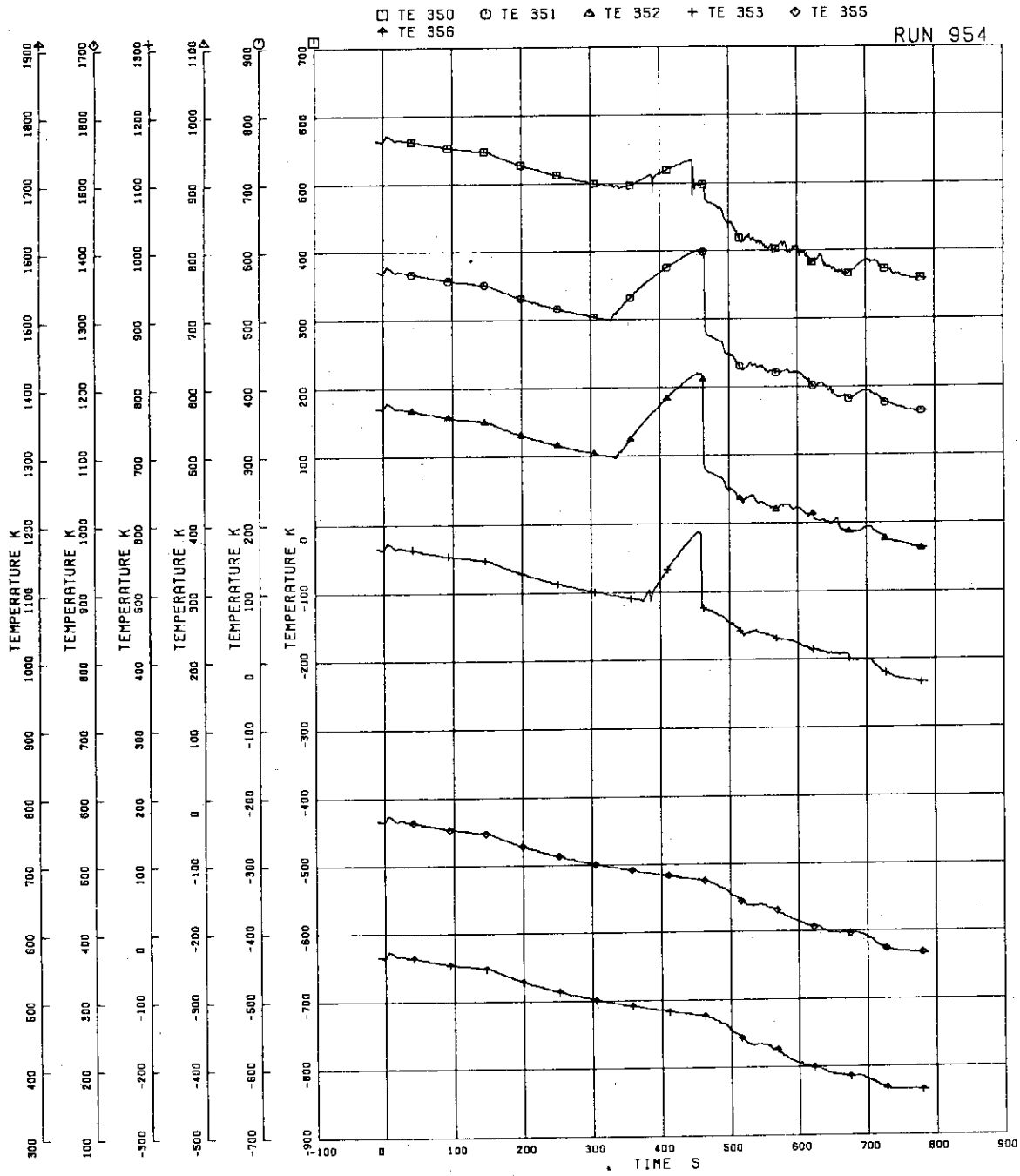

FIG.5.233 FUEL ROD SURFACE TEMPERATURE OF B77 ROD

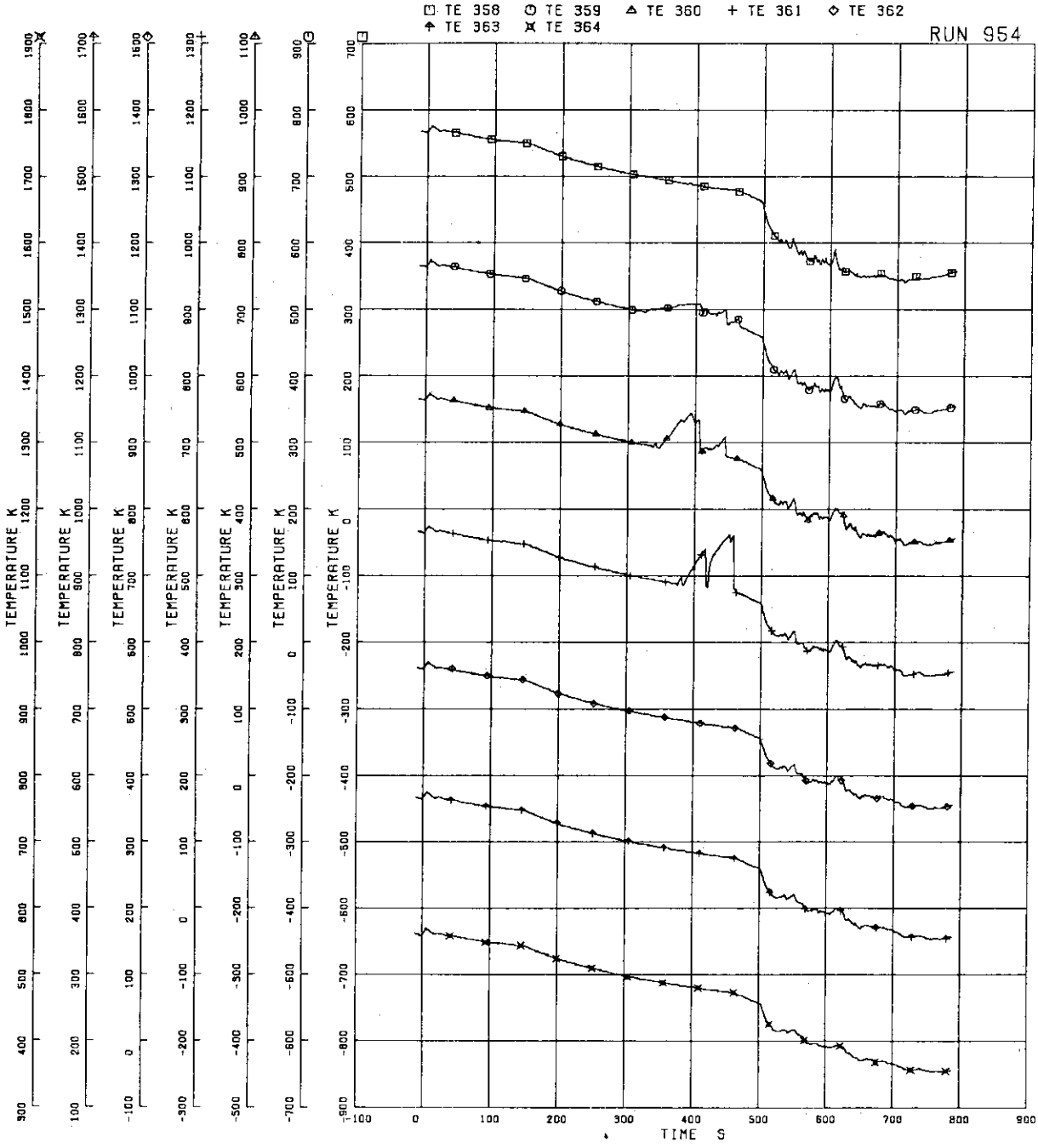

FIG.5.234 FUEL ROD SURFACE TEMPERATURE OF C11 ROD

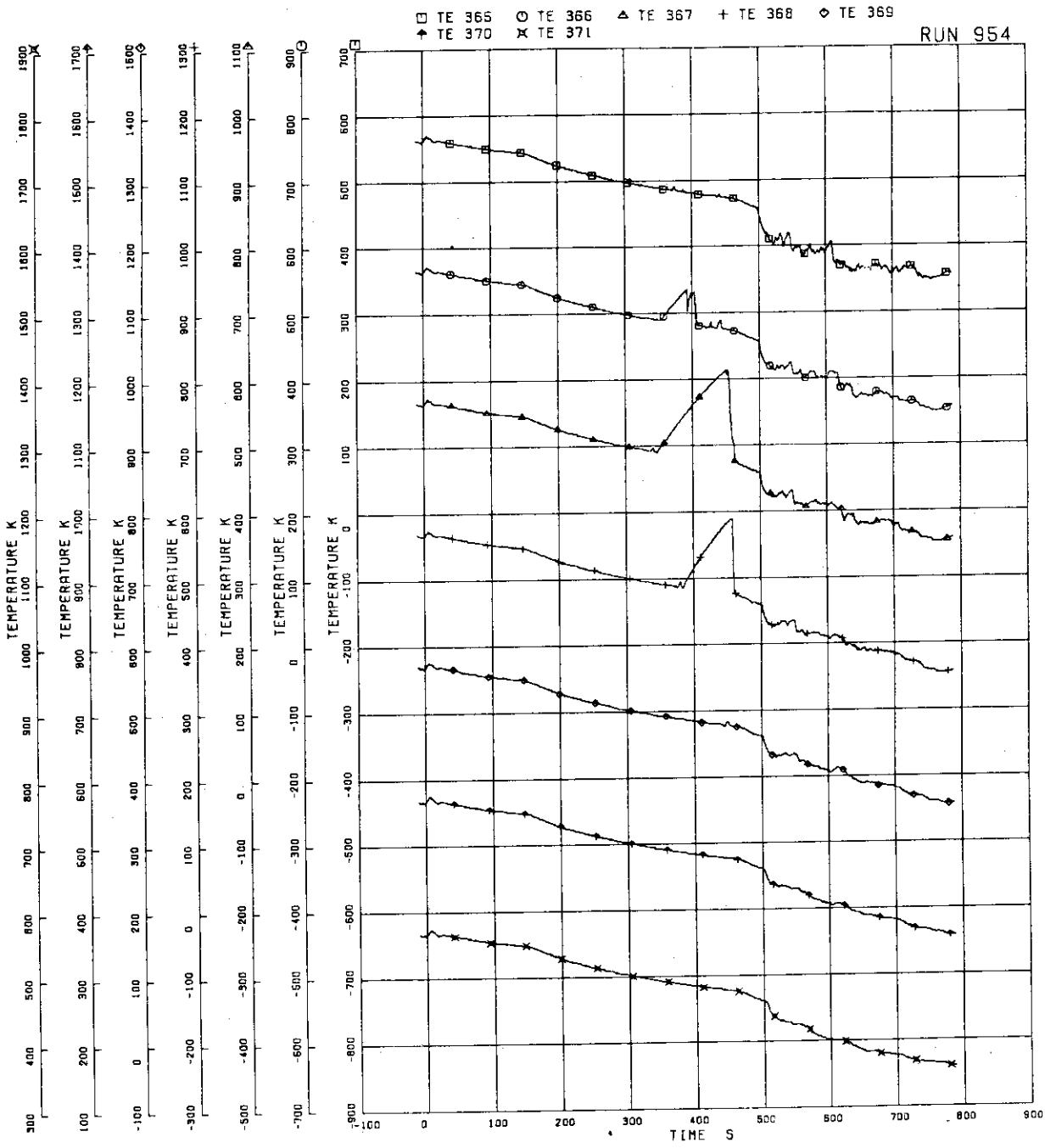

FIG.5.235 FUEL ROD SURFACE TEMPERATURE OF C13 ROD

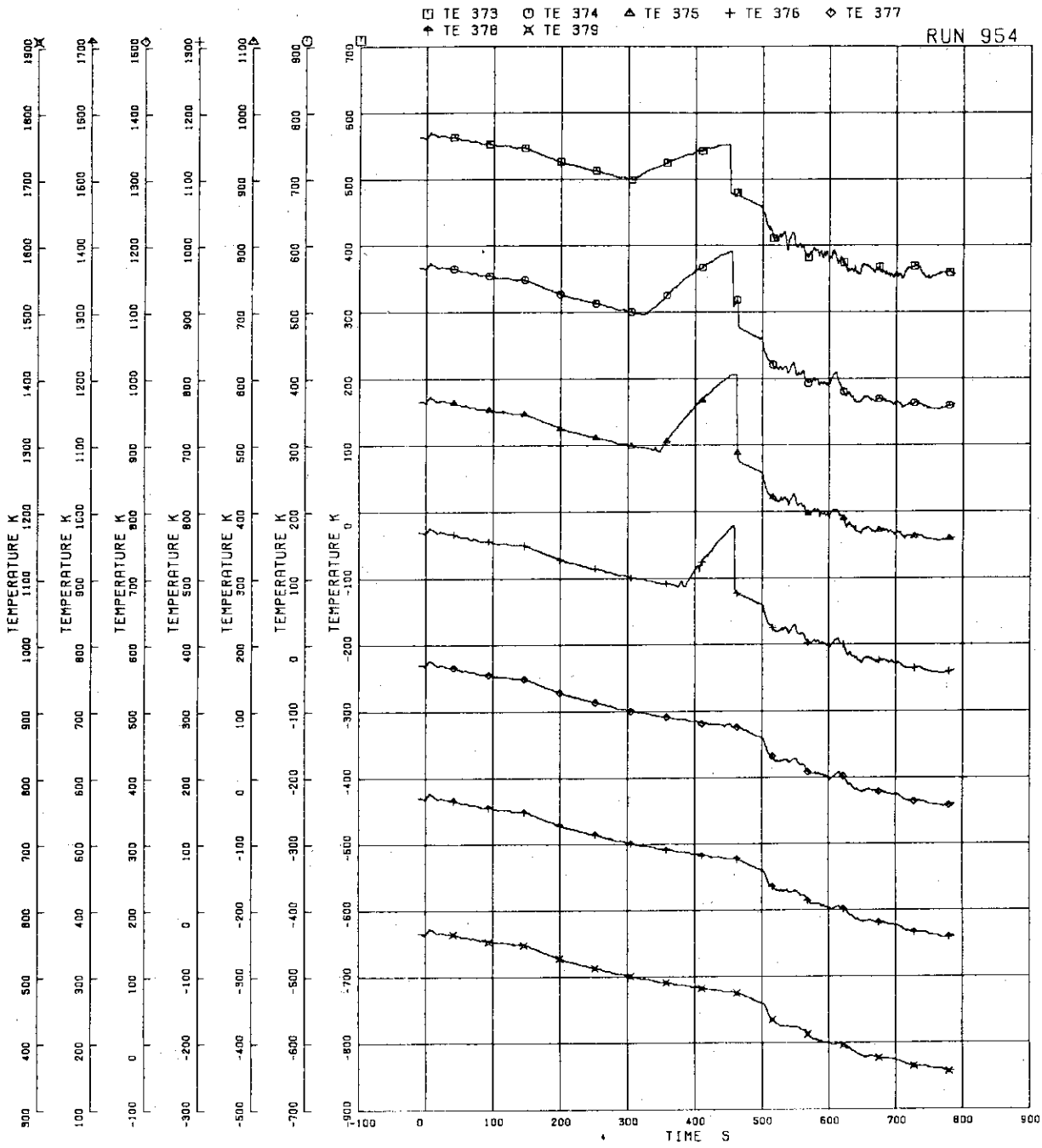

FIG.5.236 FUEL ROD SURFACE TEMPERATURE OF C22 ROD

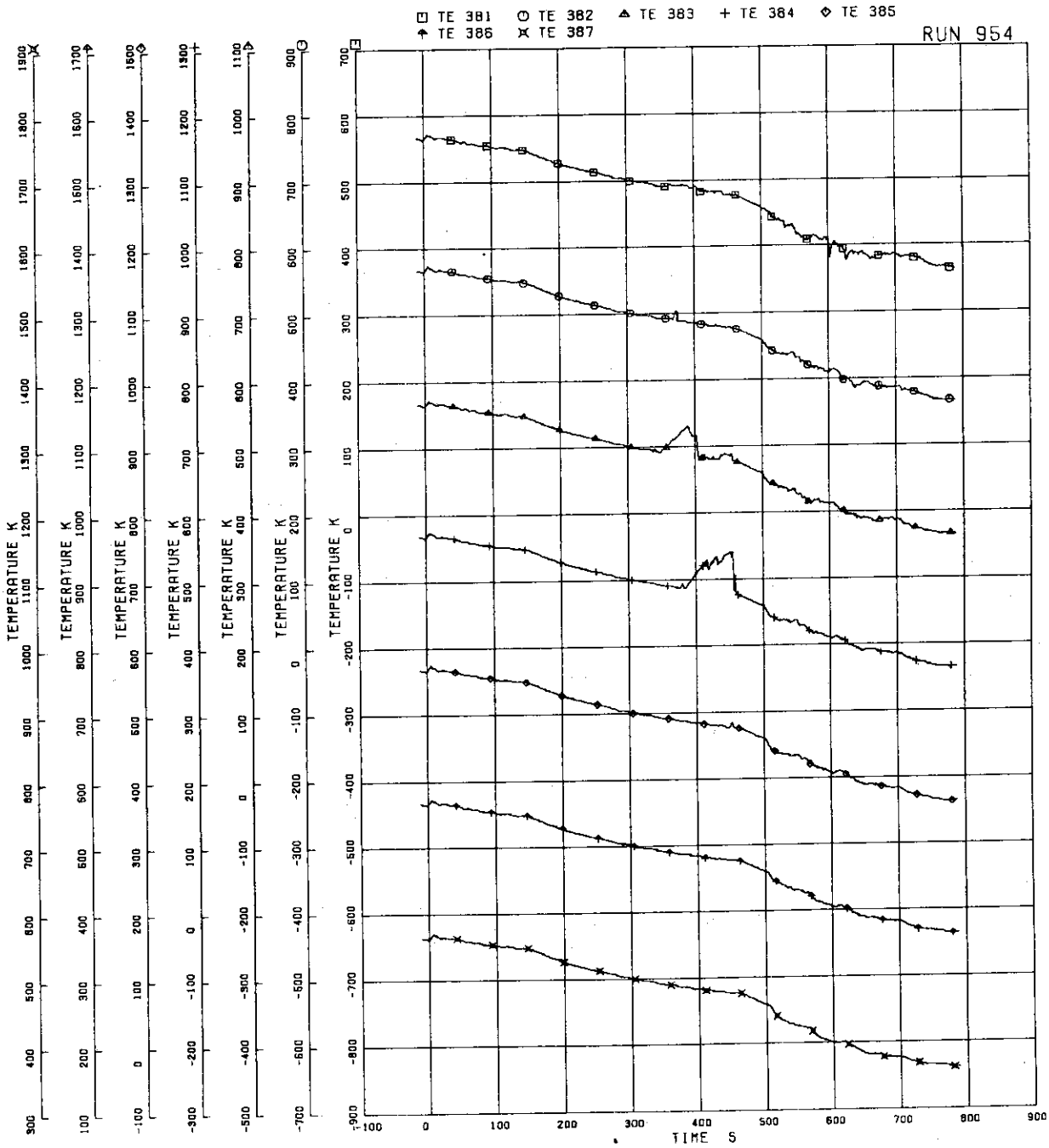

FIG.5.237 FUEL ROD SURFACE TEMPERATURE OF C33 ROD

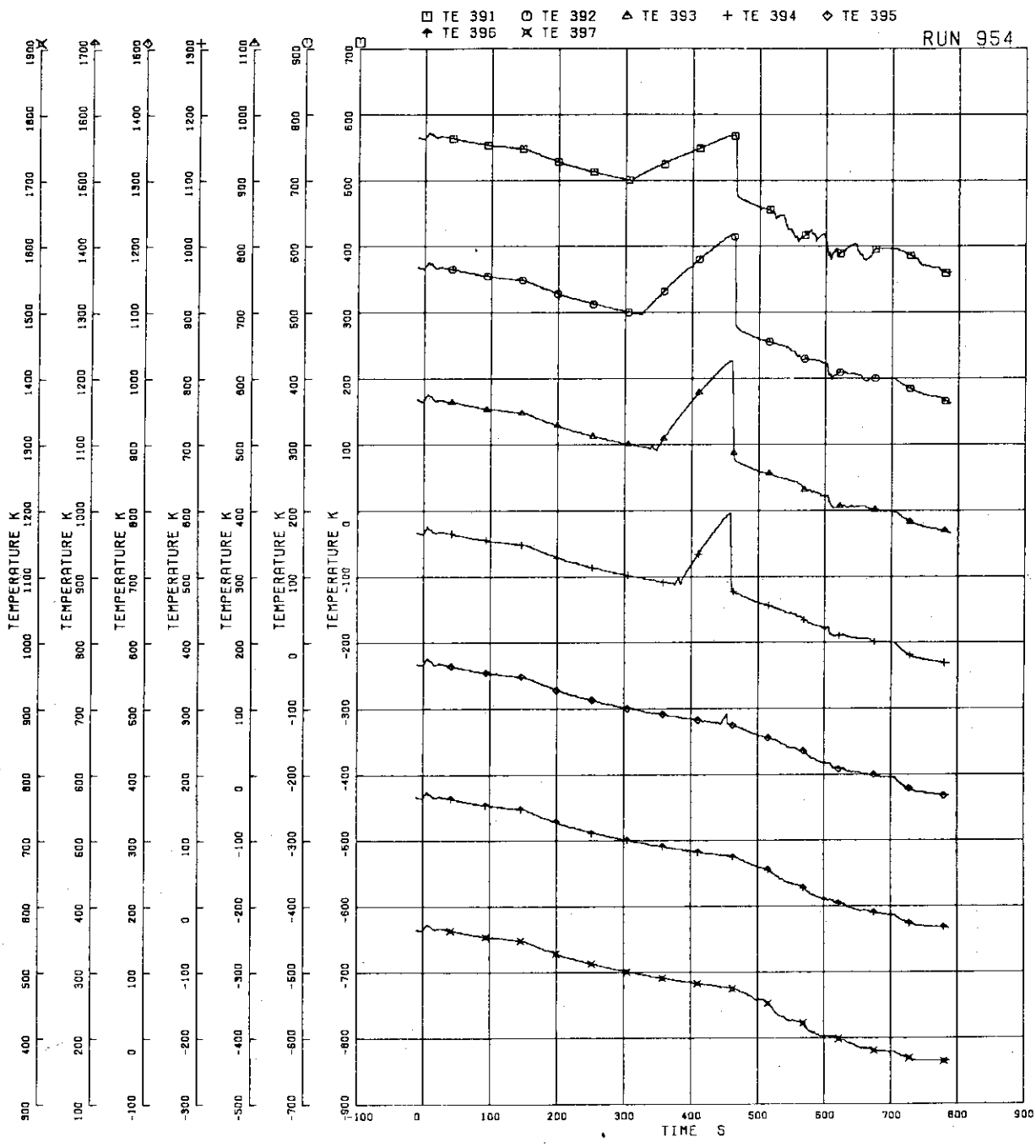

FIG.5.238 FUEL ROD SURFACE TEMPERATURE OF C77 ROD

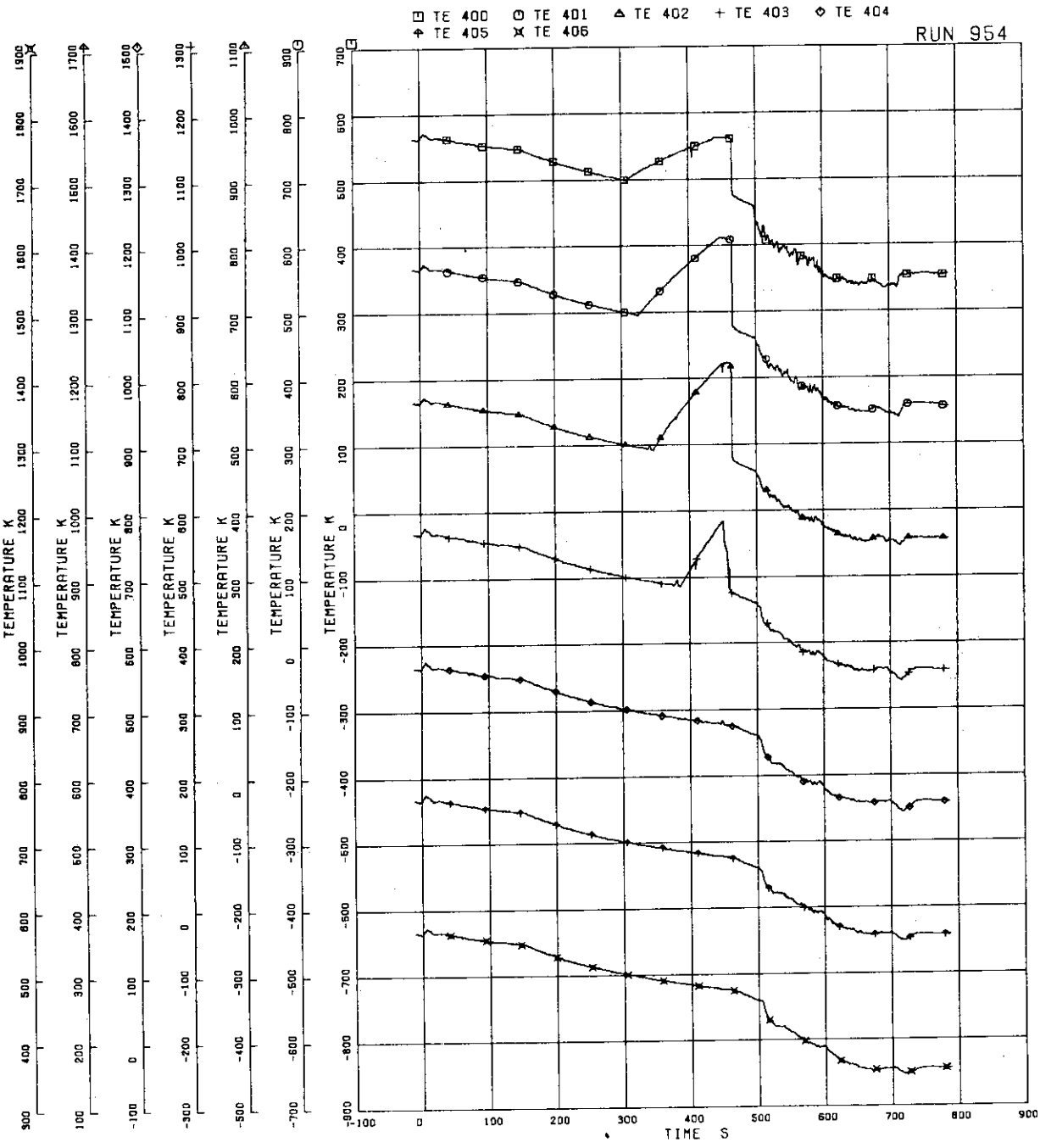

FIG.5.239 FUEL ROD SURFACE TEMPERATURE OF D22 ROD

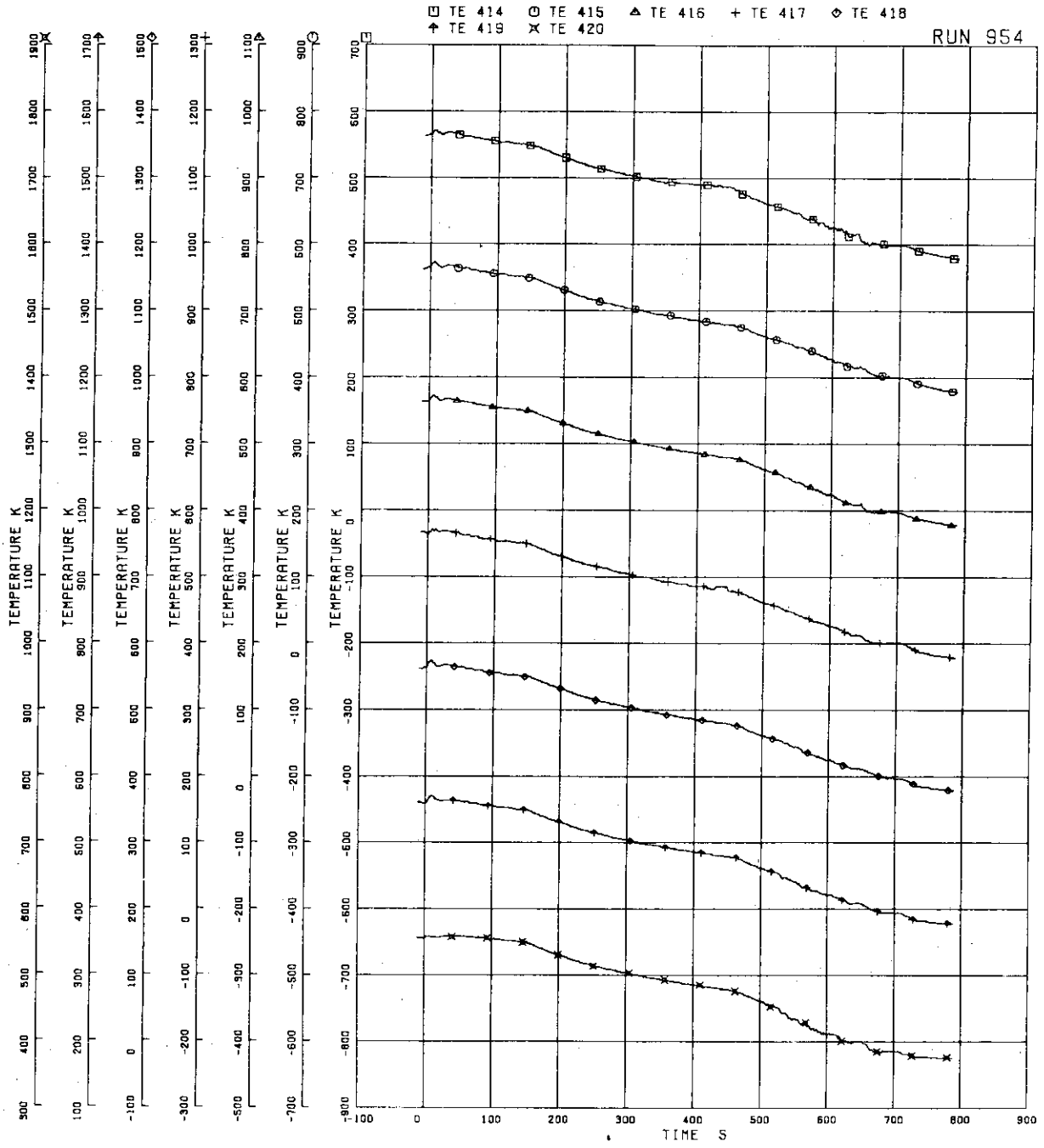

FIG.5.240 SURFACE TEMPERATURE OF WATER ROD SIMULATOR A45

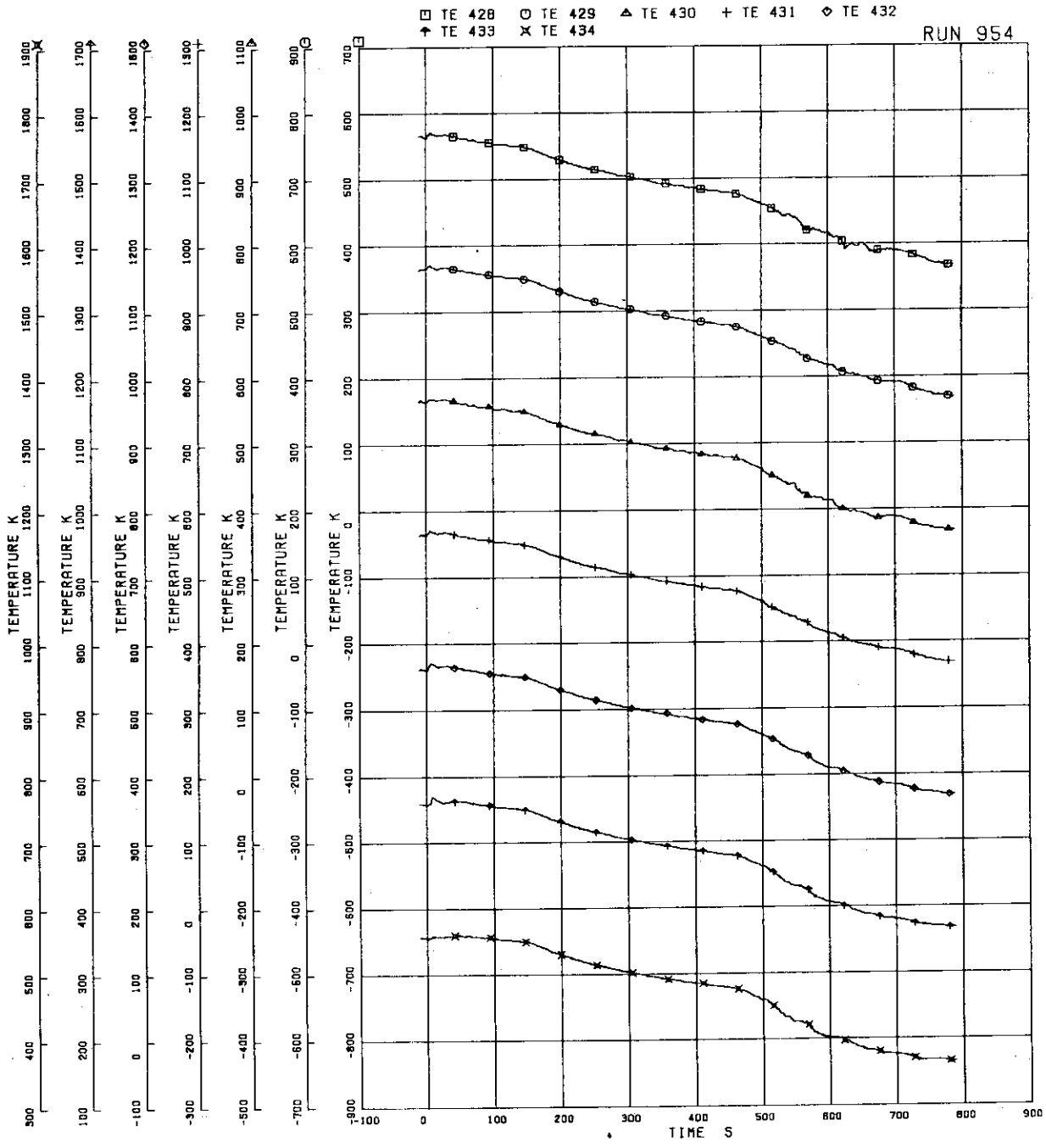

FIG.5.241 SURFACE TEMPERATURE OF WATER ROD SIMULATOR C45

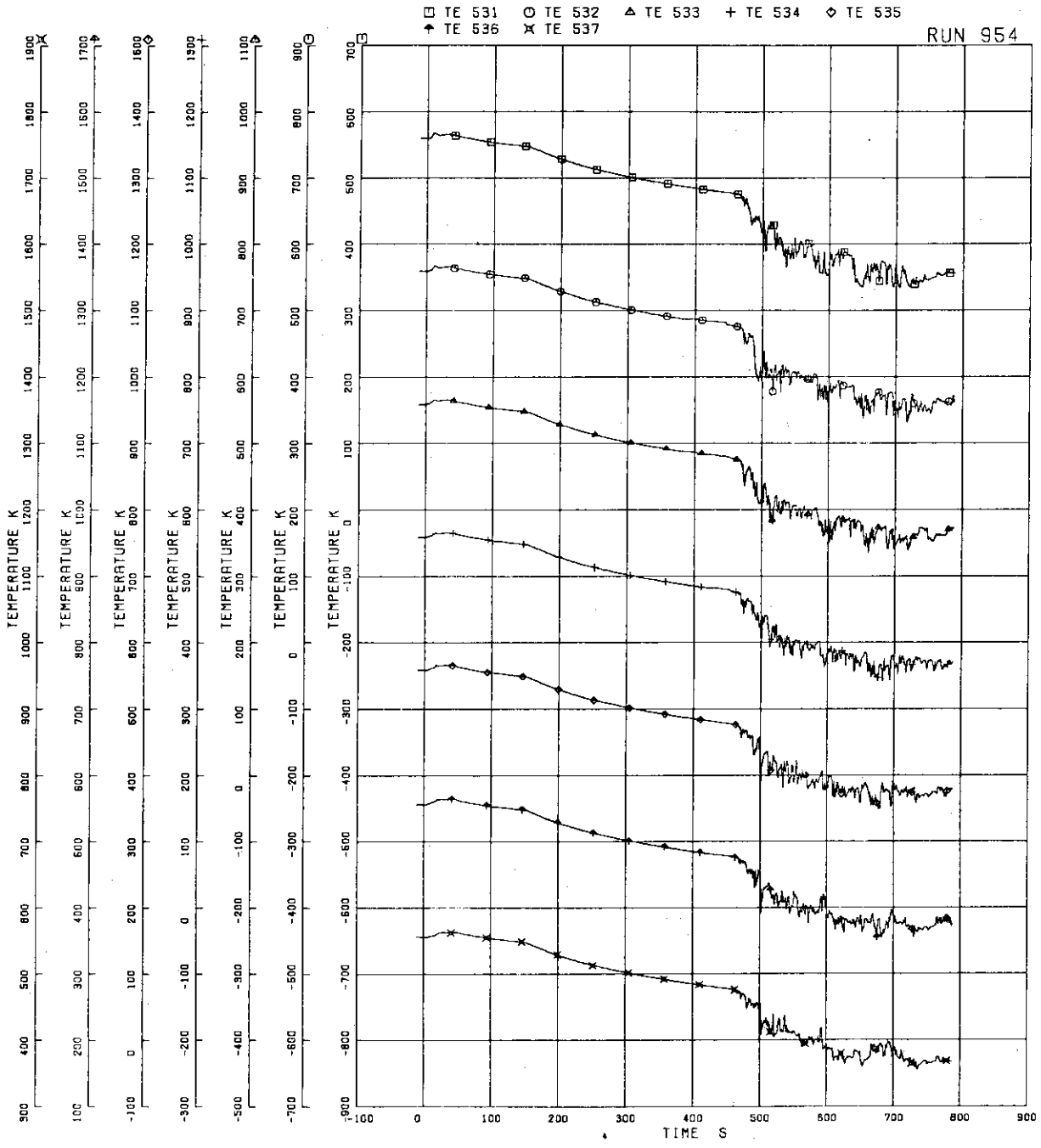

FIG.5.242 OUTER SURFACE TEMPERATURE OF CHANNEL BOX A

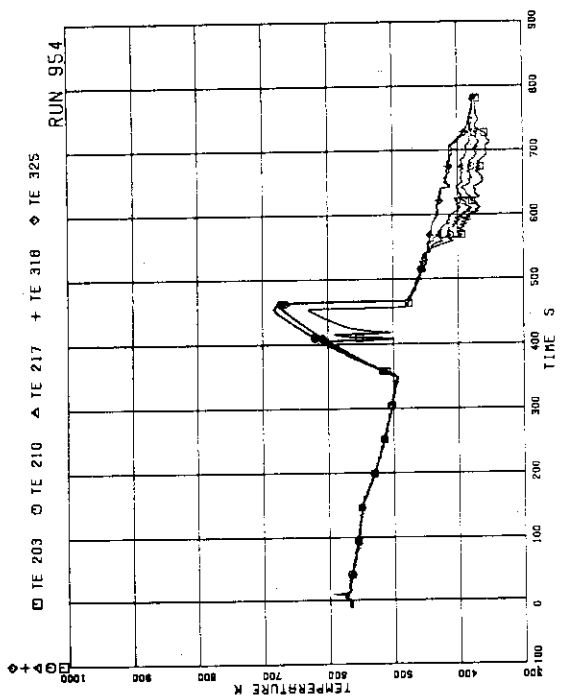

FIG.5.245 FUEL ROD SURFACE TEMPERATURE OF A11,A12,A13,A87,A88 RODS AT POSITION 3

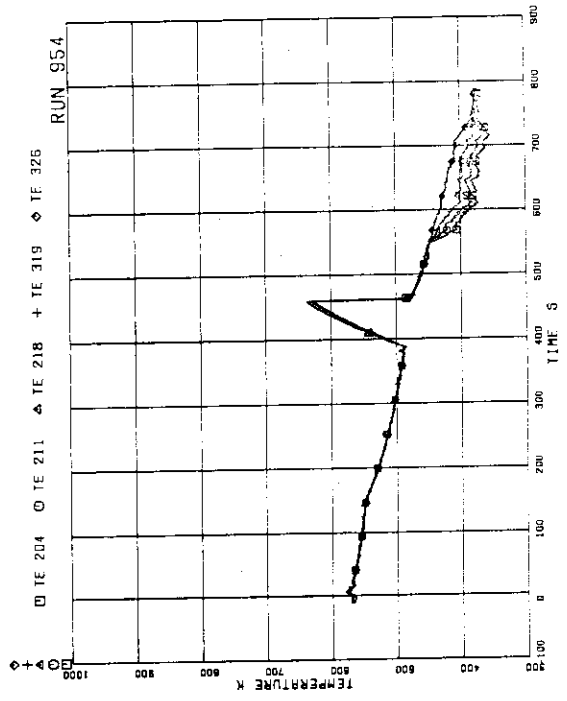

FIG.5.246 FUEL ROD SURFACE TEMPERATURE OF A11,A12,A13,A87,A88 RODS AT POSITION 4

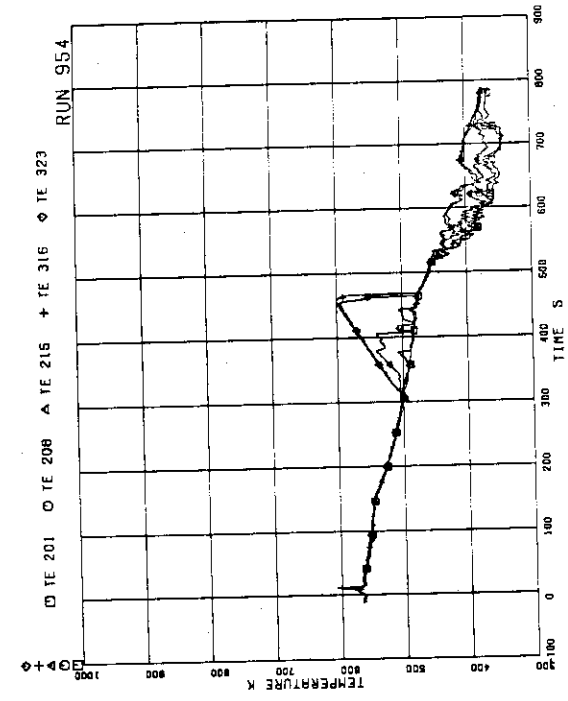

FIG.5.243 FUEL ROD SURFACE TEMPERATURE OF A11,A12,A13,A87,A88 RODS AT POSITION 1

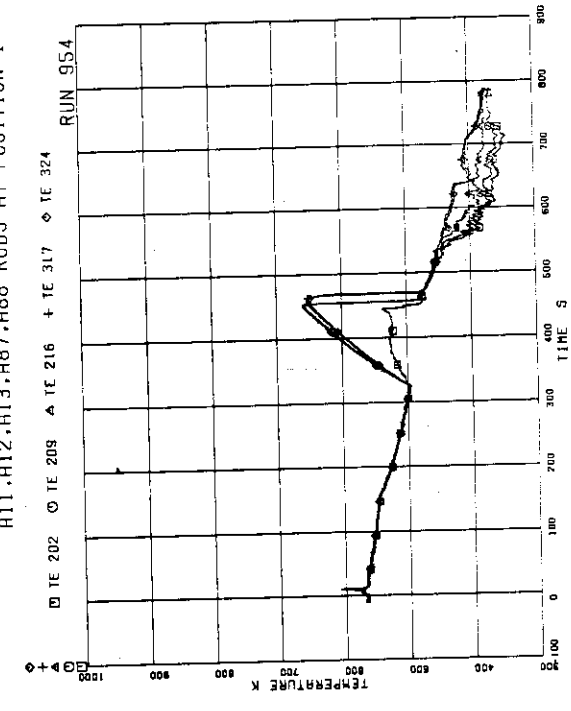

FIG.5.244 FUEL ROD SURFACE TEMPERATURE OF A11,A12,A13,A87,A88 RODS AT POSITION 2

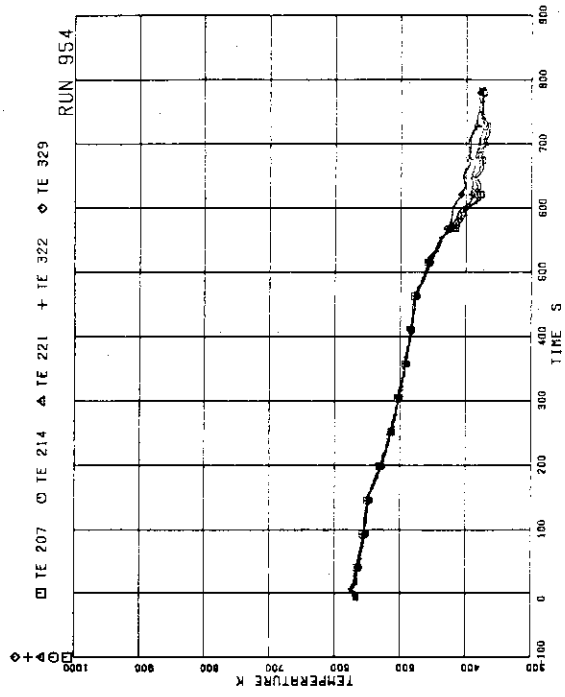

FIG.5.249 FUEL ROD SURFACE TEMPERATURE OF A11,A12,A13,A87,A88 RODS AT POSITION 7

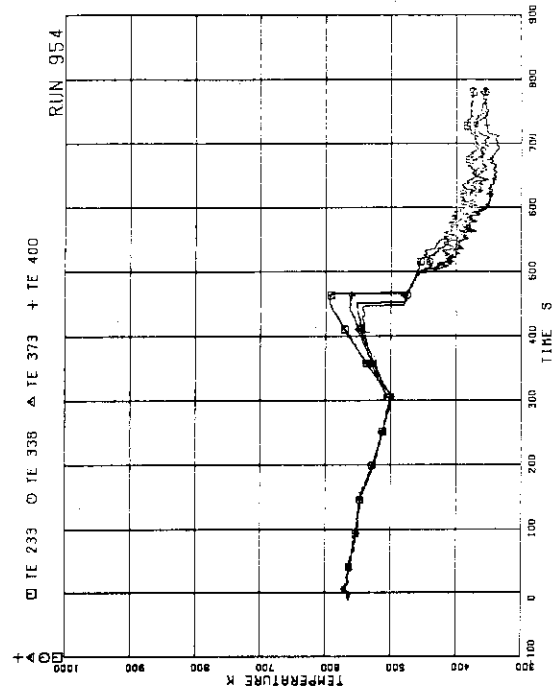

FIG.5.250 FUEL ROD SURFACE TEMPERATURE OF A22,B22,C22,D22 RODS AT POSITION 1

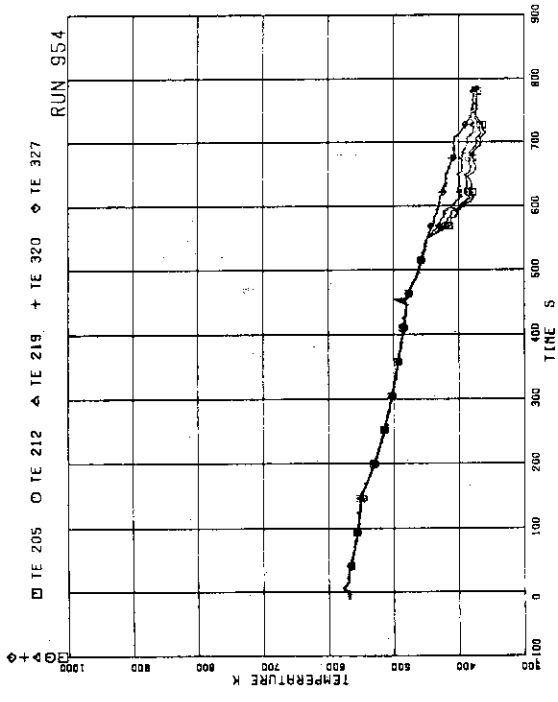

FIG.5.247 FUEL ROD SURFACE TEMPERATURE OF A11,A12,A13,A87,A88 RODS AT POSITION 5

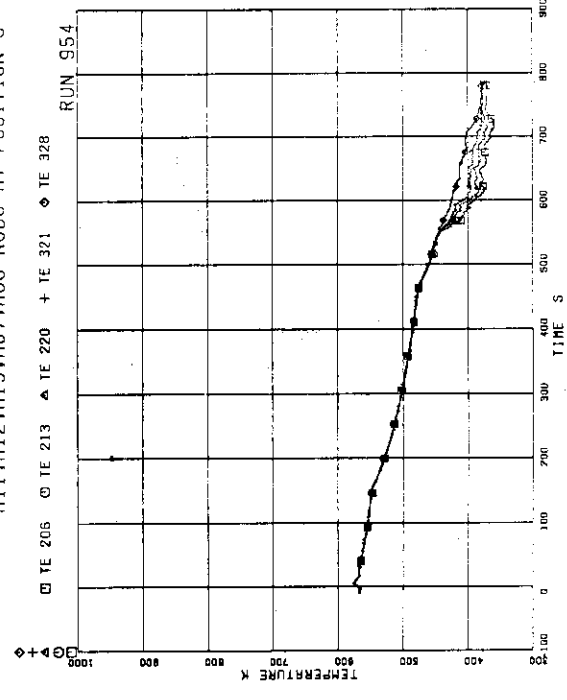

FIG.5.248 FUEL ROD SURFACE TEMPERATURE OF A11,A12,A13,A87,A88 RODS AT POSITION 6

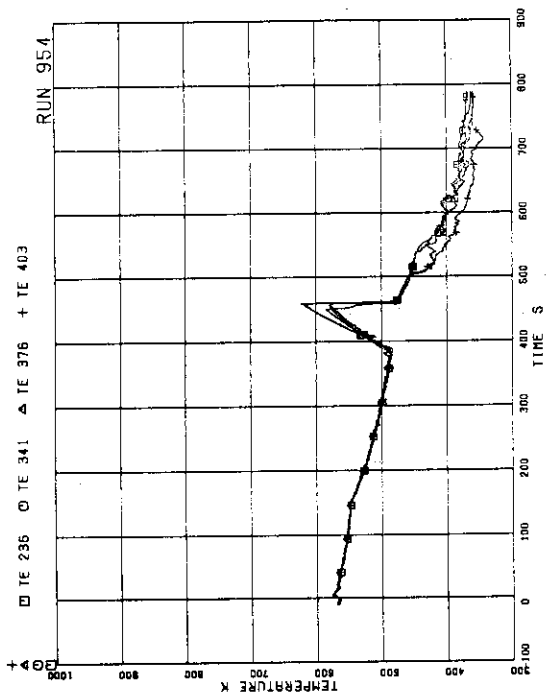

FIG.5.251 FUEL ROD SURFACE TEMPERATURE OF A22,B22,C22,D22 RODS AT POSITION 2

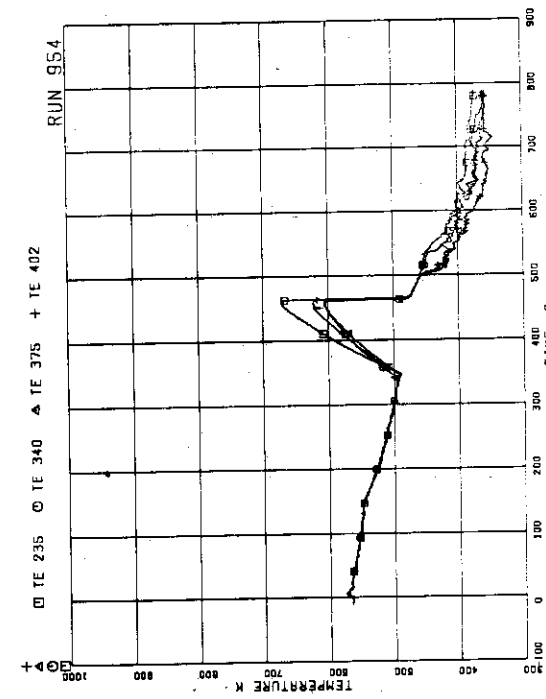

FIG.5.252 FUEL ROD SURFACE TEMPERATURE OF A22,B22,C22,D22 RODS AT POSITION 3

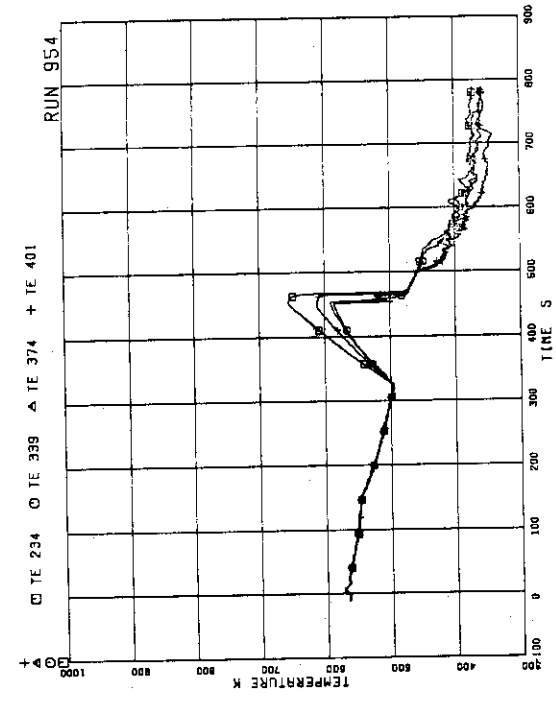

FIG.5.253 FUEL ROD SURFACE TEMPERATURE OF A22,B22,C22,D22 RODS AT POSITION 4

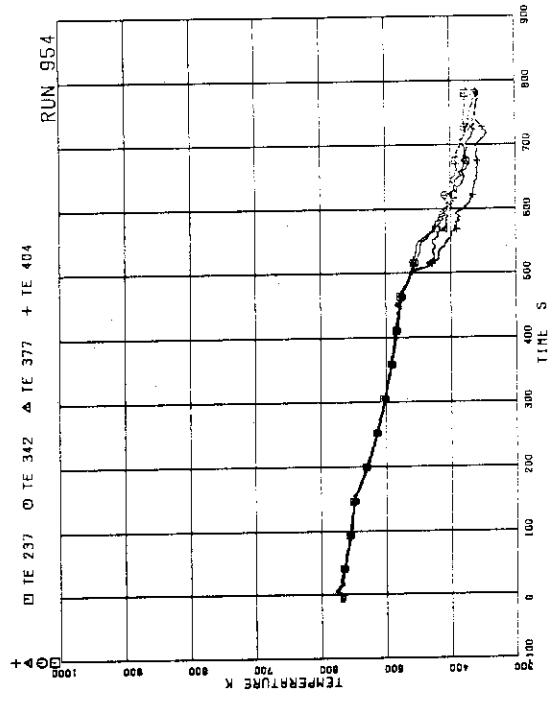

FIG.5.254 FUEL ROD SURFACE TEMPERATURE OF A22,B22,C22,D22 RODS AT POSITION 5

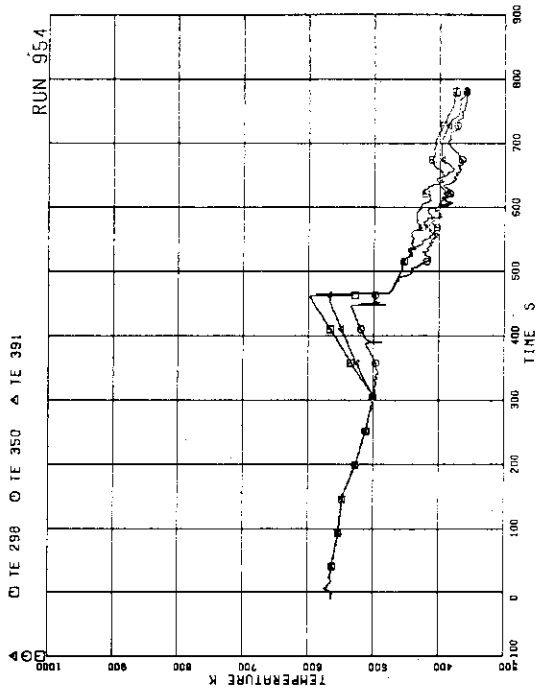

FIG.5.257 FUEL ROD SURFACE TEMPERATURE OF A77,B77,C77 RODS AT POSITION 1

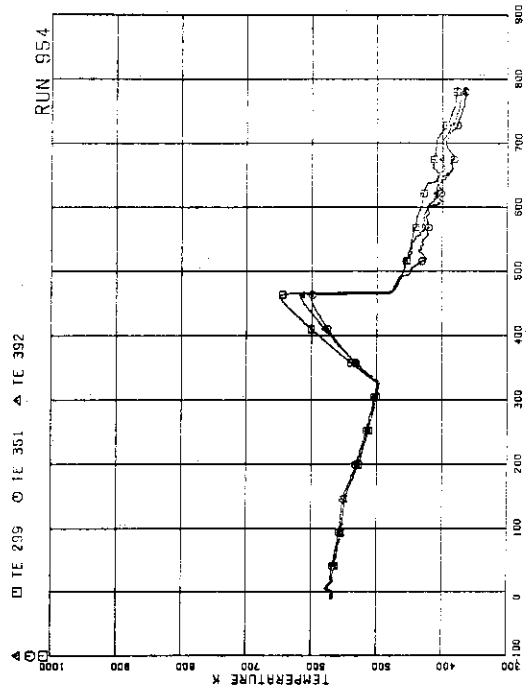

FIG.5.258 FUEL ROD SURFACE TEMPERATURE OF A77,B77,C77 RODS AT POSITION 2

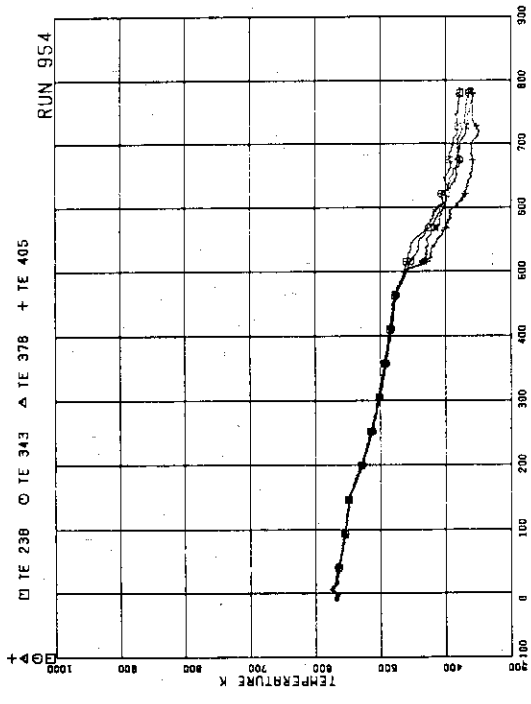

FIG.5.255 FUEL ROD SURFACE TEMPERATURE OF A22,B22,C22,D22 RODS AT POSITION 6

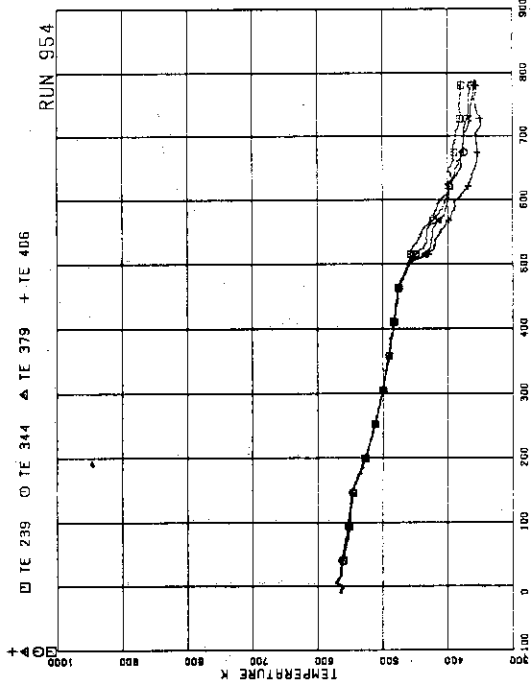

FIG.5.256 FUEL ROD SURFACE TEMPERATURE OF A22,B22,C22,D22 RODS AT POSITION 7

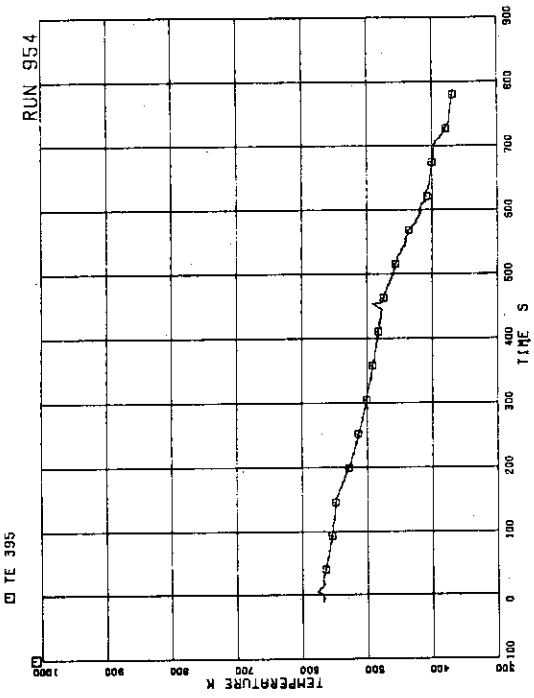

FIG.5.261 FUEL ROD SURFACE TEMPERATURE OF C77 ROD AT POSITION 5

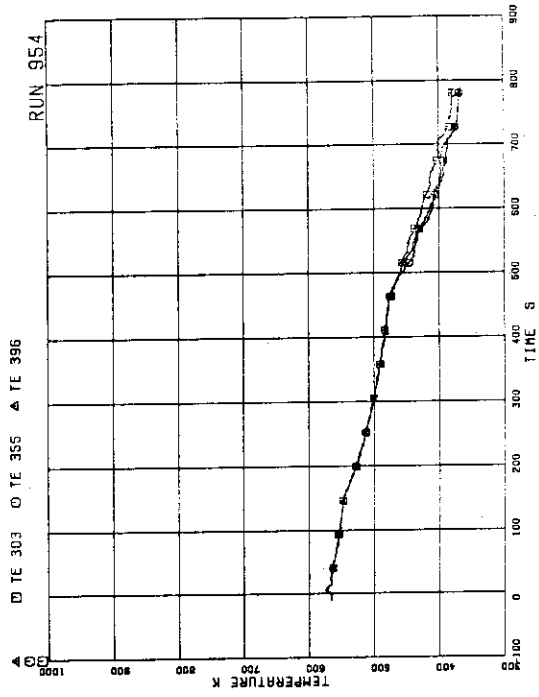

FIG.5.262 FUEL ROD SURFACE TEMPERATURE OF A77,B77,C77 RODS AT POSITION 6

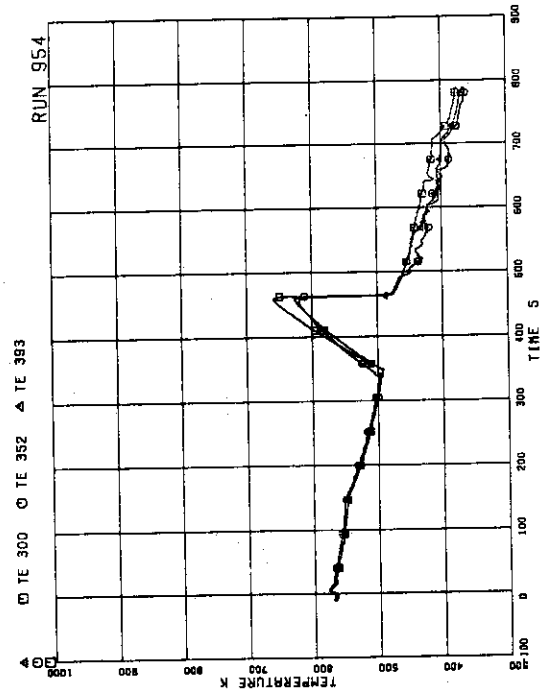

FIG.5.259 FUEL ROD SURFACE TEMPERATURE OF A77,B77,C77 RODS AT POSITION 3

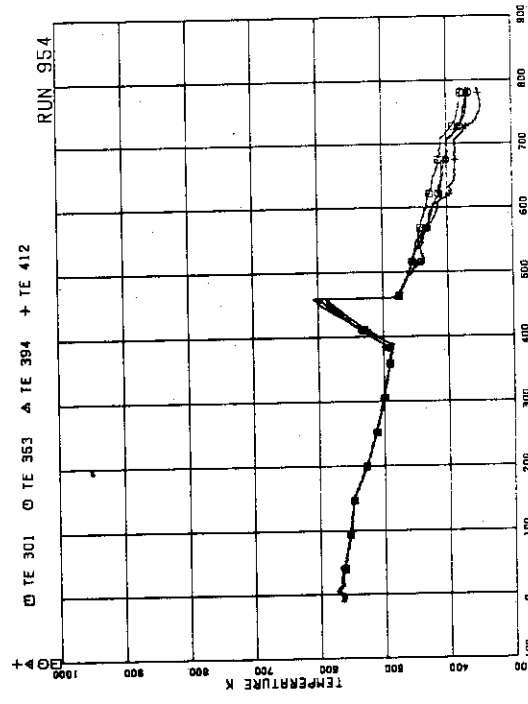

FIG.5.260 FUEL ROD SURFACE TEMPERATURE OF A77,B77,C77 RODS AT POSITION 4

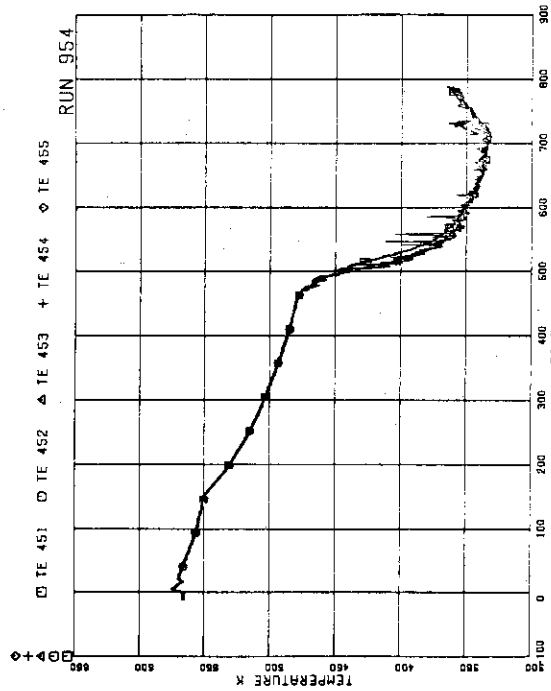

FIG.5.265 FLUID TEMPERATURE AT CHANNEL C OUTLET

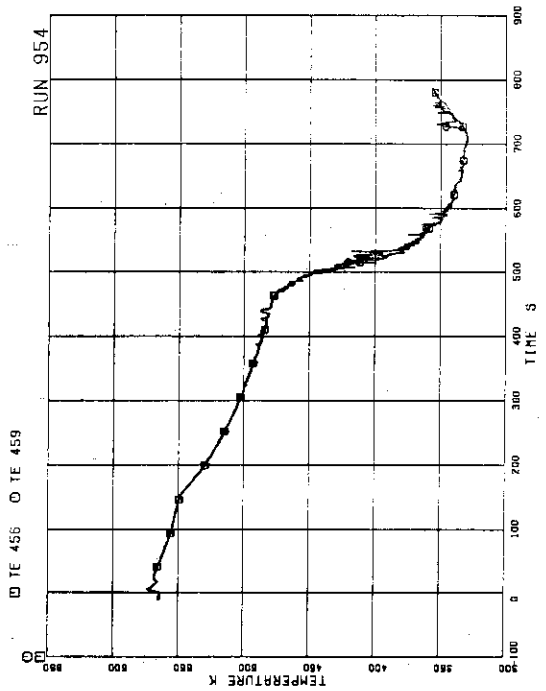

FIG.5.266 FLUID TEMPERATURE ABOVE UTP OF CHANNEL A. OPENINGS 1 AND 4

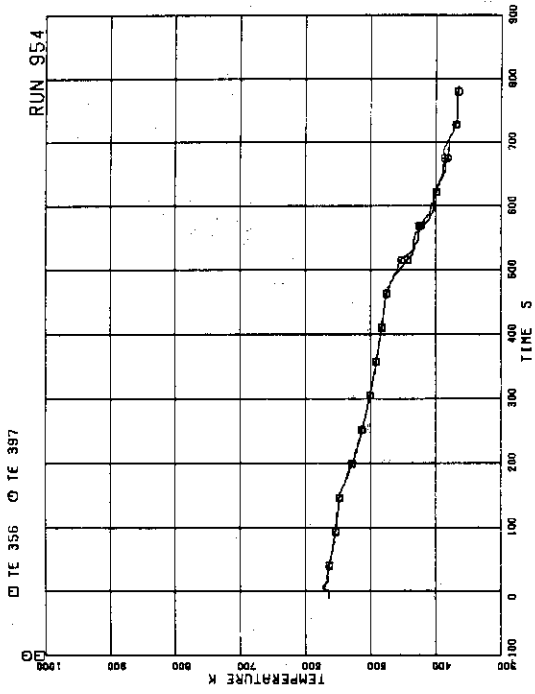

FIG.5.263 FUEL ROD SURFACE TEMPERATURE OF B77,C77 RODS AT POSITION 7

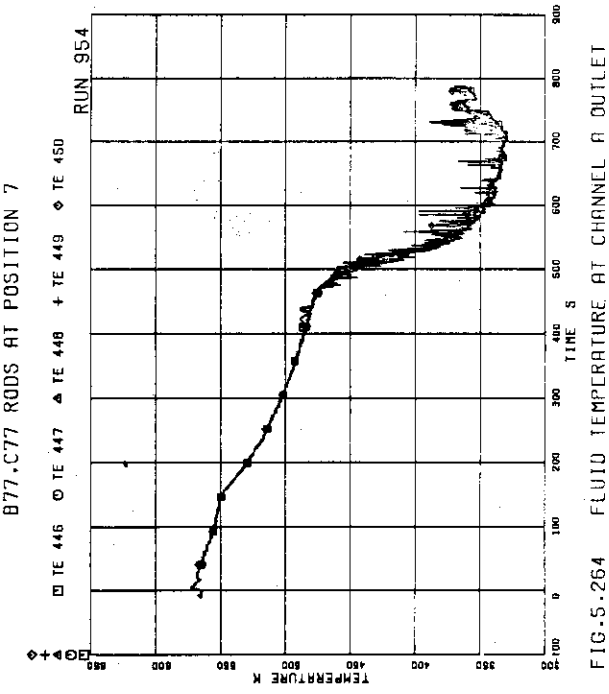

FIG.5.264 FLUID TEMPERATURE AT CHANNEL A OUTLET

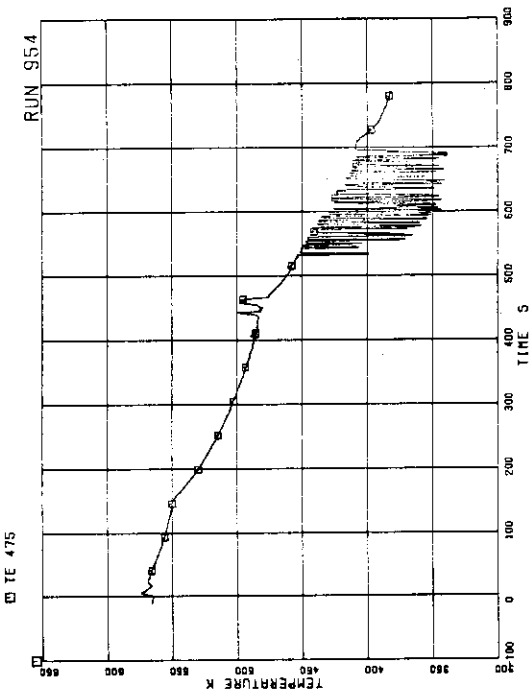

FIG.5.269 FLUID TEMPERATURE BELOW UTP OF CHANNEL A, OPENING 10

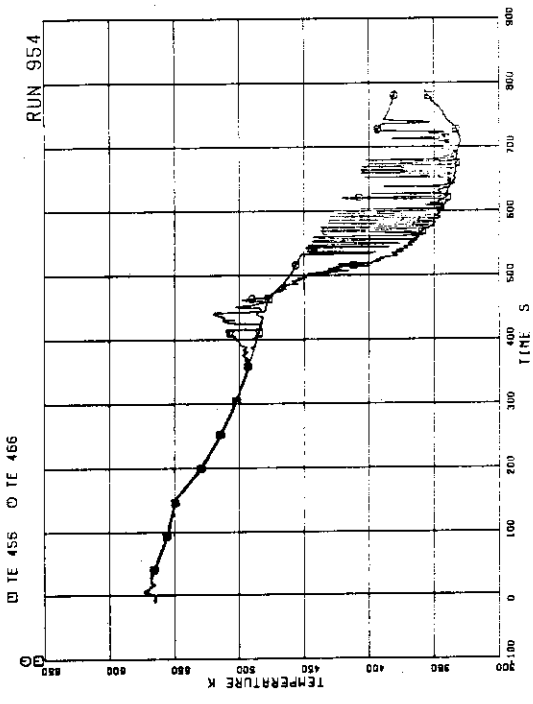

FIG.5.270 FLUID TEMPERATURE AT UTP IN CHANNEL A, OPENING 1

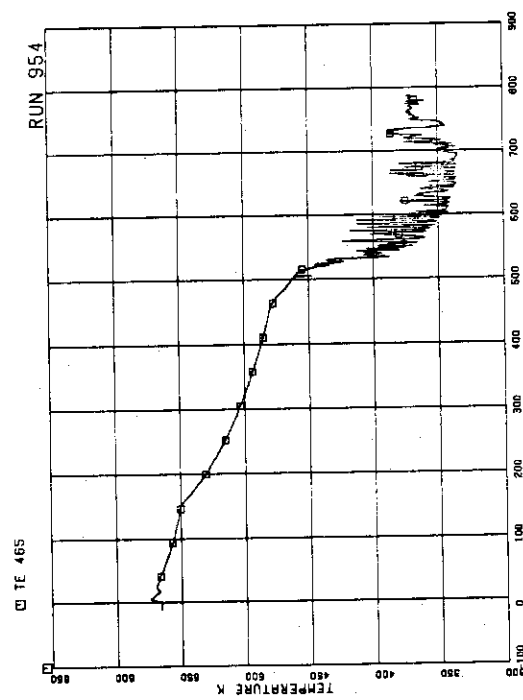

FIG.5.267 FLUID TEMPERATURE ABOVE UTP OF CHANNEL A, OPENING 10

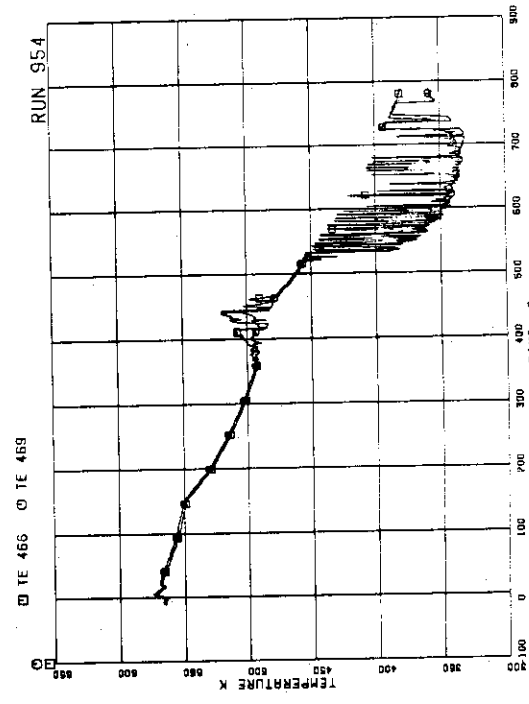

FIG.5.268 FLUID TEMPERATURE BELOW UTP OF CHANNEL A, OPENINGS 1 AND 4

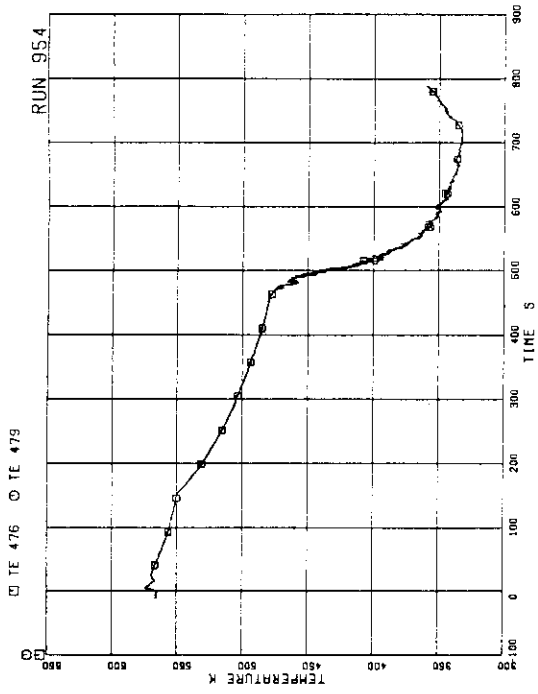

FIG.5.273 FLUID TEMPERATURE ABOVE UTP OF CHANNEL C, OPENING 1 AND 4

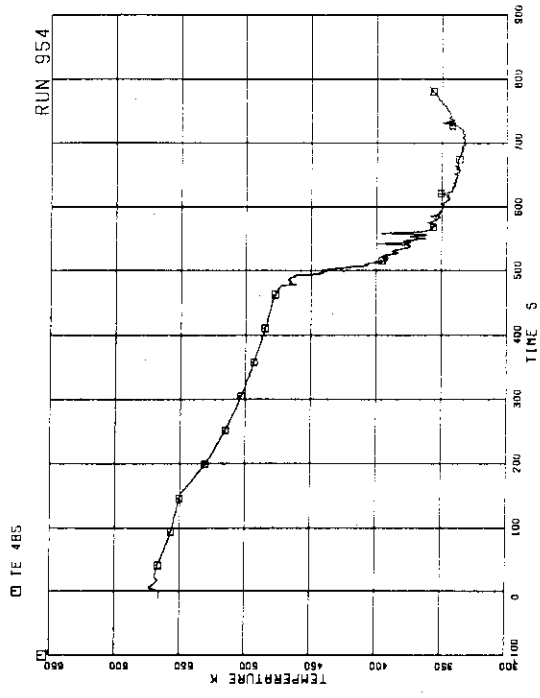

FIG.5.274 FLUID TEMPERATURE ABOVE UTP OF CHANNEL C, OPENING 10

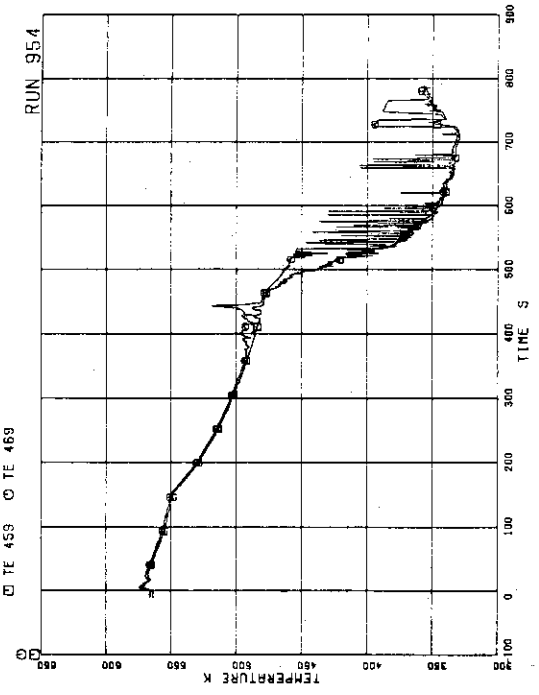

FIG.5.271 FLUID TEMPERATURE AT UTP IN CHANNEL A, OPENING 4

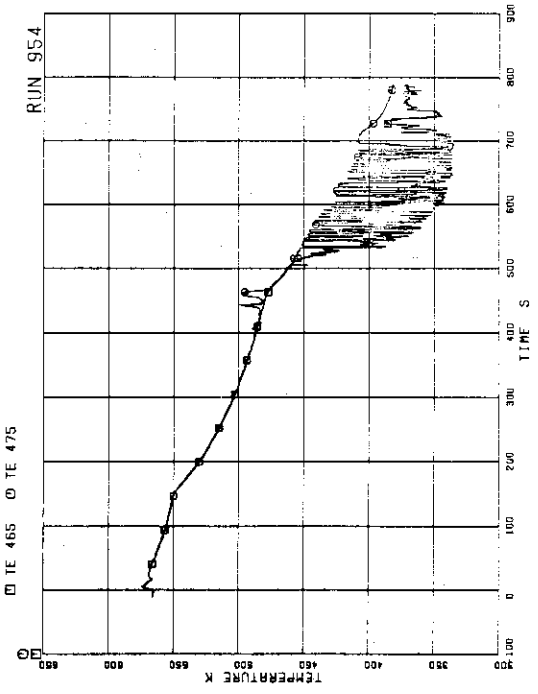

FIG.5.272 FLUID TEMPERATURE AT UTP IN CHANNEL A, OPENING 10

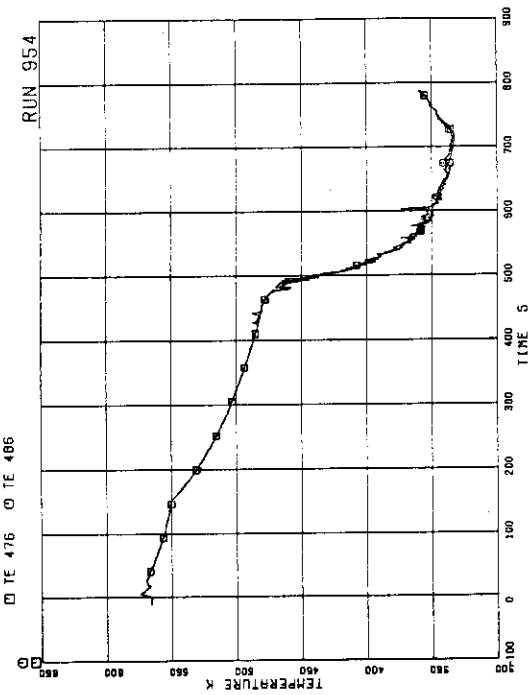

FIG.5.277 FLUID TEMPERATURE AT UTP IN CHANNEL C. OPENING 1

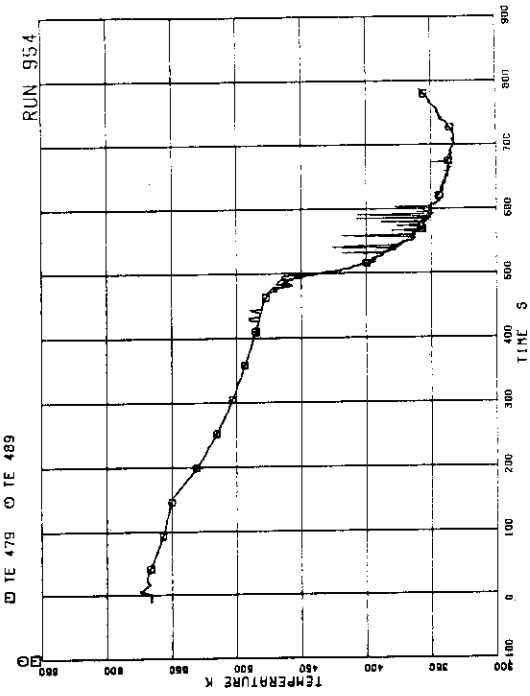

FIG.5.278 FLUID TEMPERATURE AT UTP IN CHANNEL C. OPENING 4

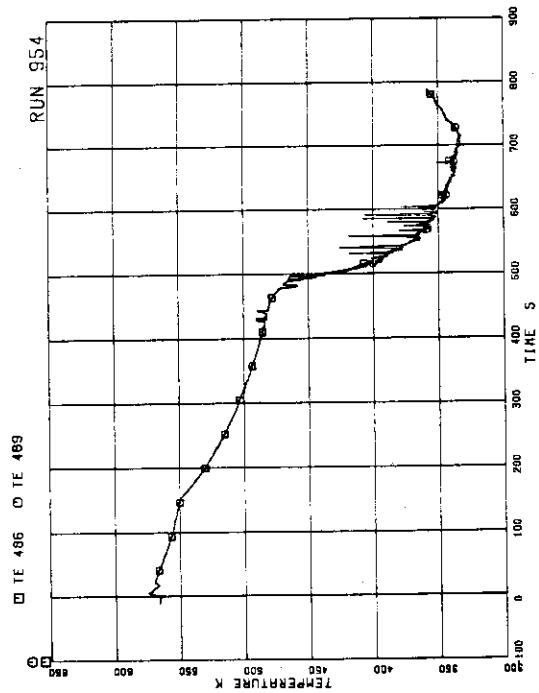

FIG.5.275 FLUID TEMPERATURE BELOW UTP OF CHANNEL C. OPENING 1 AND 4

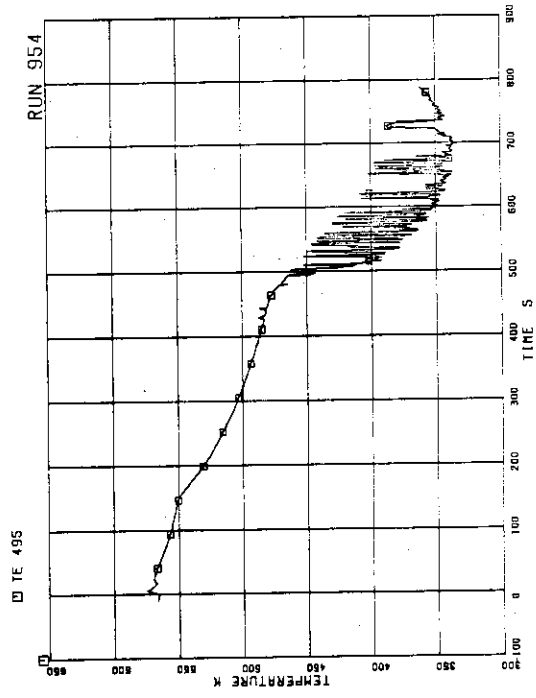

FIG.5.276 FLUID TEMPERATURE BELOW UTP OF CHANNEL C. OPENING 10

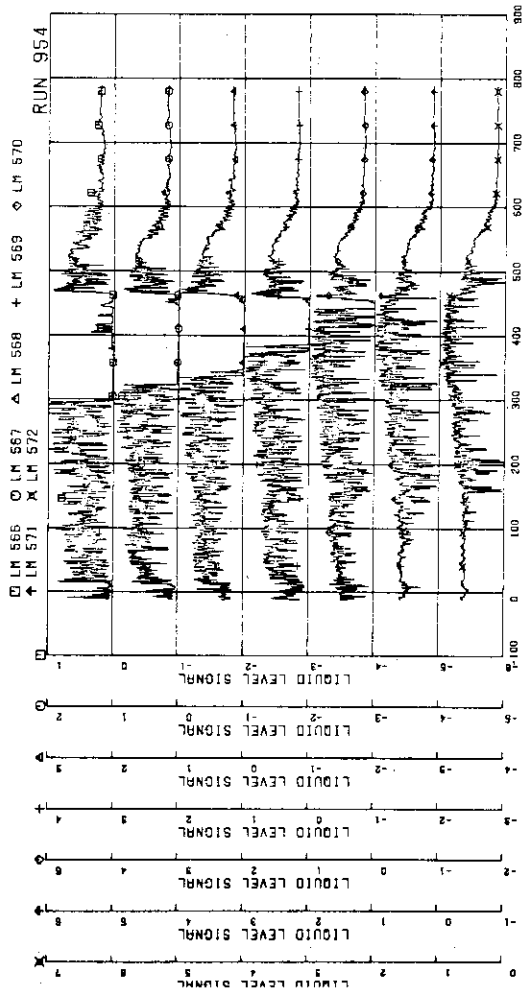

FIG.5.281 LIQUID-LEVEL SIGNAL IN CHANNEL BOX A, LOCATION A2

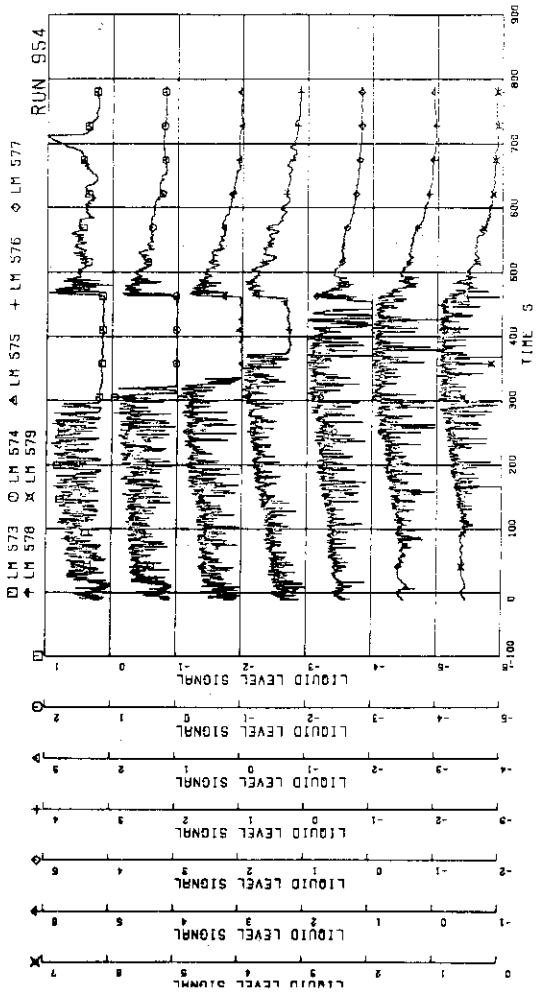

FIG.5.282 LIQUID LEVEL SIGNAL IN CHANNEL BOX B

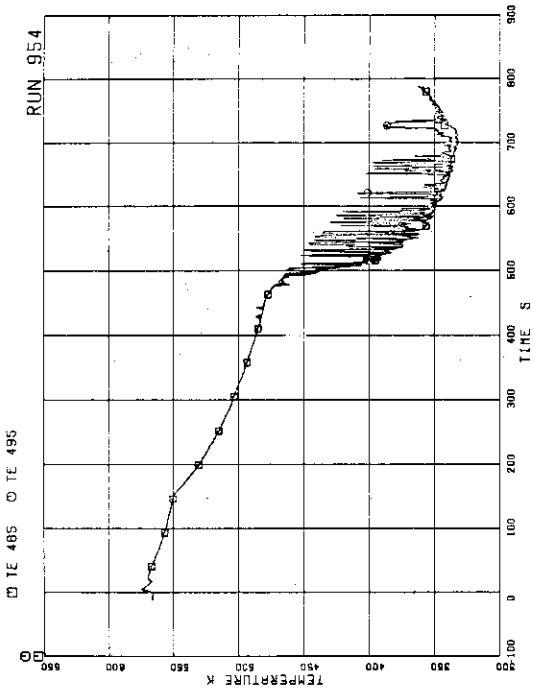

FIG.5.279 FLUID TEMPERATURE AT UTP IN CHANNEL C, OPENING 10

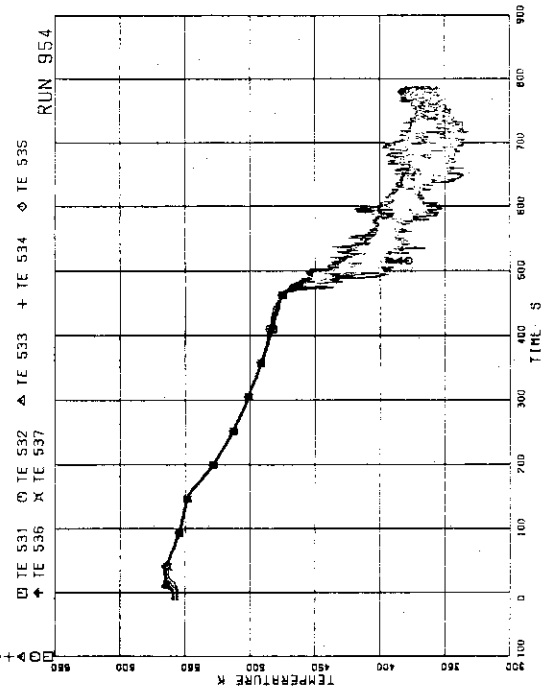

FIG.5.280 OUTER SURFACE TEMPERATURES OF CHANNEL BOX AT POSITIONS 1 TO 7

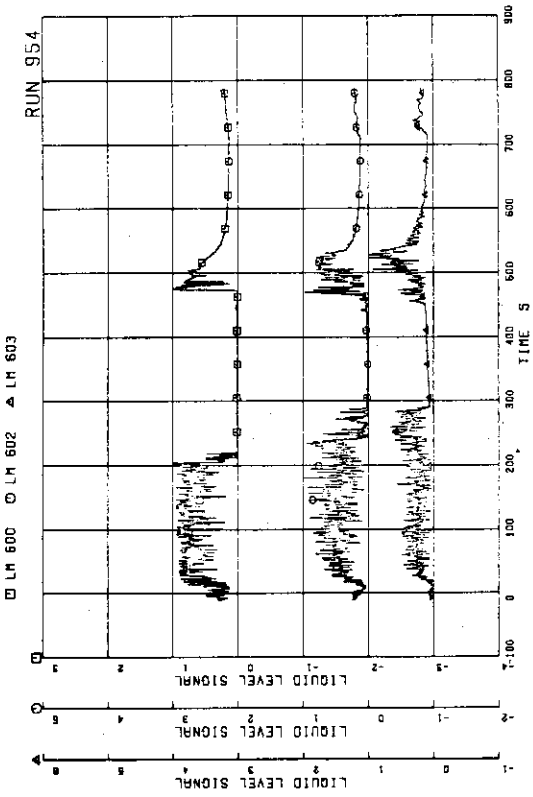

FIG.5.285 LIQUID LEVEL SIGNAL IN CHANNEL A OUTLET, CENTER

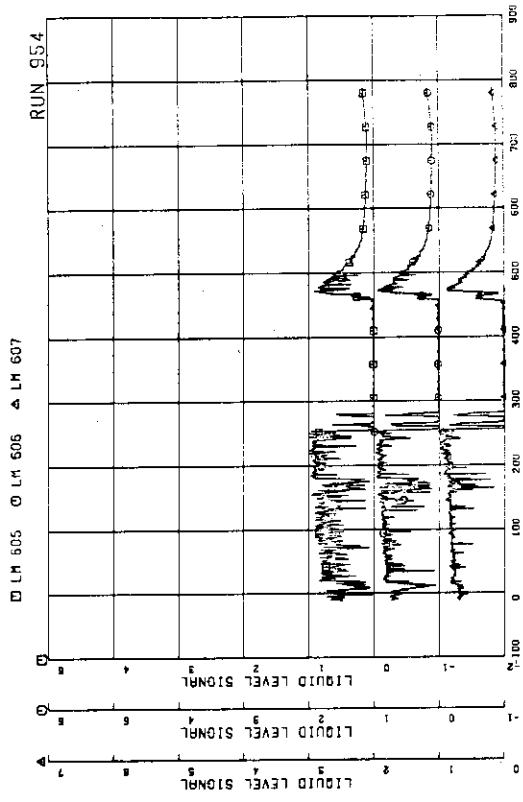

FIG.5.286 LIQUID LEVEL SIGNAL IN CHANNEL C OUTLET, LOCATION C1

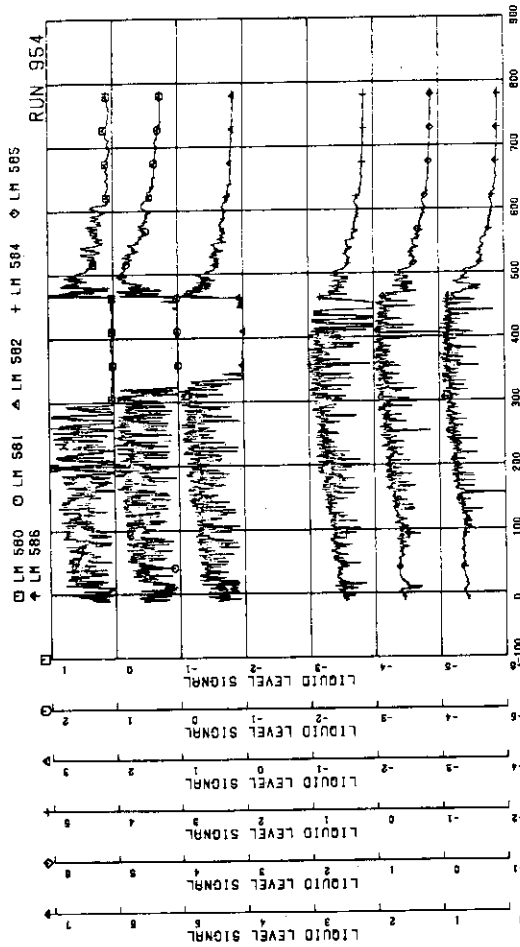

FIG.5.283 LIQUID LEVEL SIGNAL IN CHANNEL BOX C

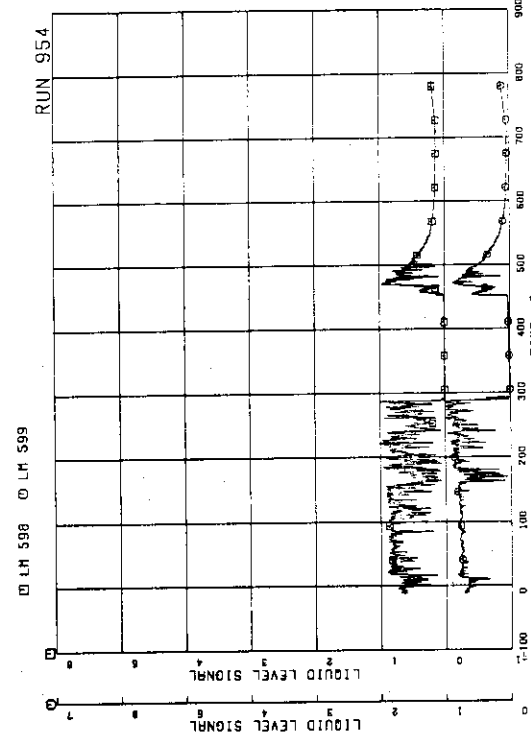

FIG.5.284 LIQUID LEVEL SIGNAL IN CHANNEL A OUTLET, LOCATION A2

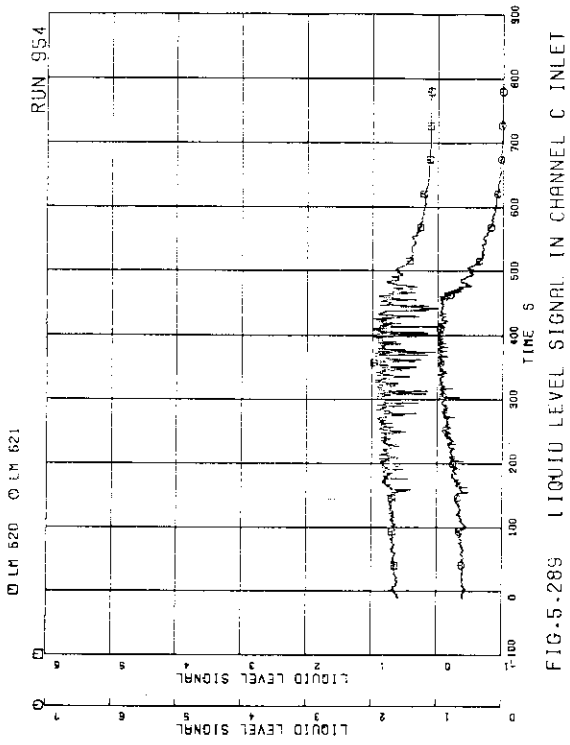

FIG.5.289 LIQUID LEVEL SIGNAL IN CHANNEL C INLET

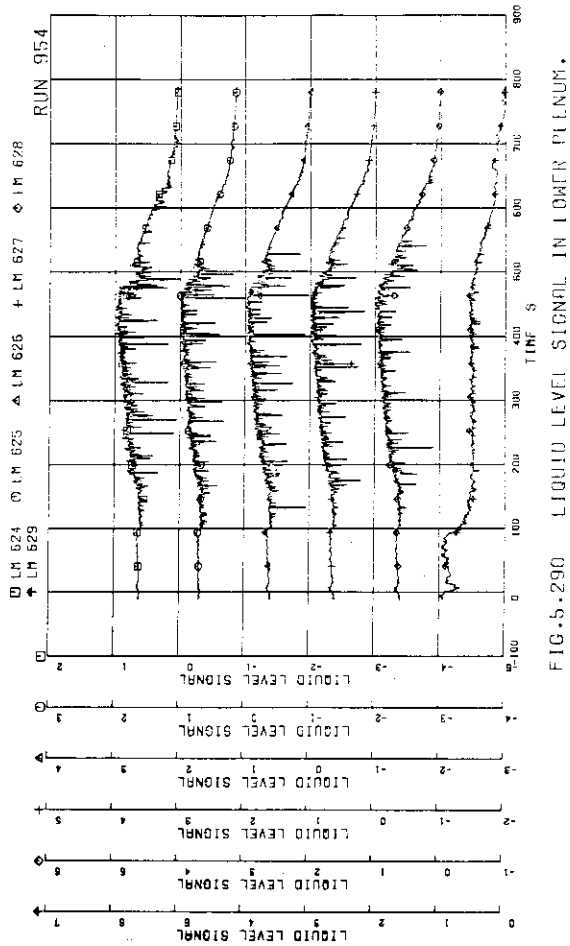

FIG.5.290 LIQUID LEVEL SIGNAL IN LOWER PLENUM, NORTH

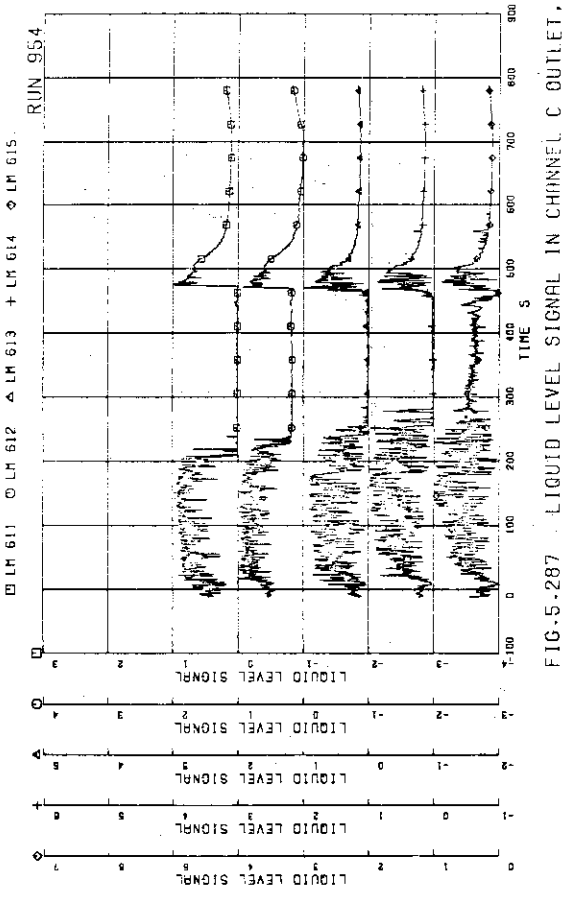

FIG.5.287 LIQUID LEVEL SIGNAL IN CHANNEL C OUTLET, CENTER

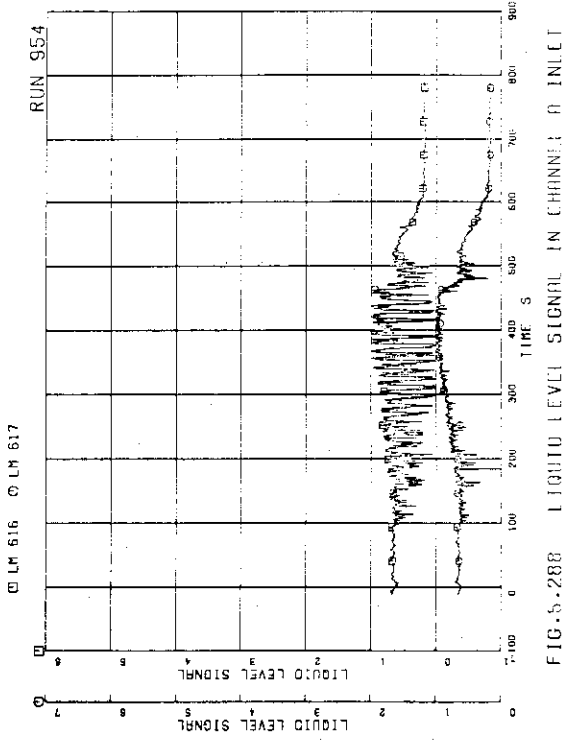

FIG.5.288 LIQUID LEVEL SIGNAL IN CHANNEL A INLET

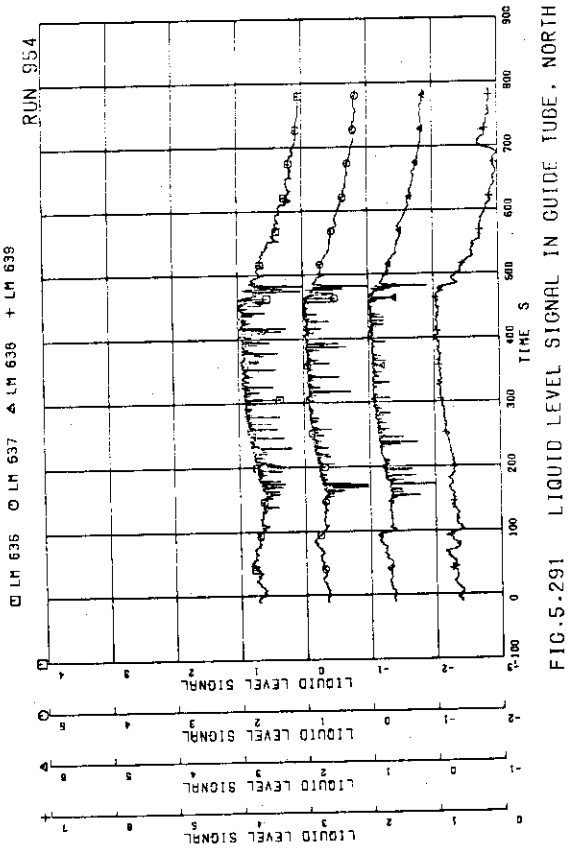

FIG.5.291 LIQUID LEVEL SIGNAL IN GUIDE TUBE, NORTH

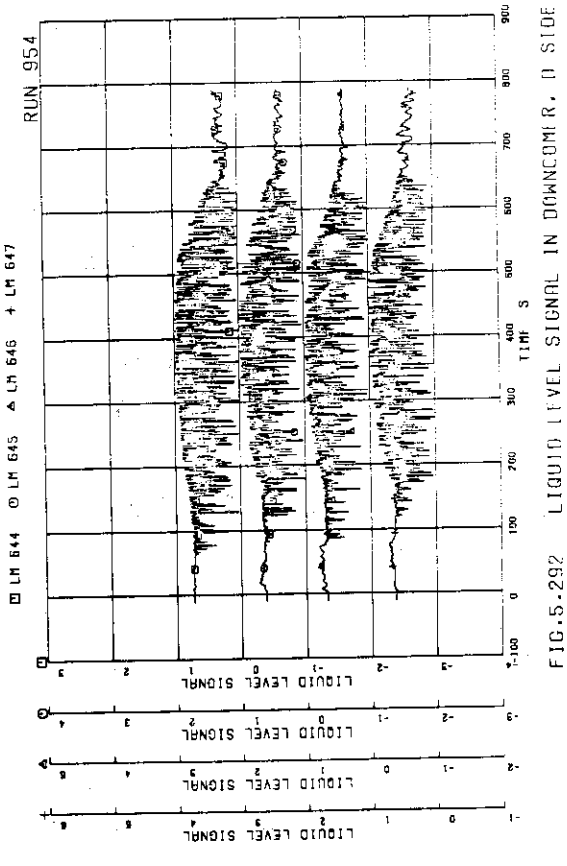

FIG.5.292 LIQUID LEVEL SIGNAL IN DOWNCOMER, D SIDE

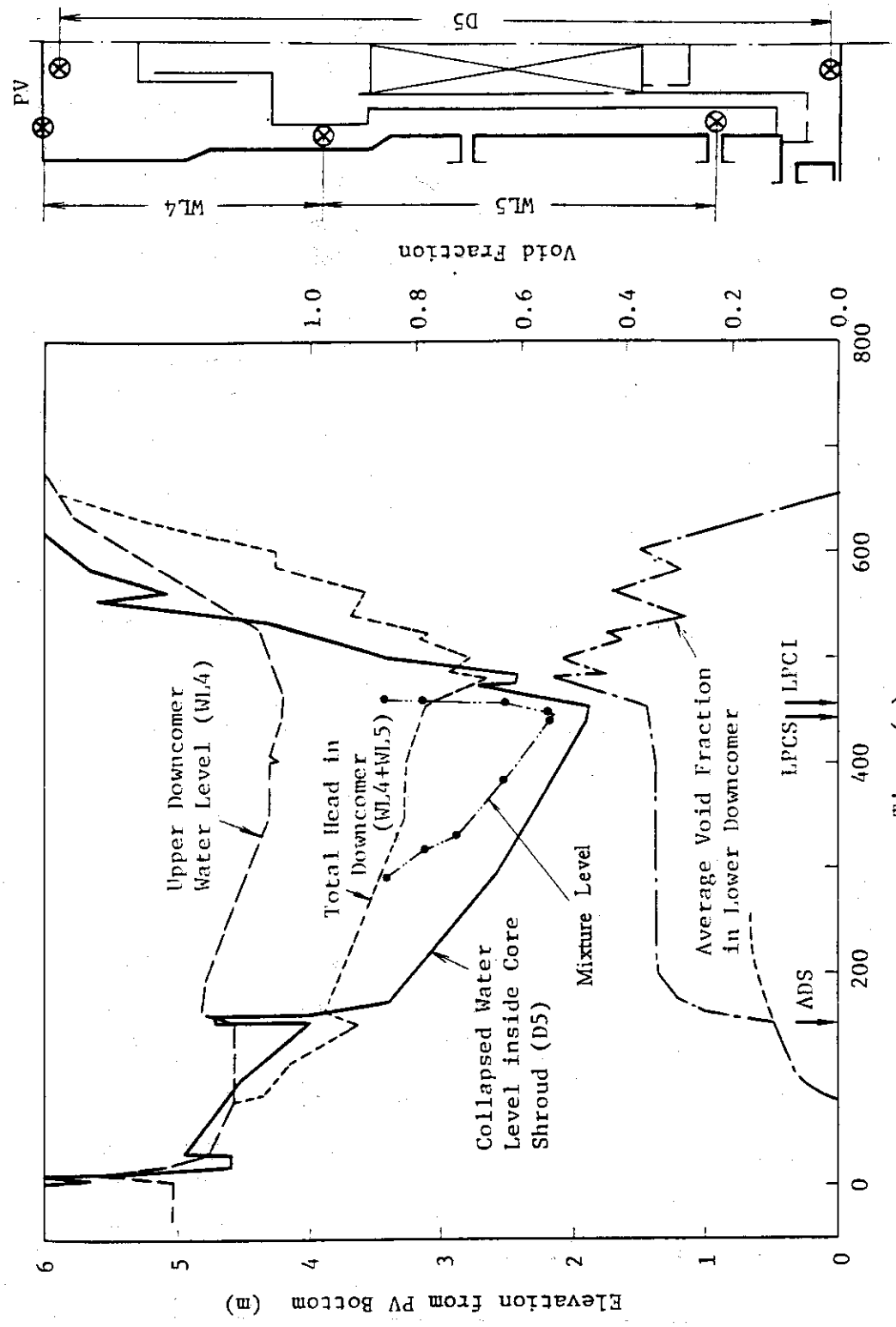

Fig. 5.293 Estimated liquid levels in pressure vessel

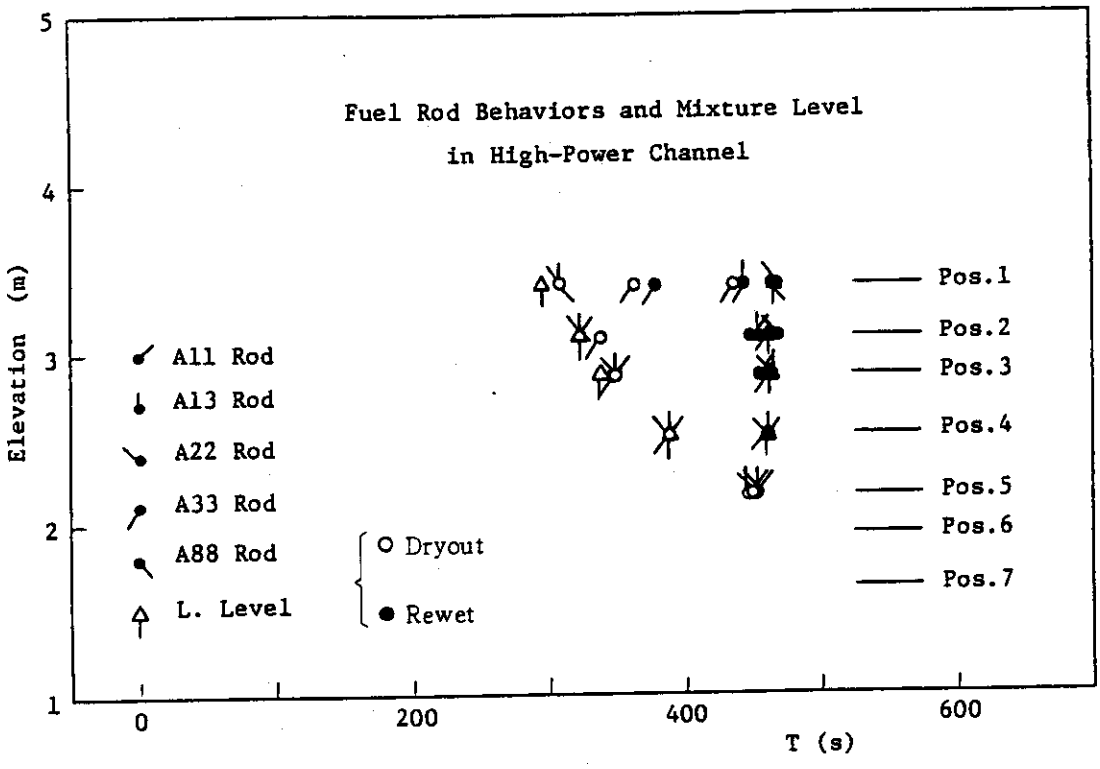

Fig. 5.294 Dryout and quench times of fuel rods in bundle A

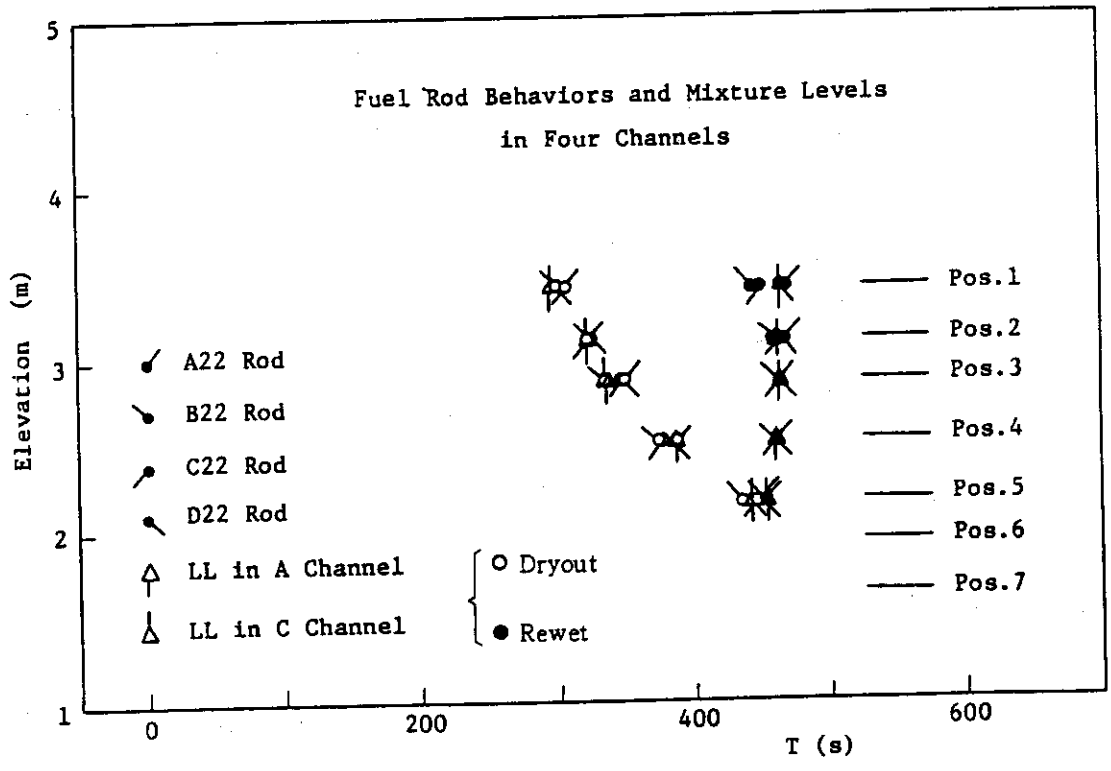

Fig. 5.295 Dryout and quench times of fuel rods in four bundles

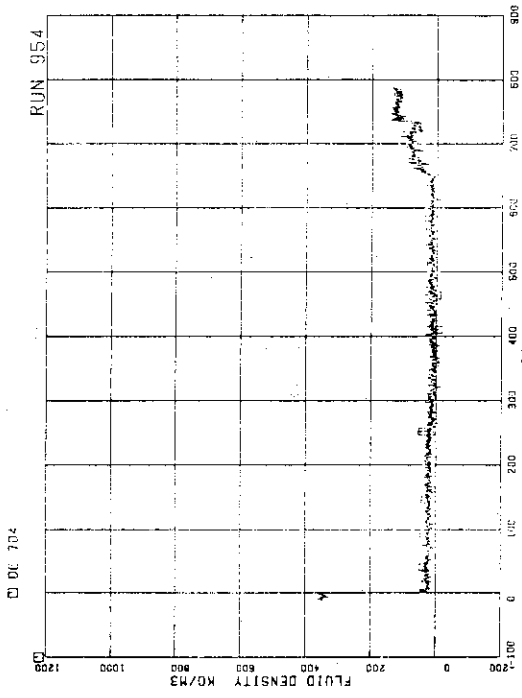

FIG.5.29[illegible] AVERAGE DENSITY IN MSL DOWN BREAK ORIFICE

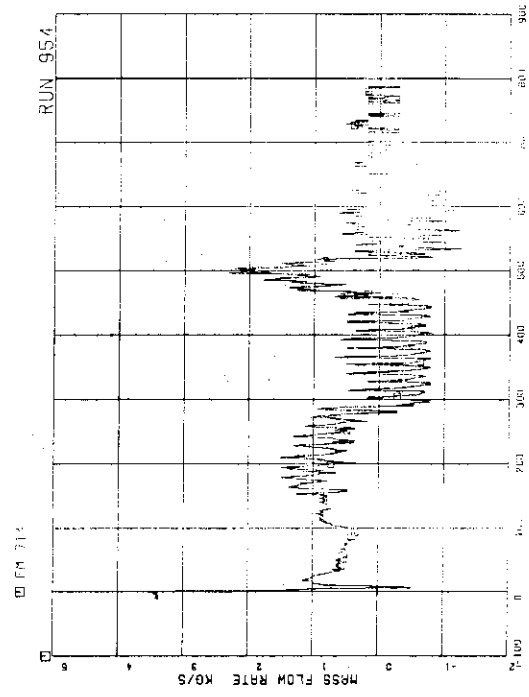

FIG.5.29[illegible] FLOW RATE AT CHANNEL OF IN[illegible]

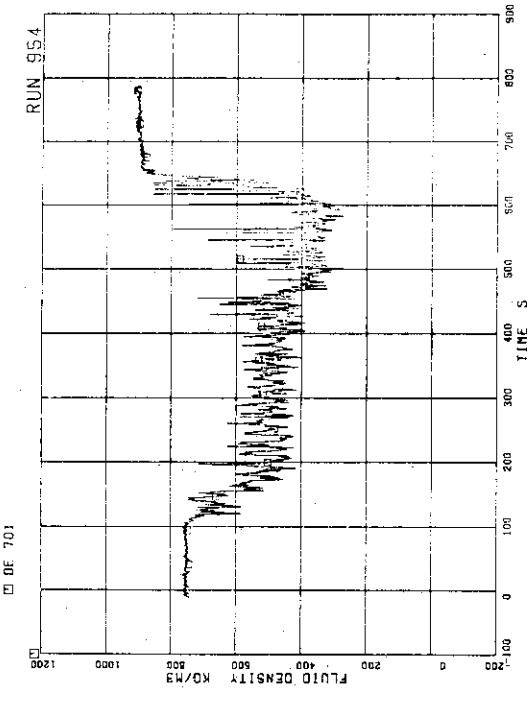

FIG.5.295 AVERAGE DENSITY AT JP-1,2 OUTLET

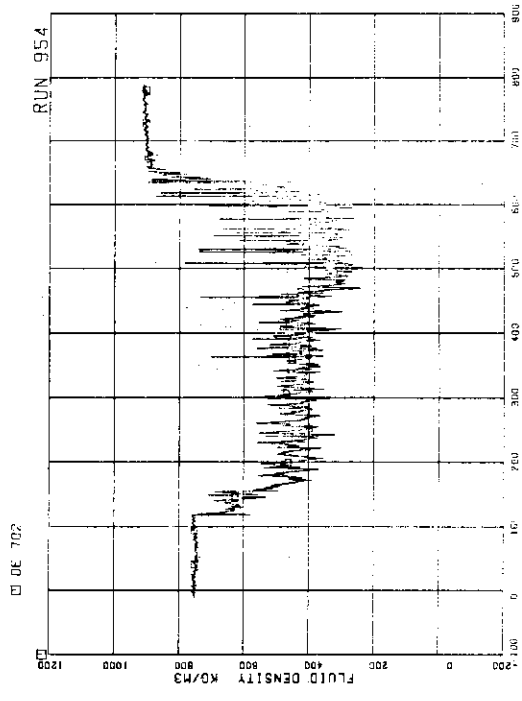

FIG.5.297 AVERAGE DENSITY AT JP 3,4 OUTLET

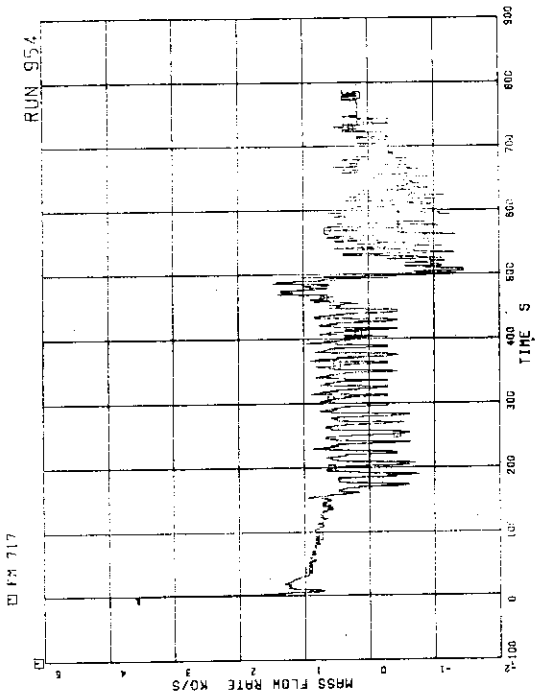

FIG.5.302 FLOW RATE AT CHANNEL D INLET

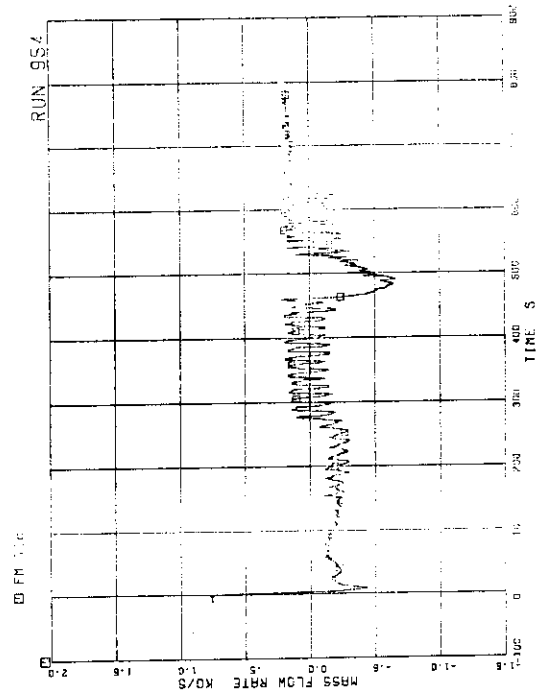

FIG.5.303 FLOW RATE AT BYPASS NO.4

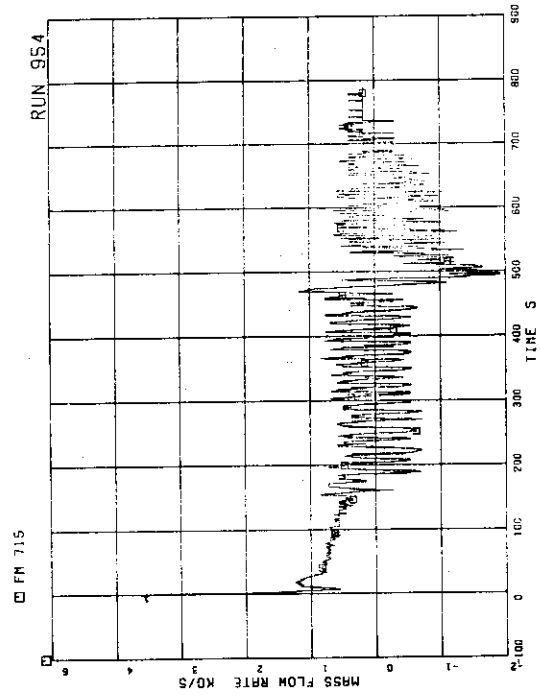

FIG.5.300 FLOW RATE AT CHANNEL B INLET

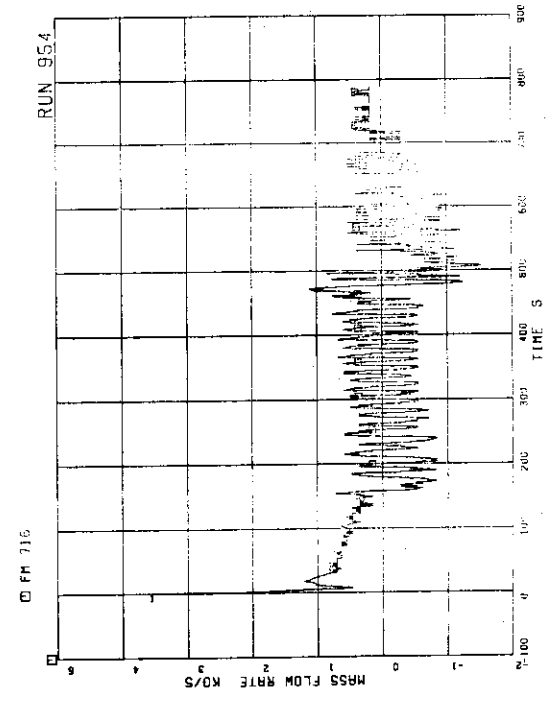

FIG.5.301 FLOW RATE AT CHANNEL C INLET

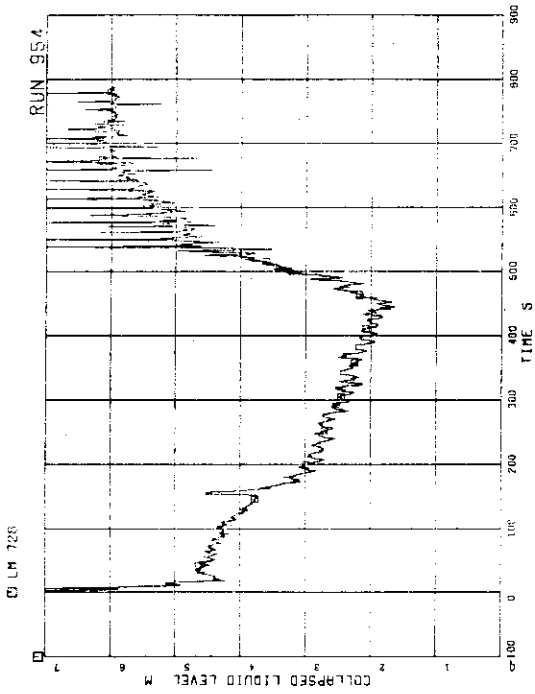

FIG.5.303 COLLAPSED LIQUID LEVEL INSIDE CORE SHROUD

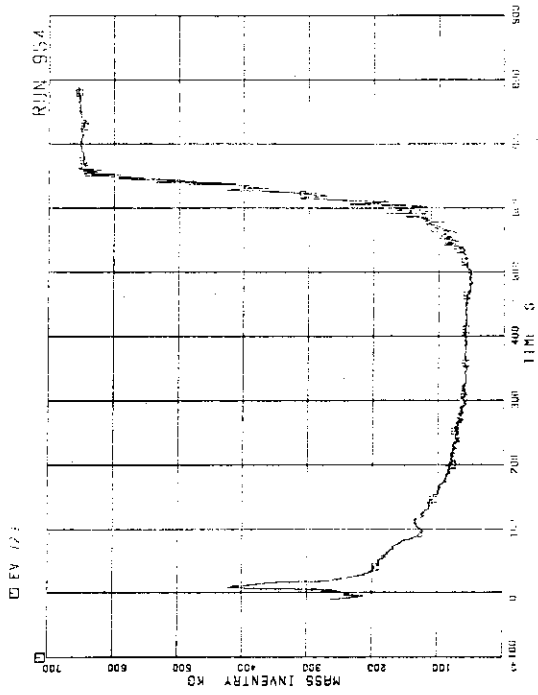

FIG.5.302 [illegible] INVENTORY IN [illegible]

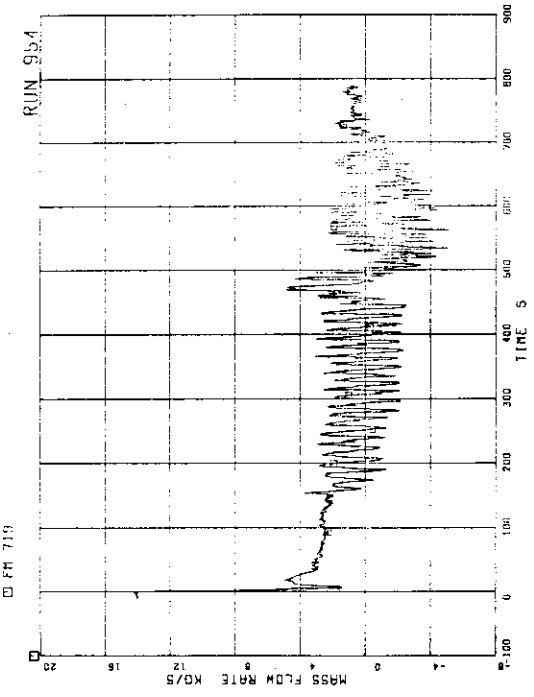

FIG.5.304 TOTAL CHANNEL INLET FLOW RATE

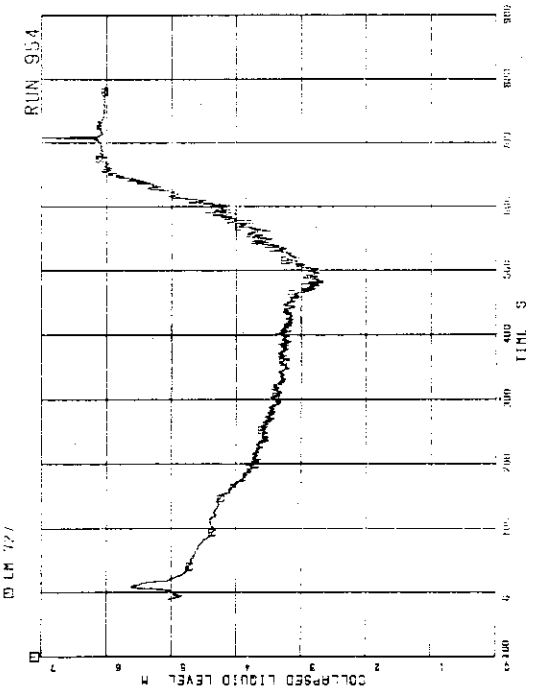

FIG.5.301 [illegible] LIQUID LEVEL IN [illegible]

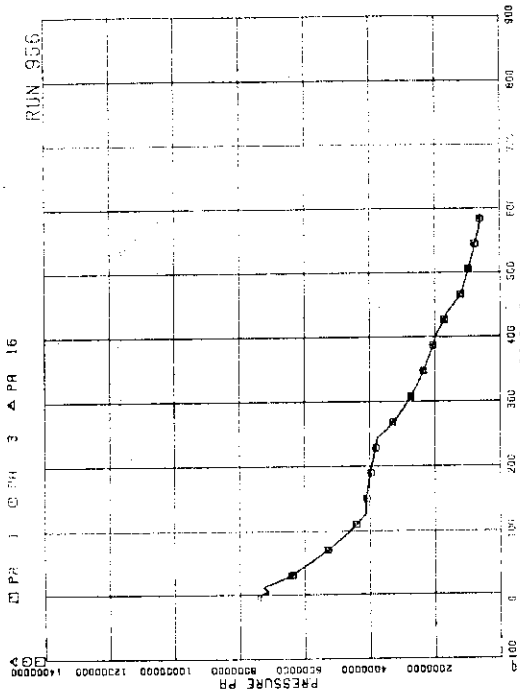

FIG.5.305 PRESSURES IN PV (PRESSURE VESSEL) AND MSL (MAIN STEAM LINE)

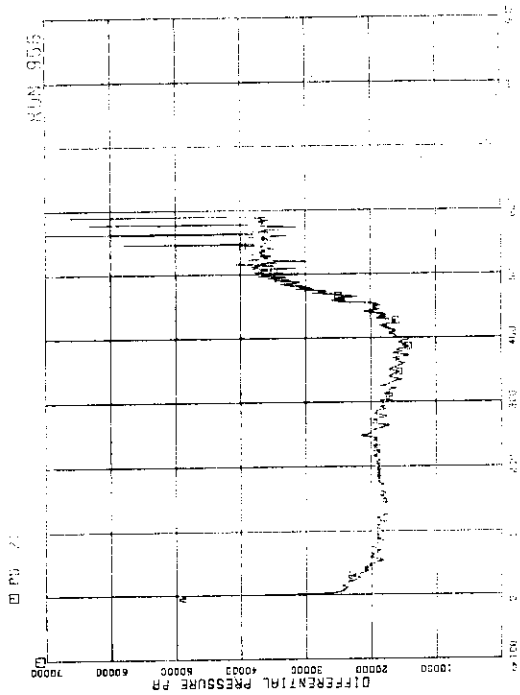

FIG.5.304

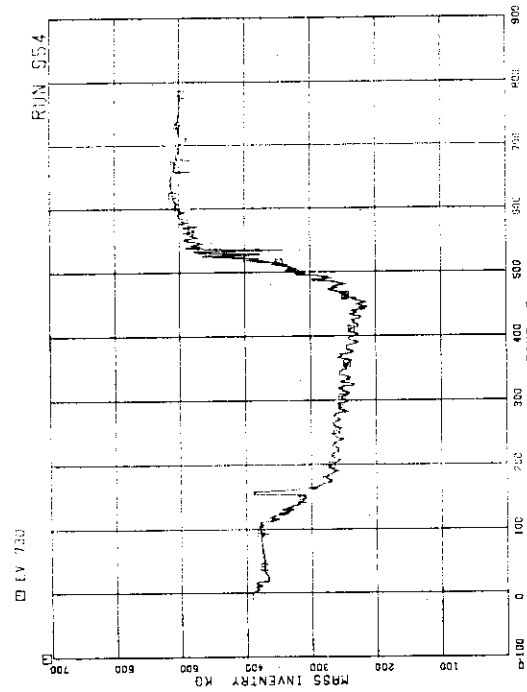

FIG.5.302 FLUID INVENTORY INSIDE CORE SHROUD

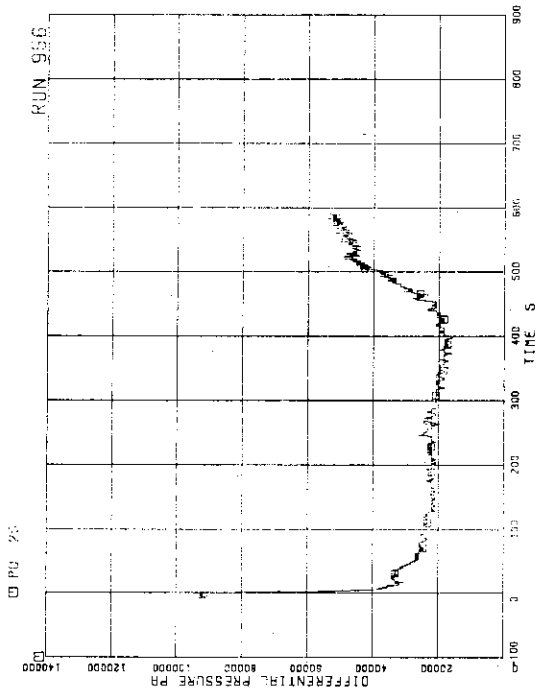

FIG.5.313 DIFFERENTIAL PRESSURE BETWEEN PV BOTTOM AND TOP

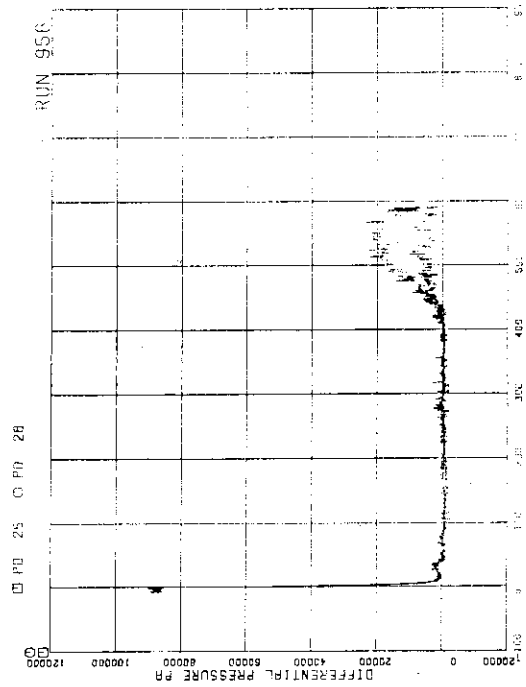

FIG.5.314 DIFFERENTIAL PRESSURE BETWEEN UP 1.2 DISCHARGE AND SUCTION

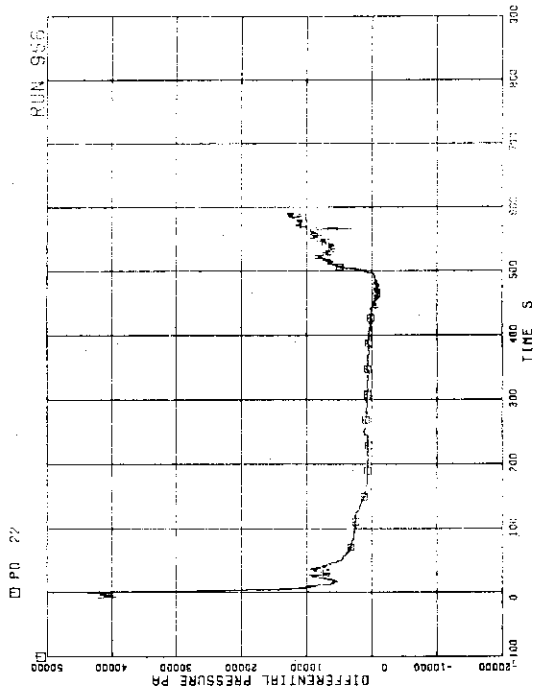

FIG.5.311 DIFFERENTIAL PRESSURE BETWEEN UP AND STEAM DOME

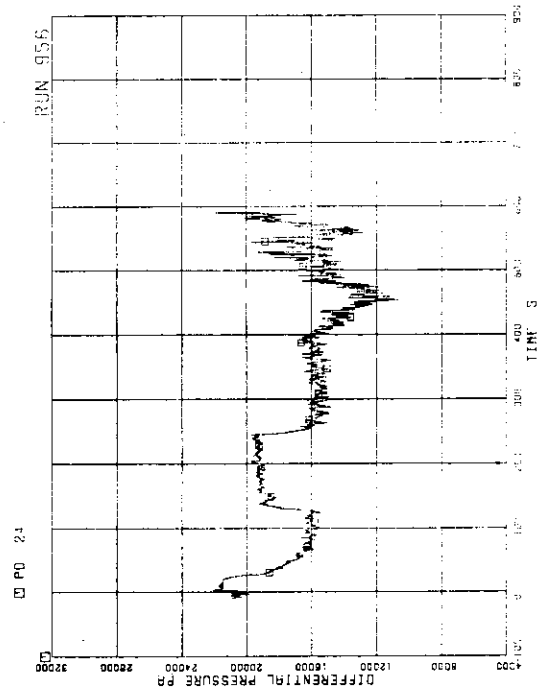

FIG.5.312 DIFFERENTIAL PRESSURE BETWEEN UP 1.2 DISCHARGE AND HEAD

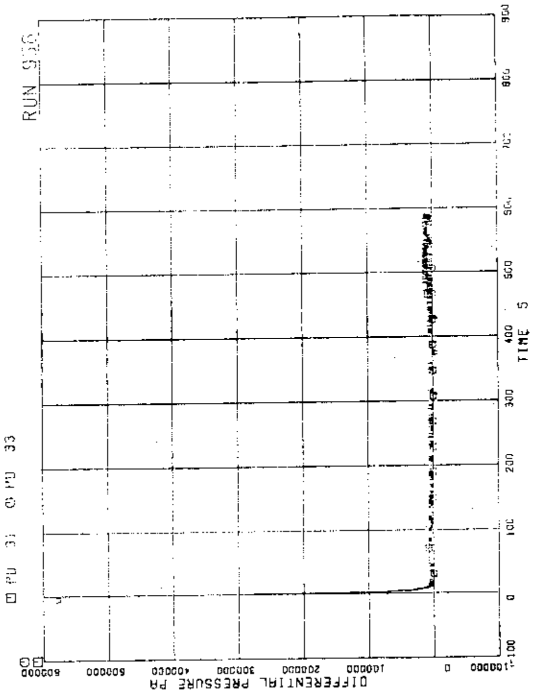

FIG.5.317 DIFFERENTIAL PRESSURE BETWEEN JP-3,4 DRIVE AND SUCTION

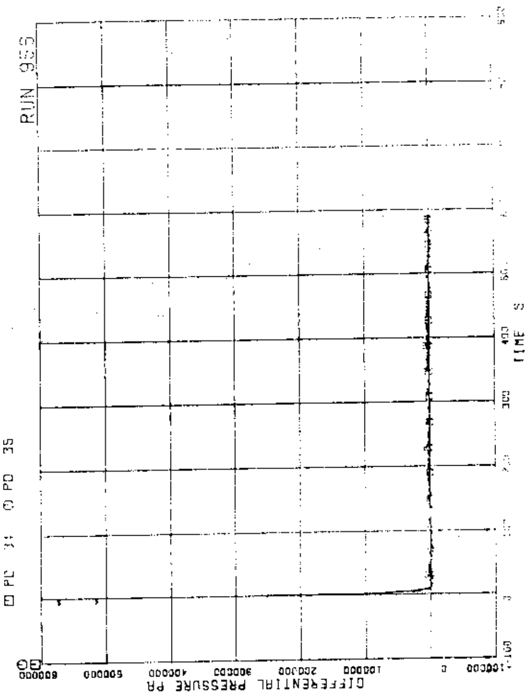

FIG.5.318 [illegible] PRESSURE [illegible] DELIVERY AND SUCTION

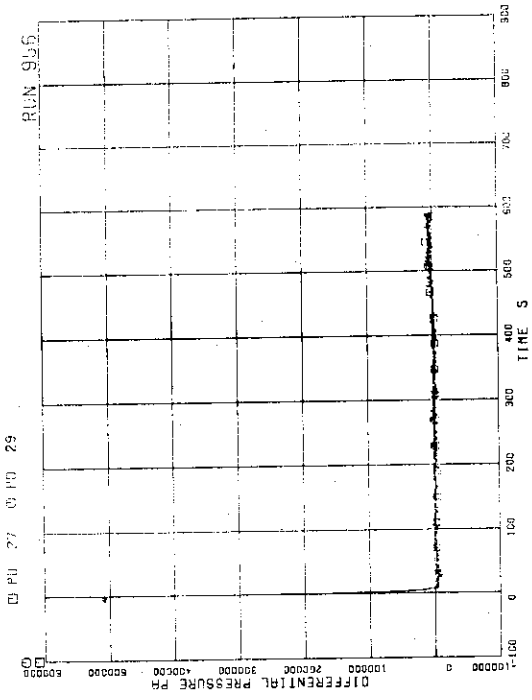

FIG.5.315 DIFFERENTIAL PRESSURE BETWEEN JP-1,2 DRIVE AND SUCTION

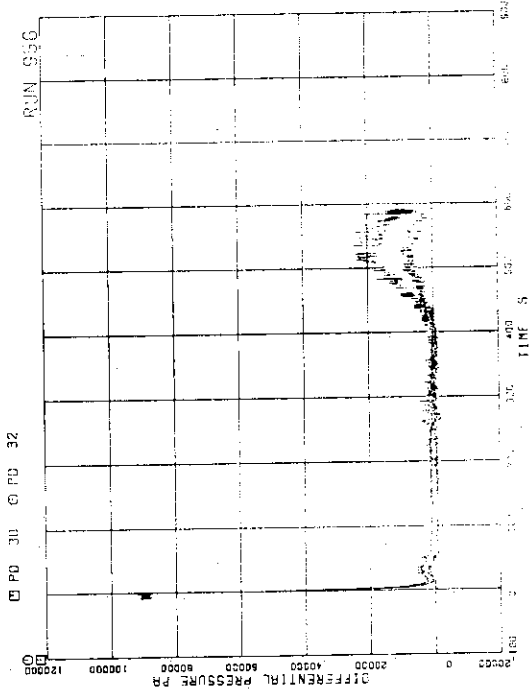

FIG.[illegible] [illegible] PRESSURE BETWEEN [illegible] 3,4 DISCHARGE AND SUCTION

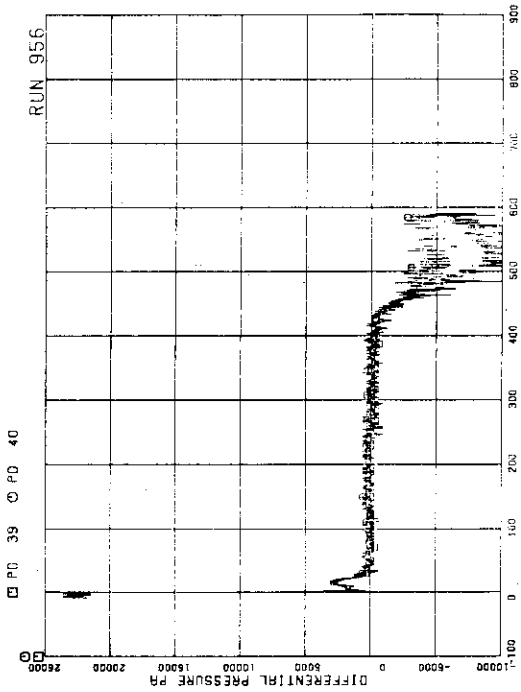

FIG.5.321 DIFFERENTIAL PRESSURE BETWEEN DC MIDDLE AND JP-1,2 SUCTION

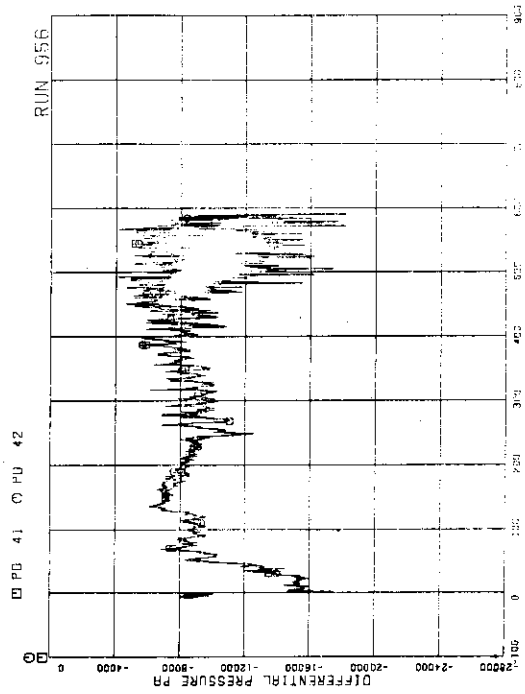

FIG.5.322 DIFFERENTIAL PRESSURE BETWEEN JP 1,2 DISCHARGE AND IP

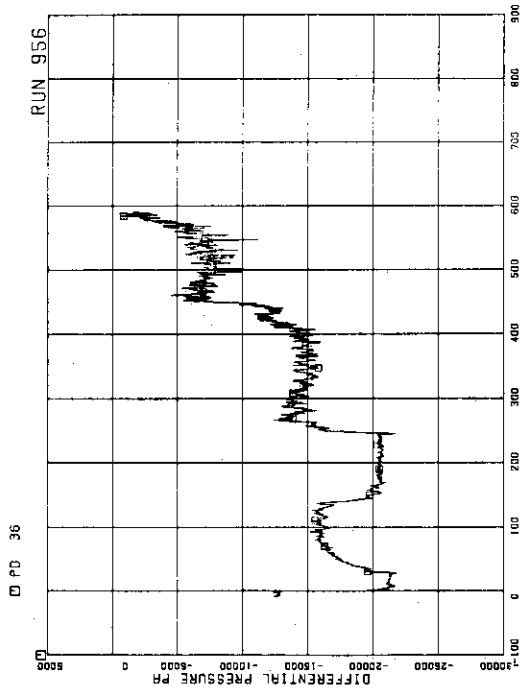

FIG.5.319 DIFFERENTIAL PRESSURE BETWEEN DC BOTTOM AND MRP1 SUCTION

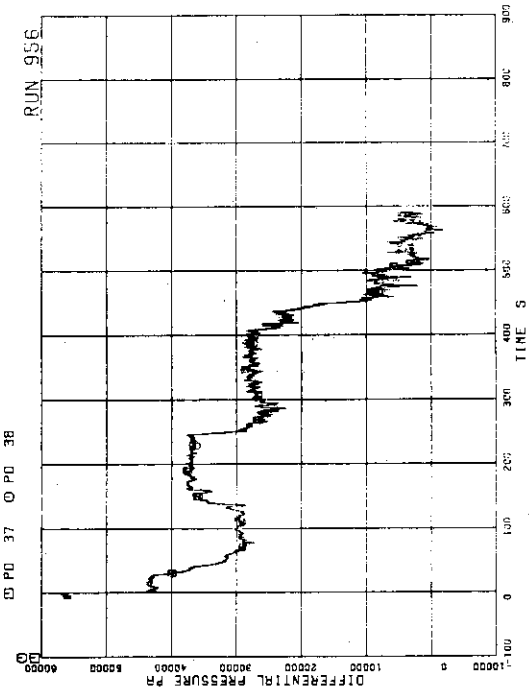

FIG.5.320 DIFFERENTIAL PRESSURE BETWEEN MRP1 DELIVERY AND JP-1,2 DRIVE

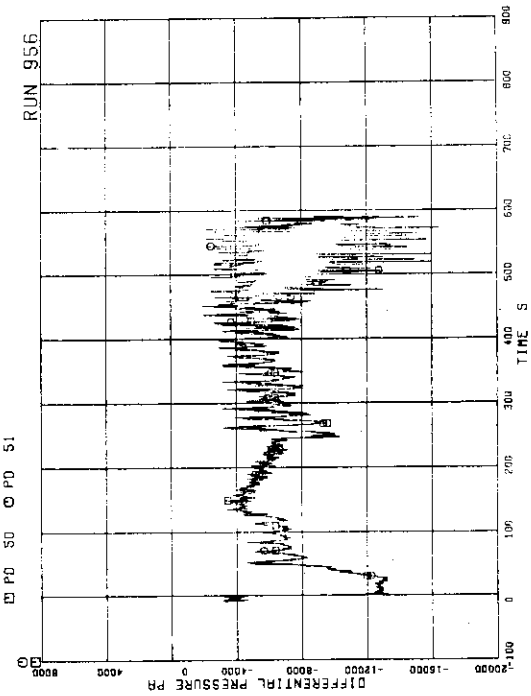

FIG.5.325 DIFFERENTIAL PRESSURE BETWEEN JP-3,4 DISCHARGE AND CONFLUENCE

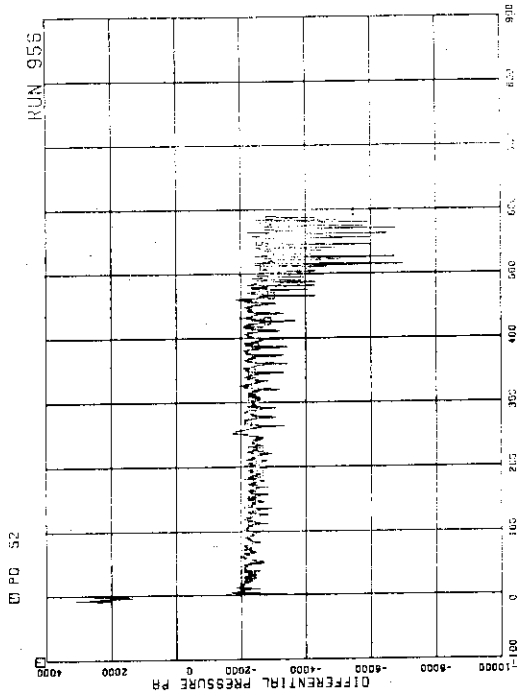

FIG.5.326 DIFFERENTIAL PRESSURE BETWEEN JP-3,4 CONFLUENCE AND LP

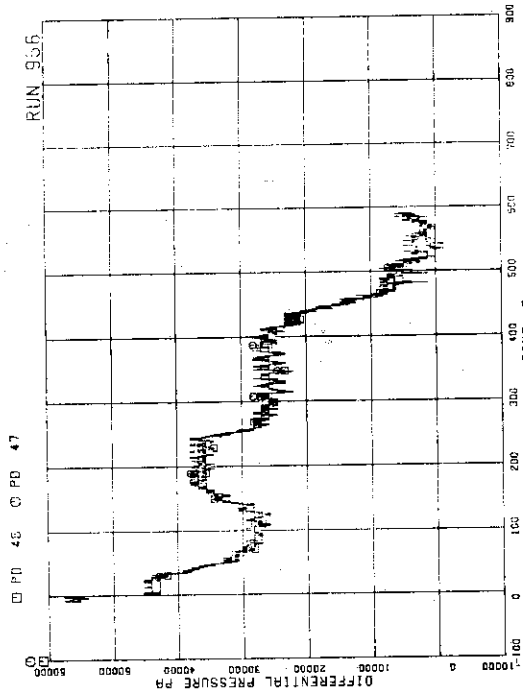

FIG.5.323 DIFFERENTIAL PRESSURE BETWEEN MRP2 DELIVERY AND JP-3,4 DRIVE

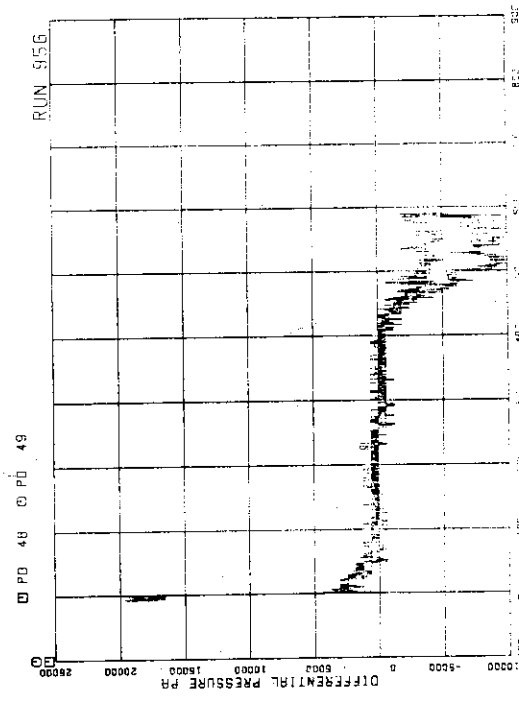

FIG.5.324 [illegible]

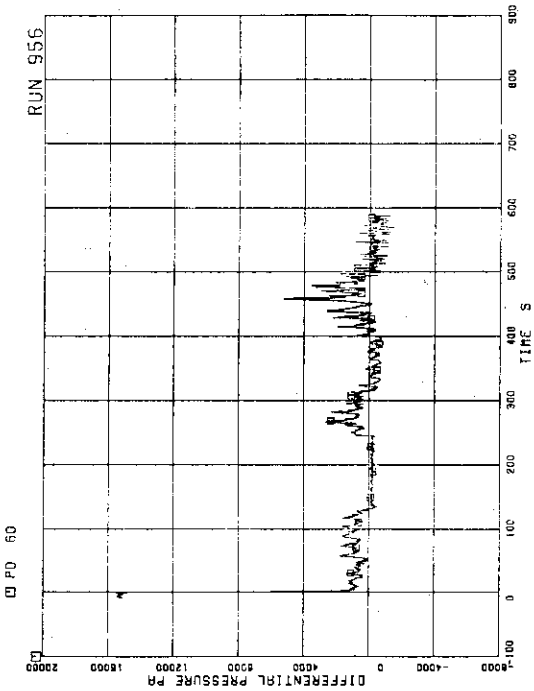

FIG.5.329 DIFFERENTIAL PRESSURE ACROSS CHANNEL INLET ORIFICE A

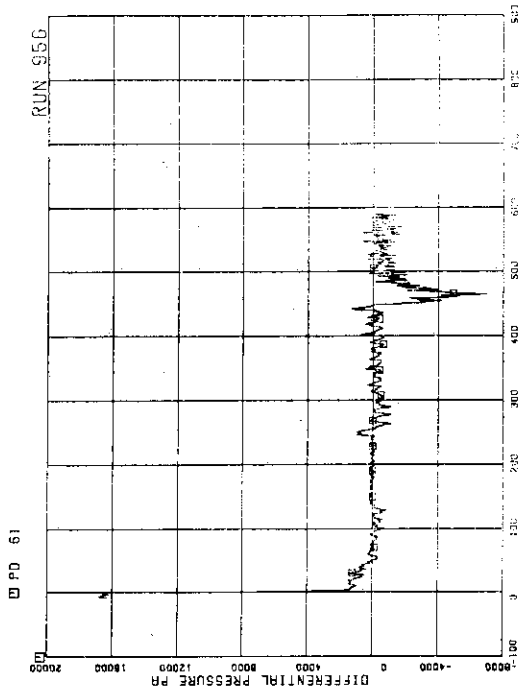

FIG.5.330 DIFFERENTIAL PRESSURE ACROSS CHANNEL INLET ORIFICE A

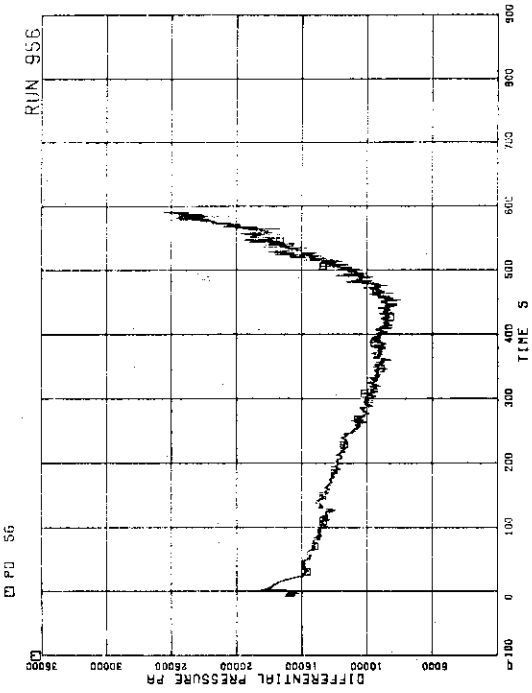

FIG.5.327 DIFFERENTIAL PRESSURE BETWEEN DC MIDDLE AND STEAM DOME

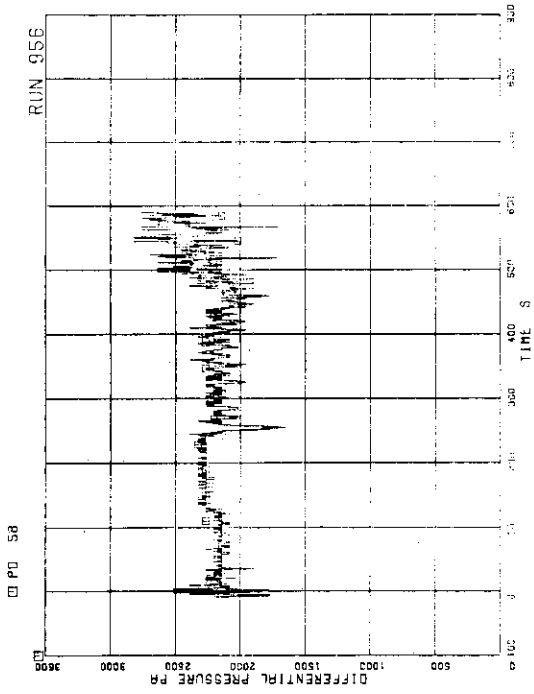

FIG.5.328 DIFFERENTIAL PRESSURE BETWEEN LP BOTTOM AND LP MIDDLE

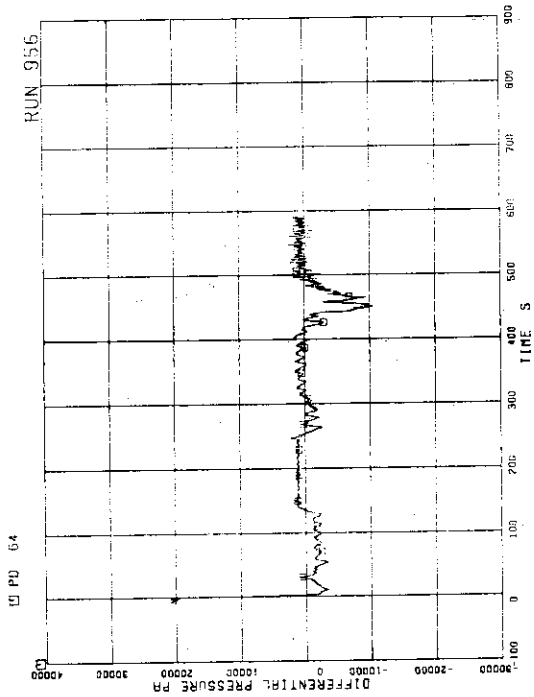

FIG.5-333 DIFFERENTIAL PRESSURE ACROSS BYPASS HOLE

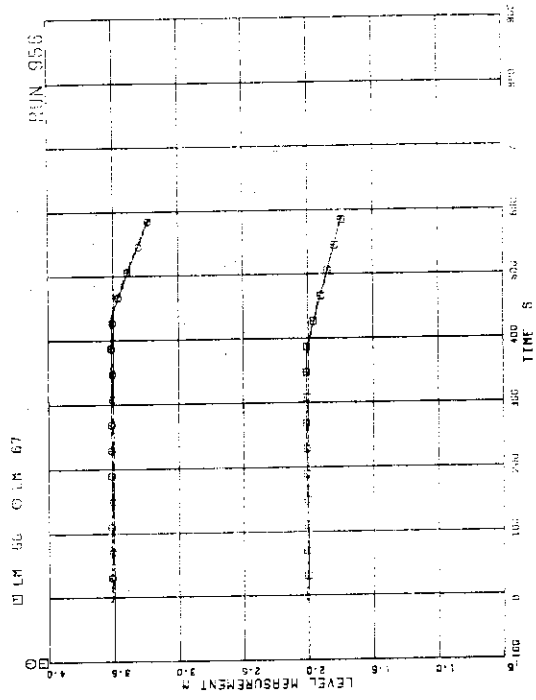

FIG.5-334 LIQUID LEVELS IN ECCS HEADER

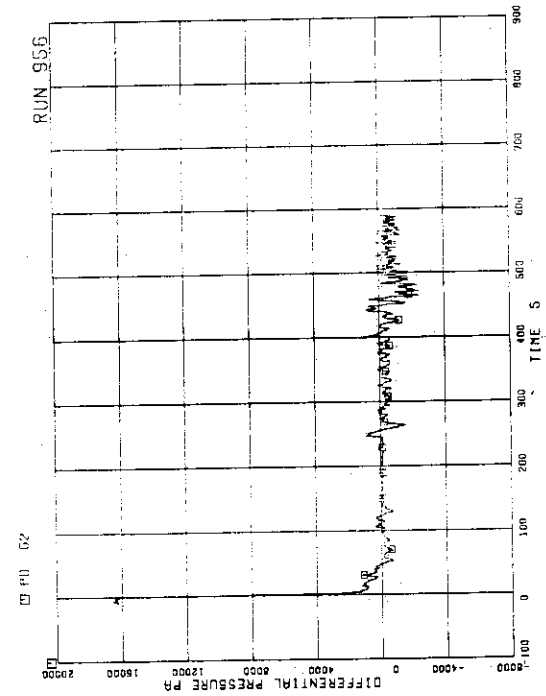

FIG.5-331 DIFFERENTIAL PRESSURE ACROSS CHANNEL INLET ORIFICE C

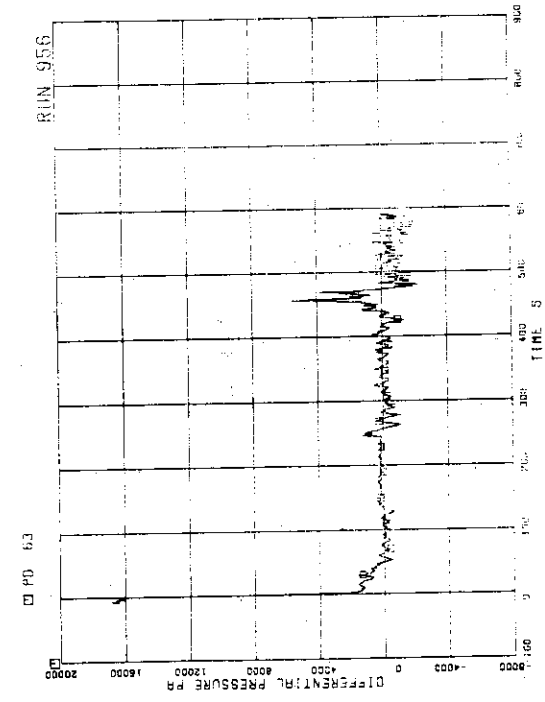

FIG.5-332 DIFFERENTIAL PRESSURE ACROSS CHANNEL INLET ORIFICE D

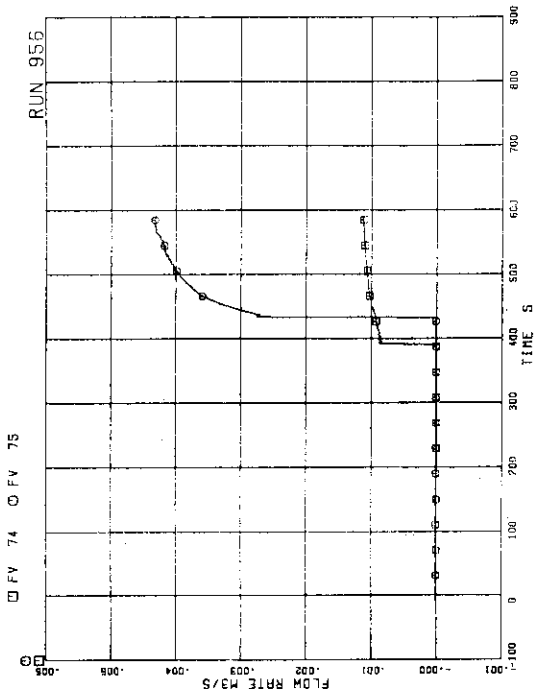

FIG.5.334 ECC INJECTION FLOW RATES

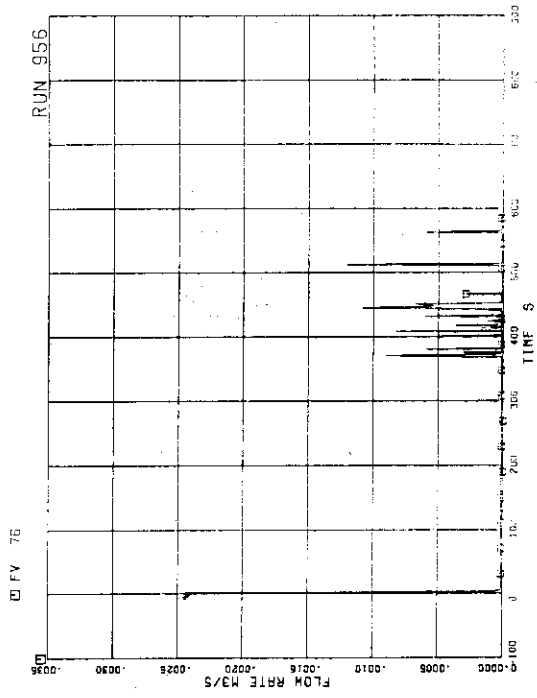

FIG.5.336 FEEDWATER FLOW RATE

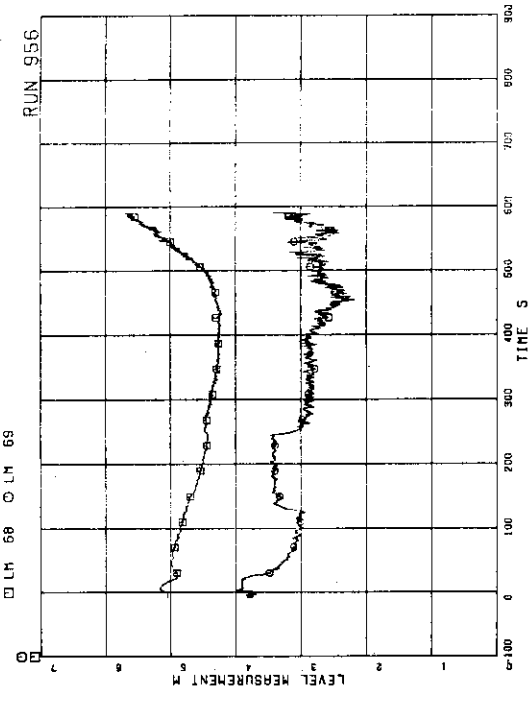

FIG.5.335 LIQUID LEVEL IN DOWNCOMER

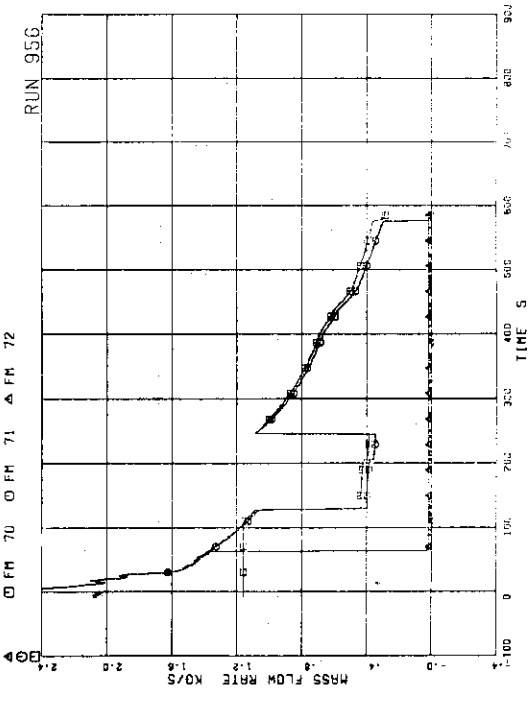

FIG.5.337 MAIN STEAM FLOW RATE IN MSL

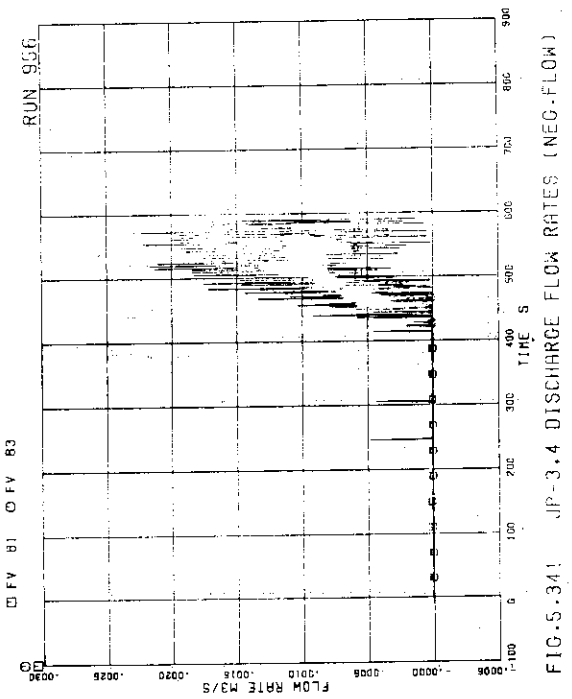

FIG.5.341 JP-3.4 DISCHARGE FLOW RATES (NEG-FLOW)

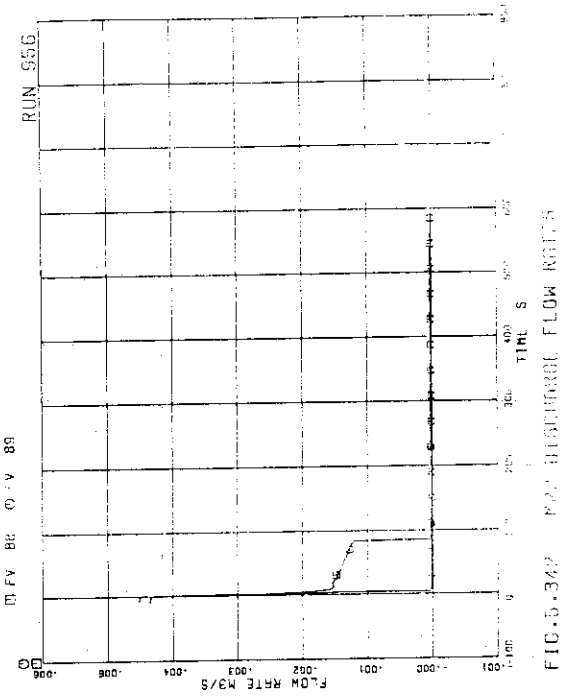

FIG.5.342

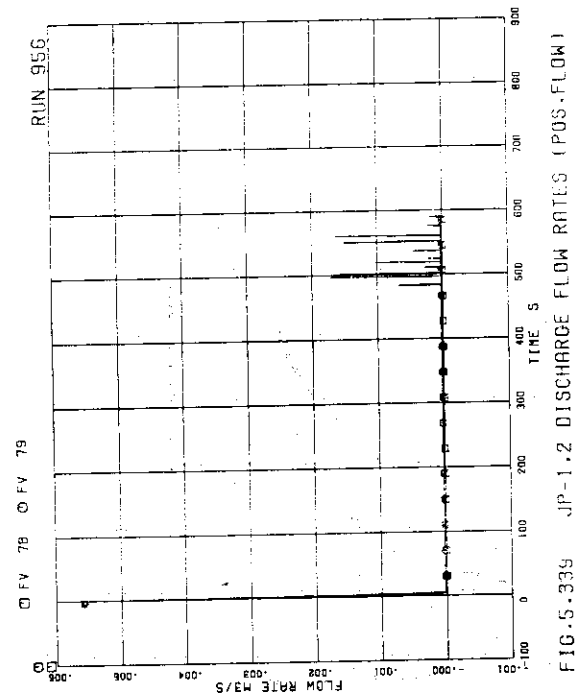

FIG.5.339 JP-1.2 DISCHARGE FLOW RATES (POS.FLOW)

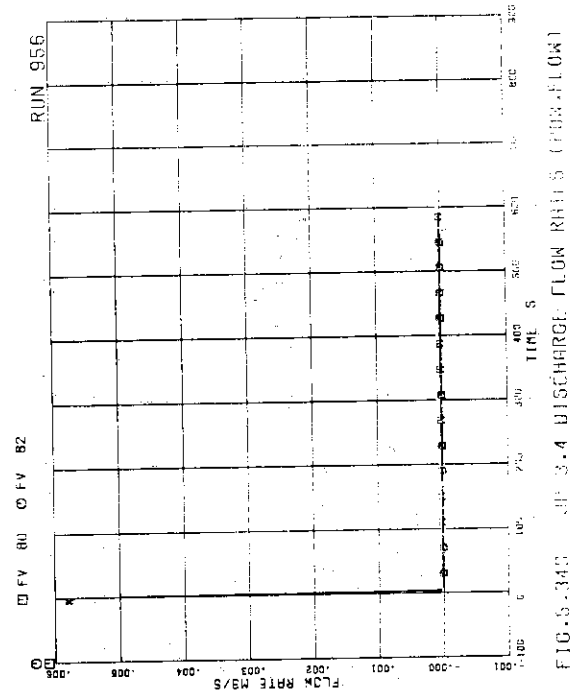

FIG.5.340

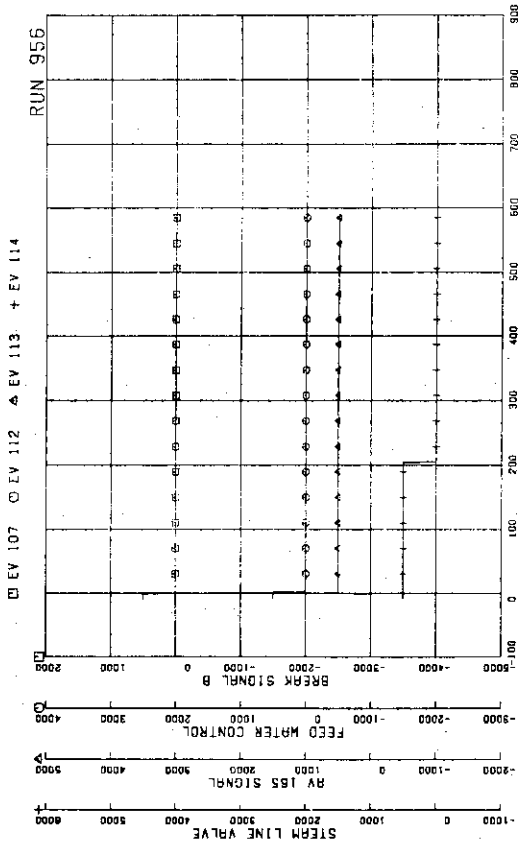

FIG.5.345 VALVE OPERATION SIGNALS

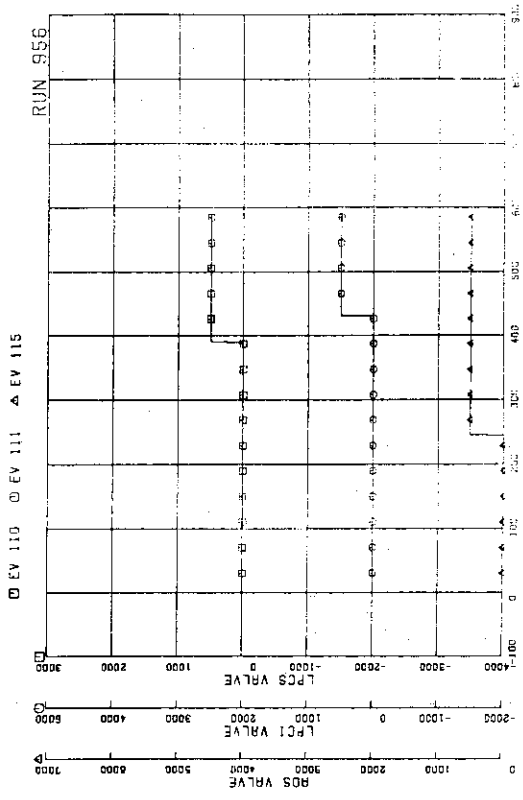

FIG.5.346 ECCS OPERATION SIGNALS

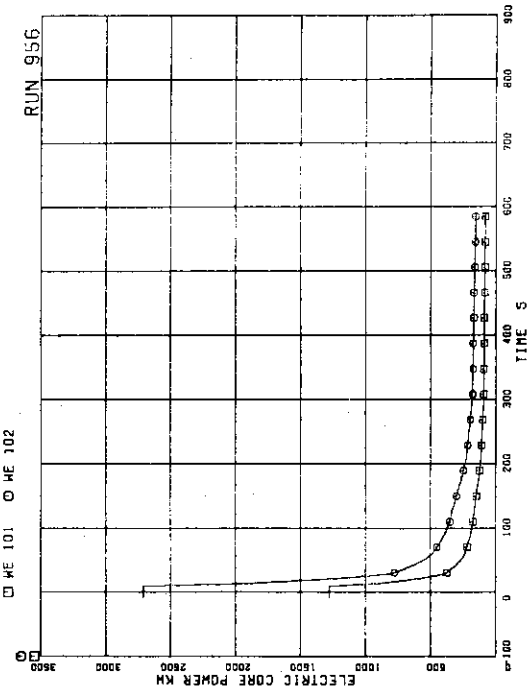

FIG.5.343 ELECTRIC CORE POWER

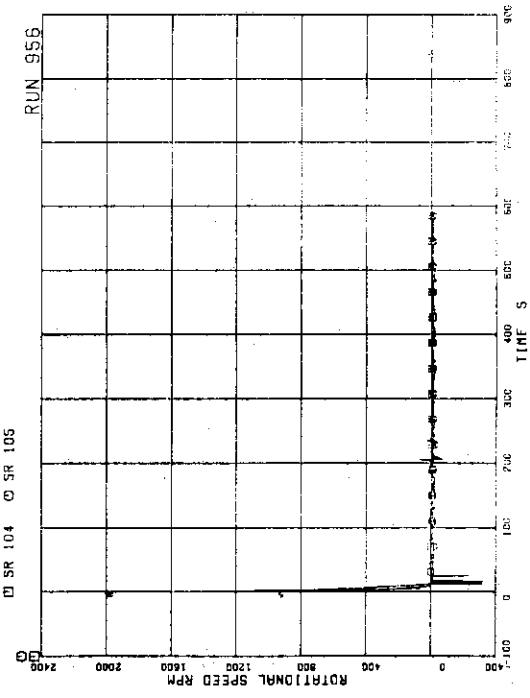

FIG.5.344 MAIN PUMP SPEEDS

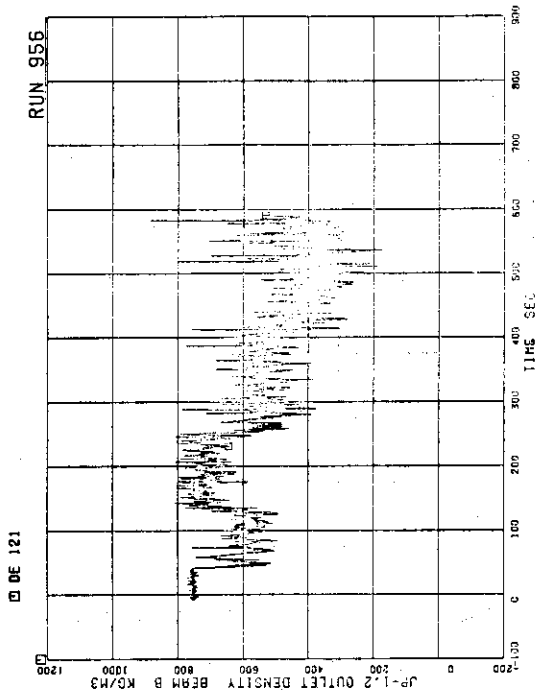

FIG.5.349 FLUID DENSITY AT JP-1,2 OUTLET, BEAM B

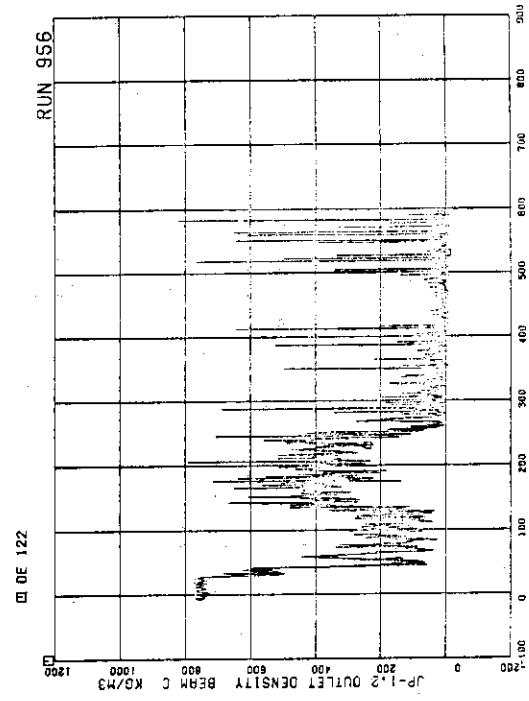

FIG.5.350 FLUID DENSITY AT JP-1,2 OUTLET, BEAM C

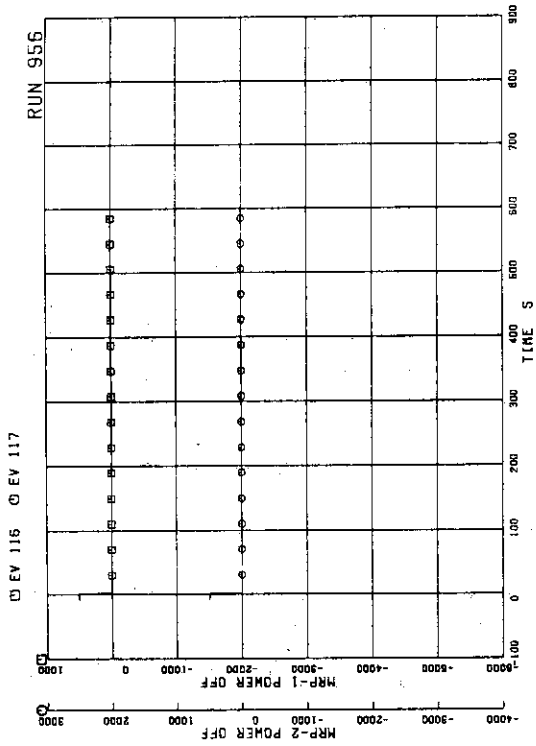

FIG.5.347 MRP OPERATION SIGNALS

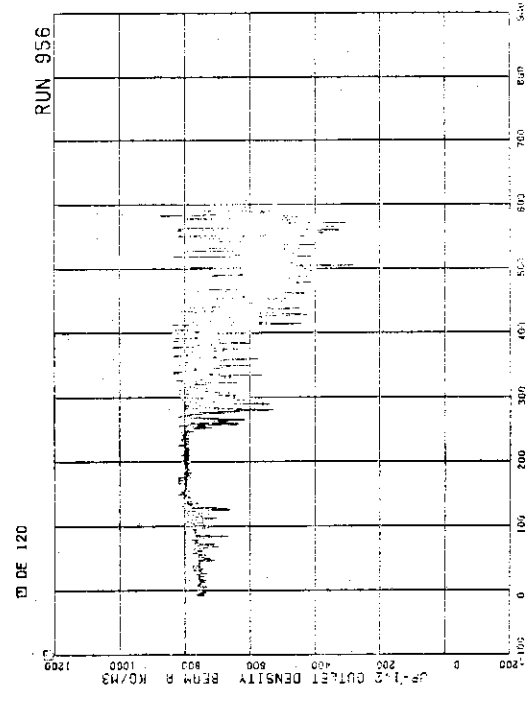

FIG.5.348 FLUID DENSITY AT JP 1,2 OUTLET, BEAM A

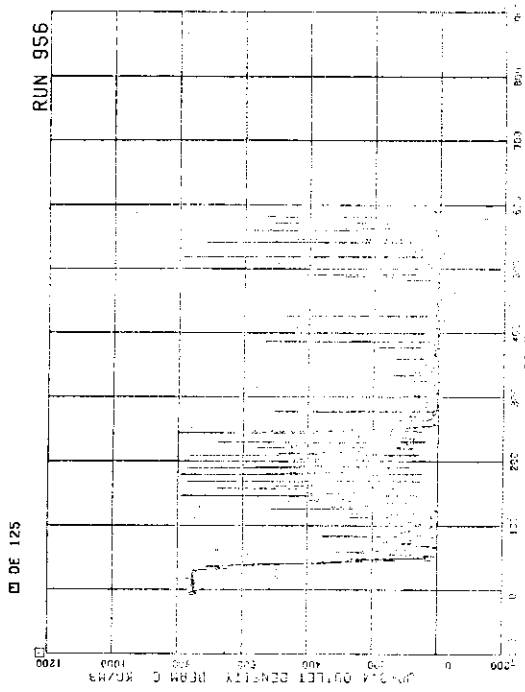

FIG.5.353 FLUID DENSITY AT JP-3,4 OUTLET, BEAM C

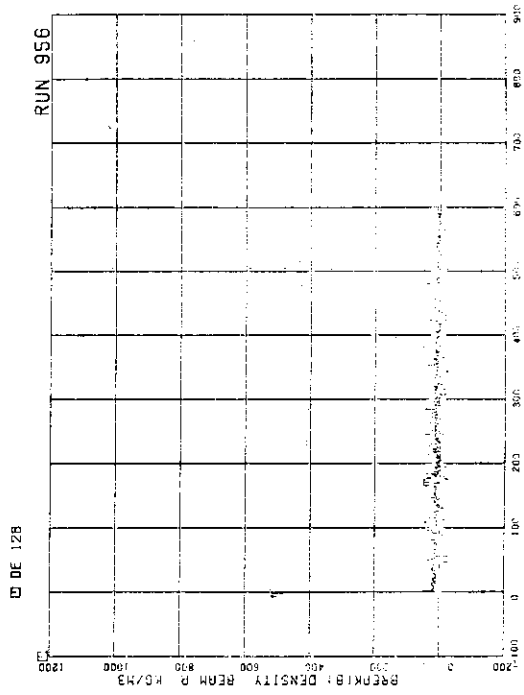

FIG.5.354 FLUID DENSITY IN MSL DOWN THL BREAK ORIFICE, BEAM A

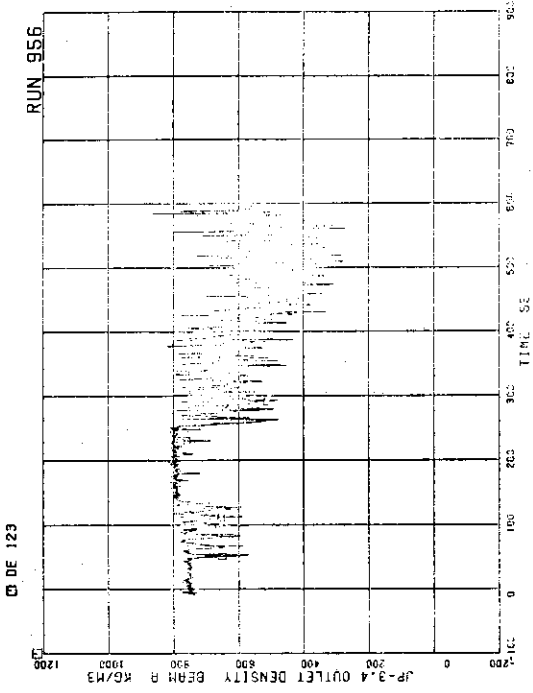

FIG.5.351 FLUID DENSITY AT JP-3,4 OUTLET, BEAM A

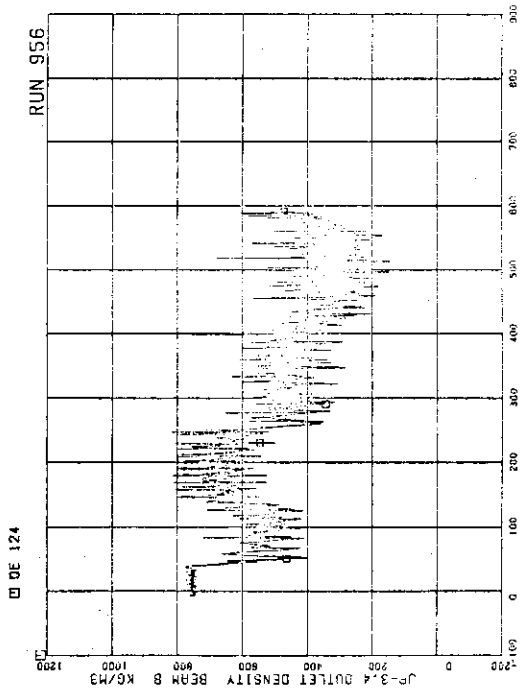

FIG.5.352 FLUID DENSITY AT JP-3,4 OUTLET, BEAM B

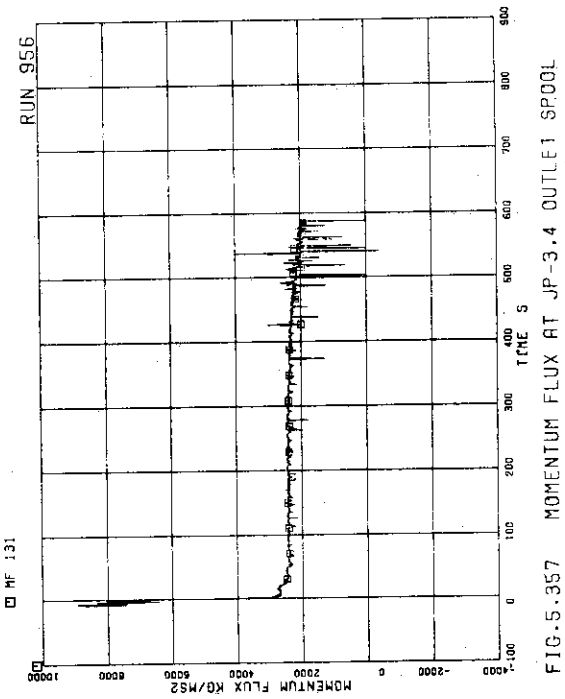

FIG.5.357 MOMENTUM FLUX AT JP-3.4 OUTLET SPOOL

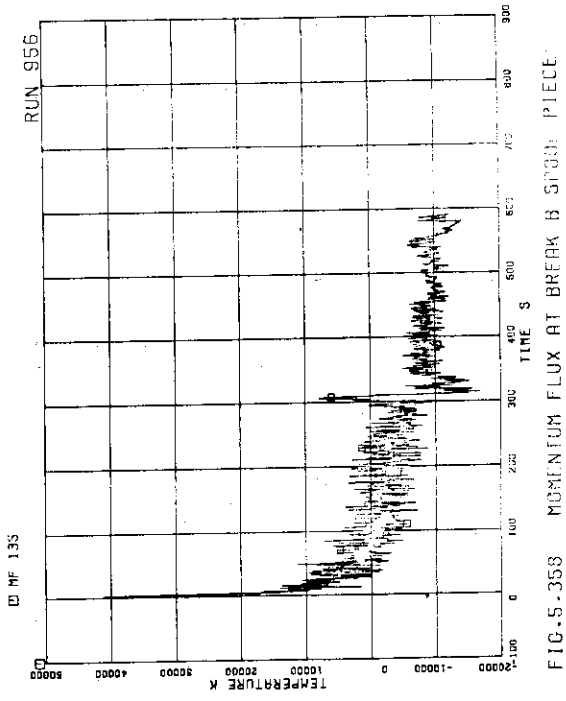

FIG.5.358 MOMENTUM FLUX AT BREAK B SPOOL PIECE (HIGH RANGE)

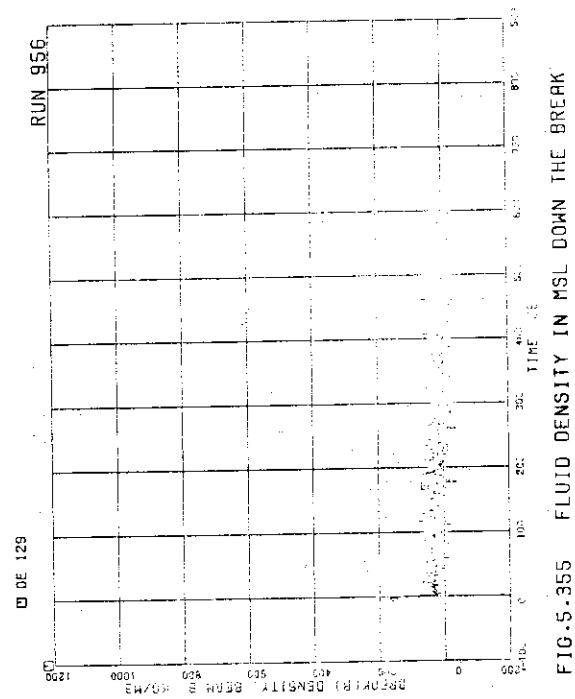

FIG.5.355 FLUID DENSITY IN MSL DOWN THE BREAK ORIFICE, BEAM B

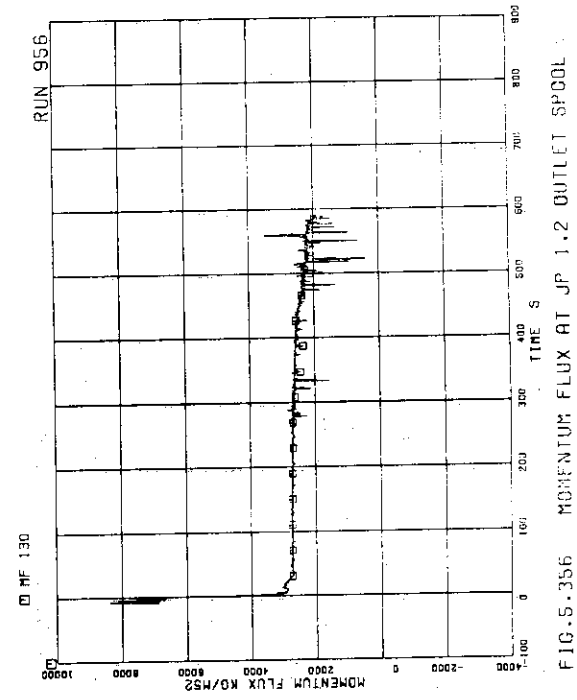

FIG.5.356 MOMENTUM FLUX AT JP 1.2 OUTLET SPOOL

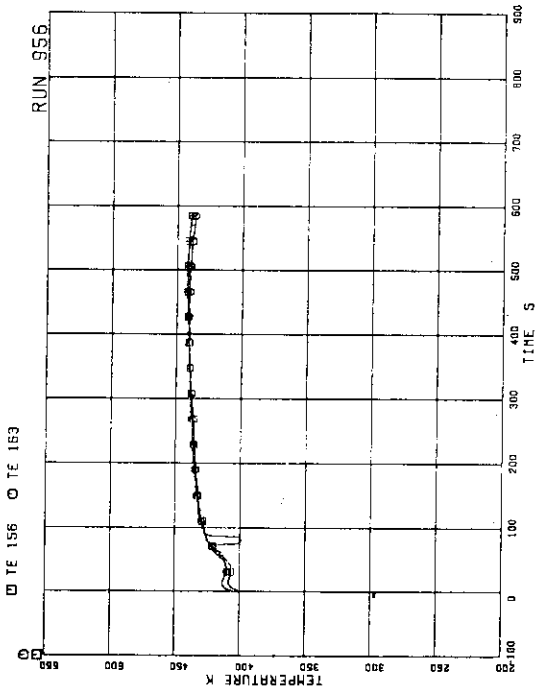

FIG.5.361 FLUID TEMPERATURE IN MSL DOWN THE BREAK ORIFICE

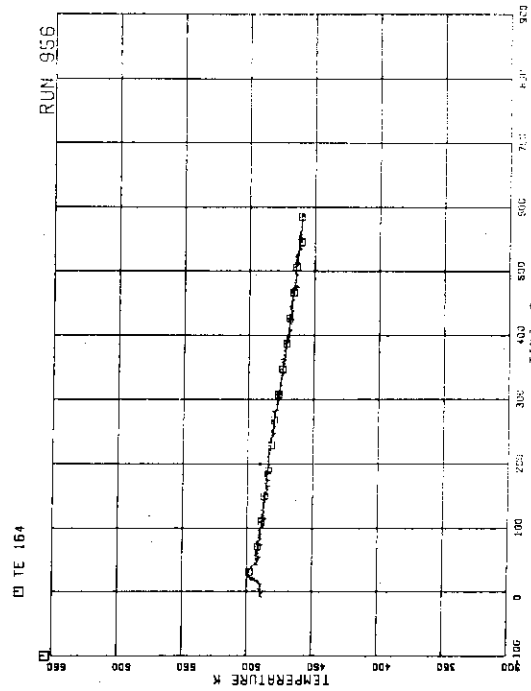

FIG.5.362 FEEDWATER TEMPERATURE

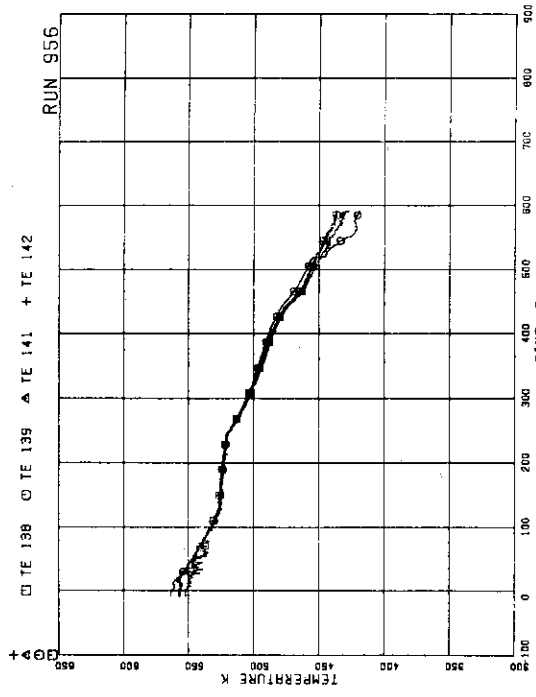

FIG.5.359 FLUID TEMPERATURES IN PV

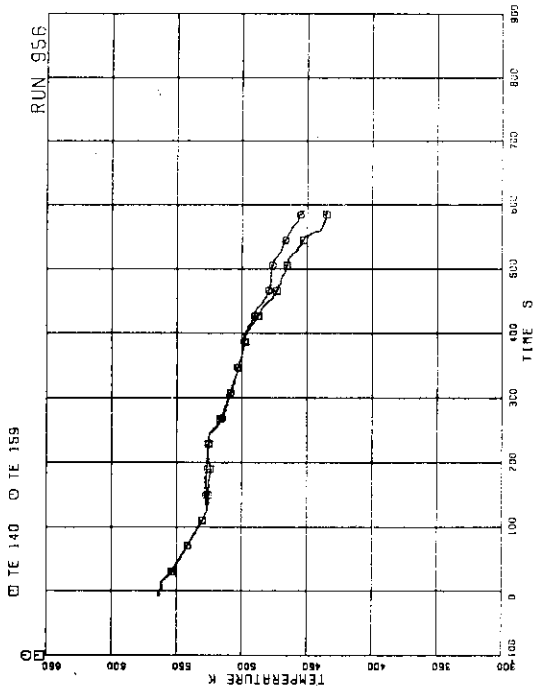

FIG.5.360 FLUID TEMPERATURE IN STEAM DUMP AND MSL

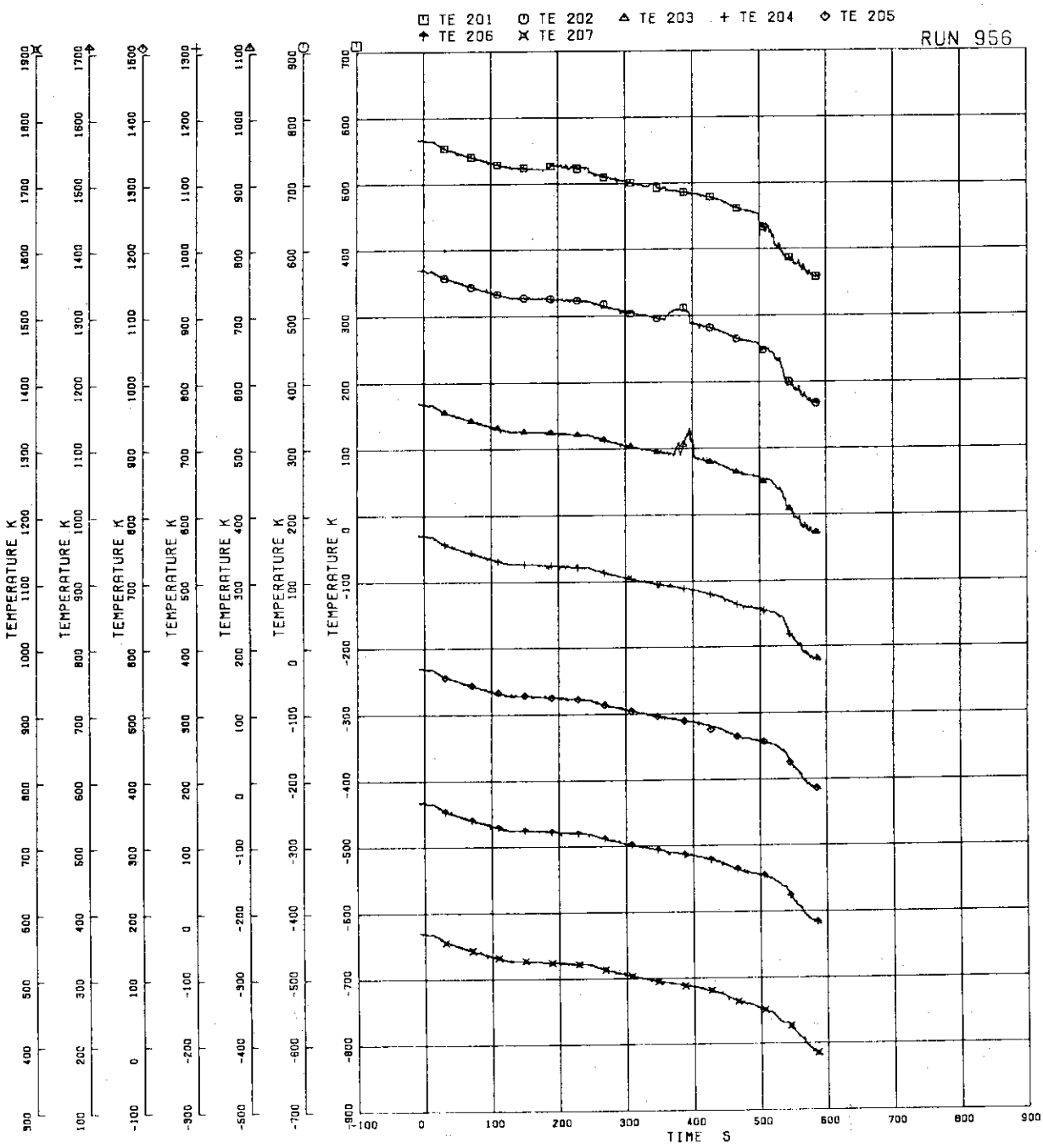

FIG.5.363 FUEL ROD SURFACE TEMPERATURE OF A11 ROD

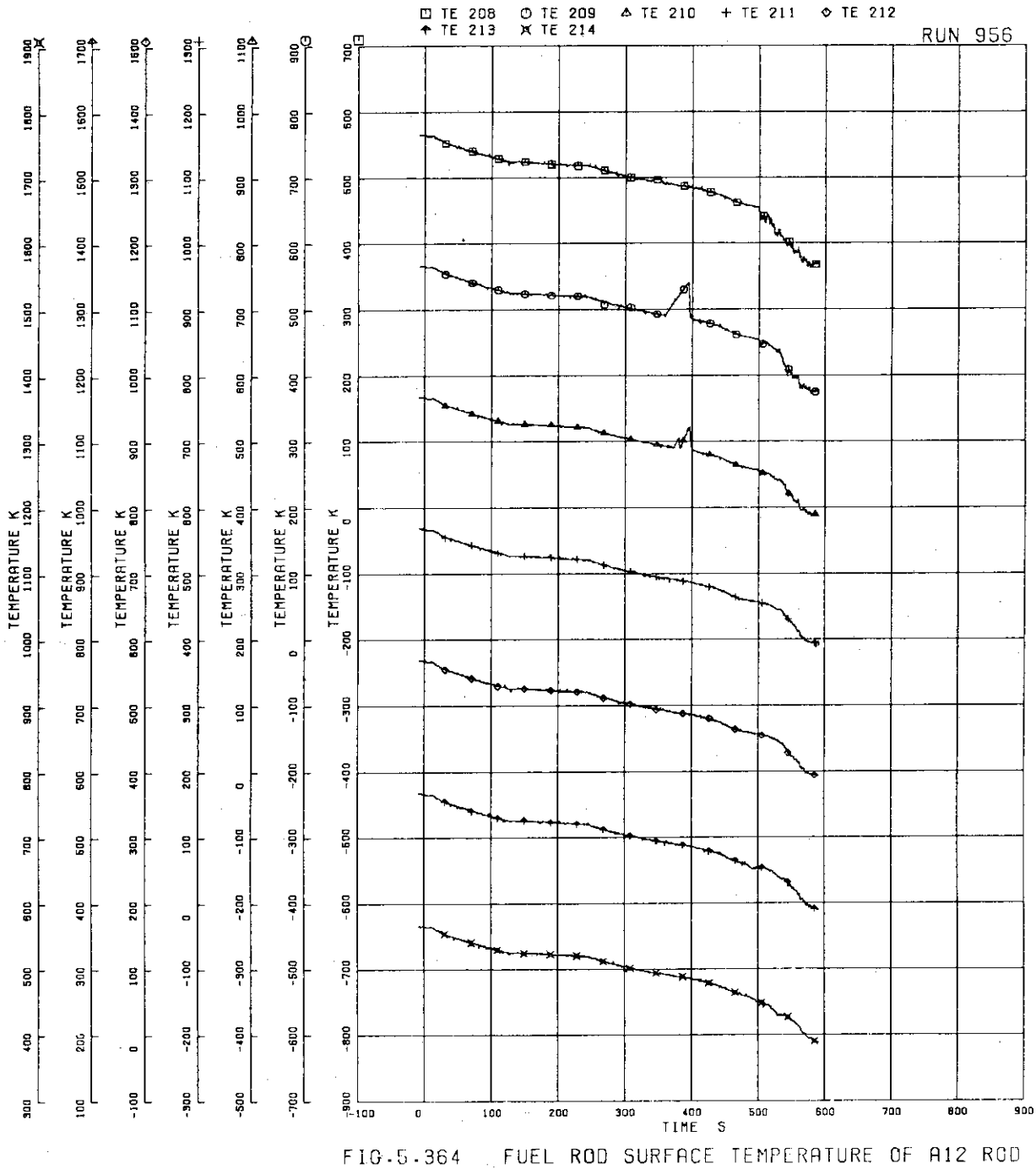

FIG.5.364 FUEL ROD SURFACE TEMPERATURE OF A12 ROD

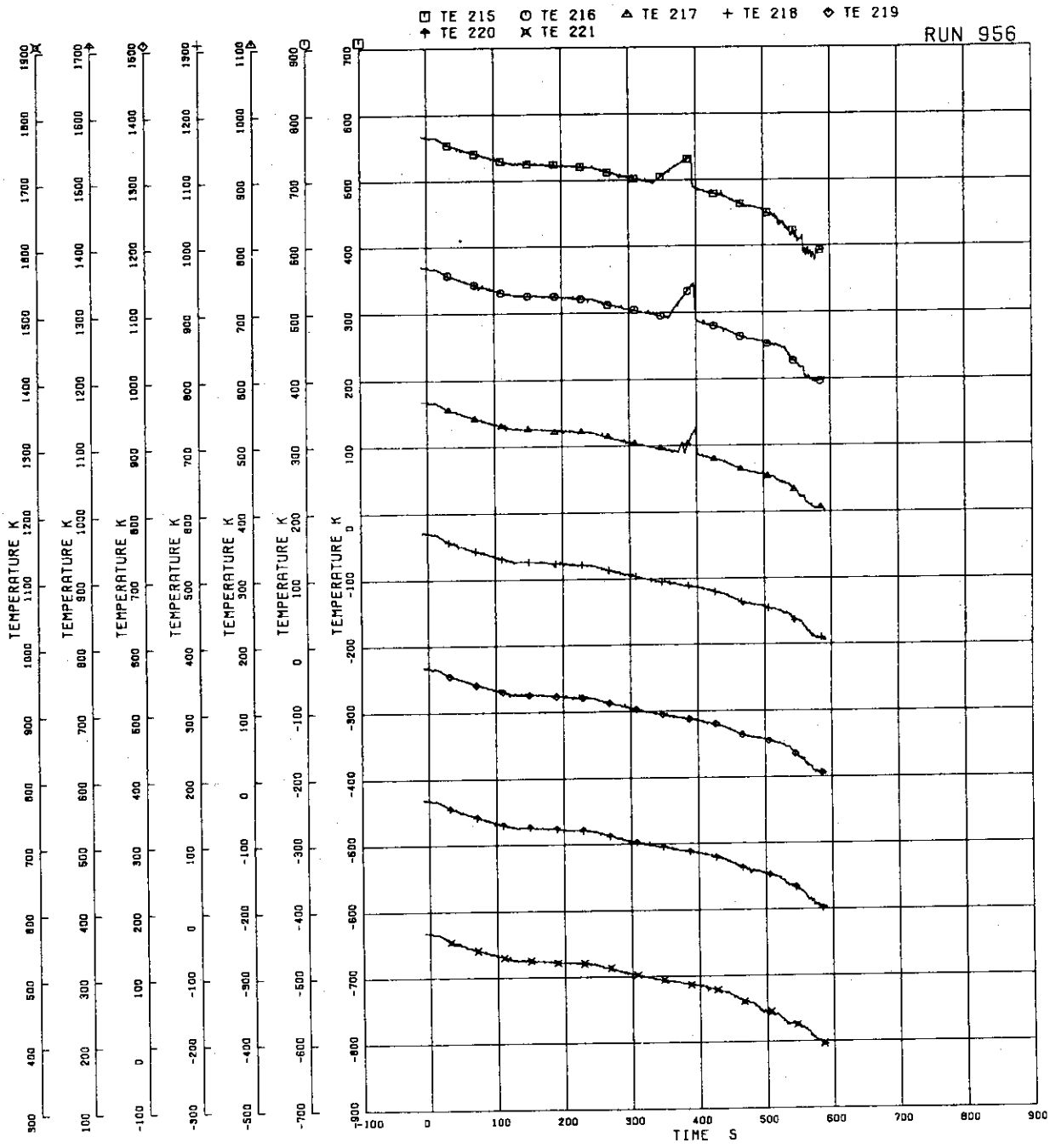

FIG.5.365 FUEL ROD SURFACE TEMPERATURE OF A13 ROD

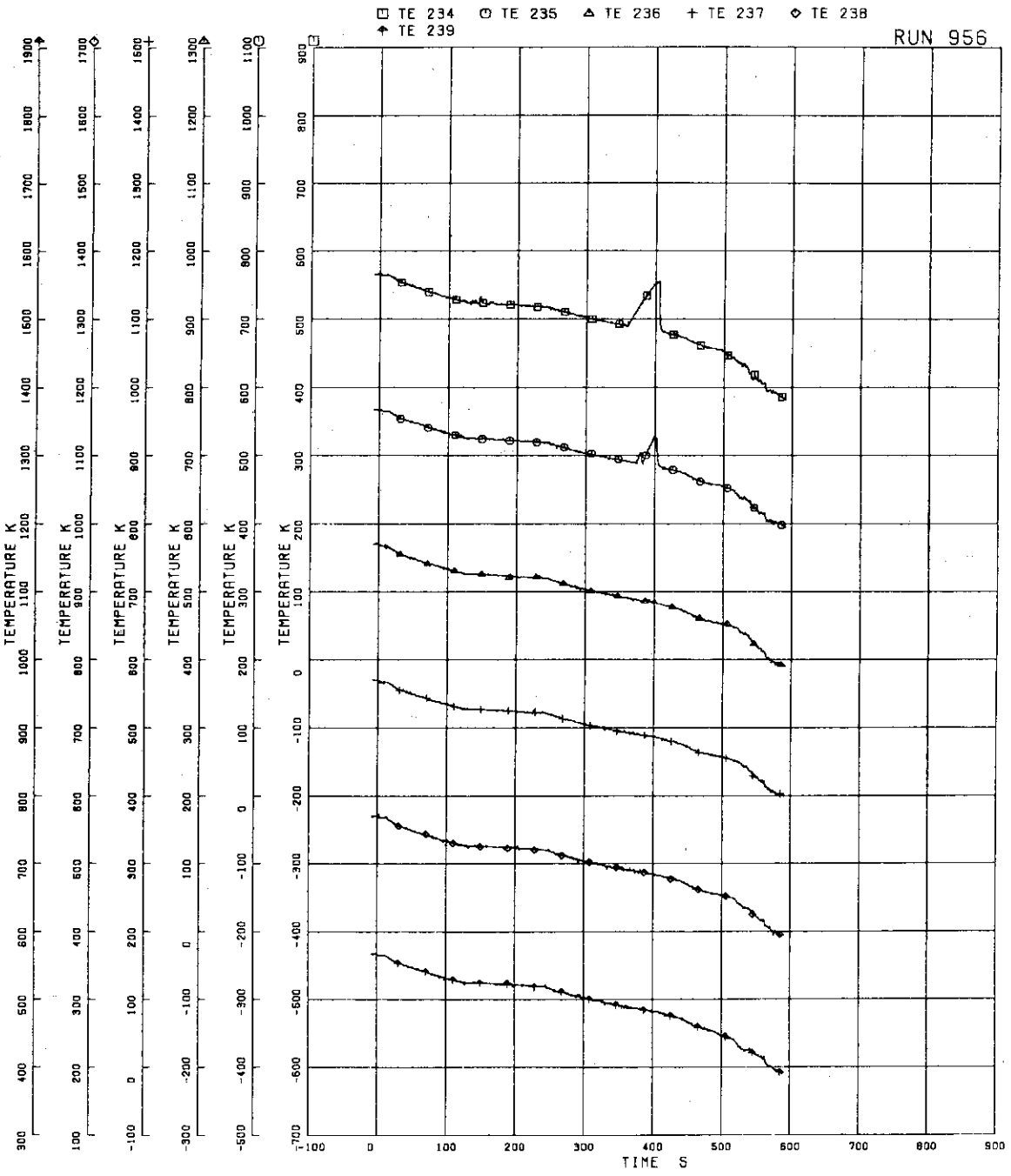

FIG.5.366 FUEL ROD SURFACE TEMPERATURE OF A22 ROD

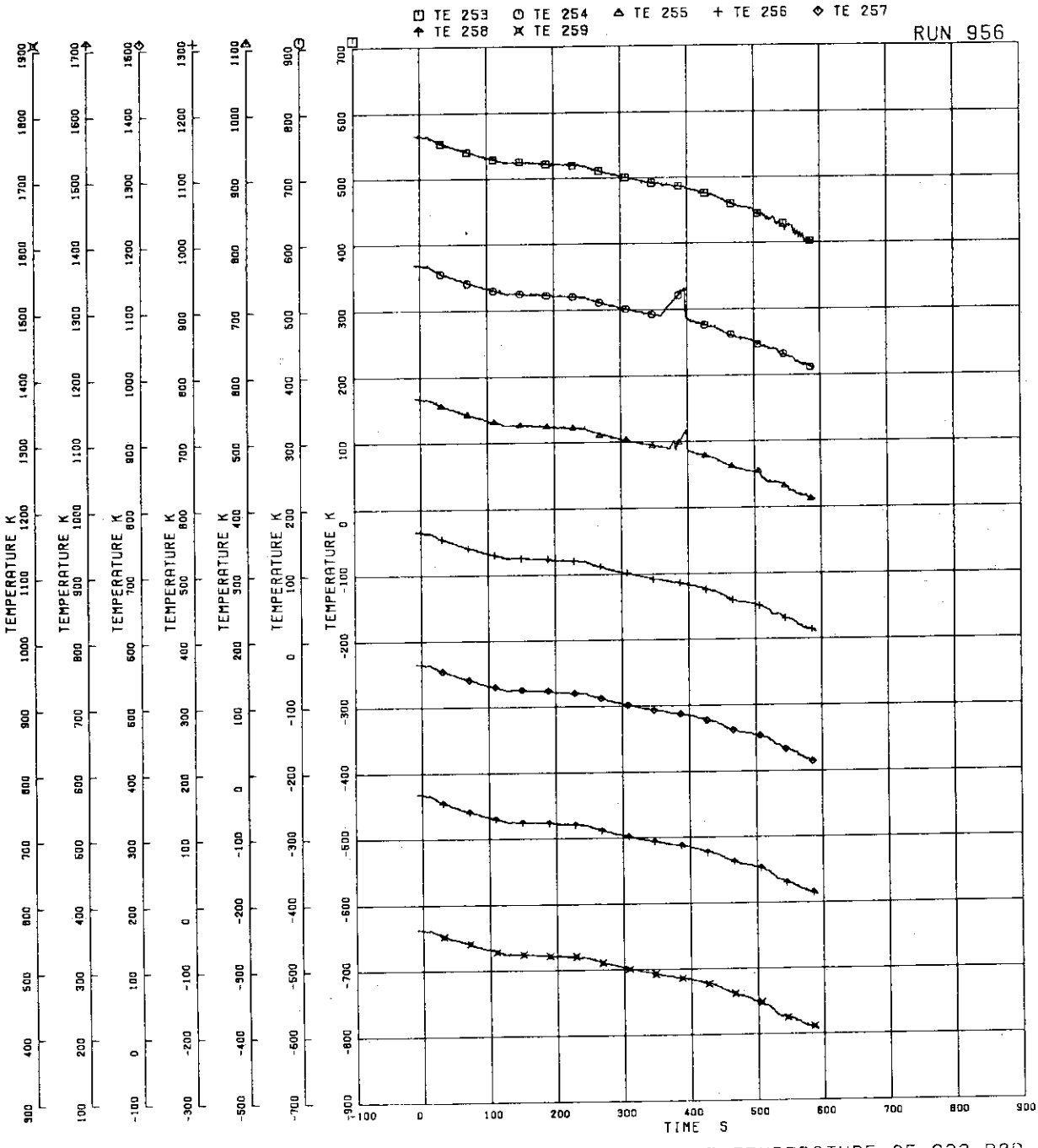

FIG.5.367 FUEL ROD SURFACE TEMPERATURE OF A33 ROD

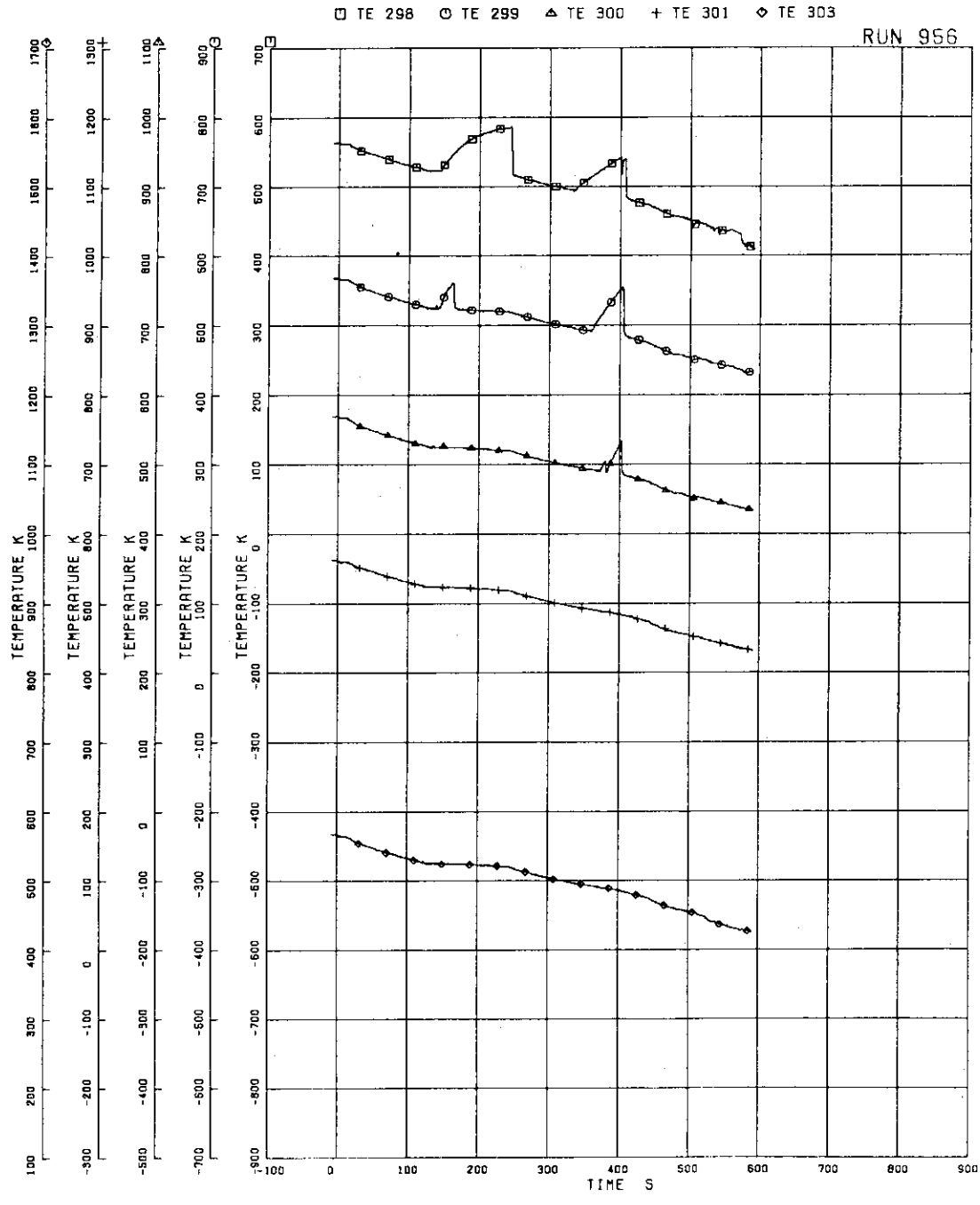

FIG.5.368 FUEL ROD SURFACE TEMPERATURE OF A77 ROD

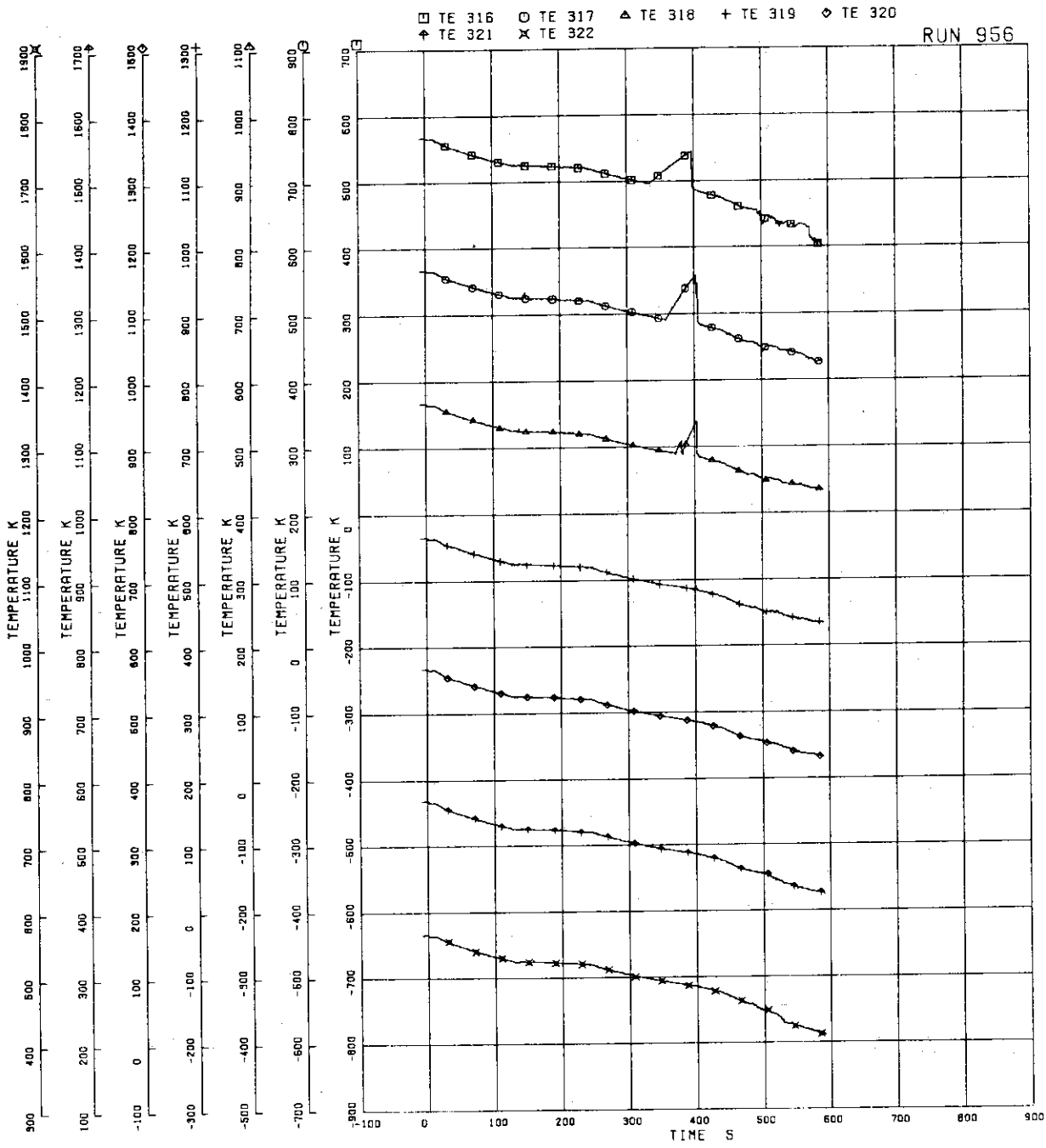

FIG.5.369 FUEL ROD SURFACE TEMPERATURE OF A87 ROD

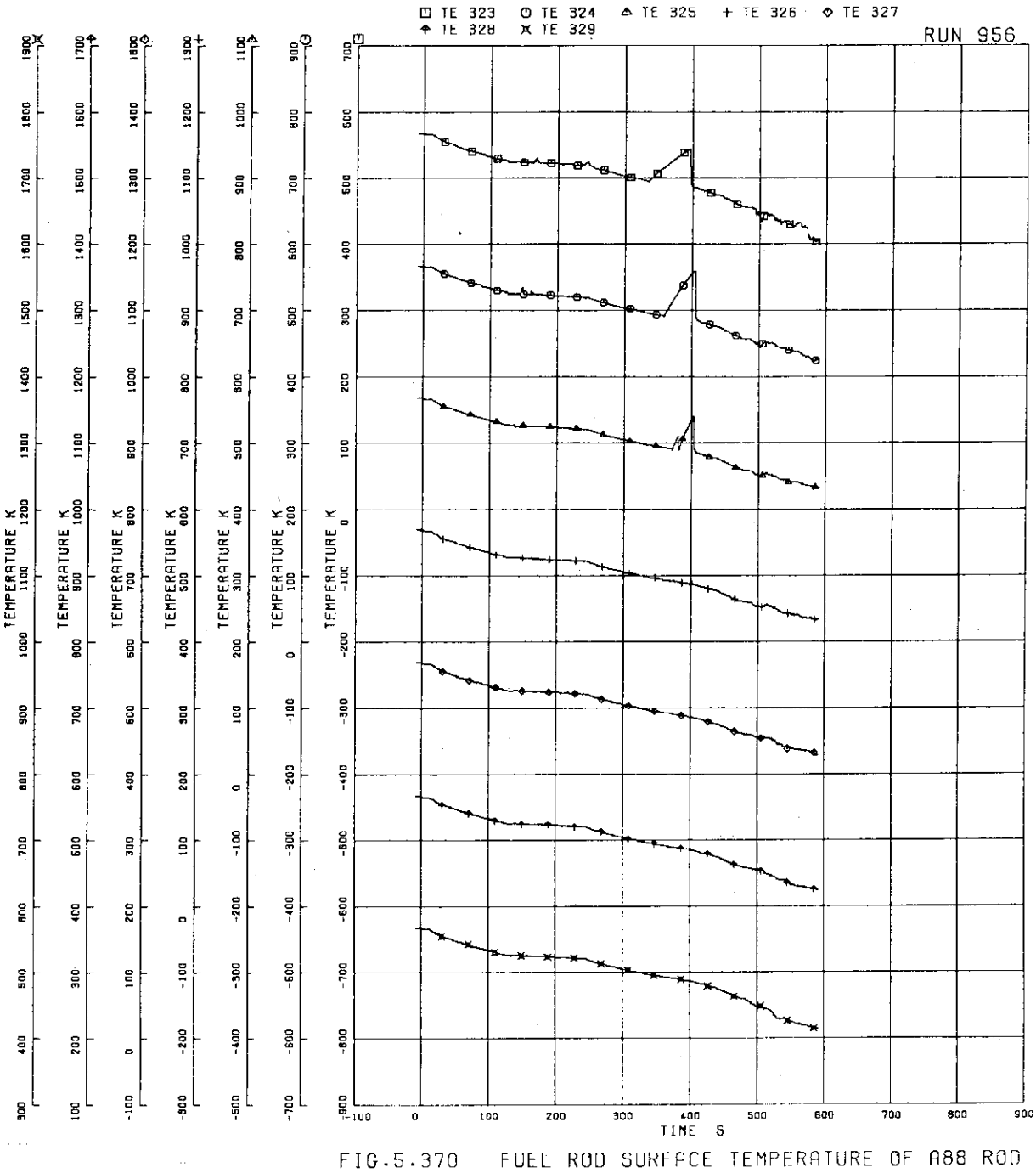

FIG.5.370 FUEL ROD SURFACE TEMPERATURE OF A88 ROD

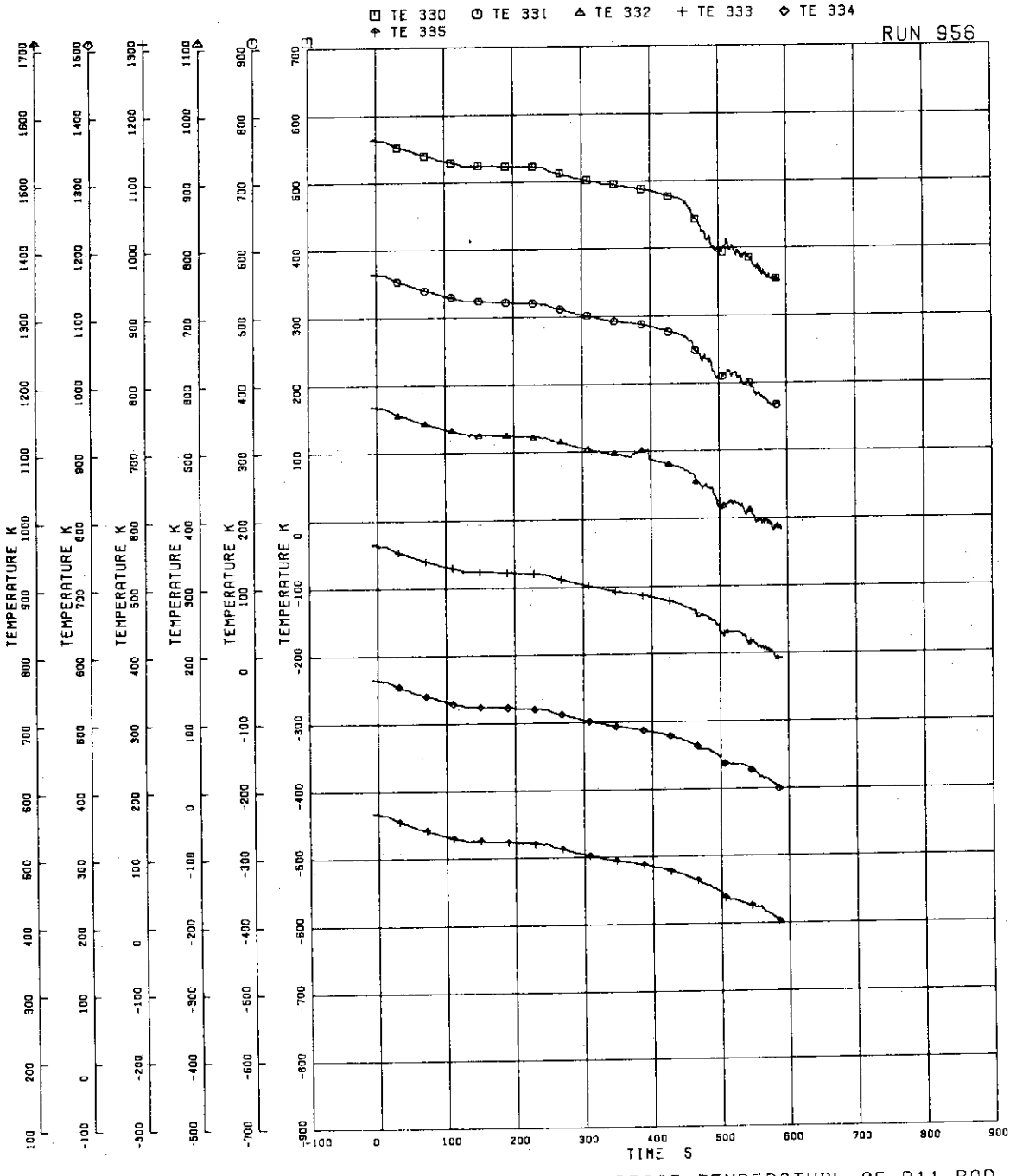

FIG.5.371 FUEL ROD SURFACE TEMPERATURE OF B11 ROD

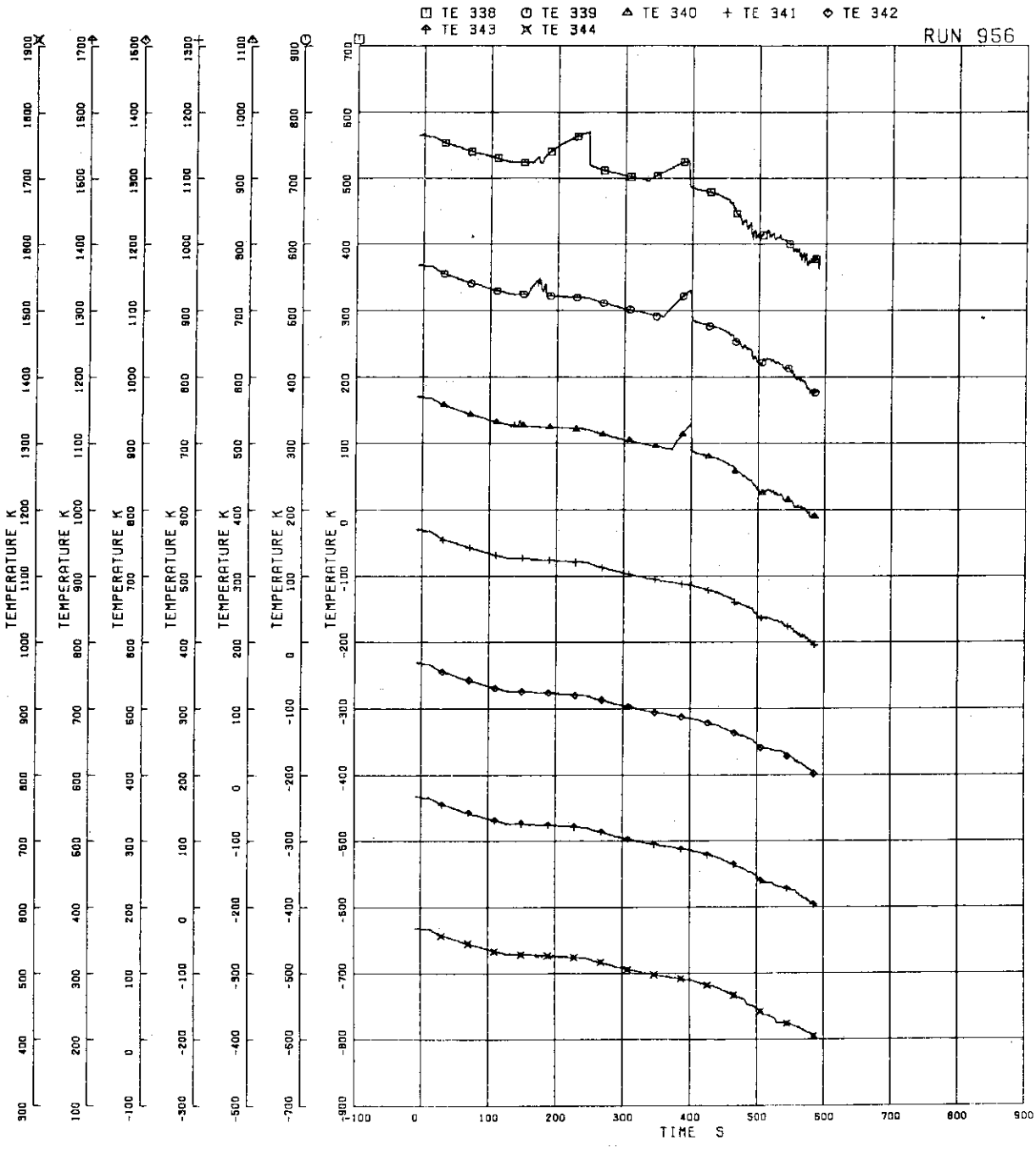

FIG.5.372 FUEL ROD SURFACE TEMPERATURE OF B22 ROD

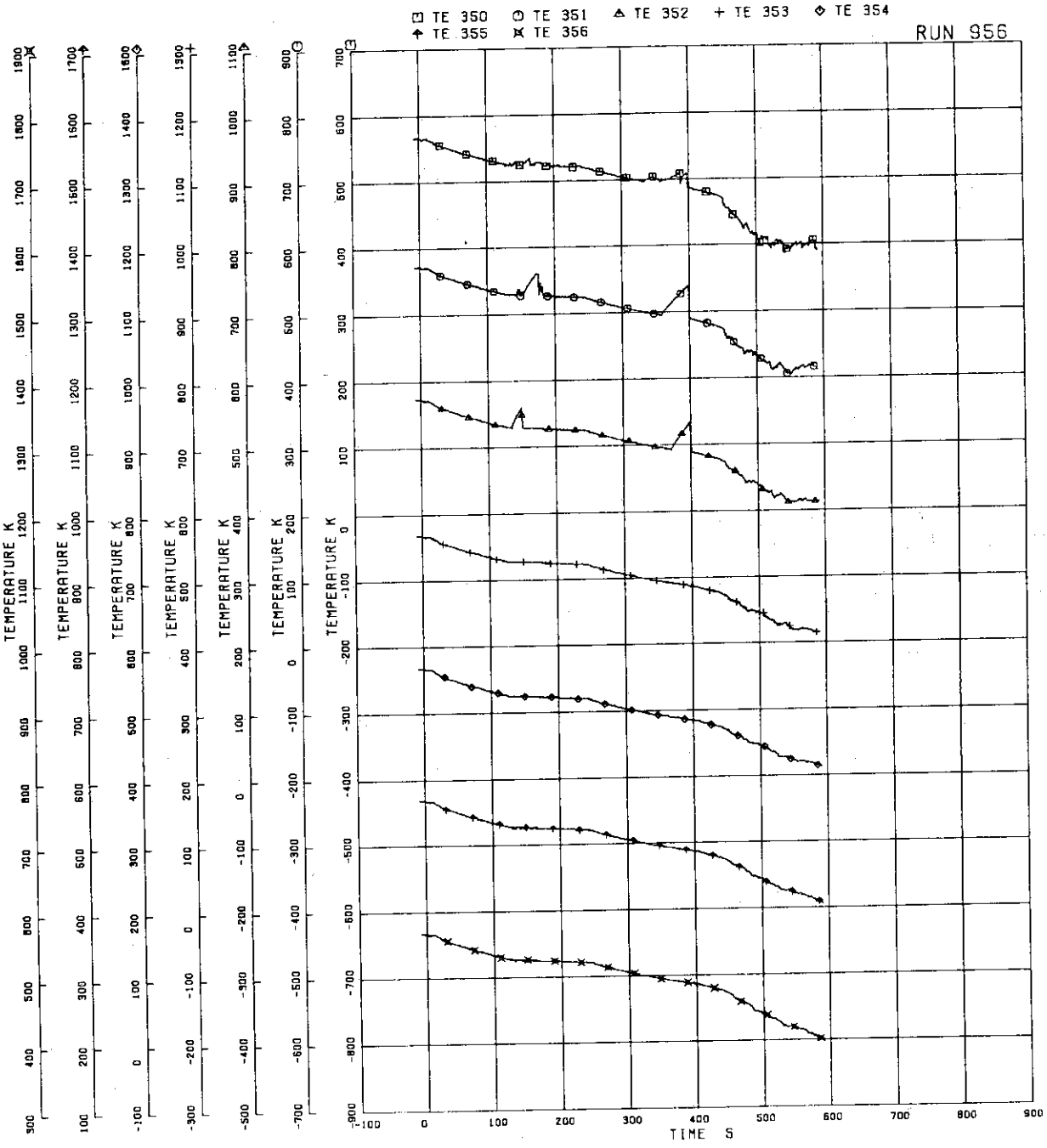

FIG.5.373 FUEL ROD SURFACE TEMPERATURE OF B77 ROD

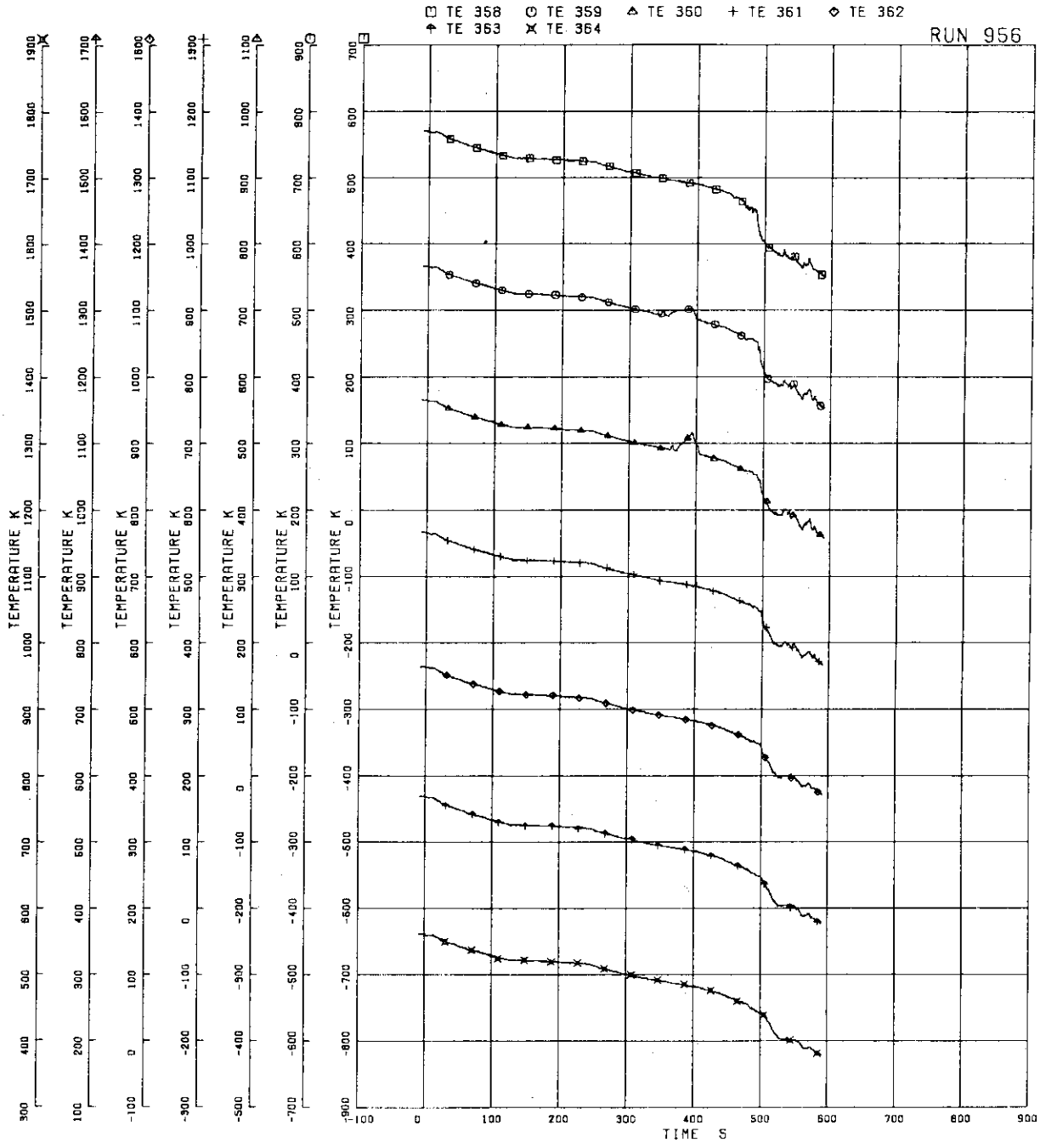

FIG.5.374 FUEL ROD SURFACE TEMPERATURE OF C11 ROD

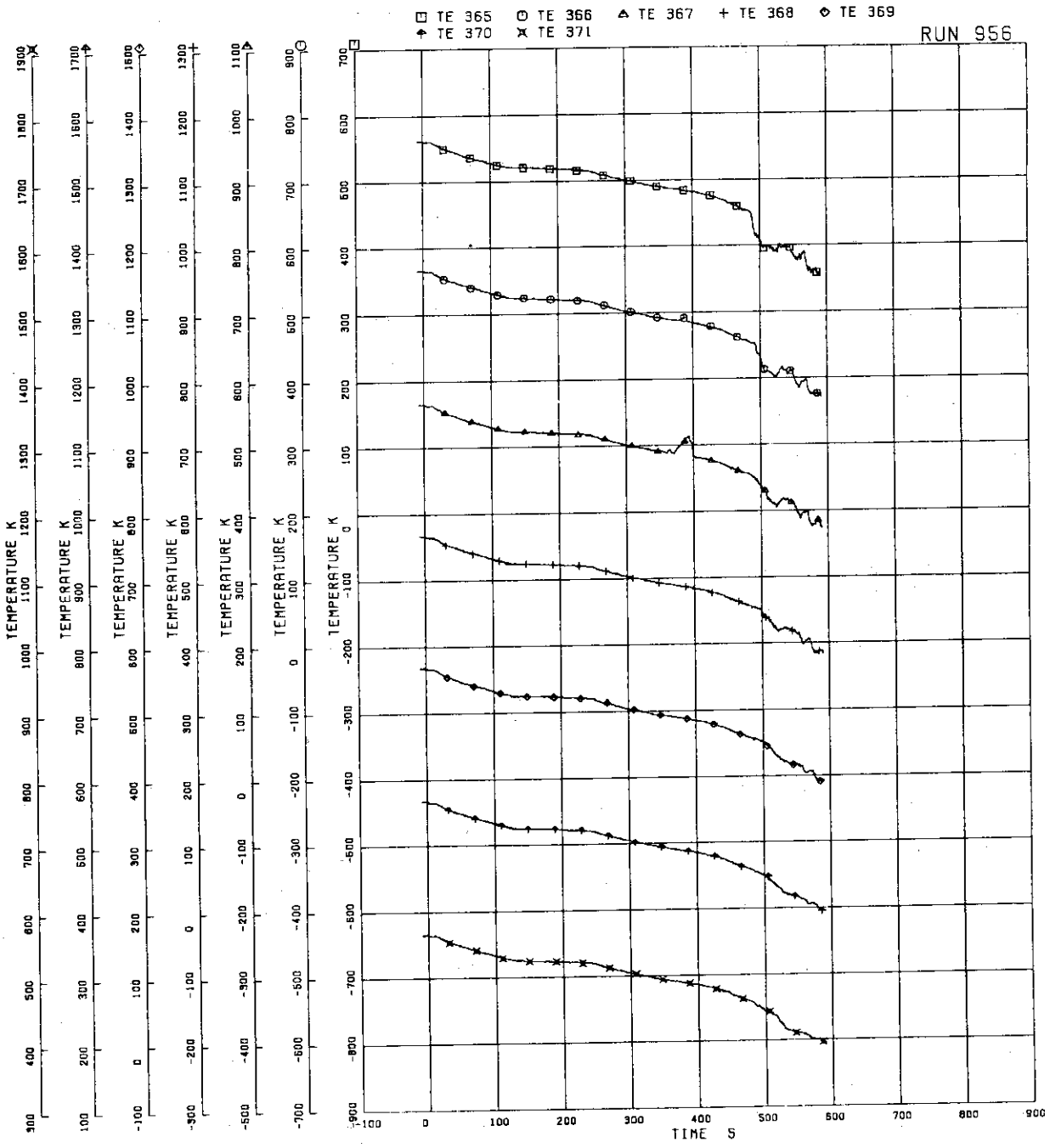

FIG.5.375 FUEL ROD SURFACE TEMPERATURE OF C13 ROD

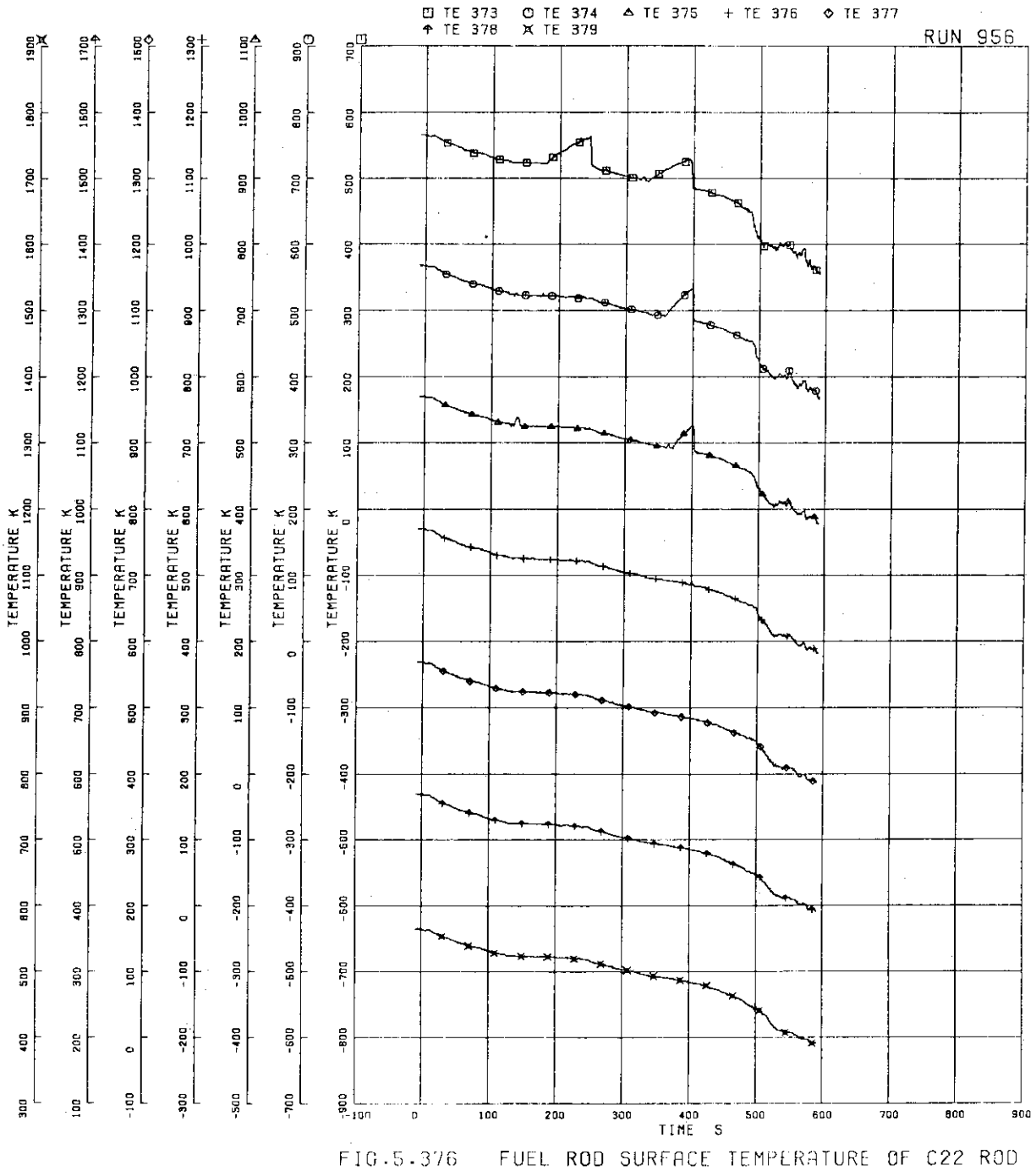

FIG.5.376 FUEL ROD SURFACE TEMPERATURE OF C22 ROD

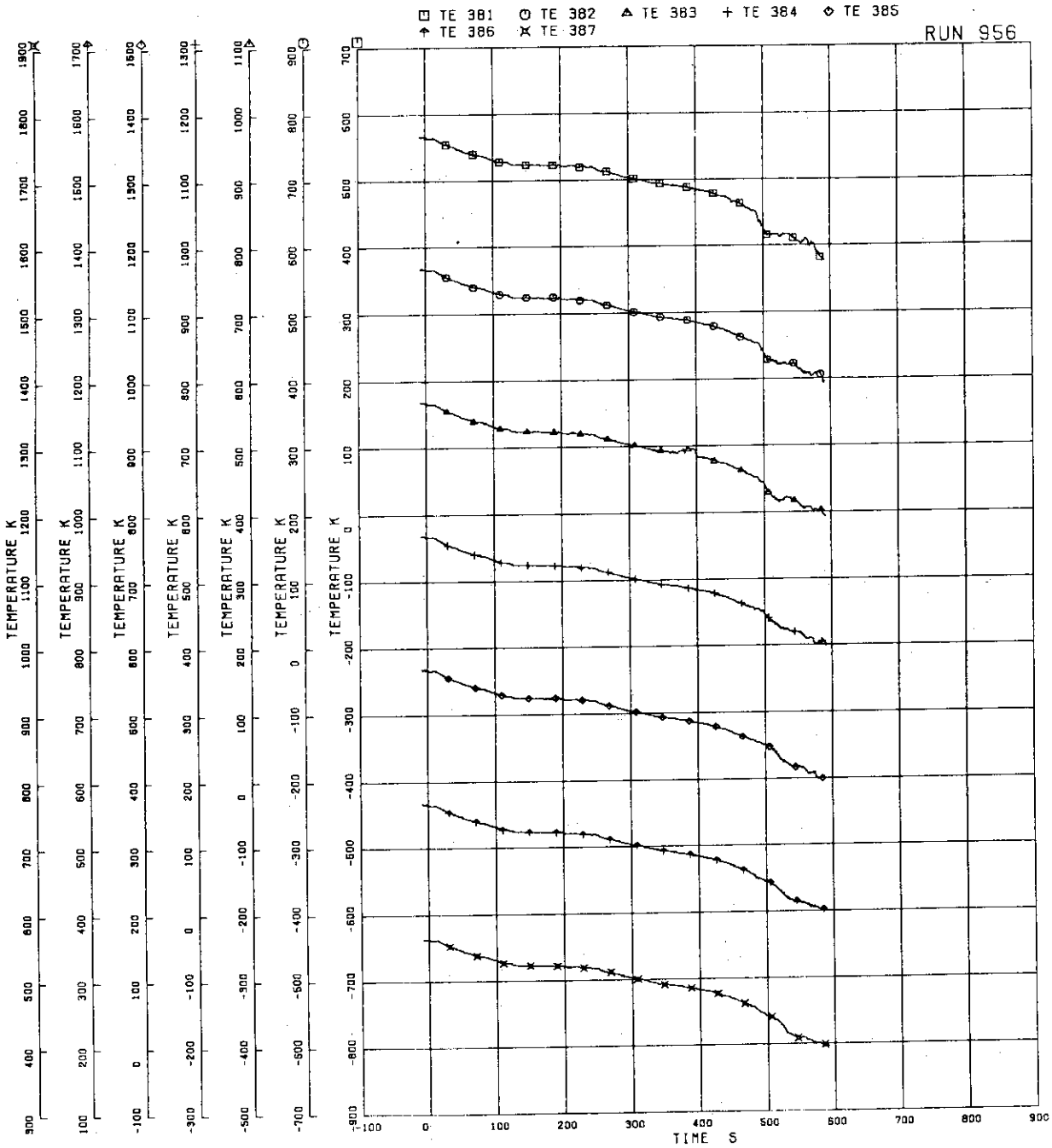

FIG.5.377 FUEL ROD SURFACE TEMPERATURE OF C33 ROD

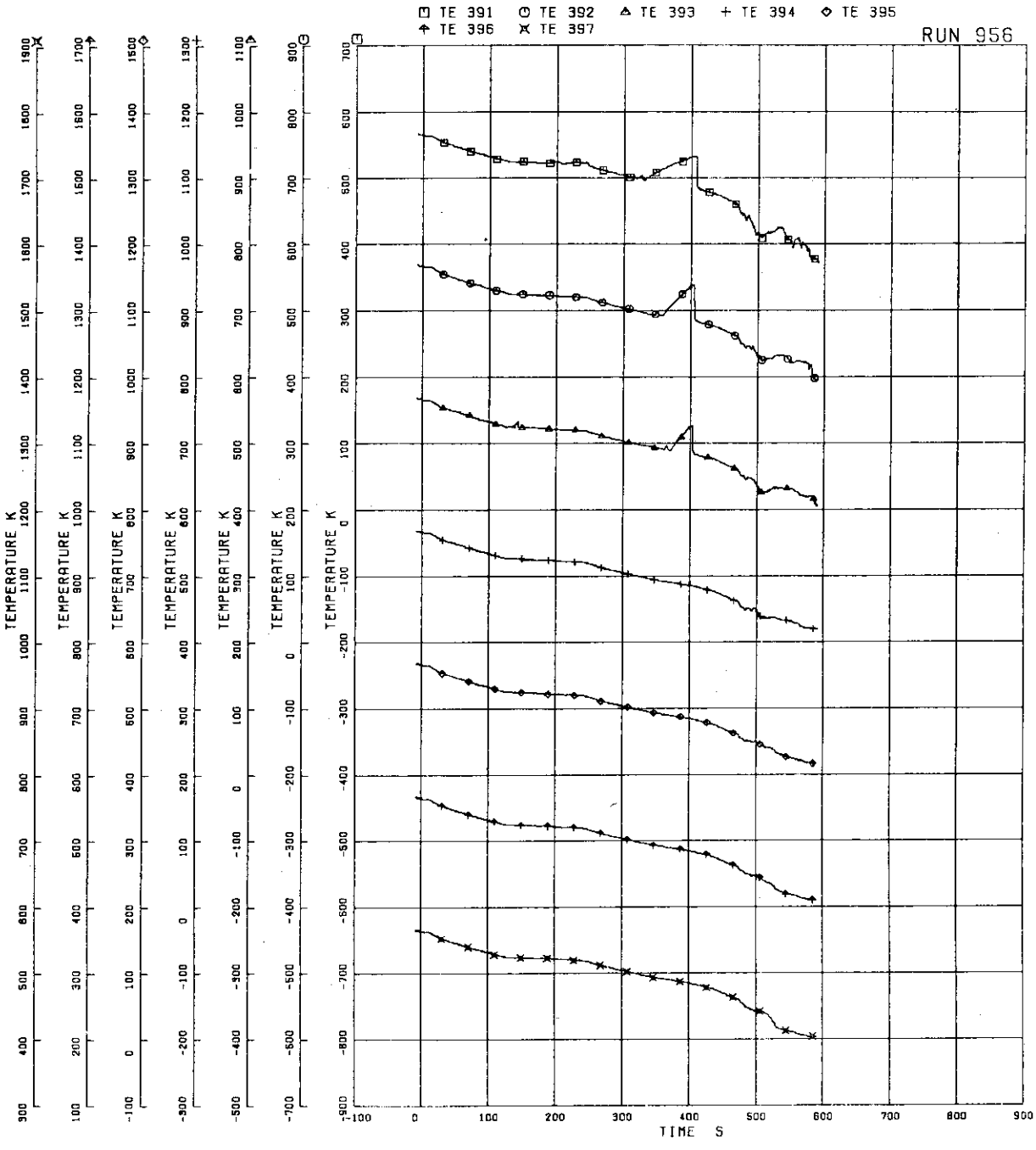

FIG.5.378 FUEL ROD SURFACE TEMPERATURE OF C77 ROD

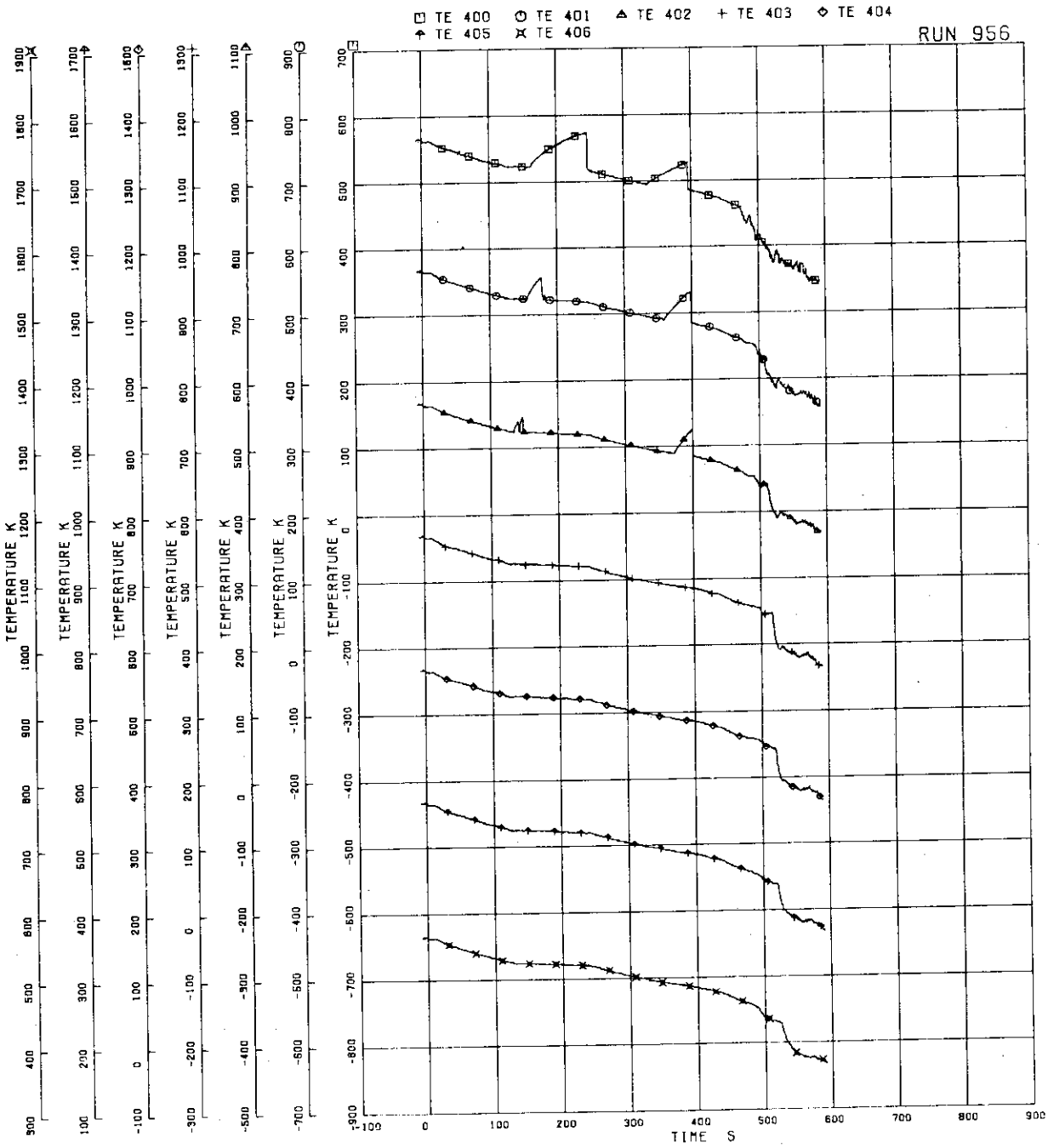

FIG.5.379 FUEL ROD SURFACE TEMPERATURE OF D22 ROD

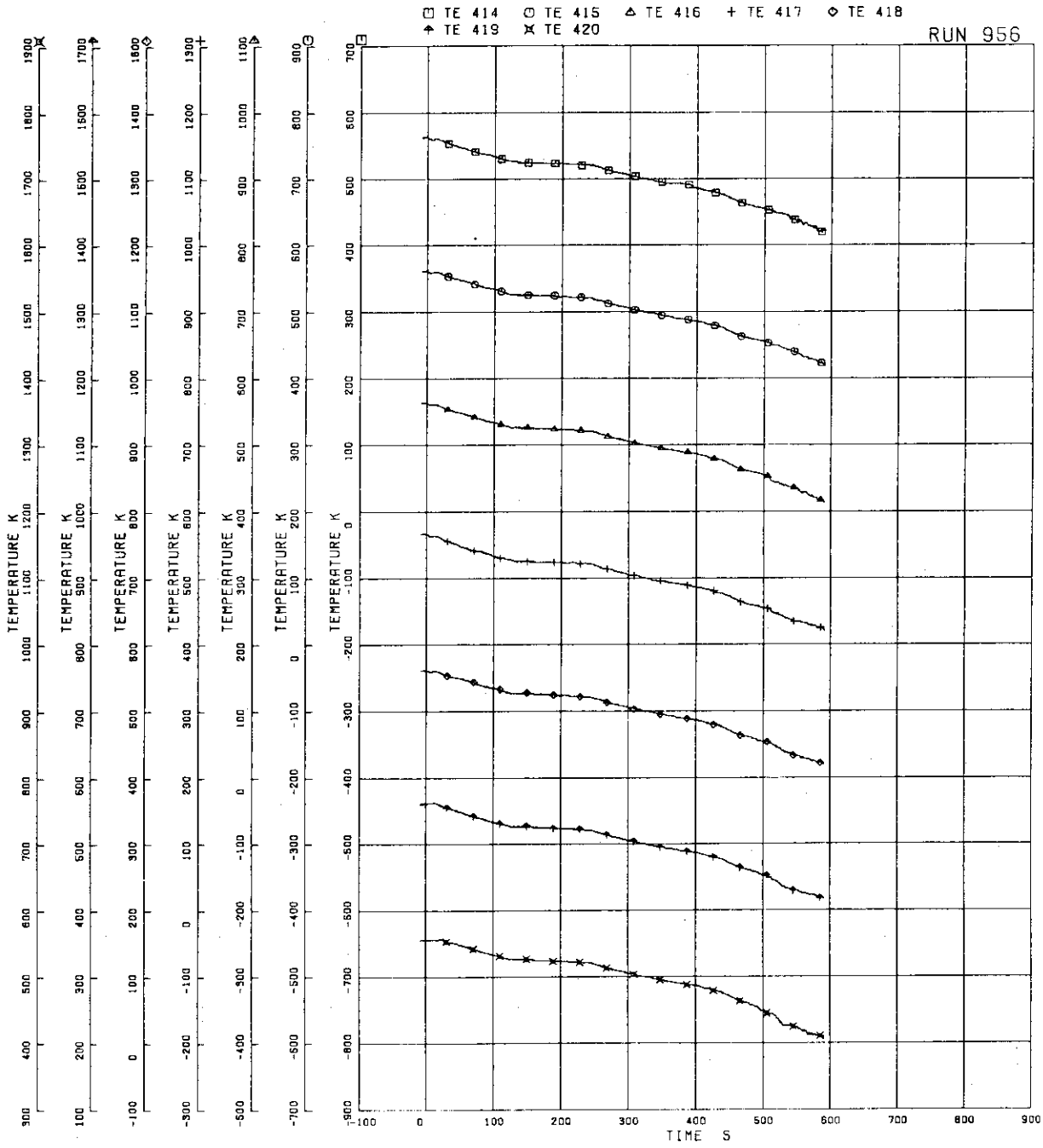

FIG.5.380 SURFACE TEMPERATURE OF WATER ROD SIMULATOR A45

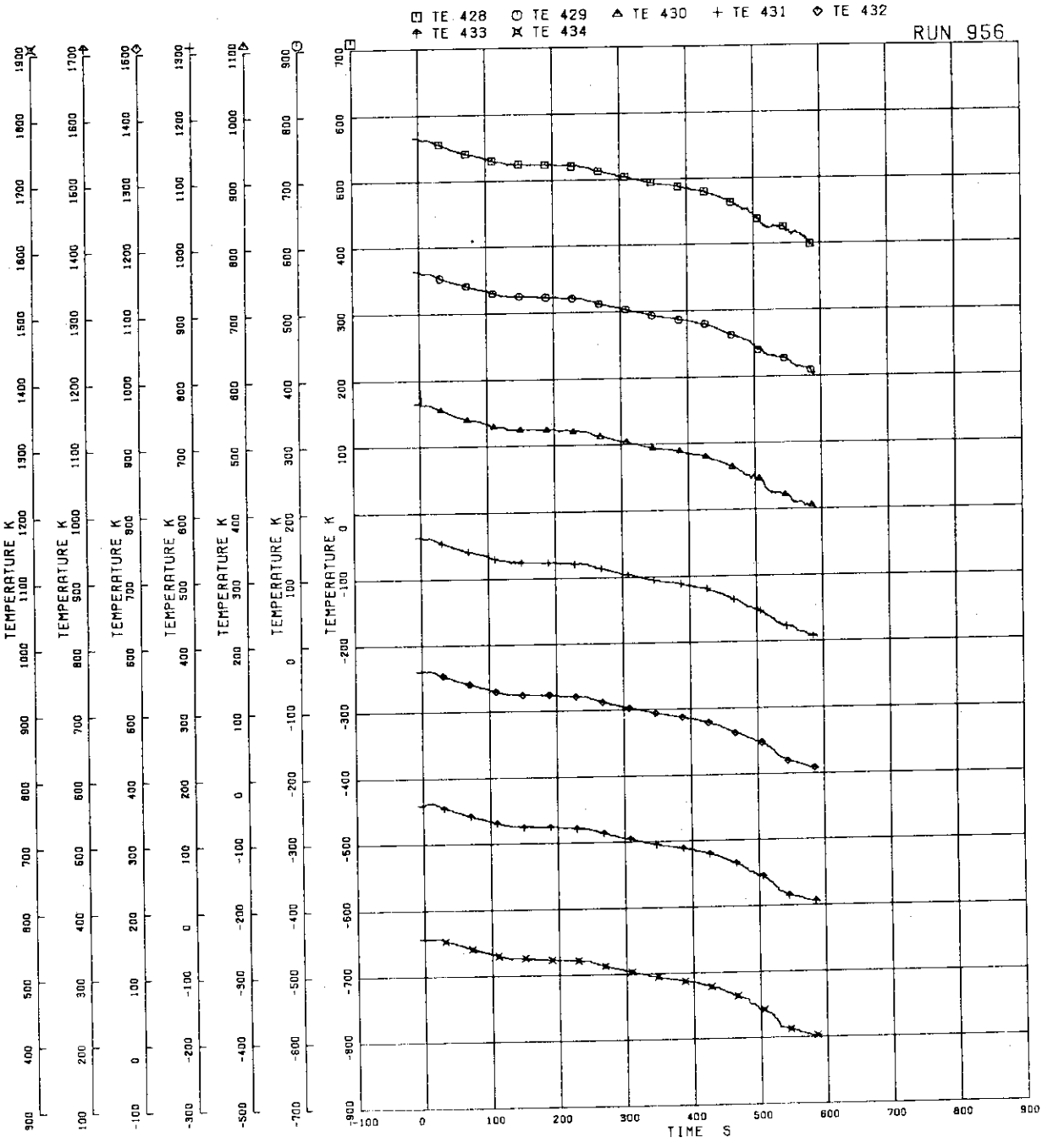

FIG.5.381 SURFACE TEMPERATURE OF WATER ROD SIMULATOR C45

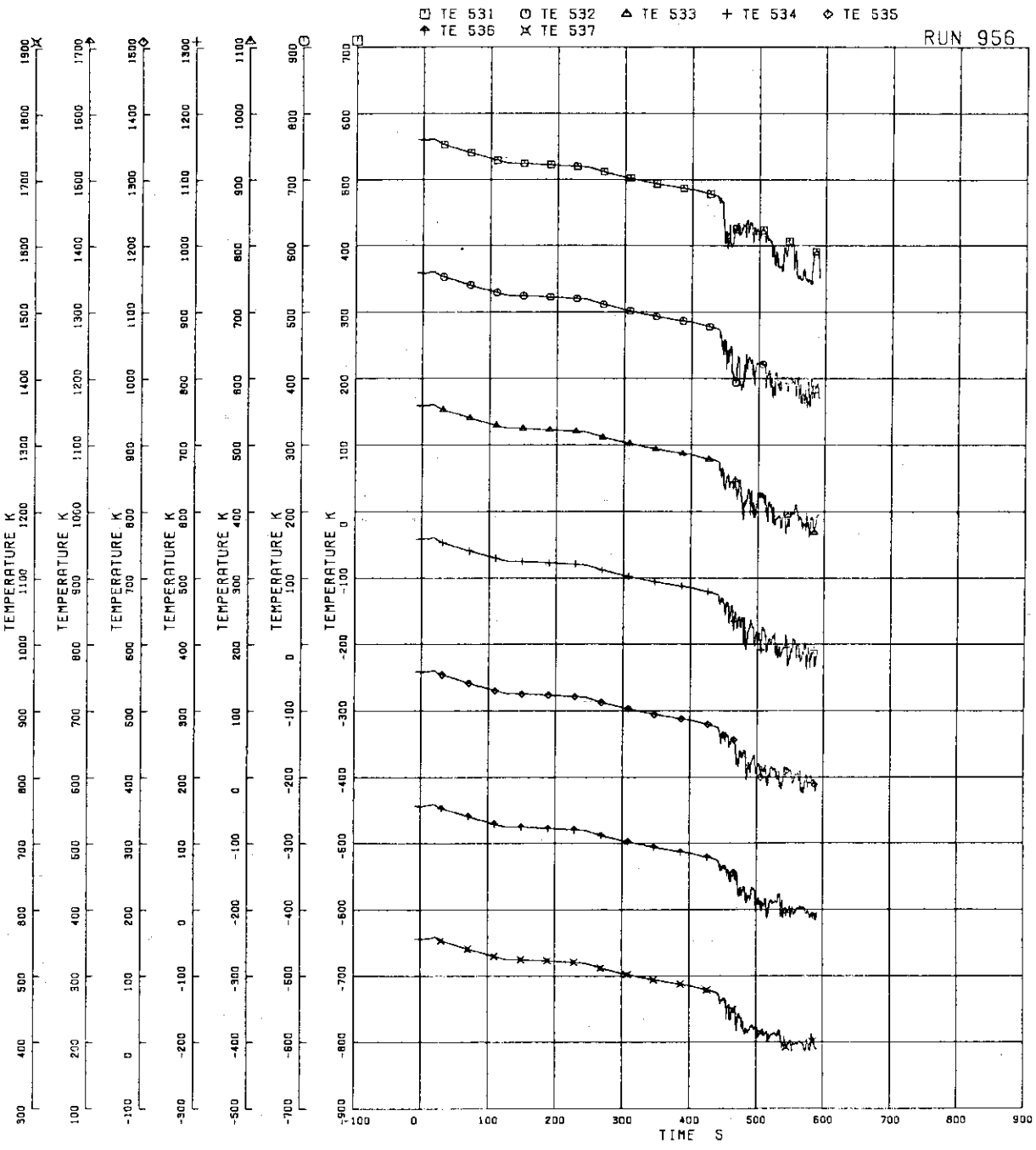

FIG.5.382 OUTER SURFACE TEMPERATURE OF CHANNEL BOX A

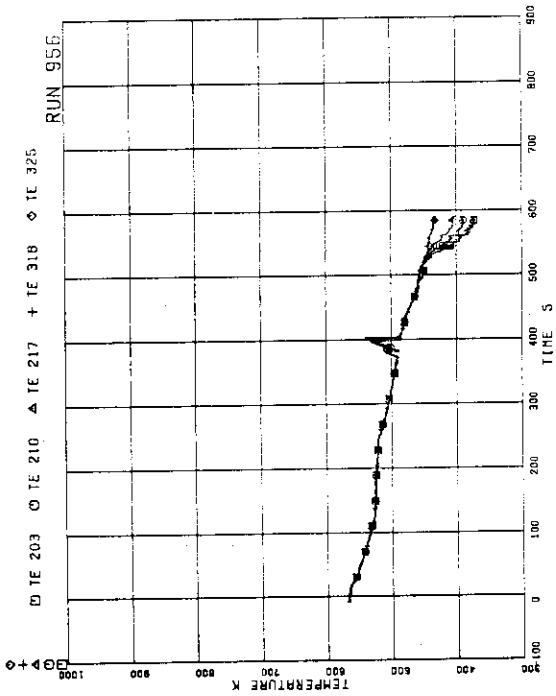

FIG.5.385 FUEL ROD SURFACE TEMPERATURE OF A11,A12,A13,A87,A88 RODS AT POSITION 3

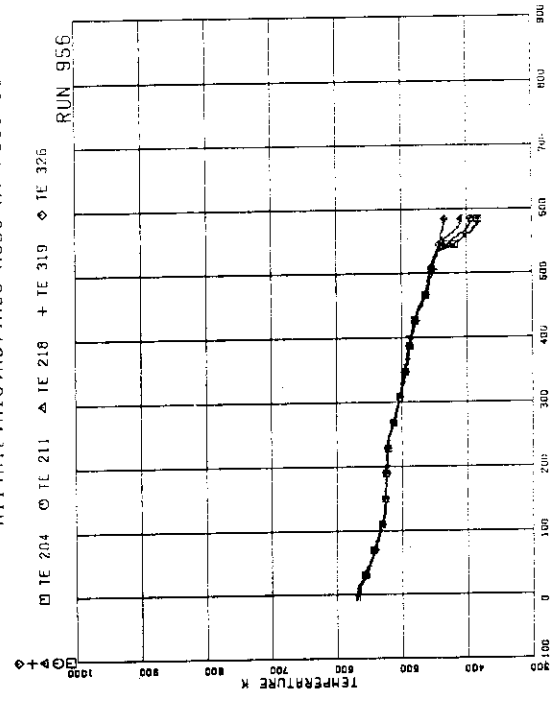

FIG.5.386 FUEL ROD SURFACE TEMPERATURE OF A11,A12,A13,A87,A88 RODS AT POSITION 4

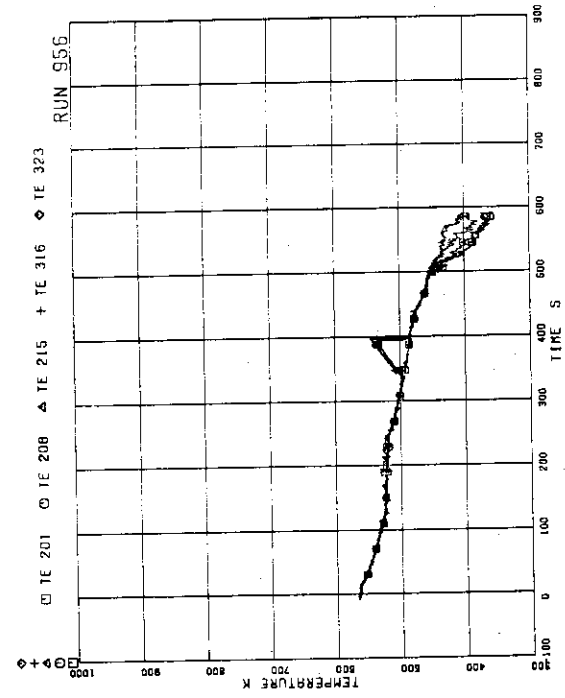

FIG.5.383 FUEL ROD SURFACE TEMPERATURE OF A11,A12,A13,A87,A88 RODS AT POSITION 1

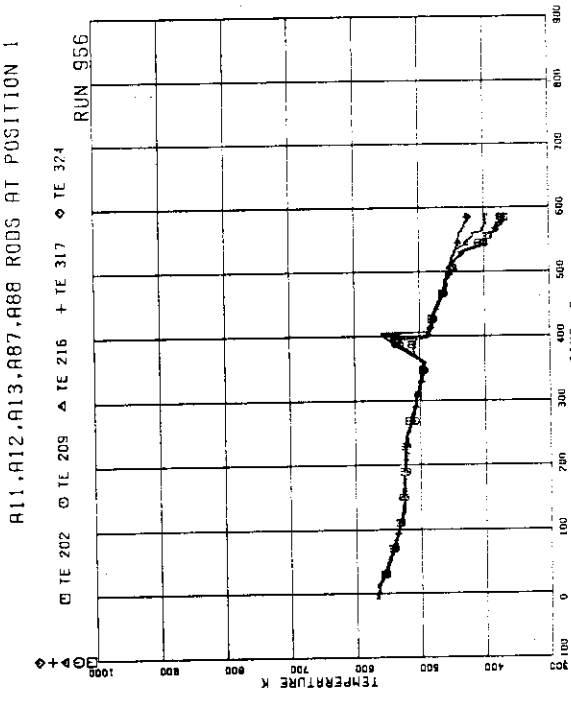

FIG.5.384 FUEL ROD SURFACE TEMPERATURE OF A11,A12,A13,A87,A88 RODS AT POSITION 2

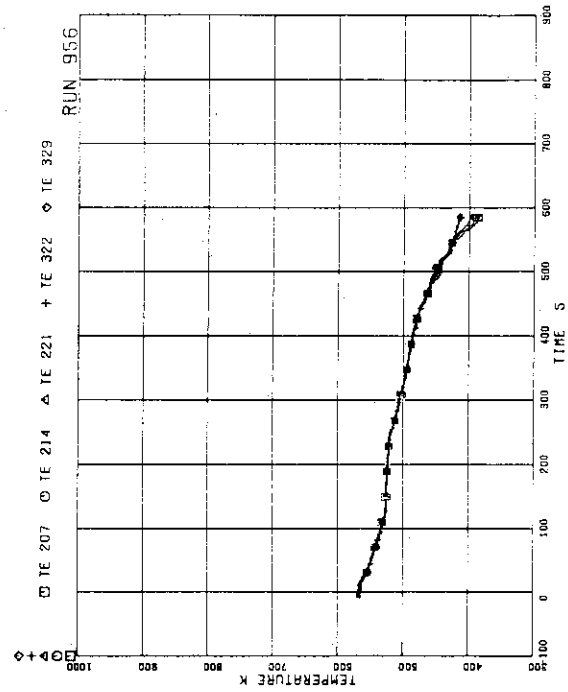

FIG.5.389 FUEL ROD SURFACE TEMPERATURE OF A11,A12,A13,A87,A88 RODS AT POSITION 7

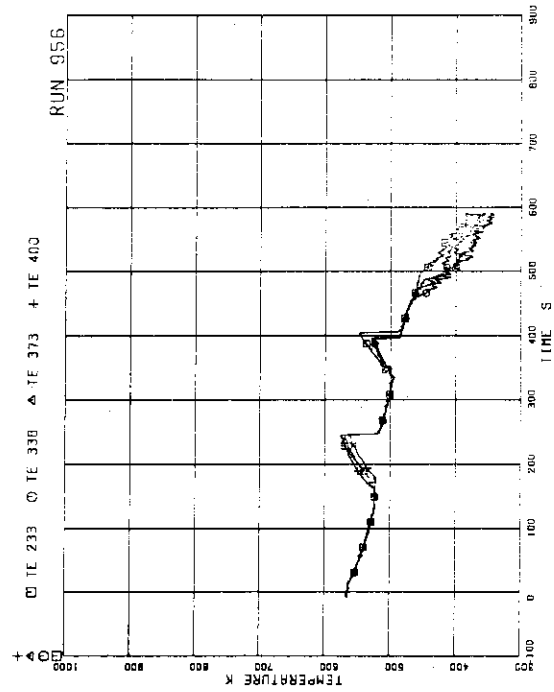

FIG.5.390 FUEL ROD SURFACE TEMPERATURE OF A22,B22,C22,D22 RODS AT POSITION 4

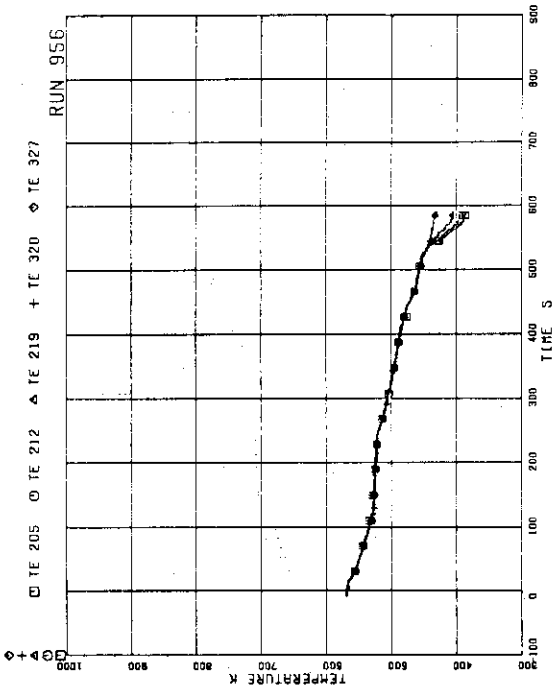

FIG.5.387 FUEL ROD SURFACE TEMPERATURE OF A11,A12,A13,A87,A88 RODS AT POSITION 5

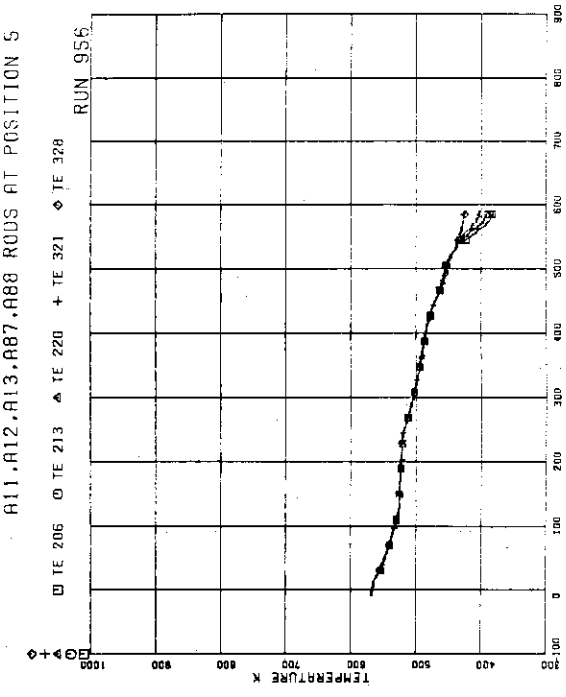

FIG.5.388 FUEL ROD SURFACE TEMPERATURE OF A11,A12,A13,A87,A88 RODS AT POSITION 6

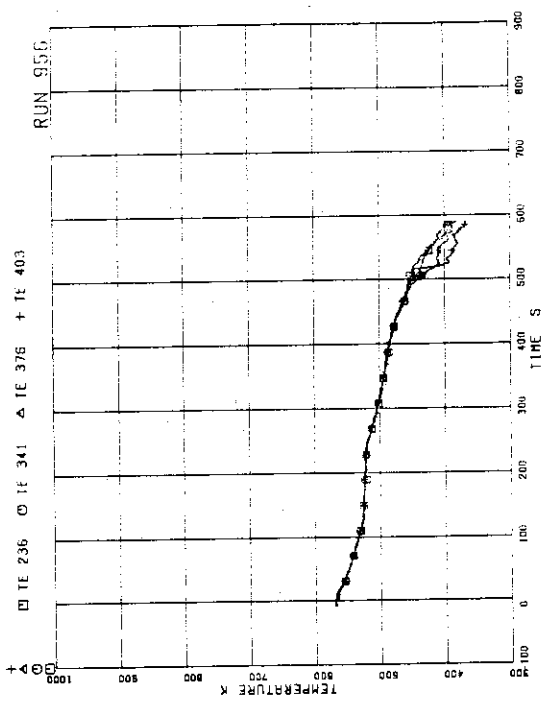

FIG.5.393 FUEL ROD SURFACE TEMPERATURE OF A22,B22,C22,D22 RODS AT POSITION 4

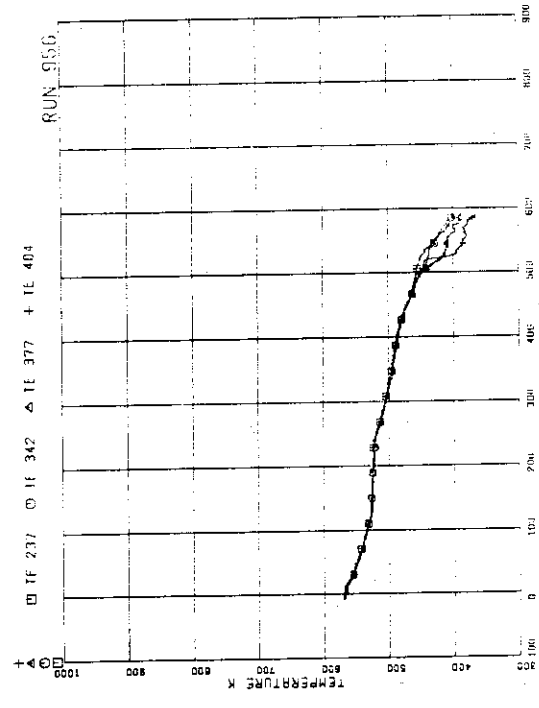

FIG.5.394 FUEL ROD SURFACE TEMPERATURE OF A22,B22,C22,D22 RODS AT POSITION 1

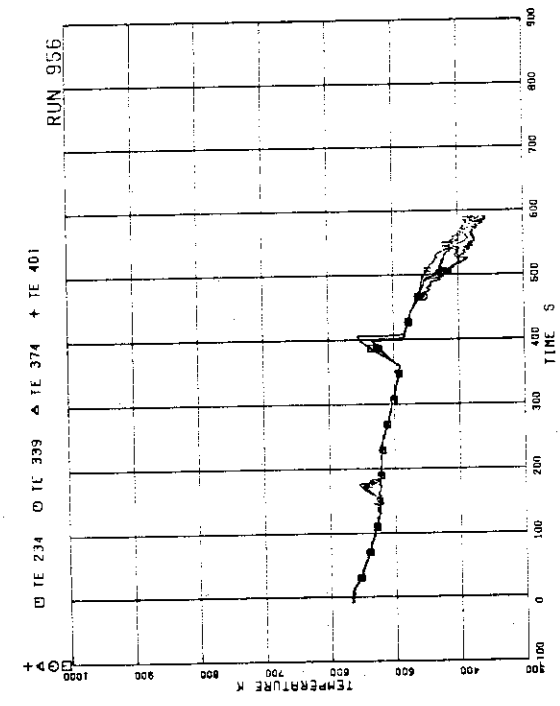

FIG.5.391 FUEL ROD SURFACE TEMPERATURE OF A22,B22,C22,D22 RODS AT POSITION 2

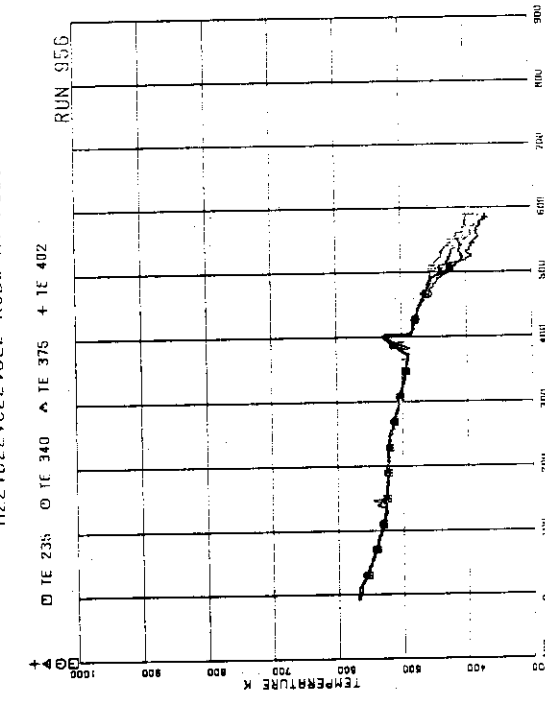

FIG.5.392 FUEL ROD SURFACE TEMPERATURE OF A22,B22,C22,D22 RODS AT POSITION 3

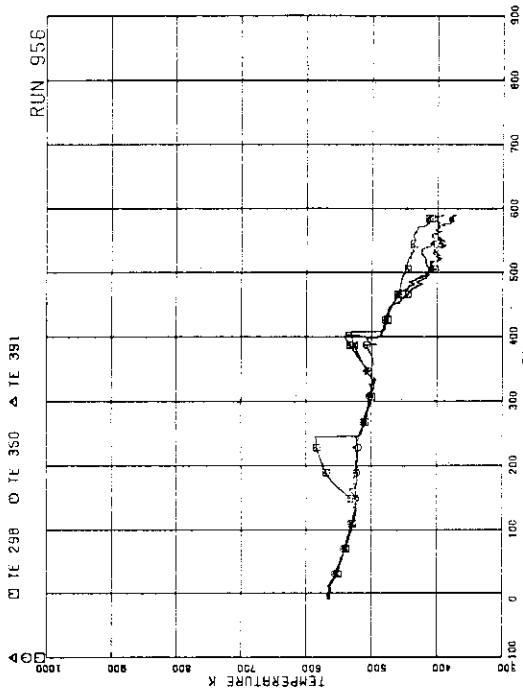

FIG.5.397 FUEL ROD SURFACE TEMPERATURE OF A77,B77,C77 RODS AT POSITION 1

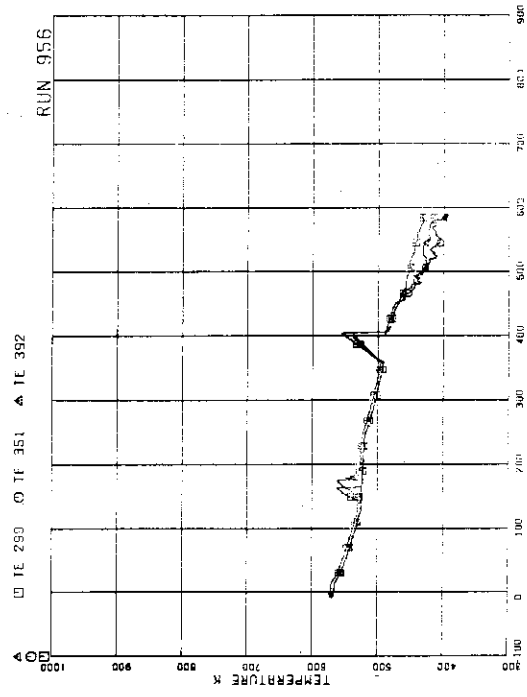

FIG.5.398 FUEL ROD SURFACE TEMPERATURE OF A77,B77,C77 RODS AT POSITION 2

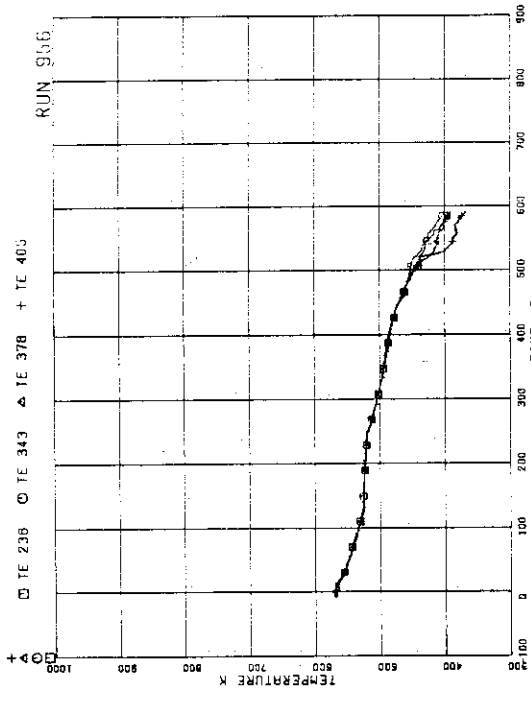

FIG.5.395 FUEL ROD SURFACE TEMPERATURE OF A22,B22,C22,D22 RODS AT POSITION 6

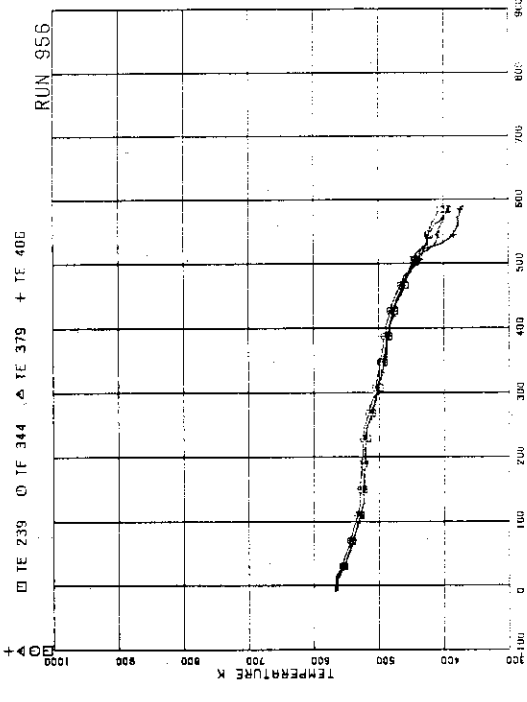

FIG.5.396 FUEL ROD SURFACE TEMPERATURE OF A22,B22,C22,D22 RODS AT POSITION 7

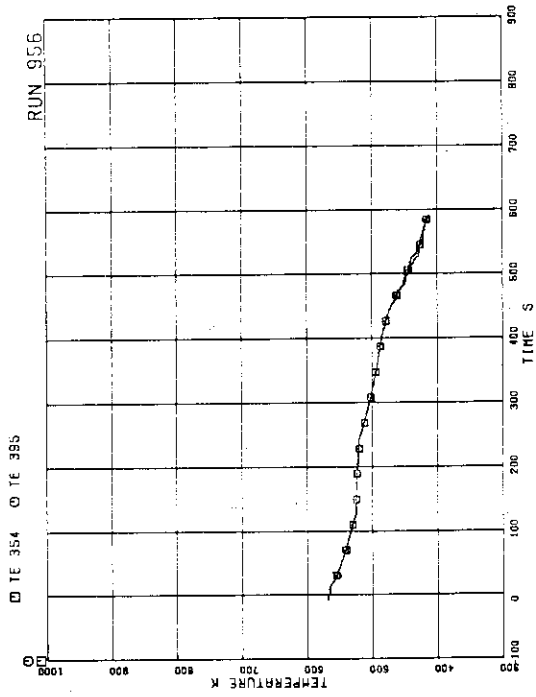

FIG.5.401 FUEL ROD SURFACE TEMPERATURE OF B77,C77 ROD AT POSITION 5

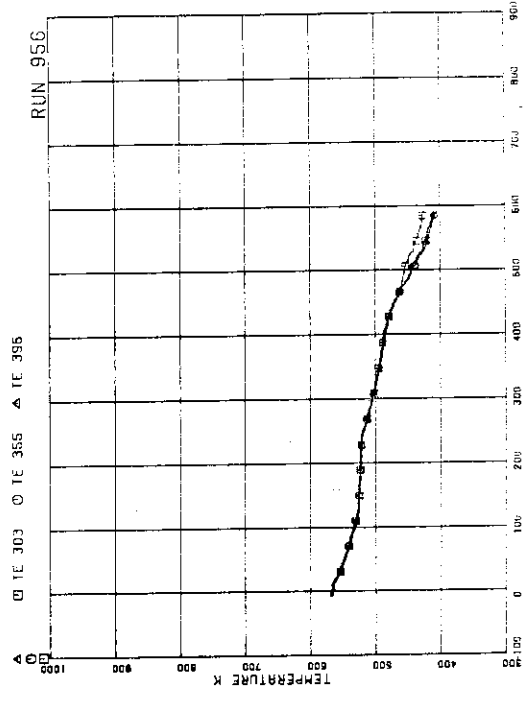

FIG.5.402 FUEL ROD SURFACE TEMPERATURE OF A77,B77,C77 RODS AT POSITION 4

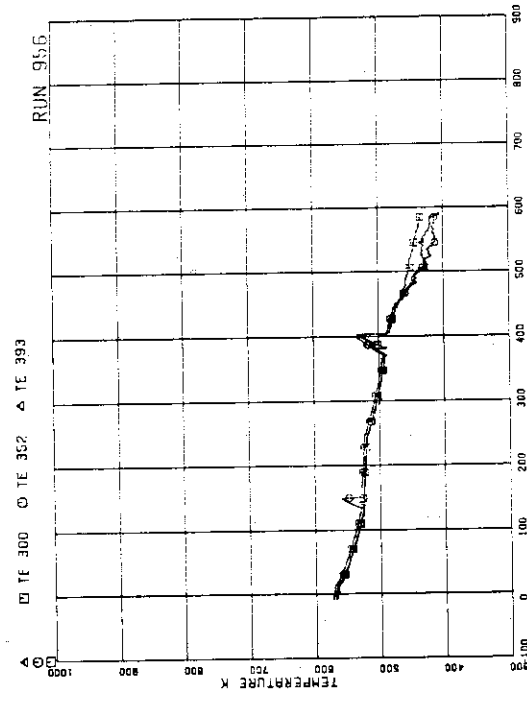

FIG.5.399 FUEL ROD SURFACE TEMPERATURE OF A77,B77,C77 RODS AT POSITION 3

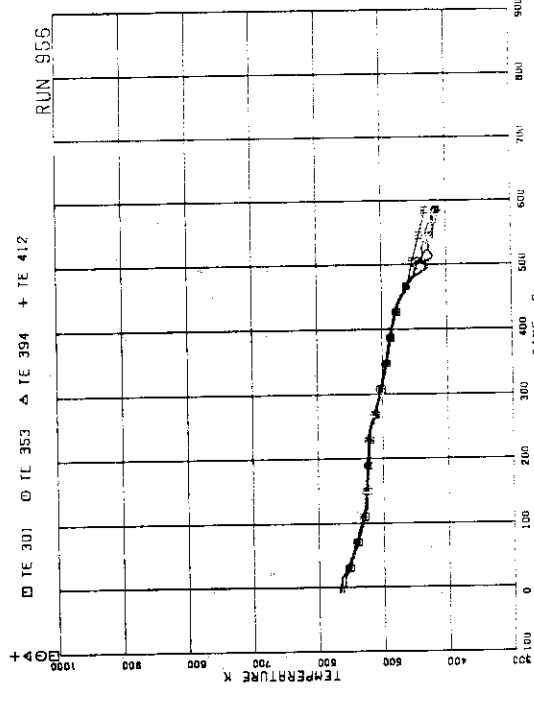

FIG.5.400 FUEL ROD SURFACE TEMPERATURE OF A77,B77,C77,D77 RODS AT POSITION 4

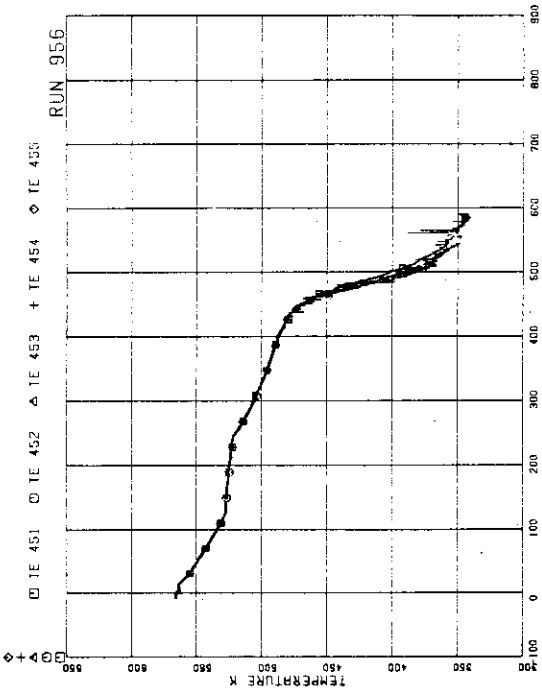

FIG.5.405 FLUID TEMPERATURE AT CHANNEL C OUTLET

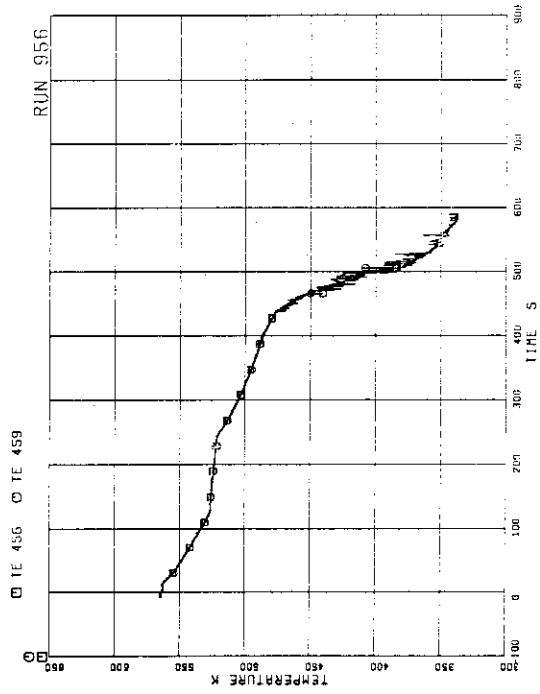

FIG.5.406 FLUID TEMPERATURE ABOVE UPP
CHANNEL A, OPENINGS 1 AND 4

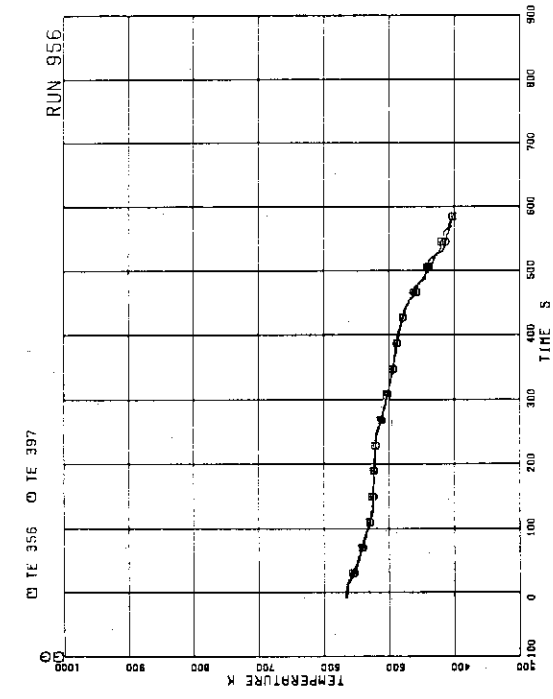

FIG.5.403 FUEL ROD SURFACE TEMPERATURE OF
B77.C77 RODS AT POSITION 7

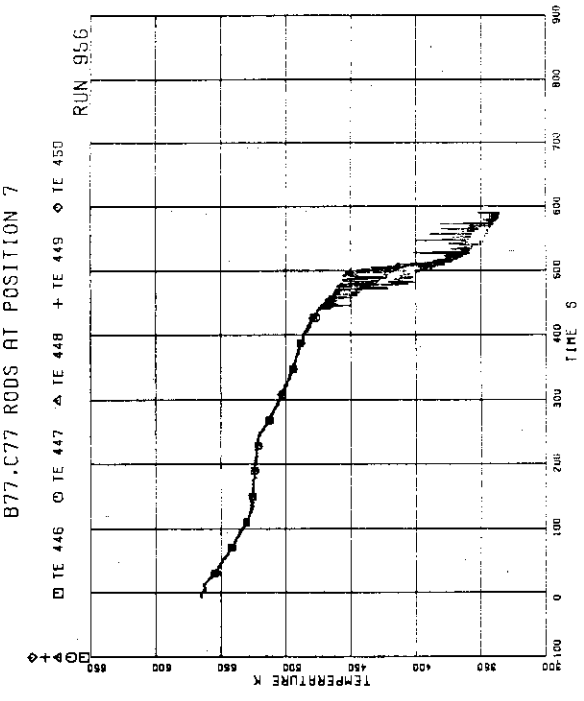

FIG.5.404 FLUID TEMPERATURE AT CHANNEL A OUTLET

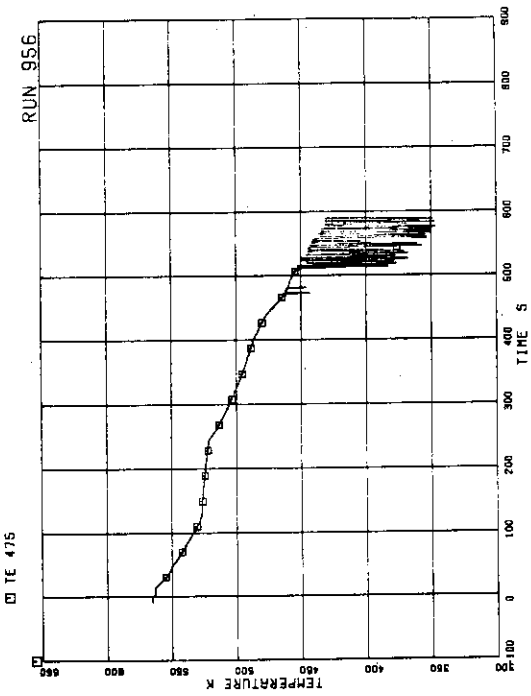

FIG.5.409 FLUID TEMPERATURE BELOW UTP OF CHANNEL A, OPENING 10

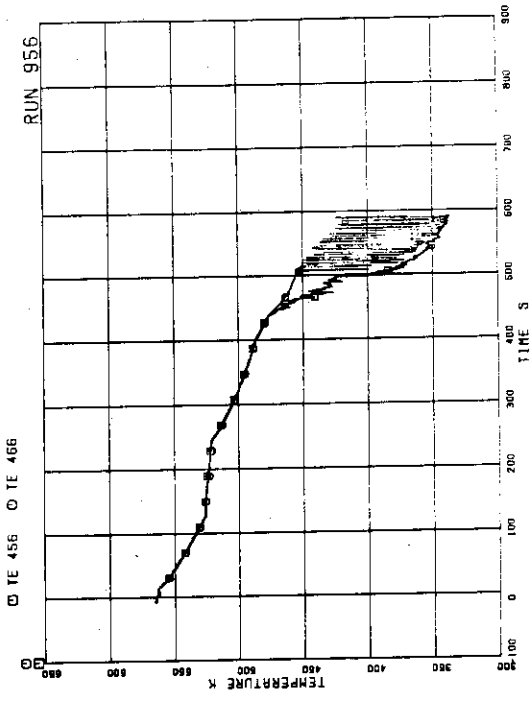

FIG.5.410 FLUID TEMPERATURE AT UTP IN CHANNEL A, OPENING 1

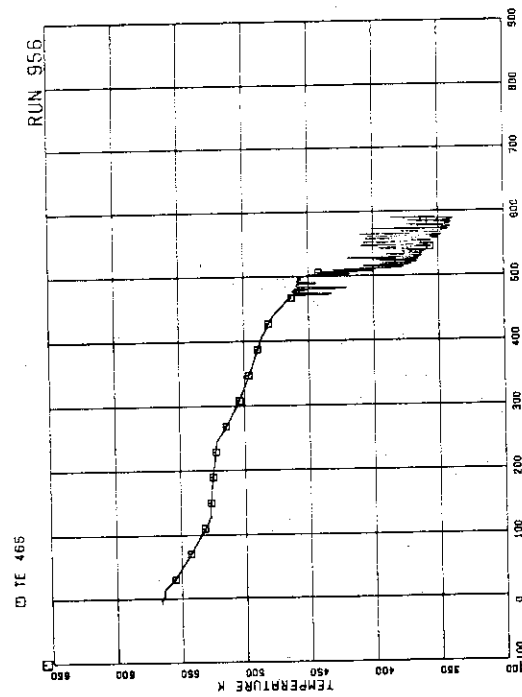

FIG.5.407 FLUID TEMPERATURE ABOVE UTP OF CHANNEL A, OPENING 10

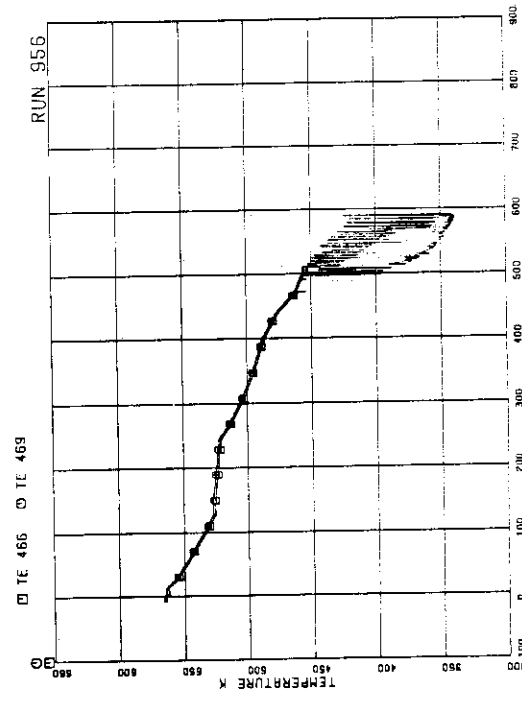

FIG.5.408 FLUID TEMPERATURE BELOW UTP OF CHANNEL A, OPENINGS 1 AND 4

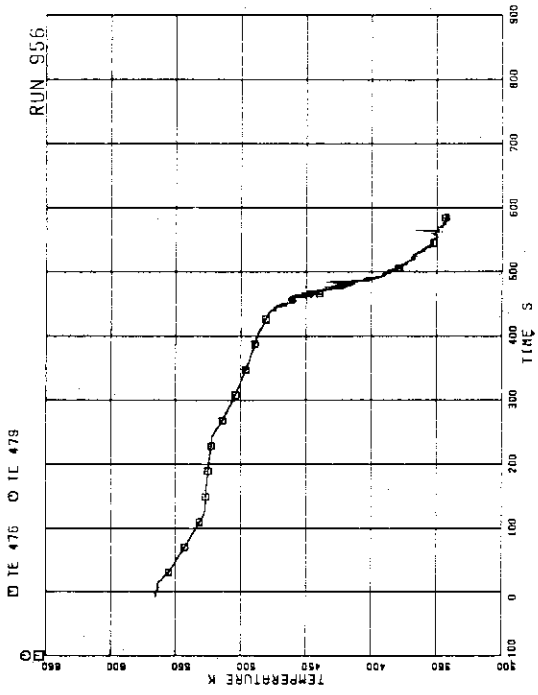

FIG.5.413 FLUID TEMPERATURE ABOVE UTP OF CHANNEL C, OPENING 1 AND 4

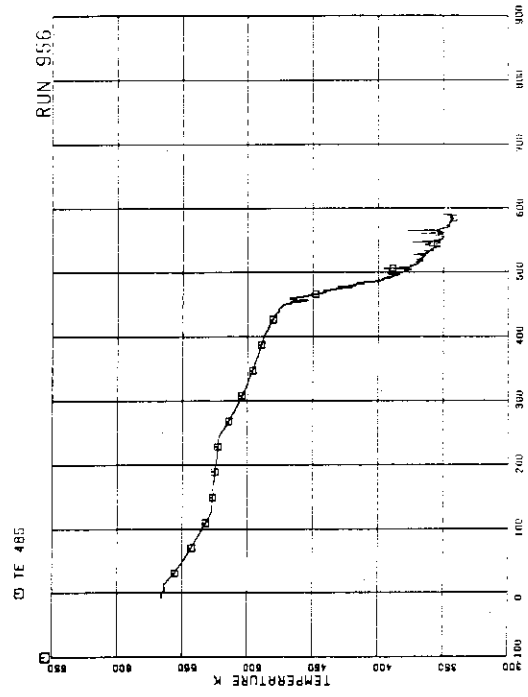

FIG.5.414 FLUID TEMPERATURE ABOVE UTP IN CHANNEL C, OPENING 10

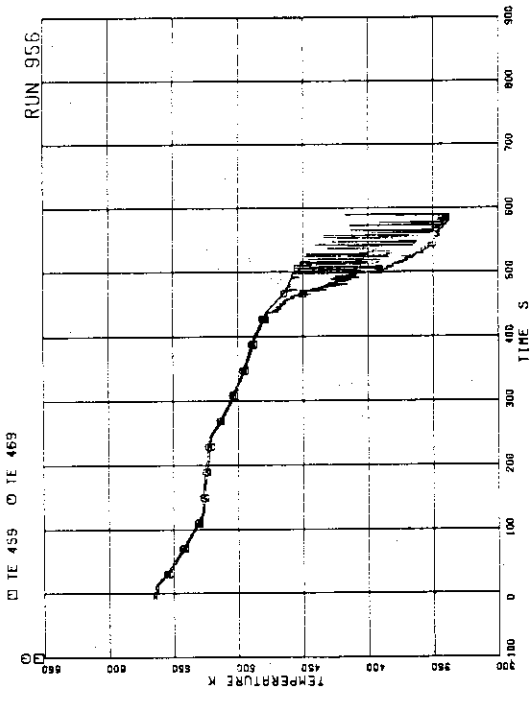

FIG.5.411 FLUID TEMPERATURE AT UTP IN CHANNEL A, OPENING 4

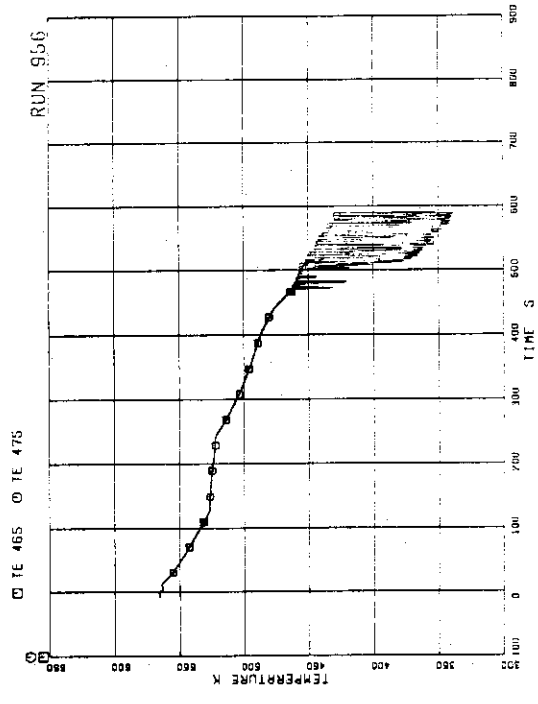

FIG.5.412 FLUID TEMPERATURE AT UTP IN CHANNEL A, OPENING 10

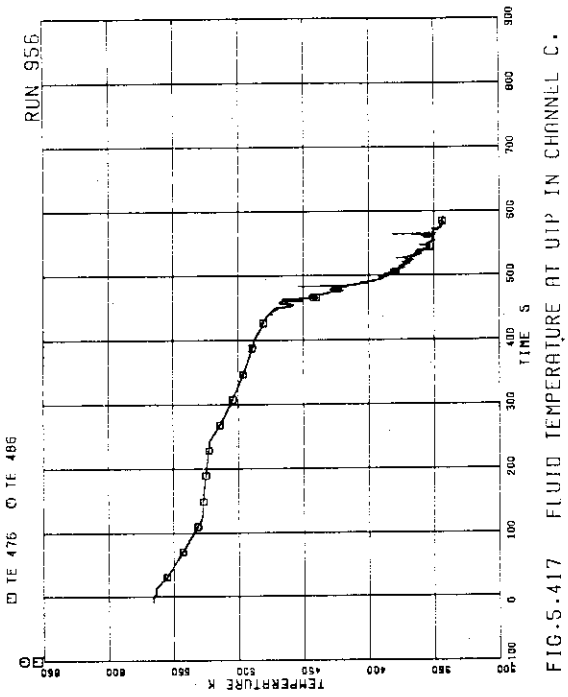

FIG.5.417 FLUID TEMPERATURE AT UTP IN CHANNEL C. OPENING 1

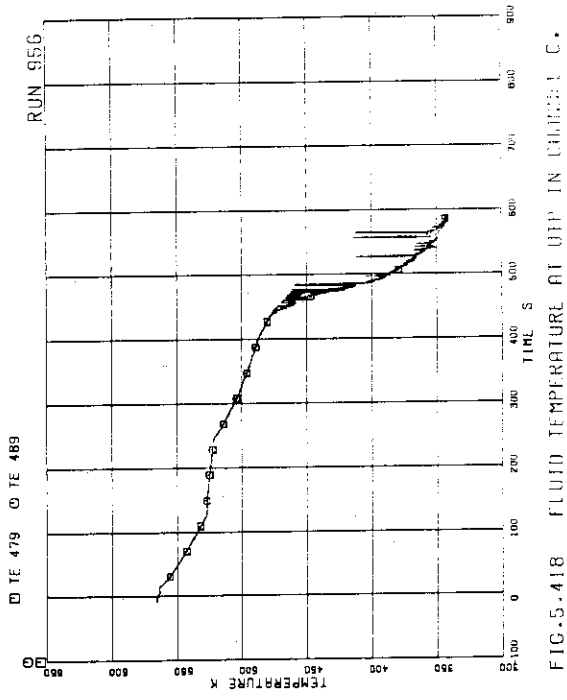

FIG.5.418 FLUID TEMPERATURE AT UTP IN CHANNEL C. OPENING 4

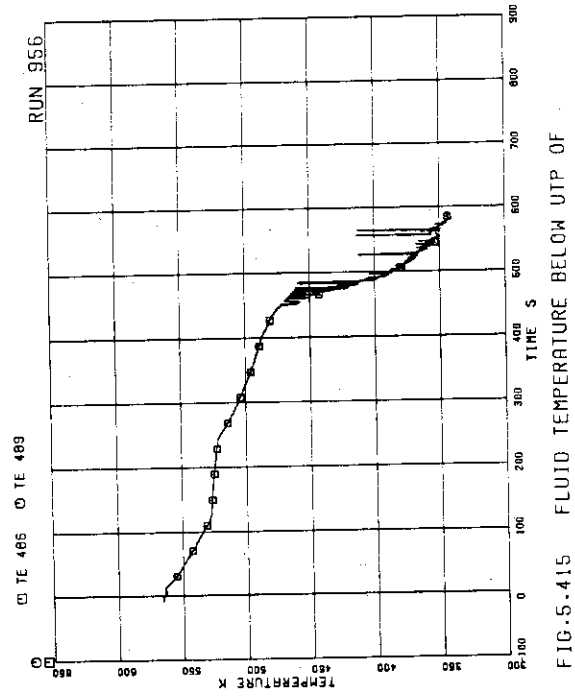

FIG.5.415 FLUID TEMPERATURE BELOW UTP OF CHANNEL C. OPENING 1 AND 4

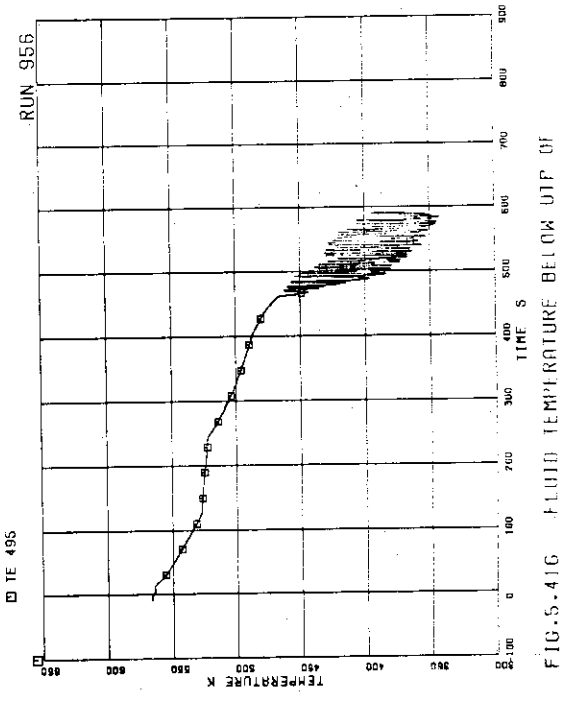

FIG.5.416 FLUID TEMPERATURE BELOW UTP OF CHANNEL C. OPENING 10

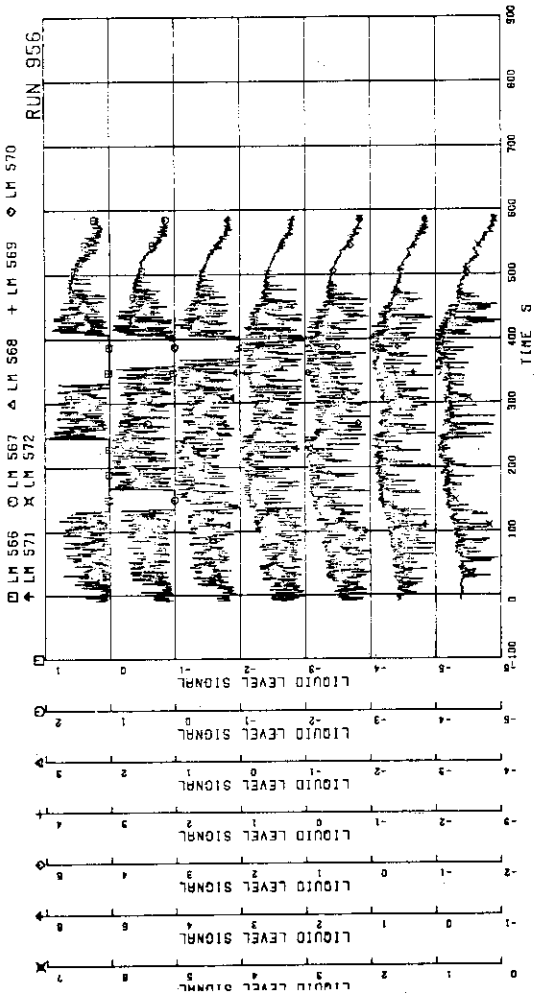

FIG.5.421 LIQUID-LEVEL SIGNAL IN CHANNEL BOX A. LOCATION A2

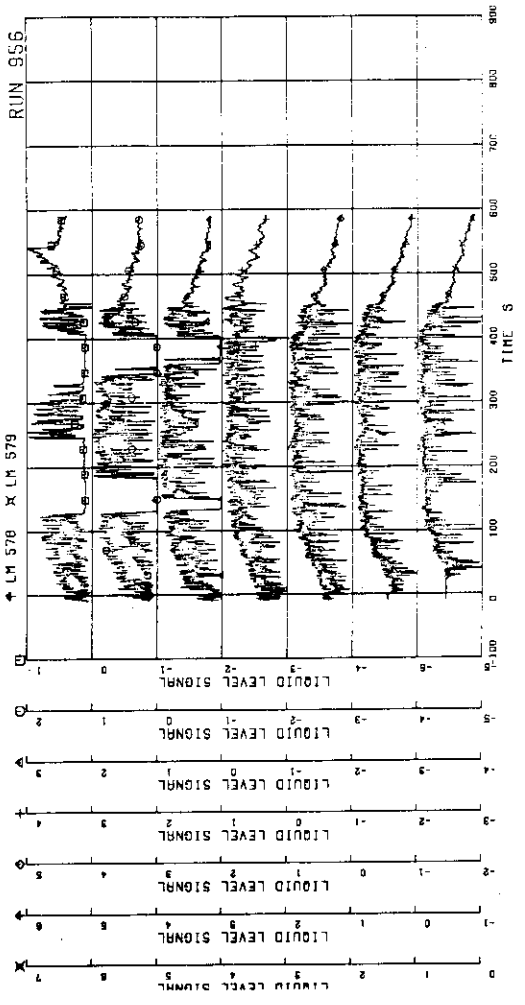

FIG.5.422 LIQUID LEVEL SIGNAL IN CHANNEL BOX B

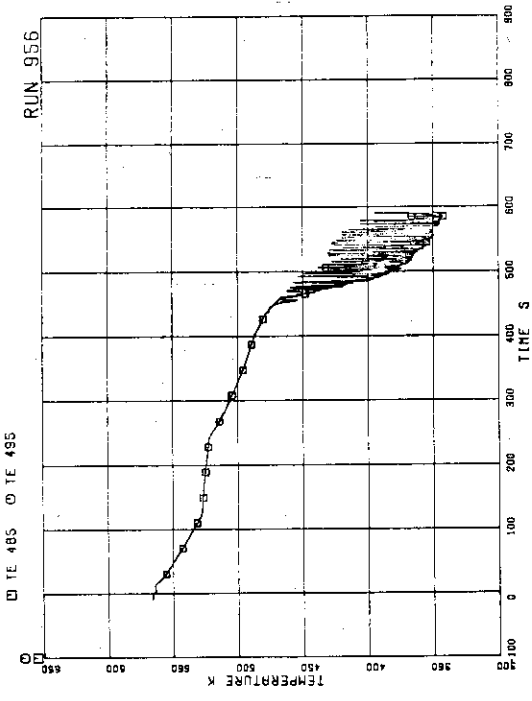

FIG.5.419 FLUID TEMPERATURE AT UTP IN CHANNEL C. OPENING 10

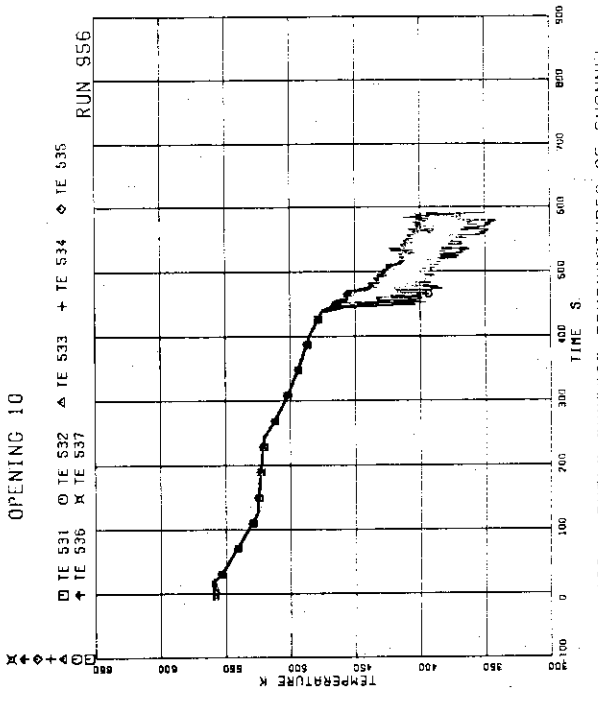

FIG.5.420 OUTER SURFACE TEMPERATURES OF CHANNEL BOX AT POSITIONS 1 TO 7

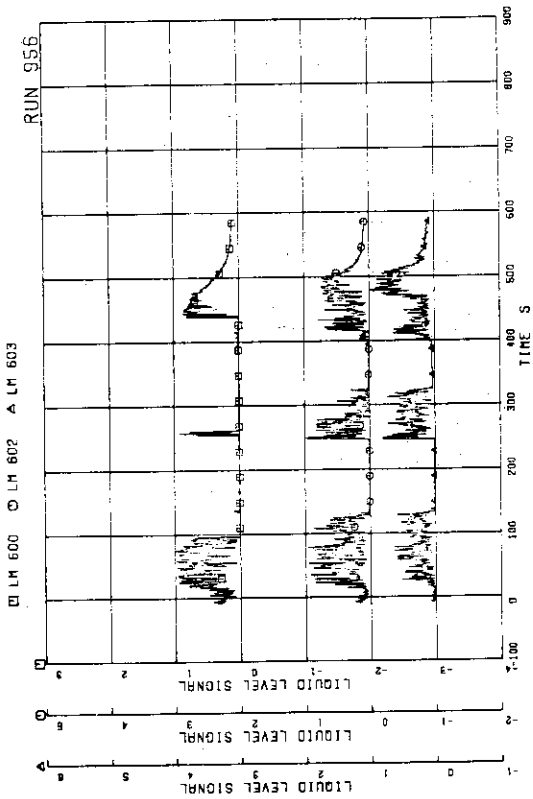

FIG.5.425 LIQUID-LEVEL SIGNAL IN CHANNEL A OUTLET, CENTER

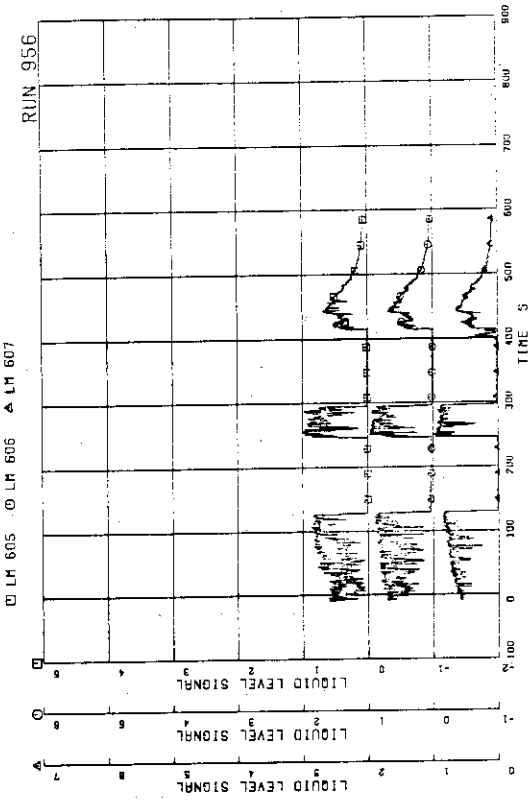

FIG.5.426 LIQUID LEVEL SIGNAL IN CHANNEL C OUTLET, LOCATION C1

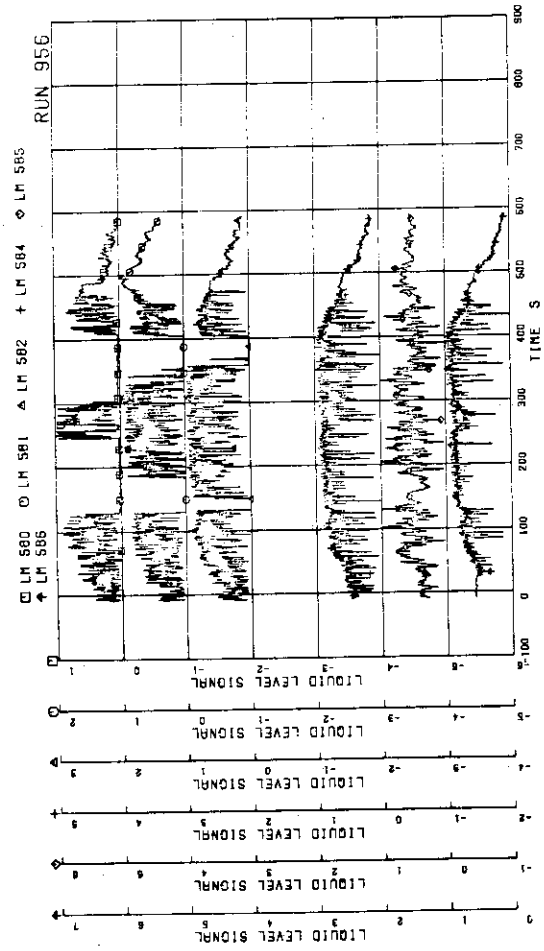

FIG.5.423 LIQUID LEVEL SIGNAL IN CHANNEL BOX C

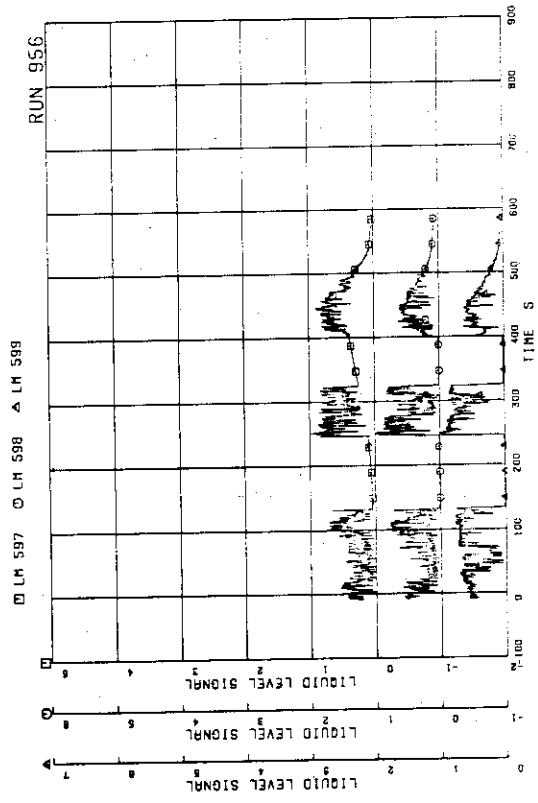

FIG.5.424 LIQUID LEVEL SIGNAL IN CHANNEL D OUTLET, LOCATION A2

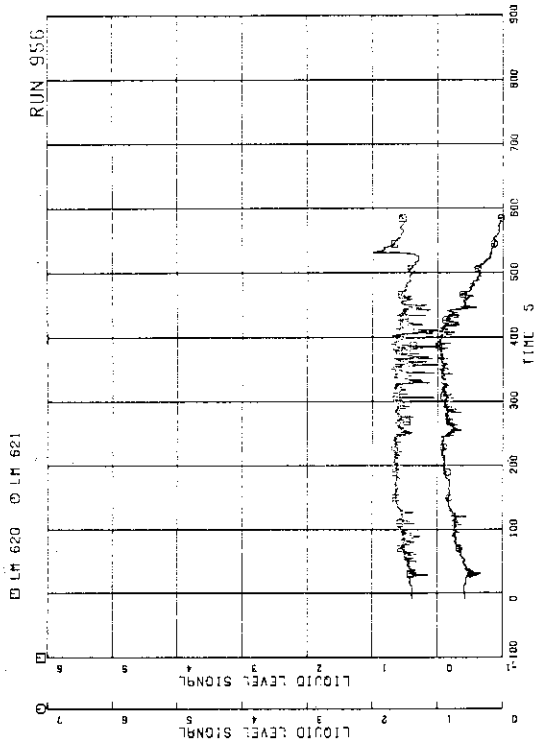

FIG.5.429 LIQUID LEVEL SIGNAL IN CHANNEL C INLET

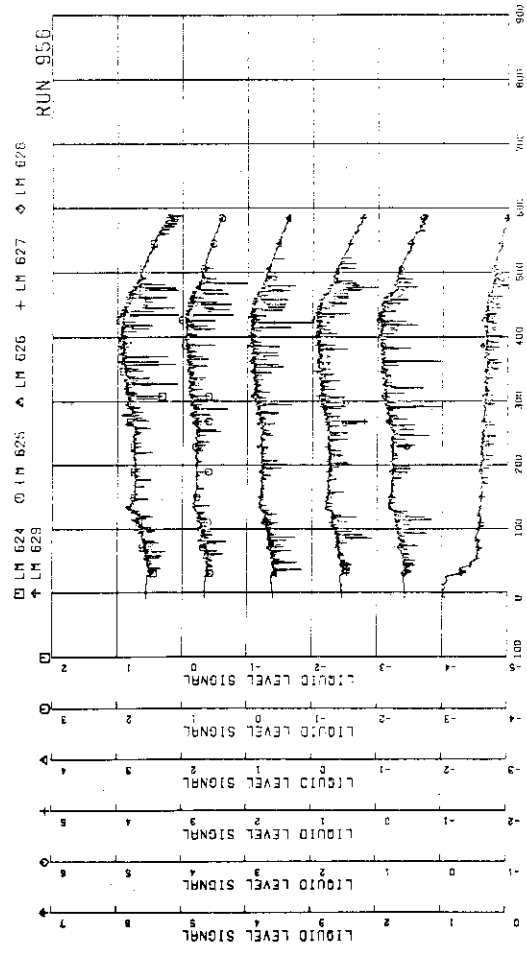

FIG.5.430 LIQUID LEVEL SIGNAL IN LOWER PLENUM, MIDDLE

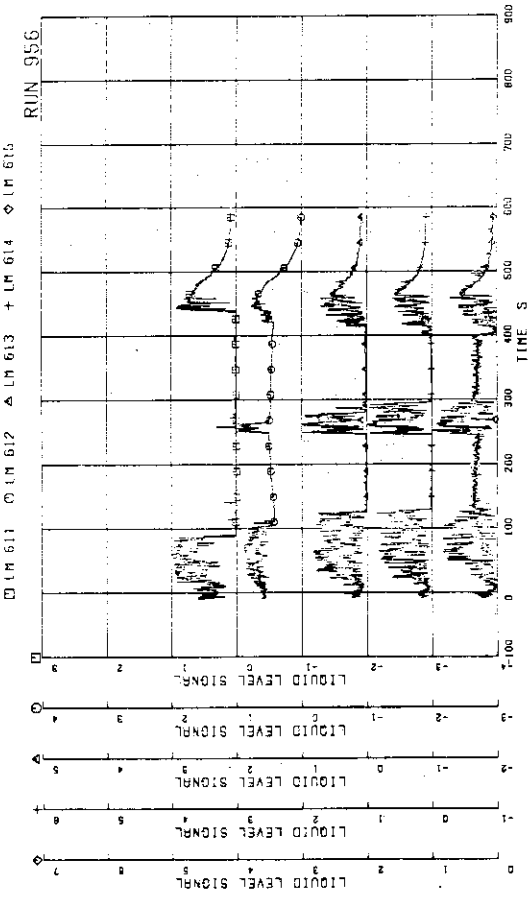

FIG.5.427 LIQUID LEVEL SIGNAL IN CHANNEL C OUTLET, CENTER

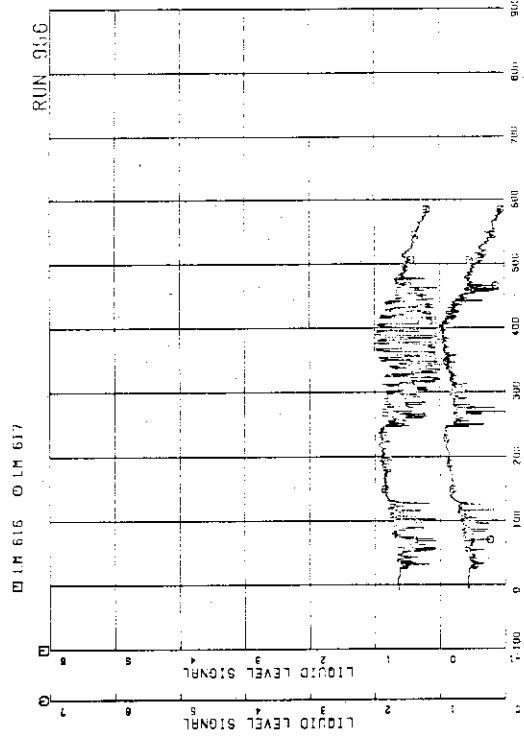

FIG.5.428 LIQUID LEVEL SIGNAL IN CHANNEL C INLET

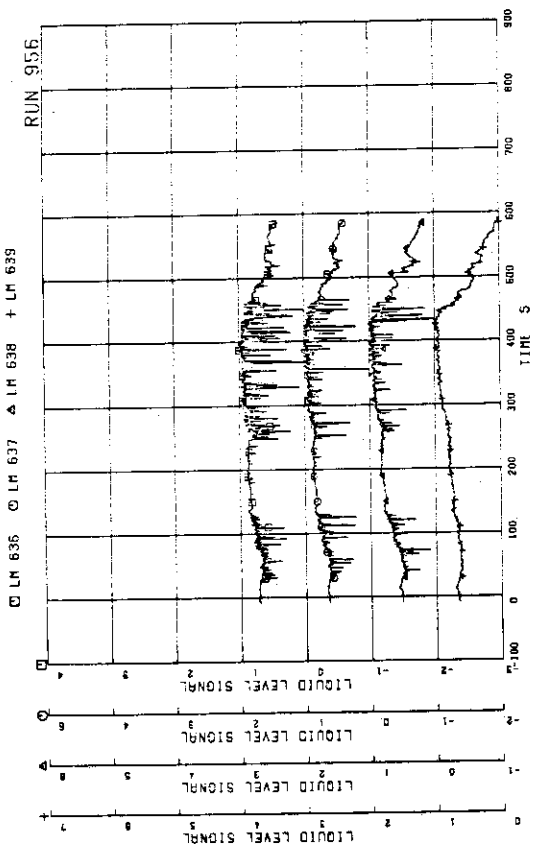

FIG.5.431 LIQUID LEVEL SIGNAL IN GUIDE TUBE, NORTH

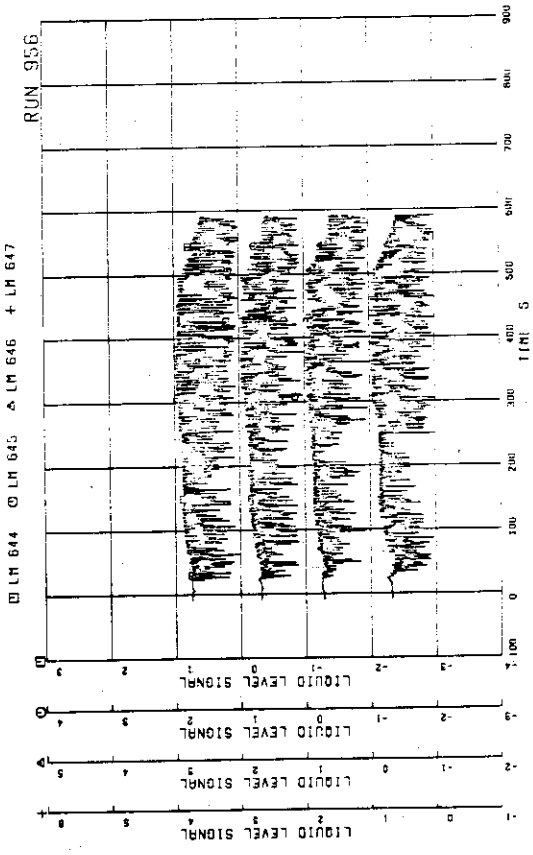

FIG.5.432 LIQUID LEVEL SIGNAL IN DOWNCOMER, B SIDE

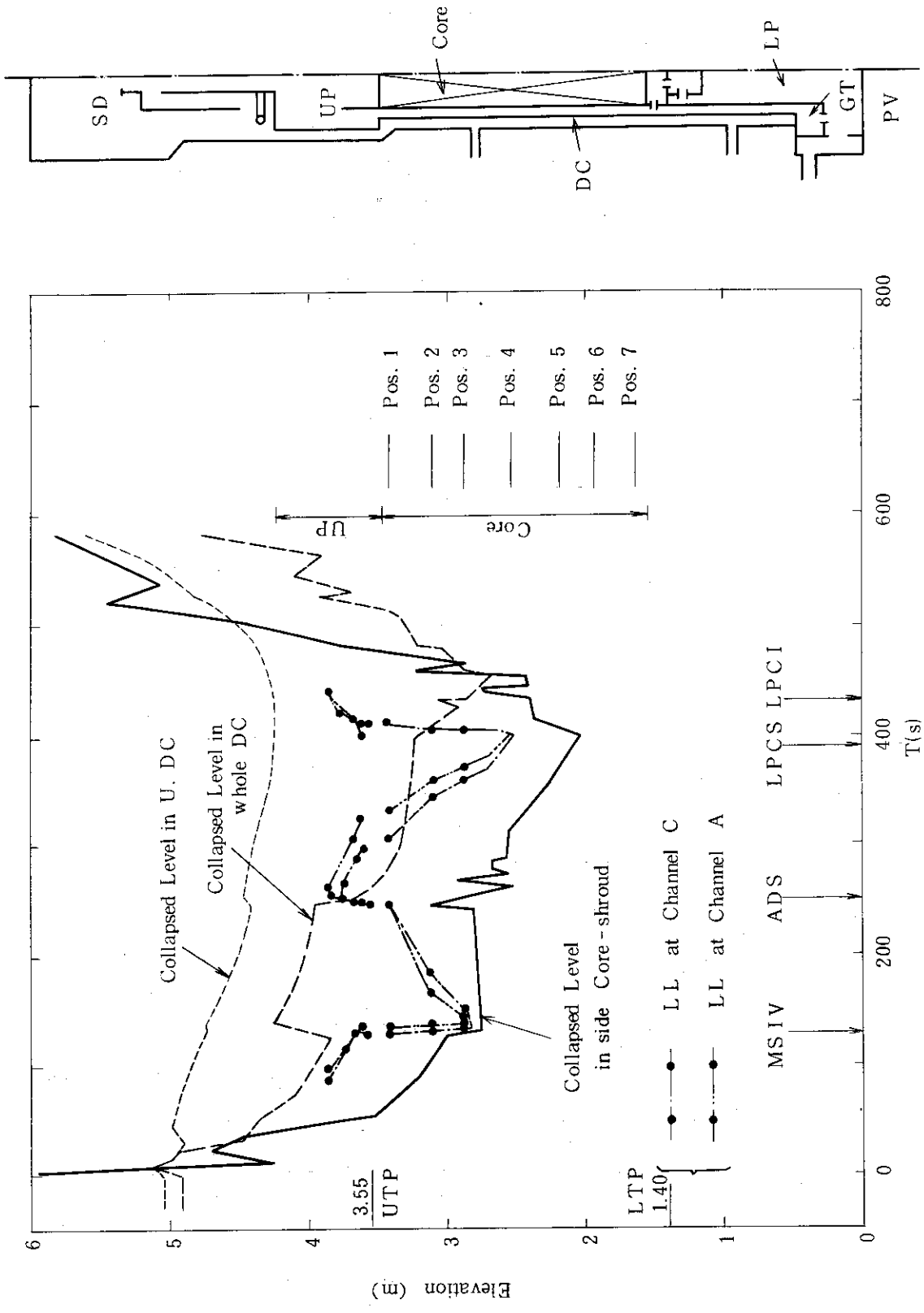

Fig. 5.433 Estimated liquid levels in pressure vessel

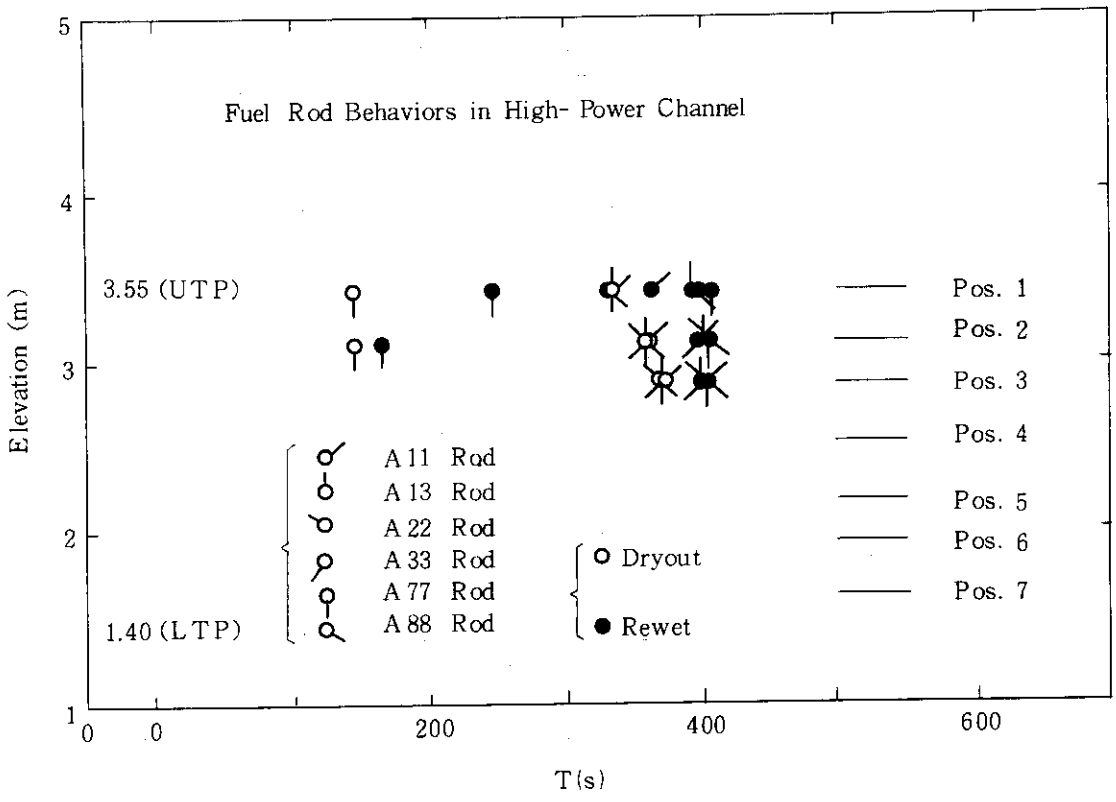

Fig. 5.434 Dryout and quench times of fuel rods in bundle A

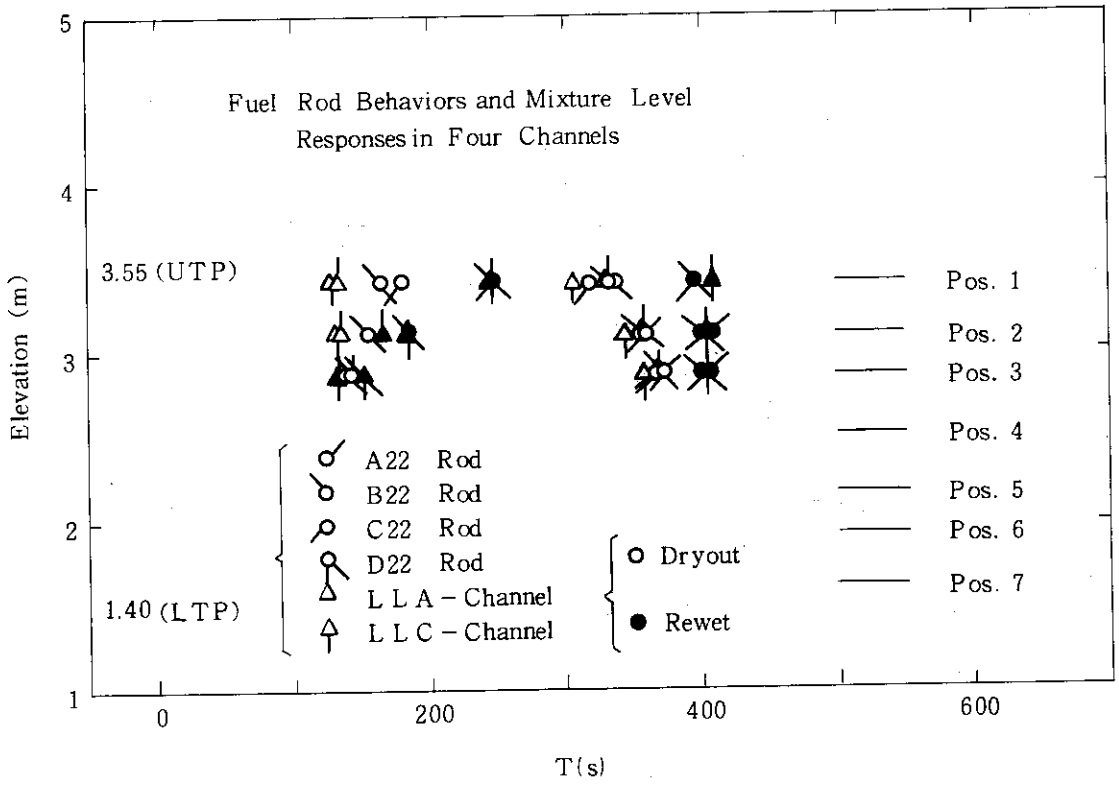

Fig. 5.435 Dryout and quench times of fuel rods in four bundles

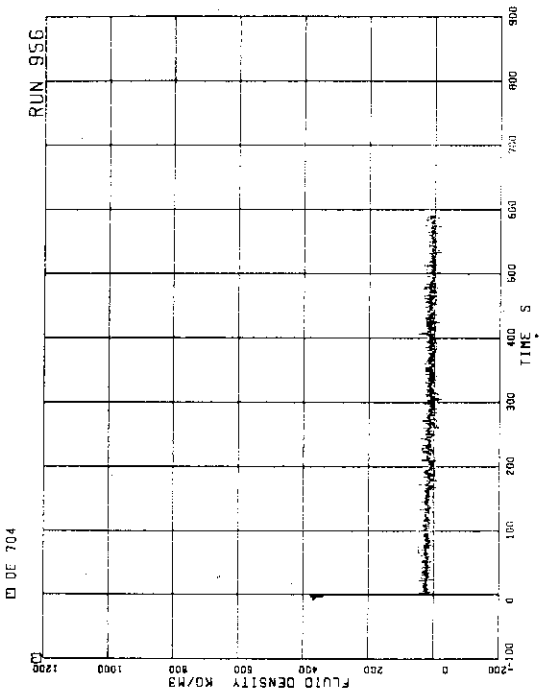

FIG.5.438 AVERAGE DENSITY AT PV SIDE OF LOOP

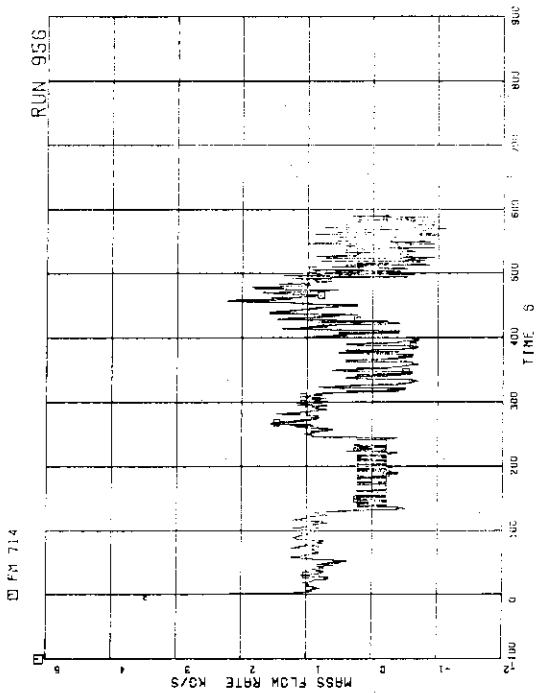

FIG.5.439 FLOW RATE AT CHANNEL A IN

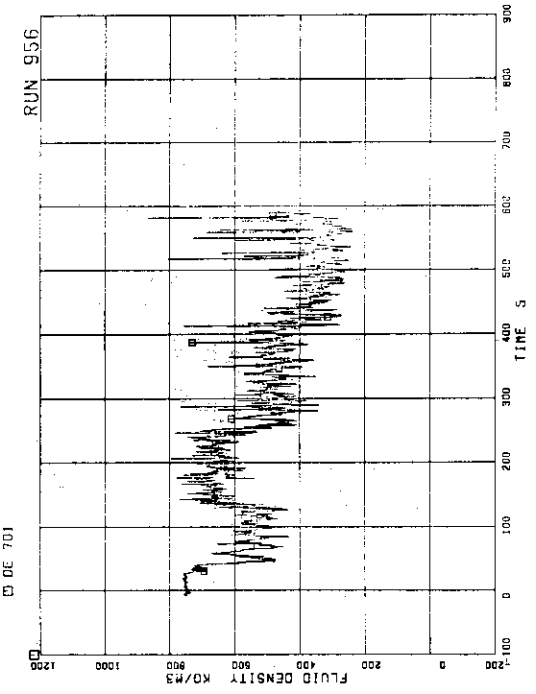

FIG.5.436 AVERAGE DENSITY AT JP-1.2 OUTLET

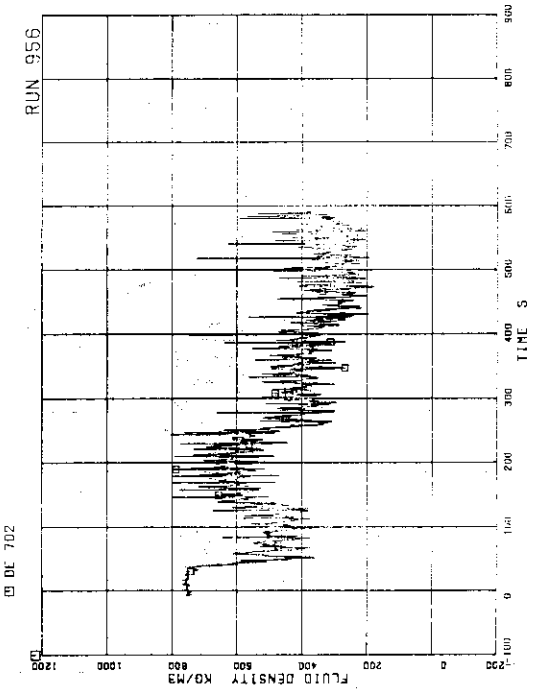

FIG.5.437 AVERAGE DENSITY IN MSL DOWN HEADER ORIFICE

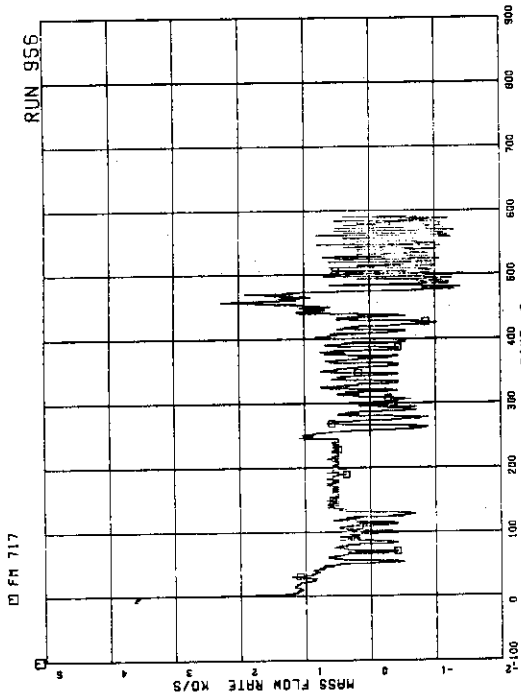

FIG.5.442 FLOW RATE AT CHANNEL D INLET

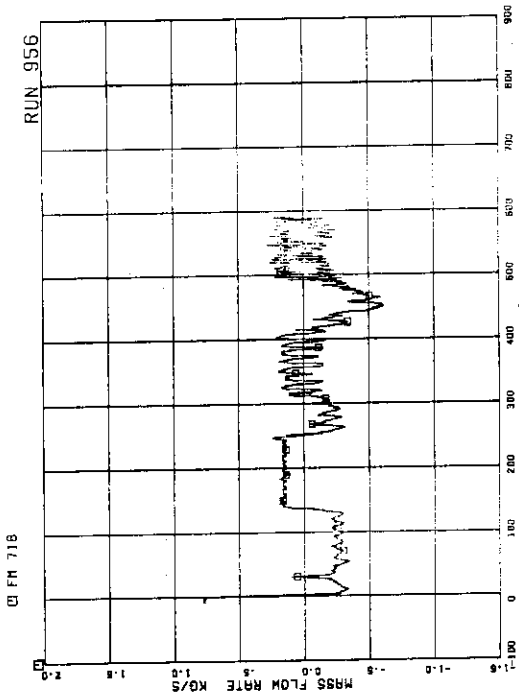

FIG.5.443 FLOW RATE AT BYPASS HOLE

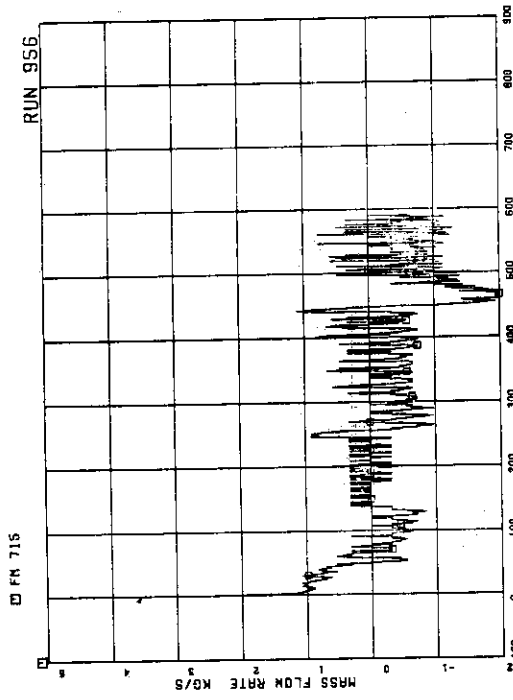

FIG.5.440 FLOW RATE AT CHANNEL B INLET

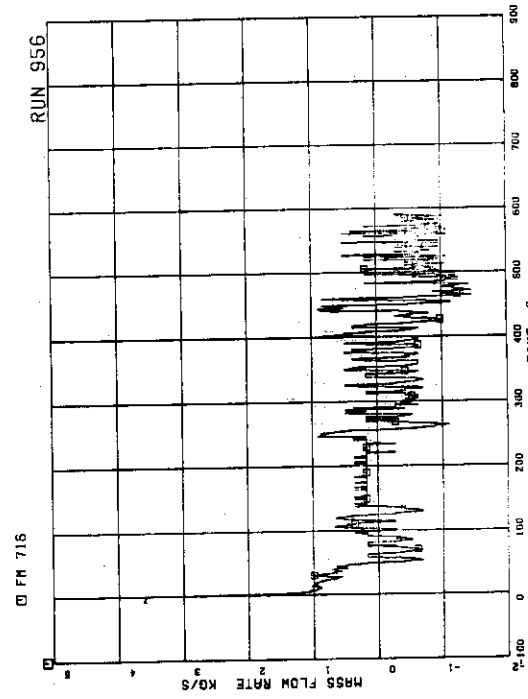

FIG.5.441 FLOW RATE AT CHANNEL C INLET

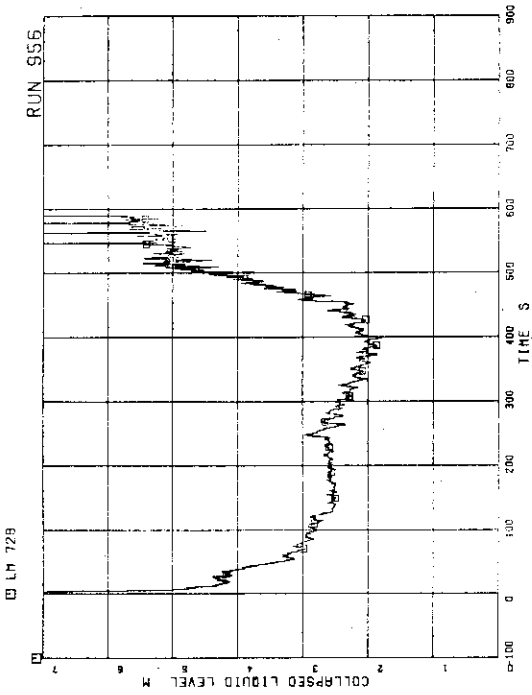

FIG.5.443 COLLAPSED LIQUID LEVEL INSIDE CORE SHROUD

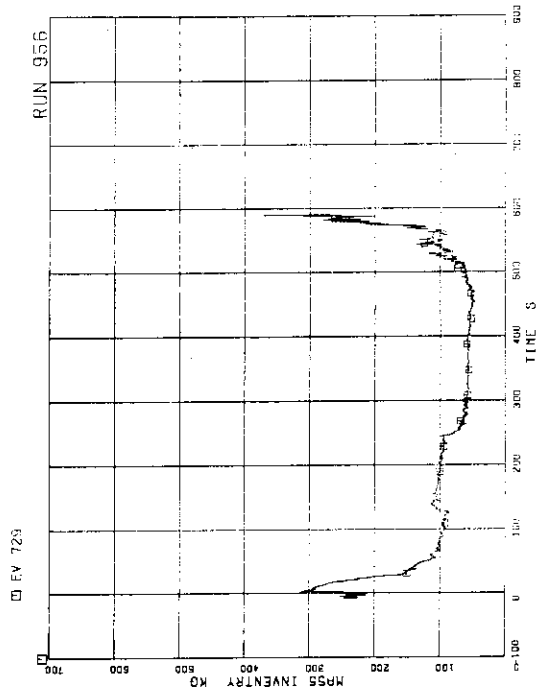

FIG. .447 FLUID INVENTORY IN DOWNCOMER

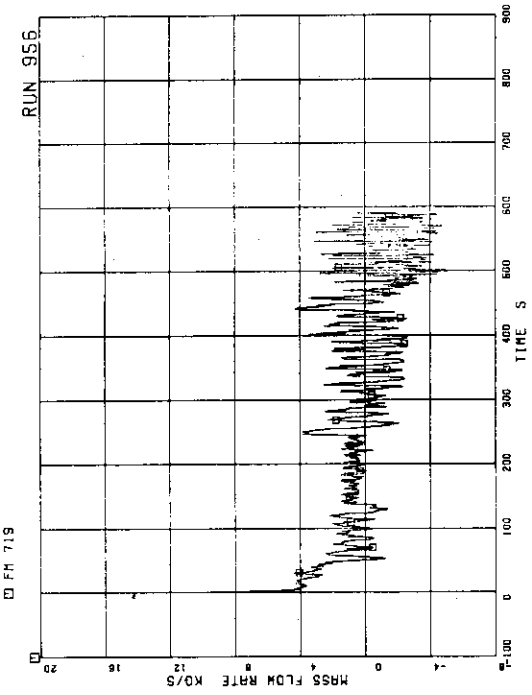

FIG.5.444 TOTAL CHANNEL INLET FLOW RATE

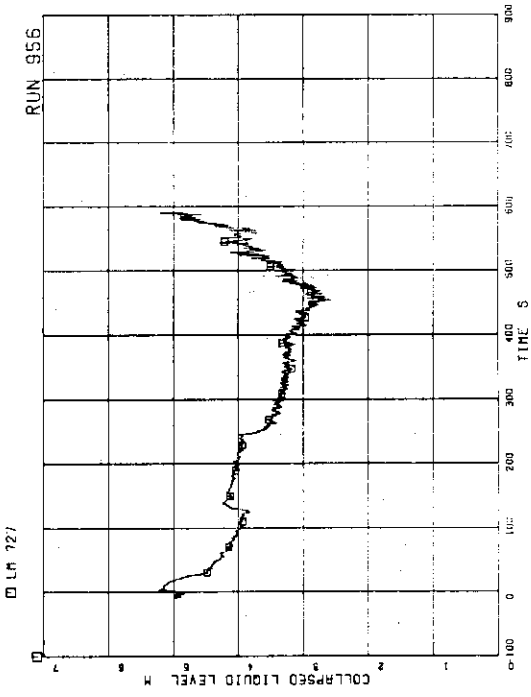

FIG.5.445 COLLAPSED LIQUID LEVEL IN DOWNCOMER

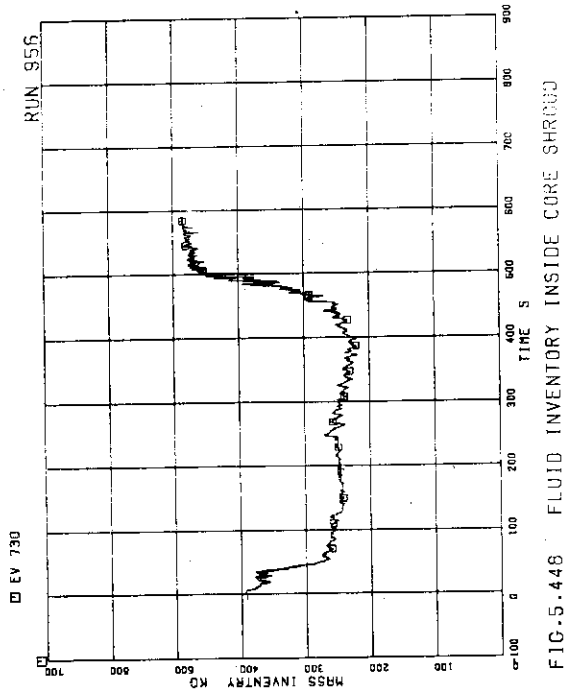

FIG.5.448 FLUID INVENTORY INSIDE CORE SHROUD

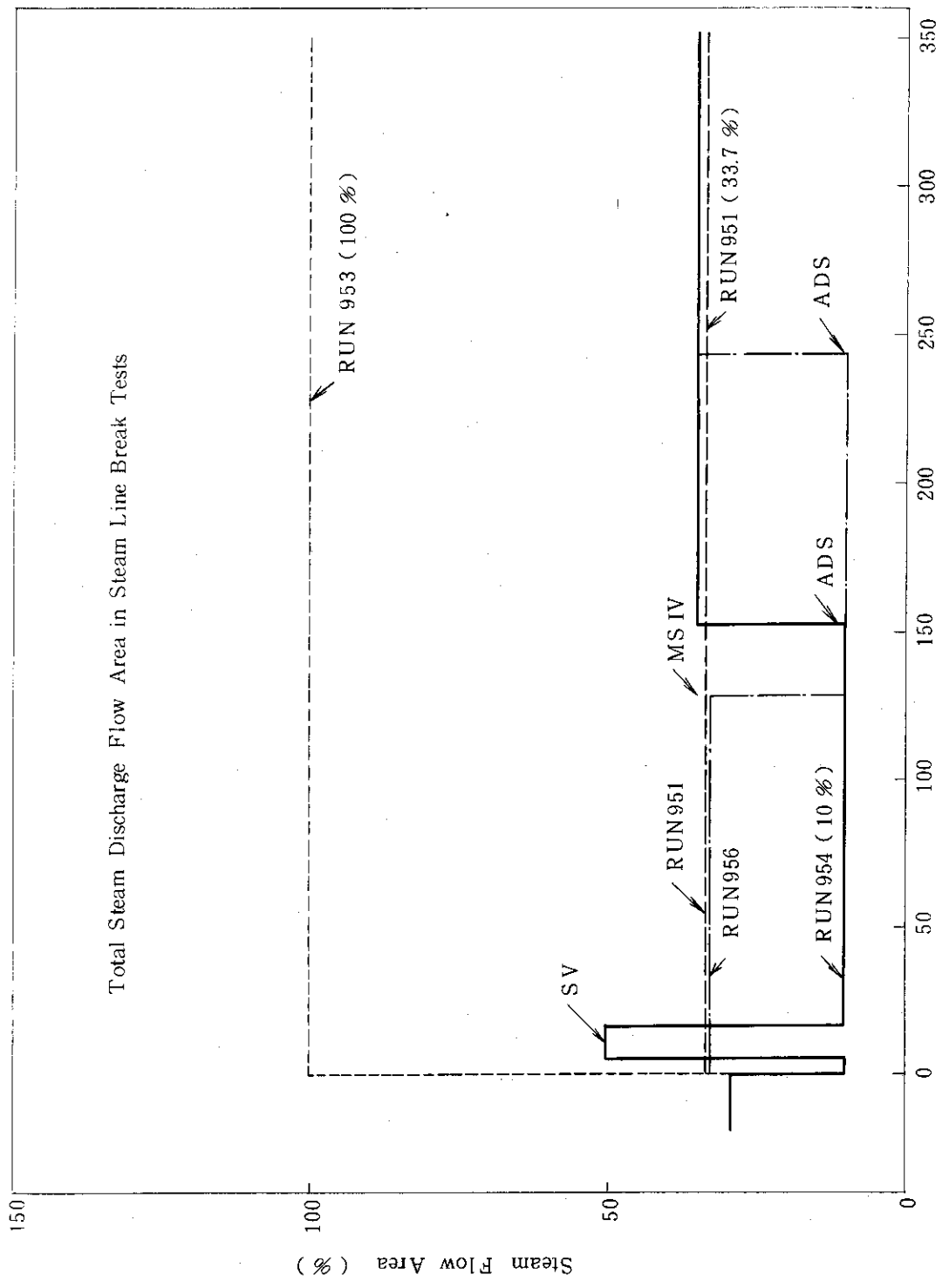

Fig. 6. 1 Total steam discharge flow area in steam line breaks

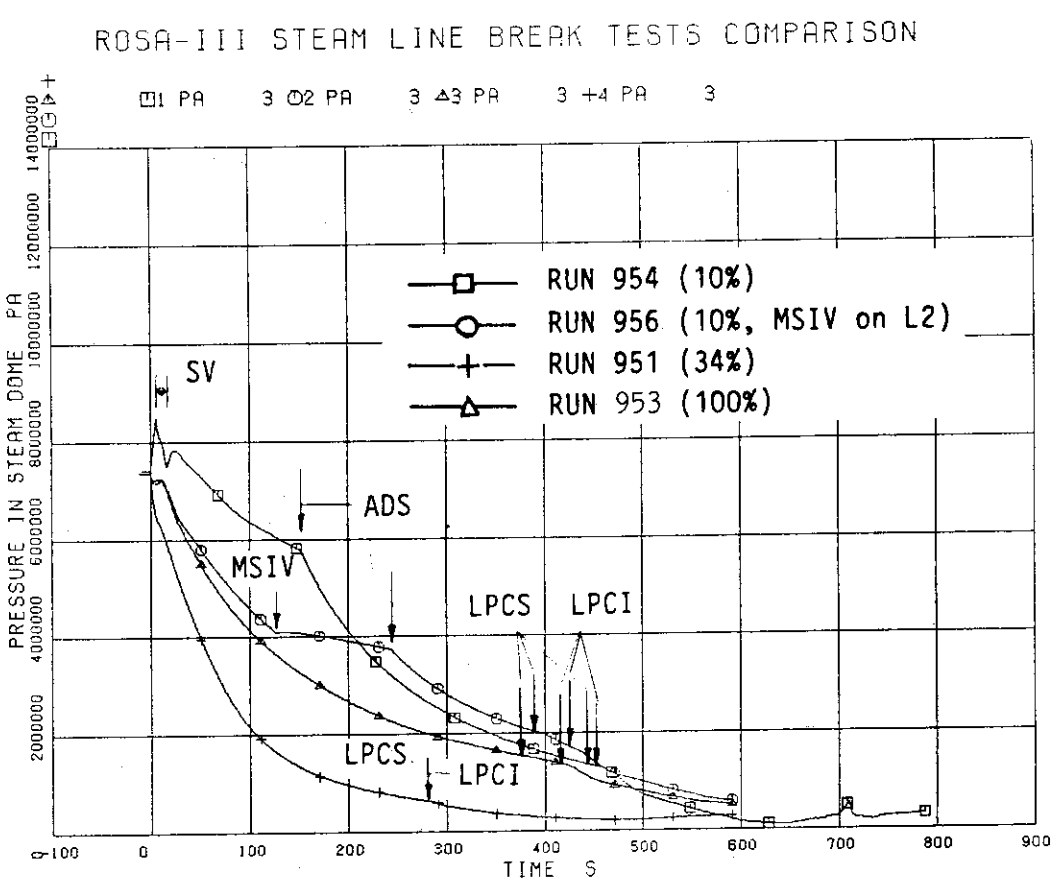

Fig. 6. 2 Comparison of steam dome pressure responses

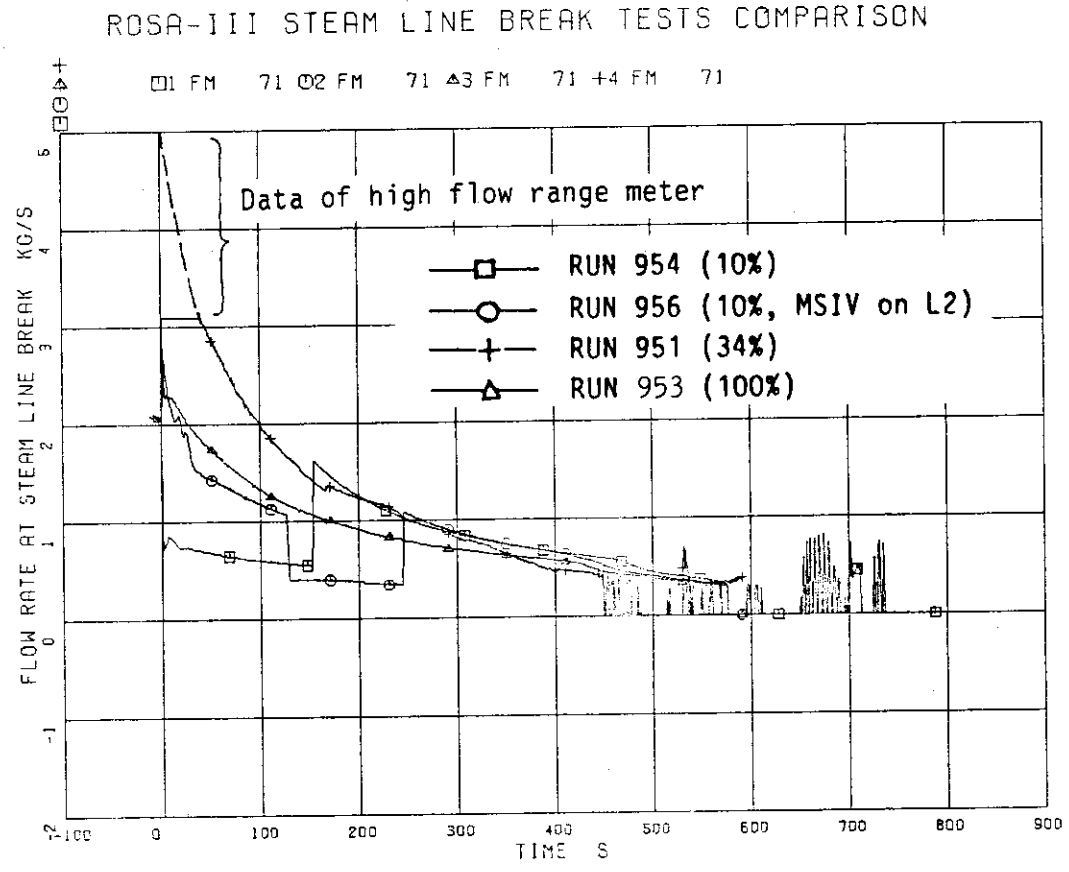

Fig. 6. 3 Comparison of steam discharge flow rates measured by an orifice-type flow meter

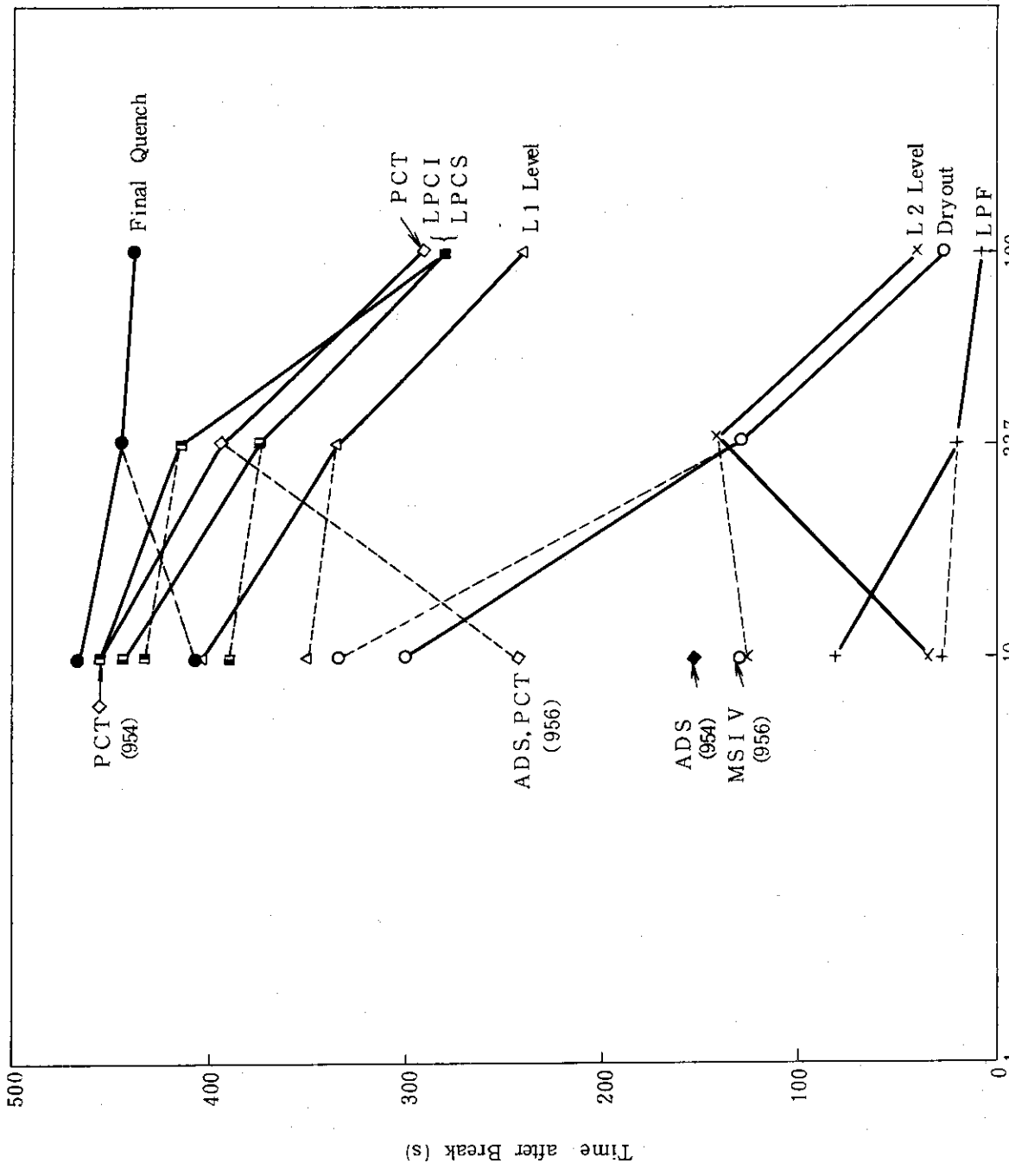

Fig. 6. 4 Times of major events related with break area

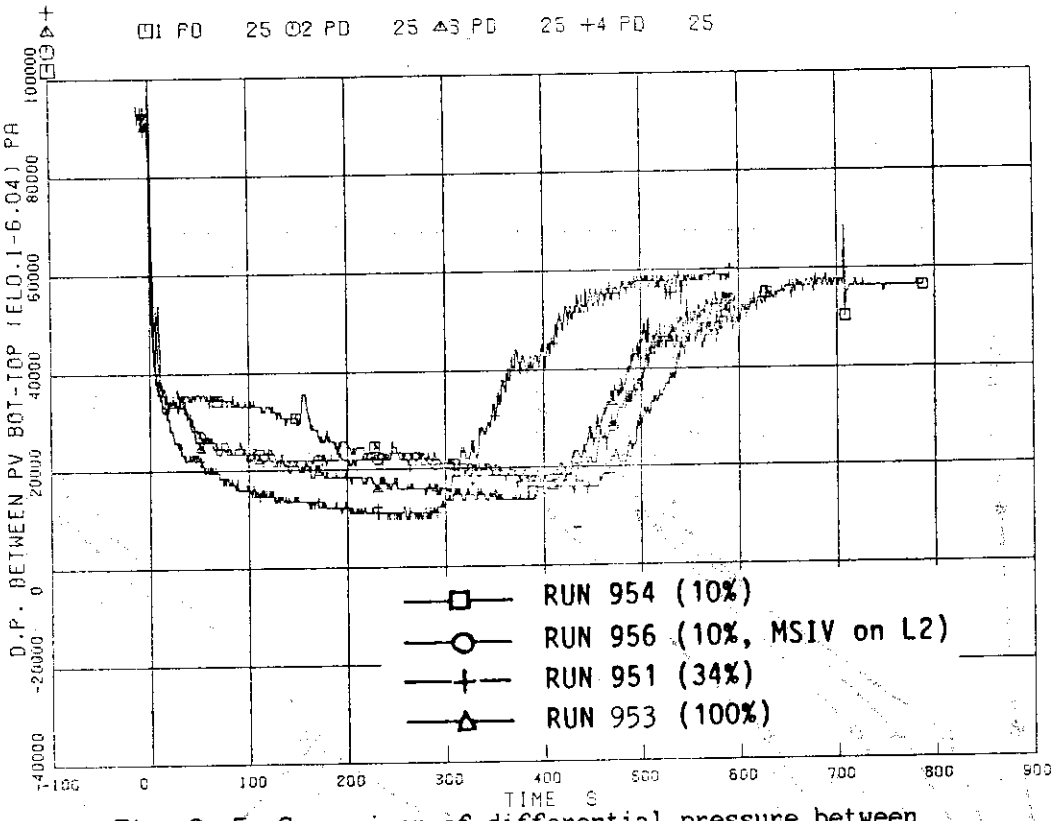

Fig. 6. 5 Comparison of differential pressure between top and bottom of PV

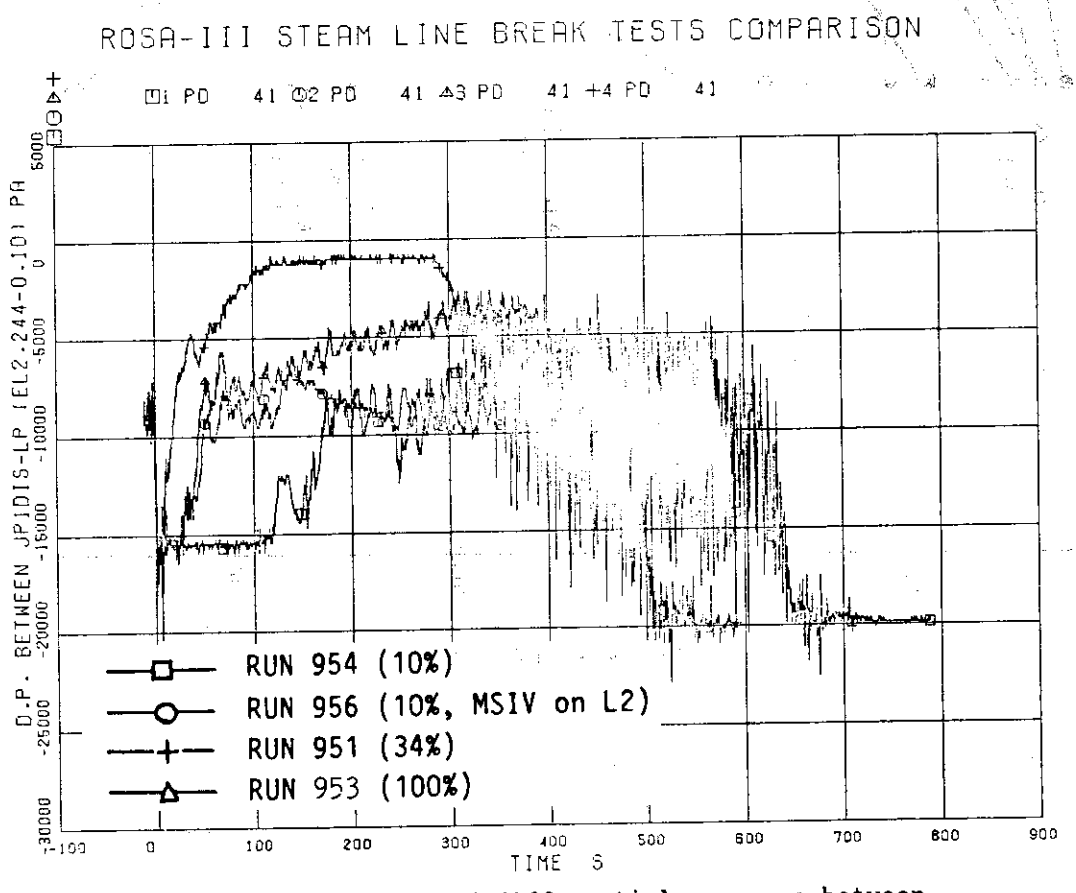

Fig. 6. 6 Comparison of differential pressure between JP1 discharge-side and lower plenum

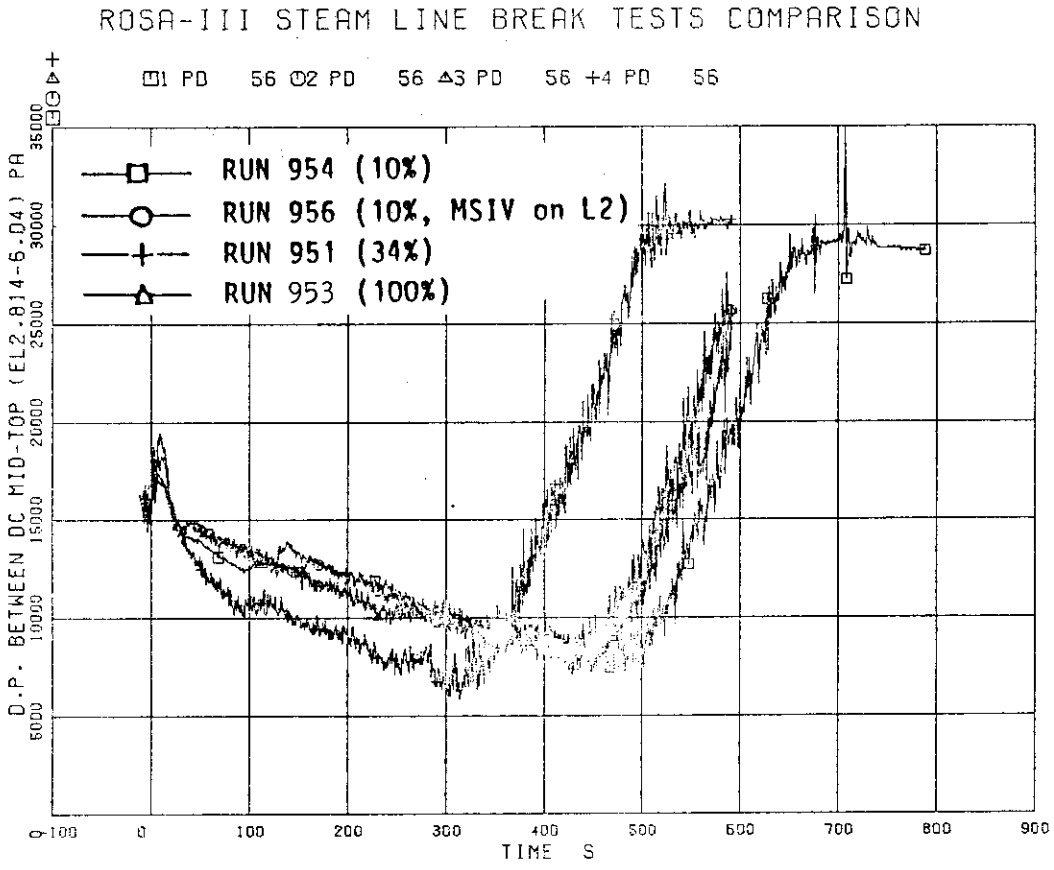

Fig. 6. 7 Comparison of differential pressure in upper downcomer

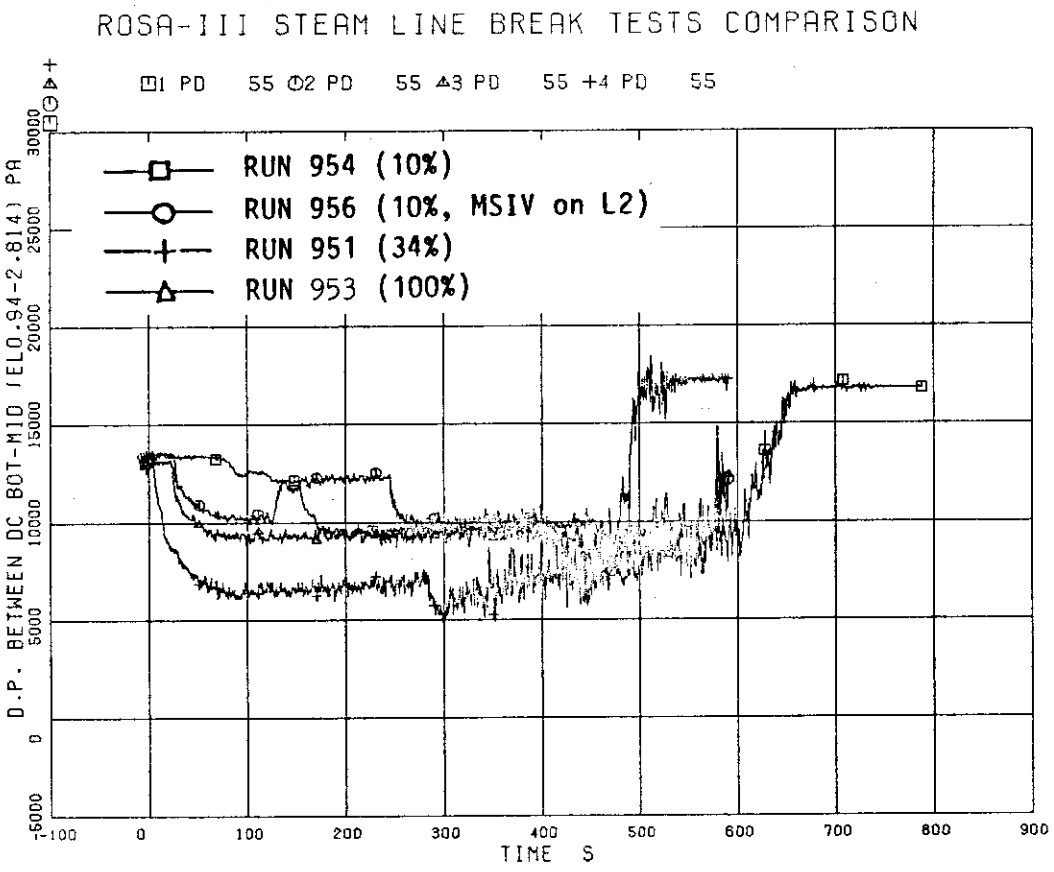

Fig. 6. 8 Comparison of differential pressure in lower downcomer

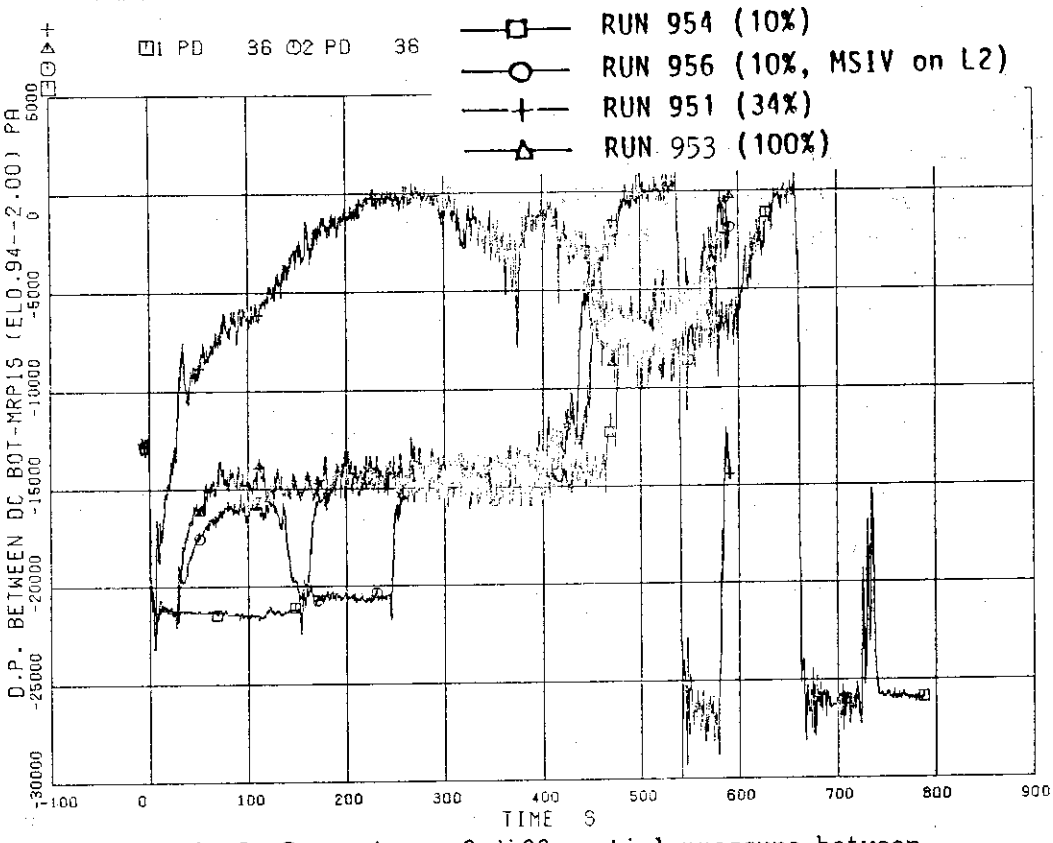

Fig. 6. 9 Comparison of differential pressure between downcomer bottom and MRP1 suction-side

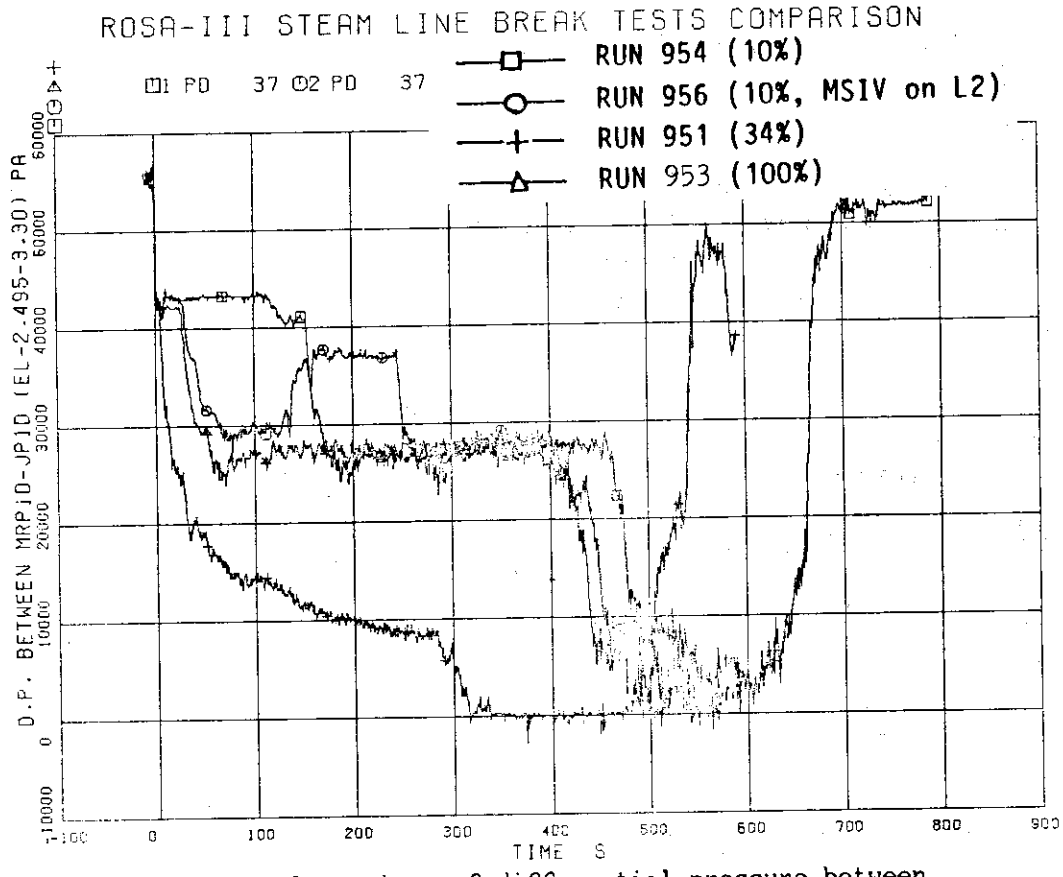

Fig. 6.10 Comparison of differential pressure between MRP1 discharge-side and JP1 drive line

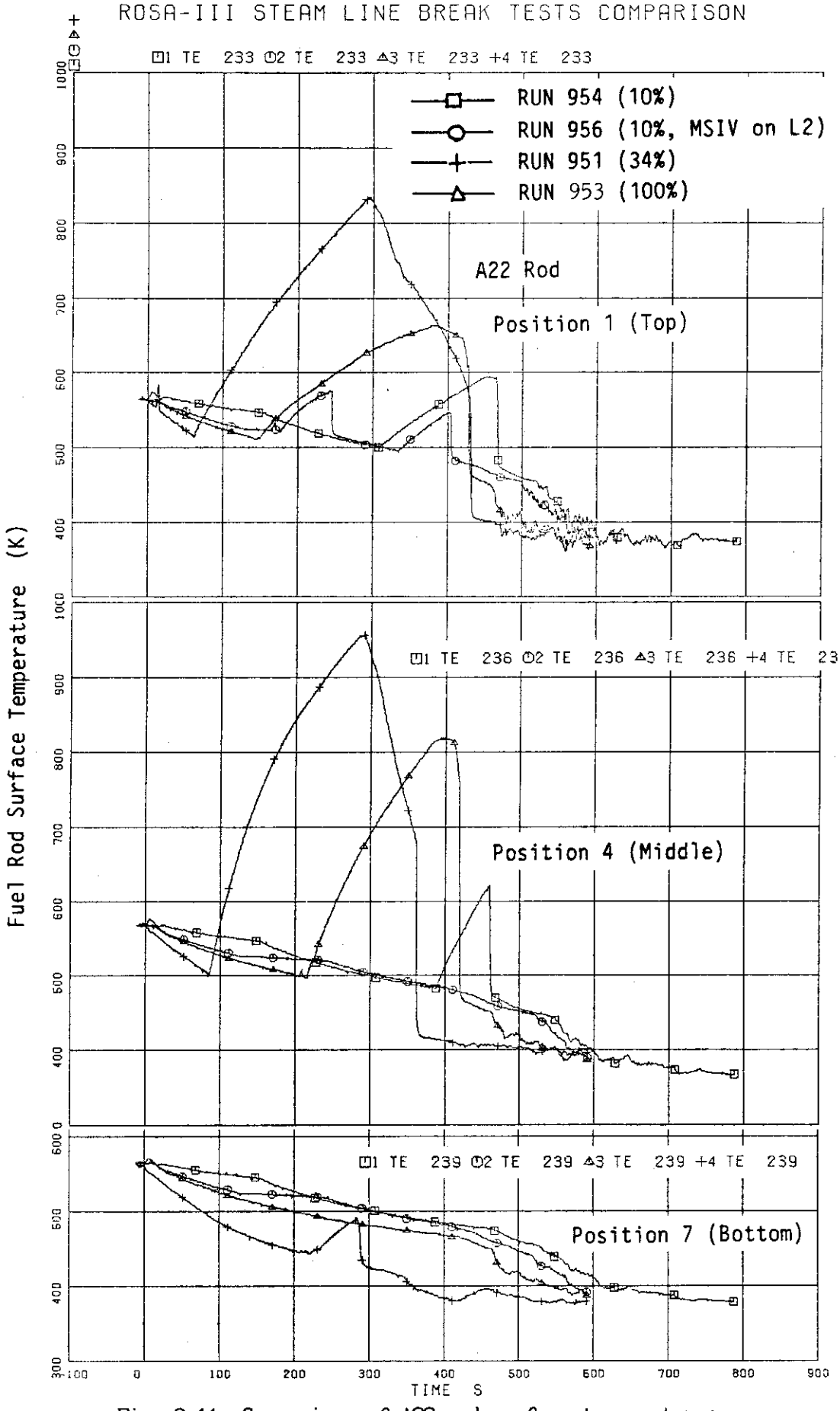

Fig. 6.11 Comparison of A22 rod surface temperatures in high power bundle A

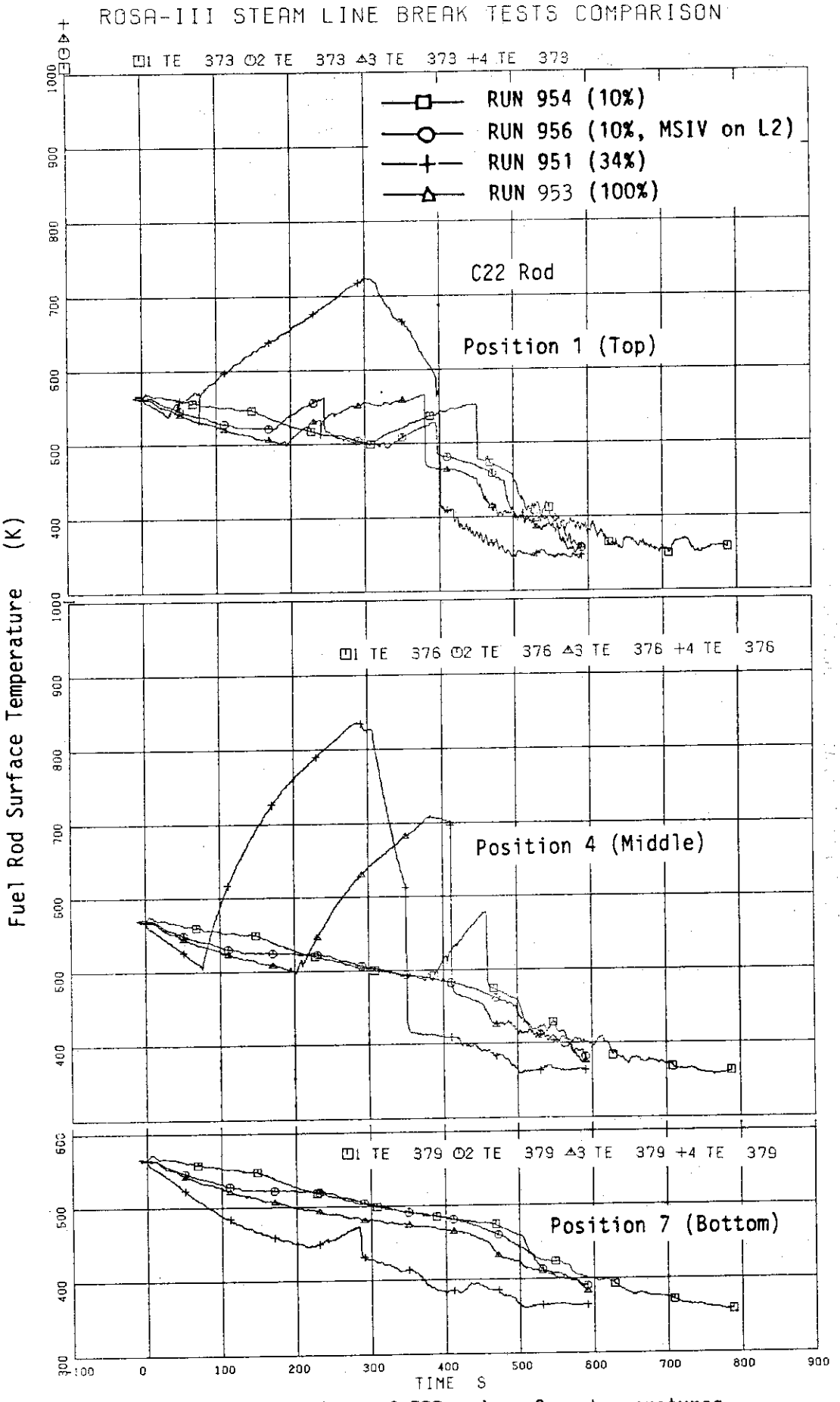

Fig. 6.12 Comparison of C22 rod surface temperatures in average power bundle C

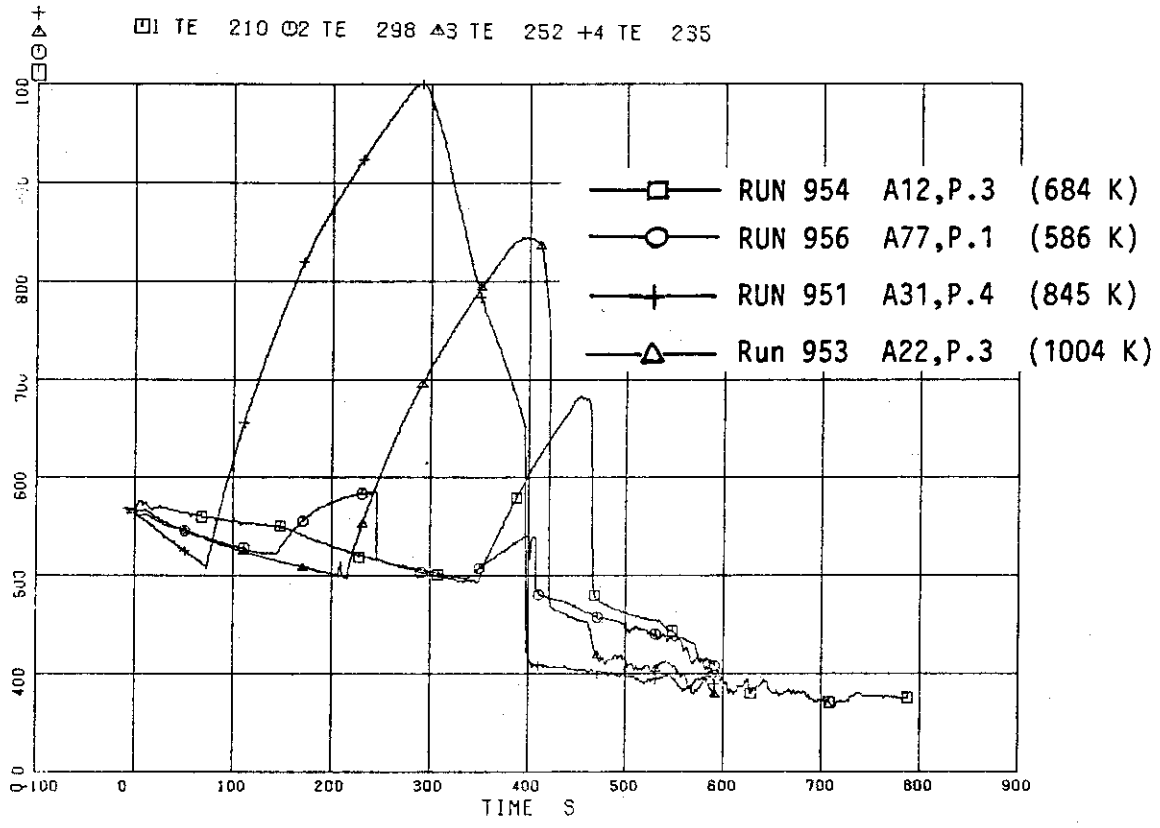

Fig. 6.13 Comparison of fuel rod surface temperatures recorded the PCT in steam line break tests

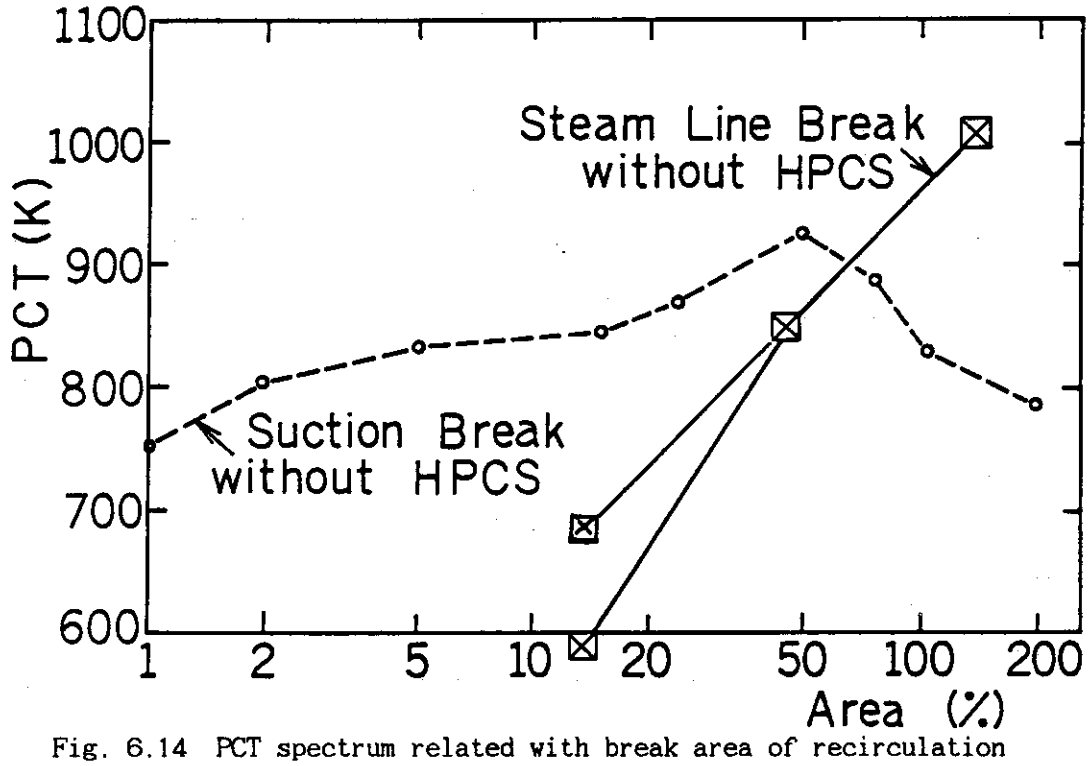

Fig. 6.14 PCT spectrum related with break area of recirculation line flow area assuming HPCS failure
(Break Area is normalized by scaled rec. line flow area)

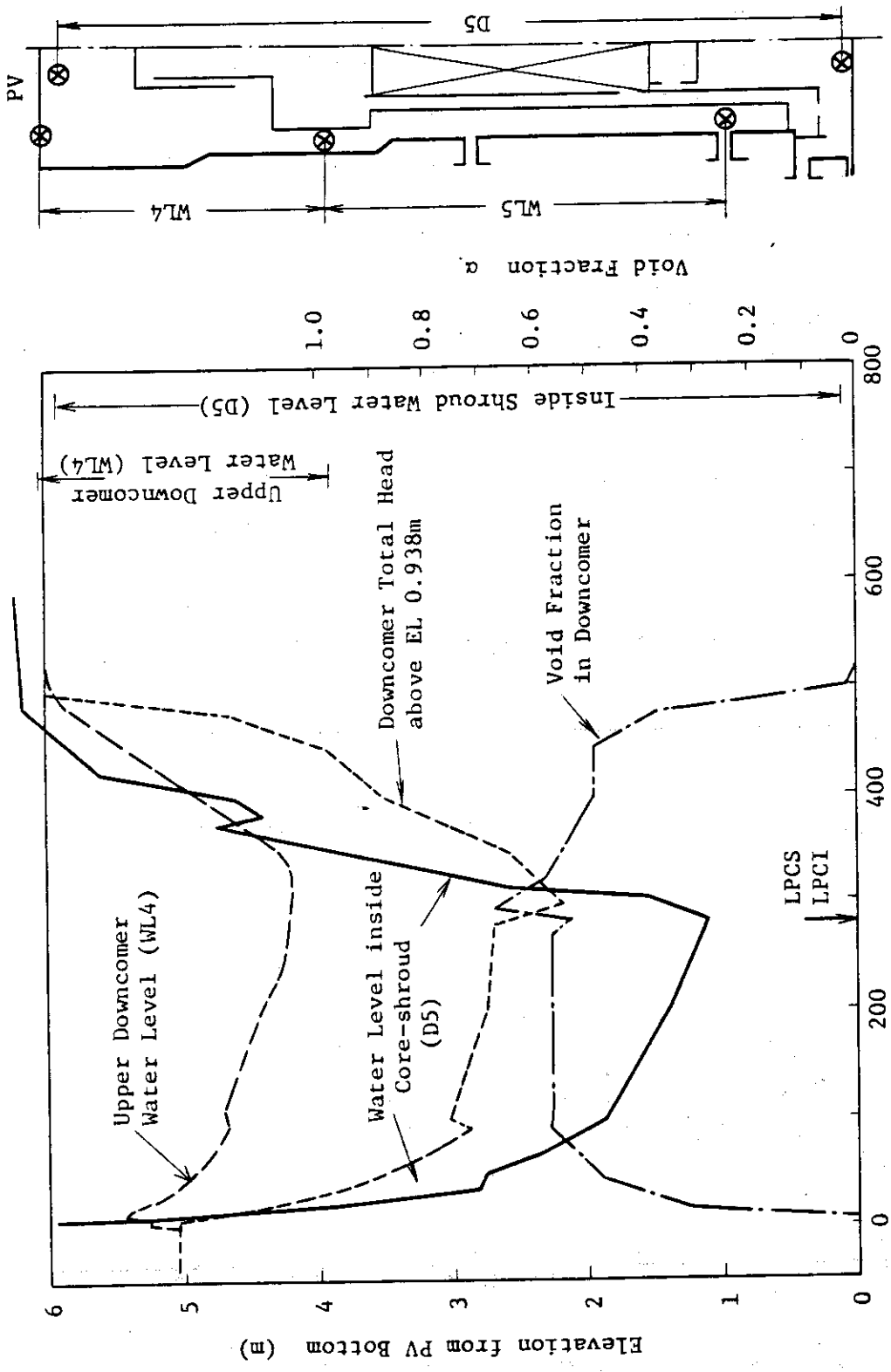

Fig. 6.15 Collapsed water levels in PV in a 100% steam line break test (RUN 953)

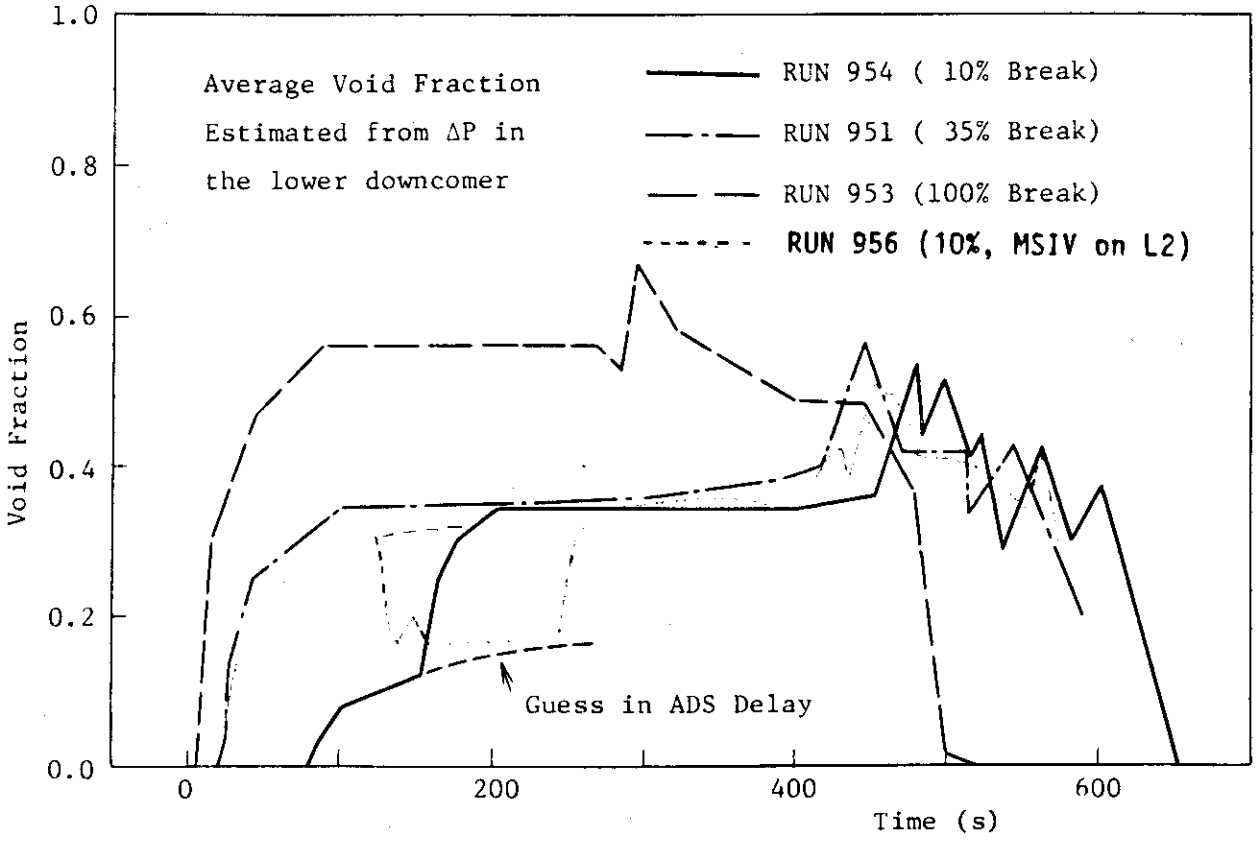

Fig. 6.16 Average void fraction in the lower downcomer estimated from diff. pressure data in steam line break tests

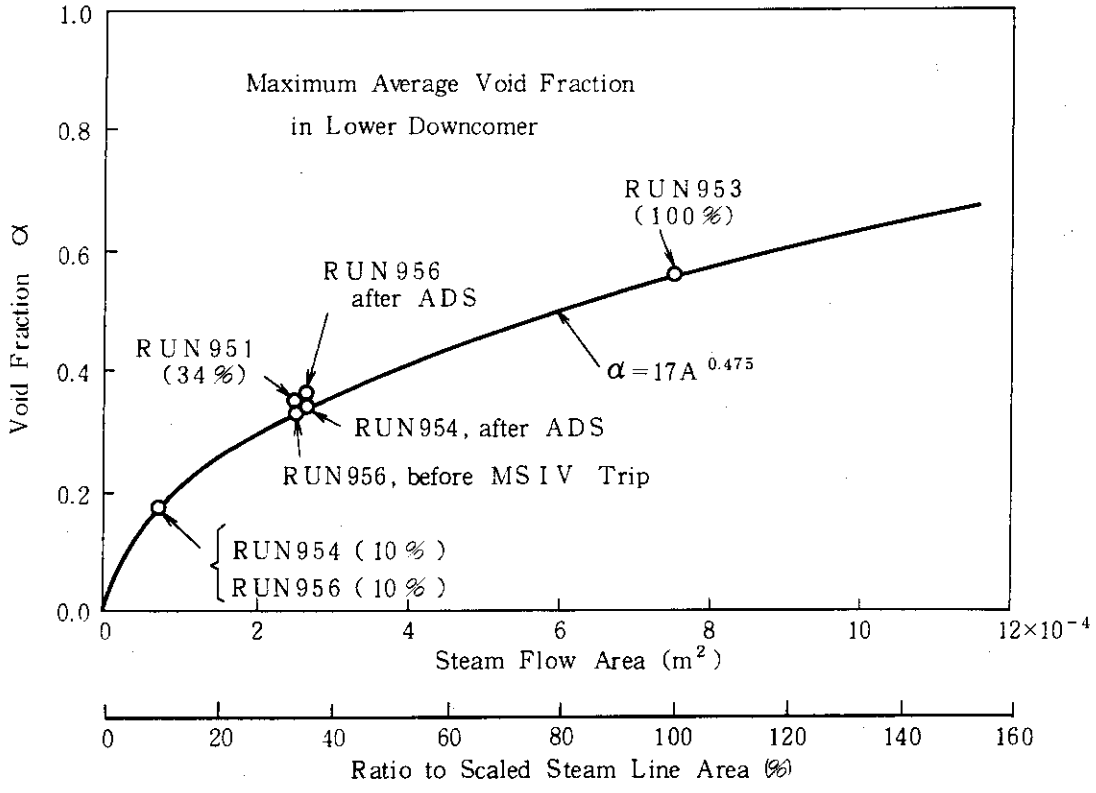

Fig. 6.17 Maximum average void fraction in lower downcomer related with total steam discharge flow area

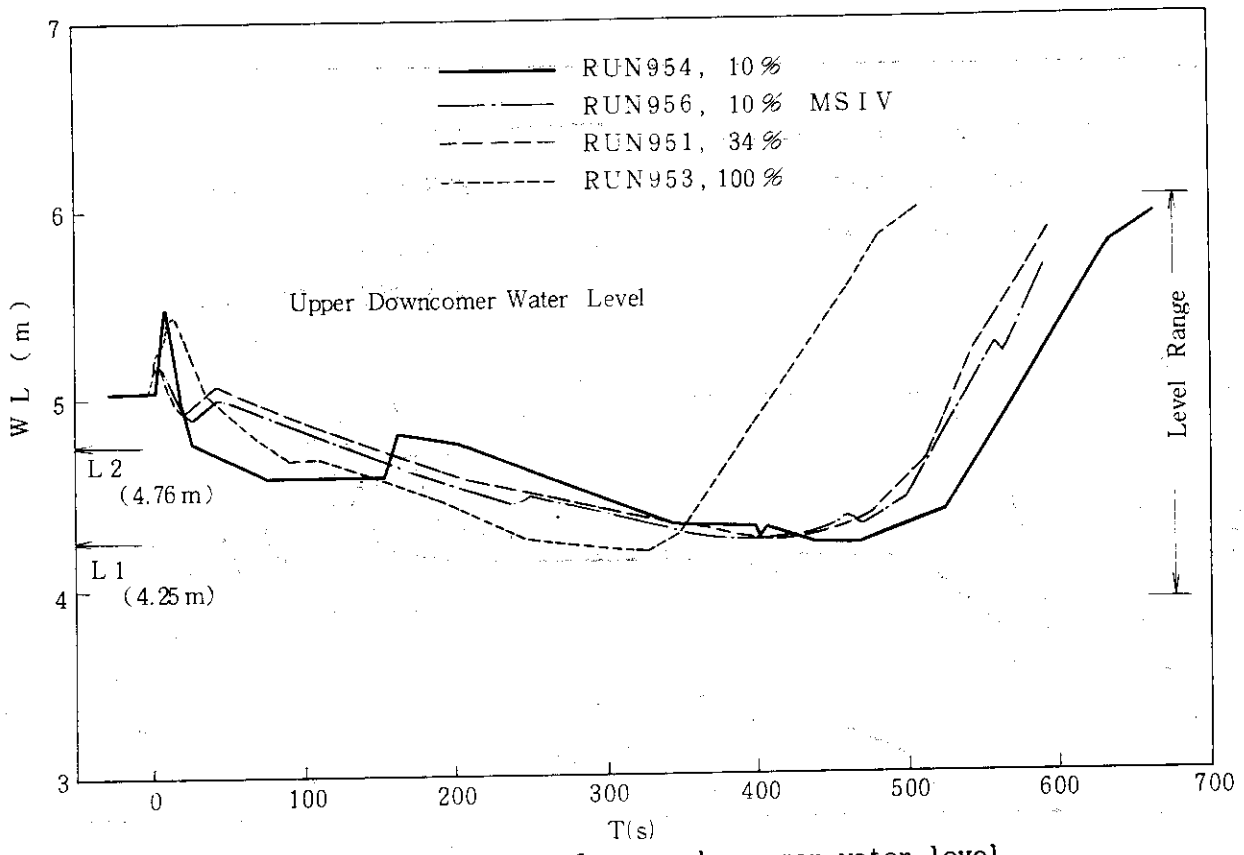

Fig. 6.18 Comparison of upper downcomer water level responses in steam line break tests

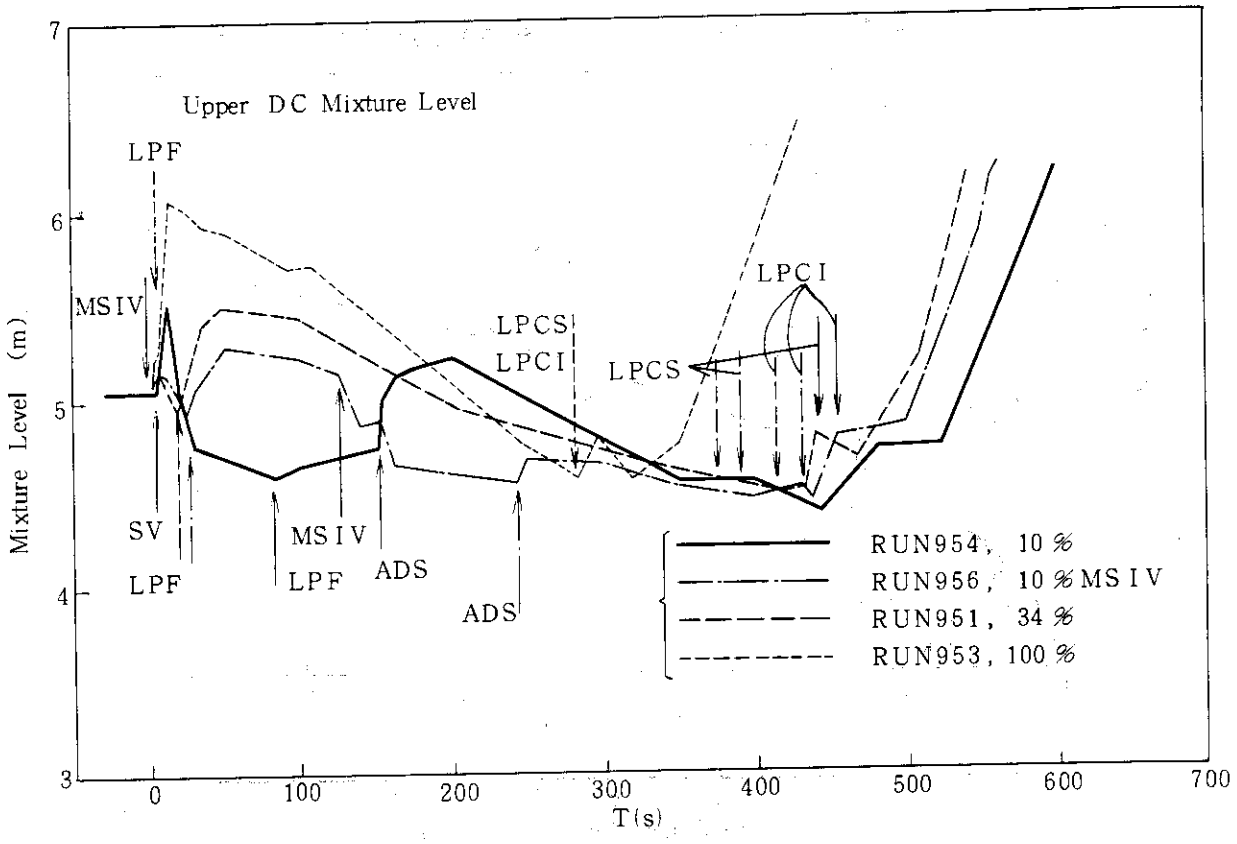

Fig. 6.19 Comparison of upper downcomer mixture level responses estimated from Fig.6.18 by assuming uniform void distribution in the downcomer

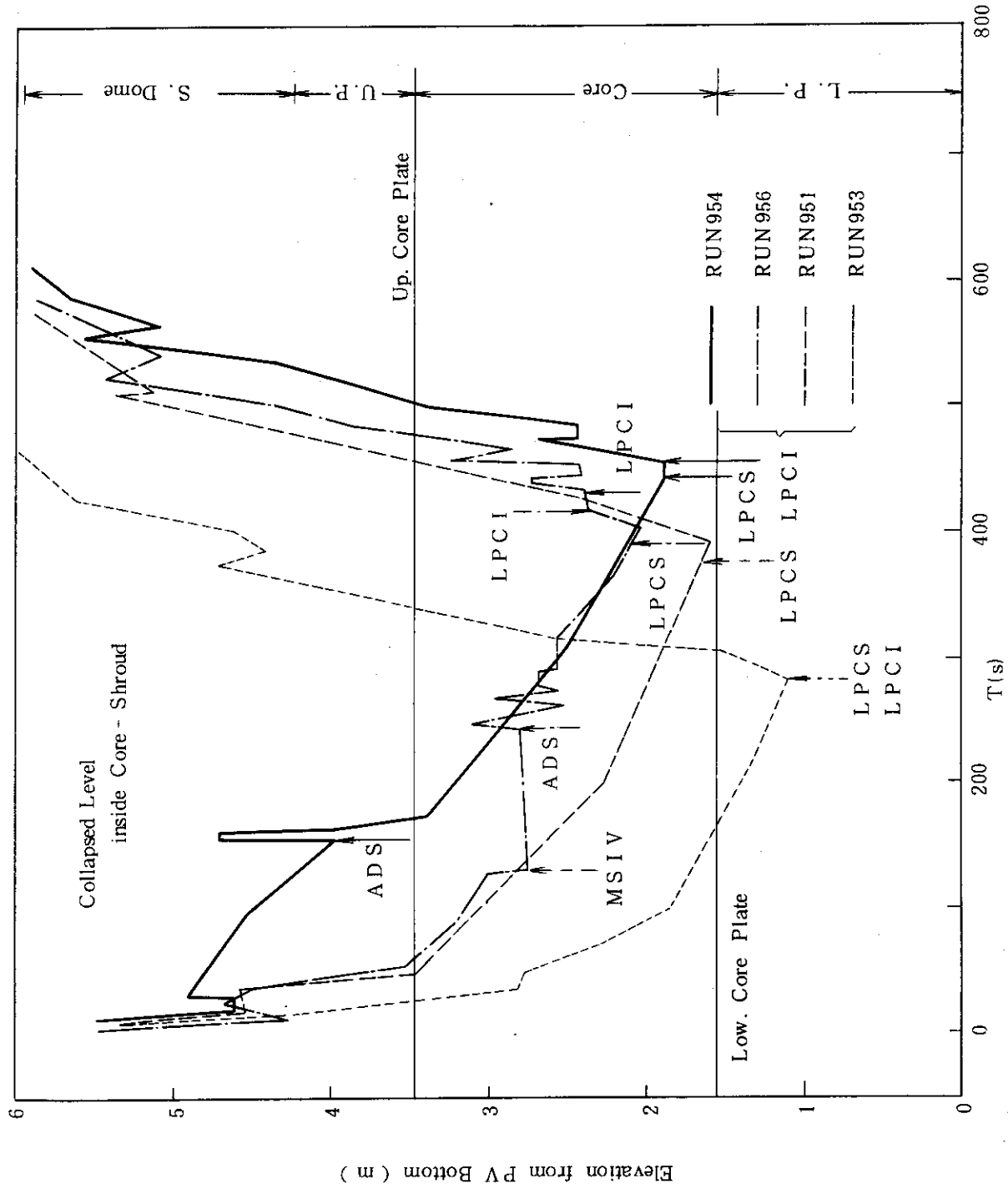

Fig. 6.20 Comparison of collapsed water level inside core-shroud in steam line break tests

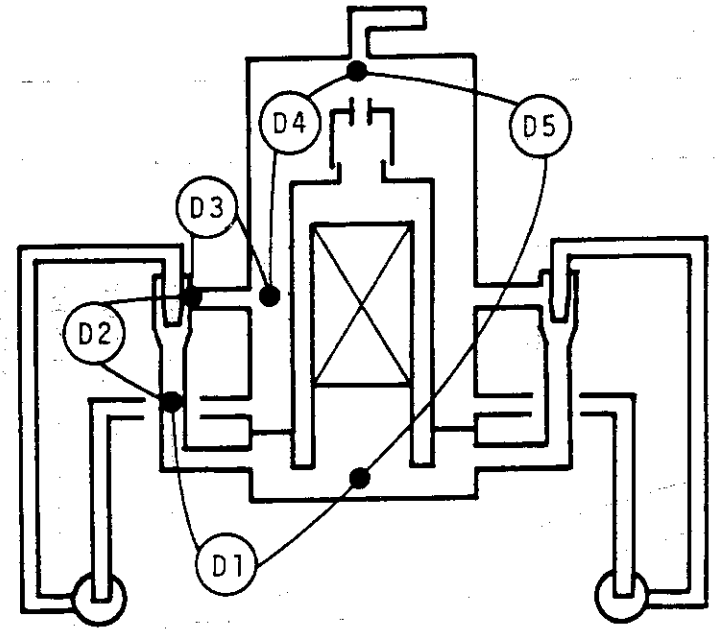

$$D5 = -D1 + D2 - D3 + D4$$

Measurement Location of Differential Pressures

D5 : DP between top and bottom of PV
(Ch.25, EL 0.10 - 5.91m)

D1 : DP between JP1 discharge and lower plenum
(Ch.41, EL 2.244 - 0.10m)

D2 : DP between JP1 discharge and suction
(Ch.26, EL 2.244 - 2.814m)

D3 : DP between DC middle and JP1 suction
(Ch.19, EL 2.814m)

D4 : DP between Dc middle and steam dome
(Ch.56, EL 2.814 - 5.91m)

Fig. 6.21 Pressure balance inside PV in terms of differential pressure data

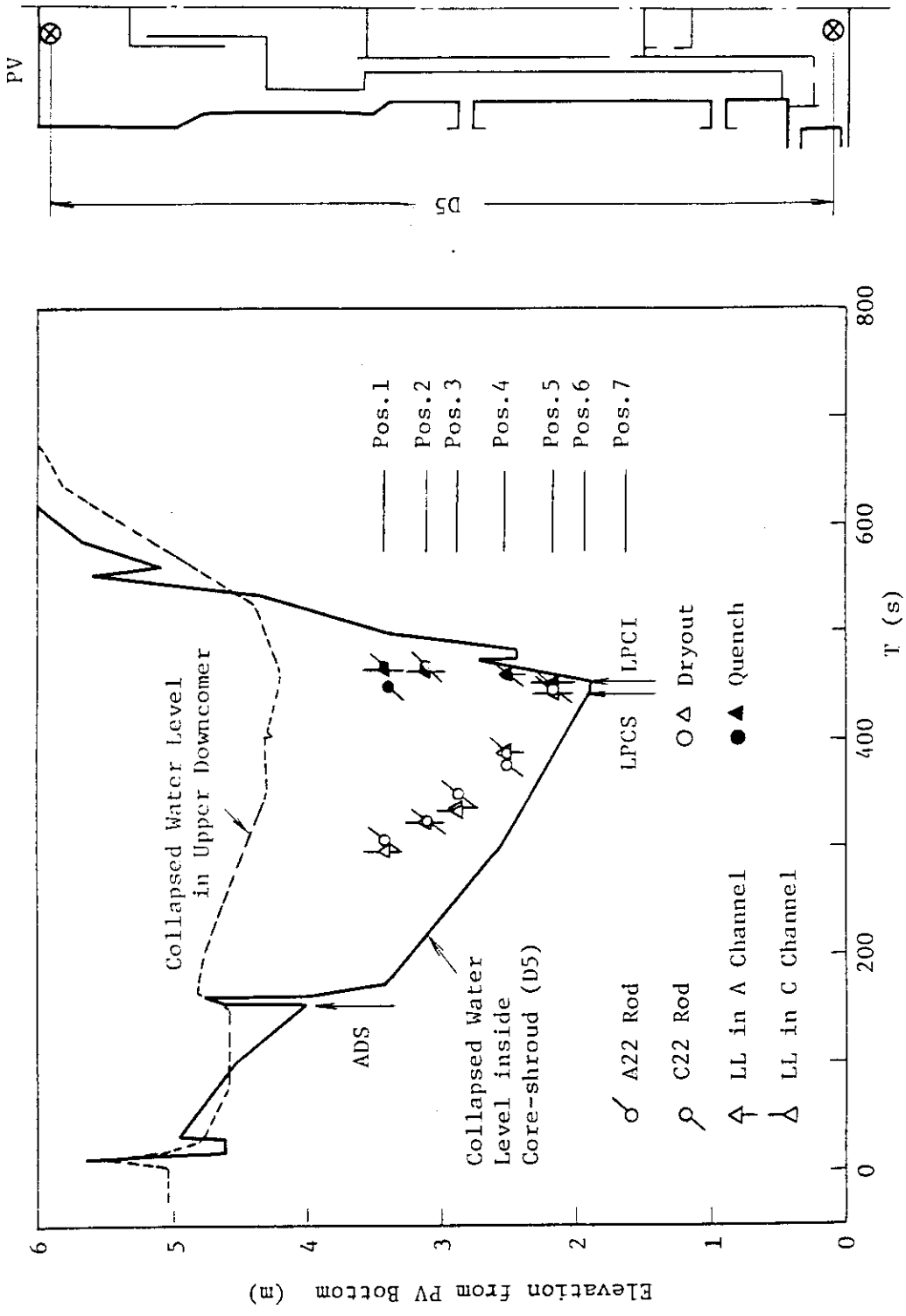

Fig. 6.22 Comparison of collapsed level, mixture level and fuel rod behaviors in PV in RUN 954

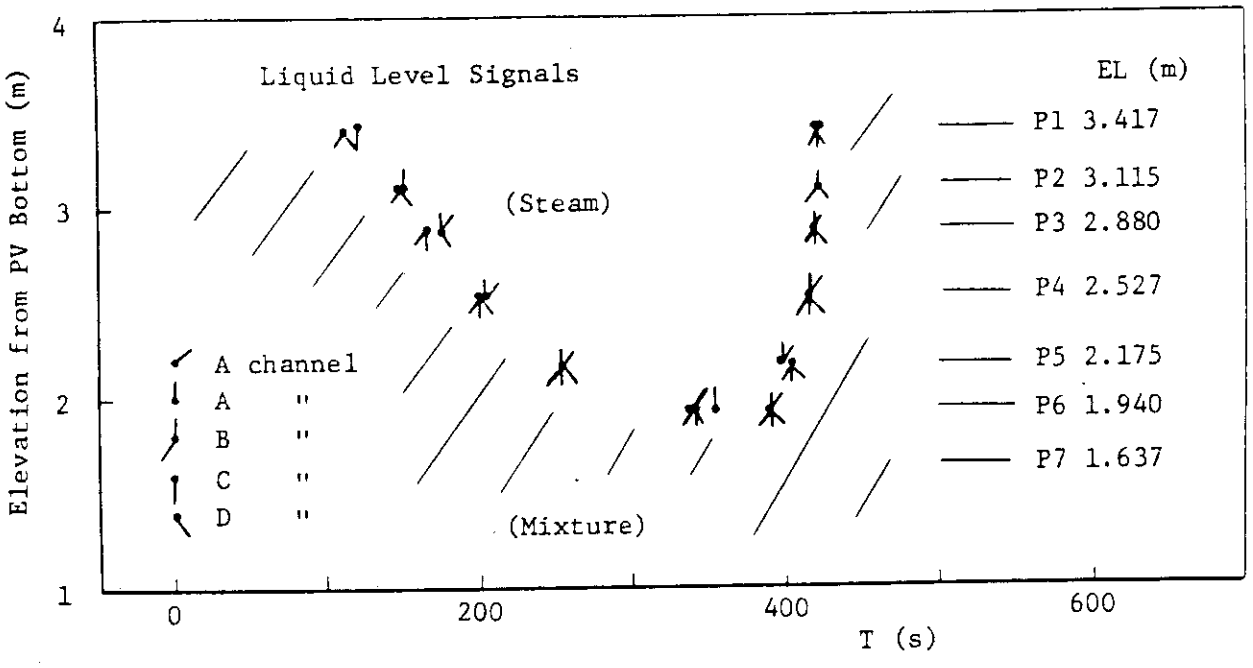

Liquid level signals in the core

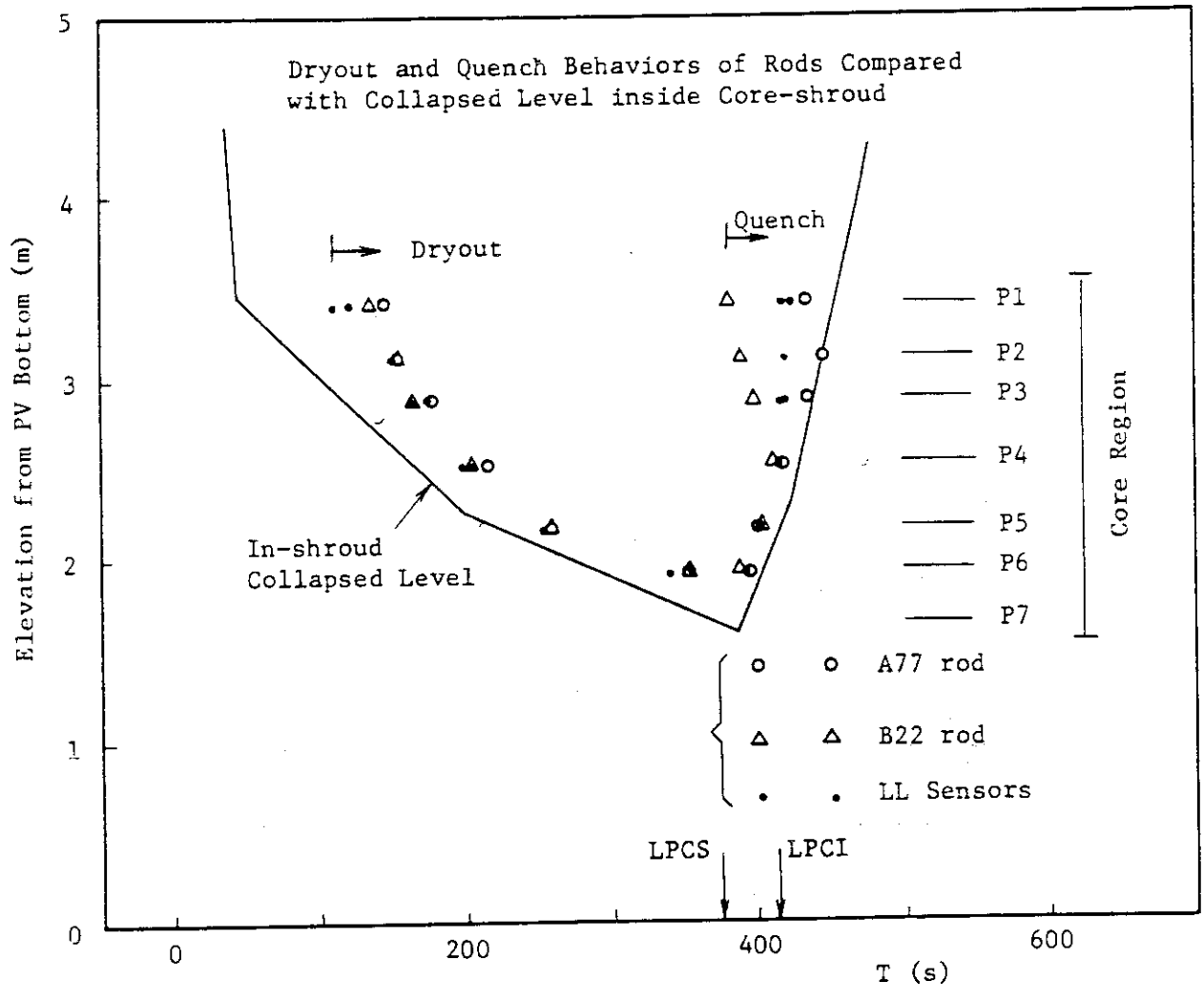

Fig. 6.23 Comparison of collapsed level, mixture level and fuel rod behaviors in PV in RUN 951

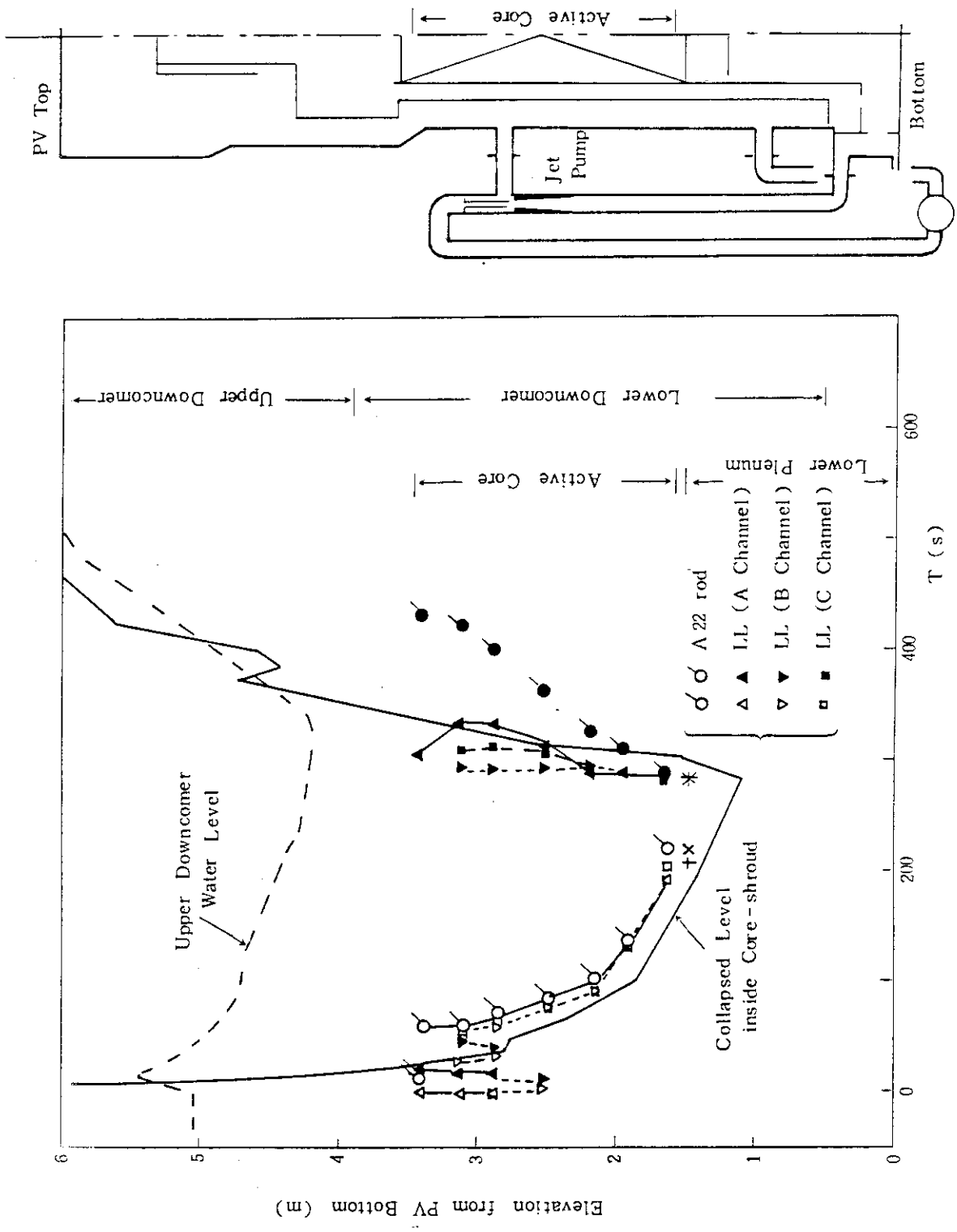

Fig. 6.24 Comparison of collapsed level, mixture level and fuel rod behaviors in PV in RUN 953